NOAA Atlas NESDIS 9

ATLAS OF SURFACE MARINE DATA 1994 VOLUME 4: ANOMALIES OF FRESH WATER FLUXES

Washington, D.C.
December 1994

U.S. DEPARTMENT OF COMMERCE
National Oceanic and Atmospheric Administration
National Environmental Satellite, Data, and Information Service

NOAA Atlas NESDIS 9

ATLAS OF SURFACE MARINE DATA 1994 VOLUME 4: ANOMALIES OF FRESH WATER FLUXES

Arlindo M. da Silva
Christine C. Young
University of Wisconsin-Milwaukee
Department of Geosciences

and

Sydney Levitus
National Oceanographic Data Center
Ocean Climate Laboratory

Washington, D.C.
December 1994

U.S. DEPARTMENT OF COMMERCE
Ronald H. Brown, Secretary

National Oceanic and Atmospheric Administration
D. James Baker, Under Secretary

National Environmental Satellite, Data, and Information Service
Robert S. Winokur, Assistant Administrator

National Oceanographic Data Center
USER SERVICES

Additional copies of this publication, as well as information about NODC data holdings, products, and services, are available on request directly from the NODC. NODC information and data are also available over the Internet through the NODC Home Page on the World Wide Web and the NODC Gopher server.

National Oceanographic Data Center
User Services Branch
NOAA/NESDIS E/OC21
Washington, DC 20235

Telephone: (202) 606-4549

Fax: (202) 606-4586

E-mail: services@nodc.noaa.gov

NODC Home Page: http://www.nodc.noaa.gov/

NODC Gopher server: gopher.nodc.noaa.gov

Contents

Acknowledgments

The work described in this atlas series would not be possible without the phenomenal work of the people in the COADS Project (Slutz *et al.* 1985; Woodruff *et al.* 1987) and the dedicated work of the observers on the many ships of the Voluntary Observing Fleet. We are particularly grateful to Scott Woodruff for long phone conversations and electronic mail messages which helped clarify many questions we had along the way. We also would like to thank Hans-Jörg Isemer for discussions regarding our wind speed correction. Special thanks go to S. Hastenrath, Y. Kushnir, and M. Rienecker for reviewing the manuscript. Most of the calculations reported here were conducted at the Department of Geosciences of the University of Wisconsin-Milwaukee (UWM). The support of Associate Dean Robert Hall and the UWM Geosciences Faculty is greatly appreciated. This work was concluded after A. da Silva joined the Data Assimilation Office of NASA's Goddard Space Flight Center; the support of R. Rood is acknowledged. At the later stages of this work C. Young has joined Systems Engineering and Security. This research has been supported by NSF grant ATM 9215811 (AMdS/CCY) and by NOAA's Climate and Global Change Program (SL/CCY). The data sets and products represented by this atlas are for distribution internationally, without restriction.

Atlas of Surface Marine Data 1994
Vol. 4: Anomalies of Fresh Water Fluxes

ARLINDO M. DA SILVA AND CHRISTINE C. YOUNG
Department of Geosciences, University of Wisconsin–Milwaukee
AND
SYDNEY LEVITUS
NOAA/National Oceanographic Data Center

Abstract

This atlas presents objectively analyzed fields of surface marine climatology and anomalies of evaporation, precipitation, constrained evaporation minus precipitation, constrained buoyancy flux, and zonal and meridional surface moisture flux over most of the global ocean. These revised monthly mean fields are derived from individual observations in the Comprehensive Ocean-Atmosphere Data Set (COADS) from January 1945 to December 1989 and are analyzed on a 1-degree by 1-degree global grid. Corrections have been made to reduce wind speed bias associated with an erroneous Beaufort equivalent scale and to consider missing Present Weather observations, from 1982 on, as representing clear weather if a cloudiness measurement is present. In addition to seasonal anomalies, maps of seasonal climatology, standard deviations, and the number of observations are presented for each quantity.

1 Introduction

The compilation of the Comprehensive Ocean-Atmosphere Data Set (COADS) as documented by Slutz *et al.* (1985) and Woodruff *et al.* (1987) has provided climate researchers with the most complete record of surface marine climate to date. The availability of this data set has contributed significantly to advancing our understanding of the atmosphere-ocean climate system. In addition to observational studies based on COADS, atmospheric and oceanic modelers have relied on this data set for boundary conditions in long-term integrations of atmospheric and oceanic circulation models.

One of the main contributions of the COADS project was to unify several historical data sets in a single, consistent format, and to subject the ship reports to the same quality control procedure. This homogenized data set is available in two forms: as monthly mean summaries in 2 by 2-degree boxes over the global oceans, and as raw individual observations. Due to the massive number of individual ship reports, the majority of researchers have used the monthly mean summaries.

In addition to the directly observed quantities (sea surface temperature, surface air temperature, etc.), COADS monthly mean summaries include a wealth of derived quantities such as moisture and pseudo oceanic fluxes, in which transfer coefficients have been ignored. In an attempt to extend and improve the oceanic fluxes in COADS, a collaborative project between the Department of Geosciences of the University of Wisconsin-Milwaukee (UWM) and the National Oceanographic Data Center/NOAA was initiated. The main goal of this project was to produce high resolution (1-degree by 1-degree), stability dependent heat and momentum fluxes, as well as evaporation, precipitation and radiational fluxes which were absent from the COADS monthly mean summaries. In addition to improved resolution and boundary layer parameterizations, a new scientific Beaufort equivalent scale was developed which reduces wind speed bias and artificial wind speed trends in the post World War II period.

Our revised monthly mean summaries (henceforth referred to as UWM/COADS monthly mean summaries) are available in the form of raw monthly means, standard deviations, and number of observations in 1 by 1-degree boxes over the global oceans, from 1945 to 1989. These raw data are made available for those users desiring to perform their own objective analysis. In addition, the monthly mean fields have

been objectively analyzed with essentially the same successive correction scheme used by Levitus (1982). It is important to note that although the analyzed fields are given with a 1-degree grid spacing, only wavelengths greater than about 770 km remain due to the smoothing effects of the analysis. Climatological half-degree by half-degree analyses have also been produced; these results will be discussed elsewhere.

In this atlas series, we present objectively analyzed seasonal mean anomalies along with climatology, standard deviations, standard error and observation density. In order to conserve space, we show seasonal averaged anomalies computed from the monthly anomalies. This volume documents the anomaly structure of fresh water fluxes for the period 1945–1989. Volume 1 describes all the computations in detail. The directly observed quantities are presented in Volume 2. Volume 3 deals with heat and momentum fluxes at the ocean surface. Additional derived quantities are included in Volume 5.

2 Data source and COADS quality control

The primary data source for this study is Release 1 of COADS which covers the period 1854–1979. For the 1980's we rely on an interim data product that preceded COADS Release 1A (recently made available). Release 1A adds more observations to the interim data base and extends it to 1992. This improved data base, which was not available in time for our calculations, will be used in future versions of our analyses.

As described below, our detailed calculations require the consideration of individual ship reports. Product 10 of COADS, the *Compressed Marine Reports* (CMR-5), contains individual reports of surface marine and atmospheric observations from merchant vessels, research vessels, buoys, and bathythermographs (Woodruff *et al.* 1987). The reports in CMR-5 include the following directly reported quantities:

- zonal and meridional wind components
- air temperature
- sea surface temperature
- sea level pressure
- dew point depression
- cloudiness
- present weather

along with quality control indicators which are briefly described next. The interested reader should consult the original COADS documentation (Slutz *et al.* 1985) for a detailed description of the quality control procedure. Note that wind, dew point depression and sea level pressure are not directly observed but rather calculated by ship personnel. When measured, the reported wind speed and direction are computed from the anemometer reading taking in consideration the ship velocity, a procedure that often introduces errors. Dew point depression is computed from the measured dry and wet bulb temperatures. Sea level pressure is computed from the measured pressure with a height correction to reduce it to sea level. WMO Publication No. 47 (e.g., WMO 1990), available yearly since 1955 (in digital form since 1973), lists all the Ships of the Voluntary Observing Fleet along with the ship instrumentation and routes. Kent and Taylor (1991) describes in some detail observing practice by VOS and the instruments they used during the VSOP-NA project (May/88 to September/90).

Quality control in COADS is implemented by means of a multiple step statistical procedure to identify "outliers." The first step is to generate *Decadal Summary Untrimmed Limits* for six variables: sea surface temperature, air temperature, air pressure, zonal wind, meridional wind, and humidity. Sextiles are calculated for each variable in every 2° box for each decade and month. Next, the first, third (the median), and fifth sextiles are averaged across latitude, longitude, month, and decade. Averaging is done for three non-overlapping periods (1854–1909, 1910–1949, 1950–79) in an attempt to separate possible climatic epochs or observational discontinuities. Further smoothing is done for the resulting 216 sets of sextile triplets (6 variables × 3 periods × 12 months). The result is three sets of smoothed lower and upper limits (σ_1, σ_5) around the smoothed mean ($\overline{x}$) for each variable, month, and 2° box. These means and limits are used to create trimming bounds for the variables. A detailed description of the statistical process can be found in Slutz *et al.* (1985), section C. Trimming flags for sea surface temperature, air temperature, humidity, wind and sea level pressure are included in CMR-5 for each observation. Note that trimming does not take into account different methods of observation within the same period, nor were bias corrections applied when the limits were generated.

We have used the COADS/CMR-5 flags to perform quality control on the data used as input to our 1-degree statistics and analysis. Table 1 summarizes the possible values of the quality control flags in COADS/CMR-5. In general, an observation is rejected if it differs from the smoothed median by more

than 3.5 "standard deviations" (flag value equal to 2) or the smoothed limits are not available (flag value equal to -999). However, over the regions climatologically covered by sea ice, this trimming procedure still yields very noisy fields. This is due to the irregular coverage of observations in ice-covered regions in both area and time. In an effort to generate smoother fields in regions where sea ice is common, a more stringent trimming criterion is used. If an observation occurs in a climatologically ice-covered region, the observation is trimmed if it differs from the smoothed median by more than 2.8 "standard deviations" (flag value equal to 1 or 2).

Table 1: Quality control flags in COADS/CMR-5, where x is is an individual observation of the variable under scrutiny, $\overline{x}$ is the smoothed median and σ_1 and σ_5 are the smoothed lower and upper median deviation. See text for details.

Flag Value	Trimming Limits	Trim?
0	$\overline{x} - 2.8\sigma_1 \leq x \leq \overline{x} + 2.8\sigma_5$	no
1	$\overline{x} - 3.5\sigma_1 \leq x < \overline{x} - 2.8\sigma_1$	if obs.
	or $\overline{x} + 2.8\sigma_5 < x \leq \overline{x} + 3.5\sigma_5$	over ice
2	$x < \overline{x} - 3.5\sigma_1$ or $x > \overline{x} + 3.5\sigma_5$	yes
-999	missing	yes

3 Known biases in COADS

The purpose of this section is to discuss some of the known biases and other problems in COADS surface marine reports. In subsequent sections, we describe our bias correction schemes for wind speed and Present Weather.

3.1 Sea surface temperature

Biases in sea surface temperature are associated with different methods of measurements (basically *bucket* and *intake*), which also respond in different ways to atmospheric conditions. On average, measurement with an uninsulated canvas bucket introduces an error of about 0.5°C due to evaporative cooling. Folland and Hsiung (1986) [see also Folland 1991] have developed a physical model for a typical canvas bucket that predicts the amount of evaporative cooling as a function of the atmospheric conditions and exposure time of the bucket. This model has been used effectively to correct the bias in bucket observations (Farmer *et al.* 1989). However, Farmer *et al.* (1989) have used the bucket correction method only for pre-World War II observations. Observations after that time were assumed to be almost exclusively measured by intake or by insulated buckets. This is consistent with the fact that the largest discontinuity in SST due to changes in measurement procedure (approximately one-half degree rise in SST around 1940) took place prior to our analysis period (Bottomley *et al.* 1990, Kushnir 1994).

Recently, the *Voluntary Observing Ships Special Observing Program for the North Atlantic* (VSOP-NA, Kent *et al.* 1993a) has found that observations of SST from insulated buckets and hull contact sensors are reliable. A constant bias of 0.35°C was found in observations from ships' intake thermometers compared to those measured by bucket.

The unreliability of the bucket/intake indicator in COADS and the lack of reliable information about the kind of bucket used make this correction impractical from individual observations. Therefore, we do not include a sea surface temperature correction in this version of our calculations.

3.2 Air temperature

Systematic errors in air temperature are believed to be caused primarily by the heating of the ship superstructure, causing biases of 0.4°–0.8°C in some regions of the tropics (Isemer and Hasse 1987 and references within). In view of this, some authors (Folland *et al.* 1984) have preferred to discard daytime observations. Although night time observations may be adequate to study long term trends in air temperature, we feel that it significantly reduces the number of observations and tends to bias the data toward a generally lower night time temperature.

Kent *et al.* (1993b) devised a method of correction for daytime surface air temperature based on wind speed and the incoming short wave radiation. Preliminary calculations by these authors indicate correcting daytime air temperature results in increases in mean sensible and latent heat fluxes of 3.3 and 1.0 W/m^2, respectively, in the North Atlantic Ocean (Kent and Taylor 1995). We intend to include such a correction in future versions of our data set, but we do not do so at this time.

3.3 Dew point temperature

Biases in dew point temperature are generally associated with contamination of the wet bulb thermometer by salt or insufficient moistening of the wet bulb thermometer wick. These instrumentation problems lead to a systematically higher value of the specific humidity. On average, the dew point temperature is biased about 0.5°C (Isemer and Hasse 1987 and references within). Since this bias is due mainly to human errors

for which no record is available, it is very difficult to devise a correction.

Kent *et al.* (1993a) have found that dew point temperature measured by psychrometers were on average lower than those reported from ships using screens. By considering the many factors that might have contributed to this discrepancy, Kent *et al.* (1993a) concluded that psychrometer observations were more reliable and a simple regression equation was devised to correct screen-measured dew point temperatures. Because of inadequate metadata in COADS/CMR-5 (there is no indicator of the method of measurement for dew point temperature) this correction could not be implemented at the present time.

3.4 Wind speed

Because wind is a key parameter for the determination of the air-sea fluxes at the ocean surface, a great deal of effort has been devoted to sort out the problems with ship winds. Wind speeds reported by ships are either directly measured with anemometers or are estimated from the *sea state*. Instrumentation problems with anemometers are believed (or better, assumed) to be non-systematic and are expected to cancel out when spatial/temporal averages are taken. Estimated winds are somewhat subjective and depend on the skill of the observer. But even when a correct identification of the sea state is made, it still needs to be converted to wind speed through a Beaufort equivalent scale.

Since 1946, a Beaufort equivalent scale developed by Simpson (1906), combined with a well defined sea state devised by Petersen (1927), has been used by meteorological weather services (Roll 1965; Isemer and Hasse 1991). This scale is known as Code 1100 and is sometimes referred to as the *old* WMO scale. It is now widely accepted that the old WMO Beaufort equivalent scale results in systematic biases when compared to anemometer measured winds. There are a few alternative Beaufort equivalent scales (WMO 1970; Cardone 1969; Kaufeld 1981), and they all suggest that the old WMO scale underestimates the winds for Beaufort numbers less than about 6 and overestimates winds for Beaufort numbers greater than about 6. As pointed out by Isemer and Hasse (1991), this systematic error causes climatological wind speeds to be underestimated, and climatological wind speed standard deviation to be overestimated in the North Atlantic Ocean. Concerning long term variability, Cardone *et al.* (1990) have shown that a Beaufort scale correction, ship anemometer height adjustment, and stability correction strongly reduce artificial trends in wind speed, and drastically improve the agreement between measured and estimated winds.

Finally, most definitions of transfer coefficients are calibrated to work with winds from a reference level of 10 m above the ocean surface. Cardone *et al.* (1990) suggest that the average ship anemometer height is actually 20 m. Kent *et al.* (1993a) shows that during VSOP-NA a typical anemometer height is in the range 15–20 m, but on modern container ships the anemometer heights are about 30 m. A common approximation is to take the 20 m wind in place of the required 10 m. Since virtually all ship anemometers are higher than 10 m, this approximation introduces a systematic error. Isemer and Hasse (1991) estimated that the 10 m wind speed is on average 93% of the wind speed at 20 m. Calculations by the authors show that for light winds under stable conditions, the surface layer has strong shear and the wind at 10 m can be as low as 40% of the wind speed at 20 m. This result suggests that a careful stability dependent correction is warranted.

The ship type indicator, however, is often incorrect or missing in COADS/CMR-5. This is particularly significant in the 1980's when large numbers of drifting buoys were placed in the southern oceans. We have found that nearly all buoy observations in the COADS/CMR-5 1980's interim product are not identified correctly. The result is that a wind observation measured at 5 m is treated as if it were taken at 20 m. Winds in regions sampled mainly by drifting buoys will be biased toward lower values. This problem has apparently been fixed in COADS Release 1A and the correct identification of buoys will be included in future analyses.

3.5 Present Weather

A code number signifying the present weather conditions is recorded as a standard part of a ship's observation. This code can be used as a proxy for precipitation, as precipitation is rarely measured on ships. Beginning in the early 1980's, the WMO no longer required Present Weather (PW) to be recorded for clear weather observations (S. Woodruff, personal communication). Previously, in clear weather episodes, the observer entered a code number indicating there was no weather observed. When the observations in the 1980's were entered into the COADS interim product, the missing clear weather observations were given the missing flag, just as truly missing PW observations were. Using such observations as they are recorded in COADS would eliminate most if not all clear weather (rainless and snowless) reports. If few clear weather reports are available, the result would be a wet bias in the 1980's precipitation. This effect would be particularly evident in climatologically clear areas, such as below the subtropical highs. In the course of this investigation, it was discovered that there is indeed a

sharp increase in the number of missing PW observations beginning in 1982.

4 Bias corrections

This section documents our bias correction procedures for wind speed and Present Weather. No additional correction is applied to the other directly observed quantities.

4.1 Wind speed

Several scientific Beaufort equivalent scales have been developed to correct WMO Code 1100 (WMO 1970; Cardone 1969; Kaufeld 1981). Data used to generate these scales have mainly been limited to the North Atlantic and North Pacific oceans. In Vol. 1, we have examined the performance of several Beaufort equivalent scales by comparing monthly mean estimated and anemometer measured wind speeds in the Northern Hemisphere oceans. The analysis was conducted for the two decades from 1970 to 1989, a period which has a good mix of estimated and measured wind observations. Taking the wind speed measurement indicator (flag WI in COADS/CMR-5) at face value, all available Beaufort equivalent scales showed climatological biases in at least some part of the wind speed range. This fact prompted the authors to empirically derive a Beaufort equivalent scale which attempts to reduce the climatological wind speed bias in COADS. After much experimentation we derived a wind speed correction of the form

$$W_{\text{new}} = x_1 W_{\text{old}} + x_2 \sqrt{W_{\text{old}}} \qquad (1)$$

where W_{old} is the WMO Code 1100 speed of the estimated wind and W_{new} is the corrected wind speed. We find that this functional form fits the relationship between measured and estimated winds reasonably well and can also accurately express the other alternative Beaufort equivalent scales. In particular, it is shown in Vol. 1 that this method also produces consistent measured/estimated wind speed standard deviations. It is important to note that the formula above is valid only for individual observations and should not be used to correct monthly mean quantities. The factors x_1 and x_2 were determined for several averaging periods (annual and monthly means), and for several regions of the world oceans by means of a least squares fit. After examining the seasonal/regional sensitivity of the correction, it was concluded that a single set of parameters x_1,x_2 based on Northern Hemisphere January data was sufficient. The chosen values are

$$x_1 = 0.7870, \qquad x_2 = 0.9547. \qquad (2)$$

This choice of parameters gives mean measured/estimated wind speeds with regression slopes within 5% of 1 and standard deviations less than 0.4 m/s (see Vol. 1). Table 2 lists equivalent wind speed for WMO Code 1100 and our new Beaufort equivalent scale. It is important to realize that this new Beaufort equivalent scale produces wind speeds valid at a 20 meter reference level. Whenever 10 meter wind speed is required, the proper conversion from 20 meters should be performed using stability dependent surface layer similarity theory. For additional details on this wind speed correction procedure, the reader is referred to Vol. 1.

Table 2: WMO Code 1100 and the revised Beaufort equivalent scale. The equivalent wind speed is given in m/s.

Beaufort Number	**Equivalent Wind Speed** Code 1100	Revised Scale
0	0	0
1	0.8	1.5
2	2.4	3.4
3	4.3	5.4
4	6.7	7.7
5	9.4	10.4
6	12.3	13.0
7	15.5	16.0
8	18.9	19.0
9	22.6	22.4
10	26.4	25.7
11	30.6	29.3
12	34.9	33.1

4.2 Present Weather

Beginning in 1982, clear weather observations are often recorded with a missing Present Weather indicator. This practice has an adverse effect on our precipitation estimates as it introduces a *wet* bias. In order to circumvent this problem we have devised a method of correction which links PW with cloudiness. It is assumed that any observer making a cloud cover observation will also make a PW observation, and vice versa. Therefore, when encountering a missing observation from 1982 and later observations, cloudiness is checked. If cloudiness is missing, PW is assumed to be missing, and is not included in the precipitation calculation. If a cloudiness observation is present, however, it is assumed that there was a PW observation and that the weather was clear. The observation is used as a clear weather observation in the precipitation calculation. As a test, PW and cloudiness

observations were checked prior to 1982. Cases in which a cloudiness observation was present but the PW observation was missing were very rare. We are confident, therefore, that our method of correcting PW is accurate.

5 Parameterizations

This section describes the parameterizations used in the production of the data set. The thermodynamic quantities described below (e.g., specific humidity, vapor pressure, etc.) are computed as in COADS (Slutz *et al.* 1985) using the software documented in Schlatter *et al.* (1981).

Symbols

B	buoyancy flux (kg $m^{-1}s^{-3}$)
c_p^{air}	specific heat of air (J $K^{-1}kg^{-1}$)
c_p^w	specific heat of water as a function of temperature and salinity (J $K^{-1}kg^{-1}$)
C_E	Dalton number (unitless)
E	evaporation rate (m s^{-1} or mm/(3hr))
F_S	flux of salt at ocean's surface (p.s.u. m s^{-1})
F_T	normalized net heat flux (K m s^{-1})
g	acceleration due to gravity (m s^{-2})
P	precipitation rate (m s^{-1} or mm/(3hr))
q	specific humidity (g kg^{-1})
q_s	saturation specific humidity at the surface (g kg^{-1}), $q_s = 0.98 q_{satur}(T_s)$
Q_{net}	net heat flux (W m^{-2})
Q_L	latent heat flux (W m^{-2})
Q_S	sensible heat flux (W m^{-2})
R_L	long wave radiation (W m^{-2})
R_S	short wave radiation (W m^{-2})
S	salinity (p.s.u.≡parts per thousand)
T_a	surface air temperature (° C or K)
T_s	sea surface temperature (° C or K)
W	wind speed, $W = \sqrt{u^2 + v^2}$ (m s^{-1})
α'	thermal expansion coefficient of sea water (K^{-1})
β'	haline coefficient of sea water (p.s.u.$^{-1}$)
ρ	air density (kg m^{-3})
ρ_w	water density as a function of temperature and salinity (kg m^{-3})
ρ_0	fresh water density as a function of temperature (kg m^{-3})

5.1 Evaporation

The bulk formula for evaporation is given by

$$E = \frac{\rho}{\rho_0} C_E W \Delta q \qquad (3)$$

The transfer coefficient C_E is estimated using the Large and Pond (1982) formulation (see Vol. 1), which gives

$$C_E = C_E(W, T_a, \Delta T, \Delta q) \qquad (4)$$

with

$$\Delta T = T_s - T_a \qquad (5)$$

$$\Delta q = q_s - q \qquad (6)$$

where ΔT is in units of ° C and Δq is unitless (grams per gram). Upon calculation, evaporation is converted from units of m/s to mm/(3 hours) in order to match the units used for precipitation. For reference, the neutral transfer coefficient is given by

$$C_{EN} = 1.2 \times 10^{-3}\,. \qquad (7)$$

Evaporation requires a complete ship report for its calculation. In practice it is difficult to obtain complete ship reports, and cases in which one or more of the quantities is missing are very common (Cardone *et al.* 1990). In order to circumvent the problem, evaporation is computed for all ship reports in which the wind and Δq data are available (neither missing nor trimmed by the quality control procedure). If a particular thermodynamic quantity is available, then it is used to compute C_E. Otherwise it is simply *filled in* with the analyzed monthly mean for that grid point and particular month.

5.2 Precipitation

Accurate measurements of precipitation at sea are extremely difficult to take. As a result, precipitation rate is not included in ship reports. However, the type of weather the ship encounters is recorded and can be used as a precipitation proxy.

Precipitation rate is estimated using the method developed by Tucker (1961). The method uses the Present Weather (PW) information of standard ship reports and relates it to precipitation rate according to a regression formula.

The PW is reported at 3 hour intervals (usually less frequently) with the results being coded from 00 to 99. Tucker considers that weather associated with codes 50 to 99 contribute significantly to precipitation. Based on data for 12 stations around the British Isles, Tucker derived a regression formula which relates precipitation during the 3 hour sampling interval to the amount of light, moderate, or heavy precipitation (x, y, and z respectively). Each PW code is then expressed as a linear combination of x, y, and z as shown in Table 3. Tucker's estimates for these coefficients are x = 1.85 mm, y = 5.66 mm, and z = 8.13 mm per 3 hour period.

Table 3: Precipitation rate in terms of x, y, and z for Present Weather codes 50 through 99 (from Tucker 1961): $x = 1.85$ mm/(3 hours), $y = 5.66$ mm/(3 hours), and $z = 8.13$ mm/(3 hours).

PW	0	1	2	3	4	5	6	7	8	9
50	0	$x/2$	$x/2$	x	y	$2y$	$x/2$	$y/2$	$x/2$	$y/2$
60	$x/2$	x	$y/2$	y	$z/2$	z	x	$(y+z)/2$	x	$(y+z)/2$
70	$x/2$	x	$y/2$	y	$z/2$	z	0	0	0	0
80	$x/2$	$y/2$	$z/2$	$x/2$	$(y+z)/4$	$x/2$	$(y+z)/4$	$x/2$	$(y+z)/2$	$x/2$
90	$(y+z)/2$	x	$(y+z)/2$	x	$(y+z)/2$	$(x+y)/2$	$(x+y)/2$	z	0	z

Because the PW does not have an adequate range to accommodate the tropics, Dorman and Bourke (1978) derived an additional correction which takes into consideration the local air temperature:

$$P_{\text{corrected}} = P_{\text{Tucker}}(a + bT_a + cT_a^2)\,. \qquad (8)$$

Dorman and Bourke (1978) give correction coefficients a, b, and c for each month of the year. The coefficients are shown in Table 4. The corrected values for P are used to calculate monthly mean precipitation rate.

The precipitation fields obtained with the formula above showed an unrealistic minimum in Spring when compared to estimates from NMC and NASA/Goddard (Schubert *et al.* 1993) reanalyses, as well as Arkin and Meisner's (1987) GOES Precipitation Index. This abrupt decrease of precipitation in spring is not present in the uncorrected P_{Tucker}, but is introduced, rather, by the correction factor $(a + bT_a + cT_a^2)$. In order to remove this spurious seasonal cycle in precipitation, we have used the annual mean of Dorman and Bourke's (1978) correction factor in our precipitation calculations: the monthly mean correction was calculated from the 12 monthly climatologies of air temperature and averaged to form the annual mean correction. This modification has little effect on the annual mean precipitation and fresh water fluxes into the ocean. The precipitation fields computed with Dorman and Bourke's (1978) original approach will be made available upon request.

5.3 Buoyancy flux

The buoyancy flux out of the ocean is computed by the formula (e.g., Schmitt *et al.* 1989)

$$B = g\rho_w\,(\alpha' F_T + \beta' F_S) \qquad (9)$$

where ρ_w is the water density at the surface, and α' and β' are the thermal expansion and haline coefficients:

$$\alpha' \;=\; -\frac{1}{\rho_w}\frac{\partial \rho_w}{\partial T_s} \qquad (10)$$

$$\beta' \;=\; \frac{1}{\rho_w}\frac{\partial \rho_w}{\partial S}\,. \qquad (11)$$

In eq. (9) $F_T = -Q_{\text{net}}/\rho_w c_p^w$ is the normalized heat flux, with Q_{net} being the net heat flux into the ocean:

$$Q_{\text{net}} = R_S - Q_L - Q_S - R_L\,. \qquad (12)$$

The flux of salt due to loss of fresh water at the surface is given by:

$$F_S = S\frac{E-P}{1-\frac{S}{1000}}\,. \qquad (13)$$

The components of net heat flux (Q_{net}) and the evaporation and precipitation rate estimates are computed from COADS individual observations as described above and adjusted using the constraints discussed in section 7. Sea surface salinity, S, however, is not part of standard ship synoptic weather reports. As salinity enters the above equation primarily as a coefficient, and as the interannual variability of salinity is only a few percent of its climatological value, we use the Levitus *et al.* (1994) monthly climatological surface salinity values in the above formula.

6 Computation of monthly statistics and objective analysis

The raw monthly fields are computed from the individual observations in the following manner:

1. The world oceans are divided into boxes with constant grid spacing in latitude and longitude. The grid we consider here is 1-degree latitude by 1-degree longitude (the same as Levitus [1982]).

2. All available (quality controlled) observations are averaged in each box for each month during the 45 year period, and the standard deviation and number of observations recorded. Bias corrections, if applicable, are made to each individual observation before averaging.

The raw monthly mean fields are then objectively analyzed to filter out spatial noise and interpolate

to gridpoints where data are missing. The objective analysis scheme used is essentially the same scheme described by Levitus (1982). This is an iterative difference-correction scheme (Cressman 1959) with a weight function developed by Barnes (1964). The procedure can be summarized as follows:

1. Determine a first guess F (see below).

2. Compute the difference between the raw observed data (O) and the first guess (F),

$$Q_{ij} = O_{ij} - F_{ij},$$

at grid point (i, j).

3. Compute the smoothed analysis increments

$$C_{ij} = \frac{\sum_{s=1}^{n} W_s Q_{i_s,j_s}}{\sum_{s=1}^{n} W_s} \qquad (14)$$

where W_s is the Barnes weight function: $W_s = \exp(-4r^2 R^{-2})$ for $r \leq \mathcal{R}$ where r is the distance between the sth gridpoint (i_s, j_s) and the analysis gridpoint (i, j). The sum on the RHS is over the region of influence, i.e., those points that are at a distance less than $\mathcal{R}$, the radius of influence.

4. Update the first guess

$$F_{ij} := F_{ij} + C_{ij}\,. \qquad (15)$$

5. Apply a 5–point nonlinear median filter to F_{ij} (Beaton and Tukey 1974; Rabiner *et al.* 1975) followed by two passes of a 5–point linear filter (Shapiro 1970). It was found that this combination effectively filters out noise with scales of the mesh-size. The two filters are applied as follows:

   (a) Non-linear. The smoothed value at the grid point (i, j) is simply the *median* value of the nine grid points in the 3 by 3 box centered at the grid point (i, j). The filter is not applied to grid points located over or adjacent to land. The median filter is used to remove noise from the data while preserving sharp gradients (Reynolds 1988; Rabiner *et al.* 1975).

   (b) Linear. The smoothed value S_{ij} at grid point (i, j) of a grid G is

$$\begin{aligned} S_{ij} &= G_{ij} + \frac{\alpha}{4}(G_{i-1,j} + G_{i+1,j} \\ &+ G_{i,j-1} + G_{i,j+1} - 4G_{ij}) \end{aligned}$$

   where α is a smoothing parameter. Two passes of the Shapiro filter are performed with $\alpha = 0.5$ for the first pass and $\alpha = -0.5$ for the second pass. The second pass is intended to restore the amplitude of the large scales which were slightly damped in the first pass (Shapiro 1970). The filter is not applied to the grid point if it is located over land or if any of the four adjacent grid points (north, south, east, and west) are located over land.

6. Repeat steps 2–5 with a different radius of influence R.

The radius of influence is decreased with each pass in order to analyze smaller scale features with each successive iteration (Cressman 1959). In practice, the smallest wavelengths are noisy. Therefore, the smallest radius of influence needs to be at least seven to eight times the average separation distance (Levitus 1982). The smallest radius of influence we use, 771 km, is over seven times the average separation distance of a 1- by 1-degree grid.

For climatologies and anomalies, 4 passes of the analysis scheme are performed with radii of influence equal to 1541 km, 1211 km, 881 km, and 771 km, as in Levitus (1982). These radii correspond to 14°, 11°, 8°, and 7° in latitude and longitude at the Equator. At 60° latitude North or South, the radii correspond to 28°, 22°, 16°, and 14° longitude. Below 40°S only the first two passes of the analysis are used in an effort to smooth the noisy data in these latitudes. The standard deviation and standard error fields are also noisy. In order to smooth them sufficiently, only two passes of the analysis are applied to those fields, using the two largest radii.

The response function for the objective analysis using four passes with radii of 1541, 1211, 881, and 771 km, but without any linear or nonlinear filter, is given in the second column of Table 5 (from Levitus 1982). As expected, the short wavelengths are damped severely while the intermediate and longer wavelengths receive moderate and little damping, respectively. Table 5 also shows the response function of the analysis including the linear filter, for both four passes and two passes of the analysis. Notice that the damping is much greater for all but the smallest wavelengths with two passes of the analysis compared to that with four passes. For extremely long wavelengths (not shown), the damping from two passes of the analysis is nearly identical to the damping from four passes.

Finally, the first guess for the analysis depends on the kind of data being analyzed:

Annual Mean Climatology:

Individual raw monthly means are averaged to produce the raw monthly mean climatologies.

Table 4: Monthly air temperature correction coefficients (from Dorman and Bourke 1978). Temperature should be given in Celsius.

	a	b	c
Jan	0.973	0.0469	0.00382
Feb	0.941	0.0412	0.00207
Mar	0.804	0.0404	0.000129
Apr	0.720	0.0603	0.000042
May	0.489	0.0678	0.000012
Jun	0.726	-0.1030	0.008885
Jul	1.734	-0.2362	0.011943
Aug	1.115	-0.1217	0.008146
Sep	0.548	0.0060	0.005140
Oct	0.671	0.0421	0.002934
Nov	0.896	0.0701	0.001350
Dec	0.985	0.0662	0.001148

Table 5: Response function for objective analysis with and without linear Shapiro filter.

wavelength	no filter	with filter	
(km)	4 passes	4 passes	2 passes
3300	1.00	1.01	0.90
2640	0.99	1.00	0.77
2200	0.97	0.98	0.65
1980	0.95	0.95	0.56
1650	0.87	0.88	0.36
1320	0.70	0.69	0.14
1100	0.49	0.49	0.07
990	0.37	0.36	0.04
880	0.23	0.22	0.01
660	0.05	0.05	0.01
550	0.02	0.02	0.01

These monthly climatologies are averaged to produce the raw annual climatology. The first guess for the annual climatology analysis is the zonal average for the individual ocean basins, following Levitus (1982).

Monthly Mean Climatologies:
The first guess for the analysis of a raw monthly climatology is the analyzed annual mean climatology.

Monthly Mean Anomalies:
From the observed raw monthly mean fields, the monthly mean analyzed climatology is subtracted to produce observed *raw* anomalies. A zero field is used as first guess in the analysis scheme.

Monthly Standard Deviation/Error:
The first guess for the analysis of the raw monthly standard deviation or standard error is the zonal average for the individual ocean basins.

7 Fine tuning of heat and fresh water fluxes

One of the applications of surface marine fluxes is the study of the heat and fresh water balances of the world oceans. Similar calculations based on surface marine data have been performed by many authors (Budyko 1956, Baumgartner and Reichel 1975, Esbensen and Kushnir 1981, Hastenrath 1982, Hsiung 1985, Oberhuber 1988, Isemer *et al.* 1989, among others.) As an example, consider the vertically integrated heat budget equation for the oceans

$$\frac{\partial H}{\partial t} + \nabla \cdot \mathcal{H} = Q_{net} \tag{16}$$

where

$$H = \text{oceanic heat content} \tag{17}$$

$$\mathcal{H} = \text{vertically integrated oceanic heat transport} = (\mathcal{H}_x, \mathcal{H}_y) \tag{18}$$

$$Q_{net} = \text{net heat flux at the surface} = R_S - (R_L + Q_L + Q_S)\ . \tag{19}$$

Integrating (16) for a sufficiently long period of time the storage term $\partial H/\partial t$ can be neglected, resulting in the balance equation

$$\nabla \cdot \overline{\mathcal{H}} = \overline{Q_{net}} \tag{20}$$

which relates the surface net heat flux to the divergence of the mean vertically integrated oceanic transport. If this equation is integrated over the globe, the

left hand side (LHS) vanishes, as the heat exchange with the continents is negligibly small. This imposes a consistency condition on the net heat fluxes:

$$\int\int_{Globe} \overline{Q_{net}}\, dx\, dy = 0\,. \tag{21}$$

As can be seen from (19), Q_{net} is computed as a residual from large, uncertain terms and the condition (21) is not guaranteed to be met. And in fact, the mean annual net heat flux calculated from our estimates of R_S, R_L, Q_L, and Q_S does not satisfy this condition. Likewise, there are imbalances between our estimates of evaporation and precipitation that cannot be accounted for by the Baumgartner and Reichel (1975) estimates of river runoff (not included in this data set).

There are two main sources of errors in estimates of surface marine fluxes from historical data. First, there are observational errors associated with instrument bias (section 4) and sampling problems associated with the uneven and inadequate data coverage of the world oceans. Second, even in the presence of perfect surface marine data, one needs to rely on bulk parameterizations which are somewhat simplified representations of complex air-sea interaction processes. The individual components that make up the net heat flux are affected by all these uncertainties. Since Q_{net} is a small residual from heat gain (incoming solar radiation) and heat loss (primarily due to evaporation) terms, its relative error is much larger than the relative error for each of the individual components.

In section 4 we have documented our attempts to reduce some of the observational biases in COADS. We also derive an additional set of corrections aimed at producing physically consistent (in the sense of approximately satisfying eq. (21) or independent oceanic measurements) surface heat and fresh water fluxes over the global oceans. To accomplish this, we perform a simple linear inverse calculation to derive small corrections for some of the bulk formula parameters, thereby producing a more physically consistent net heat flux. The technique is standard in geophysics and the development is similar to Isemer *et al.* (1989). A summary of the results follows; details of the calculation can be found in Volume 1.

7.1 Producing fine tuned fluxes

The need to adjust the flux based on measurements for a particular application will undoubtedly require users to produce their own fine tuning of the heat and fresh water fluxes. To this end, we provide users of UWM/COADS with *sensitivity fields* associated with each of the six tuning parameters p discussed in this section. In the short wave parameterization, the tuning parameter p_{Tr} is roughly associated with the transmission coefficient and water vapor absorption coefficient; p_c is related to the cloud cover coefficient. In the long wave radiation formula, p_e is associated with the parameterized water vapor effect, and p_χ with the tuning parameter for the cloud cover correction. In the latent and sensible heat flux parameterizations, we have specified a single tuning parameter for each formula (p_L and p_S), representing primarily the uncertainties in the transfer coefficients. Subsequently, the net heat flux can be written as

$$\begin{aligned} &Q_{net}(p_{Tr}, p_c, p_e, p_\chi, p_L, p_S) = \\ &\quad R_S(p_{Tr}, p_c) - R_L(p_e, p_\chi) - Q_L(p_L) - Q_S(p_S) \end{aligned} \tag{22}$$

The corresponding sensitivity fields are

$$\begin{aligned}
\mathcal{A}_{Tr} &= \frac{\partial R_S}{\partial p_{Tr}} = \frac{\partial Q_{net}}{\partial p_{Tr}} && (23)\\
&= R_S^* && (24)\\
\mathcal{A}_c &= \frac{\partial R_S}{\partial p_c} = \frac{\partial Q_{net}}{\partial p_c} && (25)\\
&= R_{\text{clear}}(1-\alpha)(-0.62c) && (26)\\
\mathcal{A}_e &= \frac{\partial R_L}{\partial p_e} = -\frac{\partial Q_{net}}{\partial p_e} && (27)\\
&= -\epsilon\sigma T_s^4 p_e \left(0.39 - 0.05\sqrt{e}\right)\left(1-\chi c^2\right) && (28)\\
\mathcal{A}_\chi &= \frac{\partial R_L}{\partial p_\chi} = -\frac{\partial Q_{net}}{\partial p_\chi} && (29)\\
&= \epsilon\sigma T_s^4 p_e \left(0.39 - 0.05\sqrt{e}\right)\left(-\chi c^2\right) && (30)\\
\mathcal{A}_L &= \frac{\partial Q_L}{\partial p_{L,E}} = -\frac{\partial Q_{net}}{\partial p_{L,E}} && (31)\\
&= Q_L^* && (32)\\
\mathcal{A}_S &= \frac{\partial Q_S}{\partial p_S} = -\frac{\partial Q_{net}}{\partial p_S} && (33)\\
&= Q_S^*\,. && (34)
\end{aligned}$$

The sensitivity fields $\mathcal{A}_{Tr}$, $\mathcal{A}_L$ and $\mathcal{A}_S$ are equal to the full unconstrained fields ($R_S^* = R_S$, $Q_L^* = Q_L$ and $Q_S^* = Q_S$) already included in UWM/COADS. The other sensitivity fields are computed either from individual observations with climatology and anomalies analyzed the same way as the other UWM/COADS fields ($\mathcal{A}_e$ and $\mathcal{A}_\chi$), or derived from analyzed fields ($\mathcal{A}_c$).

In order to produce constrained estimates of the individual heat flux components, one can calculate

$$\begin{aligned}
R_S &= R_S^* + (p_{Tr}-1)\mathcal{A}_{Tr} + (p_c-1)\mathcal{A}_c \\
&= p_{Tr}R_S^* + (p_c-1)\mathcal{A}_c && (35)\\
R_L &= R_L^* + (p_e-1)\mathcal{A}_e + (p_\chi-1)\mathcal{A}_\chi && (36)\\
Q_L &= p_{L,E}Q_L^* && (37)\\
Q_S &= p_S Q_L^* && (38)
\end{aligned}$$

where ( )* denotes the unconstrained estimate of the heat flux component as included in UWM/COADS. Likewise, constrained evaporation and precipitation fields can be computed from

$$E = p_{L,E} E^* \quad (39)$$

$$P = p_P P^* \quad (40)$$

where $p_{L,E}$ is the tuning parameter related to the uncertainties in the transfer coefficient (C_E), and p_P reflects the uncertainties in the bulk formulation of precipitation. The values of the parameters p in Table 6 can be used to produce several versions of the constrained heat and fresh water fluxes. In addition, new values for the tuning parameters can be also be calculated. Details are given in Volume 1.

7.2 Constrained fluxes in UWM/COADS

The individual heat flux components, evaporation and precipitation provided in UWM/COADS are not tuned in any way. It is left to the user to choose a particular set of tuning parameters most suitable to the application at hand. However, the net heat flux, buoyancy flux, and evaporation minus precipitation fields included in the data set have been constrained using the global balance requirement given in the first row of Table 6.

The zonally integrated meridional heat transport is shown in Fig. 1. In agreement with previous studies, our constrained heat fluxes produce a northward meridional heat transport throughout the Atlantic and a southward transport in the Indian ocean. In the Atlantic our estimate is within the error bars for Wunsch's (1984) measurement at the equator, and Hall and Bryden's (1982) measurement at 25° N. Our estimated transport at 32° N is about half the measurement of Rago and Rossby (1987) who admit their measurement is rather large. Our estimate for the southward transport in the South Pacific is somewhat smaller than previous estimates by Hsiung (1985) and Hastenrath (1982).

In the Atlantic, our constrained zonally integrated meridional fresh water transport is somewhat smaller than Schmitt *et al.*'s (1989) in the tropics (Fig. 2). At 25° N our estimate gives a southward transport of 0.23 Sv which is larger than Hall and Bryden's (1982) measured value of −0.03 Sv, but conceivably within their error bars.

While the results above suggest that our choice of tuning parameters (first row of Table 6) produces reasonable estimates of heat and fresh water fluxes, it is important to keep in mind that this choice does not produce a balanced net heat flux. When regions poleward of 65° are considered, a small imbalance

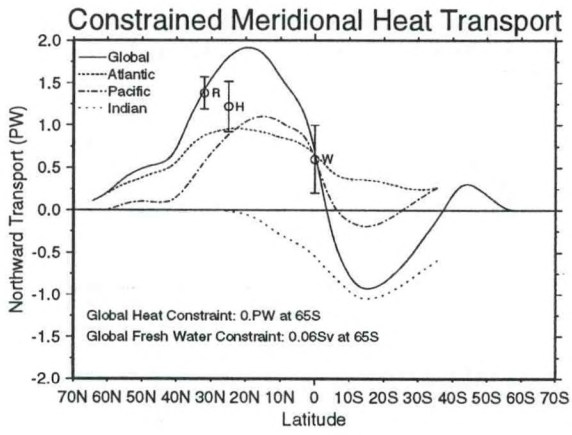

Figure 1: Meridional heat transport (1 PW = 10^{15}W) calculated from constrained net heat flux. Heat flux is constrained so that the global meridional heat transport at the southern boundary is zero and the fresh water transport at the southern boundary is 0.06 Sv. Three oceanographic measurements for Atlantic heat transport are shown with error bars: (R) Rago and Rossby [1987], (H) Hall and Bryden [1982], (W) Wunsch [1984].

(−0.06 PW) remains. It is also important to note that our choice of tuning parameters is very likely non-optimal for specific applications. We strongly encourage users to experiment with other choices of parameters.

8 Results

Table 7 lists the six fresh water flux quantities presented in this volume. Although all the analyses have been performed globally, in order to conserve space we only present maps from 40°S to 80°N, eliminating the less observed and noisier Southern and Arctic oceans. For each quantity the following information is displayed[1]:

Seasonal density of observations:

These maps document the average data coverage for each season, clearly indicating the well traveled shipping lanes. The density of observations η is defined as the mean number of observations per month per 1°× 1° box. The size of each black square is related to the value of η in each 5°box (see scale on top of page).

[1]Buoyancy flux and constrained $E - P$, derived from their analyzed component fluxes, lack figures for observation density (Figures B-1, B-2 and E-P-1, E-P-2) and standard deviation (Figures B-5 and E-P-5).

Table 6: Parameters from the simultaneous tuning of heat and fresh water fluxes. Imposed constraints on the meridional heat transport (H) and meridional fresh water transport (F) listed in the first column, with resulting transports at 25° N in the Atlantic or 65° S Global appearing in the last column. The constraint for heat flux is taken from the global balance requirement. Constraints for fresh water flux are chosen as follows: 0.06 Sv at 65° S, Peixoto and Oort (1992); 0.27 Sv at 65° S, Stommel (1980), −0.03 Sv at 25° N Atlantic, Hall and Bryden (1982). The other fresh water constraints are chosen between the unconstrained value and the value obtained when the Hall and Bryden (1982) constraint is applied.

Imposed Constraints	Tuning Parameters								Resulting Transport	
	p_{Tr}	p_c	p_e	p_χ	$p_{L,E}$	p_S	p_P	p_R	25° N	65° S
(H) 0. PW 65°S Global	0.92	1.04	1.02	0.99	1.13	1.02	1.12	1.01	0.95 PW	
(F) 0.06 Sv 65°S Global									-0.12 Sv	
(H) 0. PW 65°S Global	0.92	1.04	1.02	0.99	1.14	1.01	1.10	1.01	0.95 PW	
(F) 0.27 Sv 65°S Global									-0.10 Sv	
(H) 0. PW 65°S Global	0.93	1.04	1.02	0.99	1.14	1.01	1.04	1.01	0.95 PW	
(F) -0.03 Sv 25°N Atlantic										1.09 Sv
(H) 0. PW 65°S Global	0.92	1.04	1.02	0.99	1.14	1.01	1.09	1.01	0.95 PW	
(F) 0.5 Sv 65°S Global									-0.09 Sv	
(H) 0. PW 65°S Global	0.93	1.04	1.02	0.99	1.14	1.01	1.05	1.00	0.95 PW	
(F) 1. Sv 65°S Global									-0.06 Sv	
(H) 0. PW 65°S Global	0.93	1.04	1.02	0.99	1.15	1.01	1.01	1.00	0.95 PW	
(F) 1.5 Sv 65°S Global									-0.02 Sv	

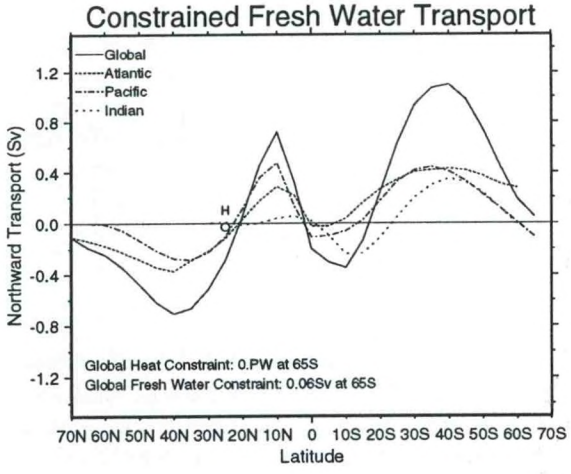

Figure 2: Meridional fresh water flux (in Sv) calculated from constrained fresh water flux. Heat flux is constrained as in the previous figure. One oceanographic measurement for Atlantic fresh water transport is shown: (H) Hall and Bryden [1982].

Table 7: Fresh water flux quantities presented in this atlas.

Parameter	Description	Units
E	evaporation rate	mm/(3 hours)
P	precipitation rate	mm/(3 hours)
E-P	E minus P rate	mm/(3 hours)
B	buoyancy flux	10^{-5}kg/(m s^3)
uq	zonal moisture flux	m/s
vq	meridional moisture flux	m/s

Decadal density of observations:

These maps document the increase in data coverage in the last 3 decades. The density of observations η is defined as the mean number of observations per month per 1°× 1° box. The size of each black square is related to the value of η in each 5°box (see scale on top of page). A much more detailed description of the data coverage evolution in the period 1945-89 can be found in Young *et al.* (1993) where the location of each sea surface temperature observation is displayed for each month from January/45 to December/89.

Seasonal climatology:

Computed from monthly mean analyzed climatology. Units are given in Table 7.

Seasonal interannual standard deviation:

Computed from the analyzed monthly anomalies and averaged seasonally. The interannual standard deviation for a 1° × 1° box for a par-

ticular month is given by

$$\sigma_{\text{int}} = \sqrt{\frac{\sum_{y=1}^{N}(a_y)^2}{N-1}} \qquad (41)$$

where a_y is the anomaly value for year number y and N is the total number of years (45 in this case).

Seasonal standard deviation:

The total standard deviation for a month in a single 1° × 1° box with more than one observation is given by

$$\sigma = \sqrt{\frac{\sum_{i=1}^{n}(x_i - \bar{x})^2}{n-1}} \qquad (42)$$

where x_i is the value for observation number i during the desired month and $\bar{x}$ is the average of all x_i's for that particular month. The total number of observations over the 45–year period for that month and box is n. The *seasonal standard deviation* fields are computed by objectively analyzing these total standard deviation fields for each month and then averaging seasonally. Units are given in Table 7.

Seasonal anomalies:

Computed from analyzed monthly mean anomalies. The anomalies are computed from the analyzed 45-year climatology for each month. Units are given in Table 7.

The contour interval ("ci" for short) along with units and season information (DJF for December-January-February, MAM for March-April-May, etc.) are displayed in a box on the continent of Asia for each map.

A detailed exposition of the spatial and temporal structure of the anomaly fields is beyond the scope of this atlas. In particular, study of the impact of our bias corrections and comparison with other authors is underway and will be reported elsewhere. Several other projects are in progress to document the decadal/interannual variability of the atmosphere-ocean system which in turn will provide guidance regarding the quality of the data set and hopefully point to ways to improve it in future releases. The maps presented here are intended to serve as a reference for researchers engaged in observational or modeling studies using our revised data sets.

9 Limitations and shortcomings of the data sets

A description of surface marine data sets could not be complete without a discussion of the remaining problems and limitations for which solutions may never be found. Because ship reports are probably the only comprehensive observational record available of the surface marine climate, this data source will undoubtedly continue to be used in studies of the ocean-atmosphere system. As large uncertainties are present, it is imperative that researchers remember that an analysis of surface marine data is an evolving process. Continual improvement will be necessary as more data or metadata become available, physical parameterizations are improved, and advances in data assimilation techniques become available. The corrections we have reported here are, at best, a step in the right direction, but much remains to be done. In the remainder of this section, we discuss some of the remaining problems. This list is by no means exhaustive.

The first, and most uncontrollable, errors exist in the ship reports themselves. Marine and atmospheric measurement techniques and the recording of these observations are not perfect. Some errors are introduced through poor instrumentation. Surface air temperature can be biased due to heating of a ship's superstructure during the day and inadequate shelter ventilation (Isemer and Hasse 1987; Ramage 1984; Kent *et al.* 1993a,b). Sea surface temperature observations taken via ship intake will be biased compared to those taken by insulated bucket or hull sensors.

Many of the biases are impossible to correct due to the lack of instrumentation information as discussed in section 3. A proper homogenization of the measured wind speeds requires the knowledge of the precise anemometer height information which is not included in COADS/CMR-5 at the present time; an average anemometer height of 20 m has been assumed in our calculations. In addition, the flag WI in COADS/CMR-5, which allows the discrimination between measured and estimated winds, is not reliable (Slutz *et al.* 1985, Cardone *et al.* 1990). Our wind speed bias correction procedure takes the WI flag at face value and consequently is affected by this uncertainty. Any systematic bias in the anemometer winds remains to be evaluated.

Even when an observation is considered accurate and unbiased, the recording stage may result in errors (Slutz *et al.* 1985). Some observations are taken in different units (such as Fahrenheit vs. Celsius) without documentation. Coding practices change but are not implemented by all observers on the same date. Ship positions may be erroneous. The transfer of written records to digital form can also introduce error. Some recording errors were repaired by the compilers of COADS, but some miscoded errors undoubtedly remain. The tendency for ships to avoid stormy weather also introduces a fair weather bias into the

observations when considered as a whole, although this bias is less problematic in the tropics.

After we deal with the correctable biases and calculate raw fields, error can be introduced by the analysis scheme as well. One problem with the successive correction method used in our analysis is the introduction of unrealistic features (Levitus 1982). Objective analysis of the sort used here fills in the gaps by interpolating/extrapolating smoothed data from remote regions, but cannot compensate entirely for poor sampling. This effect is particularly troublesome in the tropics and southern oceans where observations are clumped along ship tracks with data void areas in between. As a result, bull's eye type features often remain in analyzed fields, particularly in anomaly fields.

The analysis of anomaly values rather than the observed data can result in spurious extrema. For example, the analysis has problems handling positive definite quantities such as fractional cloud cover which only take values between 0 and 1. The analysis procedure can produce full field values (climatology plus anomalies) less than 0 in broad clear areas or values greater than 1 in broad overcast regions. The climatology fields in the data set have been corrected so that positive definite quantities (cloudiness, relative and specific humidity, vapor pressure, precipitation, etc.) have a minimum value of zero. Maximum limits have not been applied to the climatology, however, nor have the full field values been corrected to their valid ranges. The only additional correction made to the anomaly fields was to force the 45-year mean monthly anomaly to equal zero at each grid point.

It should always be kept in mind that although the analyzed fields are given on a $1° \times 1°$ grid, only features with wavelength greater than 770 km (1300 km or greater for regions below 40°S and for standard deviation fields) are retained. The reader is referred to Levitus (1982) or Daley (1991) for additional discussions of the limitations of the objective analysis technique. A higher resolution climatological analysis has been performed on a half-degree by half-degree grid where features with wavelength greater than 386 km are retained. These results will be presented elsewhere.

In contrast to our analysis method, modern data assimilation techniques are assisted by some sort of dynamic constraint: a model is used to provide a first guess for the analysis or to ensure a proper balance of the analyzed fields (Daley 1991). In this first version of our analysis, we concentrated on bias corrections and calculations from individual observations, using a successive correction method to grid the data. Current four dimensional atmospheric reanalysis efforts (Schubert *et al.* 1993; Kalnay and Jenne 1991; Bengtsson and Shukla 1988) will provide several estimates of surface marine fields which would prove useful to validate and assess the limitations of our approach. We are also making available the raw, unanalyzed fields to allow researchers to develop their own objective analyses/data assimilation system from the monthly mean data.

10 Summary and plans for future work

We have described the results of a collaborative project between the Department of Geosciences of the University of Wisconsin-Milwaukee and the National Oceanographic Data Center to produce high resolution analyses of surface marine fields for climate variability studies. Our work is based on individual surface marine reports prepared by the COADS project (Slutz *et al.* 1985). We have corrected wind speed and cloudiness biases in the original COADS reports and produced monthly means and other statistics on 1° boxes over the global oceans. Although we have attempted to create objectively analyzed fields that can be used as is, we have documented several shortcomings and limitations of the data sets which we hope will be taken into consideration by the careful researcher. Analyzed fields of this sort are estimates of the *true* surface marine climate, and we hope to improve these estimates by inclusion of additional data/metadata and overall improvements in our analysis system.

An immediate improvement concerns the use of COADS Release 1A (COADS/1A) which was not available at the time of this calculation. For the 1980's, our analysis is based on the so-called *interim* product. COADS/1A includes several delayed ship and buoy sources in the 1980's, and other sources not included in the interim product. COADS/1A contains more elaborate duplicate elimination, some corrections to the data, and more quality control flags. Furthermore, COADS/1A adopts a more complete report format including ship ID call sign, buoy number and identification of platform type whenever feasible (S. Woodruff, personal communication). All these extra data and metadata should improve our analysis significantly. In addition, the dew point and air temperature corrections proposed by Kent *et al.* (1993a,b) will be implemented, as metadata permit.

Ultimately, the use of these data to address scientific issues in the dynamics of the ocean-atmosphere climate system will establish the strengths and weaknesses of the data sets and hopefully provide clues for further improvements. For this reason, and to ensure the widest possible distribution, the objective

analyses as well as the raw monthly means on which they are based are being made available internationally, without restriction, on various magnetic media as well as CD-ROM.

References

Arkin, P. A., and B. N. Meisner, 1987: The relationship between large-scale convective rainfall and cloud cover over the western hemisphere during 1982–84. *Mon. Wea. Rev.*, **115**, 51–74.

Barnes, S. L., 1964: A technique for maximizing details in numerical weather map analysis. *J. Appl. Meteor.*, **3**, 396–409.

Baumgartner, A., and E. Reichel, 1975: *The World Water Balance.* Elsevier, 179 pp.

Beaton, A. E., and J. W. Tukey, 1974: The fitting of power series, meaning polynomials, illustrated on band-spectroscopic data. *Technometrics*, **16**, 147–185.

Bengtsson, L., and J. Shukla, 1988: Integration of space and in situ observations to study global climate change. *Bull. Amer. Meteor. Soc.*, **69**, 1130–1143.

Bottomley, M., C. K. Follund, J. Hsiung, R. E. Newell and D. E. Parker, 1990: *Global Ocean Surface Temperature Atlas.* Joint Meteorol. Off./Mass. Inst. Techno. Proj., supported by U. S. Dept. of Energy, U. S. Natl. Sci. Found., and U. S. Off. of Nav. Res., funded by U. K. Depts. of Energy and Environ., Her Majesty's Stationery Office, London, 20 pp., 313 plates.

Budyko, M. I., 1956: *The Heat Balance of the Earth's Surface*, translated by N. A. Stepanova, 1958. U. S. Dept. of Commerce, Washington D. C. 259 pp.

Cardone, V. J., 1969: Specification of the wind distribution in the marine boundary layer for wave forecasting. Report TR69-1, New York University, New York, NY, 131 pp. [NTIS AD 702 490].

Cardone, V. J., J. G. Greenwood and M. Cane, 1990: On trends in historical marine wind data. *J. Climate*, **3**, 113–127.

Cressman, G. P., 1959: An operational objective analysis scheme. *Mon. Wea. Rev.*, **87**, 329–340.

Daley, R., 1991: *Atmospheric Data Analysis.* Cambridge University Press, Cambridge, 457pp.

Dorman, C. E., and R. H. Bourke, 1978: A temperature correction for Tucker's ocean rainfall estimates. *Q. J. Royal Meteor. Soc.*, **104**, 765–773.

Esbensen, S. K. and J. Kushnir, 1981: The heat budget of the global oceans: An atlas based on estimates from marine surface observations. Oregon State University Climate Research Institute Rep. No. 29, 27 pp.

Farmer, G., T. M. L. Wigley, P. D. Jones and M. Salmon, 1989: Documenting and explaining recent global-mean temperature changes. *Final Report to Natural Environment Research Council.*, Climate Research Unit, University of East Anglia, U. K.

Folland, C. K., 1991: Sea temperature bucket models used to correct historical SST data in the Meteorological Office. Climate Research Technical Note No. 14, British Meteorological Office, England.

Folland, C. K., and J. Hsiung, 1986: Correction of seasonally varying biases in uninsulated bucket sea surface temperature data using a physical model. Met. Office Synoptic Climatology Branch Memo No. 154.

Folland, C. K., D. E. Parker and F. E. Kates, 1984: World wide marine temperature fluctuations 1856–1981. *Nature*, **310**, 670–673.

Hall, M. M., and H. L. Bryden, 1982: Direct estimates and mechanisms of ocean heat transport. *Deep–Sea Res.*, **29**, 339–359.

Hastenrath, S., 1982: On meridional heat transports in the world ocean. *J. Phys. Oceanogr.*, **10**, 159-170.

Hsiung, J., 1985: Estimates of global oceanic meridional heat transport. *J. Phys. Oceanogr.*, **15**, 1405–1413.

Isemer, H.–J. and L. Hasse, 1987: *The Bunker Atlas of the North Atlantic Ocean. Vol. 2: Air–sea interactions.* Springer Verlag, 252 pp.

———, 1991: The scientific Beaufort equivalent scale: Effects on wind statistics and climatological air–sea flux estimates in the North Atlantic ocean. *J. Climate*, **4**, 819–836.

Isemer, H.–J., J. Willebrand and L. Hasse, 1989: Fine adjustment of large air-sea energy flux parameterizations by direct estimates of ocean heat transport. *J. Climate*, **2**, 1173–1184.

Kalnay, E., and R. Jenne, 1991: Summary of the NMC/NCAR reanalysis workshop of April 1991. *Bull. Amer. Meteor. Soc.*, **72**, 1897–1904.

Kaufeld, L., 1981: The development of a new Beaufort equivalent scale. *Meteor. Rundsch.*, **34**, 17–23.

Kent, E. C. and P. K. Taylor, 1991: Ships observing marine climate: a catalogue of the Voluntary Observing Ships Participating in the VSOP-NA. *Marine and Oceanographic Activities Report 25*, WMO, Geneva, 123pp.

Kent, E. C. and P. K. Taylor, 1995: A comparison of heat flux estimates for the North Atlantic ocean. *J. Phys. Oceanogr.*. In press.

Kent, E. C., P. K. Taylor, B. S. Truscott and J. S. Hopkins, 1993a: The accuracy of voluntary observing ships' meteorological observations – Results of the VSOP-NA. *J. Atmos. & Oceanic Tech.*, **10**, 591–608.

Kent, E. C., R. J. Tiddy and P. K. Taylor, 1993b: Correction of marine daytime air temperature observations for radiation effects. *J. Atmos. & Oceanic Tech.*, **10**, 900–906.

Kushnir, Y., 1994: Interdecadal variations in North Atlantic sea surface temperature and associated atmospheric conditions. *J. Climate*, **7**, 141–157.

Large, W., and S. Pond, 1982: Sensible and latent heat flux measurements over the ocean. *J. Phys. Oceanogr.*, **12**, 464–482.

Levitus, S., 1982: Climatological Atlas of the World Ocean, NOAA Prof. Paper No. 13, U. S. Government Printing Office, Washington D. C., 17 fiches, 173 pp.

Levitus, S., R. Burgett and T. Boyer, 1994: *World Ocean Atlas 1994, Volume 3: Salinity.* NOAA Atlas NESDIS 3, U. S. Government Printing Office, Washington D. C., 99pp.

Oberhuber, J. M., 1988: An Atlas Based on the COADS Data Set: The Budgets of Heat, Buoyancy, and Turbulent Kinetic Energy at the Surface of the Global Ocean. Report No. 15, Max-Planck Institut für Meteorology.

Peixoto, J. P., and A. H. Oort, 1992: *Physics of Climate.* American Institute of Physics, 520pp.

Petersen, P., 1927: Zur Bestimmung der Windstärke auf See. *Ann. Hydrogr.*, **55**, 69–72.

Rabiner, L. R., M. R. Sambur and C. E. Schmidt, 1975: Applications of a nonlinear smoothing algorithm to speech processing. *IEEE Transactions on Acoustics, Speech, and Signal Processing*, **ASSP–23**, 552–557.

Rago, T. T., and H. T. Rossby, 1987: Heat transport into the North Atlantic Ocean north of 27°N latitude. *J. Phys. Oceanogr.*, **17**, 854–871.

Ramage, C. S., 1984: Can shipboard measurements reveal secular changes in tropical air–sea heat flux? *J. Climate Appl. Meteor.*, **23**, 187–193.

Reynolds, R. W., 1988: A real–time global sea surface temperature analysis. *J. Climate*, **1**, 75–86.

Roll, H. U., 1965: *Physics of the Marine Atmosphere.* Int. Geophys. Ser., Vol. 7, 426 pp.

Schlatter, T. W., and D. V. Baker, 1981: Algorithms for thermodynamic calculations. NOAA/ERL PROFS Program Office, Boulder, CO, 34 pp.

Schmitt, R. W., P. S. Bogden and C. E. Dorman, 1989: Evaporation minus precipitation and density fluxes for the North Atlantic. *J. Phys. Oceanogr.*, **19**, 1208–1221.

Schubert, S. D., R. B. Rood and J. Pfaendtner, 1993: An assimilated dataset for earth sciences applications. *Bull. Amer. Meteor. Soc.*, **74**, 2331–2342.

Shapiro, R., 1970: Smoothing, filtering, and boundary effects. *Rev. of Geophys. and Space Phys.*, **8**, 359–387.

Simpson, G. C., 1906: The velocity equivalents of the Beaufort scale. Rep. of Director of Meteorological Office No. 180, London.

Slutz, R. J., S. J. Lubker, J. D. Hiscox, S. D. Woodruff, R. L. Jenne, D. H. Joseph, P. M. Steurer and J. D. Elms, 1985: COADS, Comprehensive Ocean–Atmosphere Data Set, Release 1. Climate Research Program, Environmental Research Laboratory, Boulder, CO, 262 pp.

Stommel, H. 1980: Assymetry of interoceanic freshwater and heat fluxes. *Proc. Natl. Acad. Sci. USA*, **77**, 2377–2381.

Tucker, G. B., 1961: Precipitation over the North Atlantic Ocean. *Q. J. Royal Meteor. Soc.*, **87**, 147–158.

Woodruff, S. D., R. J. Slutz, R. L. Jenne and P. M. Steurer, 1987: A comprehensive ocean–atmosphere data set. *Bull. Amer. Meteor. Soc.*, **68**, 1239–1250.

World Meteorological Organization (WMO), 1970: Reports on marine science affairs. Rep. No. 3: The Beaufort scale of wind force. WMO, Geneva, Switzerland, 22pp.

World Meteorological Organization (WMO), 1990: International list of selected, suplementary and auxiliary ships. *WMO Publ. No. 47*, World Meteorological Organization, Geneva.

Wunsch, C., 1984: An eclectic Atlantic Ocean circulation model. Part I: The meridional flux of heat. *J. Phys. Oceanogr.*, **14**, 1712–1733.

Young, C. C., A. M. da Silva and S. Levitus, 1993: Monthly Distribution of SST Observations in COADS: 1945-89. *Tech. Rep. Geosci. 93.01*, University of Wisconsin-Milwaukee, 275pp.

11 Evaporation rate

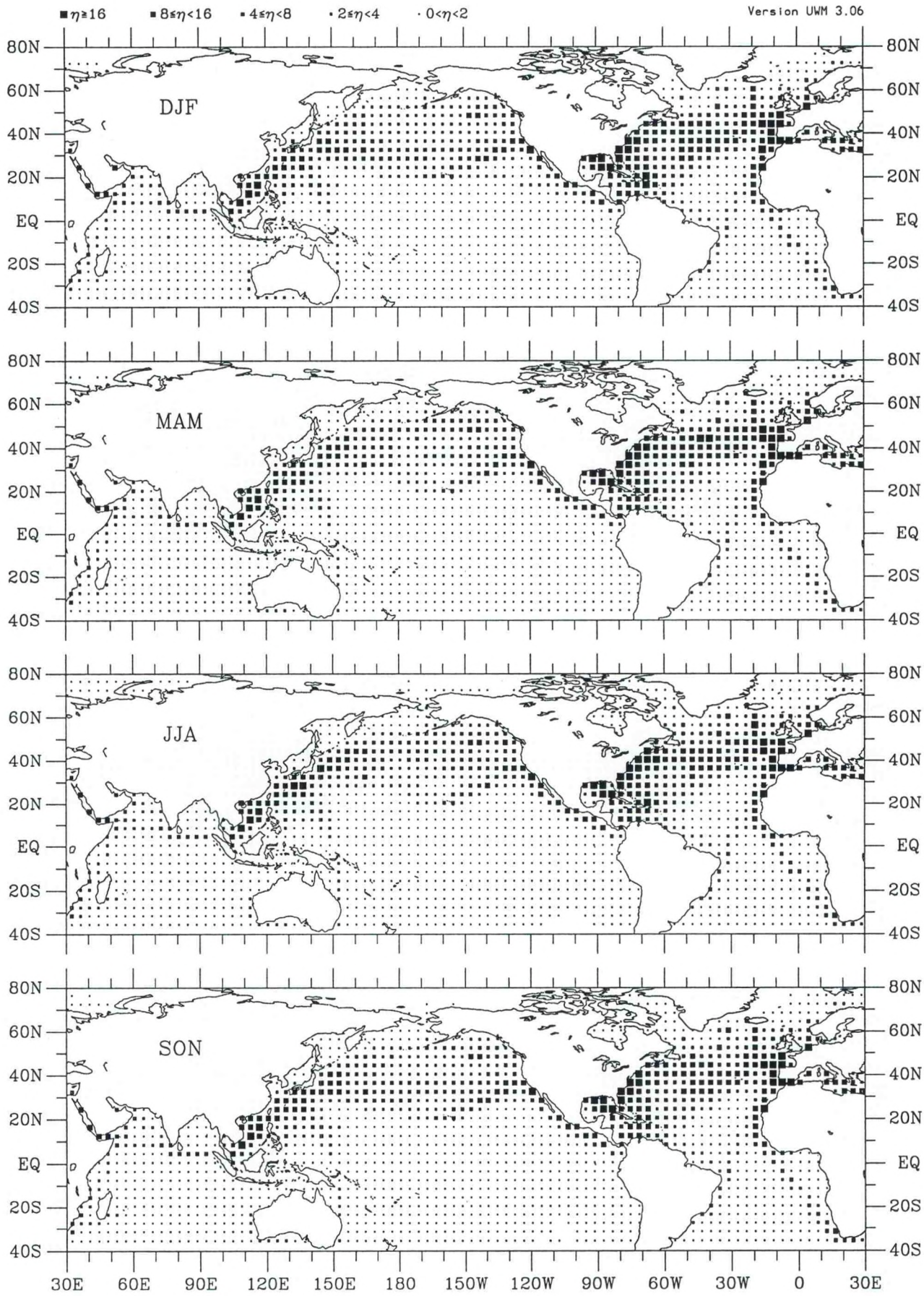

Figure E−1. Evaporation seasonal observation density (1945−89).

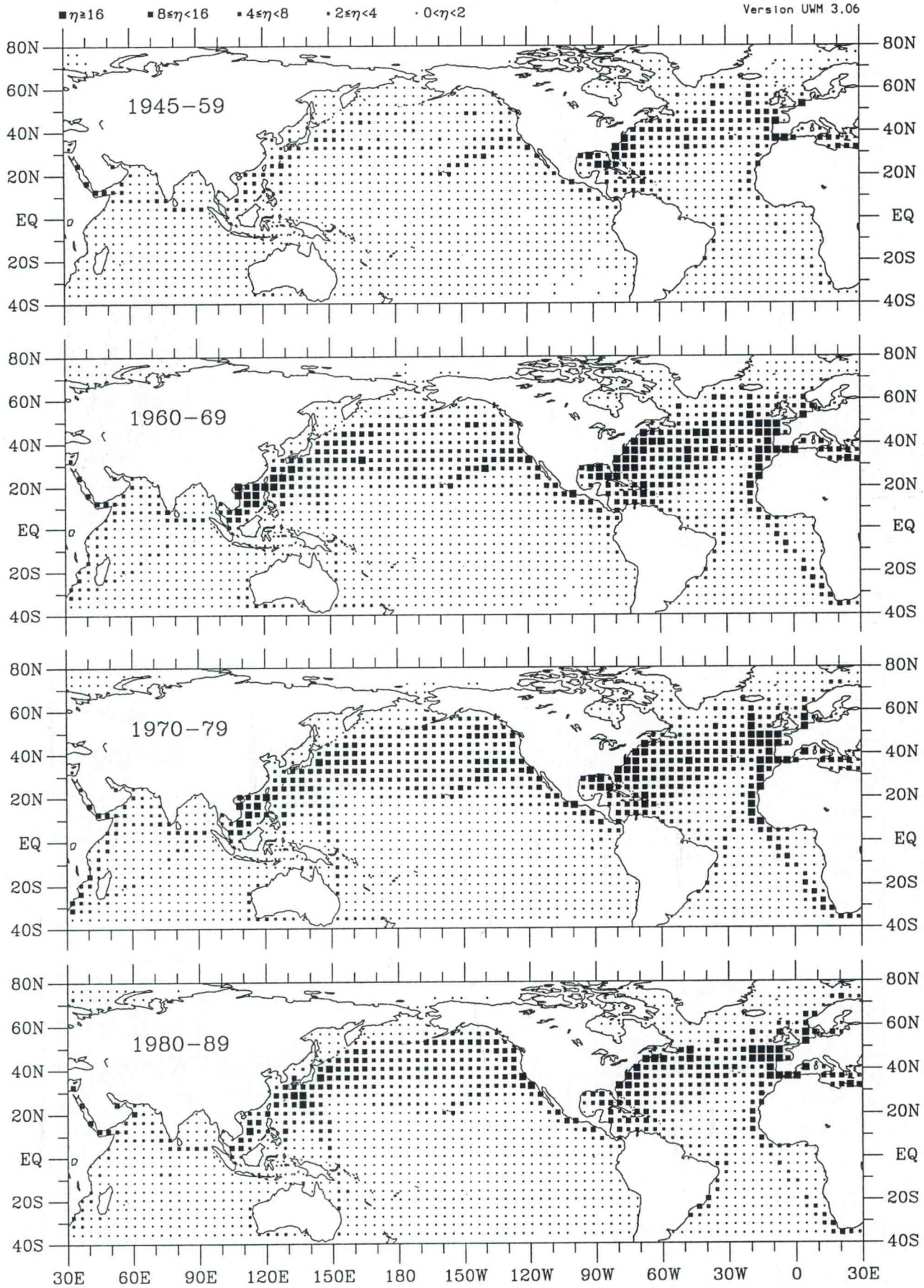

Figure E-2. Evaporation decadal observation density.

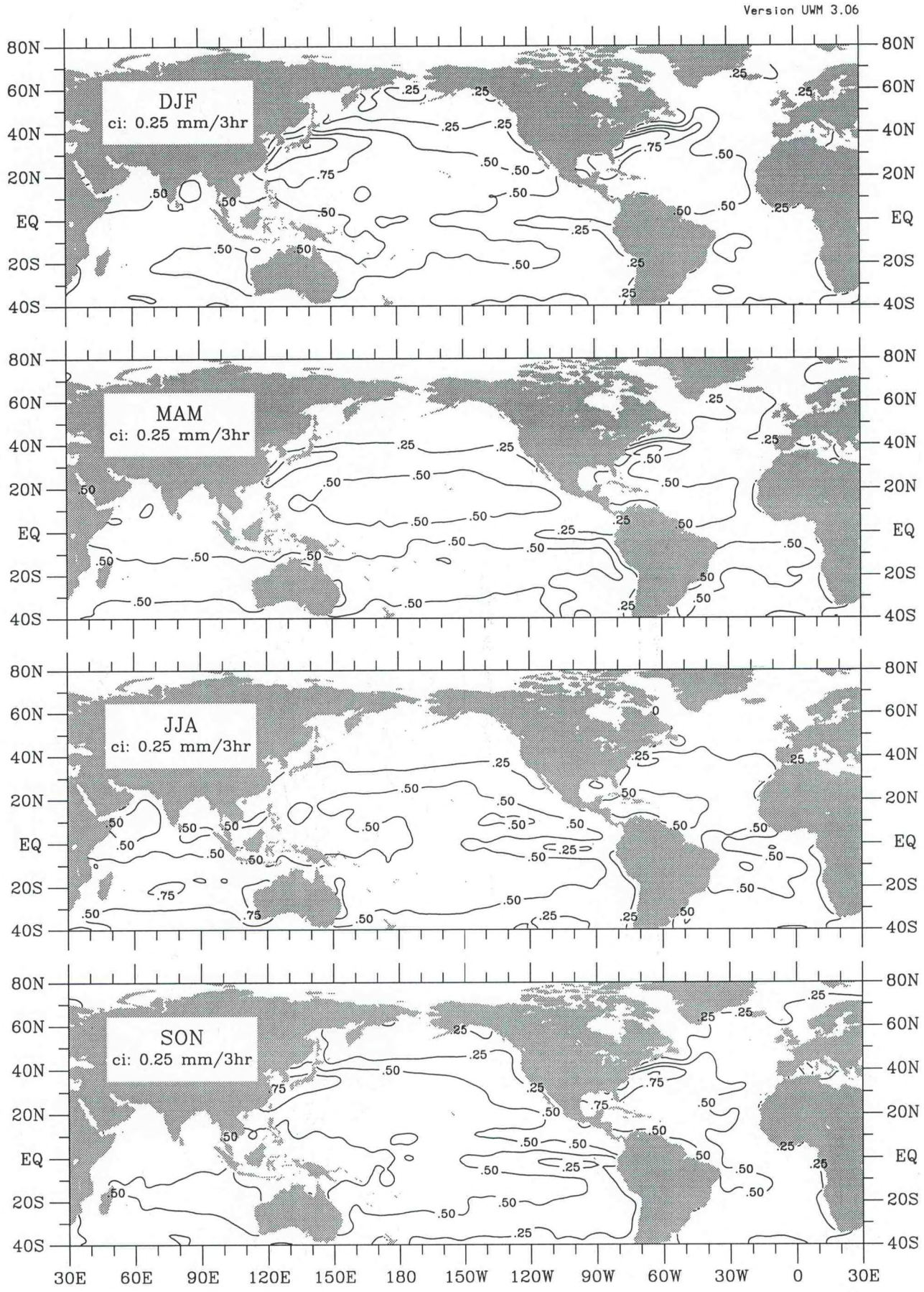

Figure E-3. Evaporation seasonal climatology (1945-89).

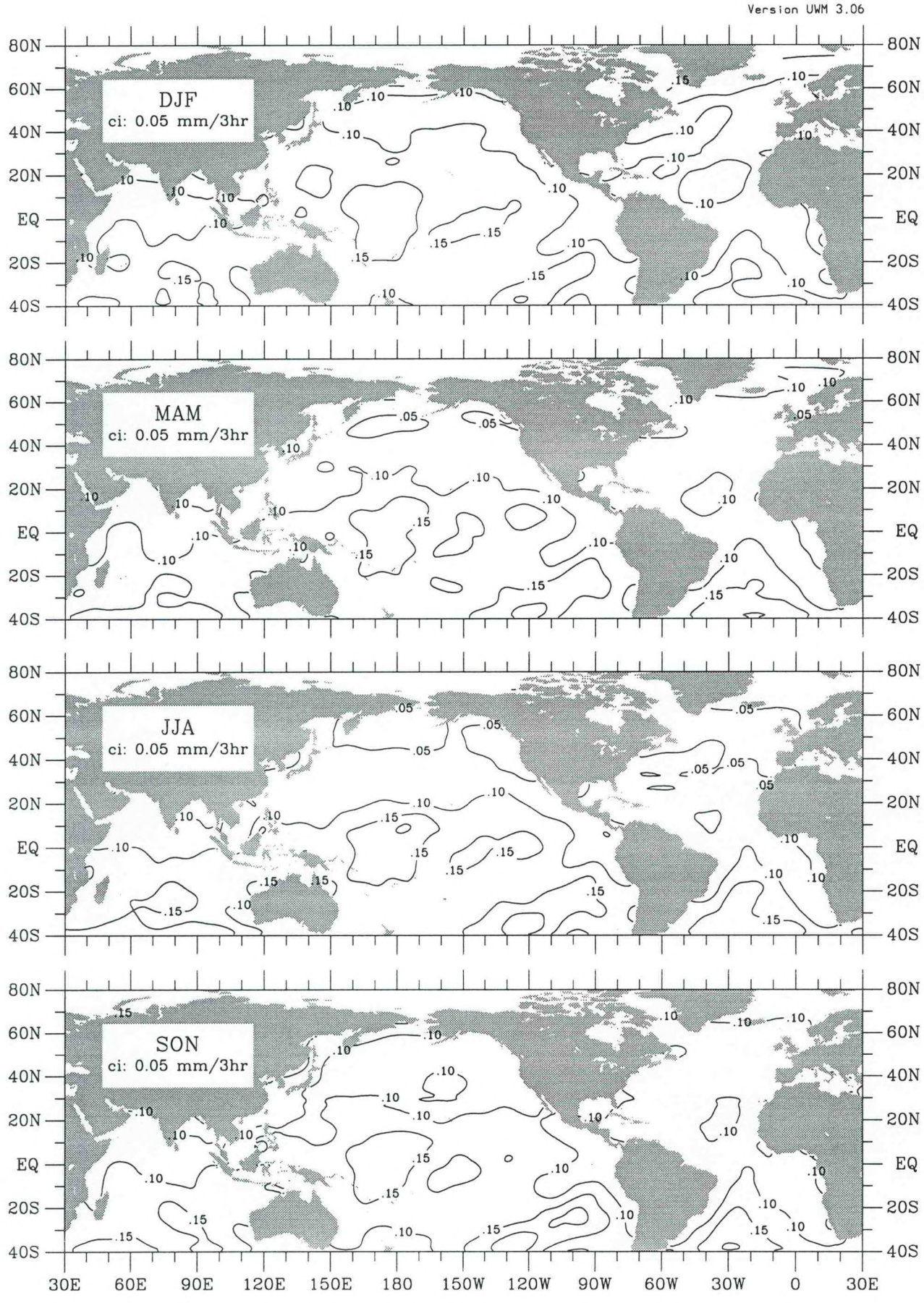

Figure E-4. Evaporation seasonal interannual std dev (1945-89).

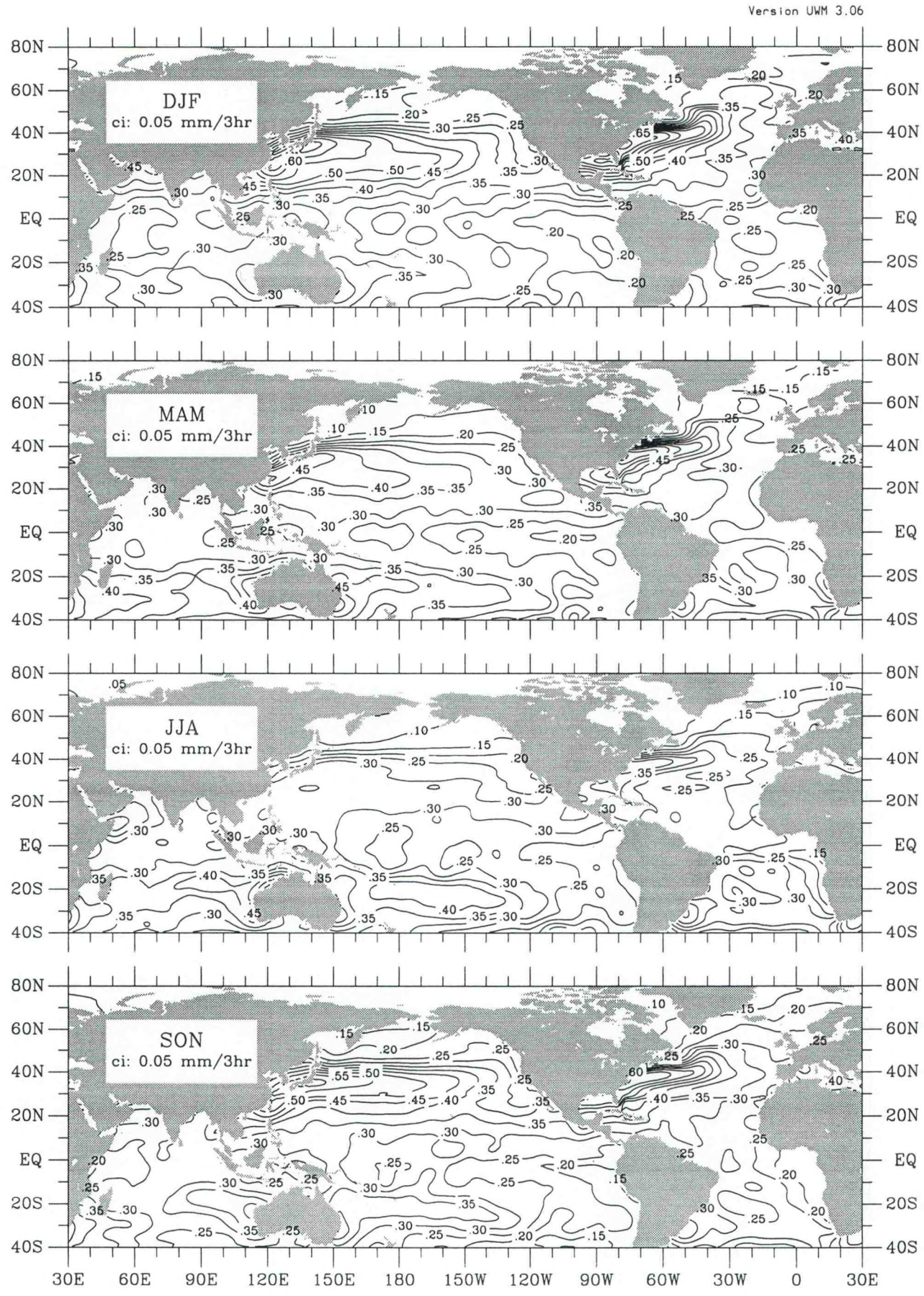

Figure E-5. Evaporation seasonal standard deviation (1945-89).

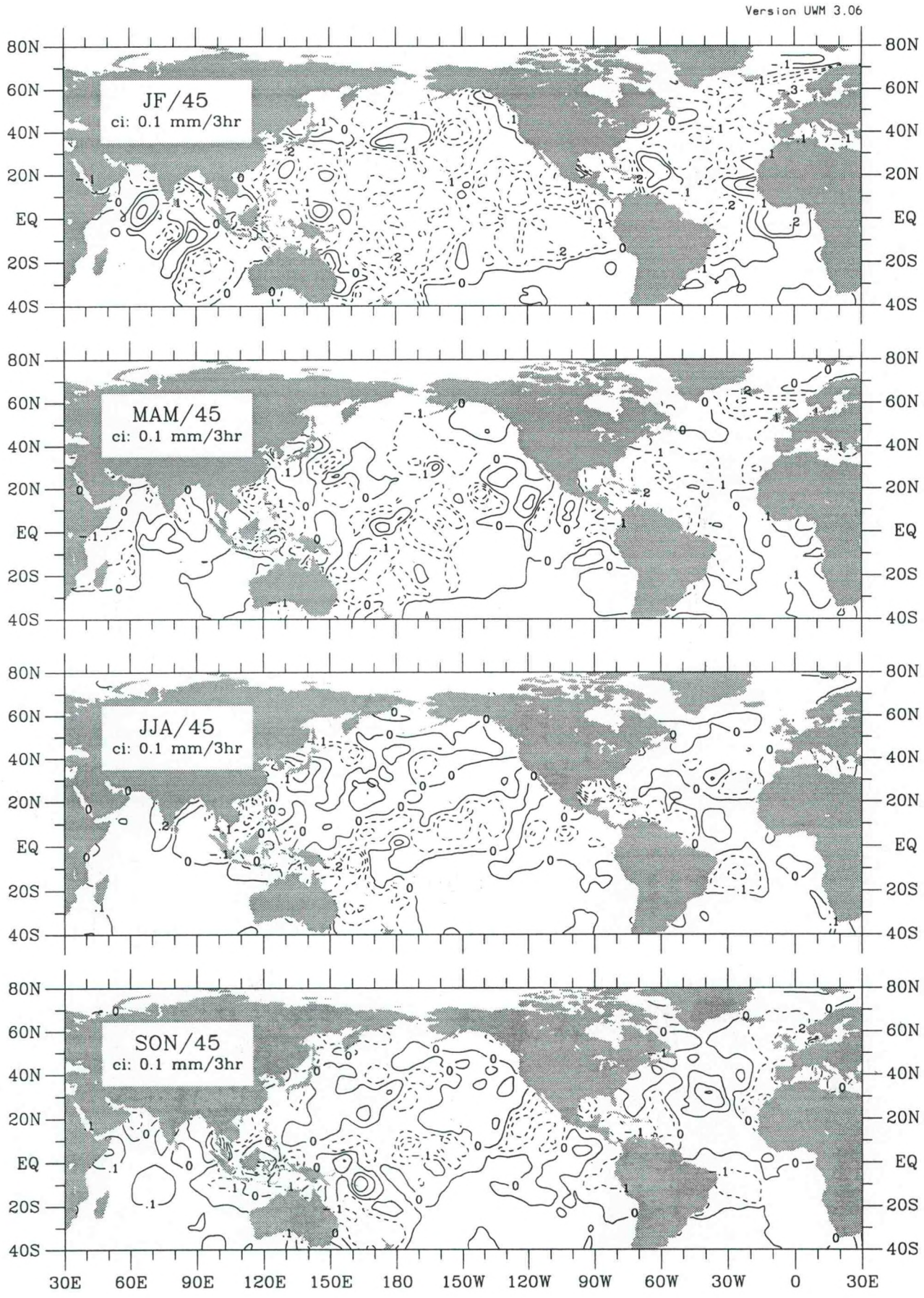

Figure E-6. Evaporation seasonal anomaly for 1945.

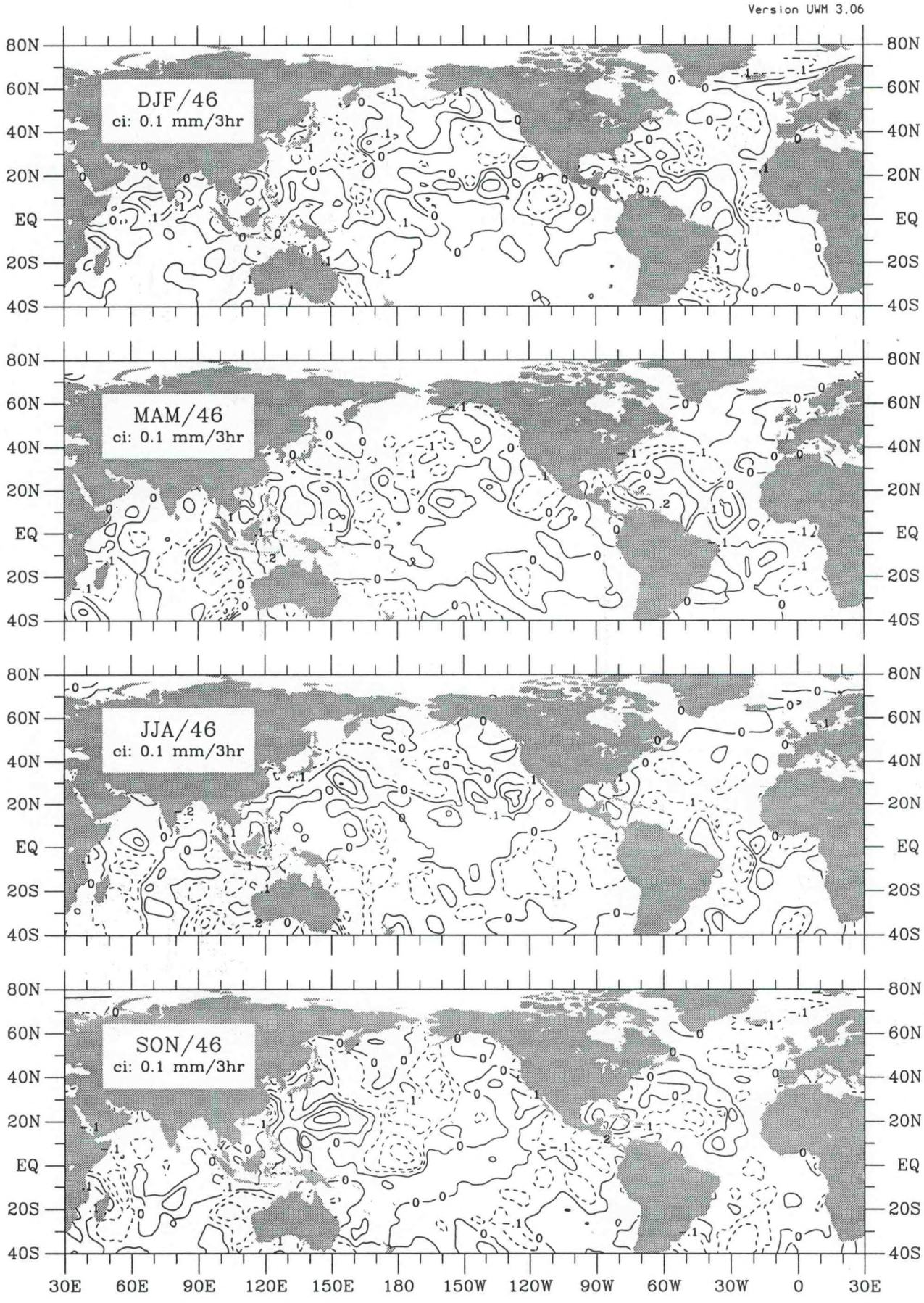

Figure E-7. Evaporation seasonal anomaly for 1946.

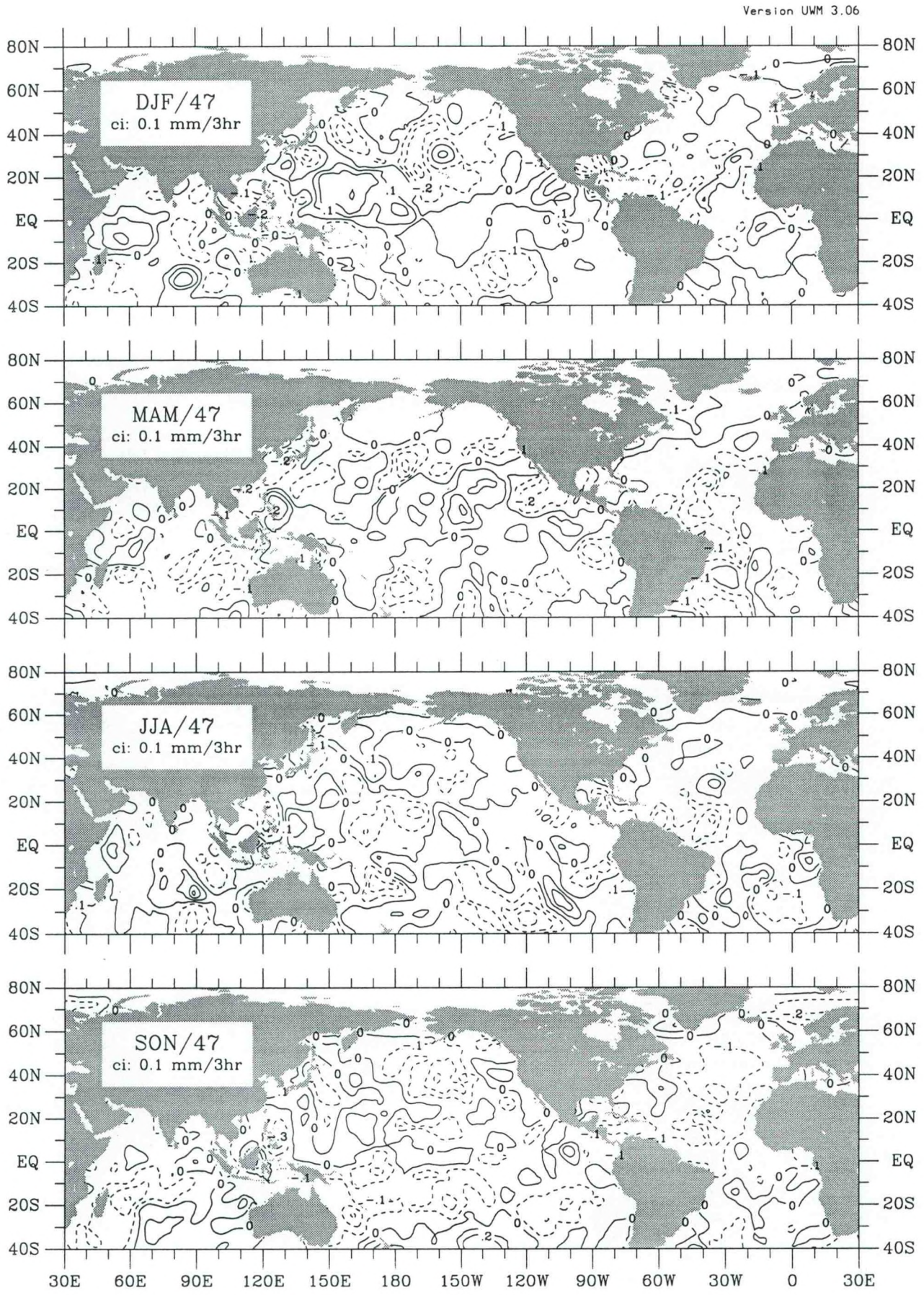

Figure E-8. Evaporation seasonal anomaly for 1947.

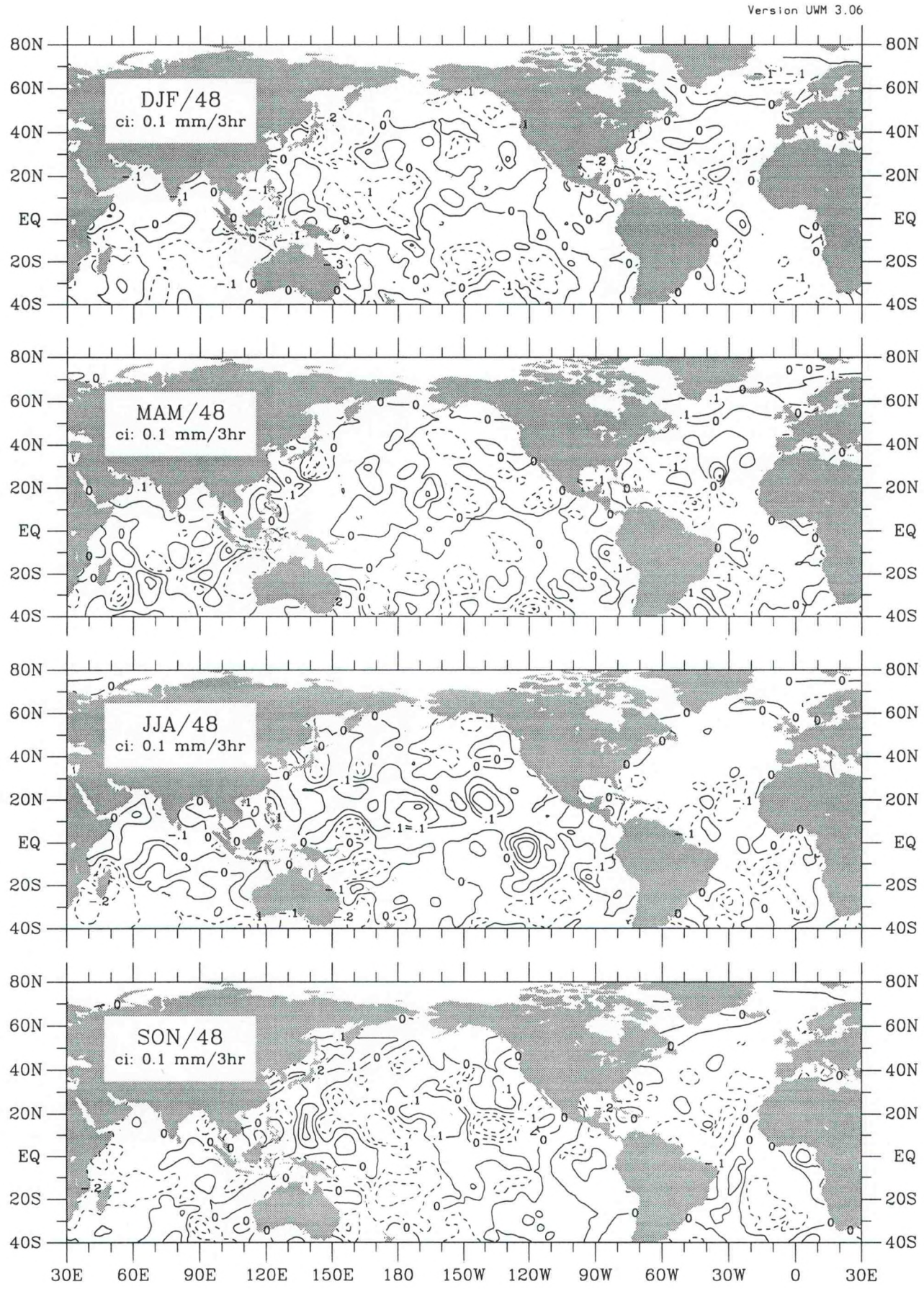

Figure E-9. Evaporation seasonal anomaly for 1948.

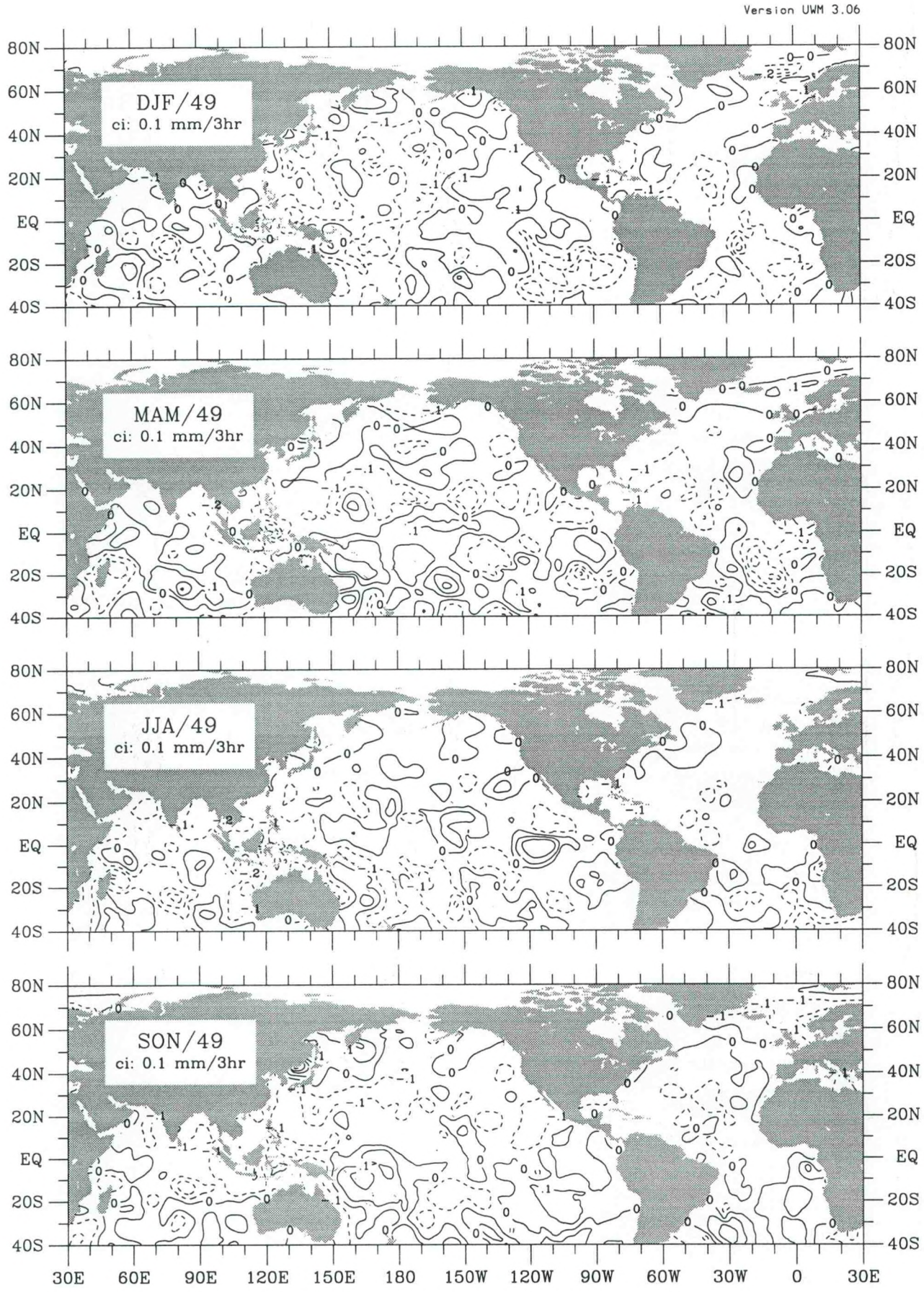

Figure E-10. Evaporation seasonal anomaly for 1949.

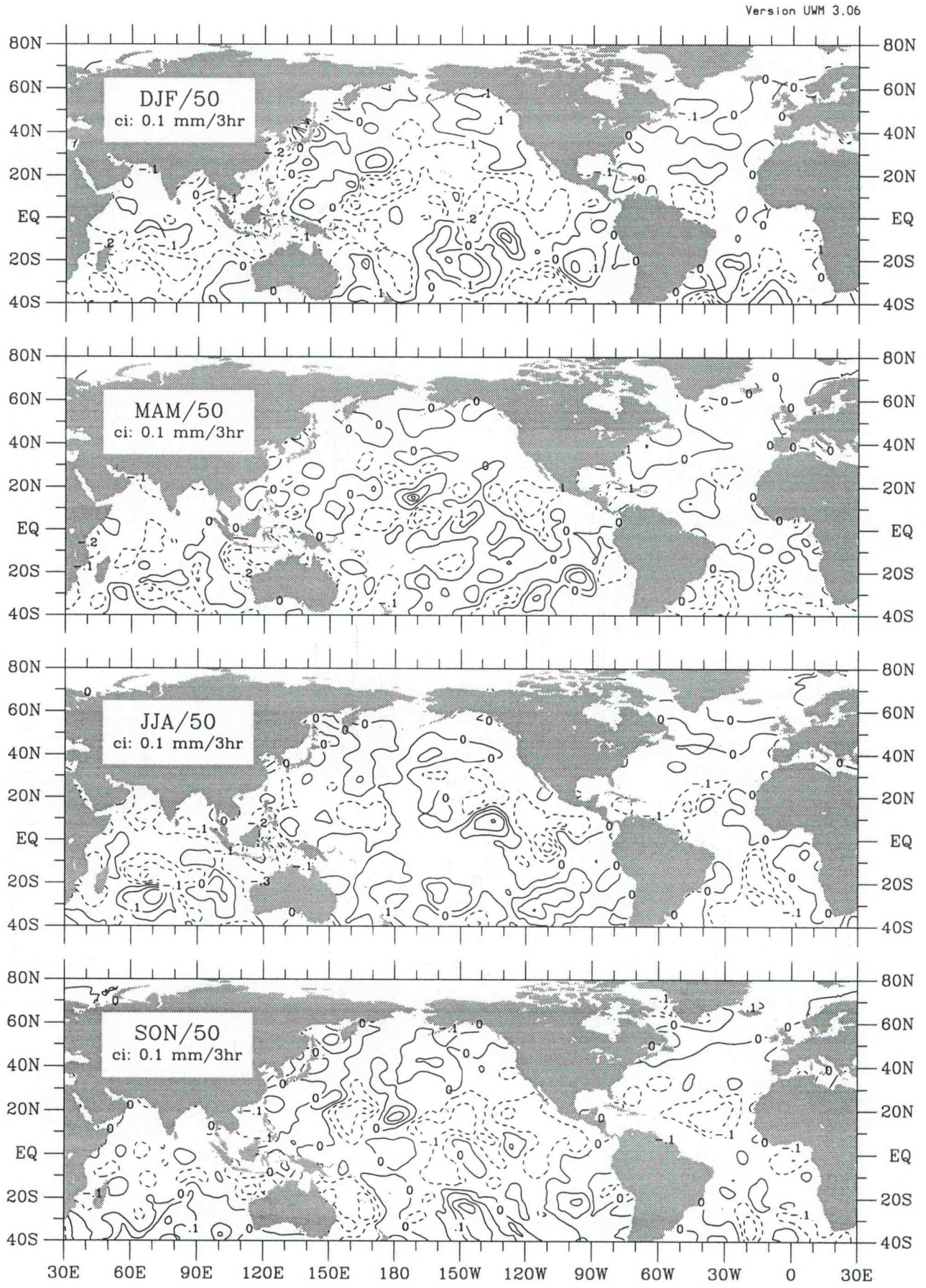

Figure E-11. Evaporation seasonal anomaly for 1950.

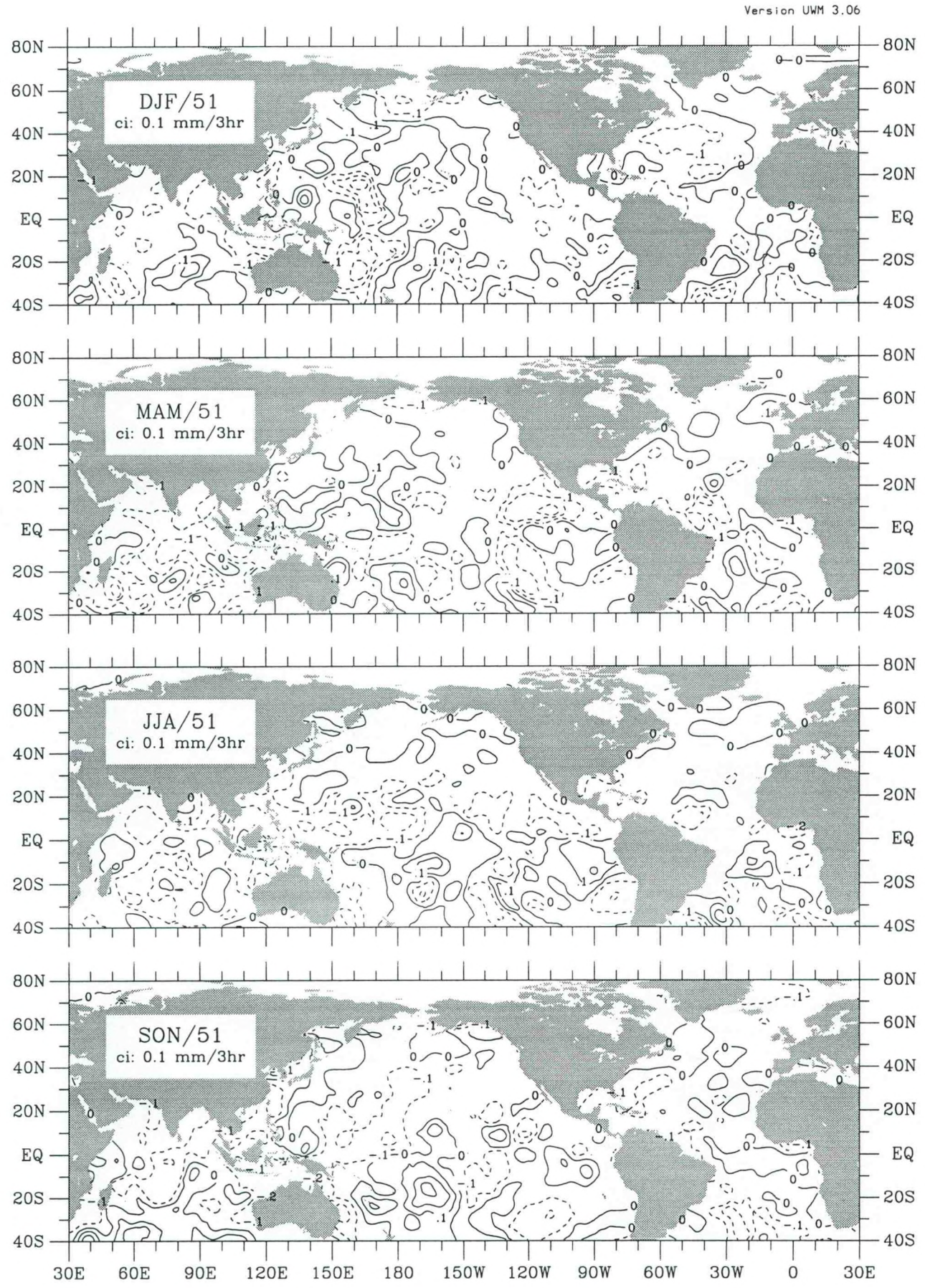

Figure E-12. Evaporation seasonal anomaly for 1951.

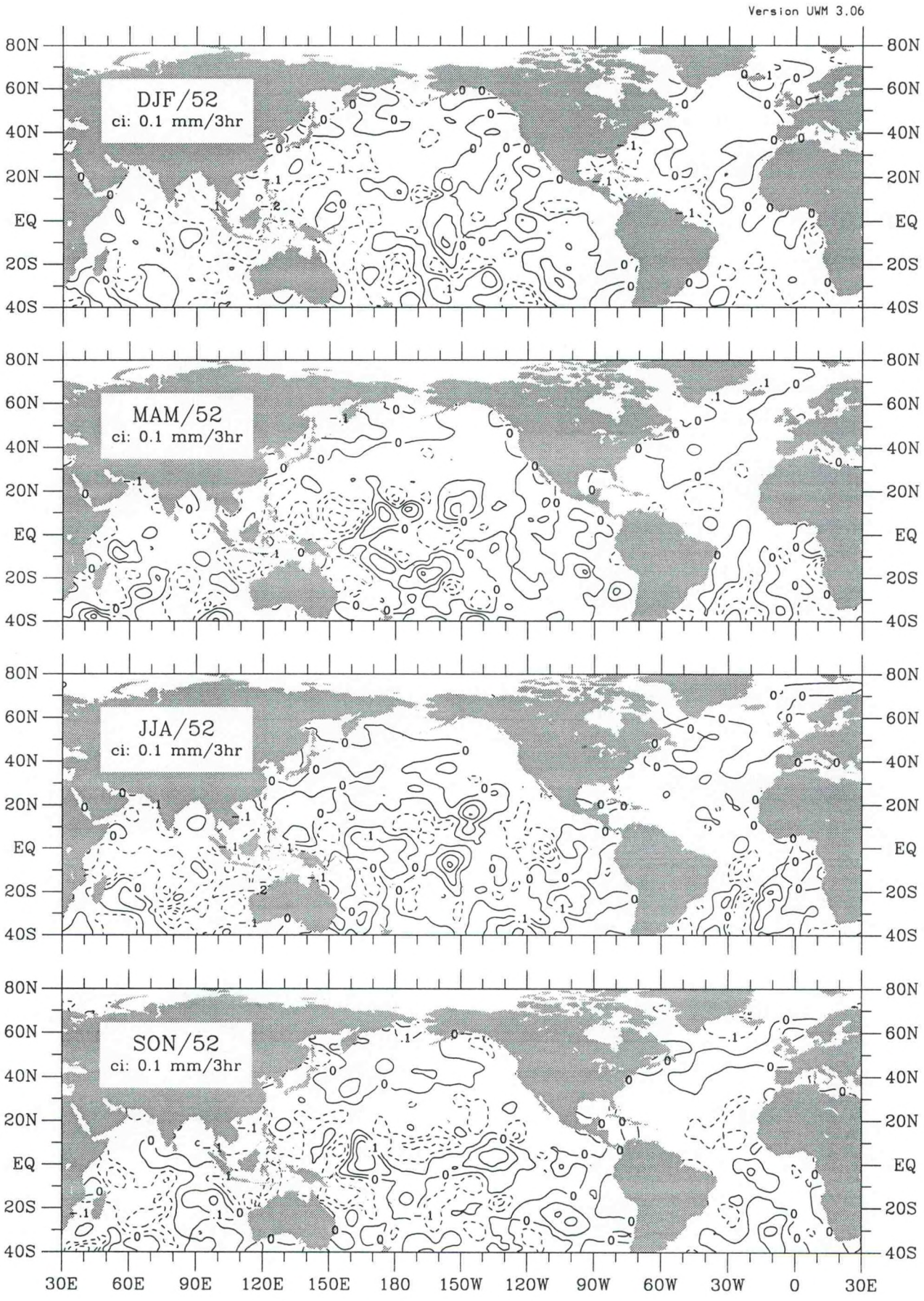

Figure E-13. Evaporation seasonal anomaly for 1952.

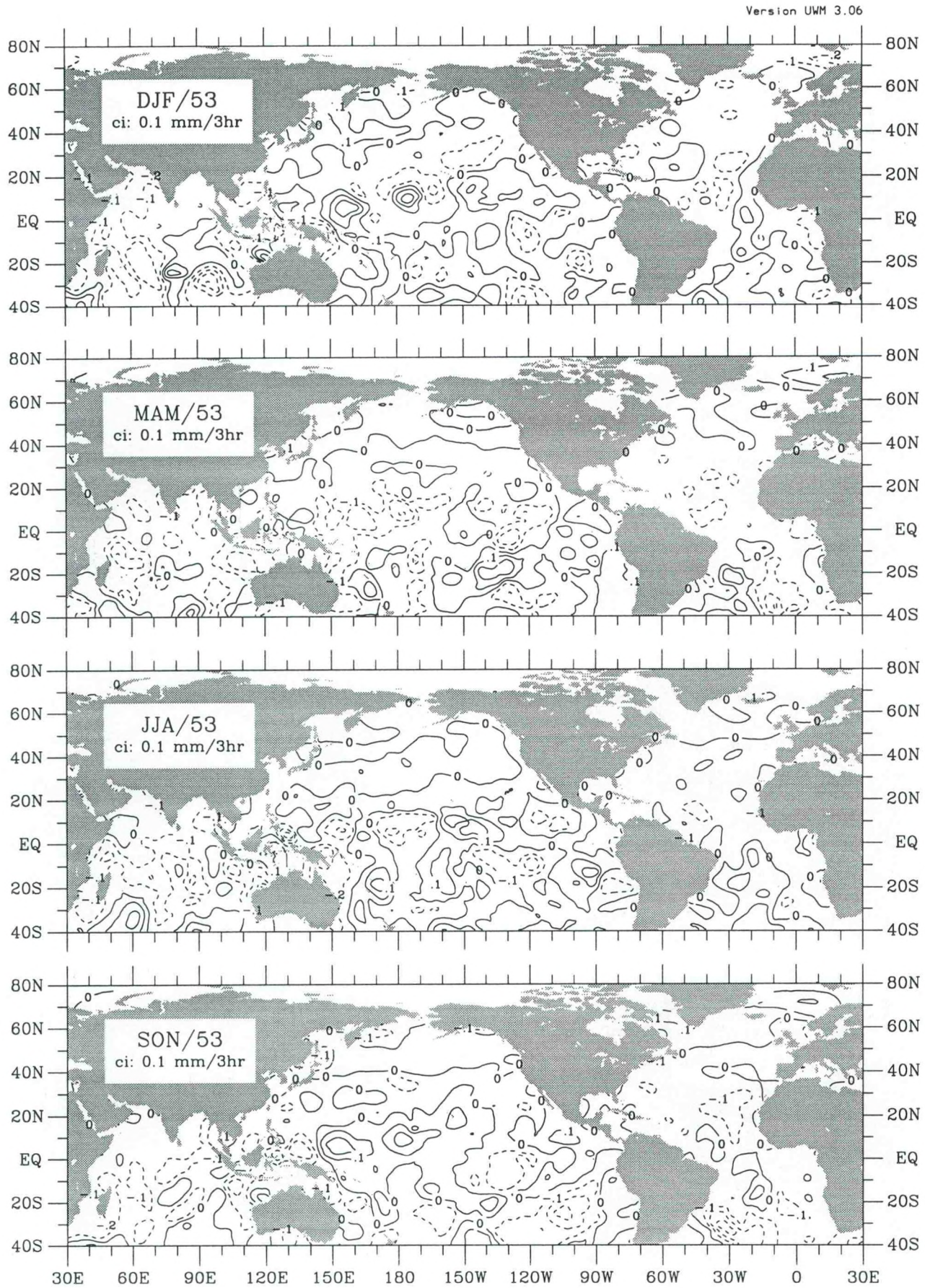

Figure E-14. Evaporation seasonal anomaly for 1953.

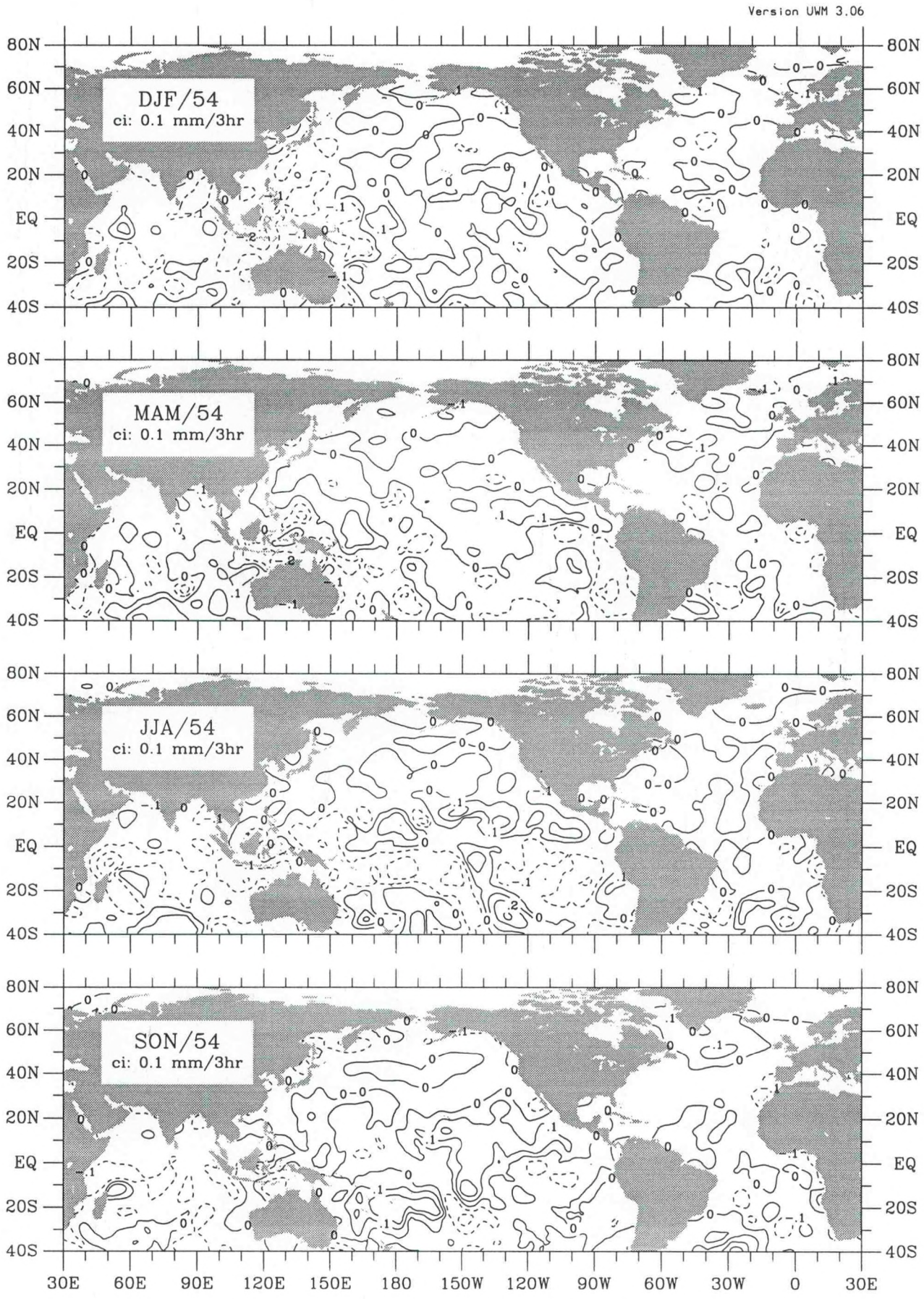

Figure E-15. Evaporation seasonal anomaly for 1954.

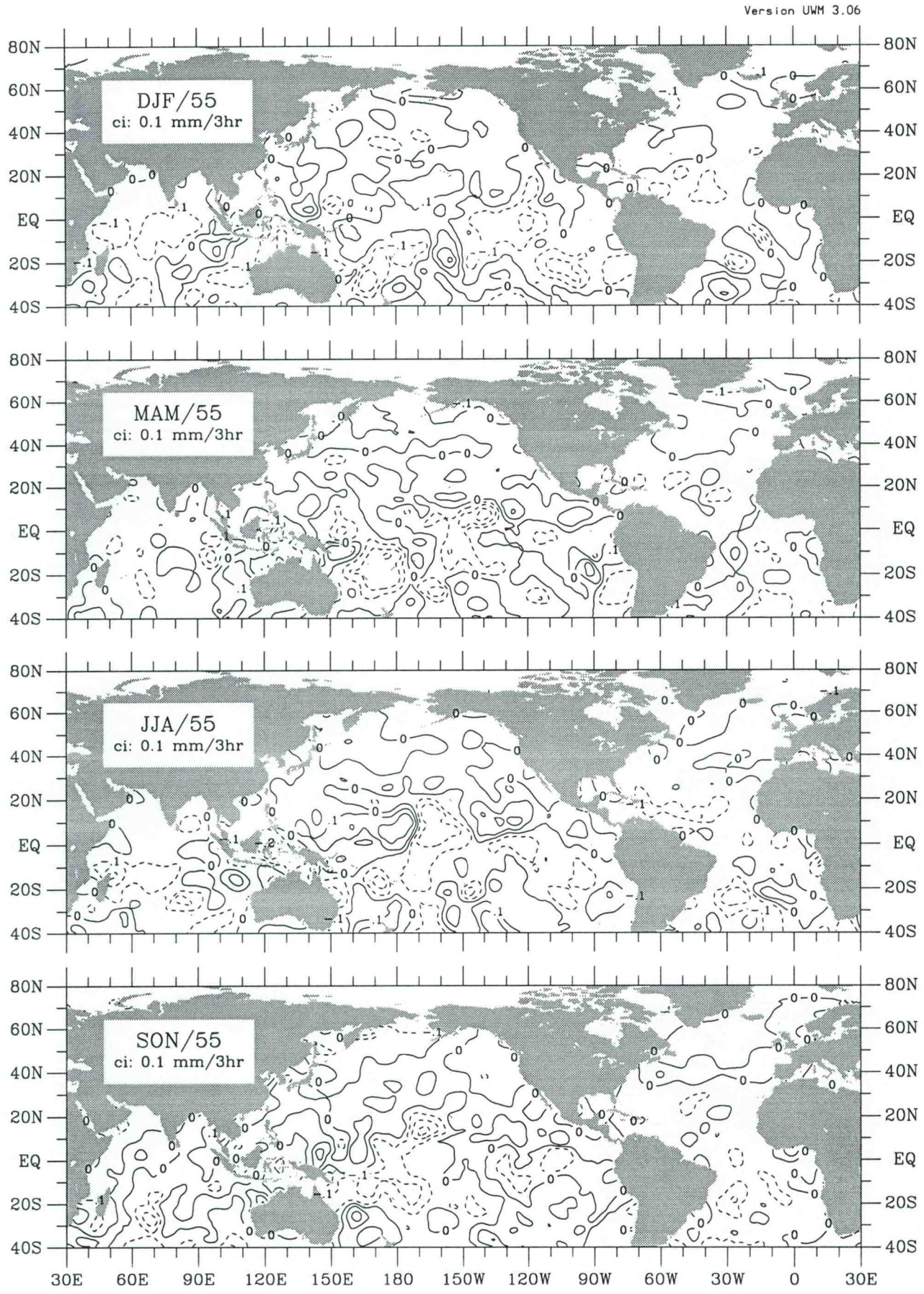

Figure E-16. Evaporation seasonal anomaly for 1955.

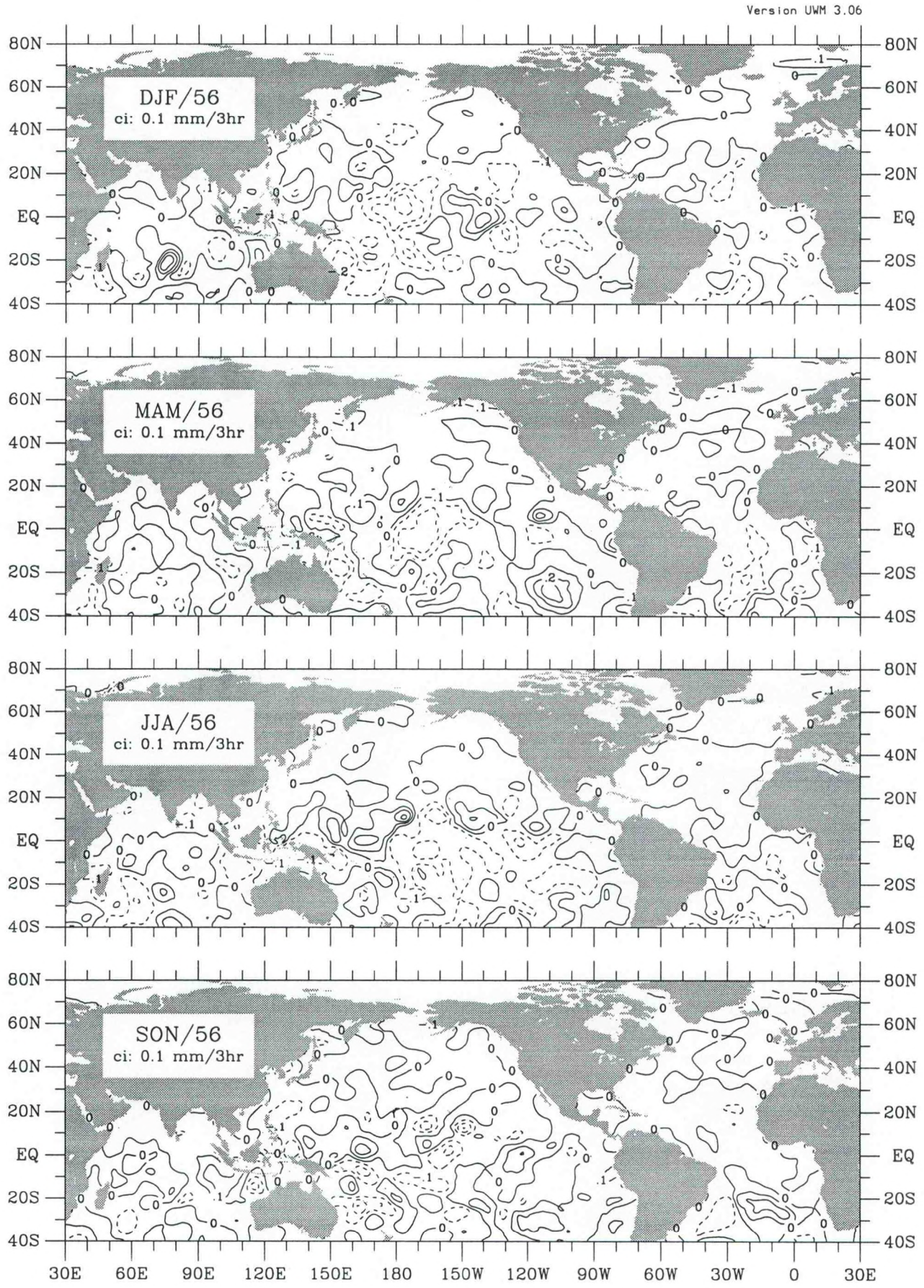

Figure E-17. Evaporation seasonal anomaly for 1956.

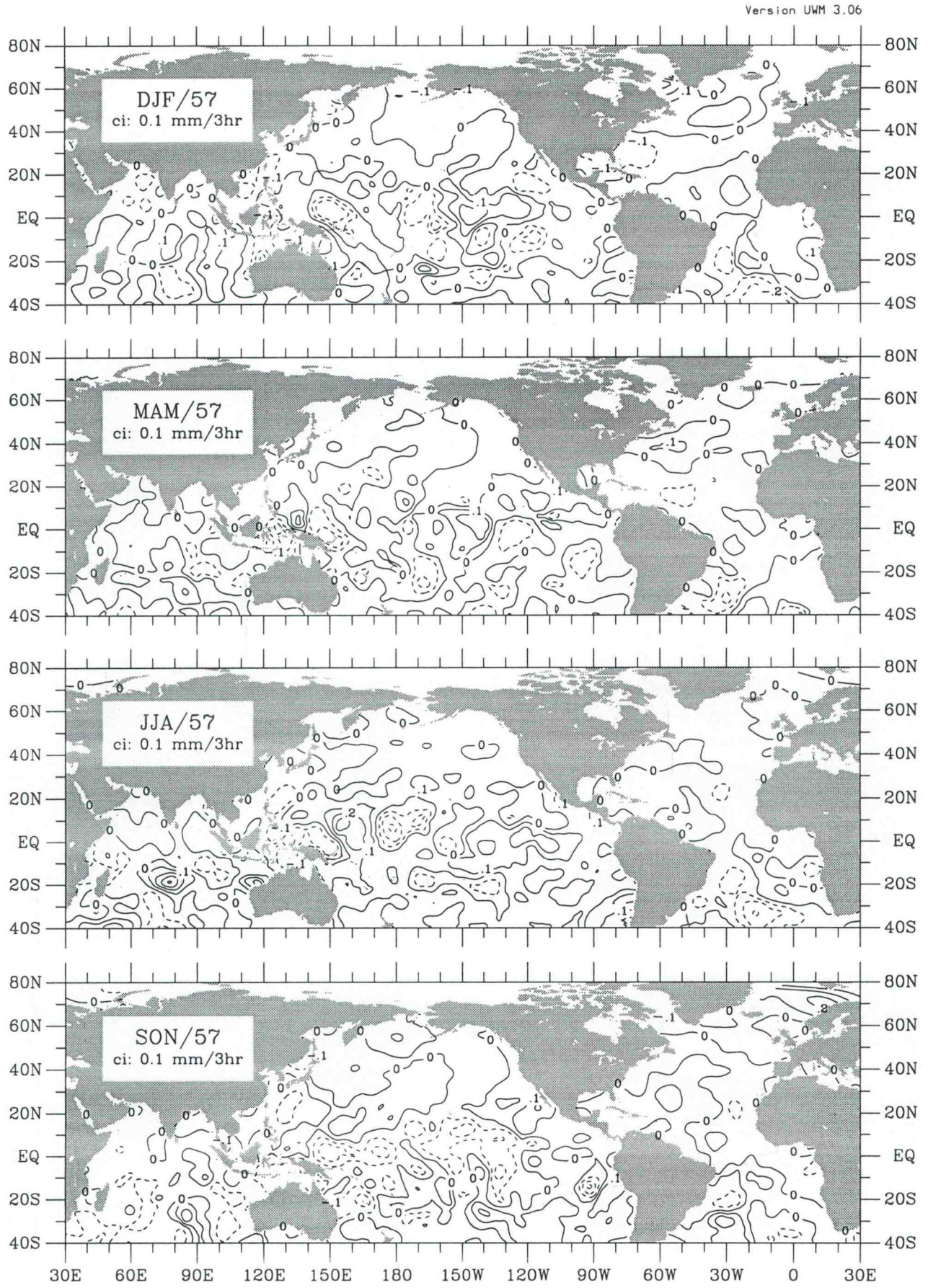

Figure E-18. Evaporation seasonal anomaly for 1957.

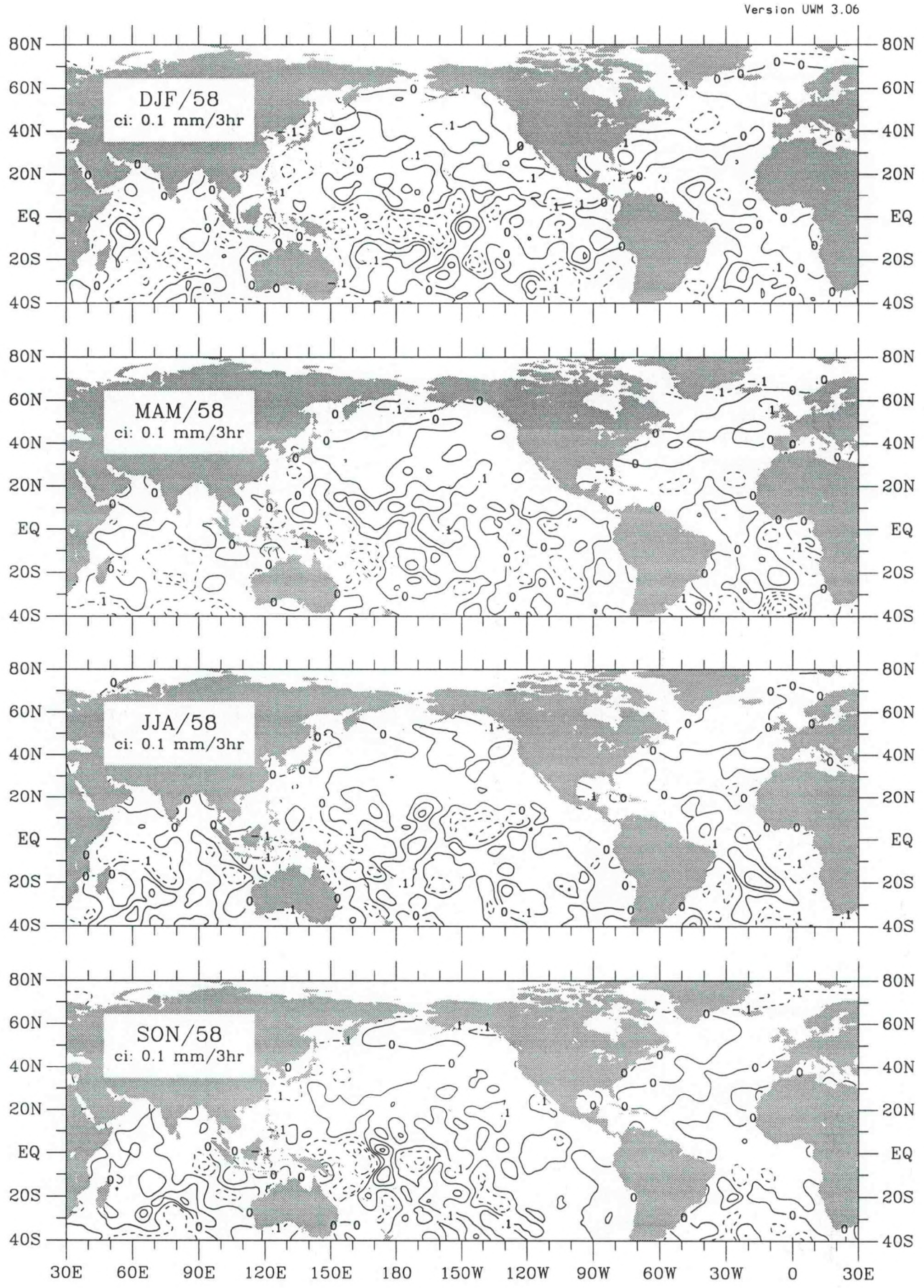

Figure E-19. Evaporation seasonal anomaly for 1958.

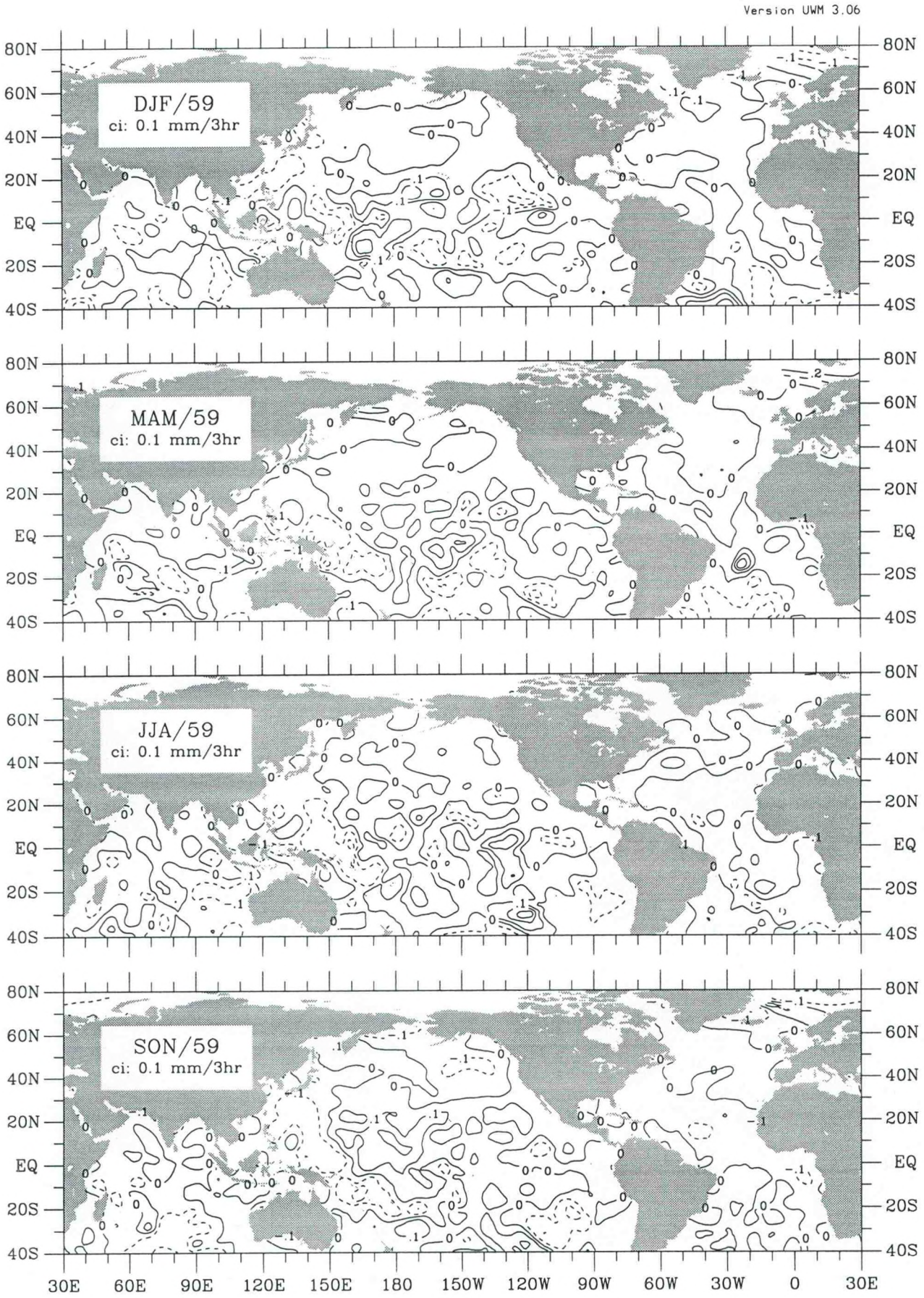

Figure E-20. Evaporation seasonal anomaly for 1959.

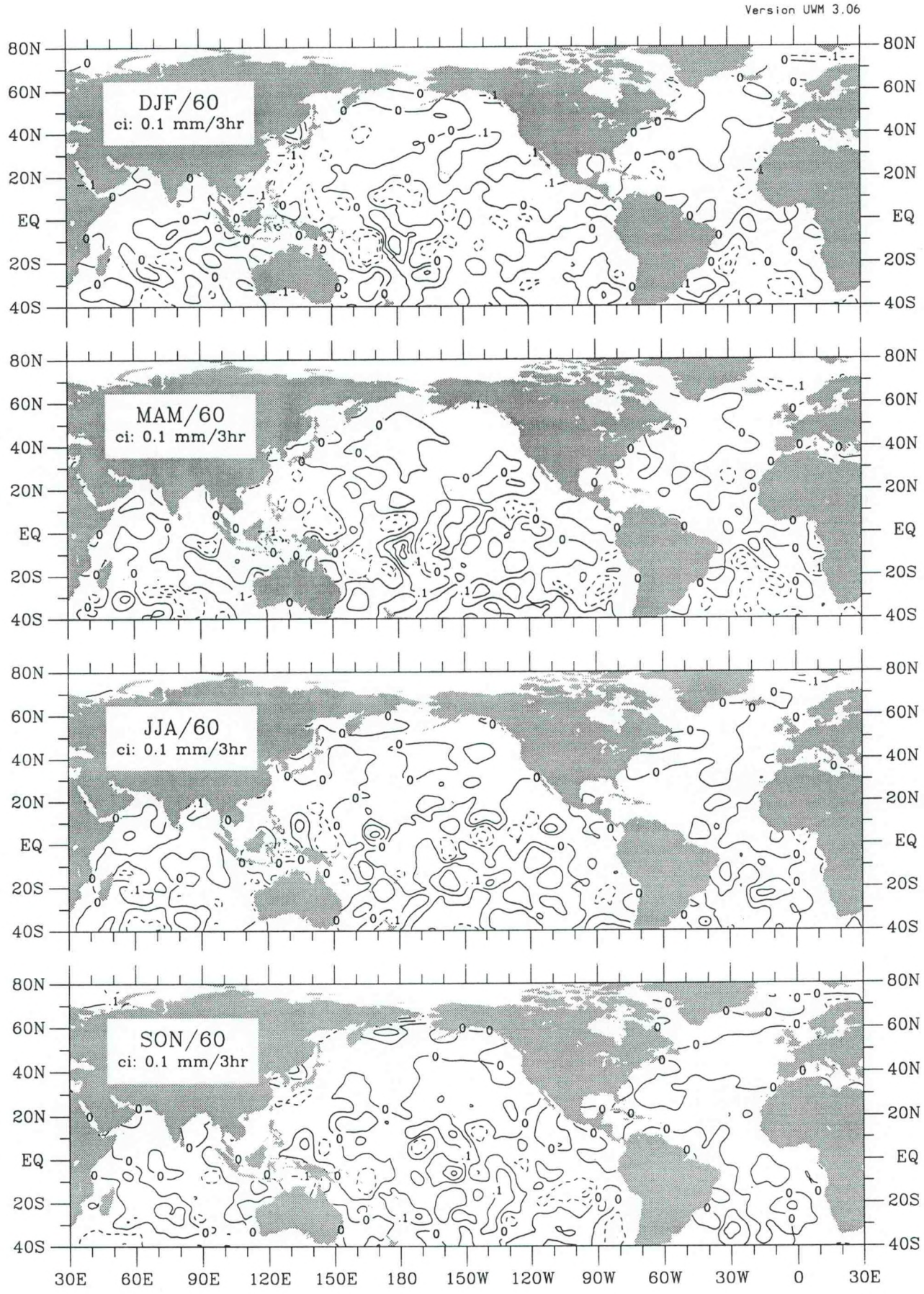

Figure E-21. Evaporation seasonal anomaly for 1960.

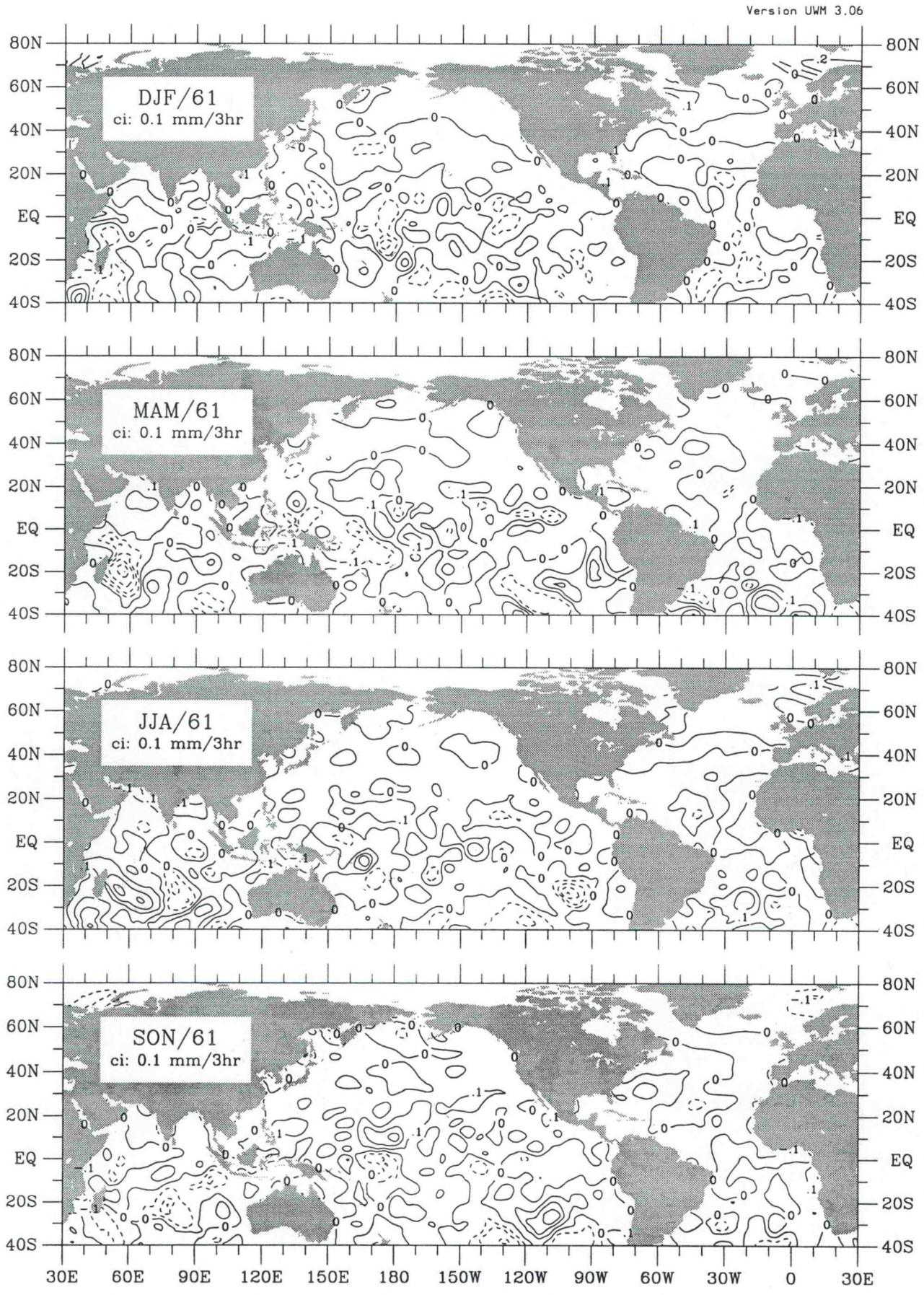

Figure E-22. Evaporation seasonal anomaly for 1961.

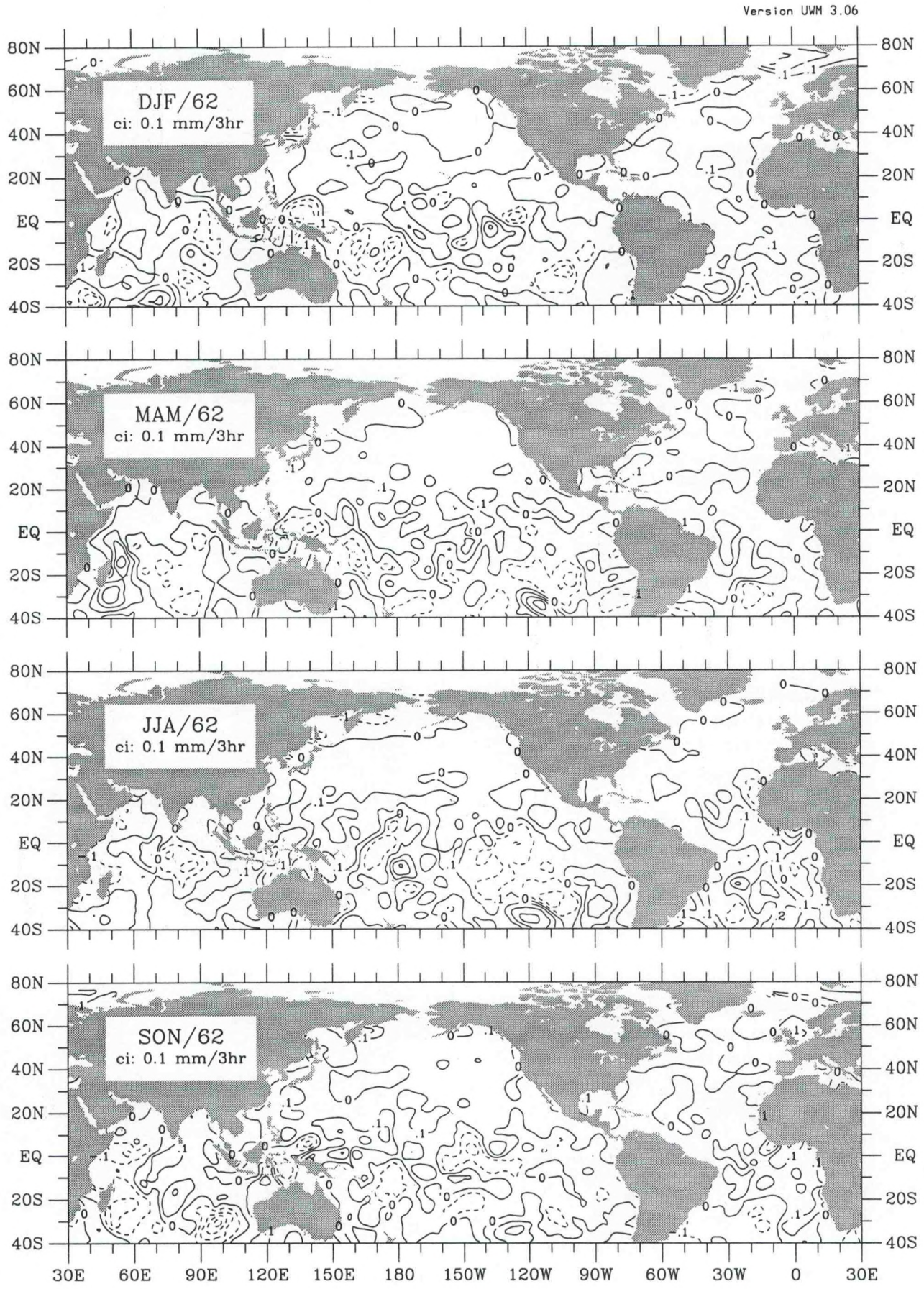

Figure E-23. Evaporation seasonal anomaly for 1962.

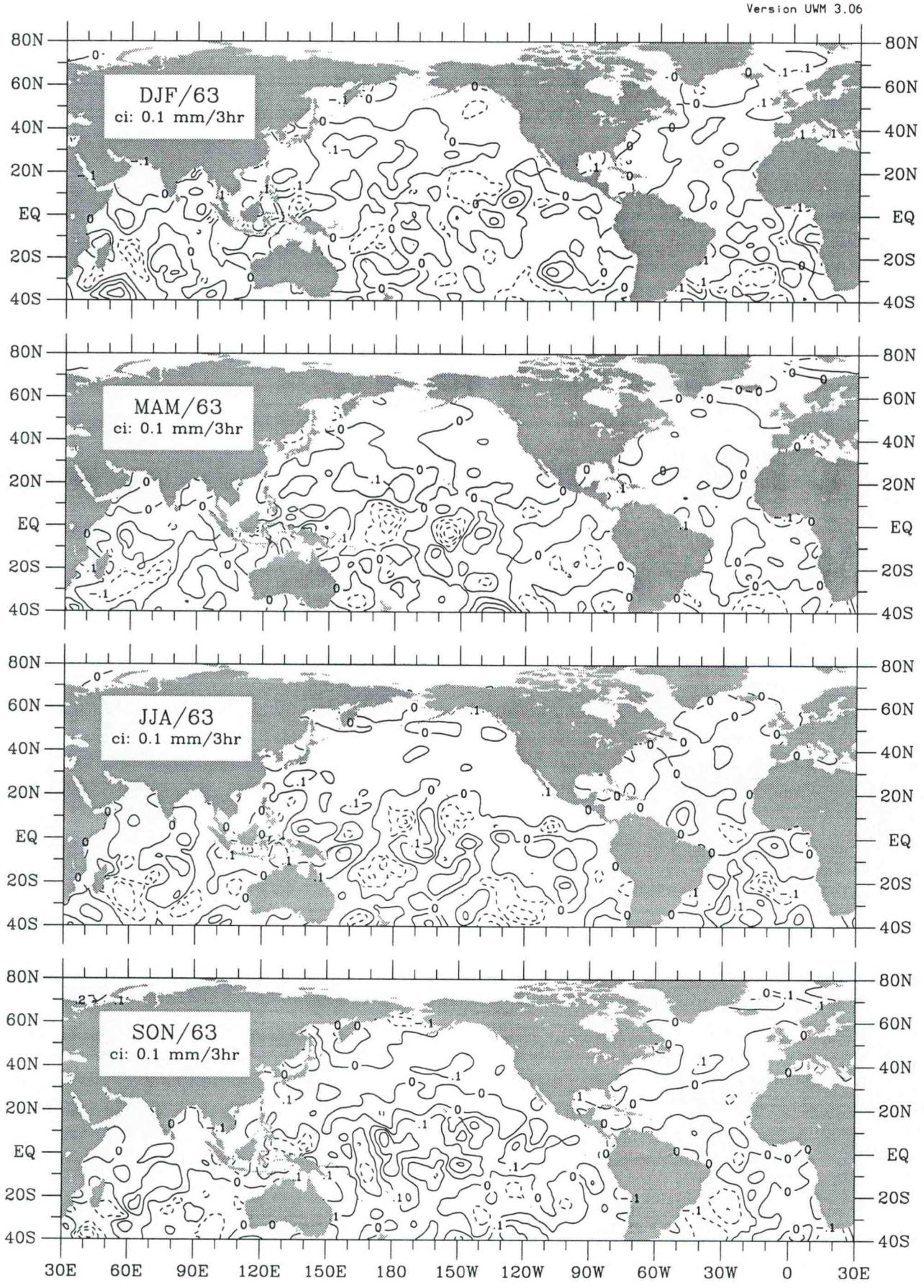

Figure E-24. Evaporation seasonal anomaly for 1963.

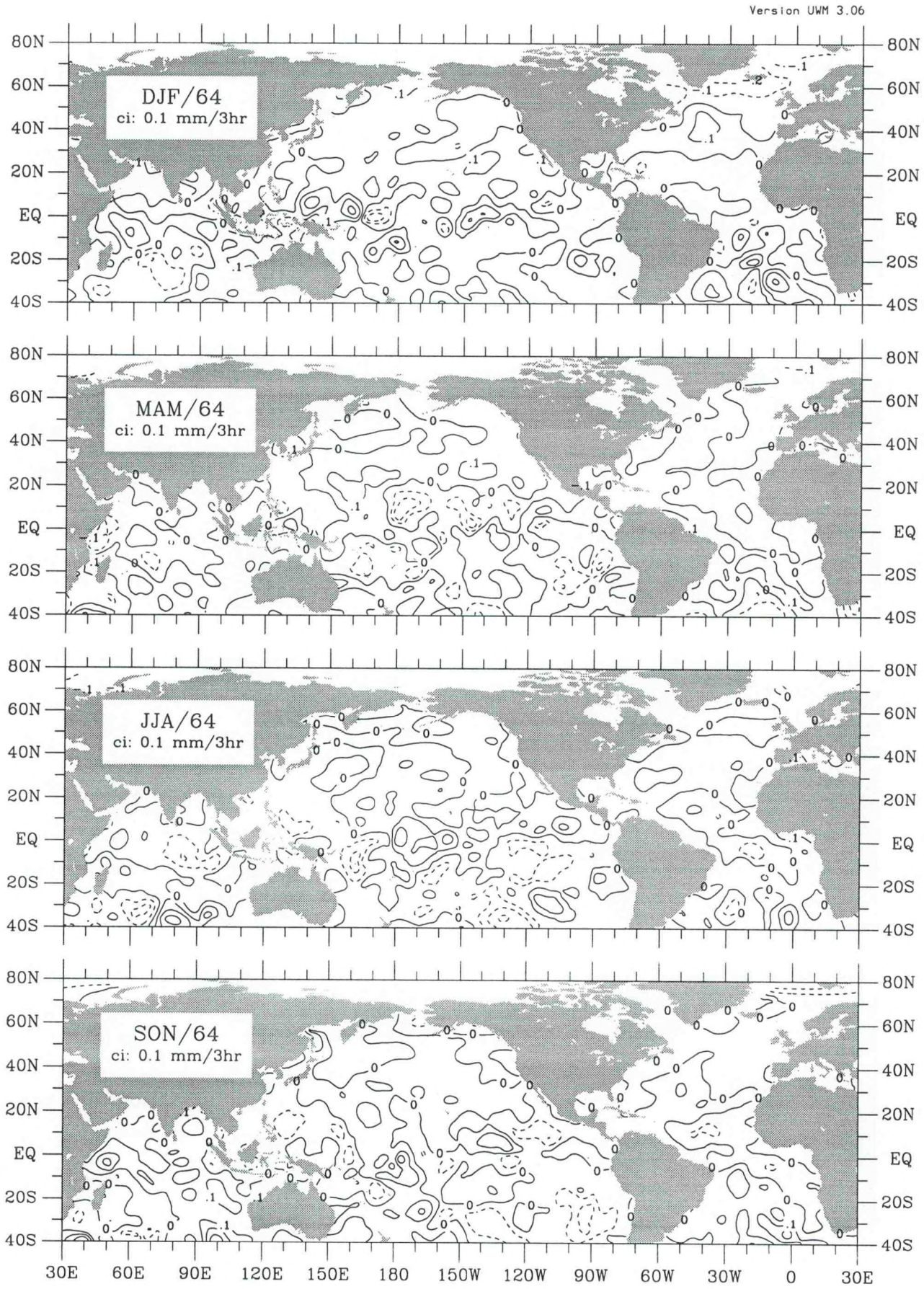

Figure E-25. Evaporation seasonal anomaly for 1964.

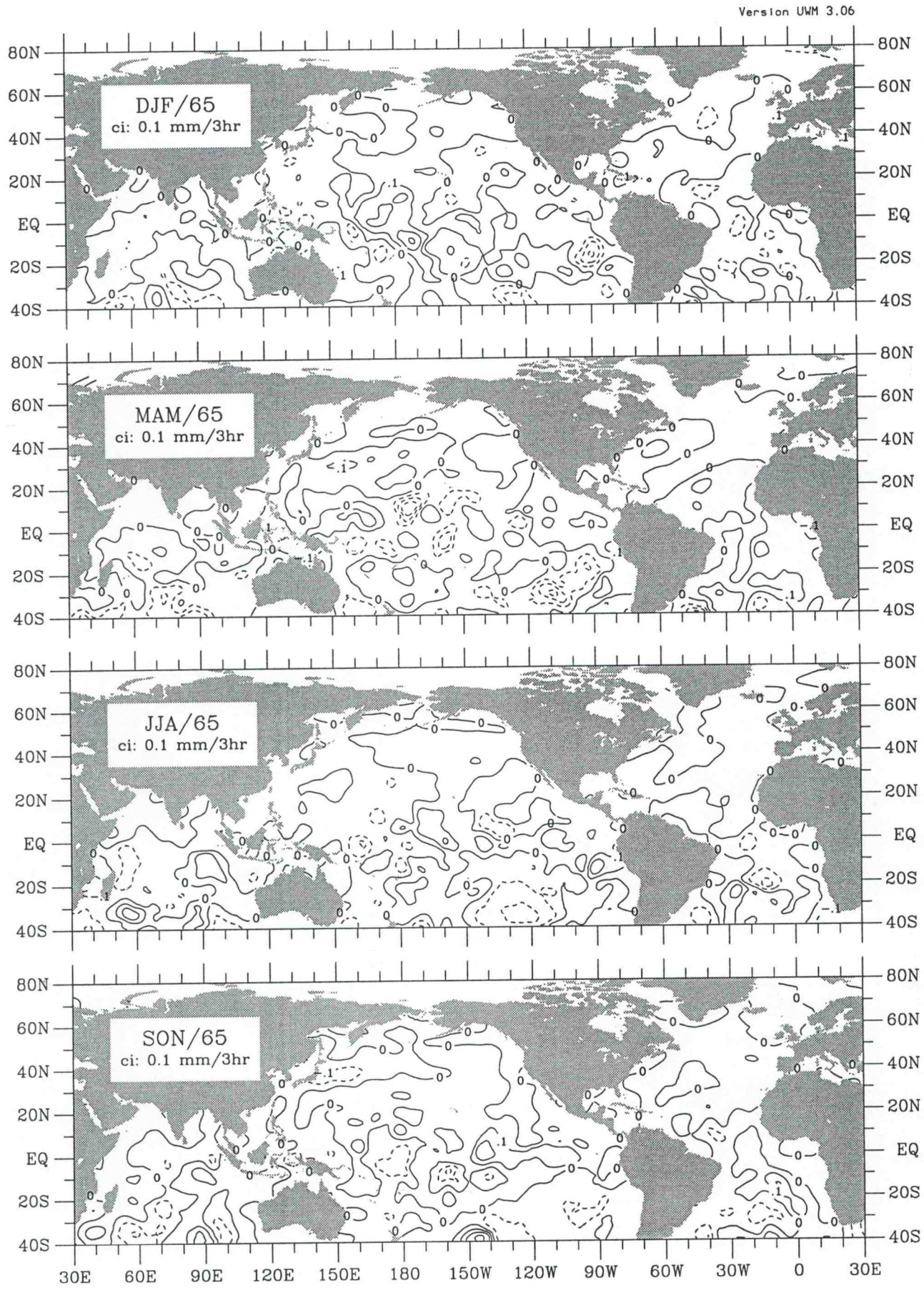

Figure E-26. Evaporation seasonal anomaly for 1965.

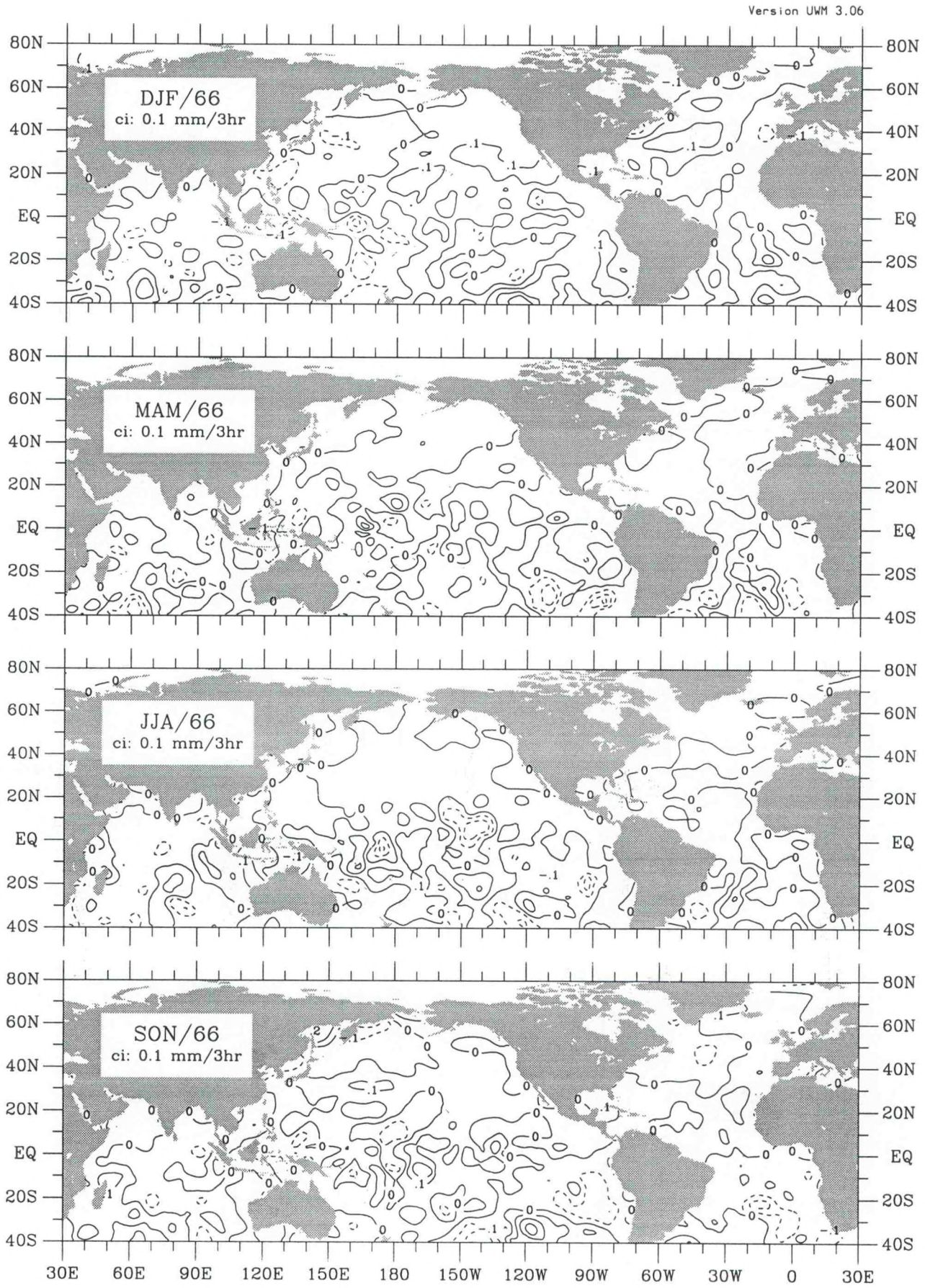

Figure E-27. Evaporation seasonal anomaly for 1966.

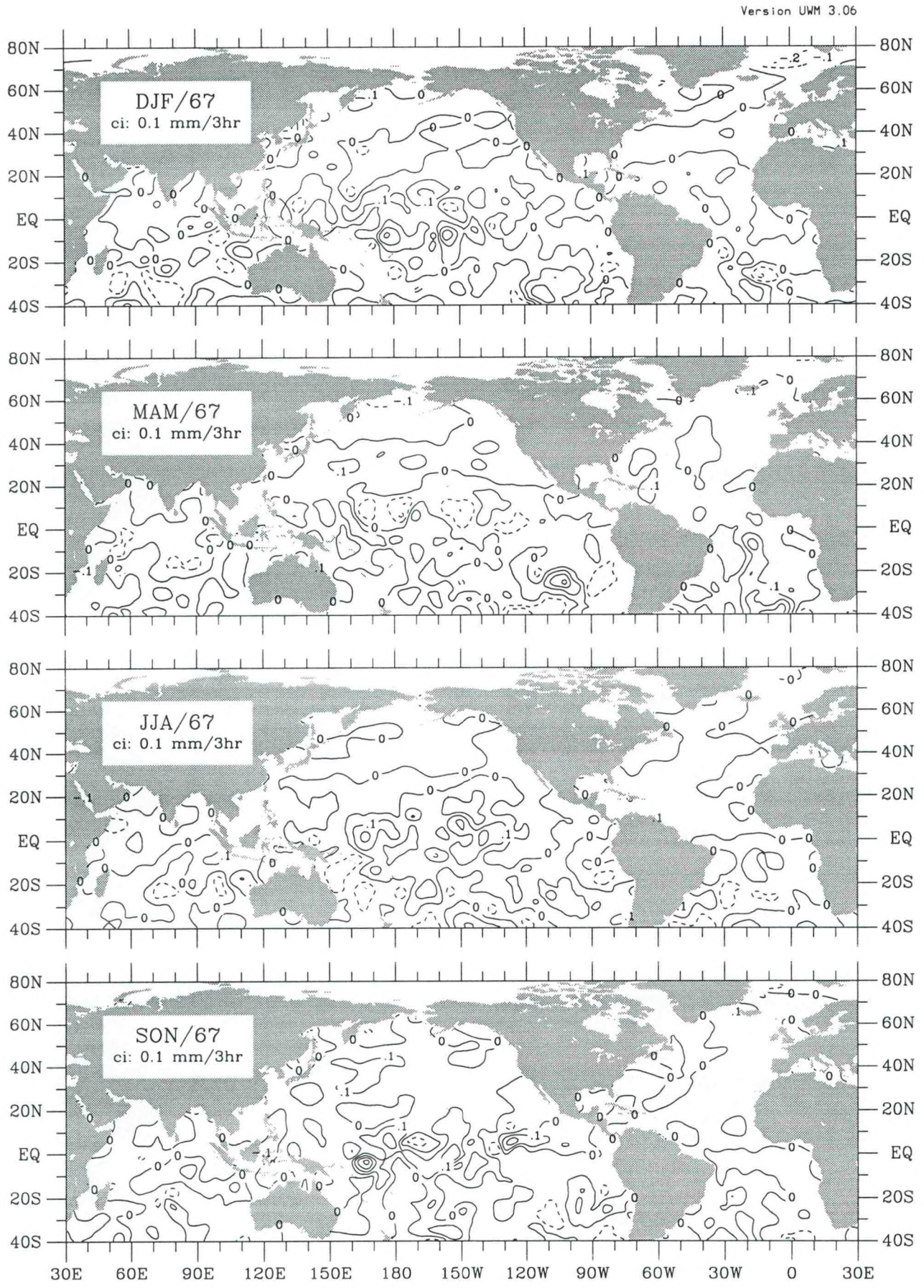

Figure E-28. Evaporation seasonal anomaly for 1967.

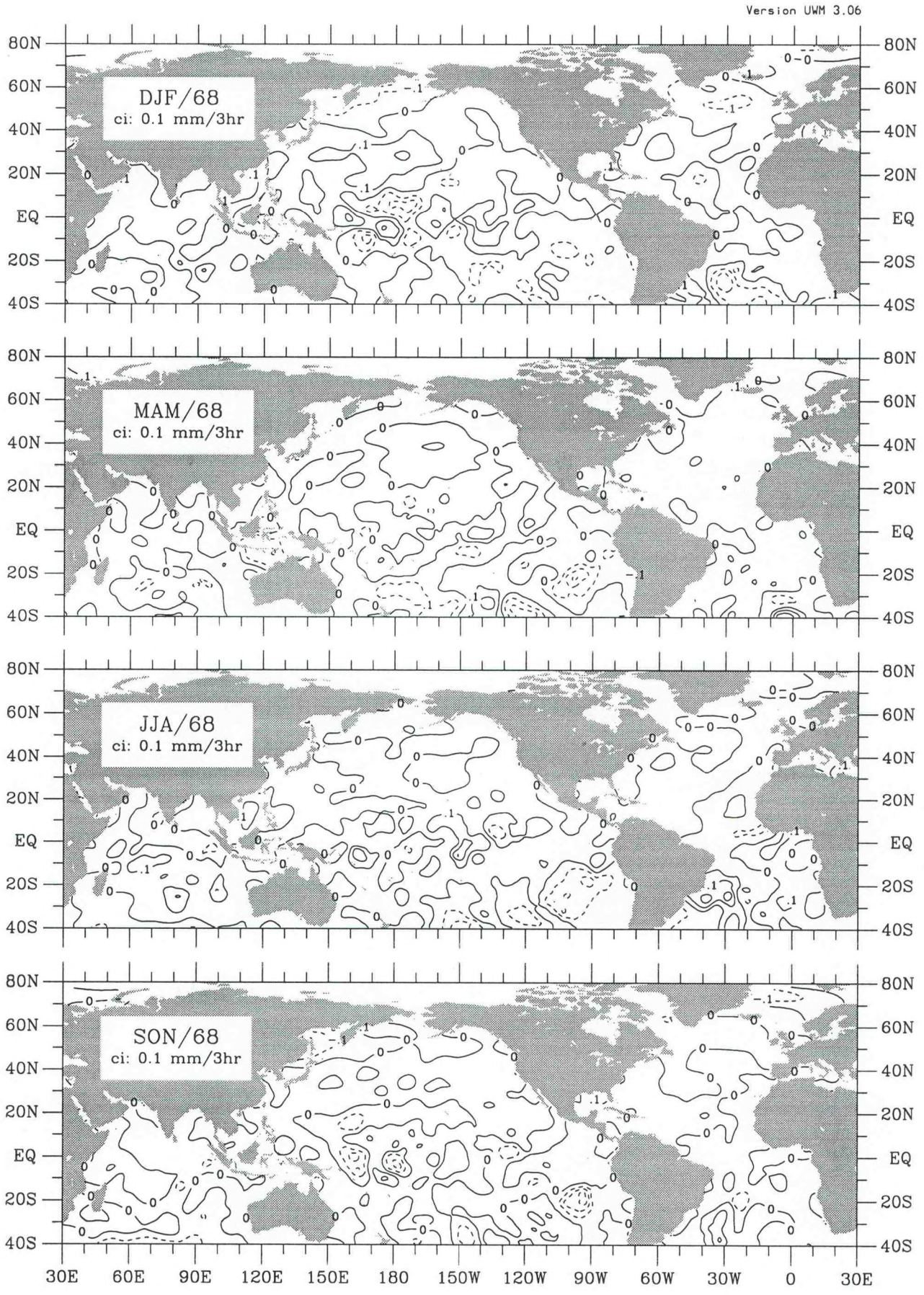

Figure E-29. Evaporation seasonal anomaly for 1968.

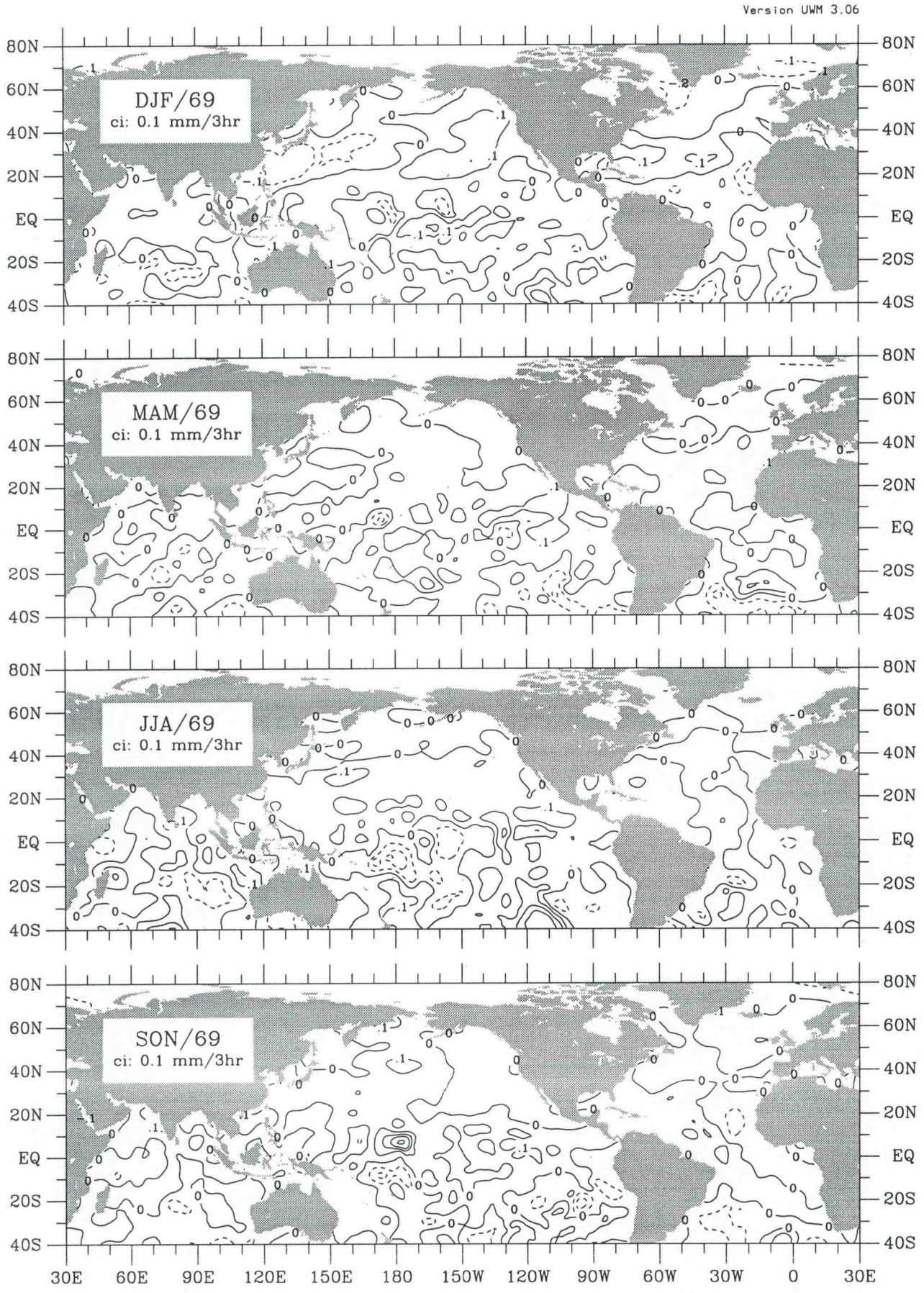

Figure E-30. Evaporation seasonal anomaly for 1969.

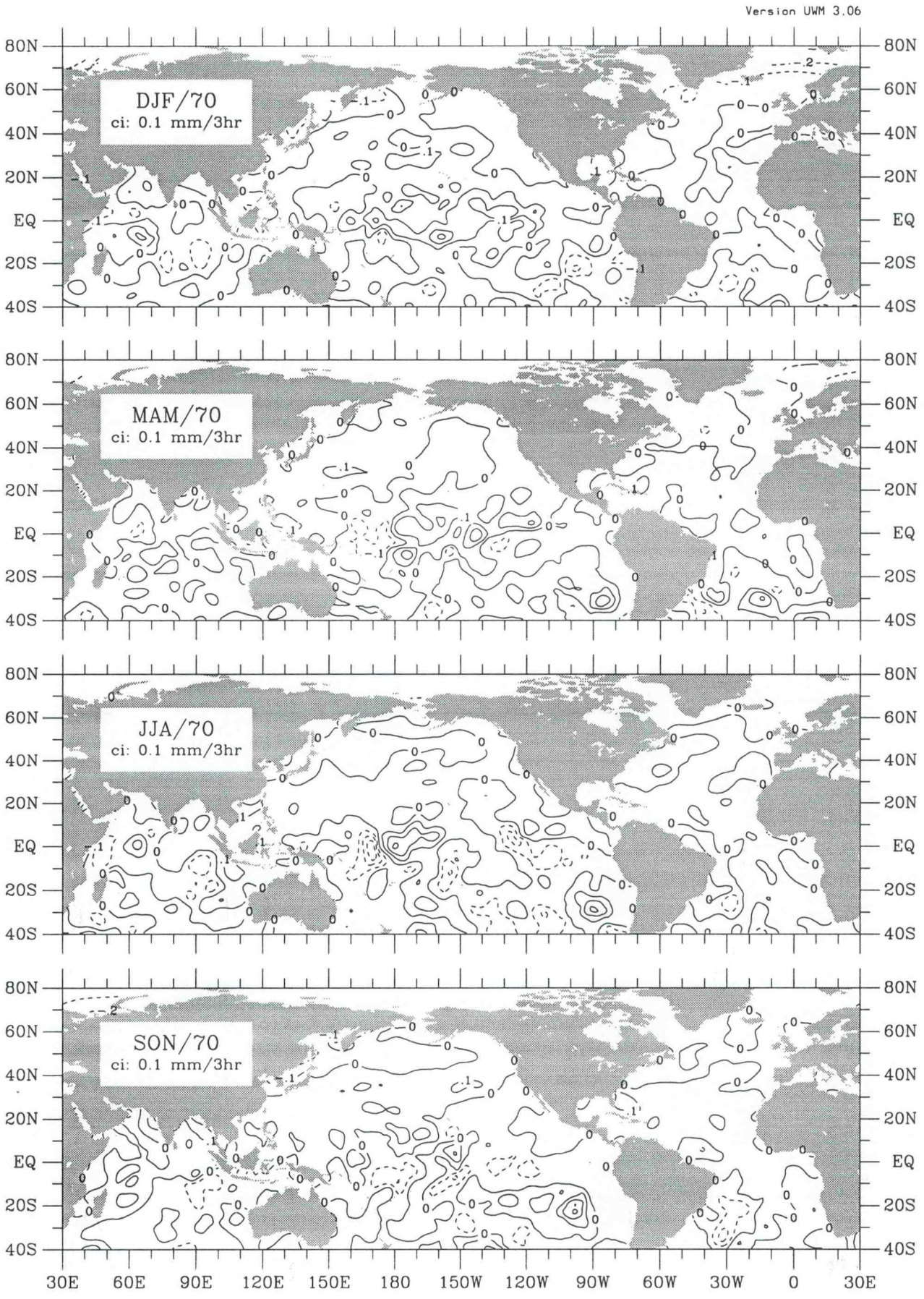

Figure E-31. Evaporation seasonal anomaly for 1970.

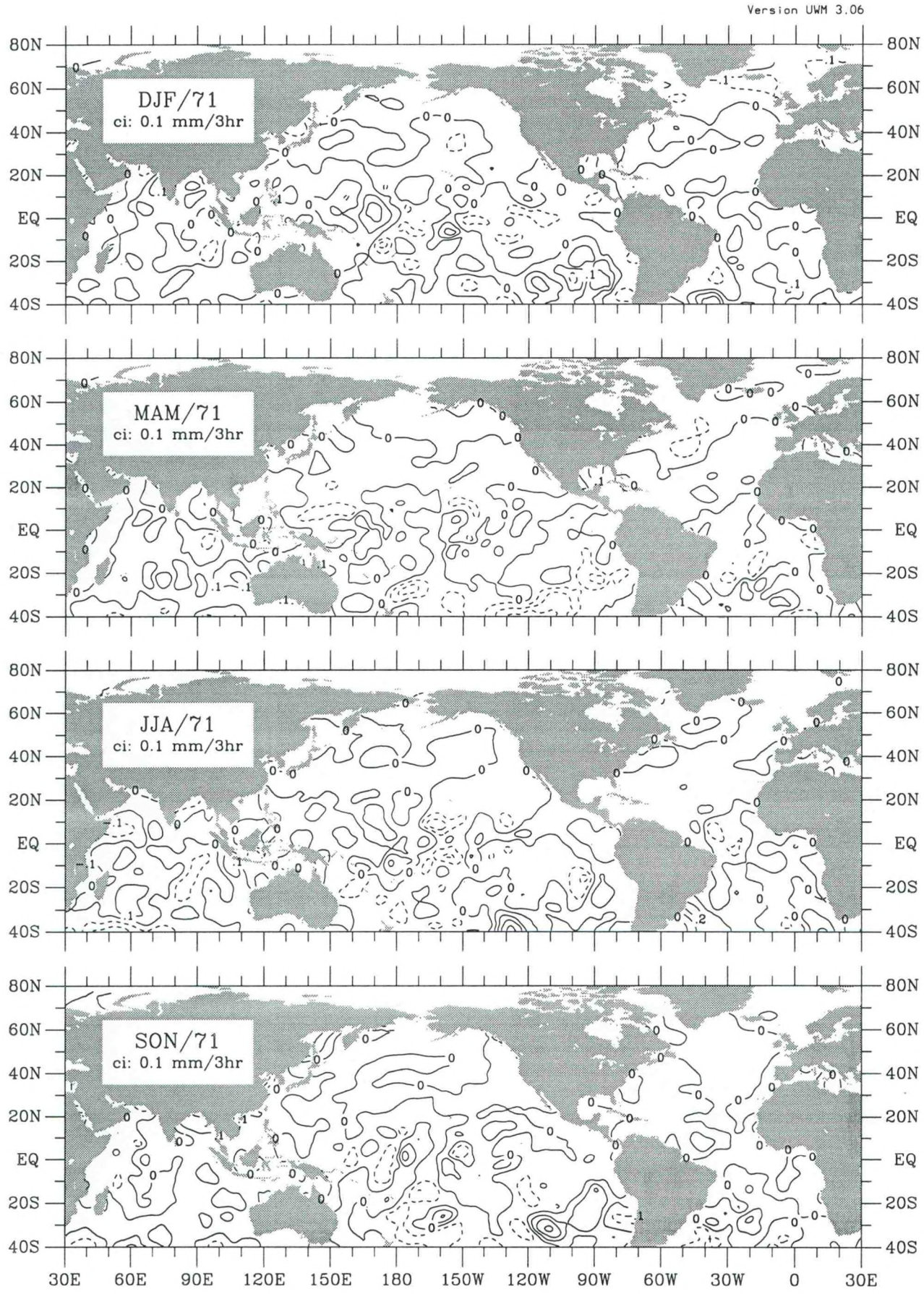

Figure E-32. Evaporation seasonal anomaly for 1971.

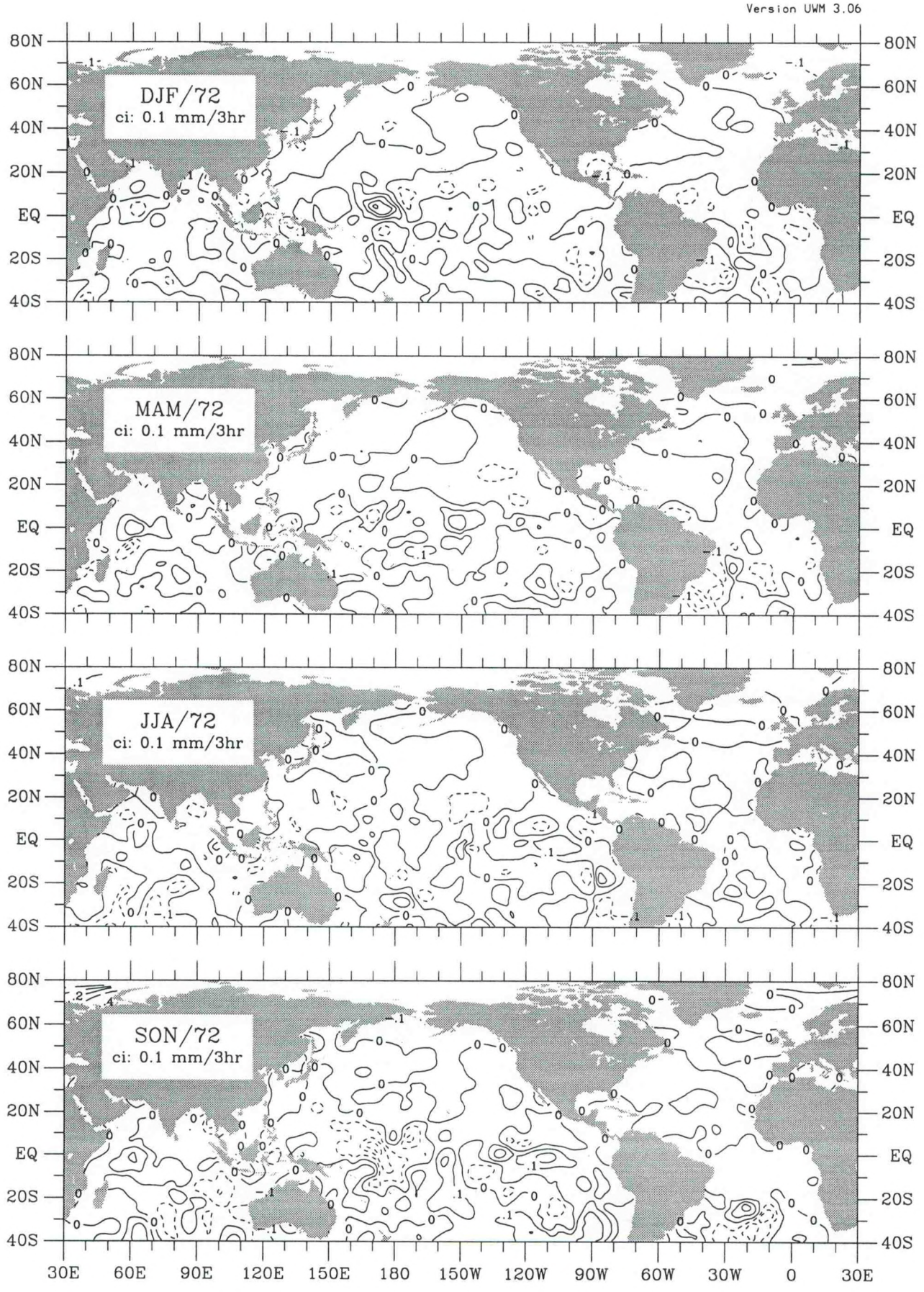

Figure E-33. Evaporation seasonal anomaly for 1972.

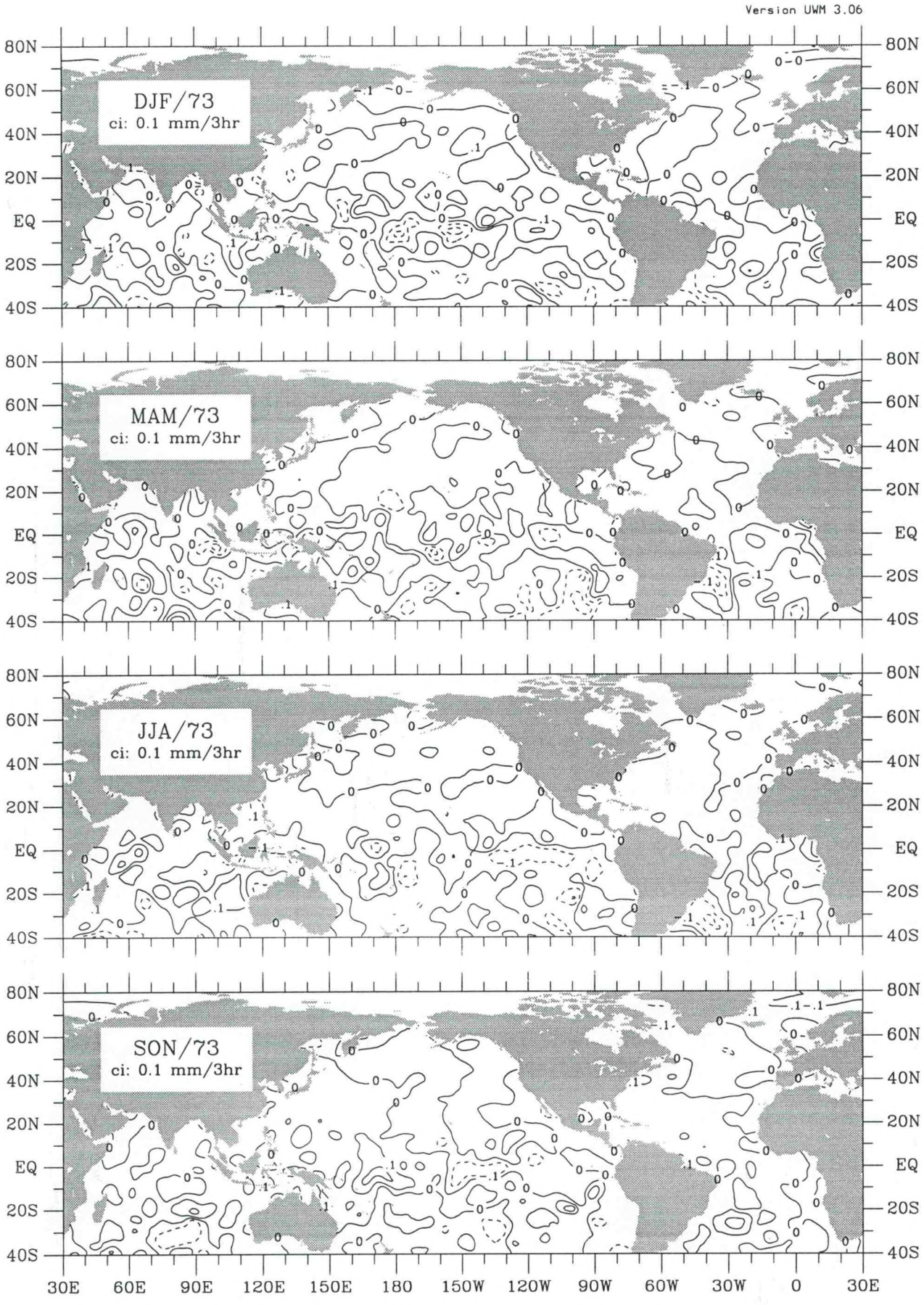

Figure E-34. Evaporation seasonal anomaly for 1973.

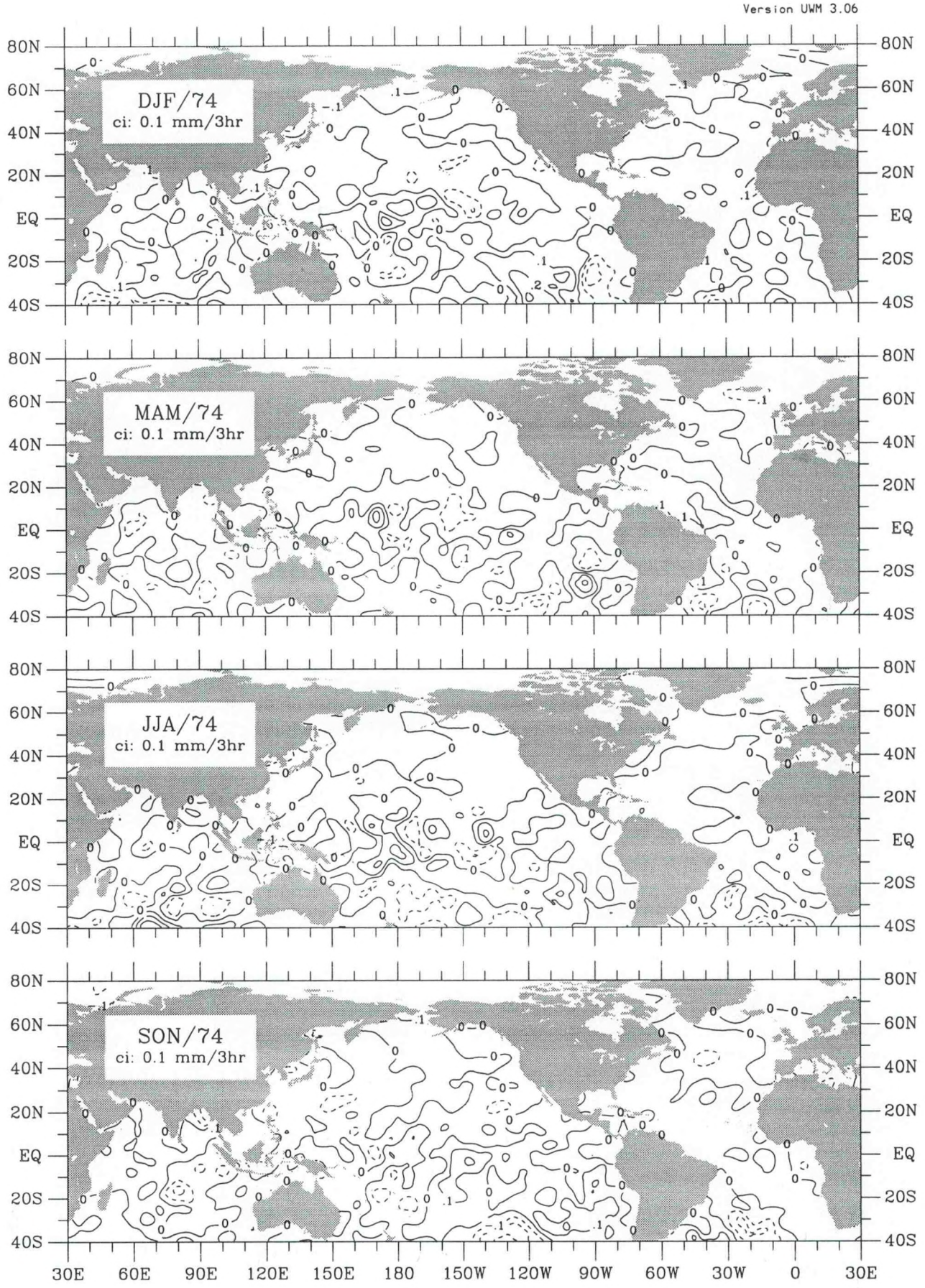

Figure E-35. Evaporation seasonal anomaly for 1974.

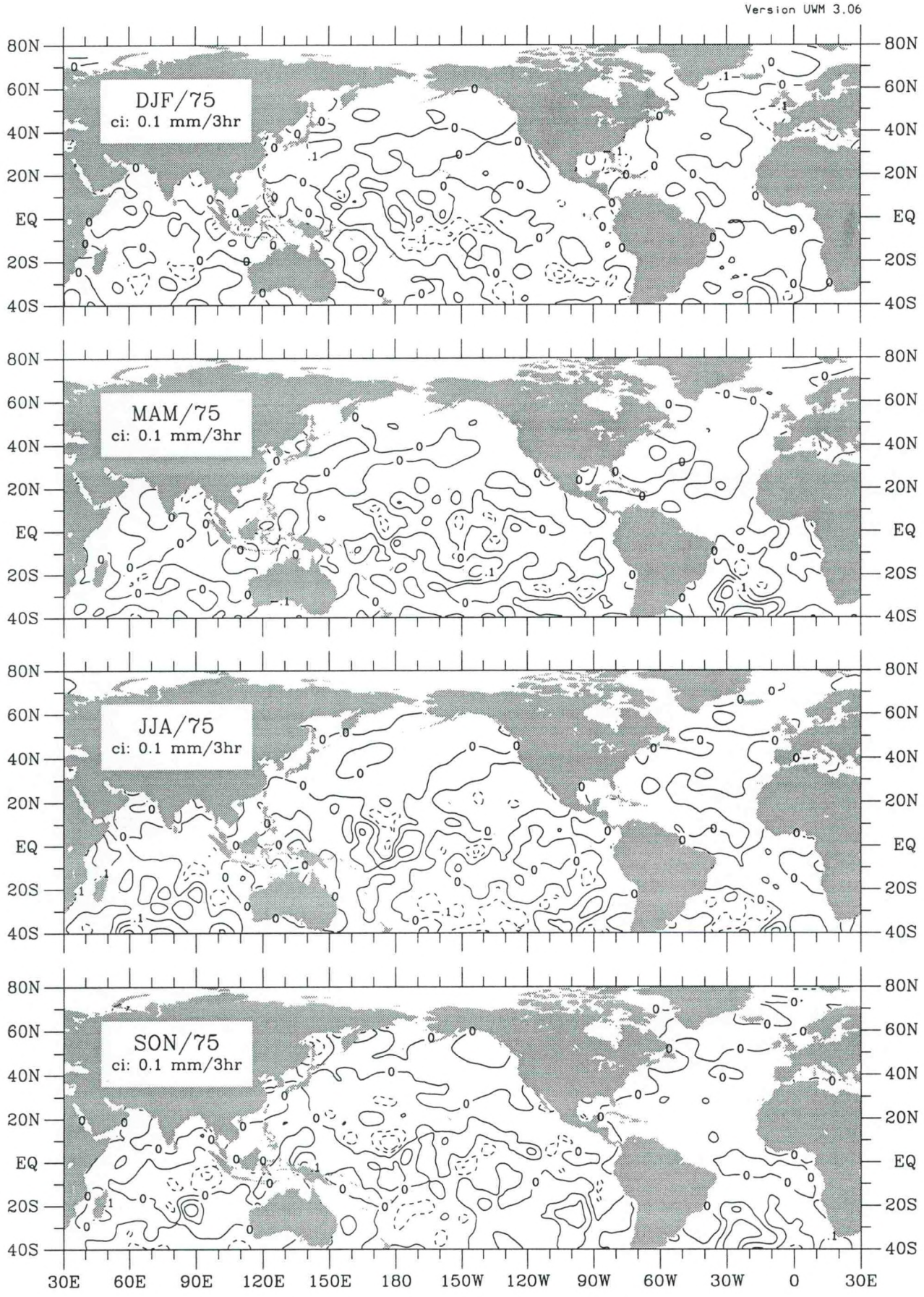

Figure E-36. Evaporation seasonal anomaly for 1975.

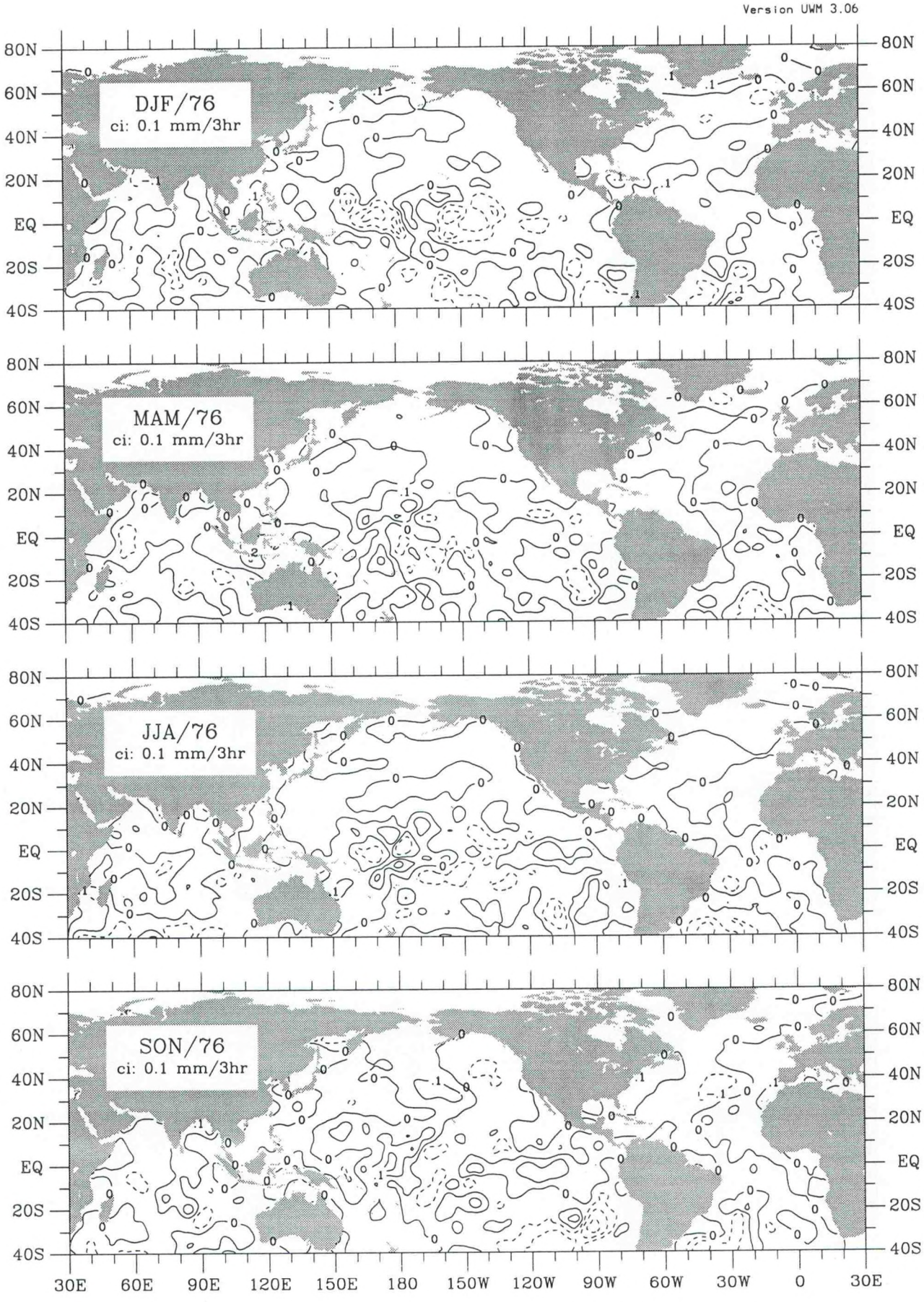

Figure E-37. Evaporation seasonal anomaly for 1976.

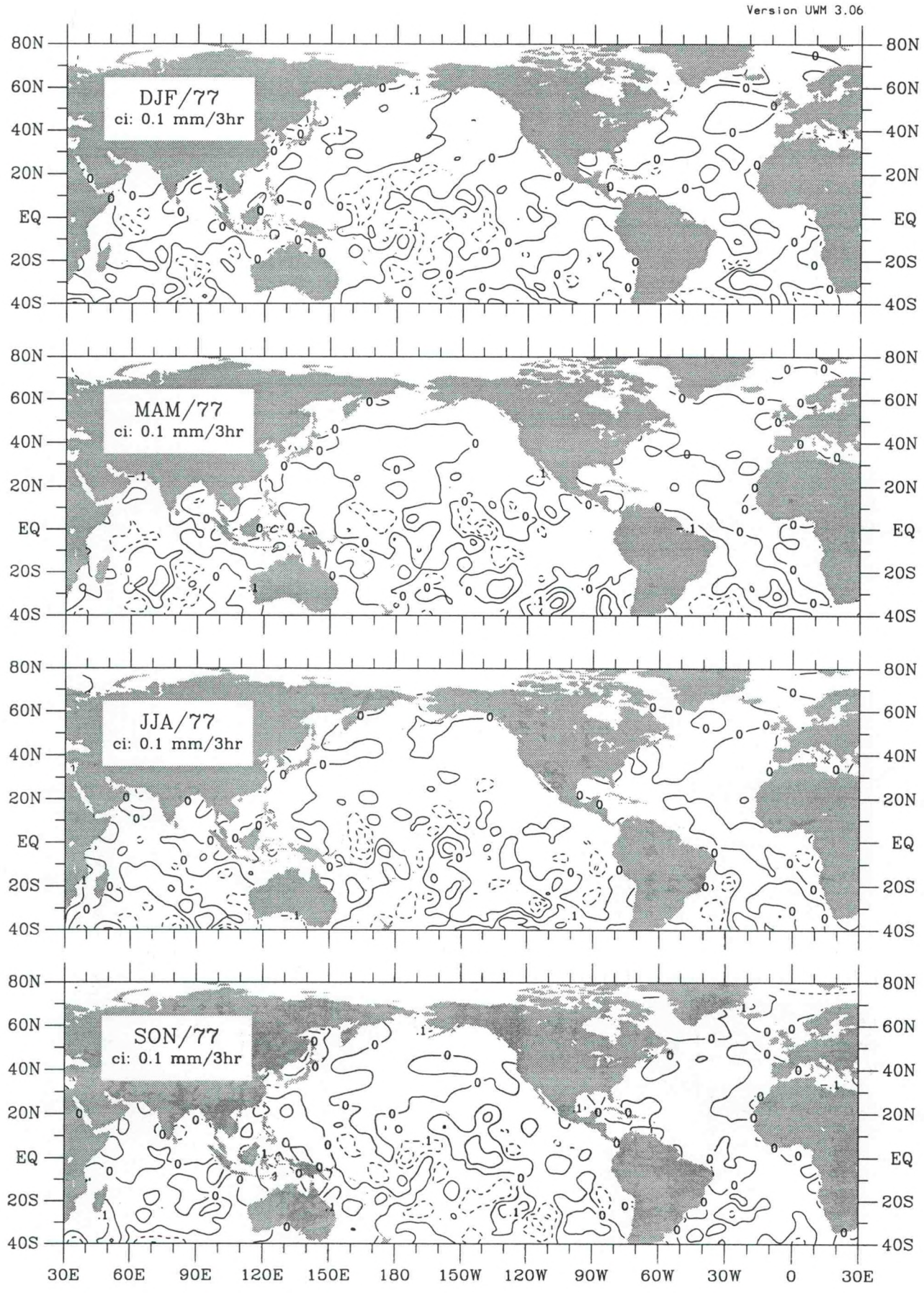

Figure E-38. Evaporation seasonal anomaly for 1977.

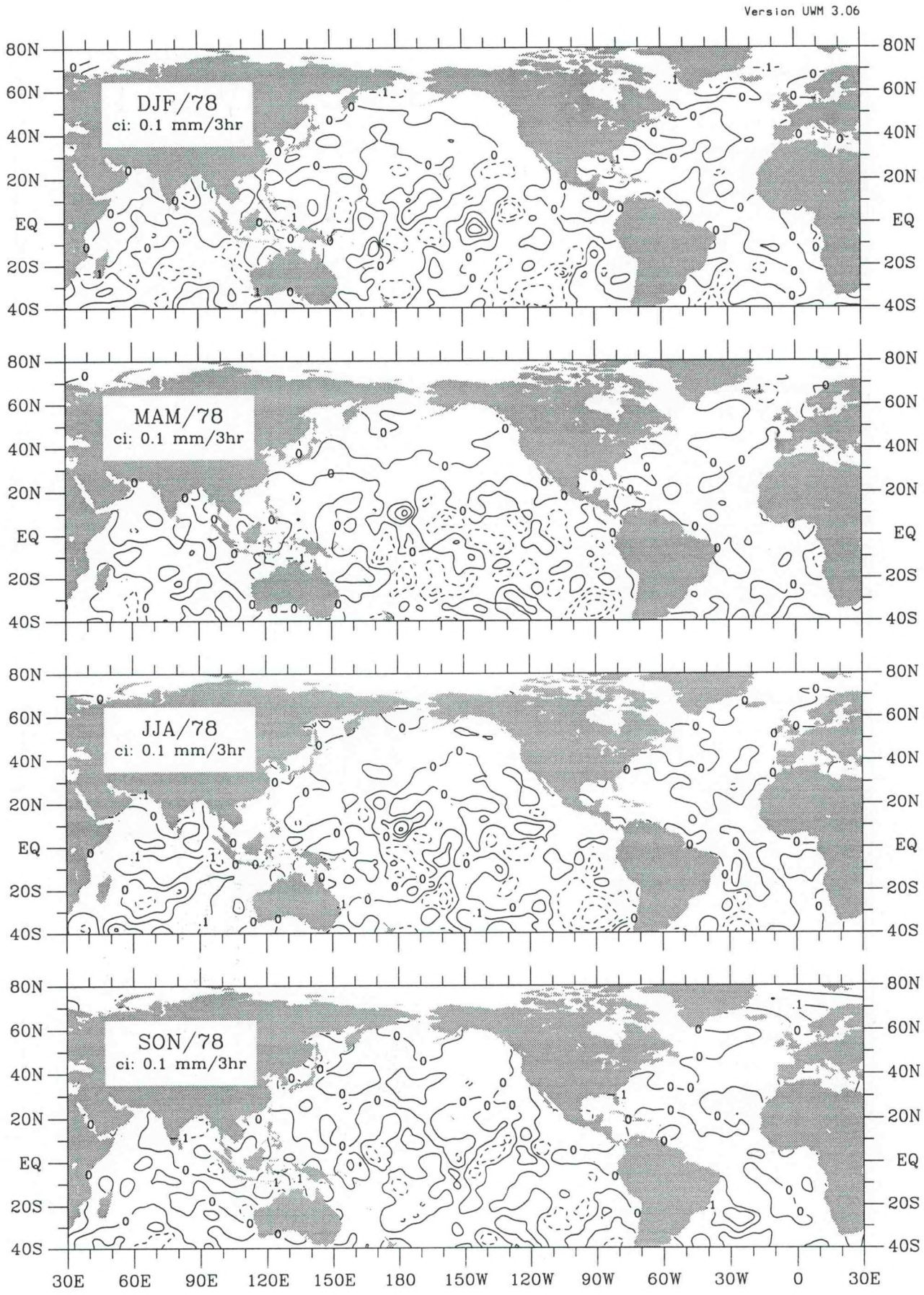

Figure E-39. Evaporation seasonal anomaly for 1978.

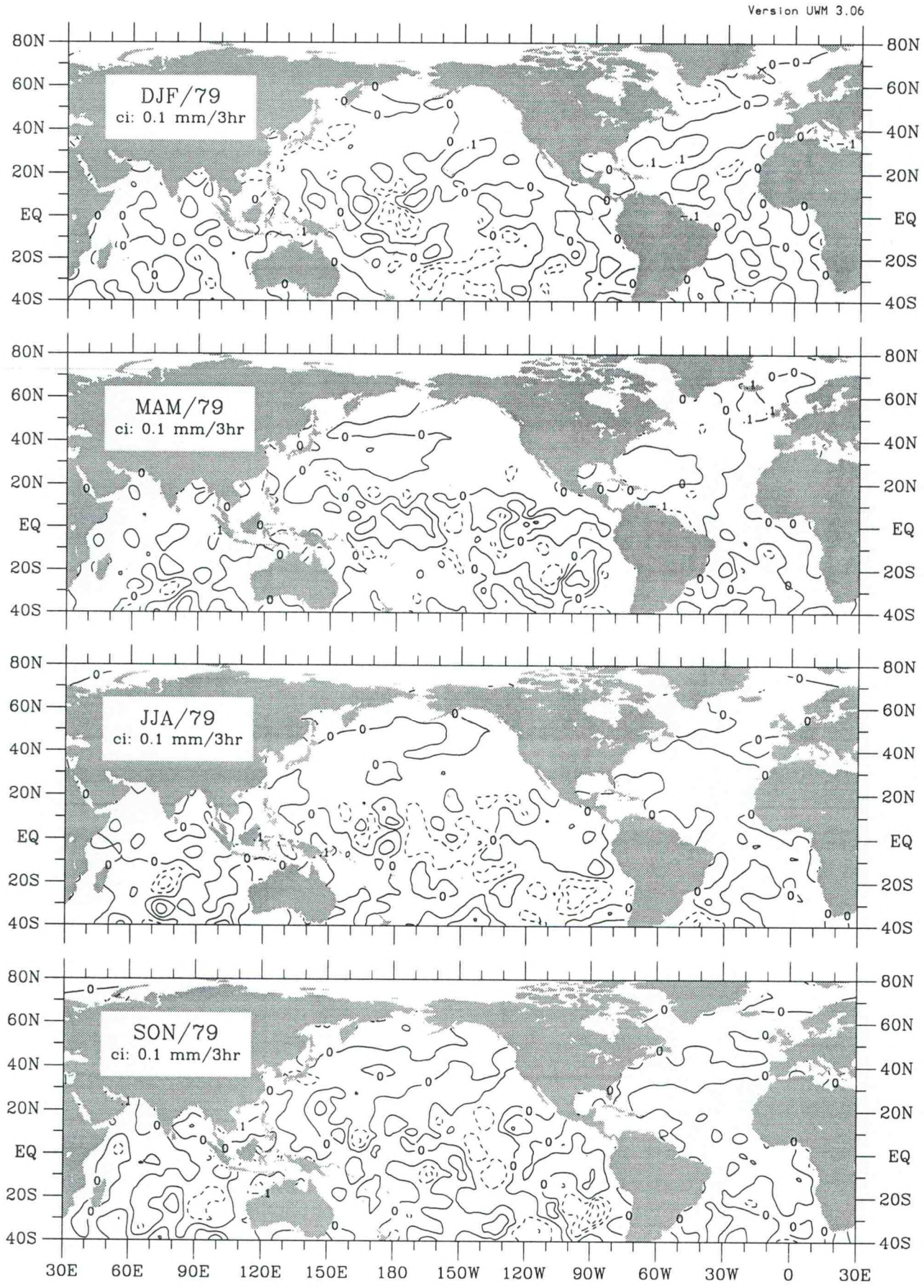

Figure E-40. Evaporation seasonal anomaly for 1979.

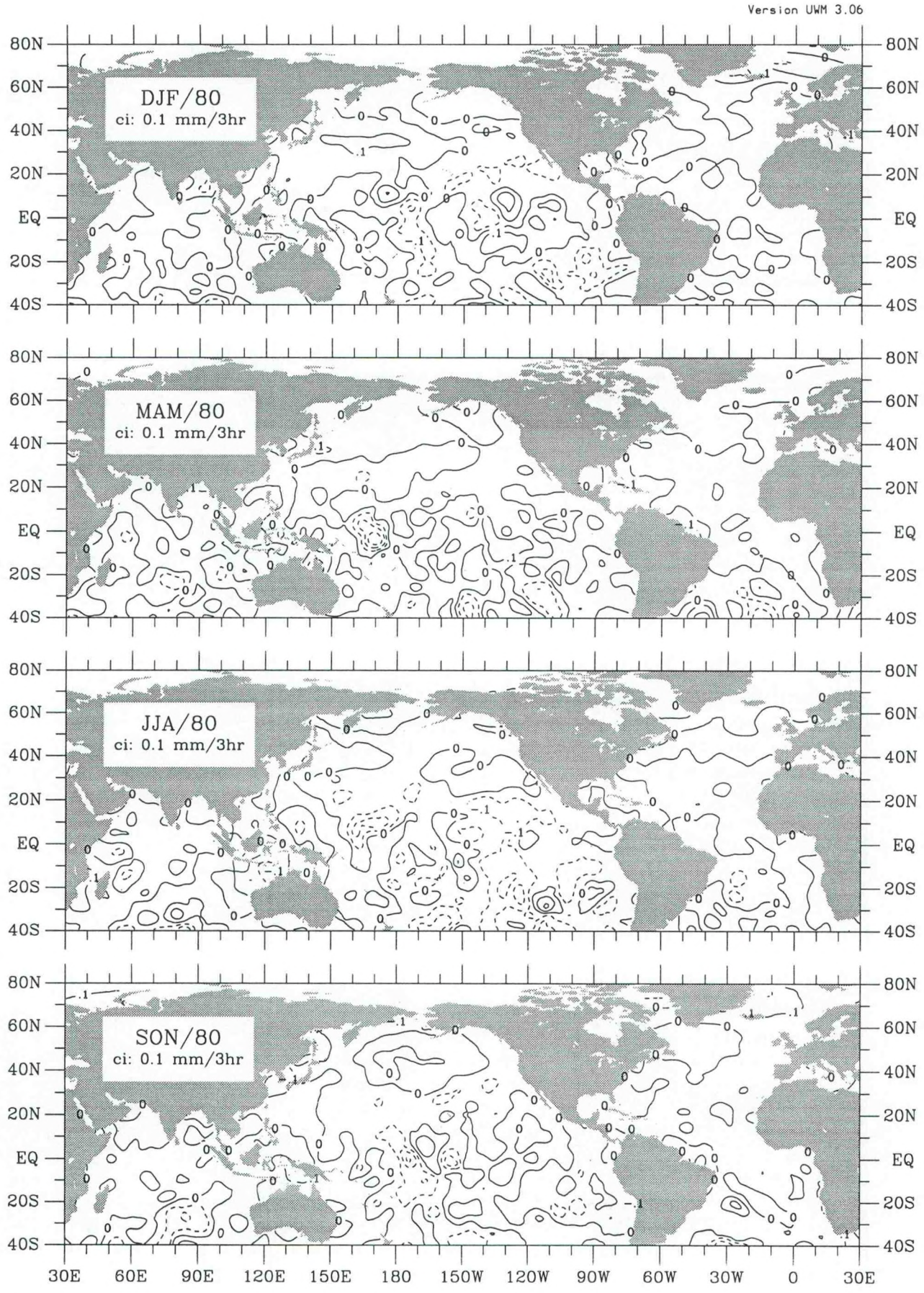

Figure E-41. Evaporation seasonal anomaly for 1980.

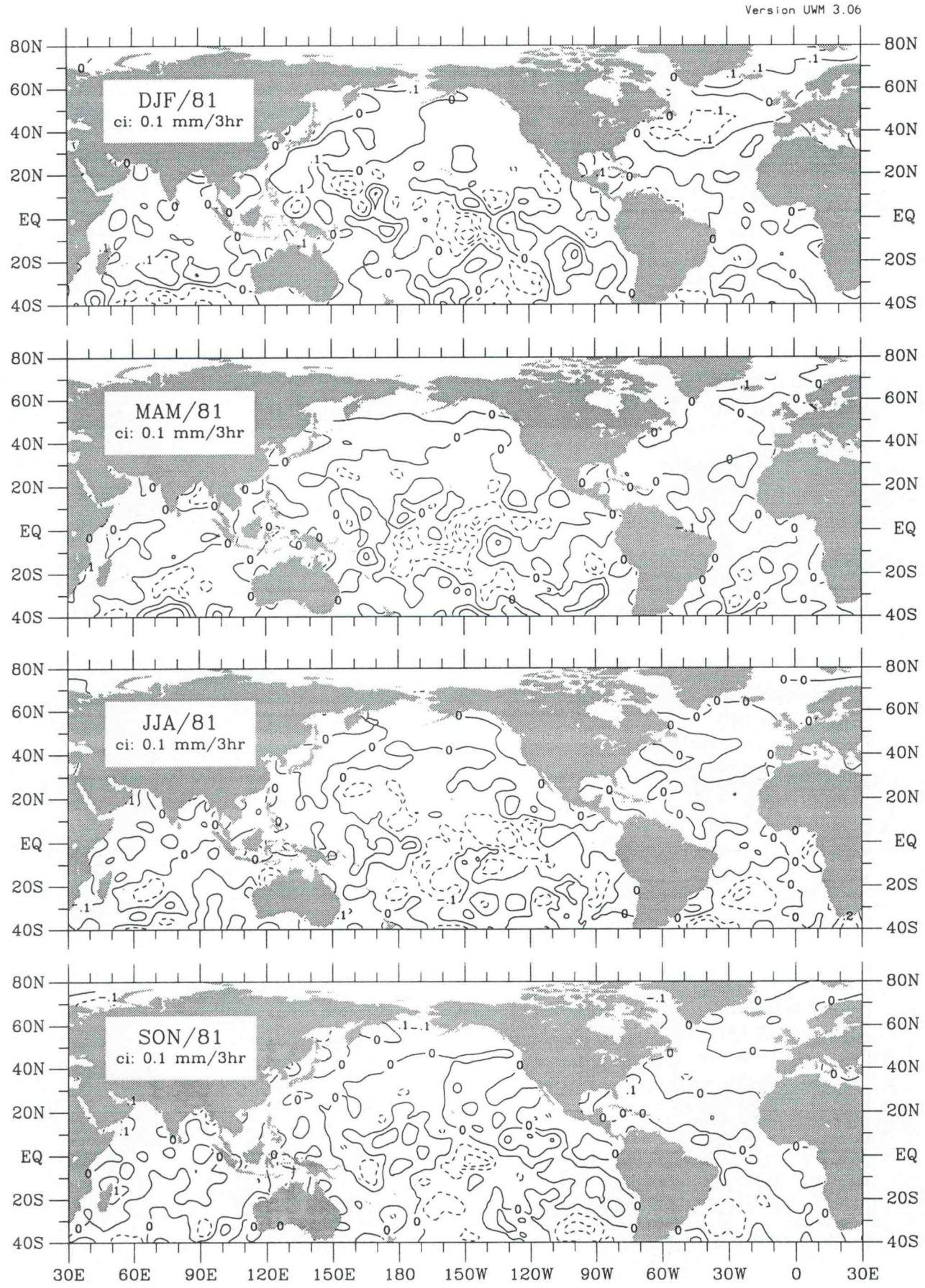

Figure E-42. Evaporation seasonal anomaly for 1981.

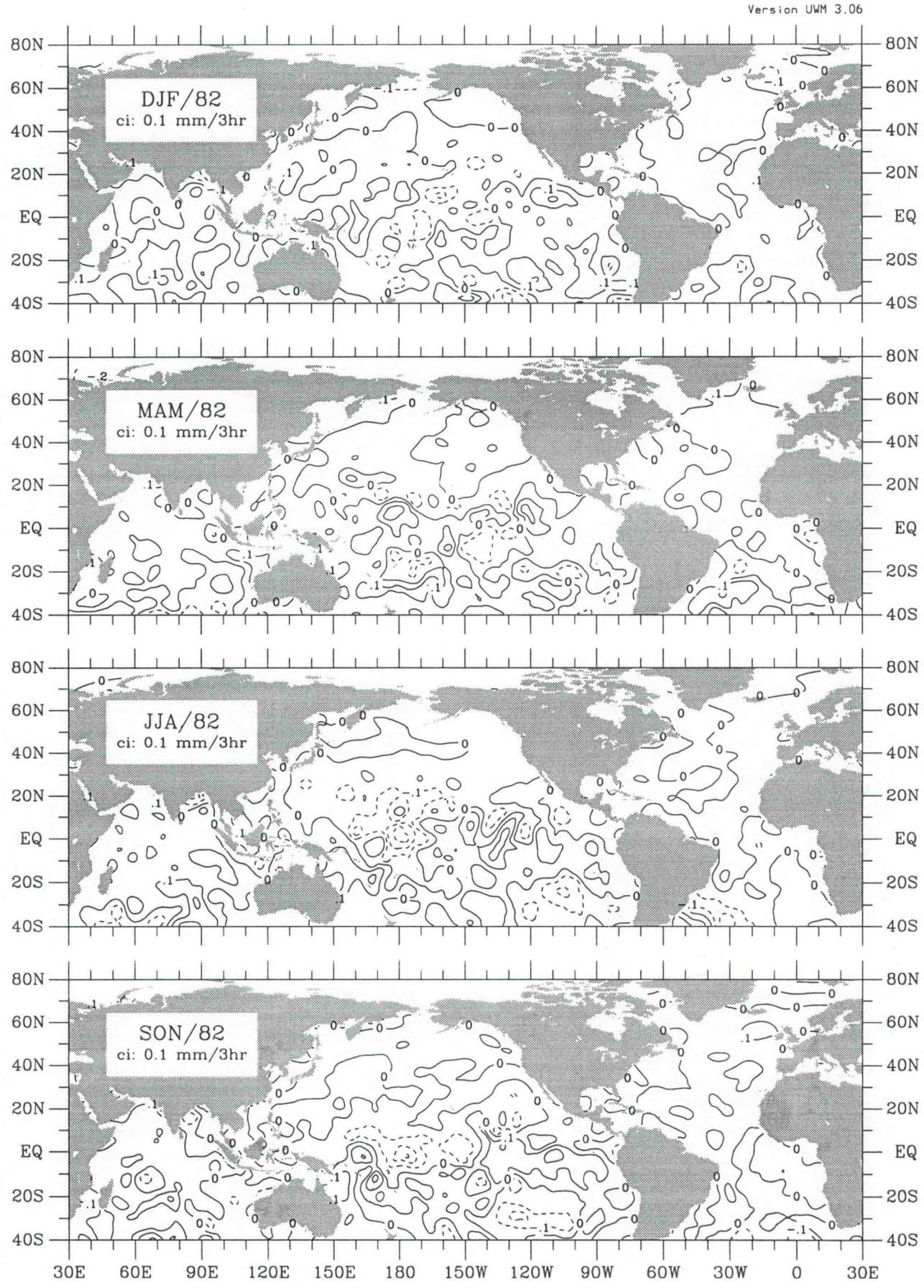

Figure E-43. Evaporation seasonal anomaly for 1982.

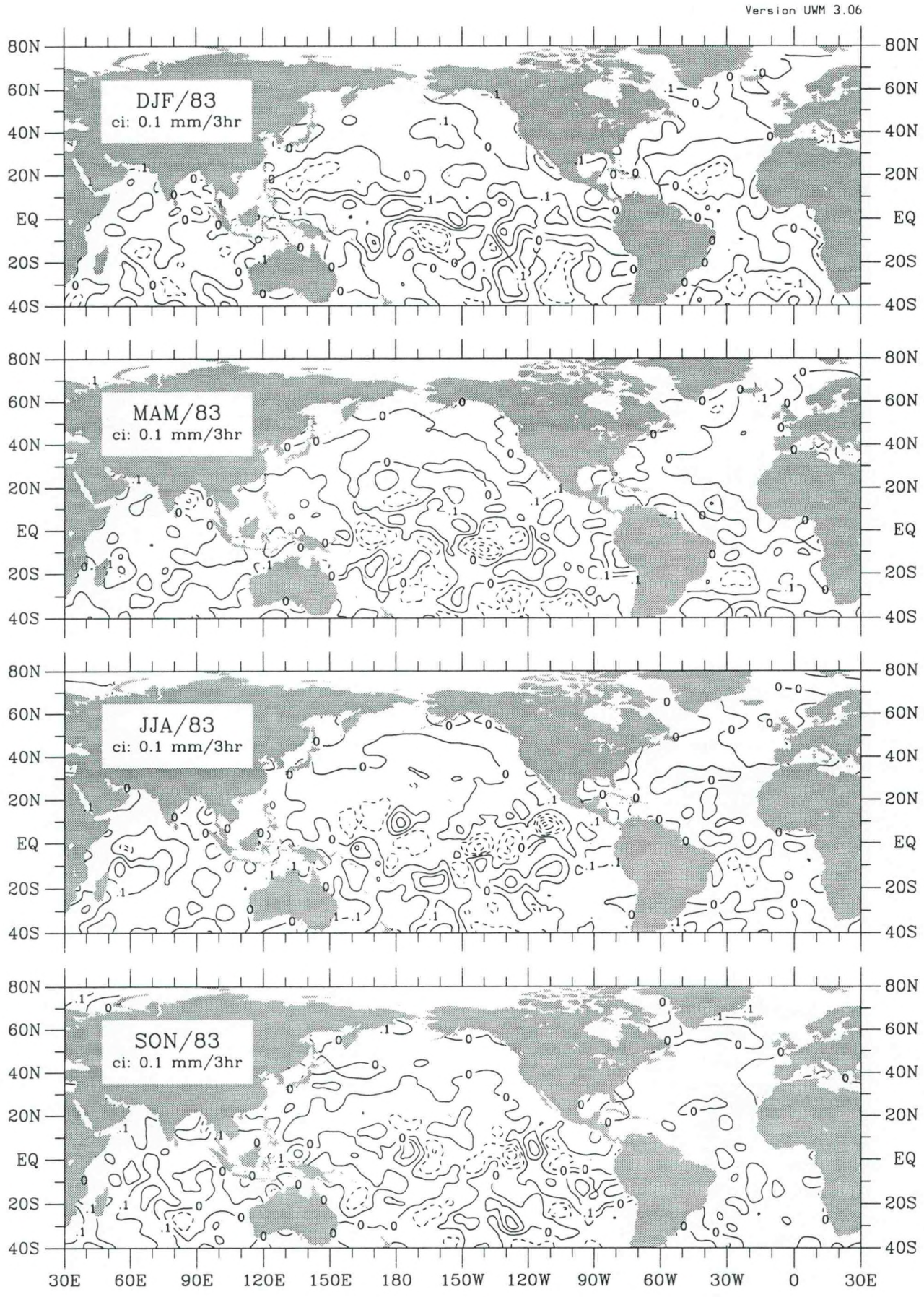

Figure E-44. Evaporation seasonal anomaly for 1983.

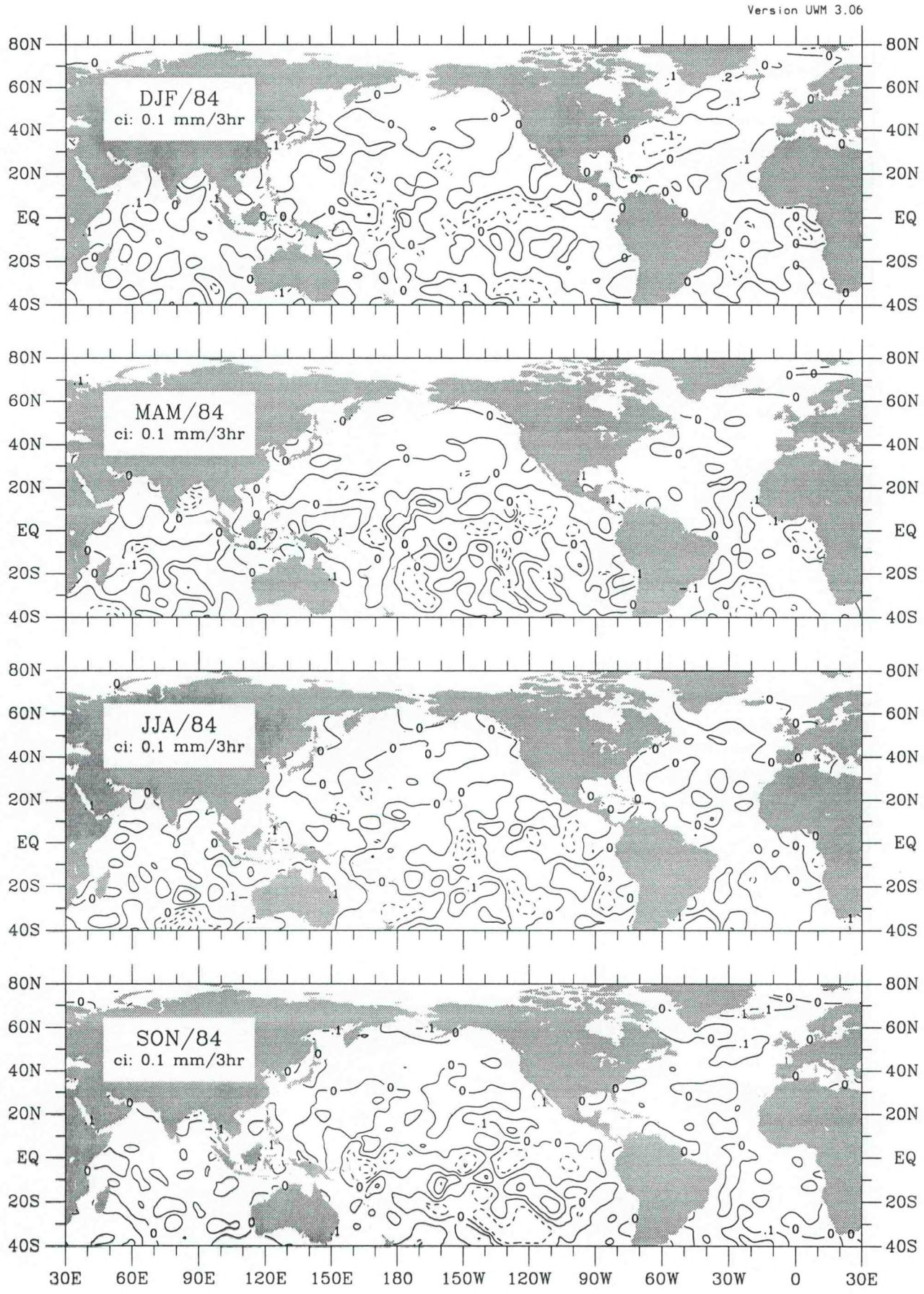

Figure E-45. Evaporation seasonal anomaly for 1984.

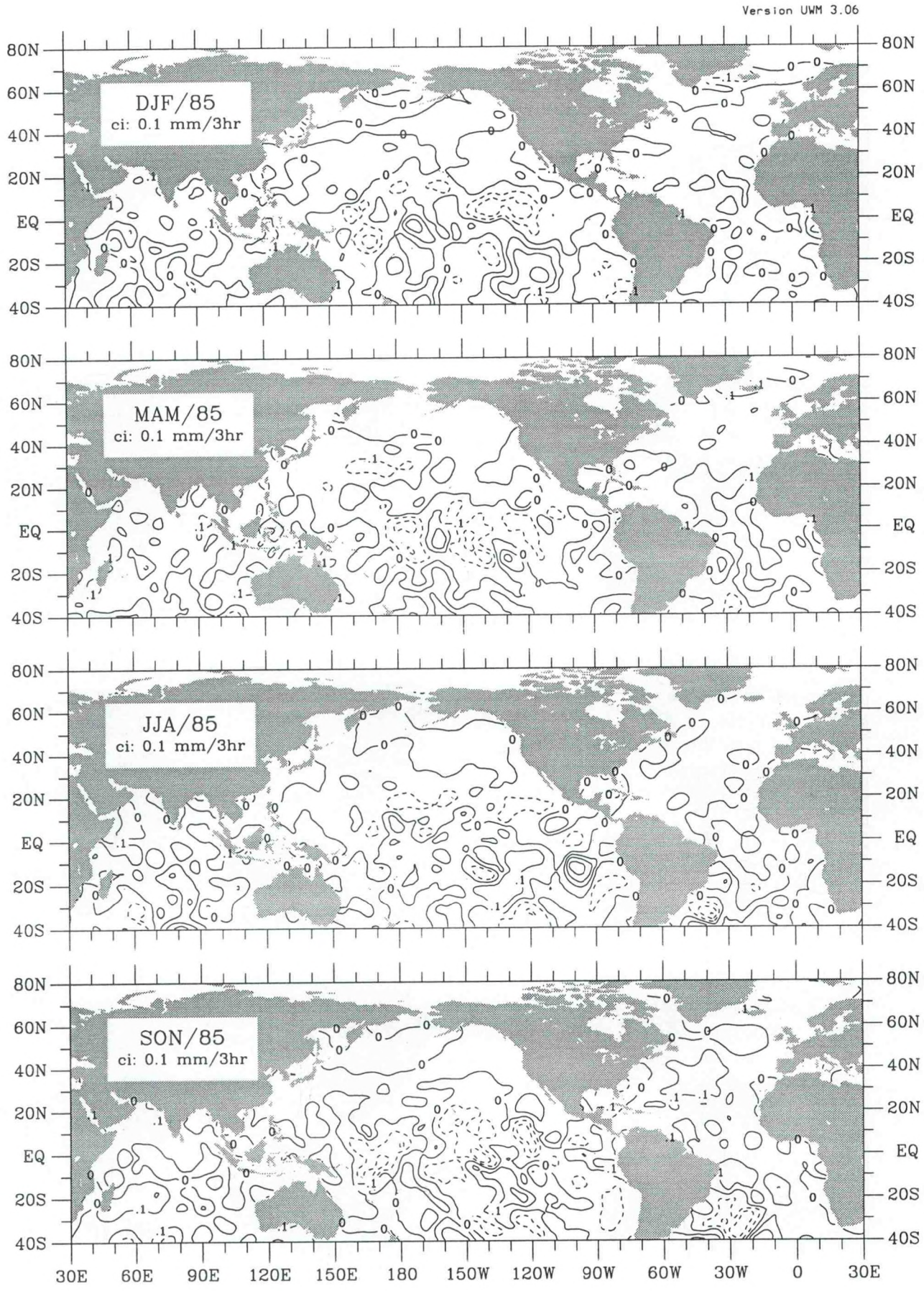

Figure E-46. Evaporation seasonal anomaly for 1985.

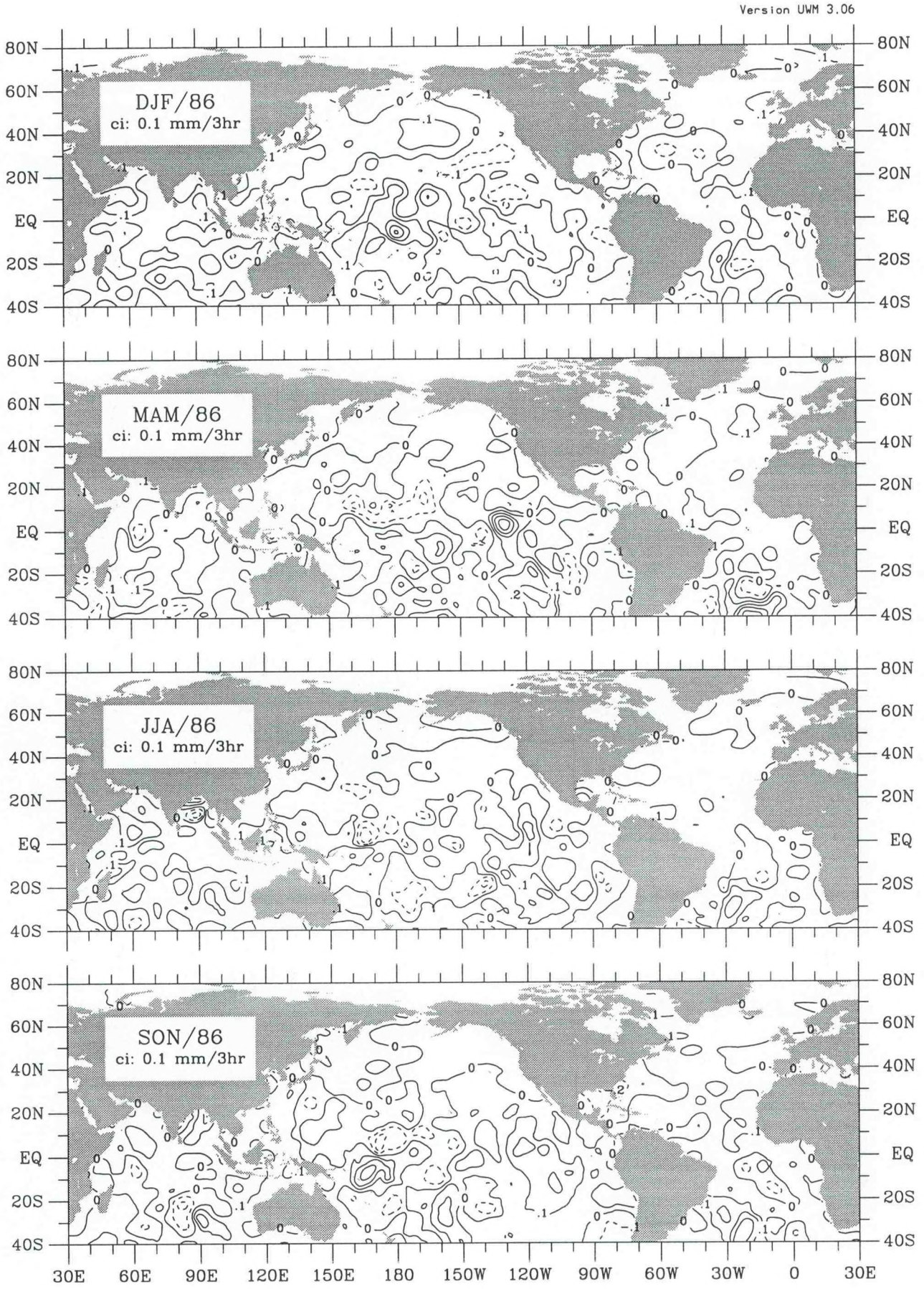

Figure E-47. Evaporation seasonal anomaly for 1986.

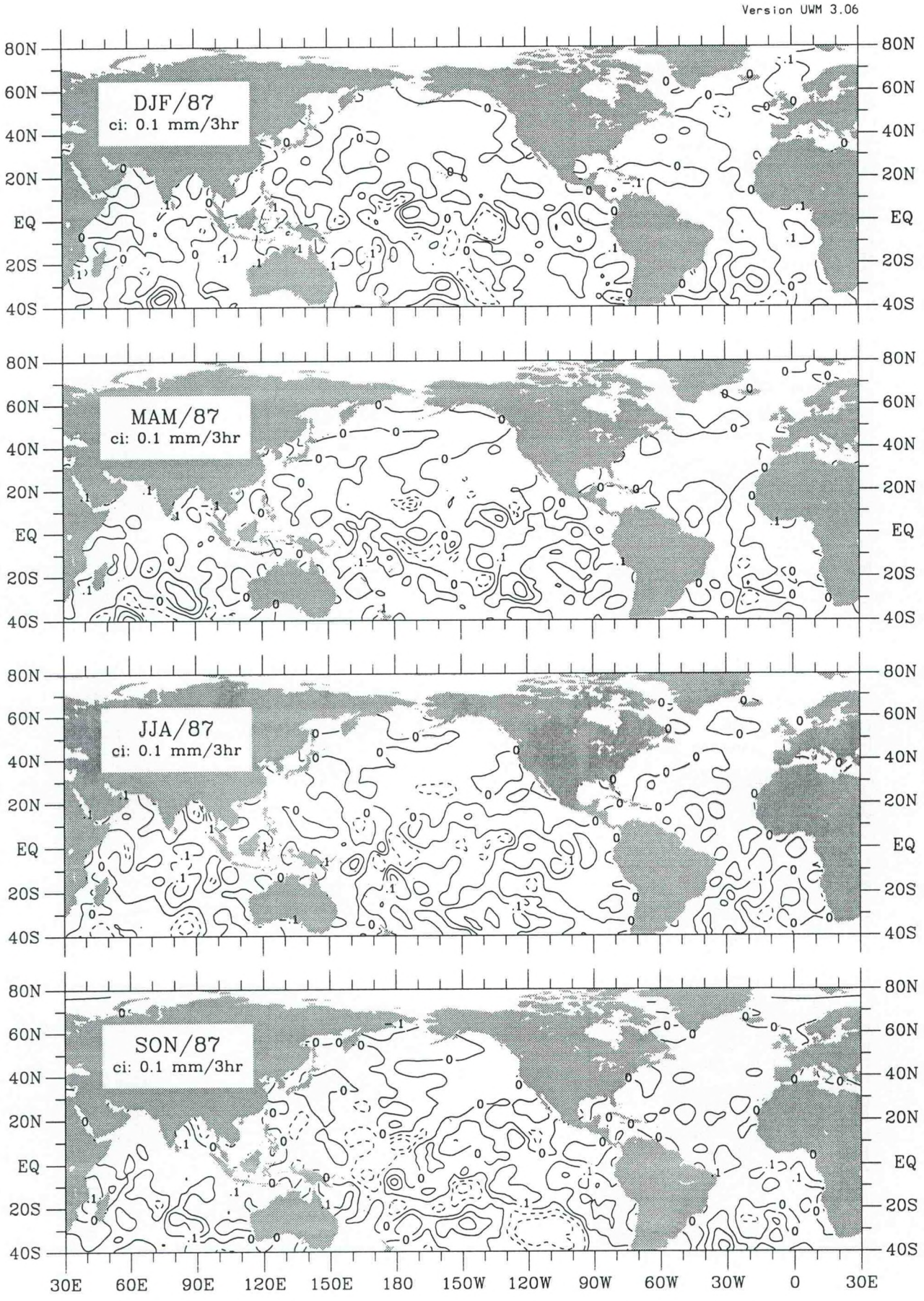

Figure E-48. Evaporation seasonal anomaly for 1987.

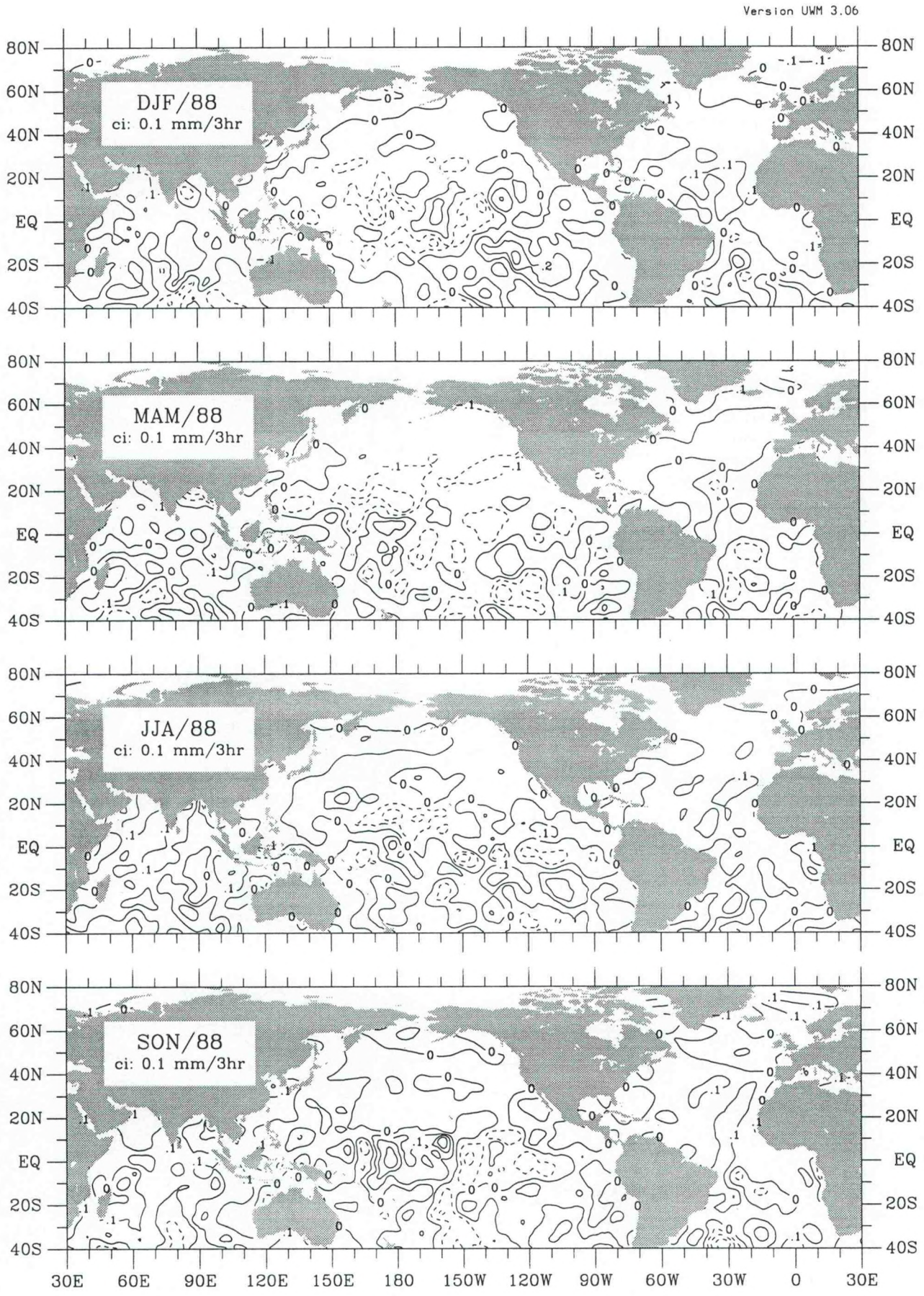

Figure E-49. Evaporation seasonal anomaly for 1988.

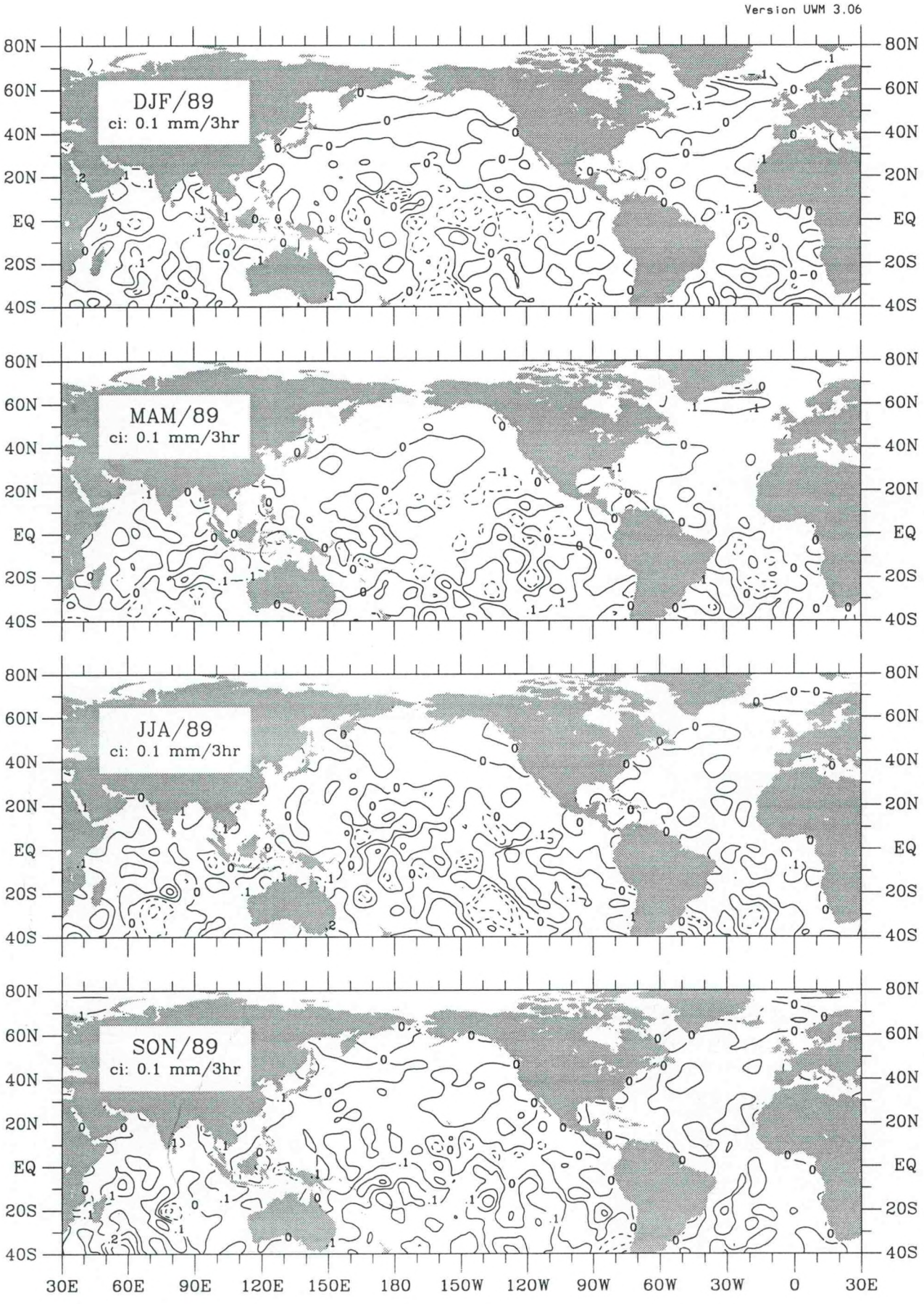

Figure E-50. Evaporation seasonal anomaly for 1989.

12 Precipitation rate

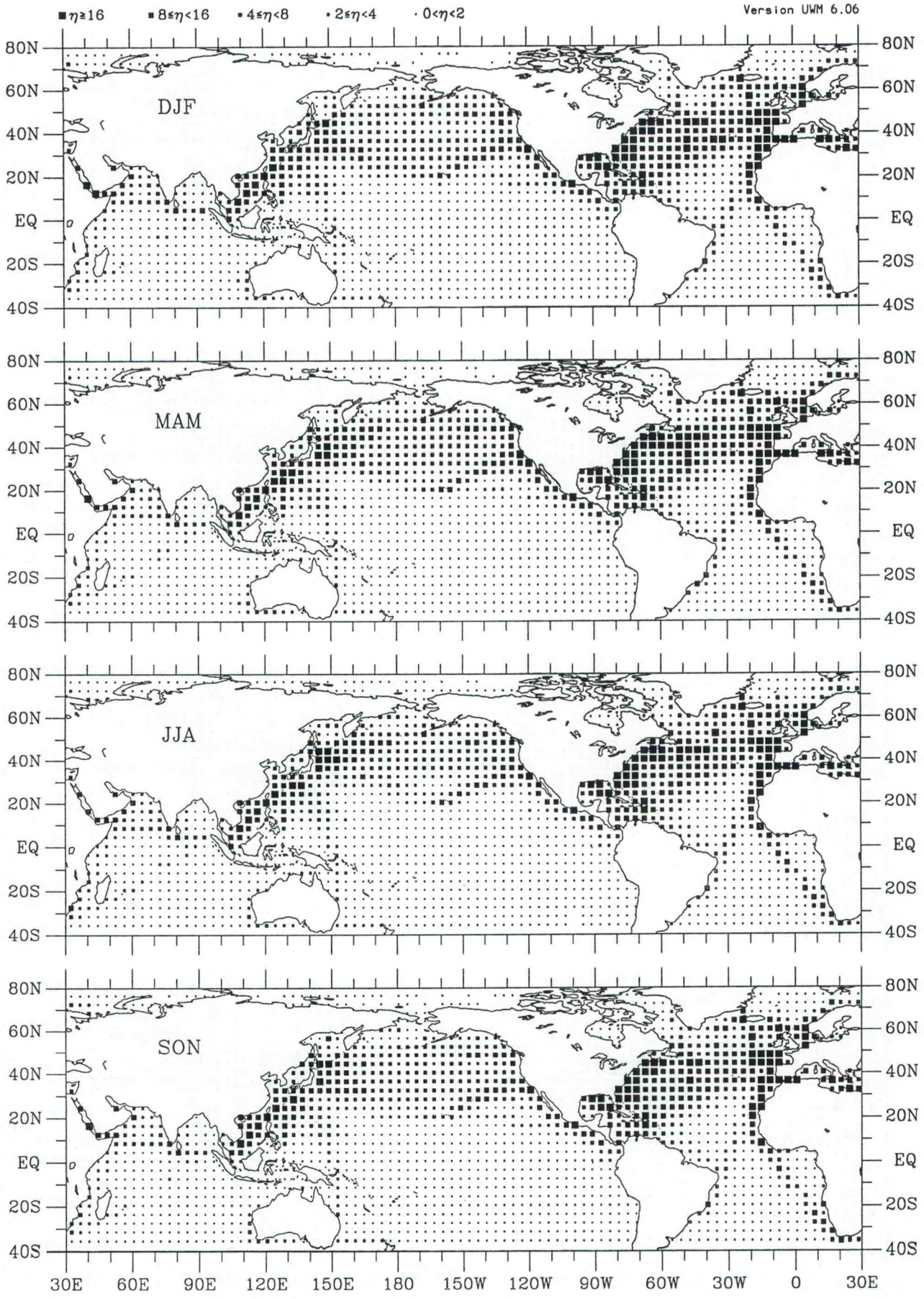

Figure P–1. Precipitation seasonal observation density (1945–89).

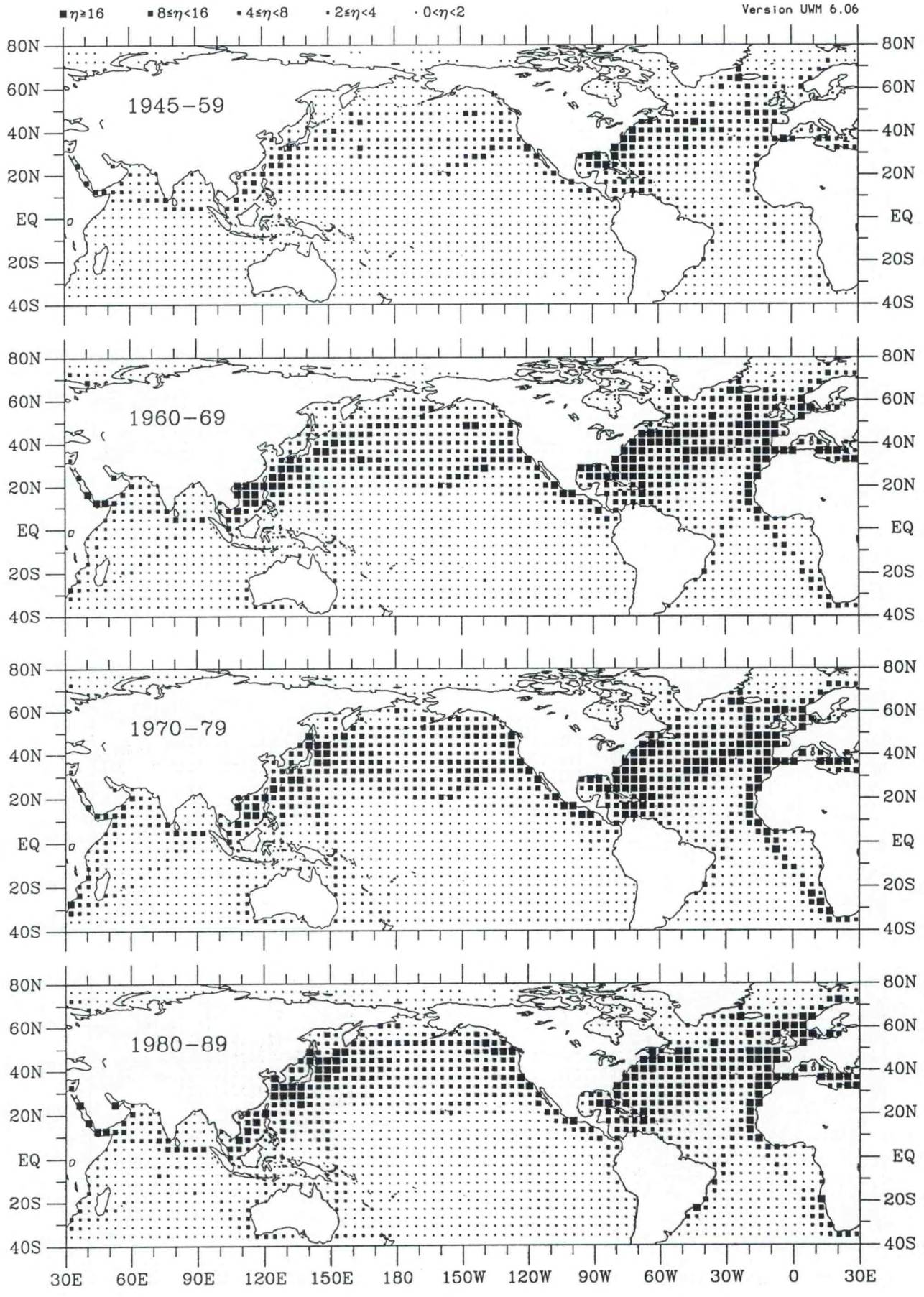

Figure P-2. Precipitation decadal observation density.

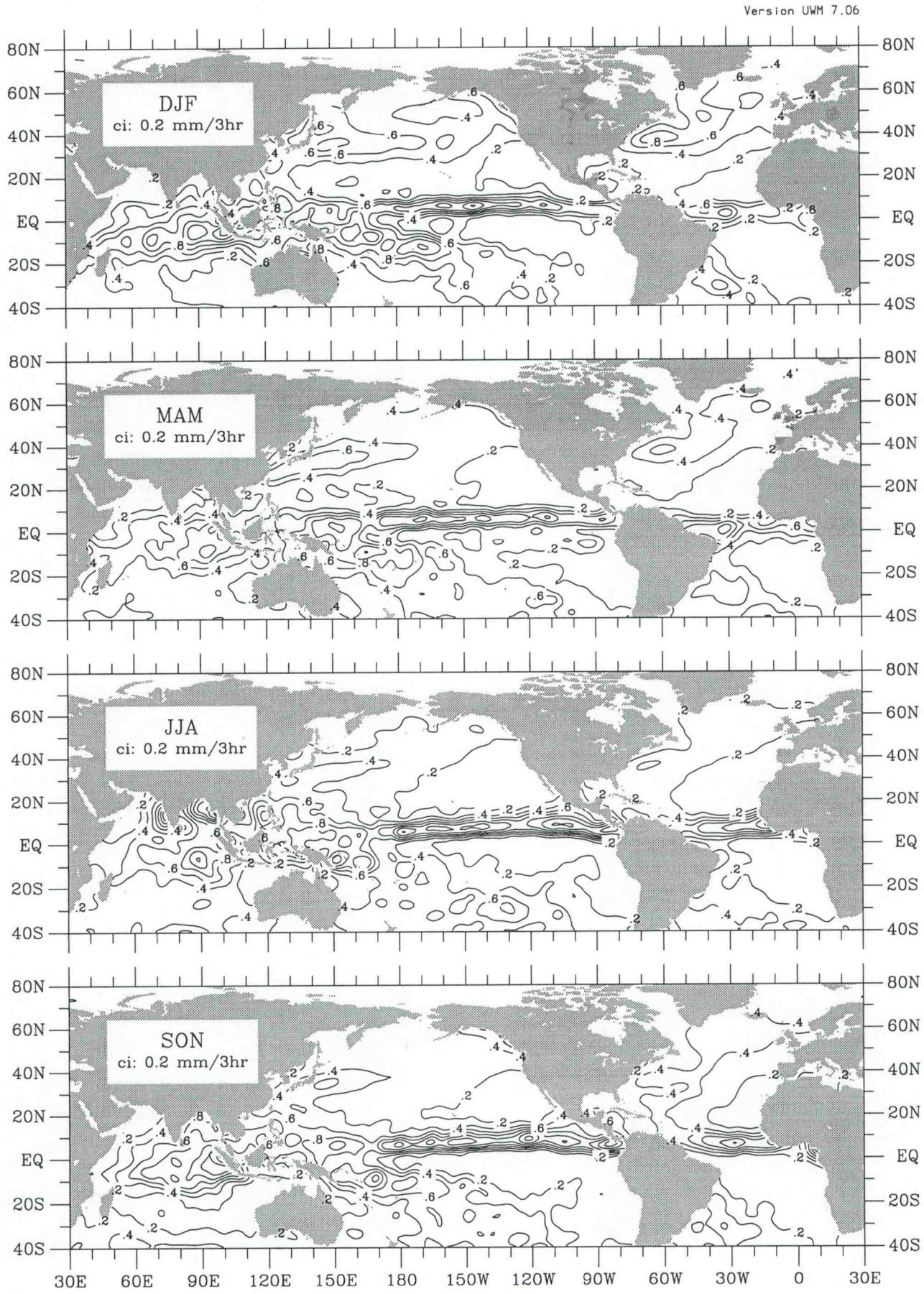

Figure P–3. Precipitation seasonal climatology (1945–89).

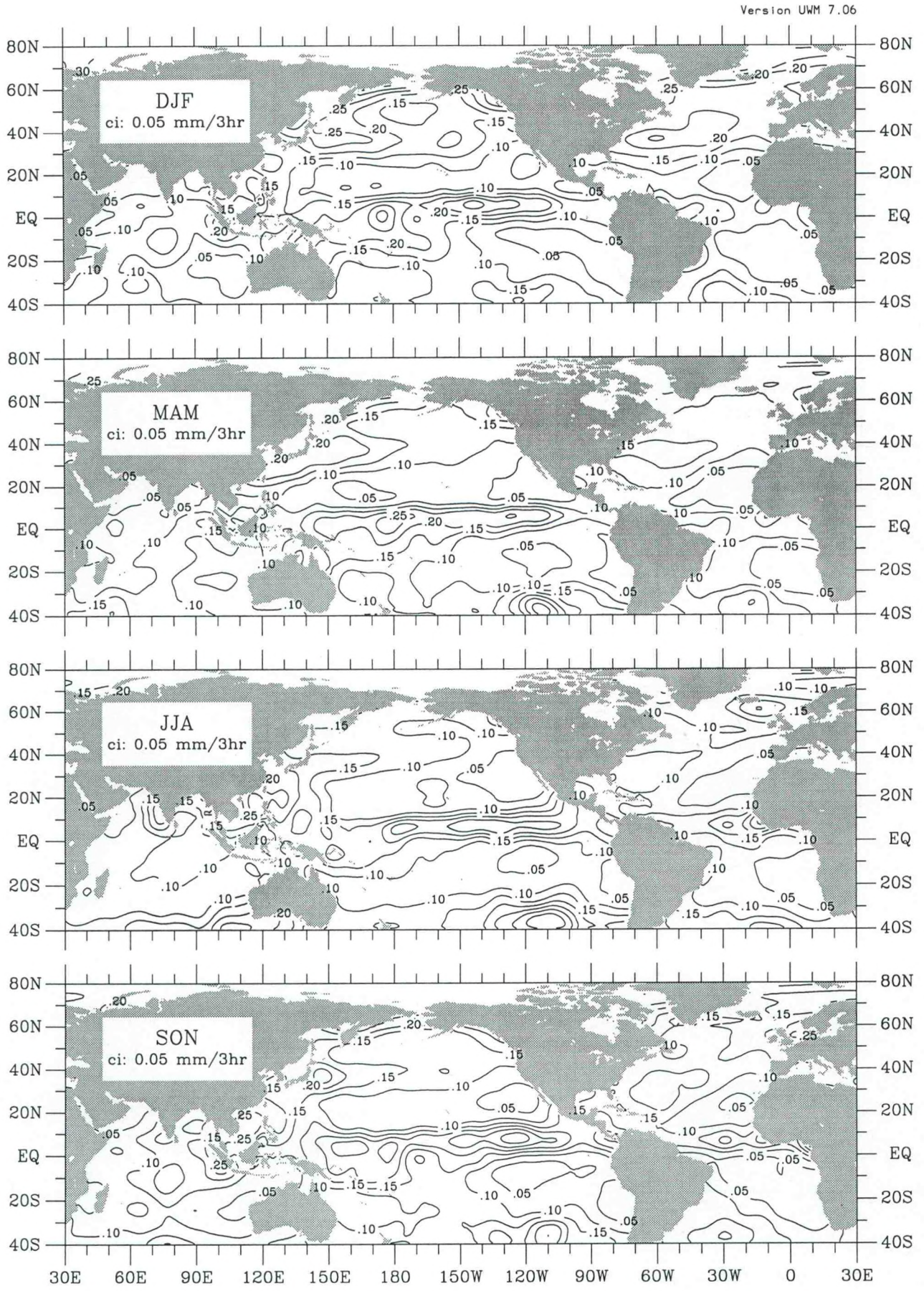

Figure P–4. Precipitation seasonal interannual std dev (1945–89).

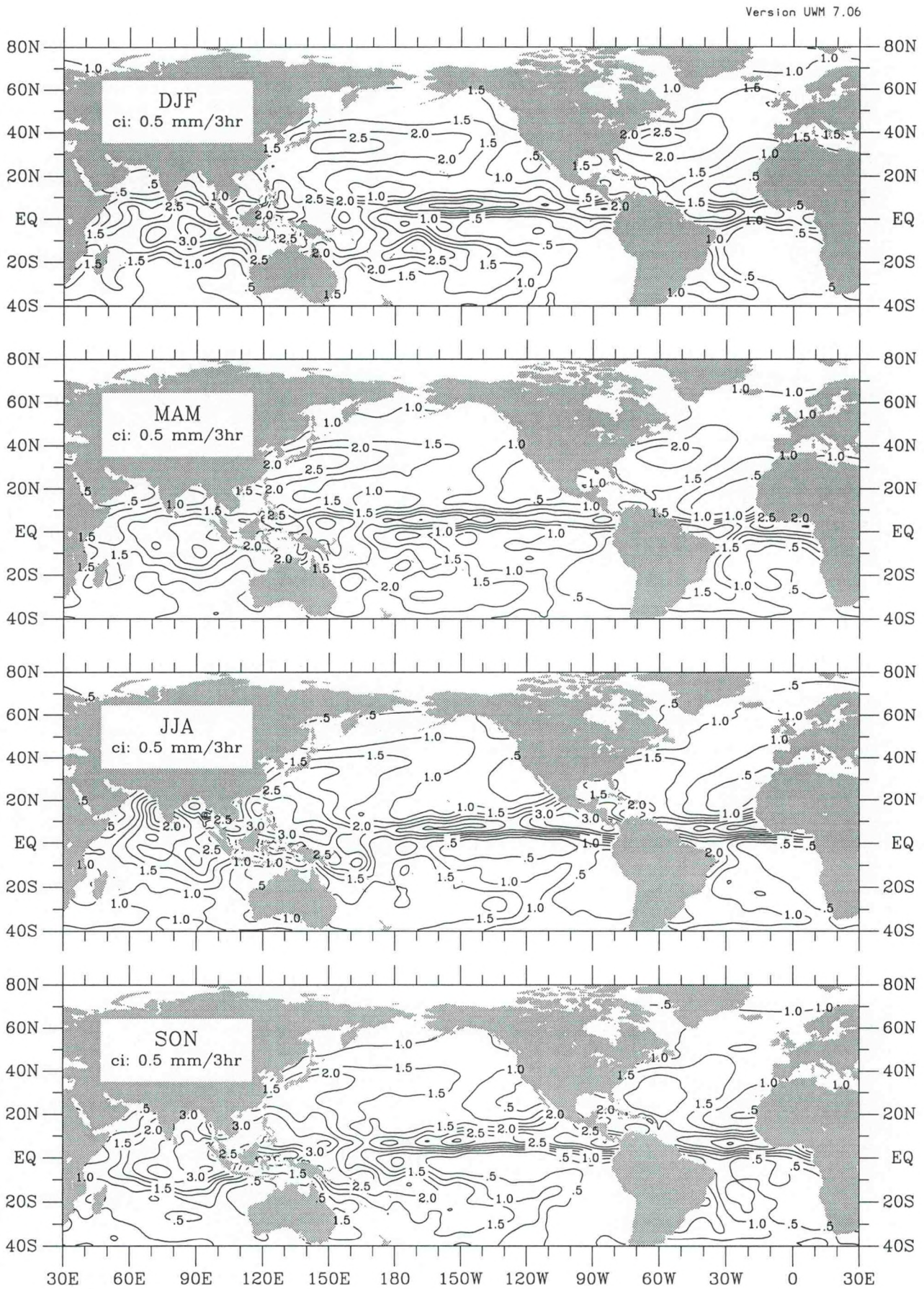

Figure P–5. Precipitation seasonal standard deviation (1945–89).

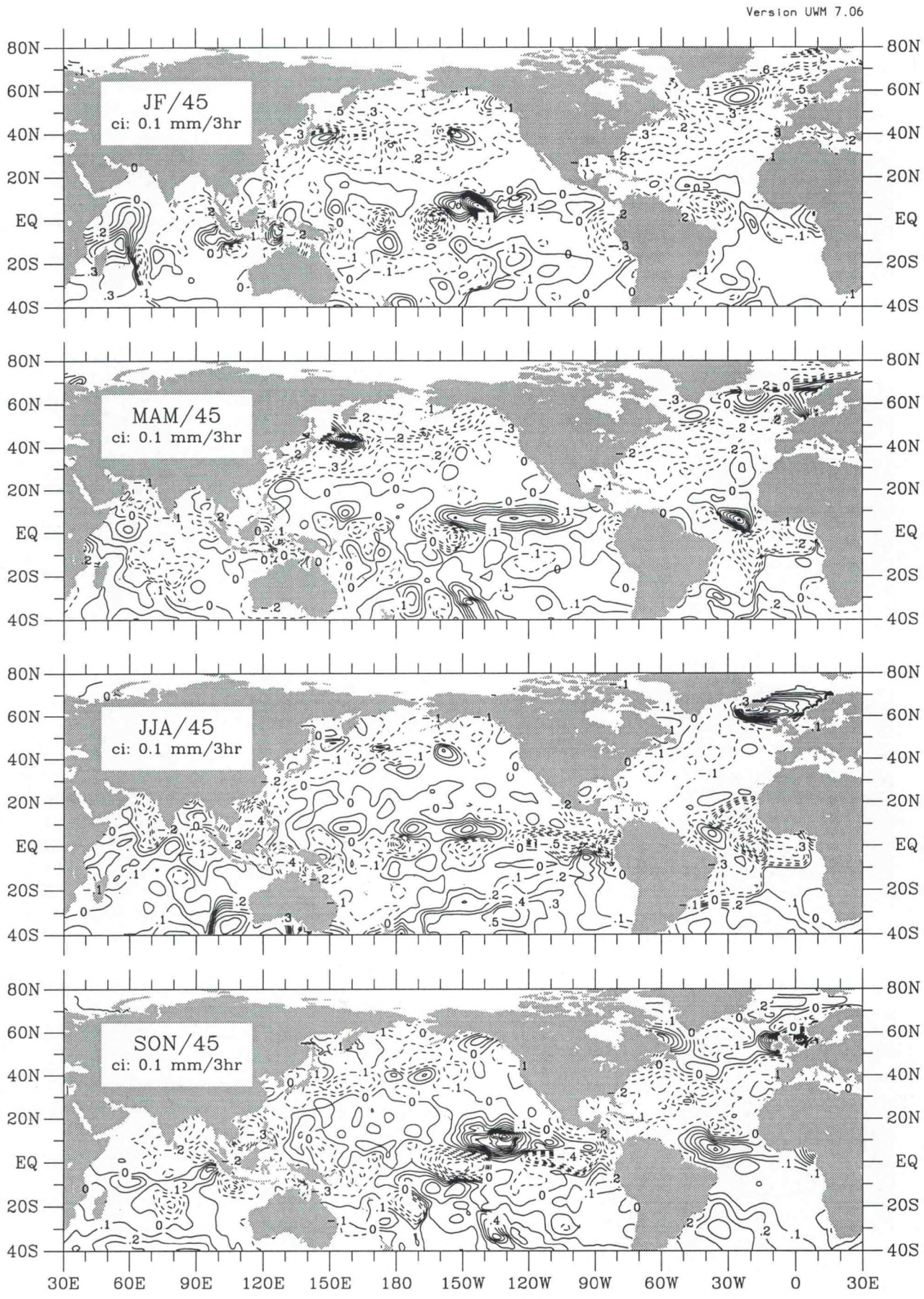

Figure P–6. Precipitation seasonal anomaly for 1945.

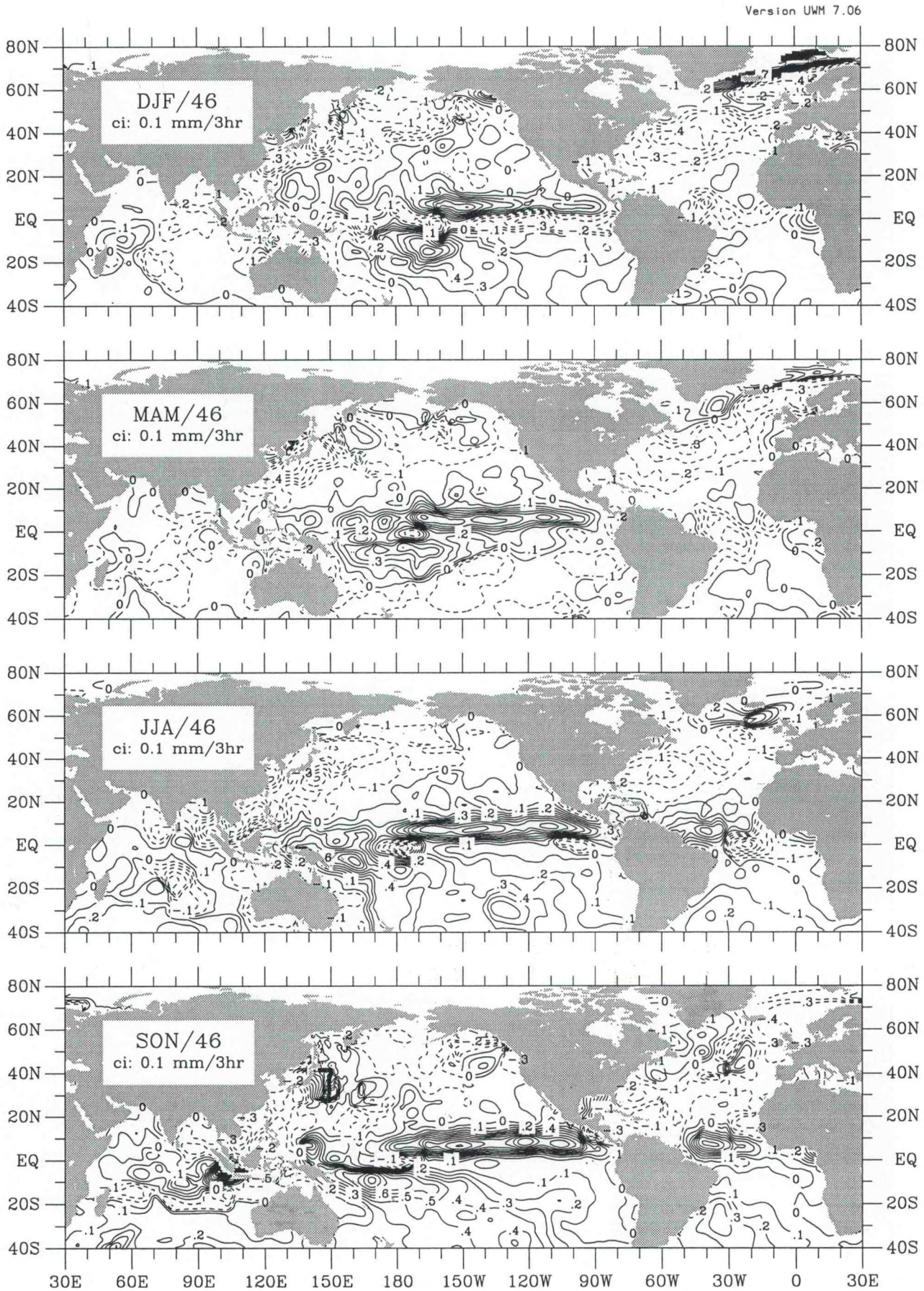

Figure P–7. Precipitation seasonal anomaly for 1946.

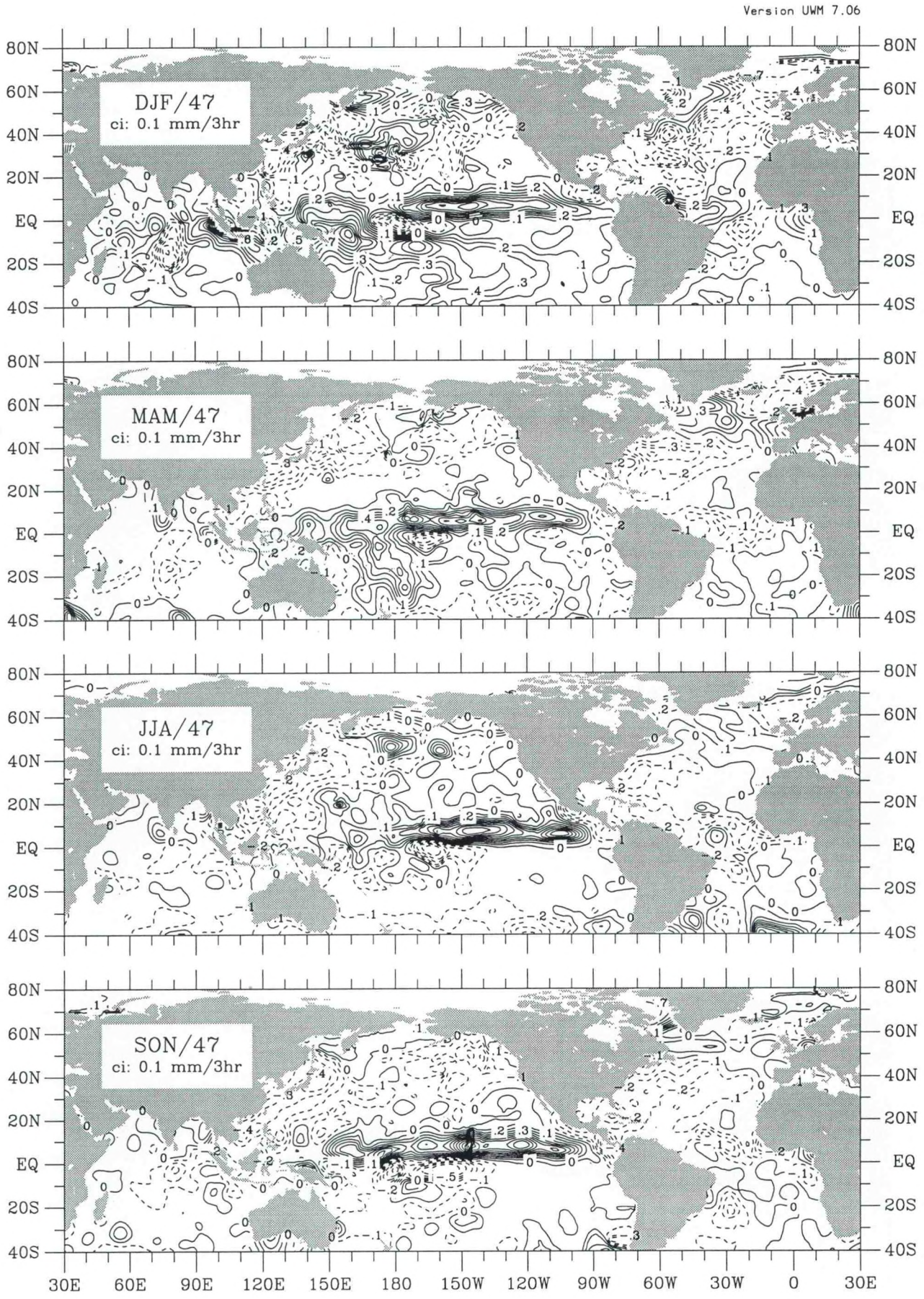

Figure P-8. Precipitation seasonal anomaly for 1947.

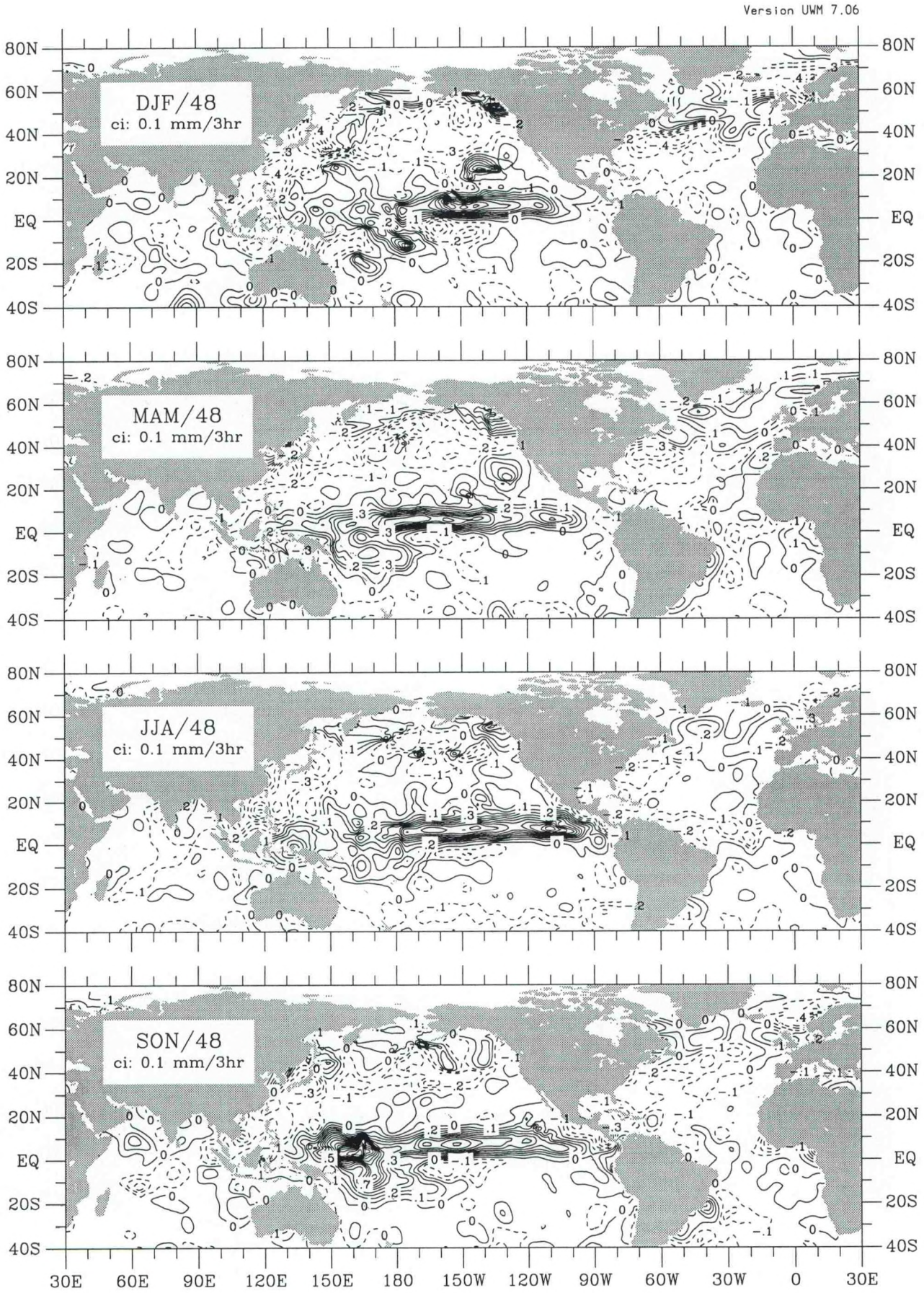

Figure P-9. Precipitation seasonal anomaly for 1948.

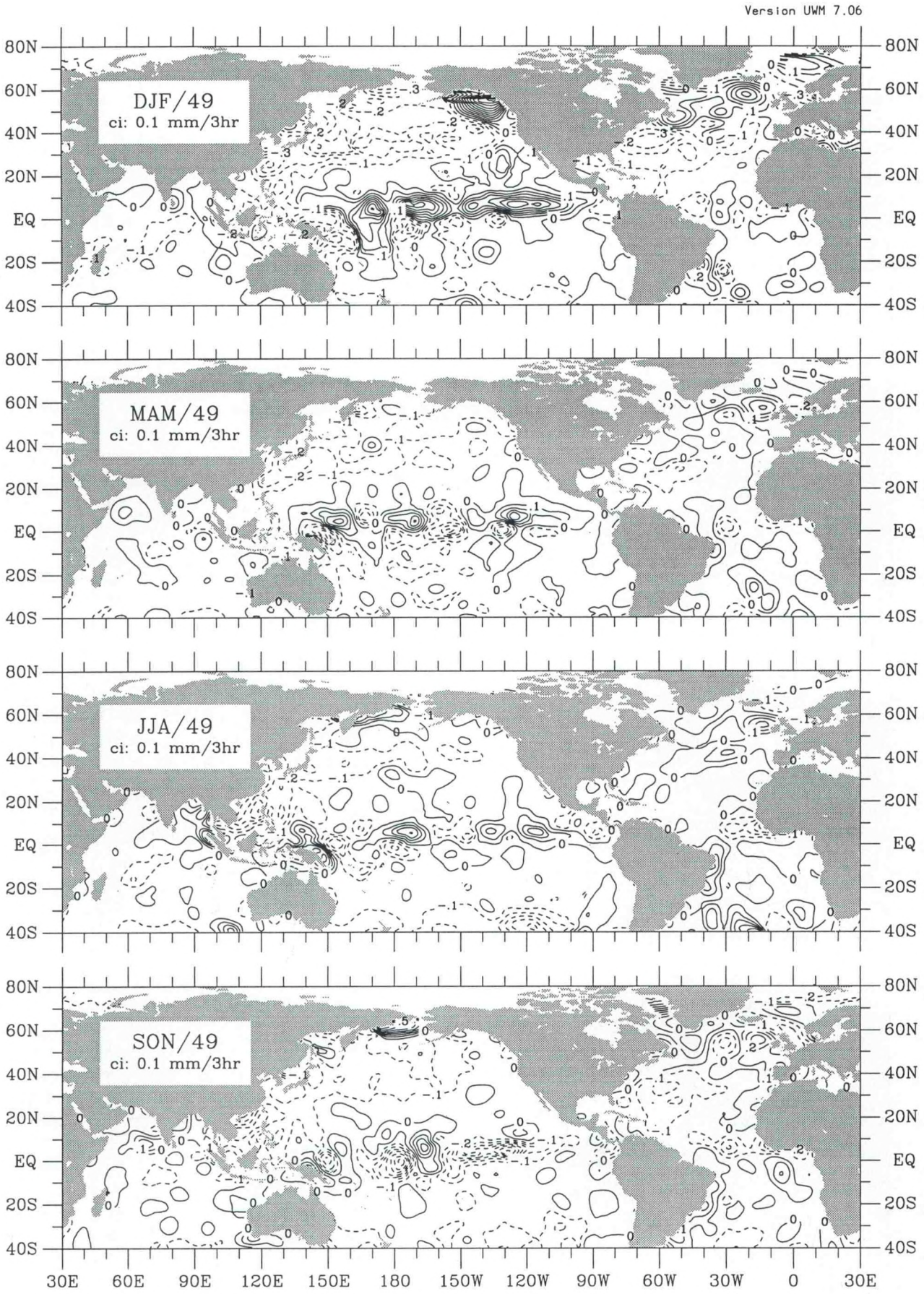

Figure P-10. Precipitation seasonal anomaly for 1949.

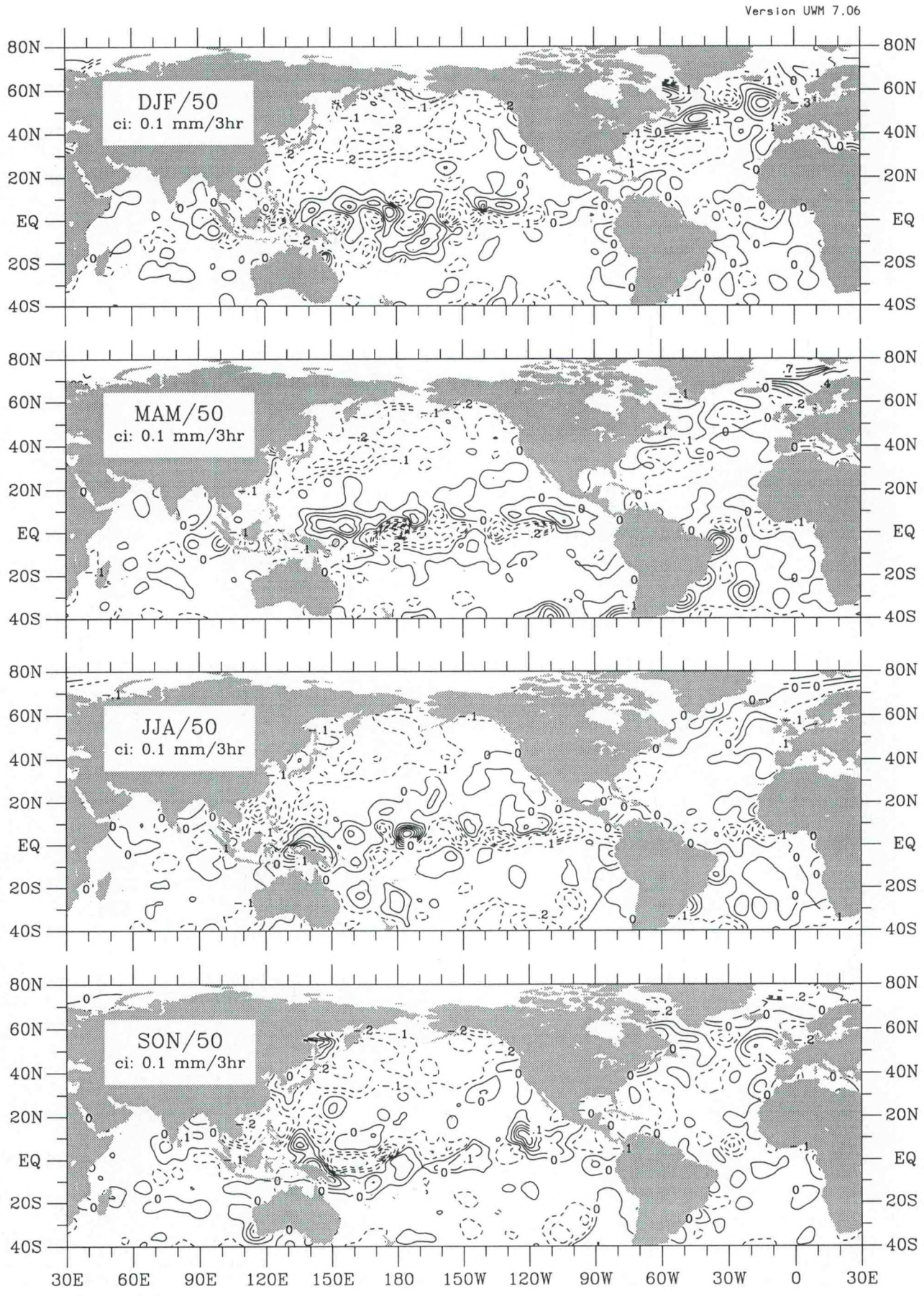

Figure P-11. Precipitation seasonal anomaly for 1950.

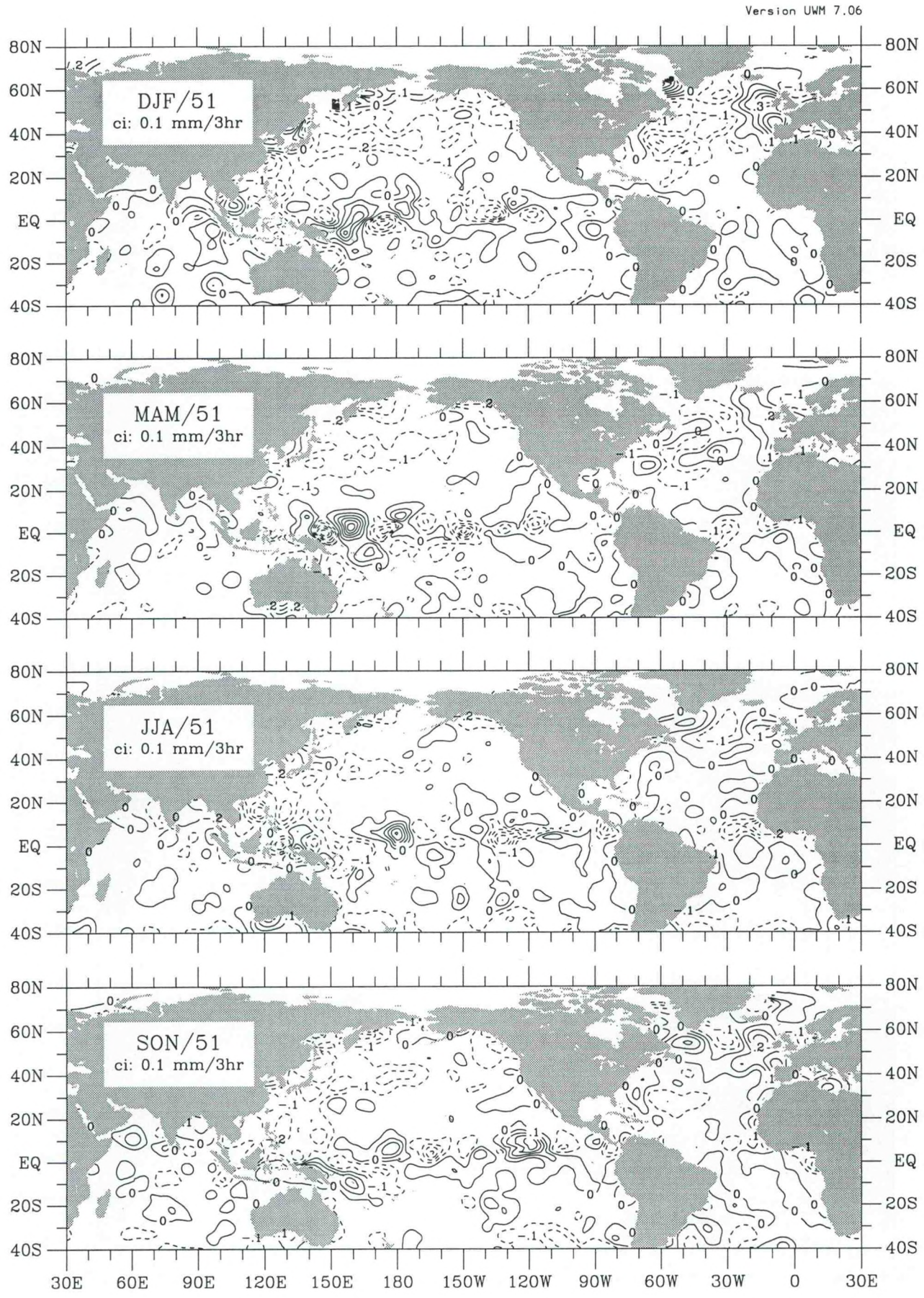

Figure P-12. Precipitation seasonal anomaly for 1951.

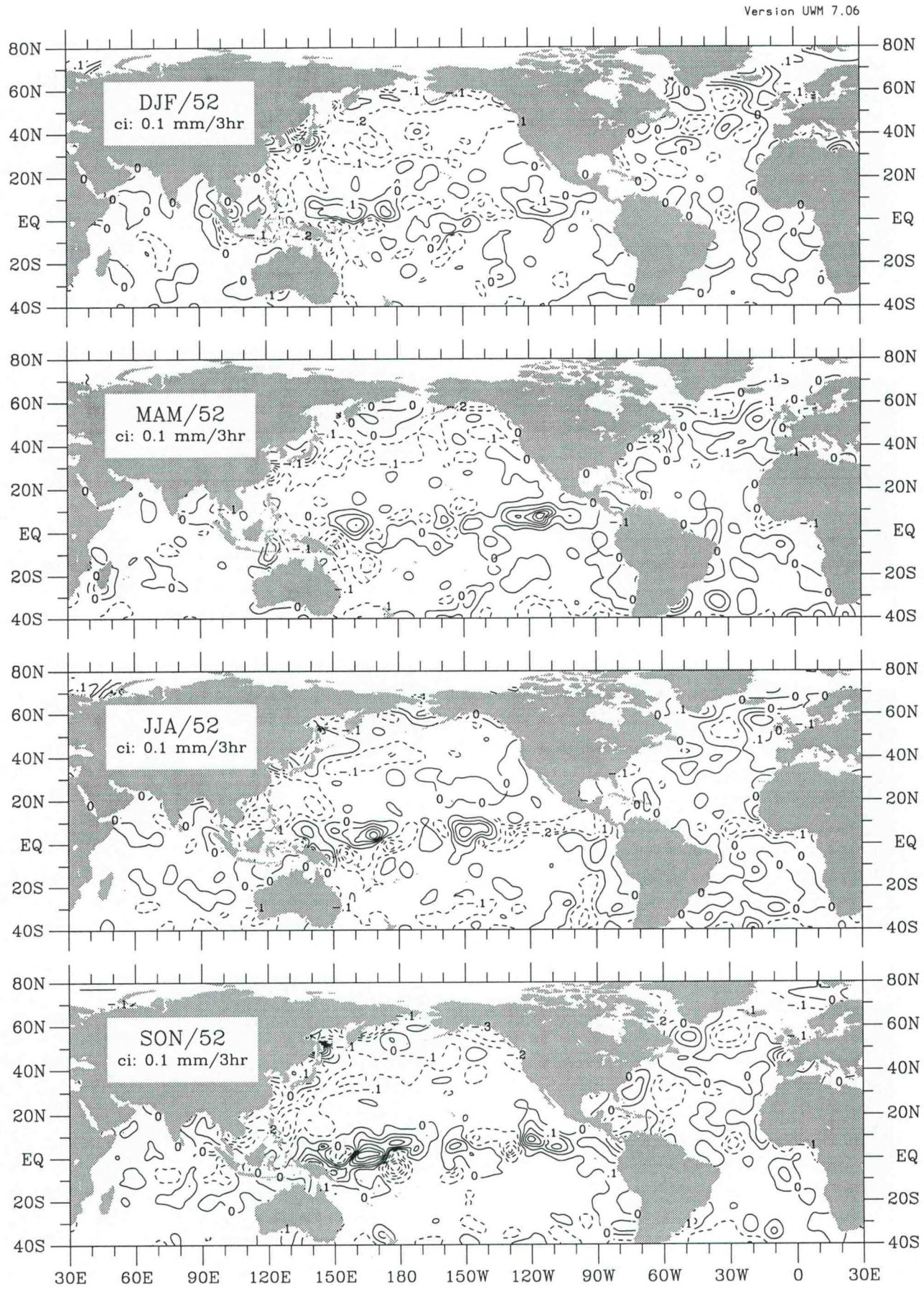

Figure P-13. Precipitation seasonal anomaly for 1952.

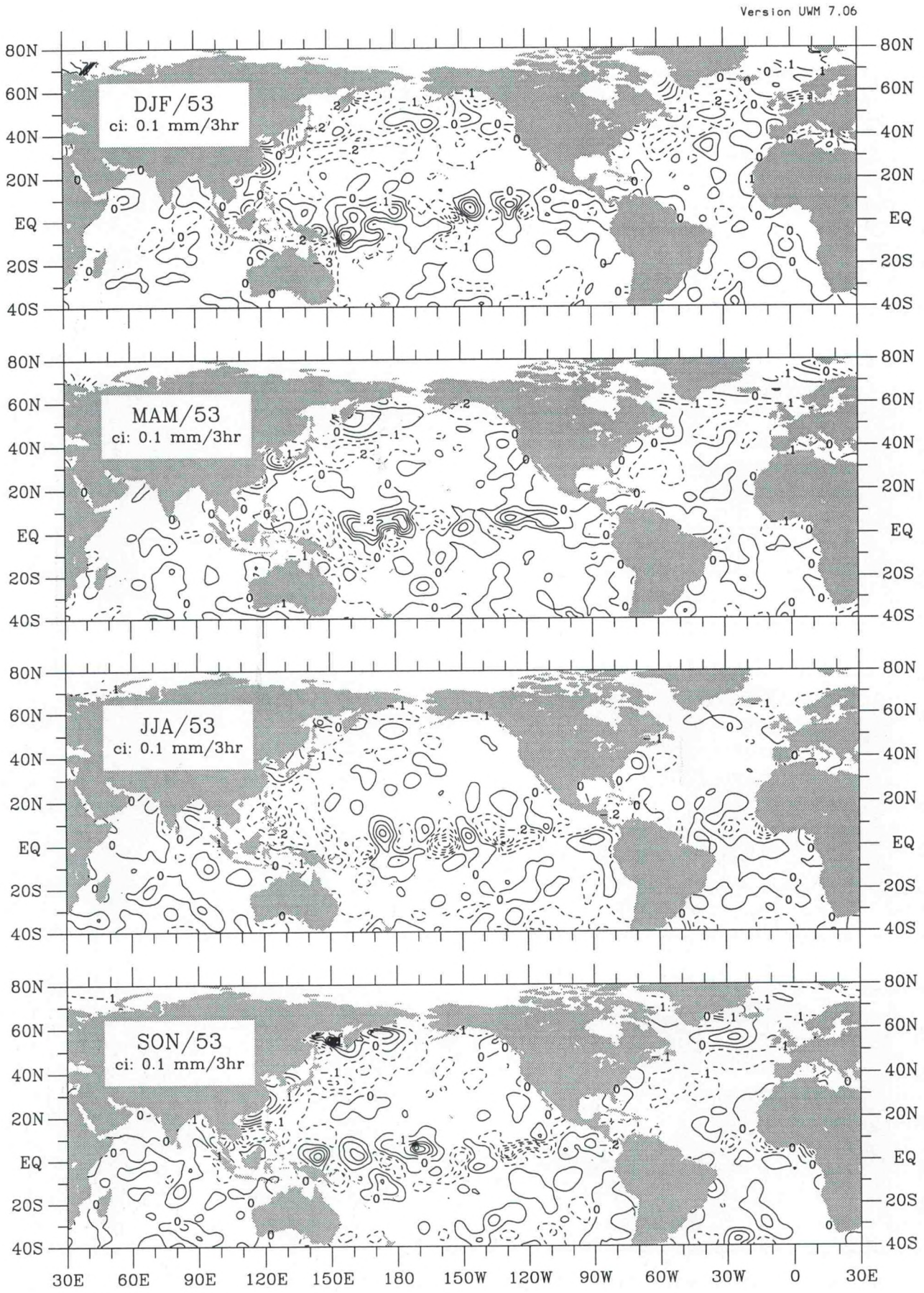

Figure P-14. Precipitation seasonal anomaly for 1953.

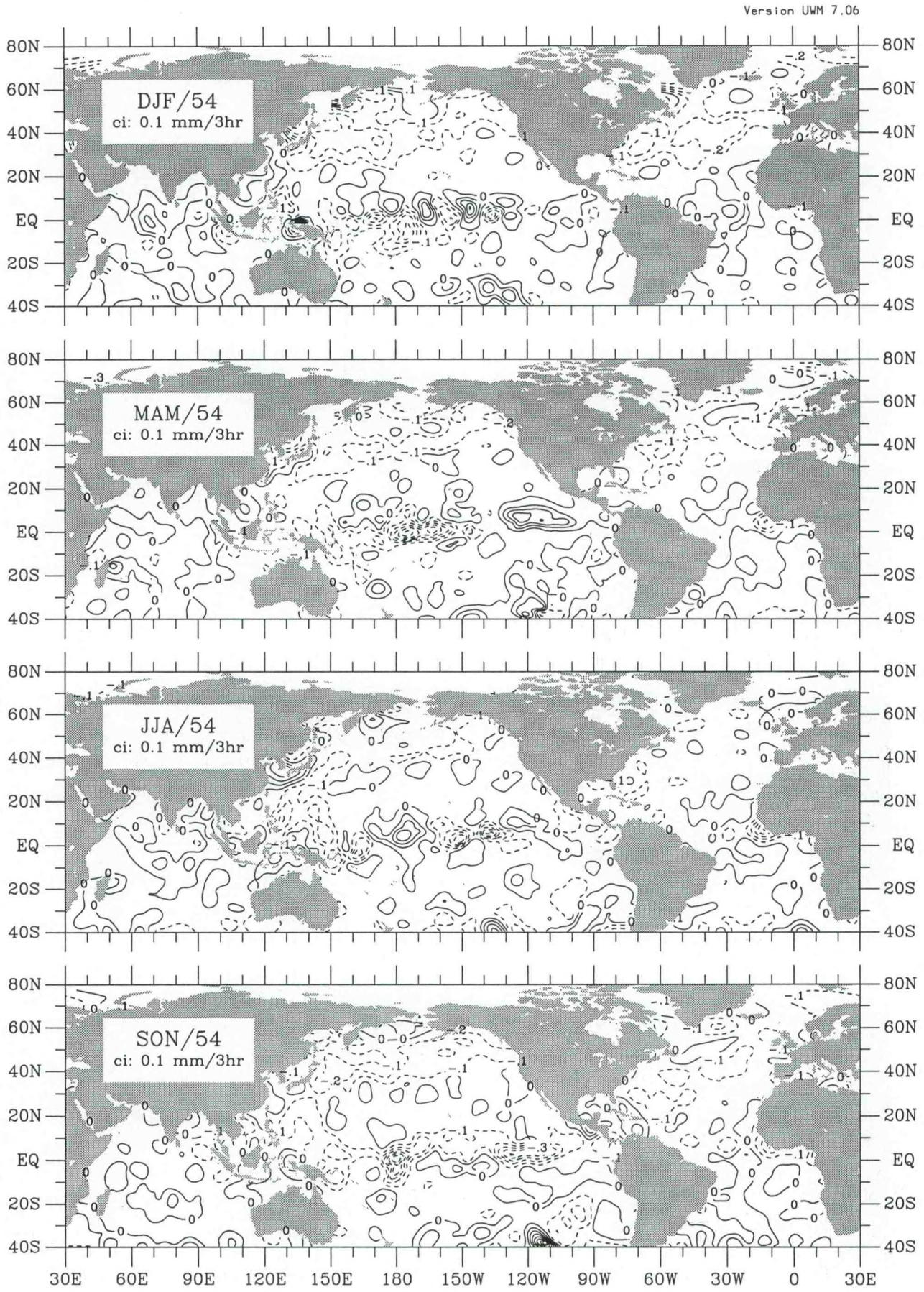

Figure P-15. Precipitation seasonal anomaly for 1954.

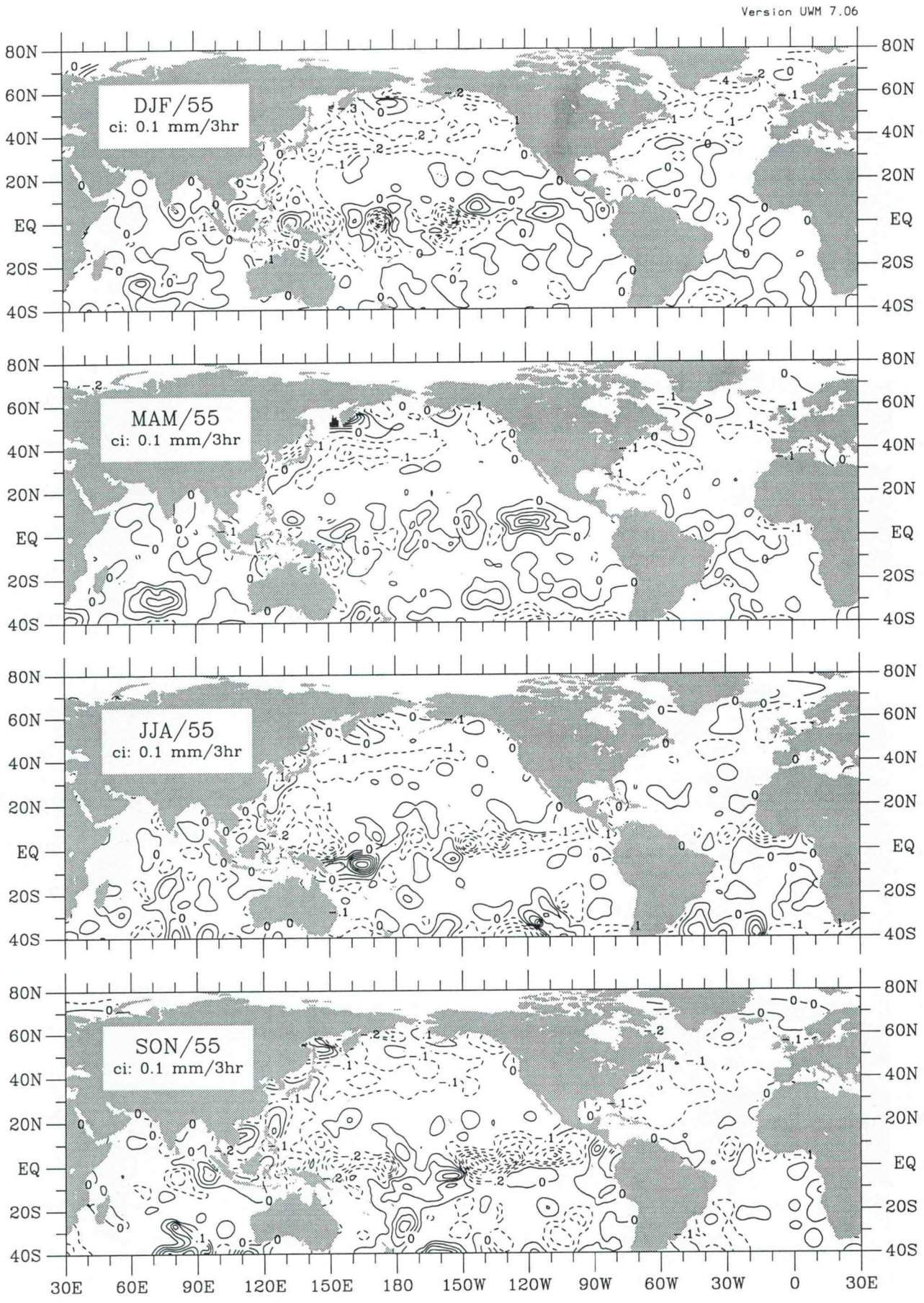

Figure P-16. Precipitation seasonal anomaly for 1955.

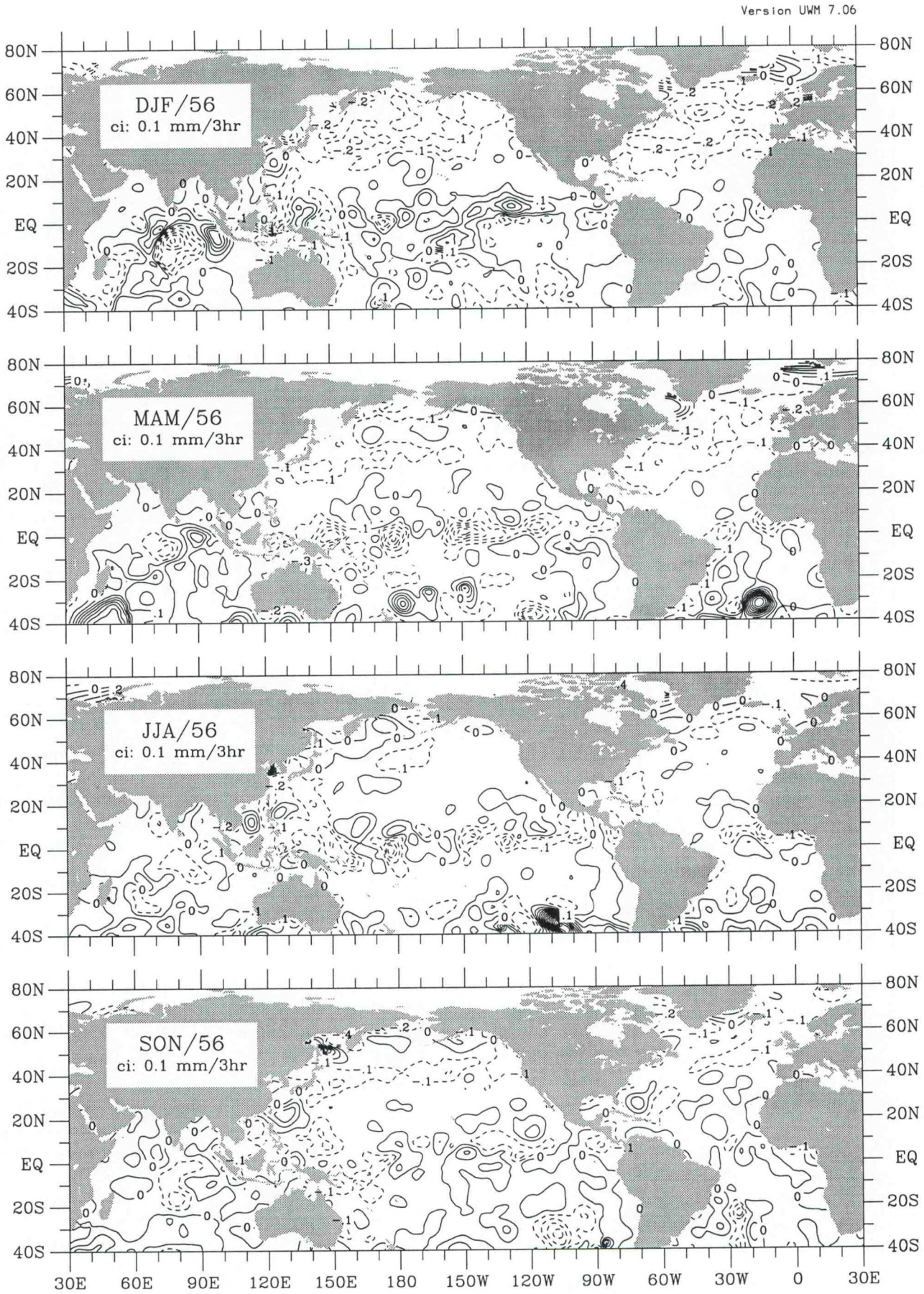

Figure P-17. Precipitation seasonal anomaly for 1956.

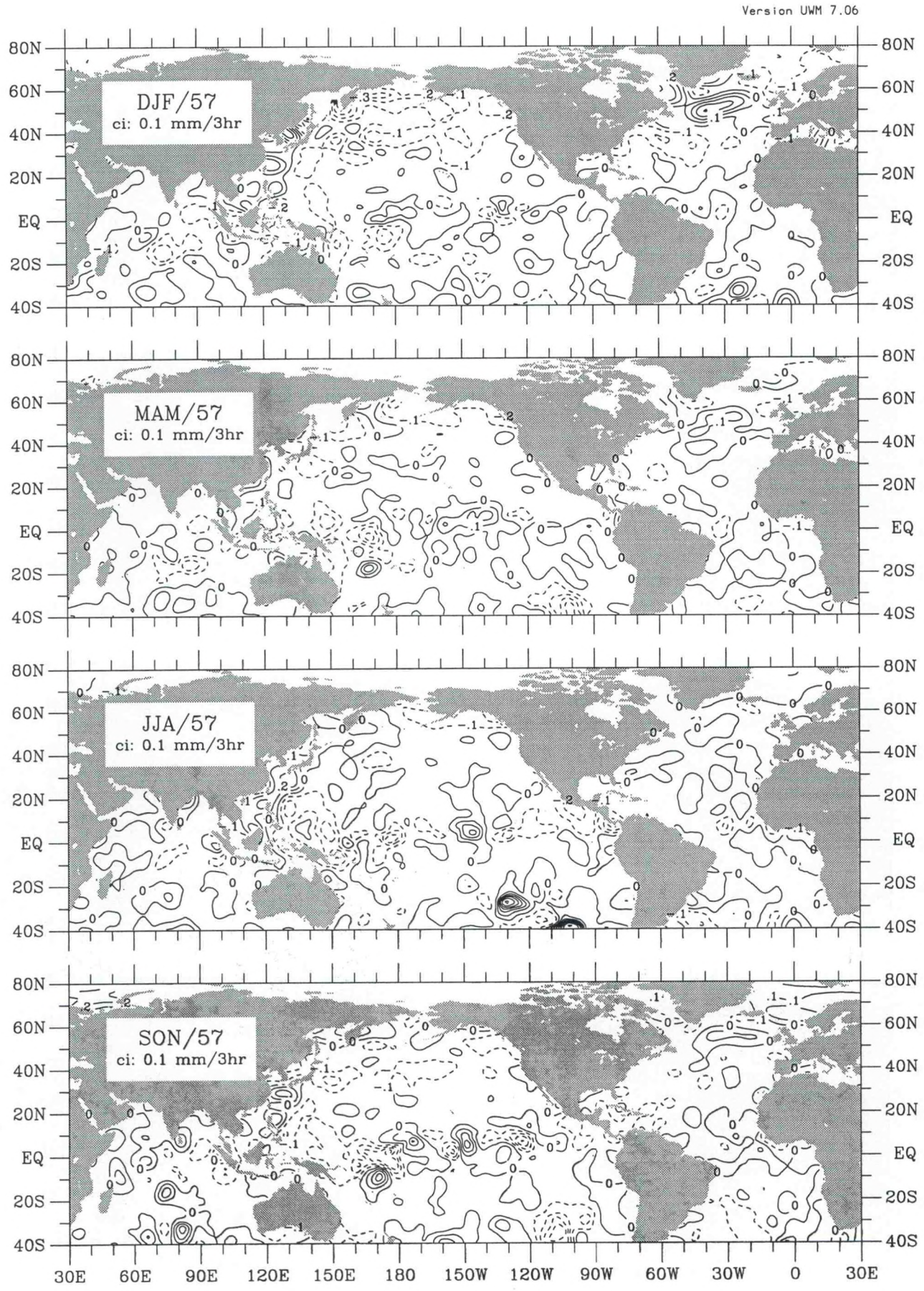

Figure P–18. Precipitation seasonal anomaly for 1957.

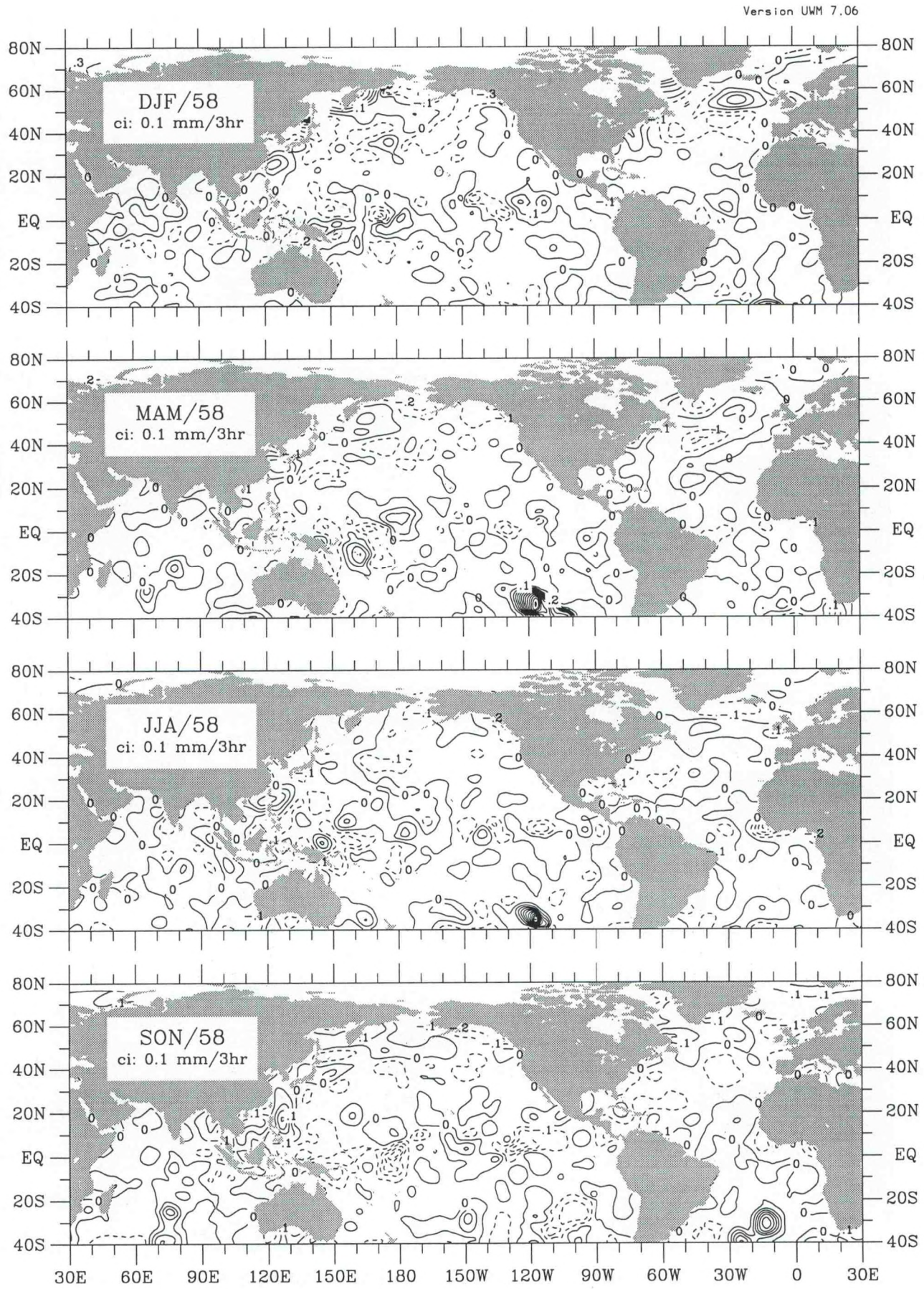

Figure P-19. Precipitation seasonal anomaly for 1958.

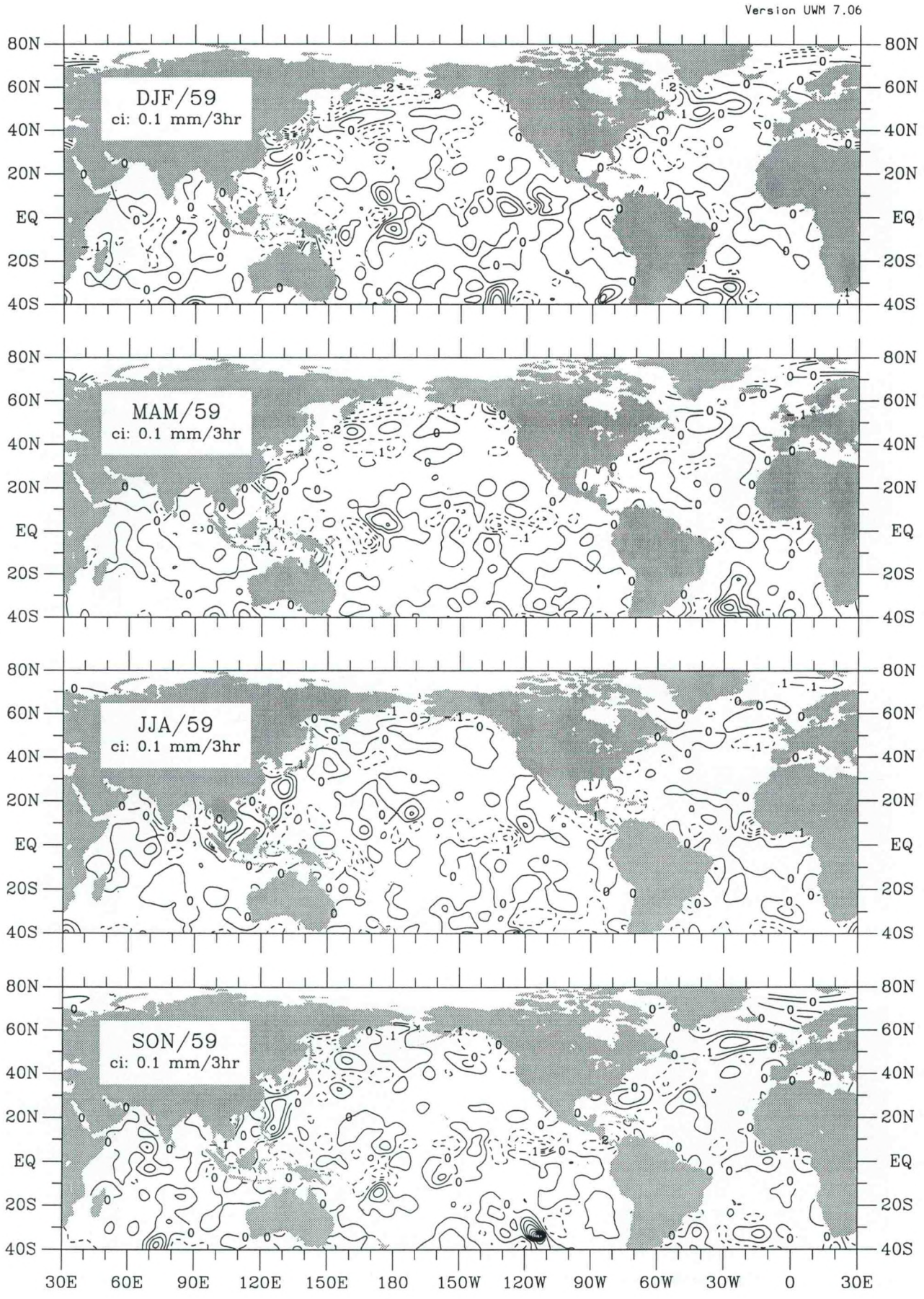

Figure P–20. Precipitation seasonal anomaly for 1959.

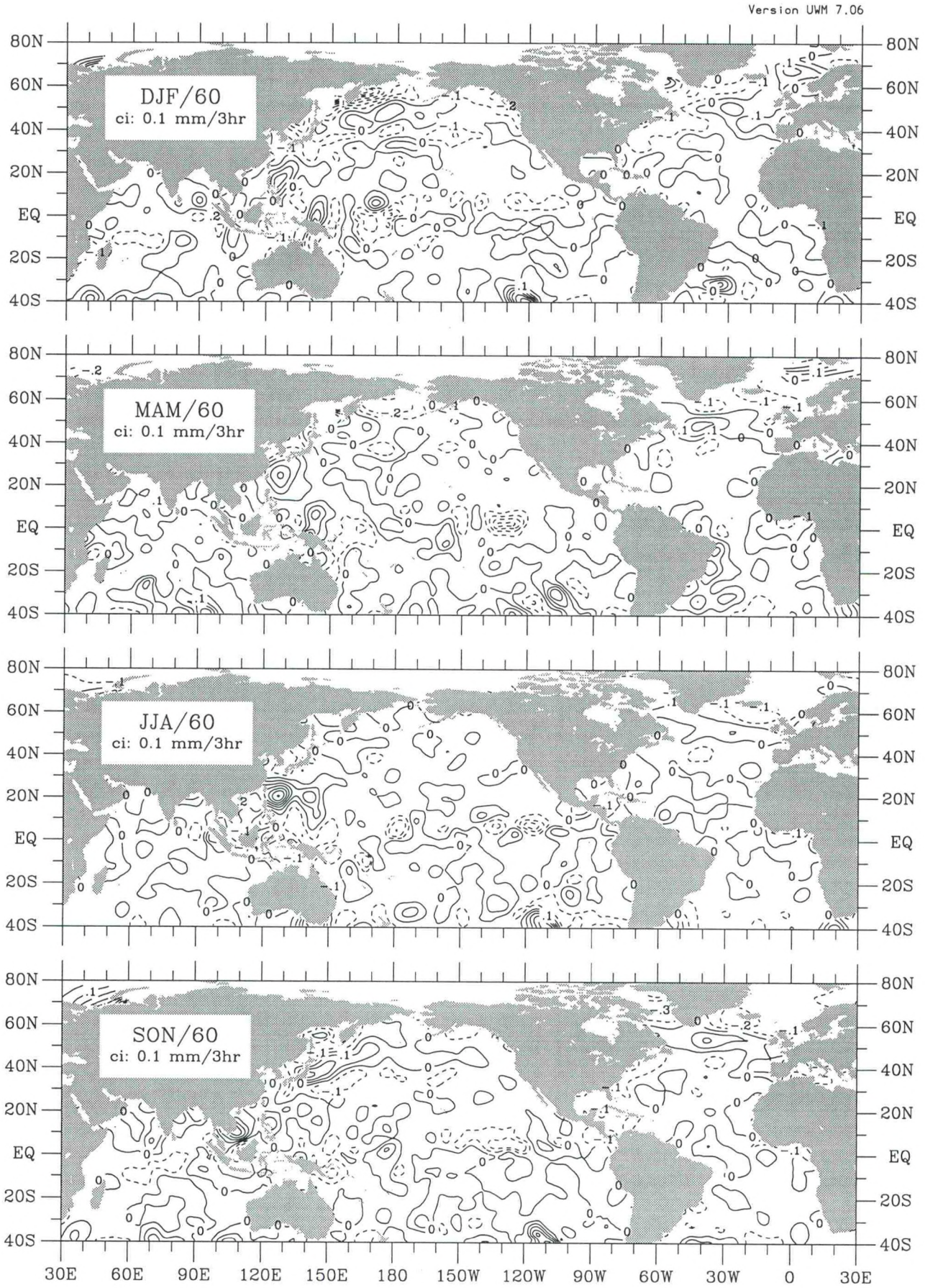

Figure P-21. Precipitation seasonal anomaly for 1960.

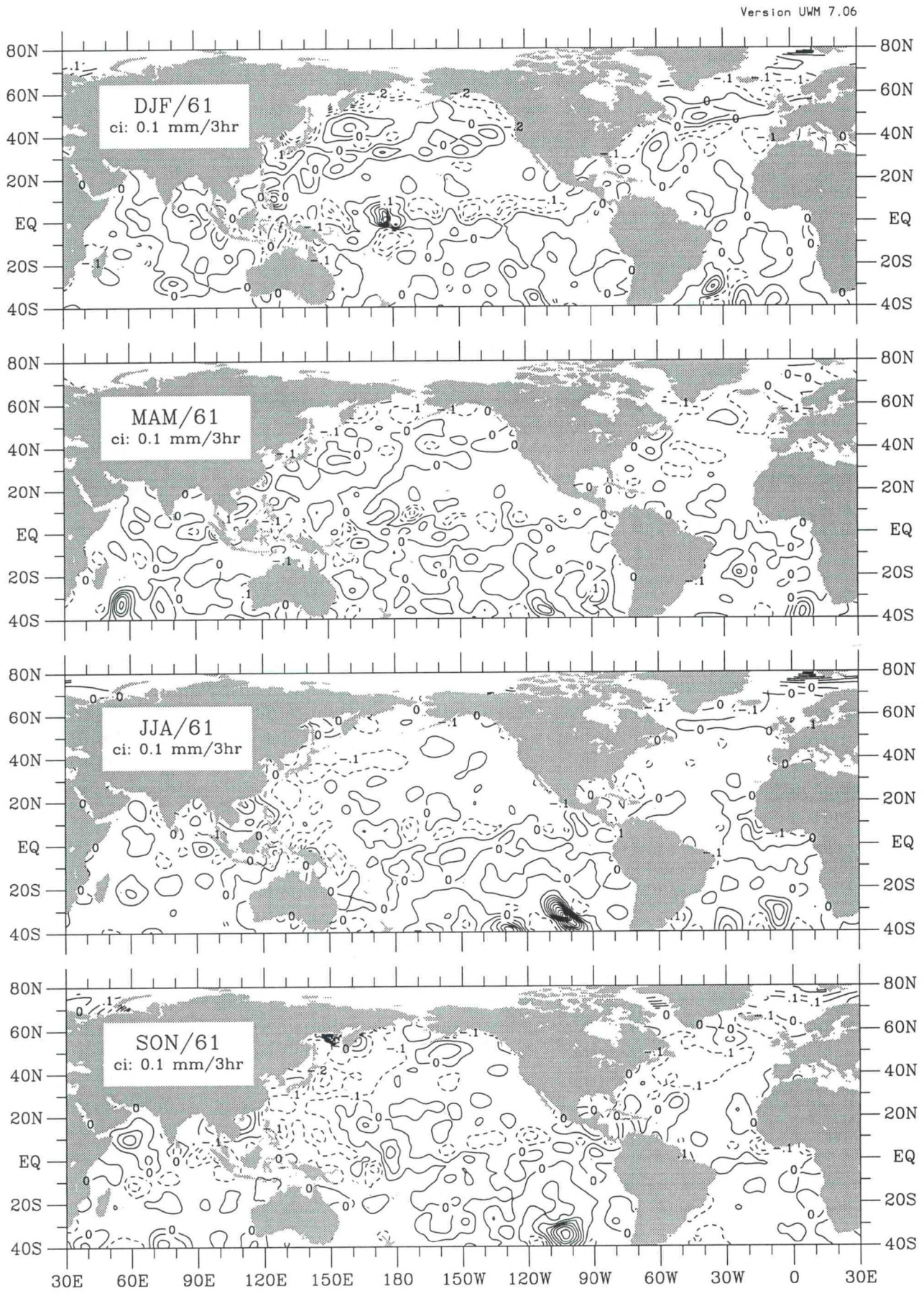

Figure P-22. Precipitation seasonal anomaly for 1961.

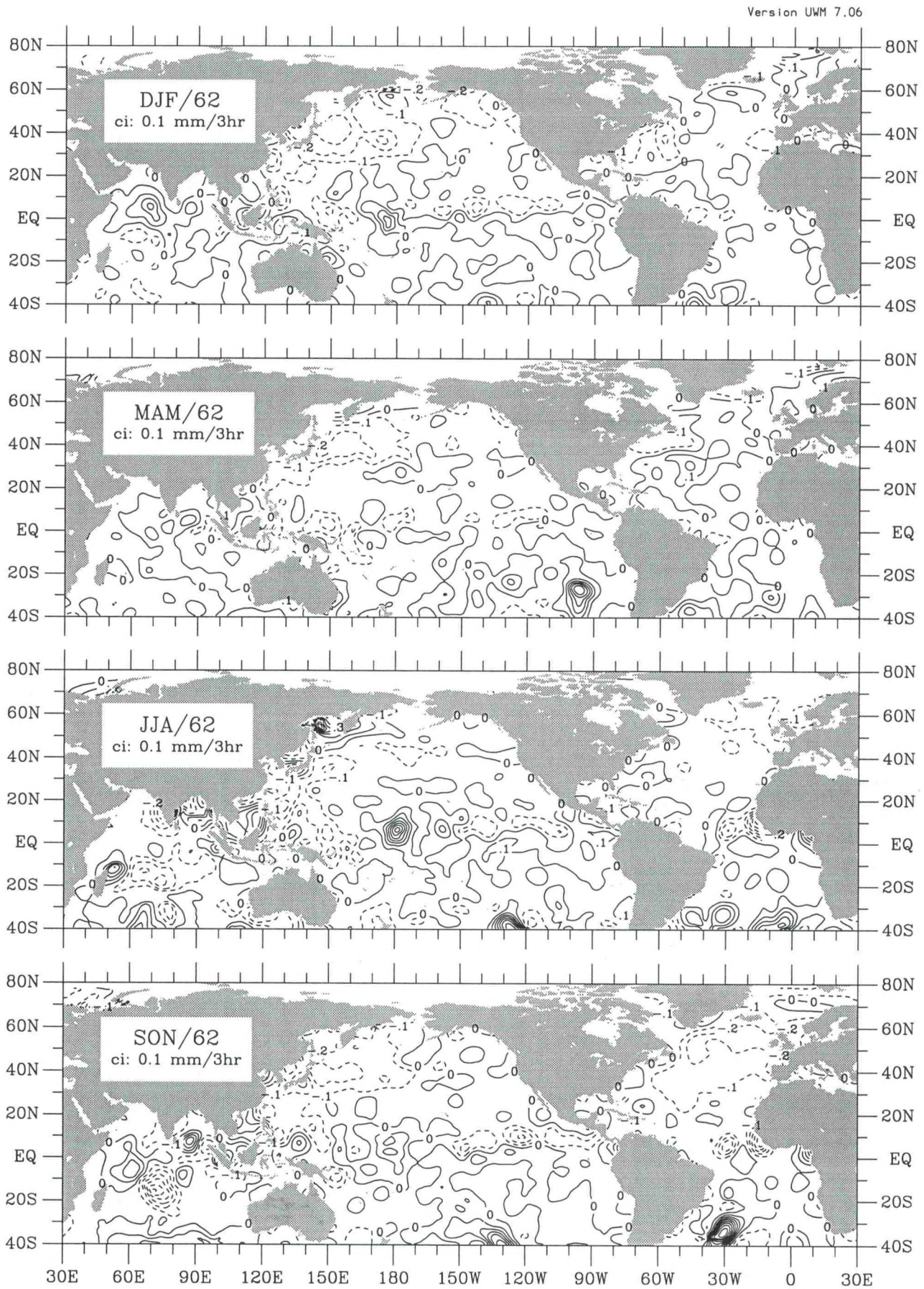

Figure P-23. Precipitation seasonal anomaly for 1962.

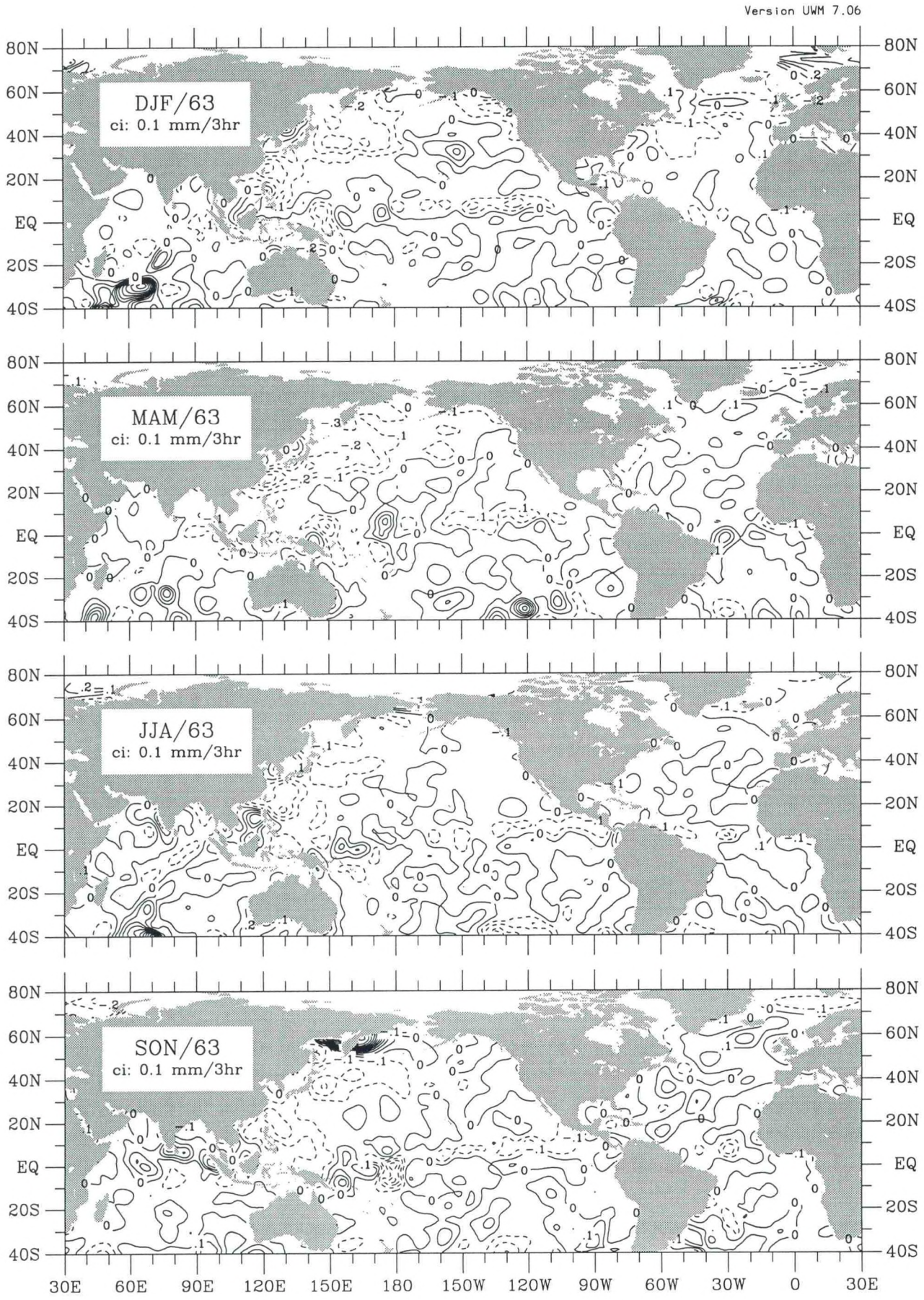

Figure P-24. Precipitation seasonal anomaly for 1963.

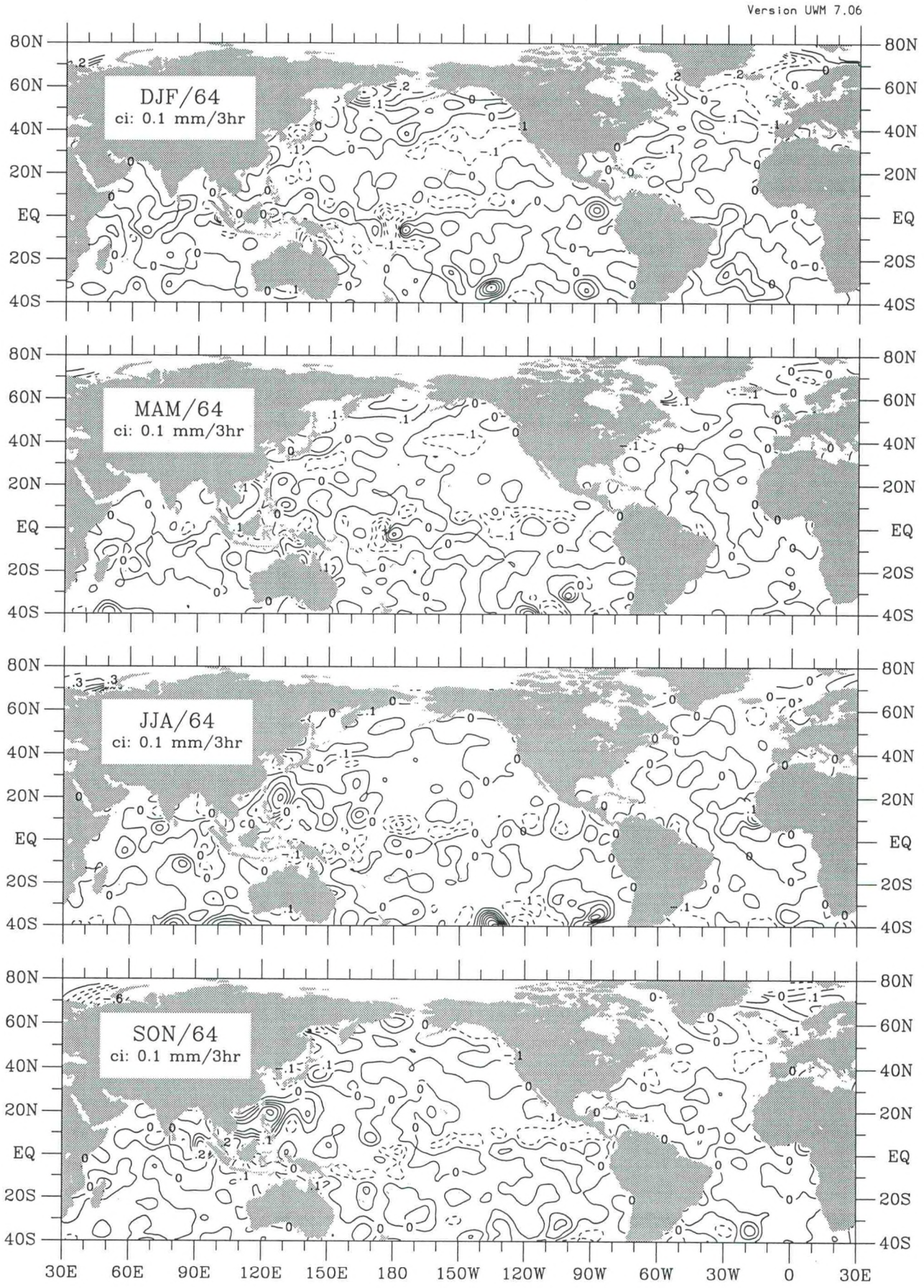

Figure P-25. Precipitation seasonal anomaly for 1964.

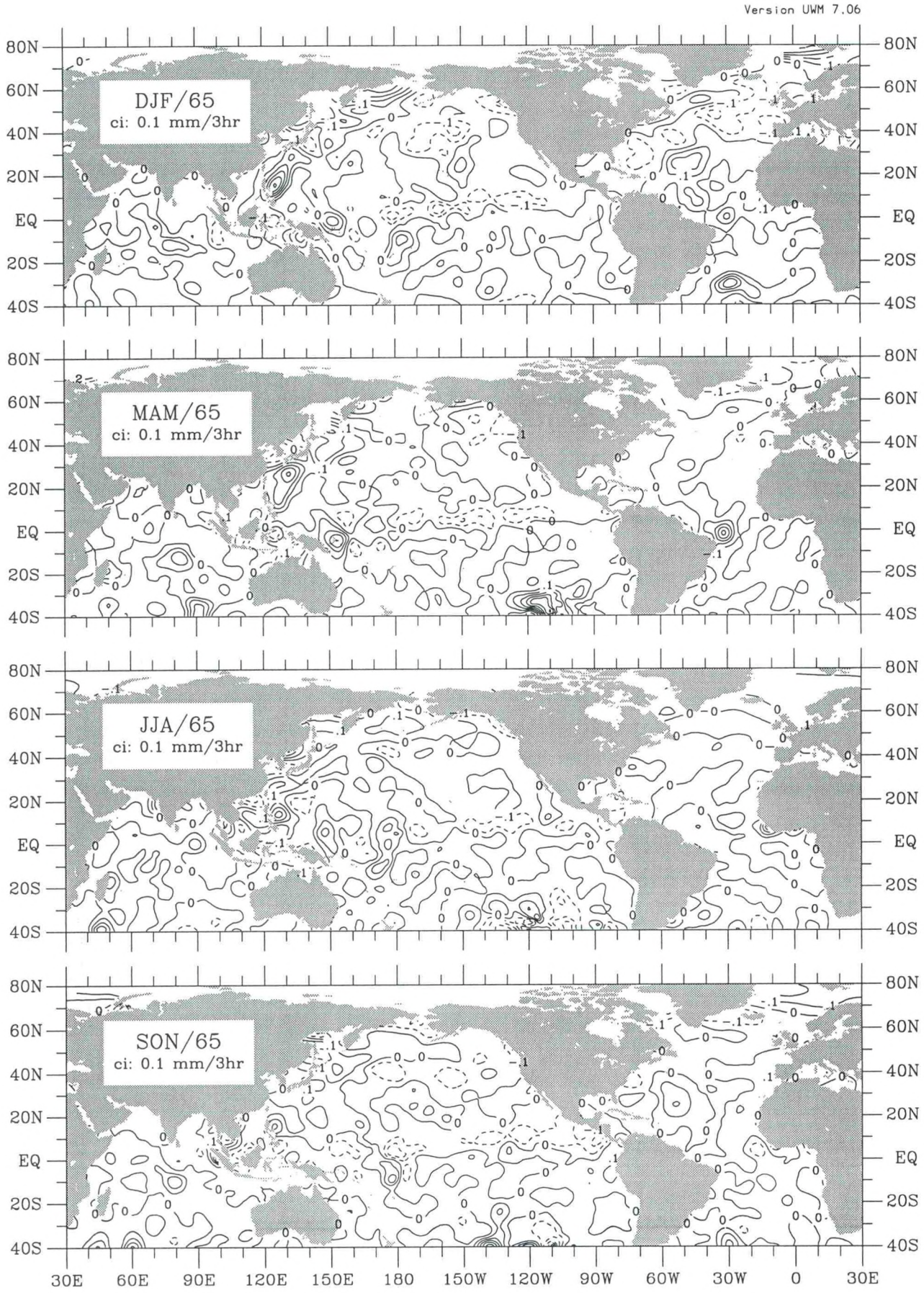

Figure P-26. Precipitation seasonal anomaly for 1965.

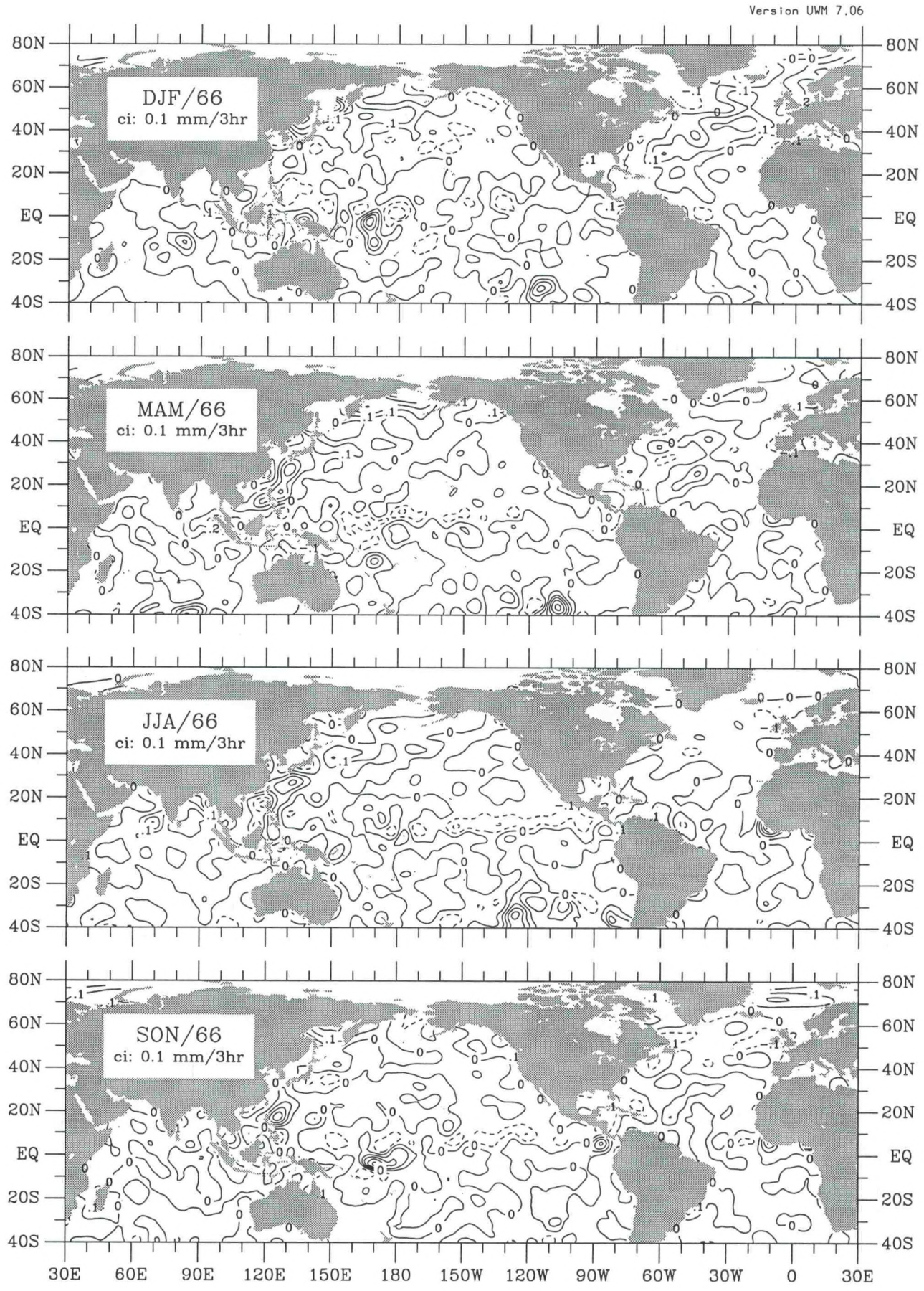

Figure P–27. Precipitation seasonal anomaly for 1966.

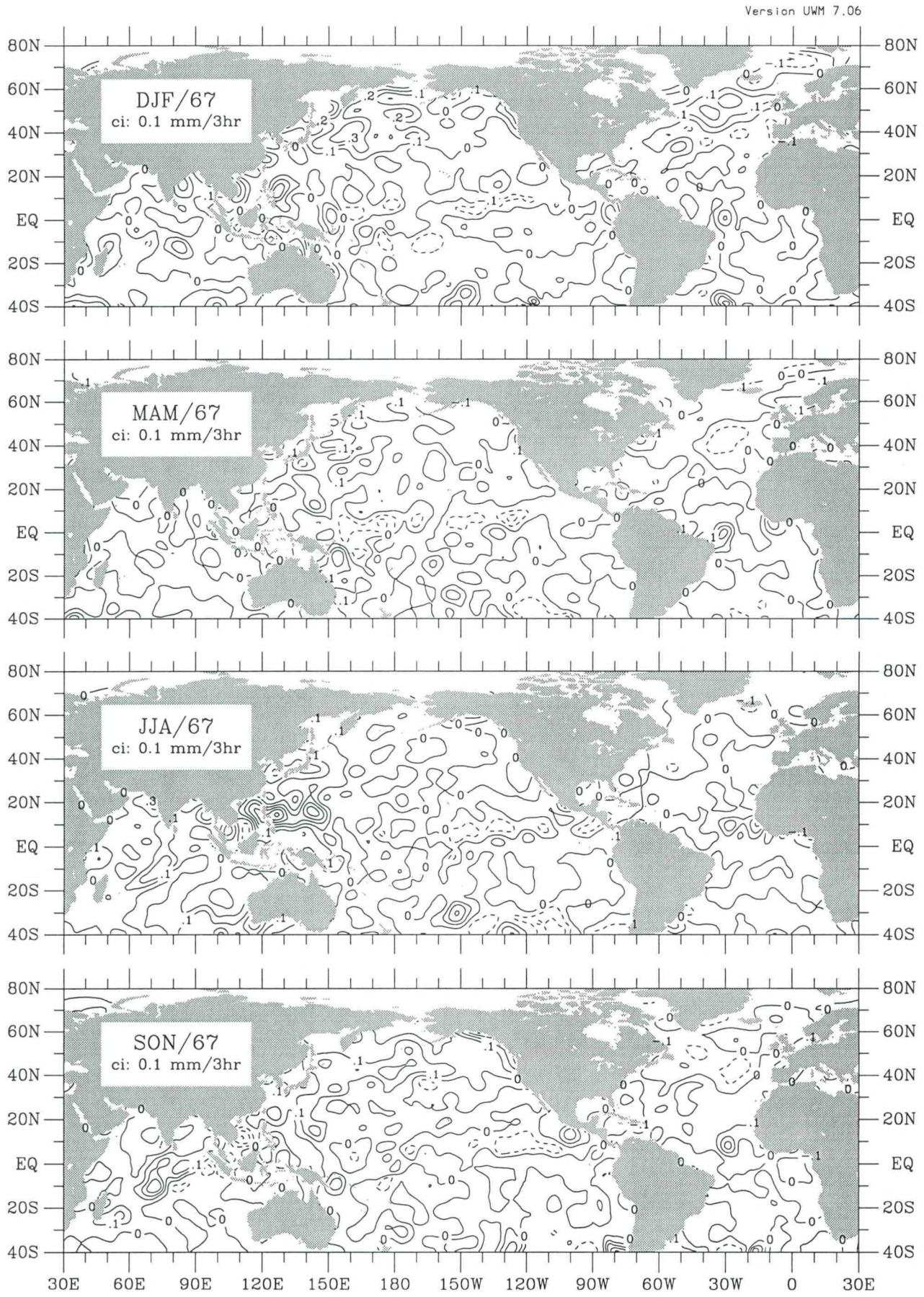

Figure P-28. Precipitation seasonal anomaly for 1967.

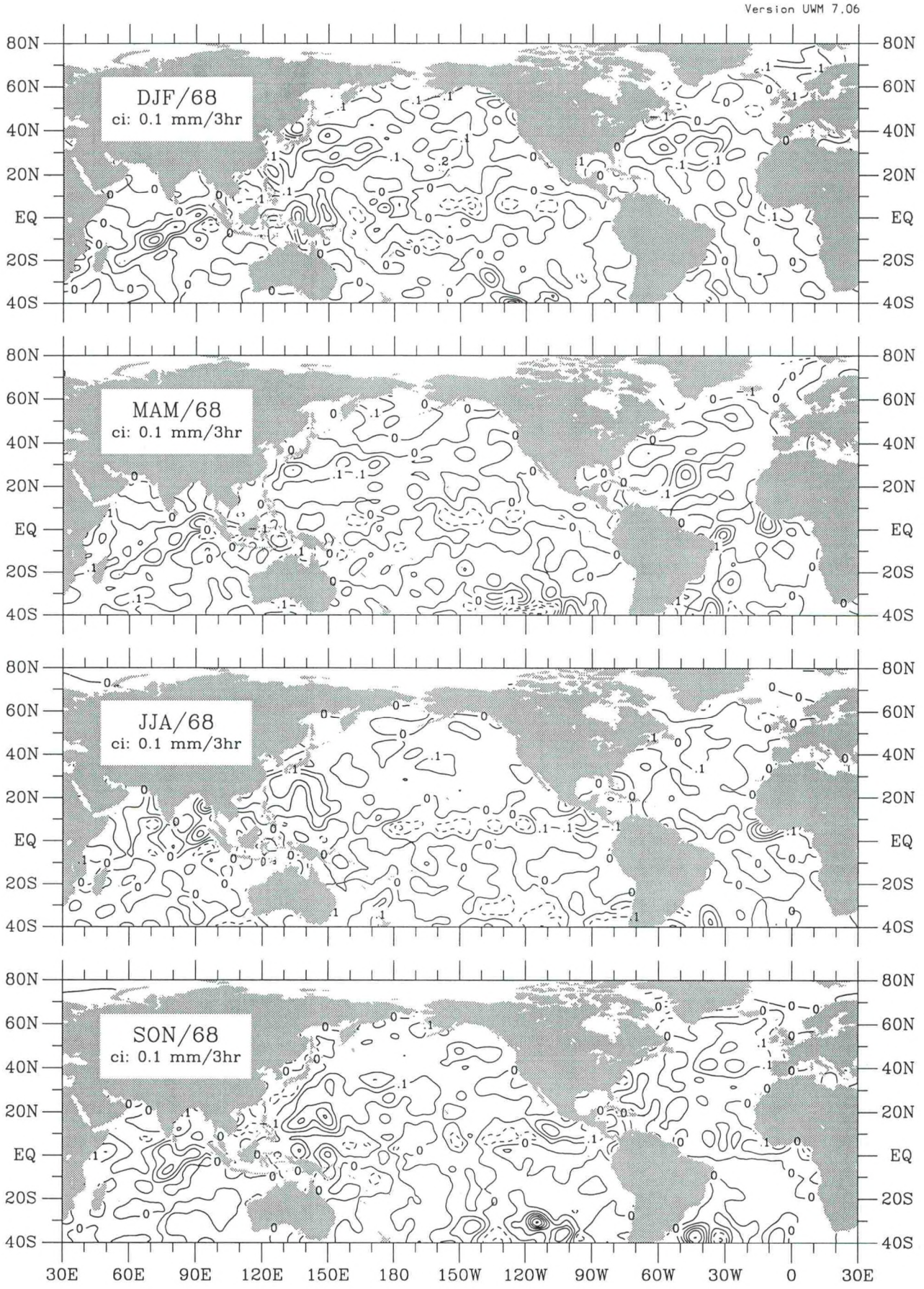

Figure P-29. Precipitation seasonal anomaly for 1968.

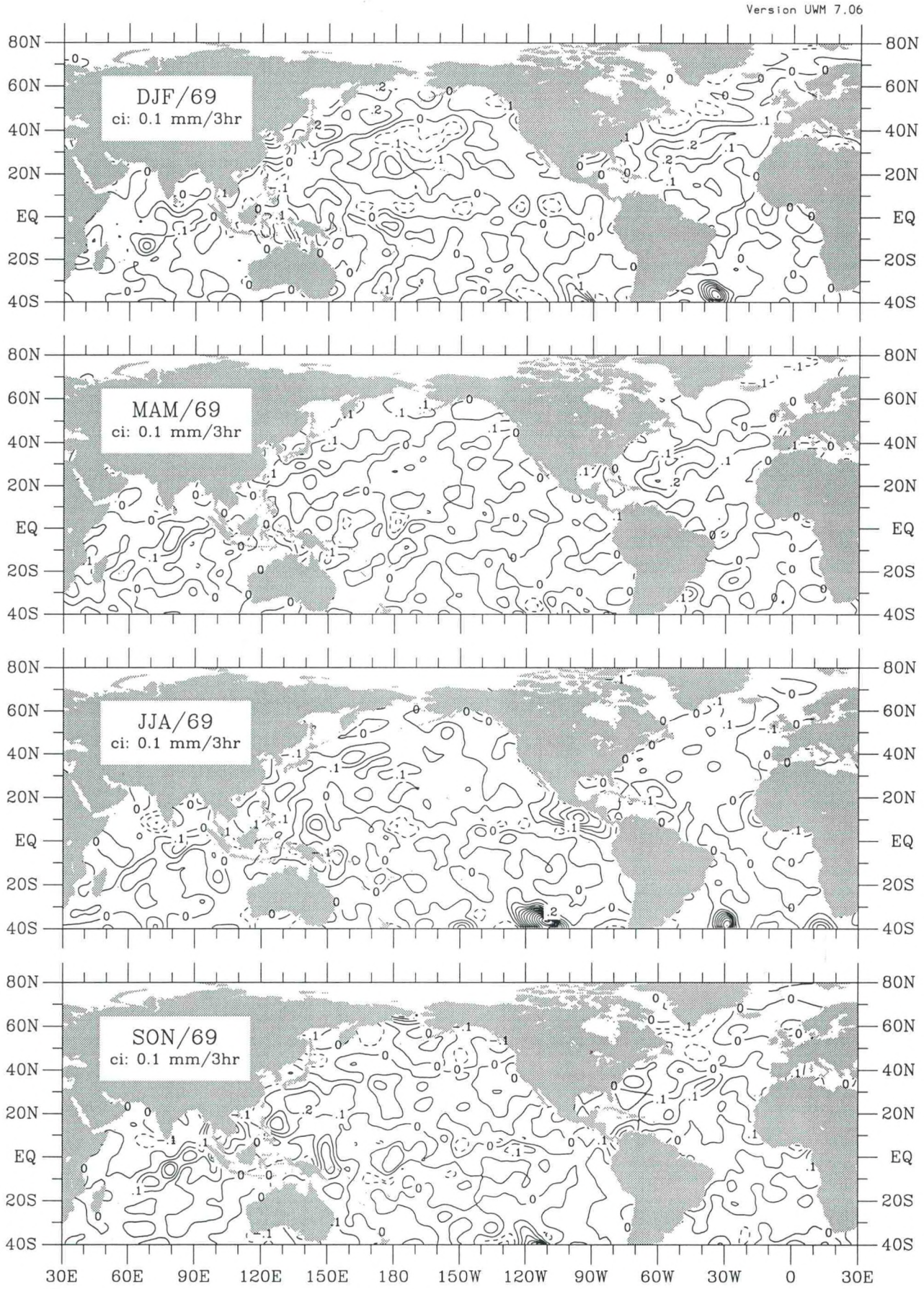

Figure P-30. Precipitation seasonal anomaly for 1969.

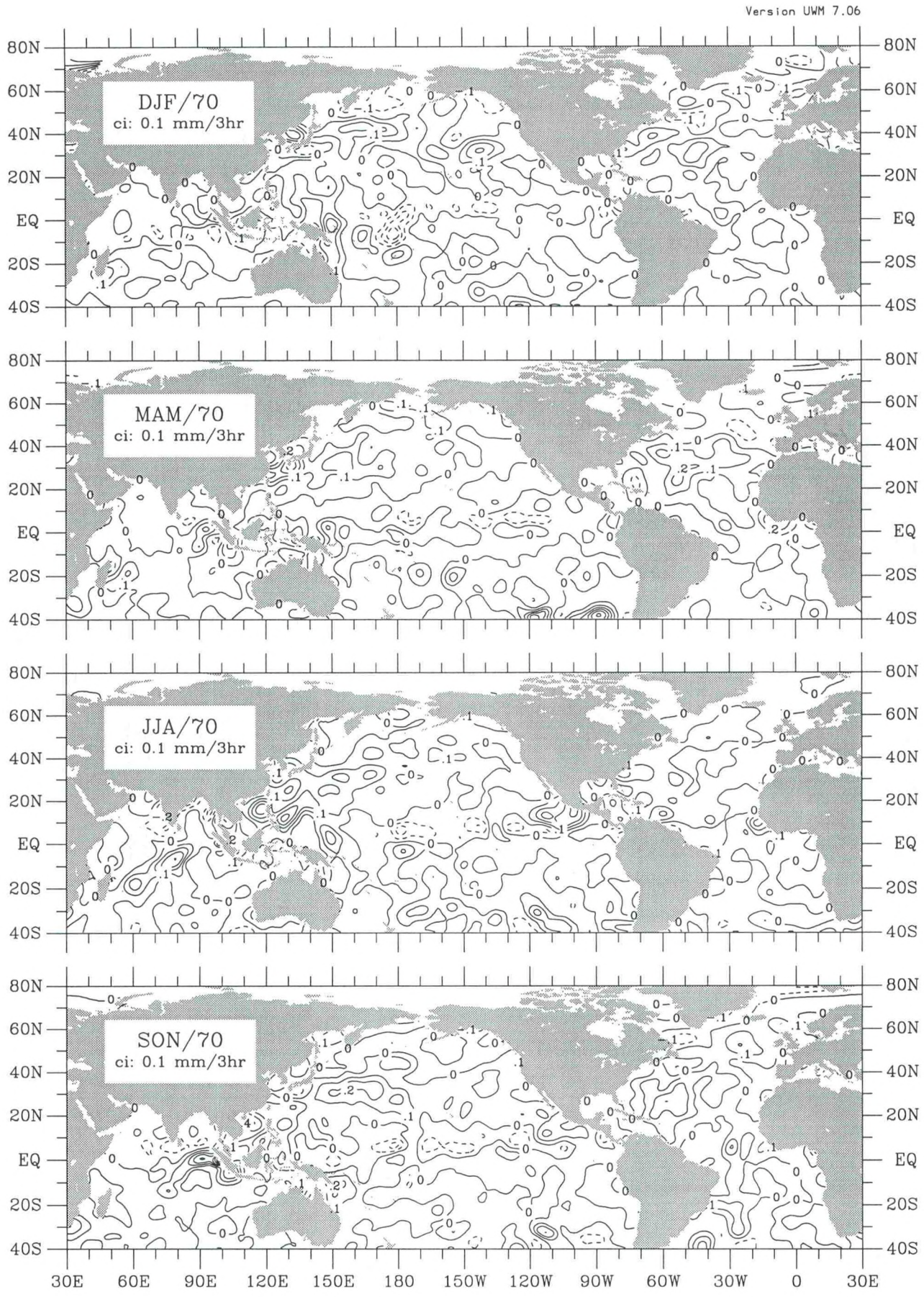

Figure P-31. Precipitation seasonal anomaly for 1970.

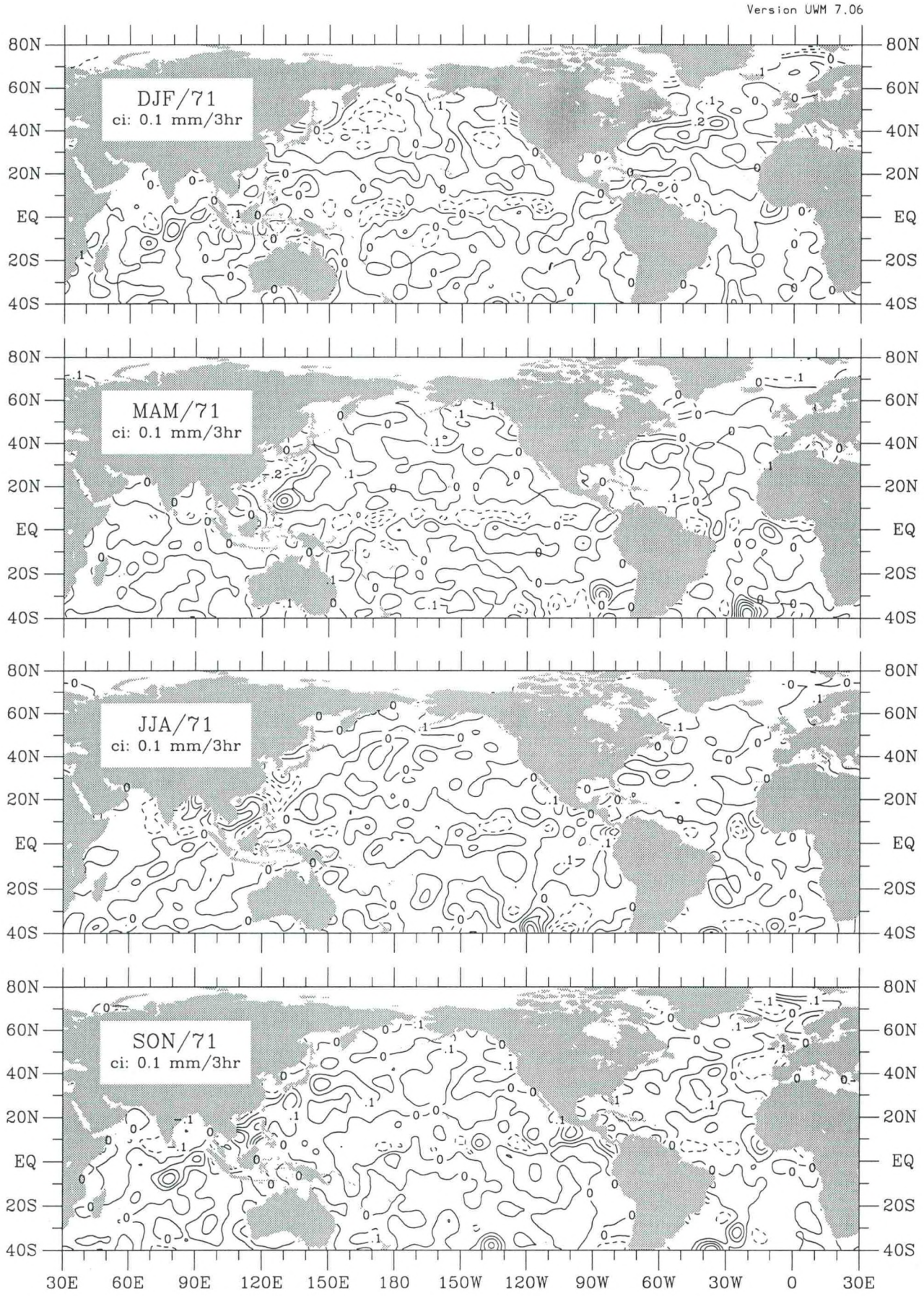

Figure P-32. Precipitation seasonal anomaly for 1971.

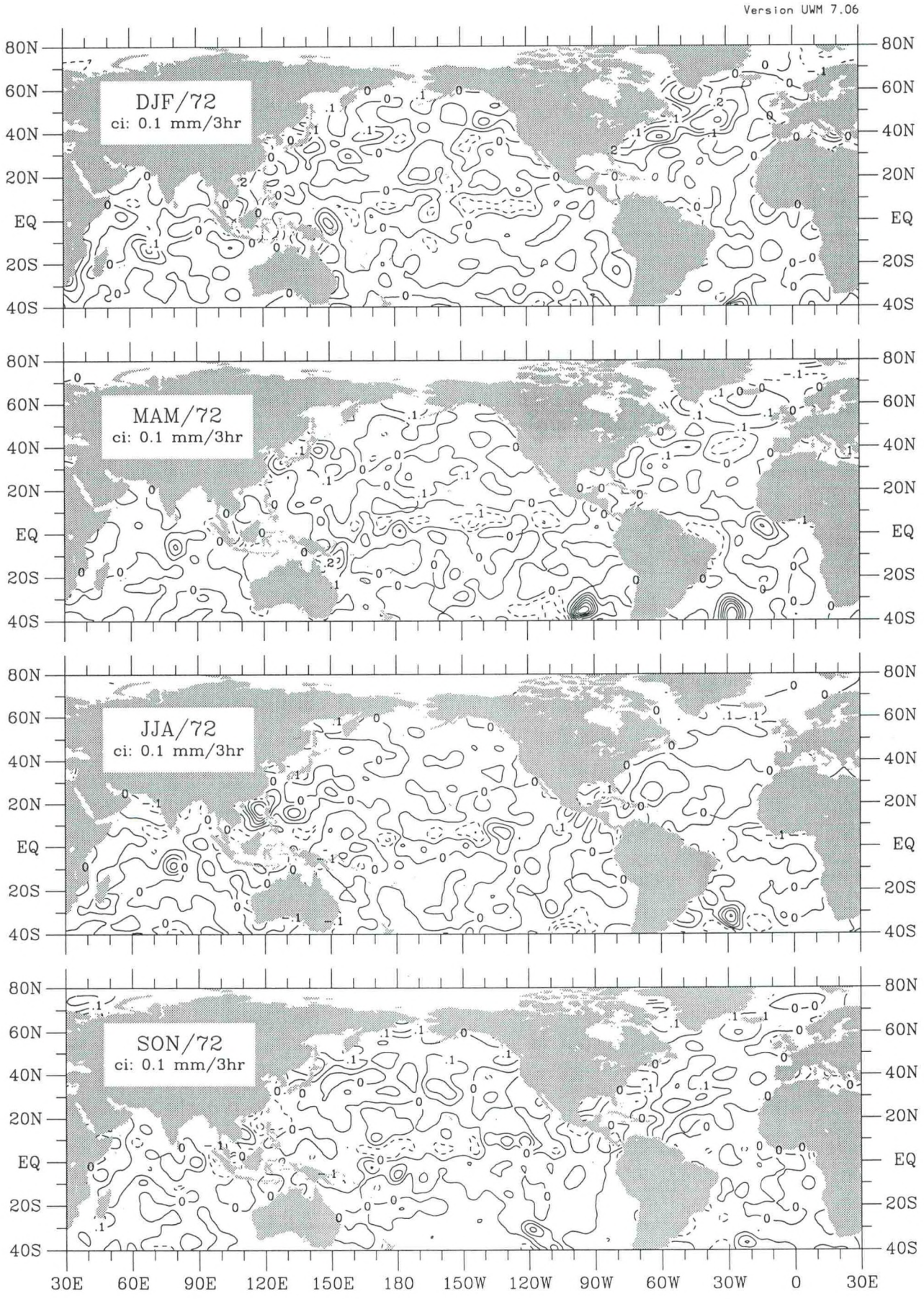

Figure P-33. Precipitation seasonal anomaly for 1972.

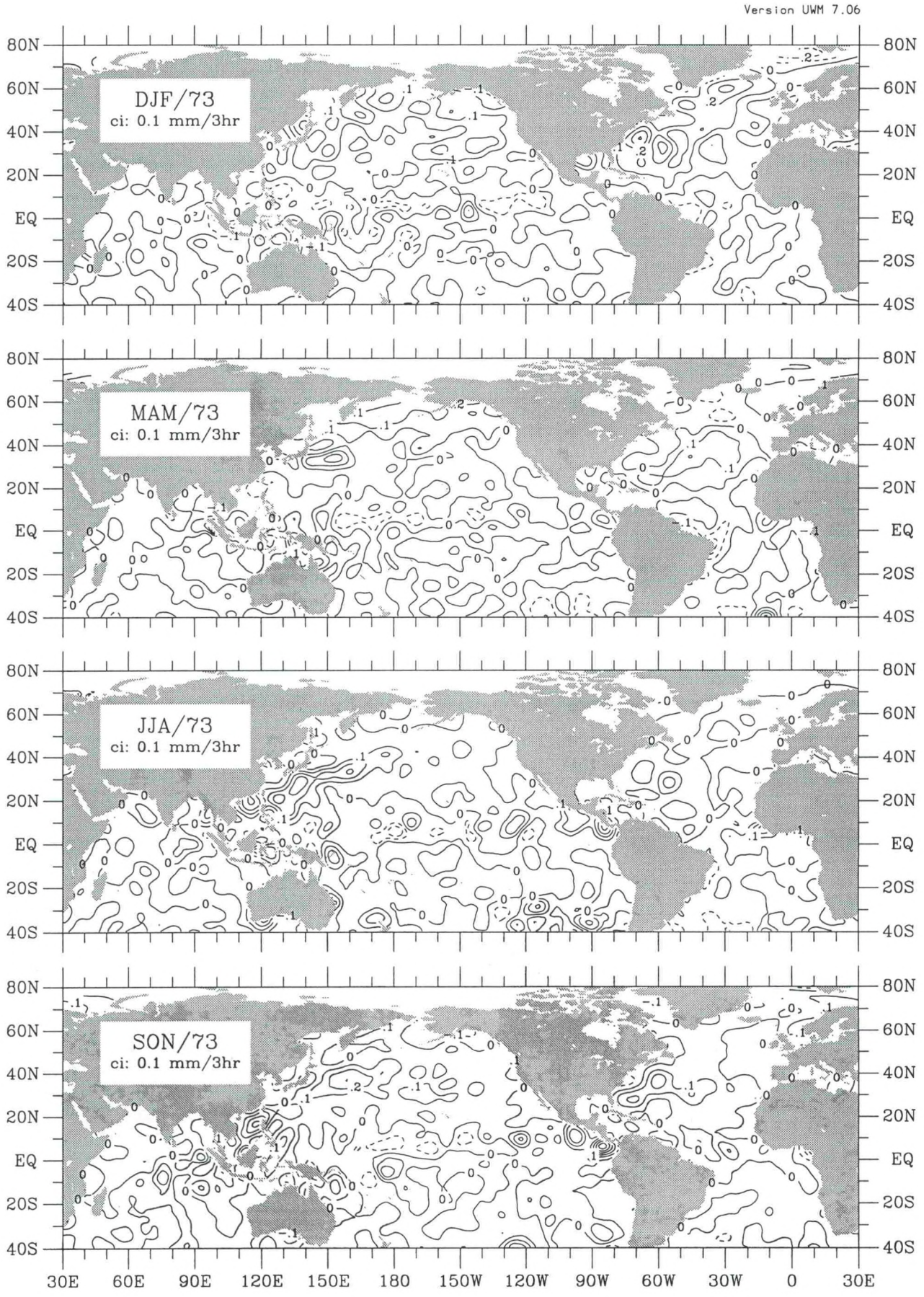

Figure P-34. Precipitation seasonal anomaly for 1973.

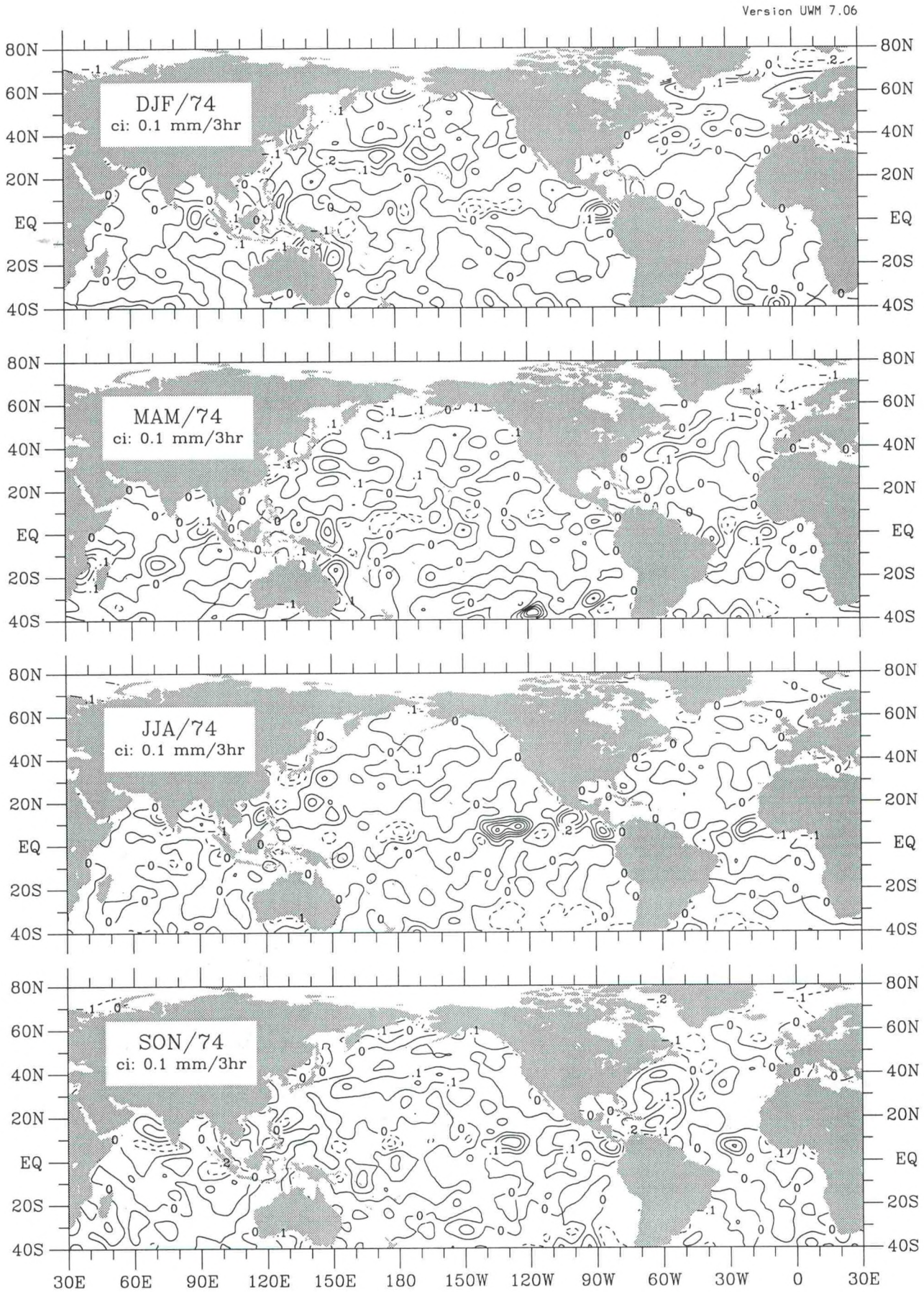

Figure P-35. Precipitation seasonal anomaly for 1974.

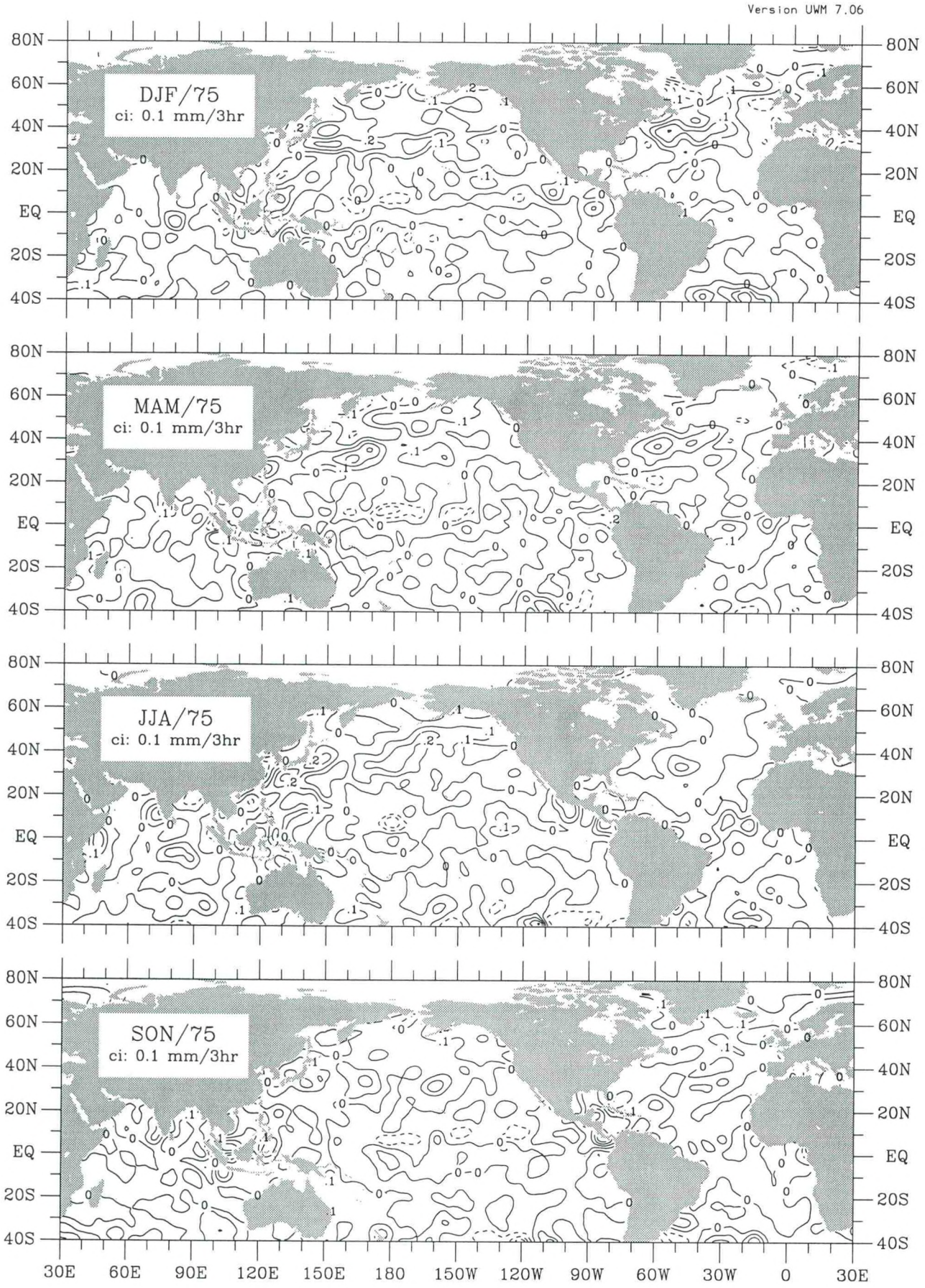

Figure P-36. Precipitation seasonal anomaly for 1975.

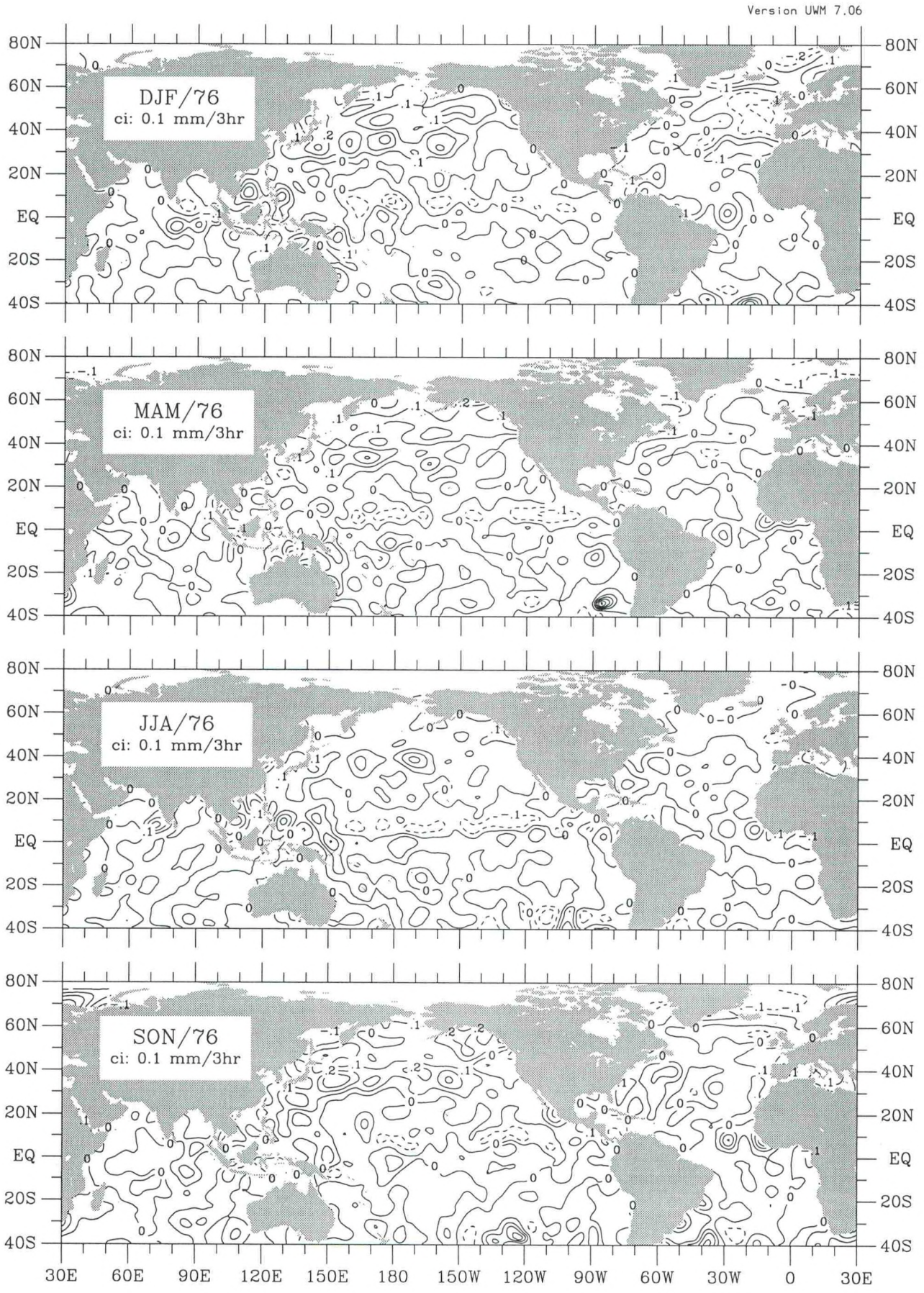

Figure P–37. Precipitation seasonal anomaly for 1976.

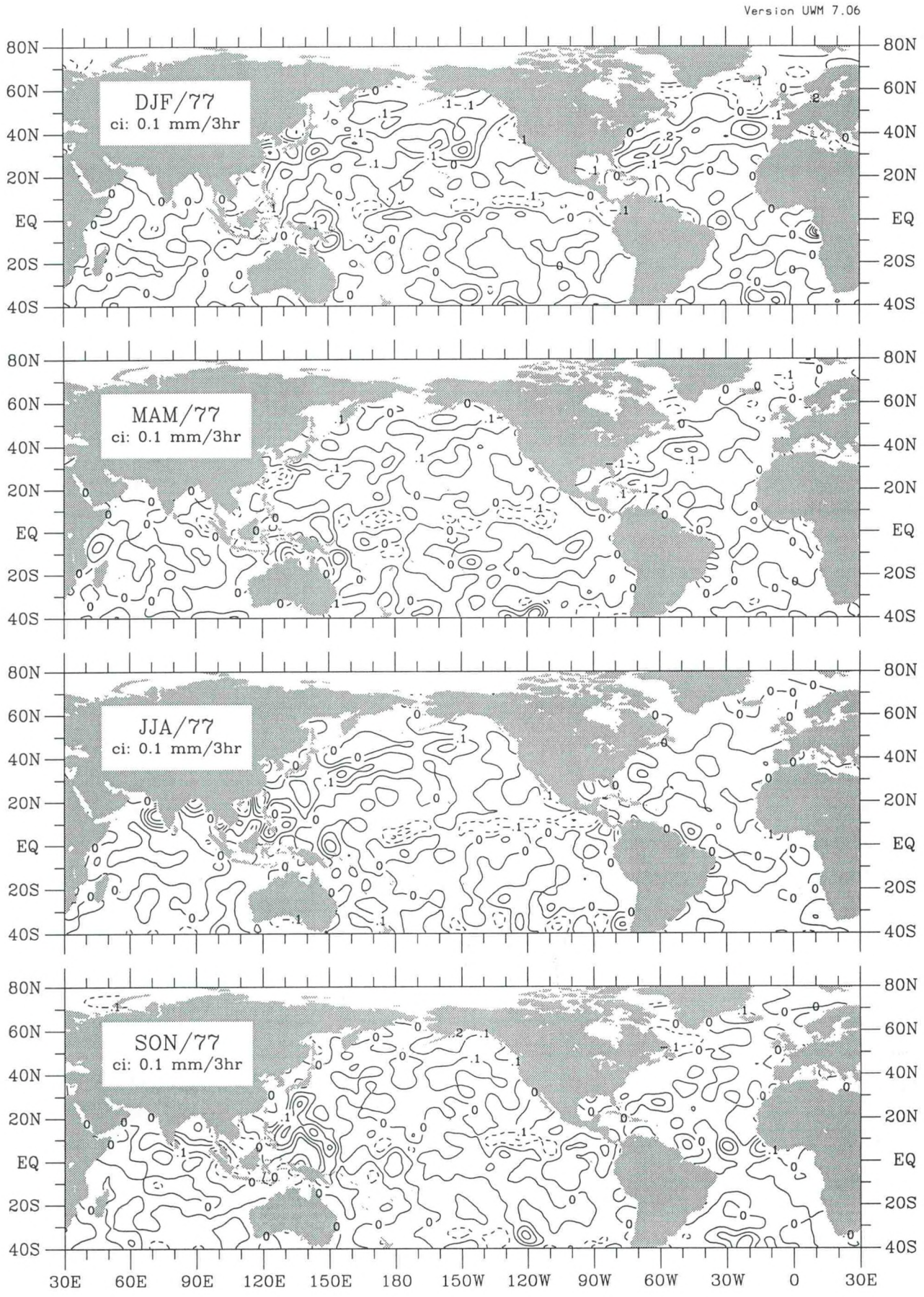

Figure P-38. Precipitation seasonal anomaly for 1977.

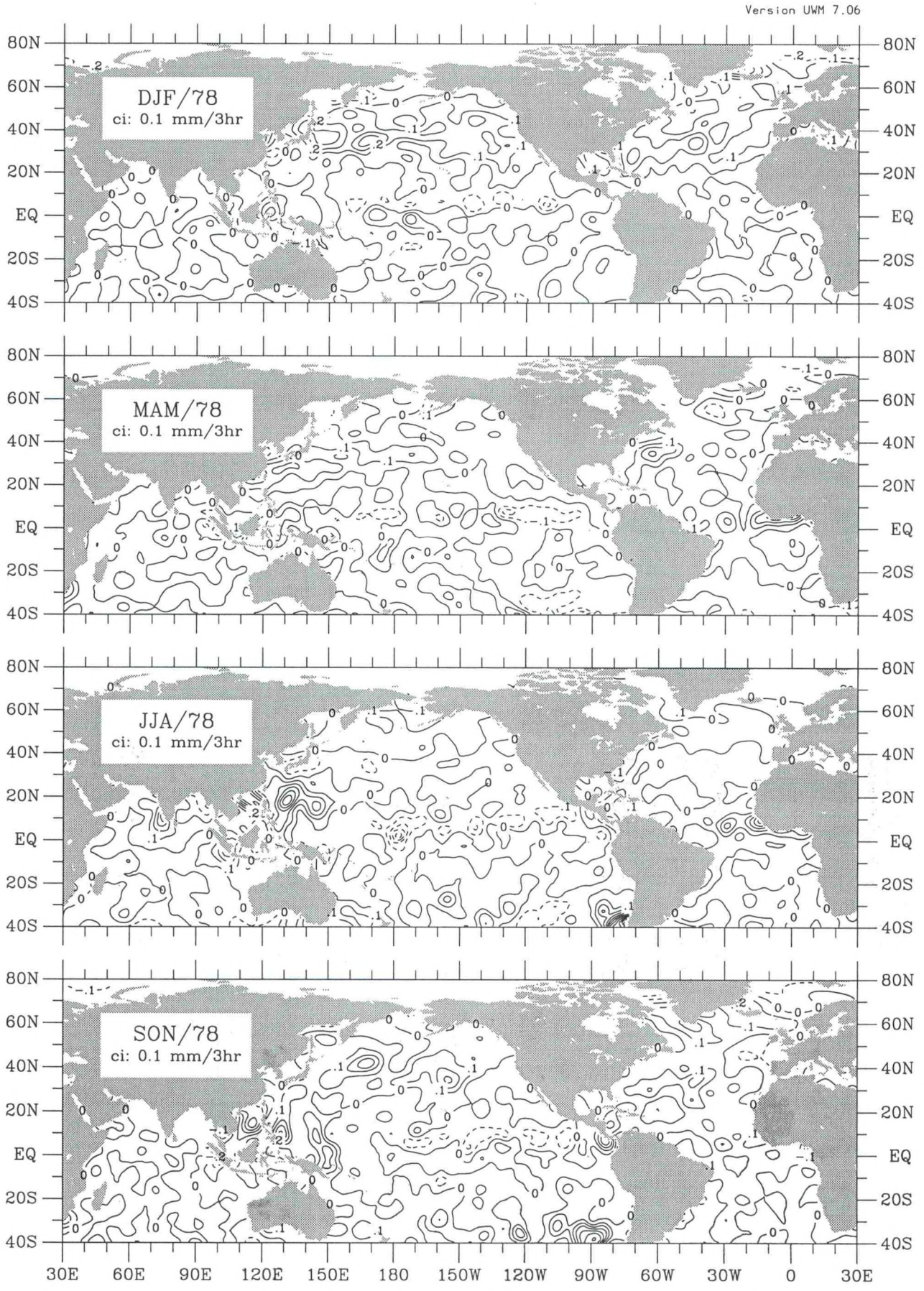

Figure P-39. Precipitation seasonal anomaly for 1978.

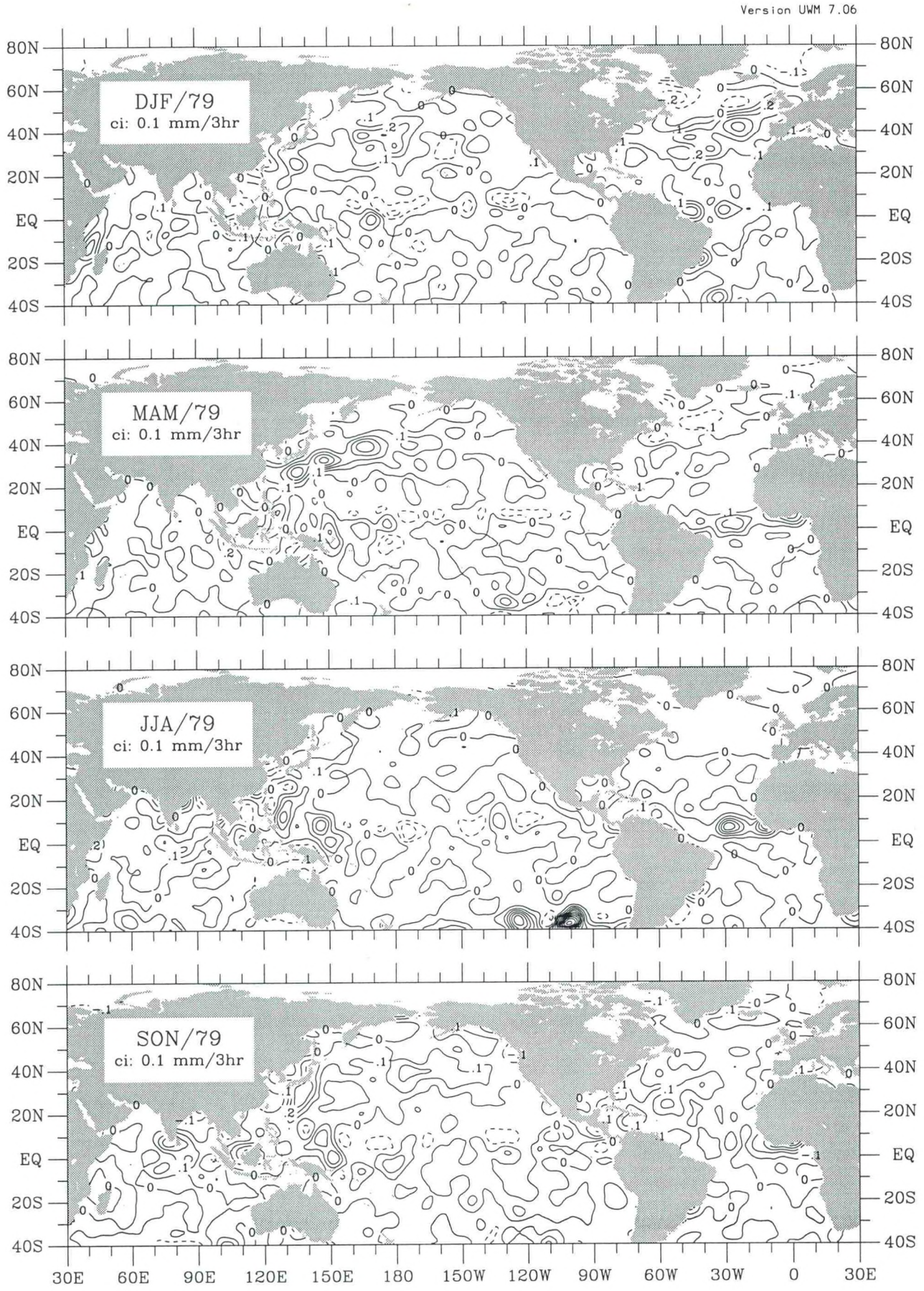

Figure P-40. Precipitation seasonal anomaly for 1979.

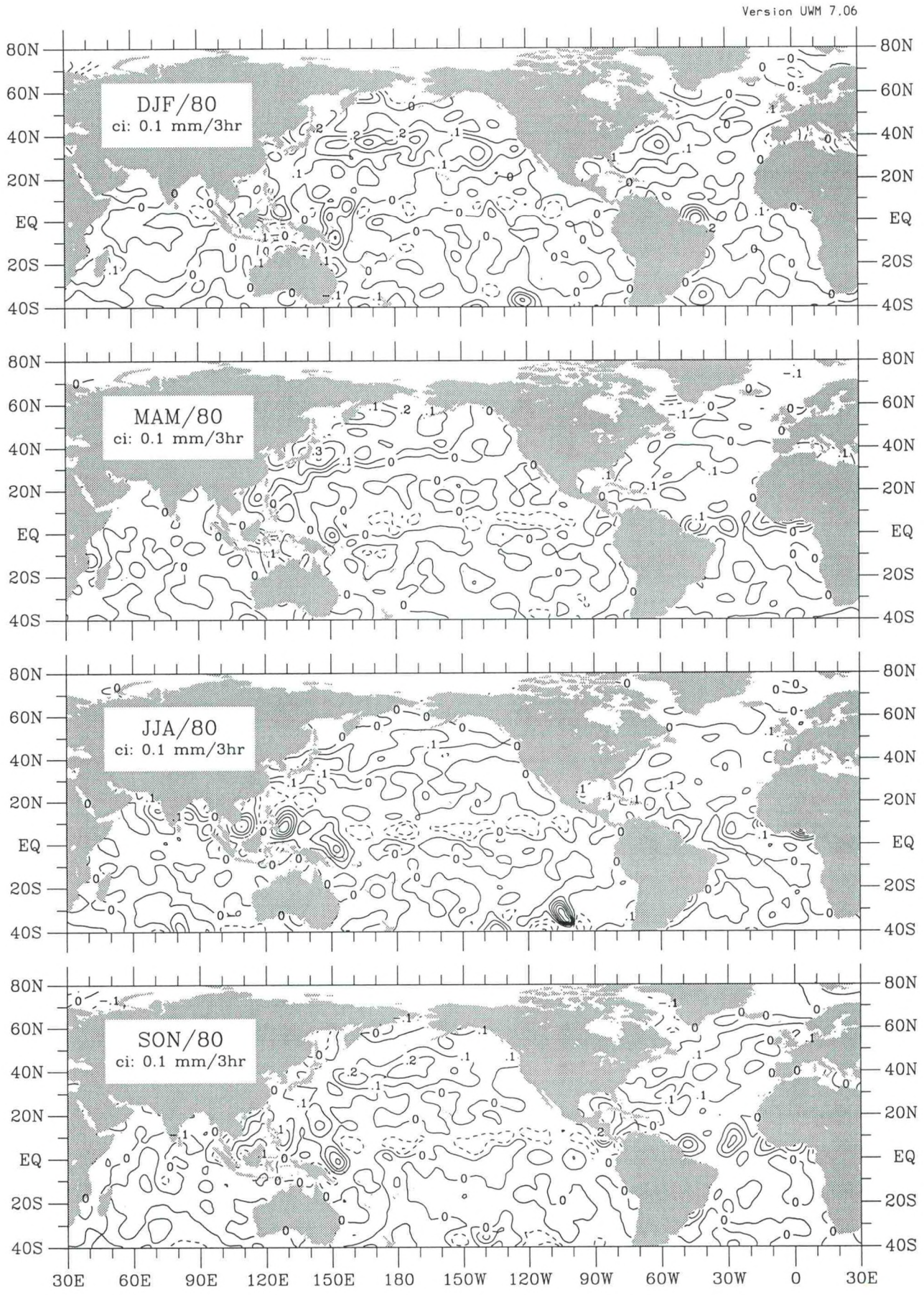

Figure P-41. Precipitation seasonal anomaly for 1980.

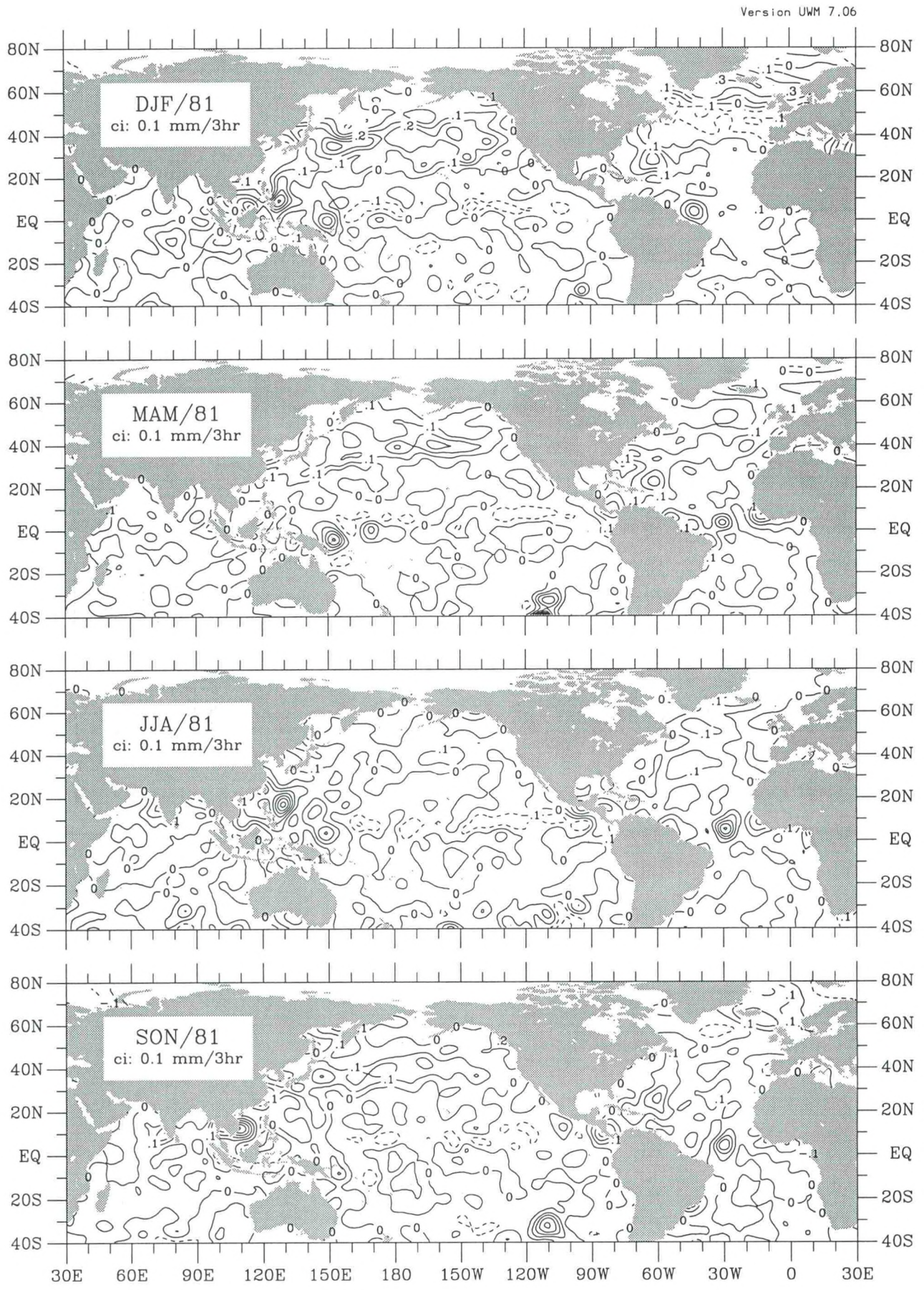

Figure P-42. Precipitation seasonal anomaly for 1981.

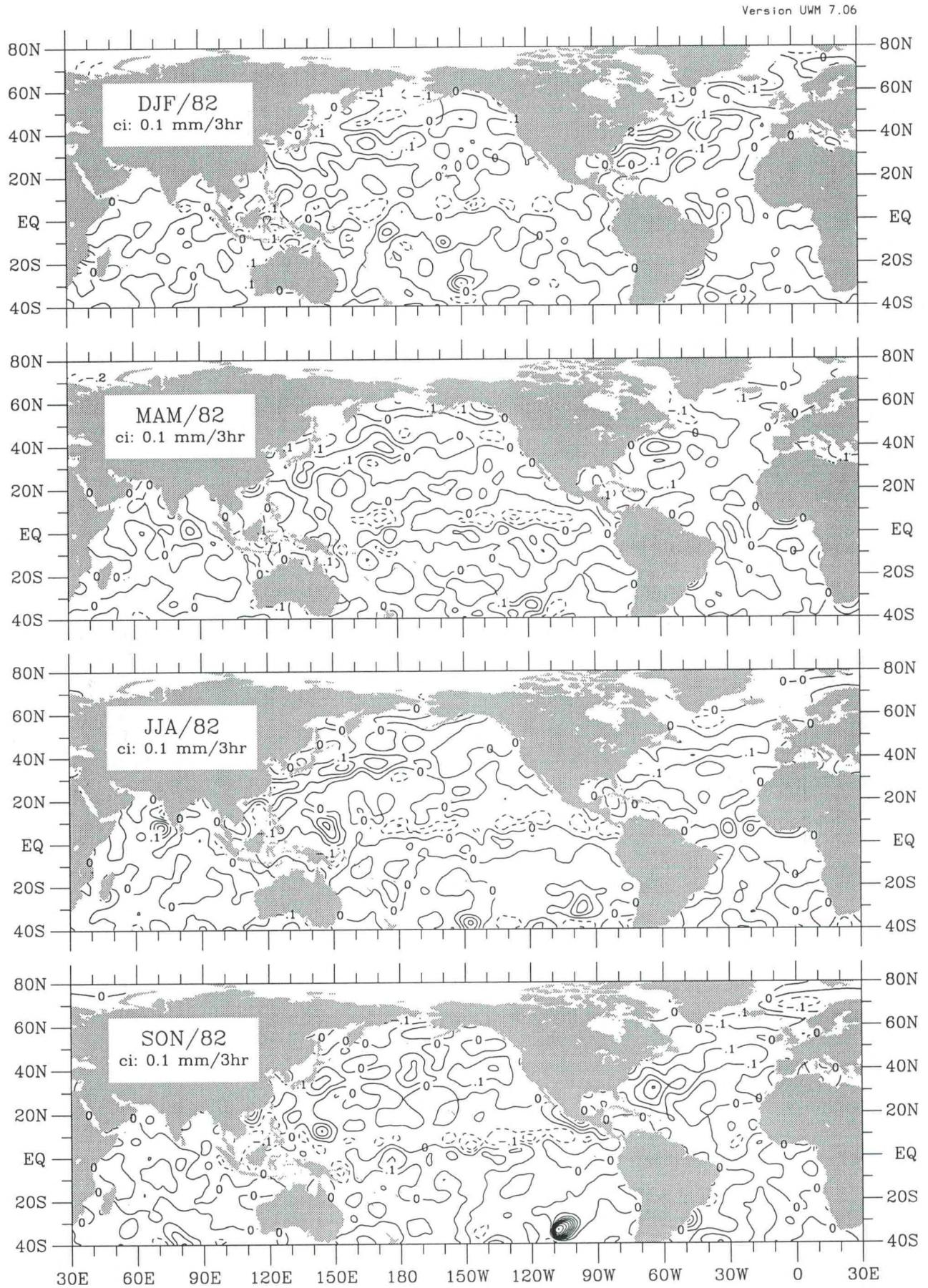

Figure P-43. Precipitation seasonal anomaly for 1982.

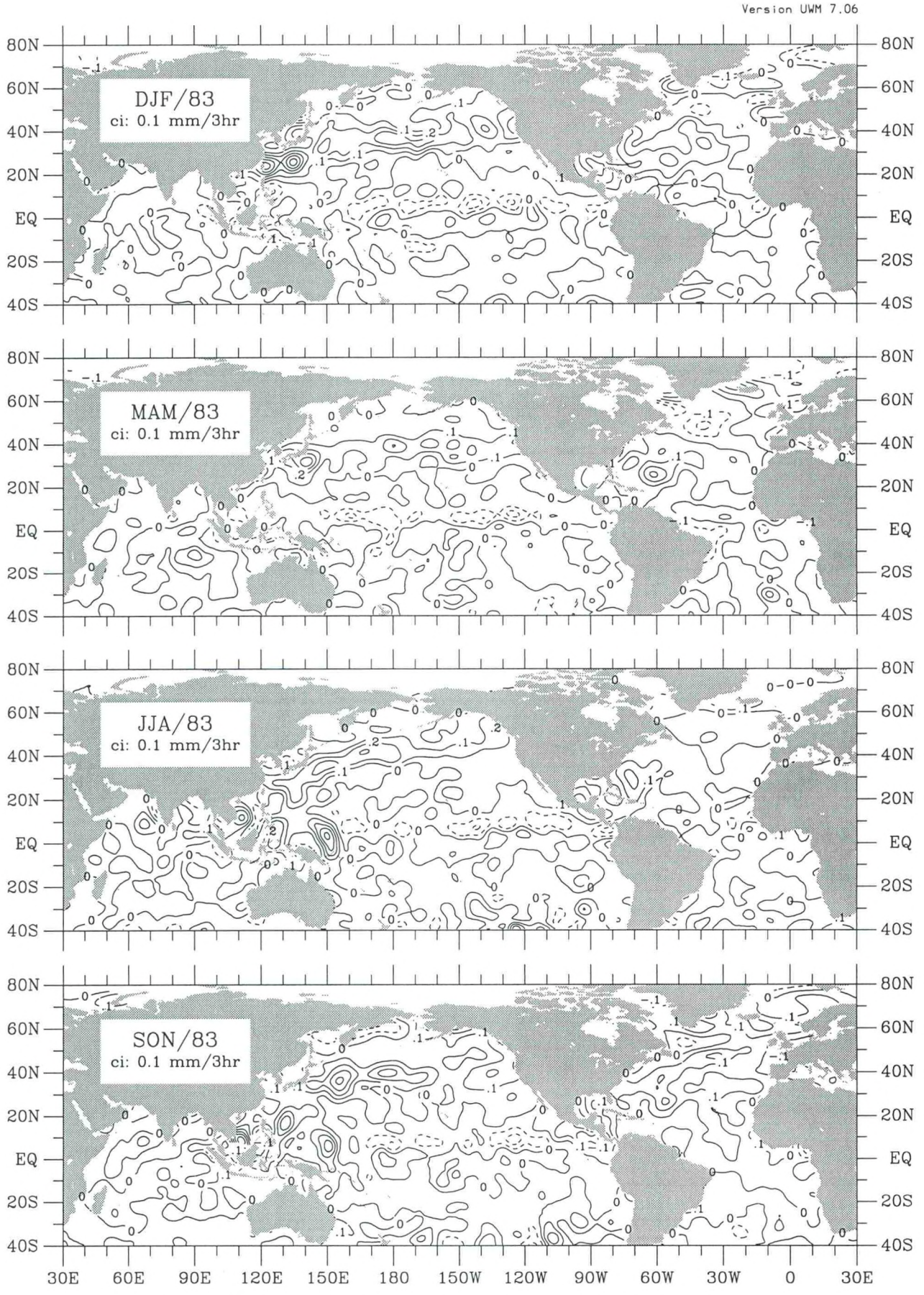

Figure P-44. Precipitation seasonal anomaly for 1983.

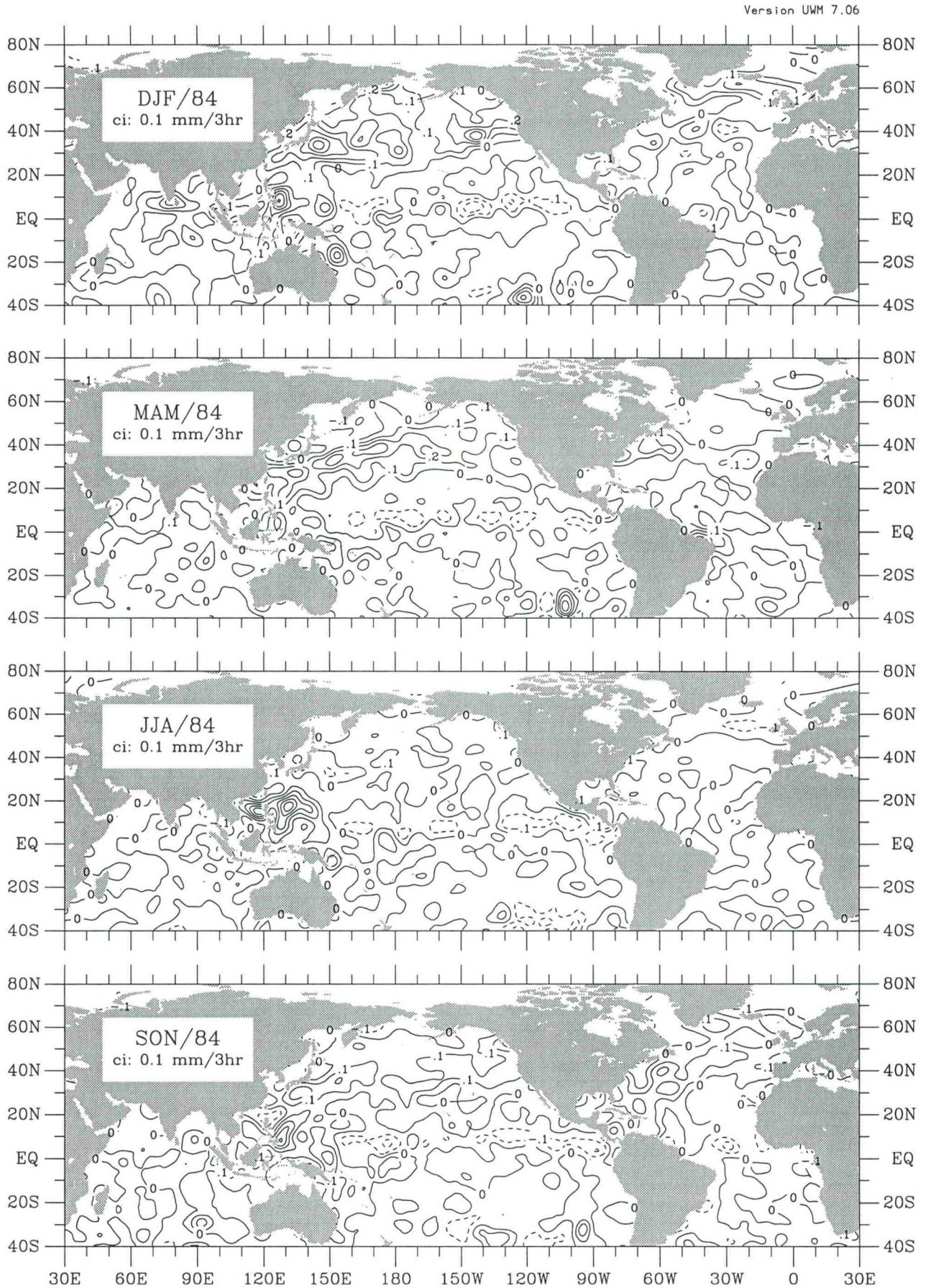

Figure P-45. Precipitation seasonal anomaly for 1984.

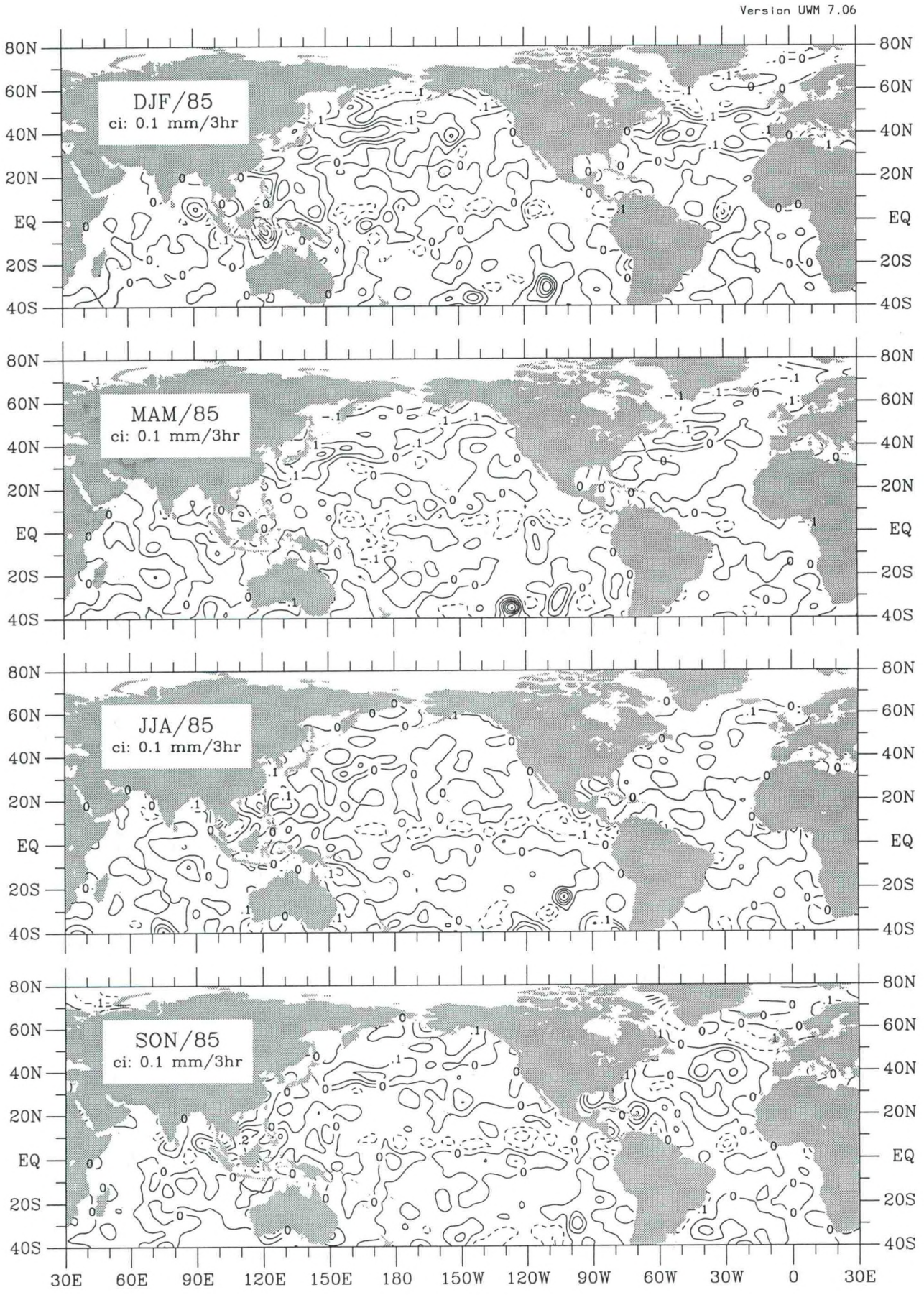

Figure P-46. Precipitation seasonal anomaly for 1985.

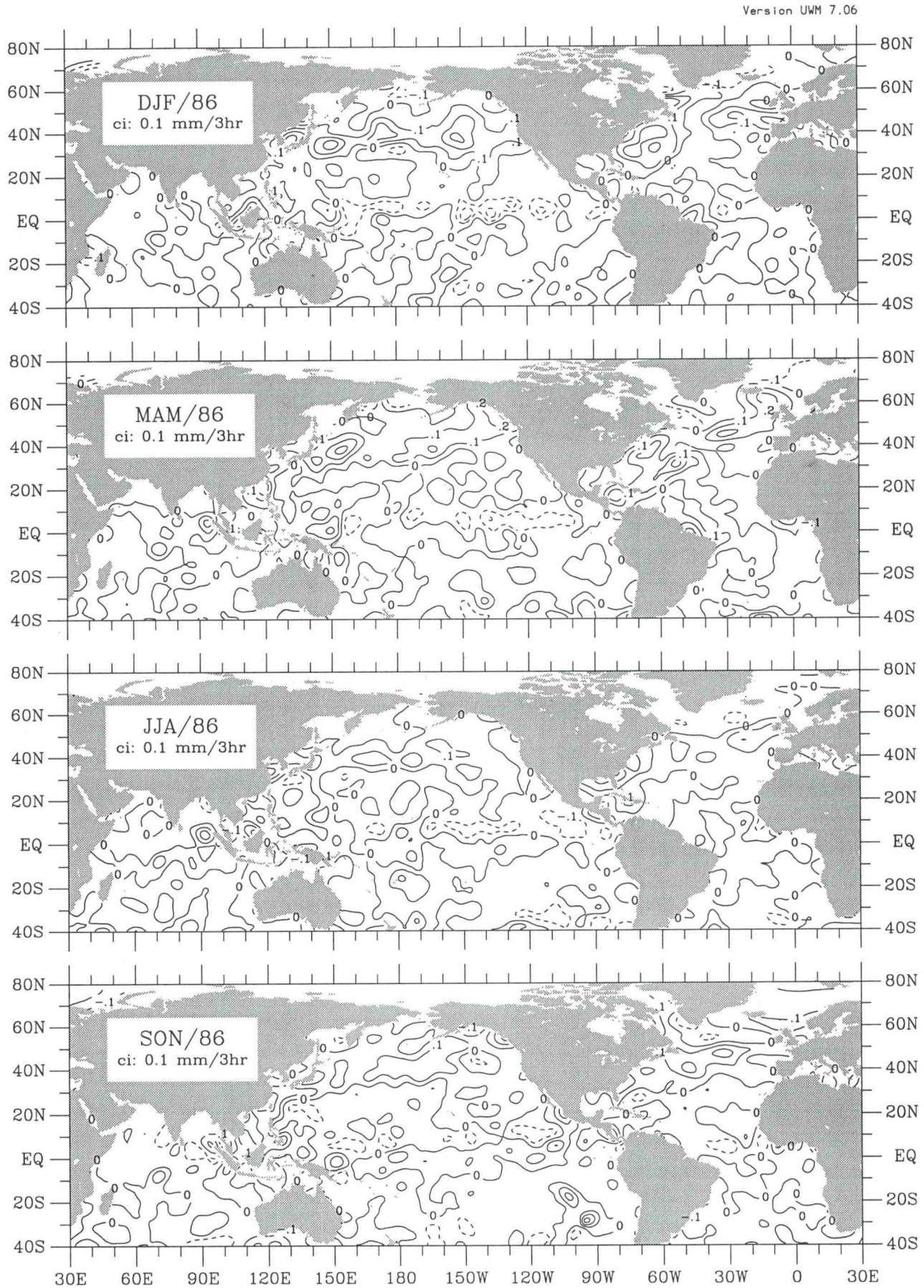

Figure P-47. Precipitation seasonal anomaly for 1986.

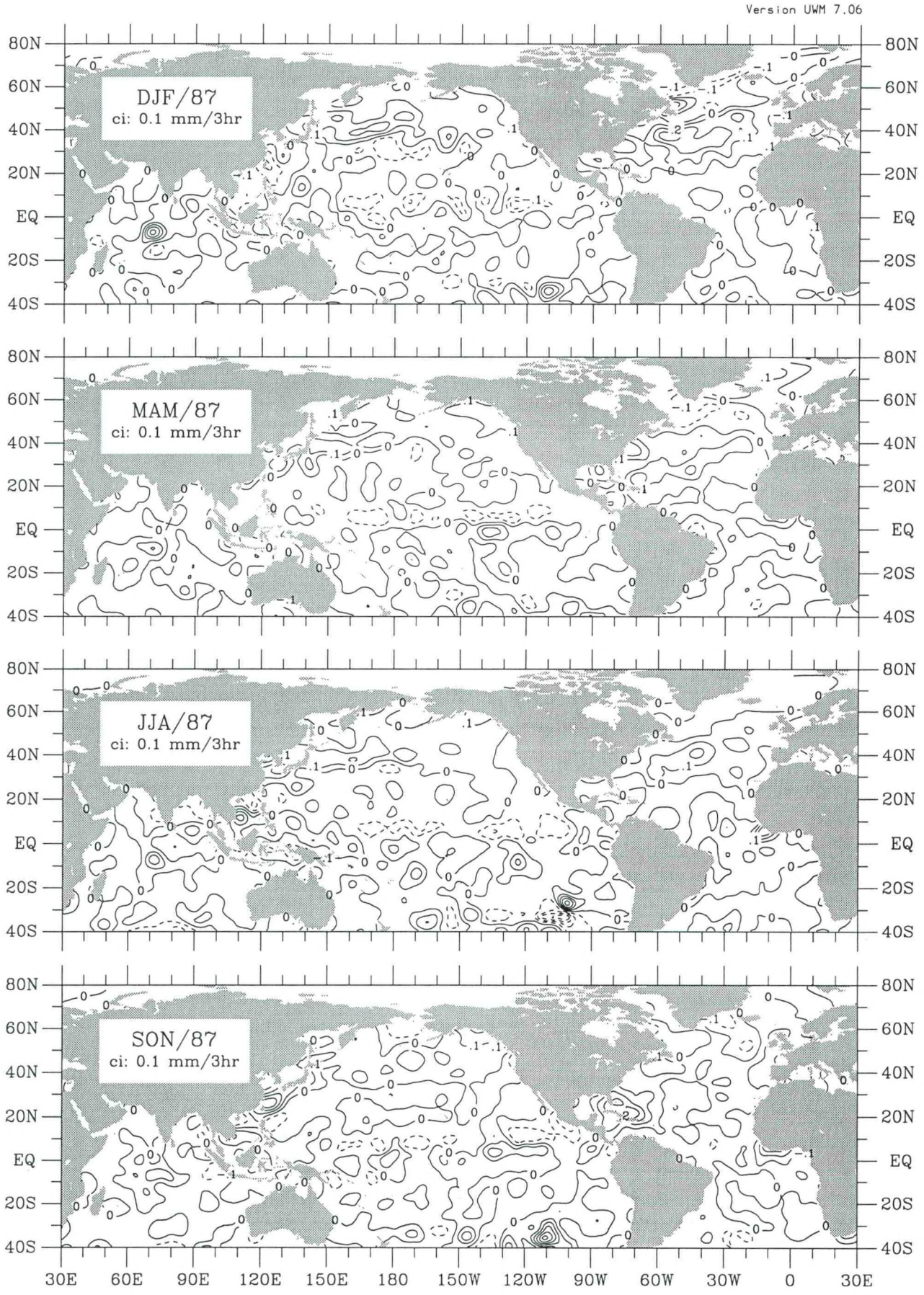

Figure P-48. Precipitation seasonal anomaly for 1987.

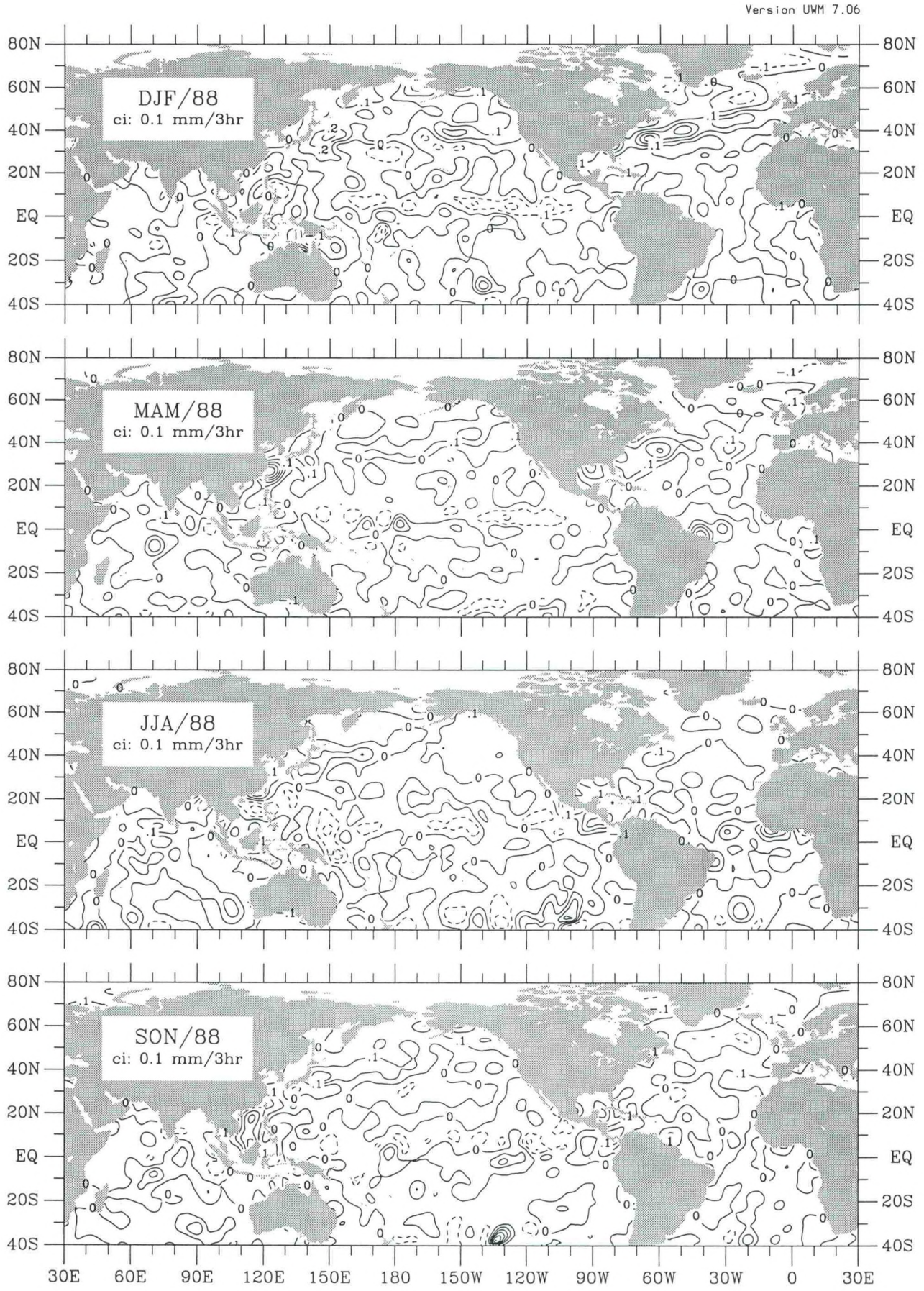

Figure P-49. Precipitation seasonal anomaly for 1988.

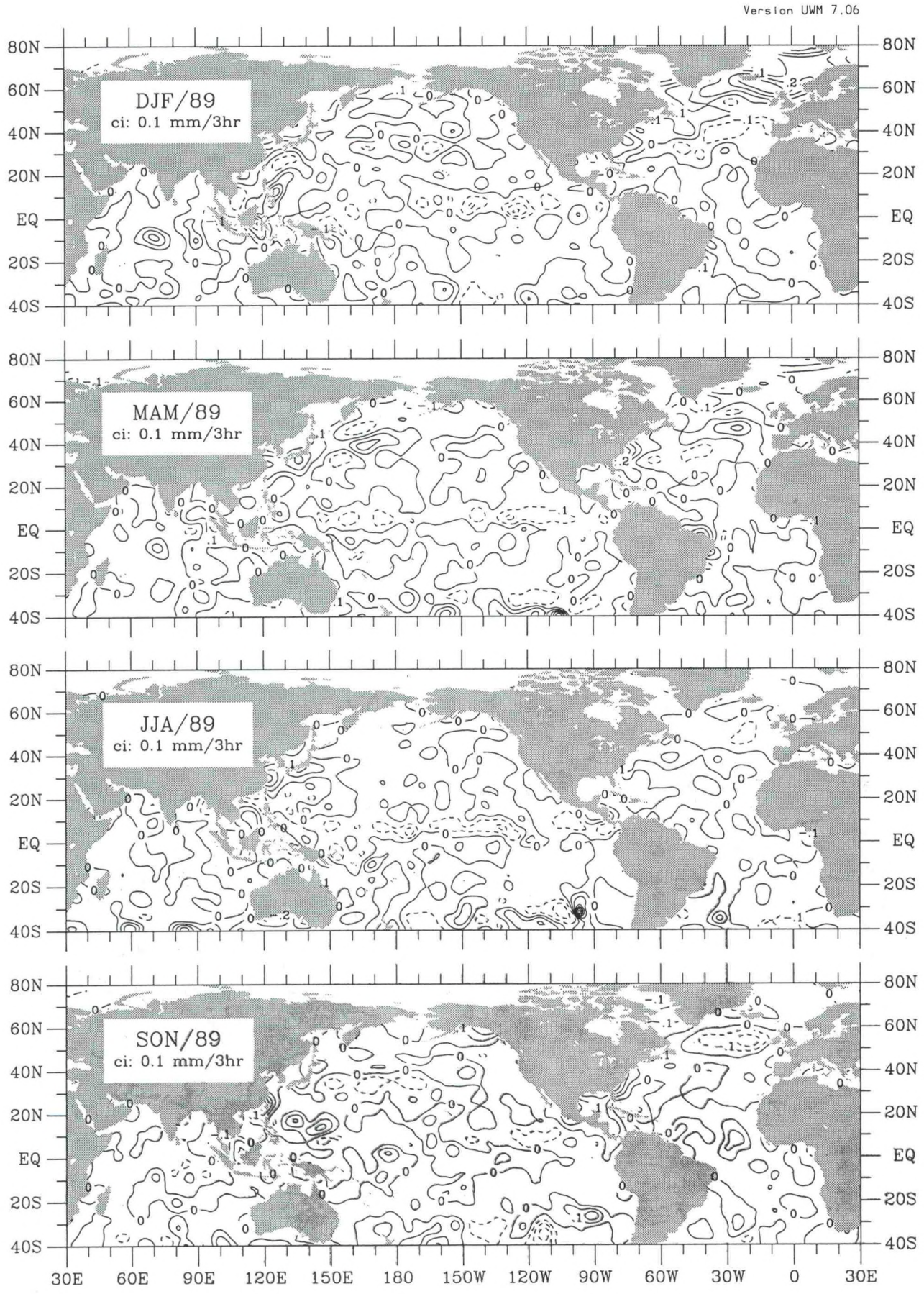

Figure P-50. Precipitation seasonal anomaly for 1989.

13 Constrained E-P rate

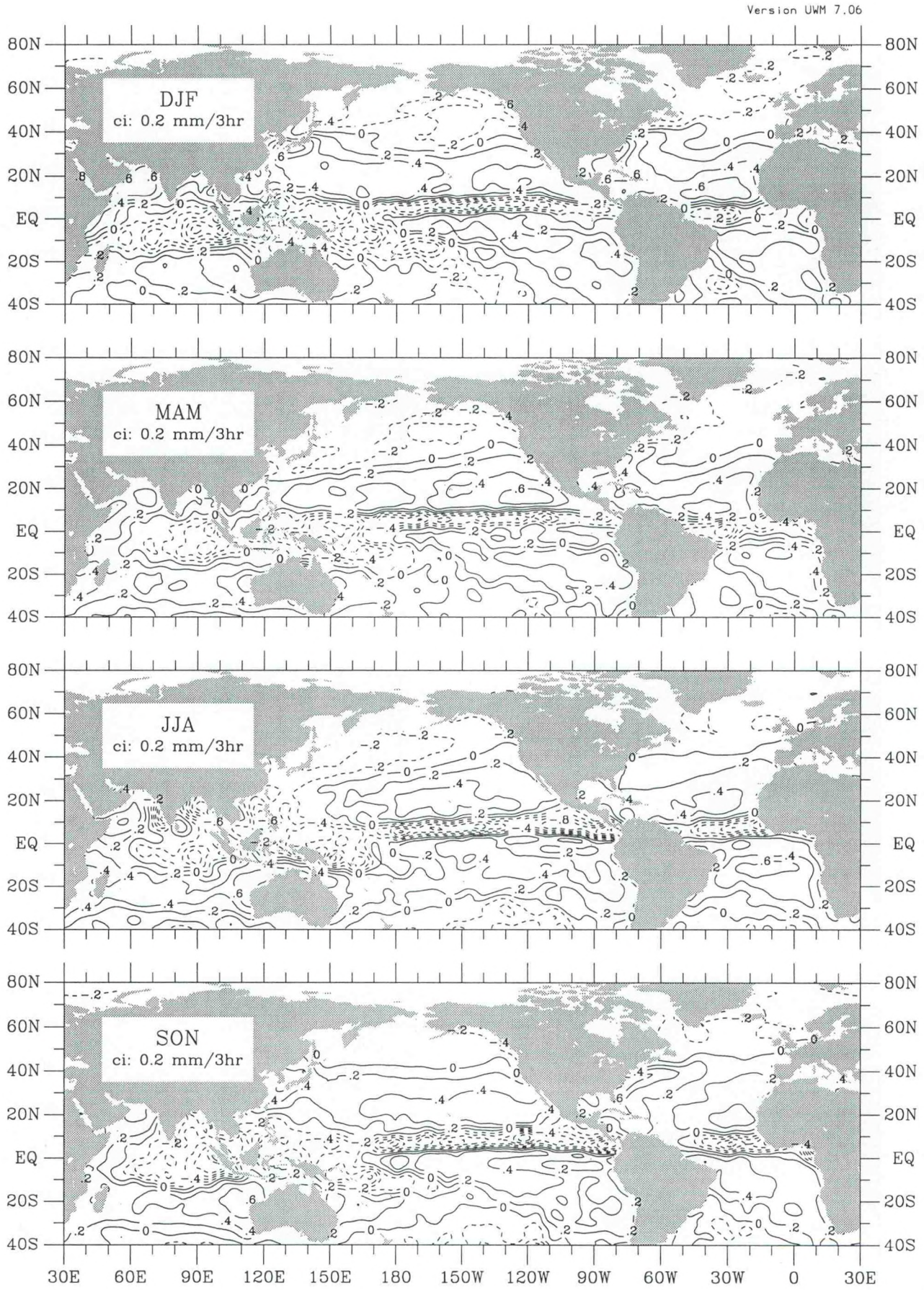

Figure E–P–3. E minus P seasonal climatology (1945–89).

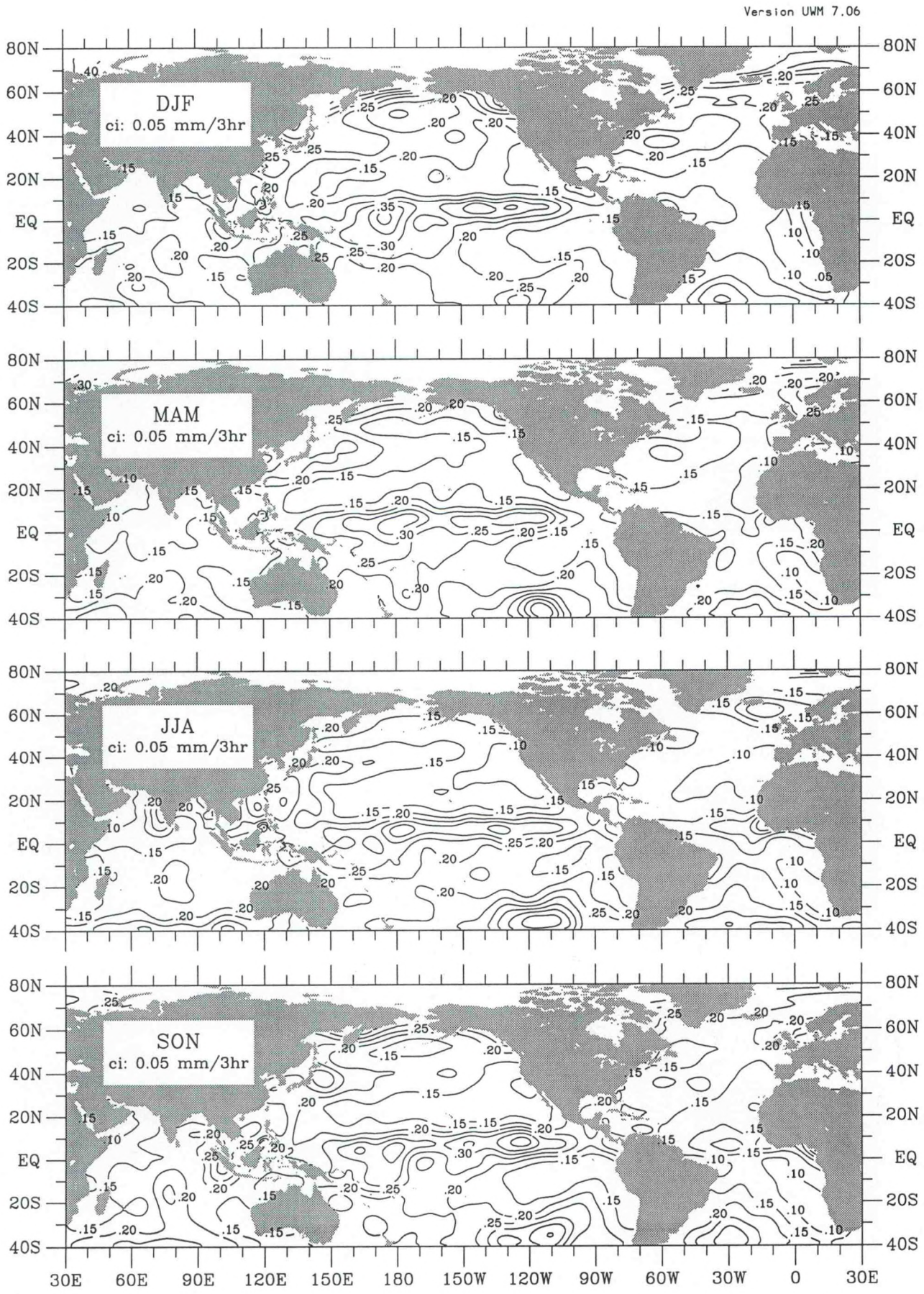

Figure E−P−4. E minus P seasonal interannual std dev (1945−89).

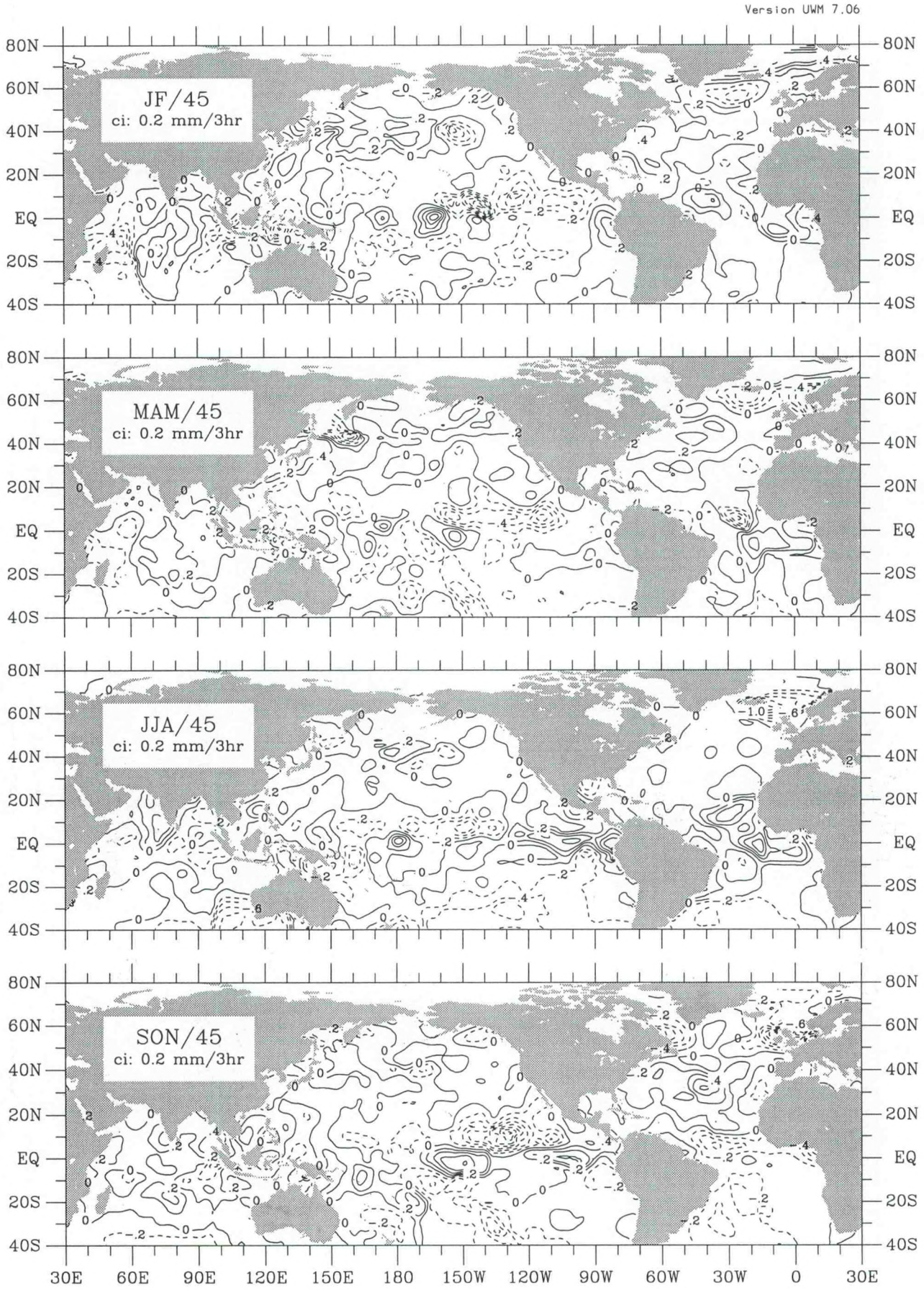

Figure E–P–6. E minus P seasonal anomaly for 1945.

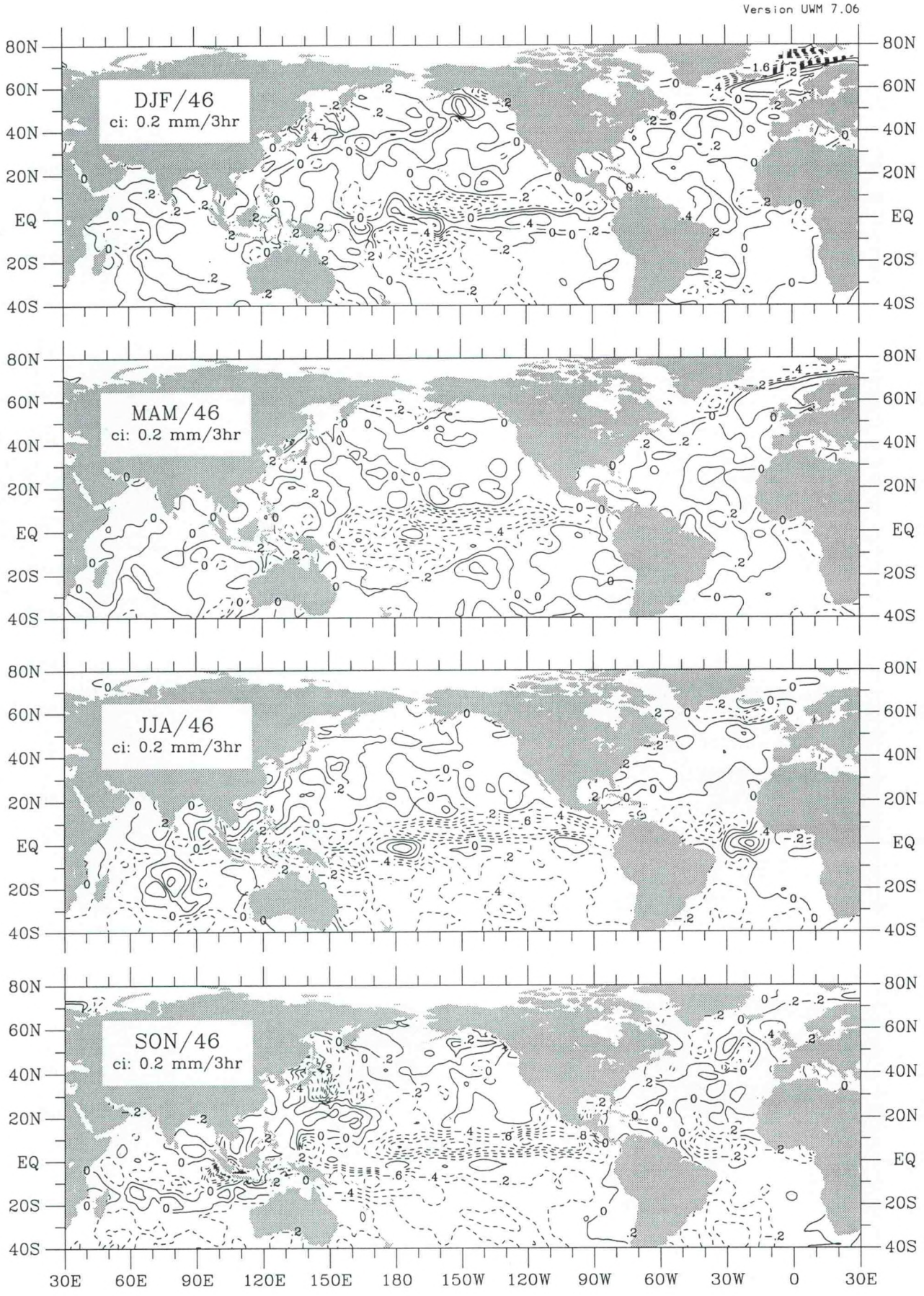

Figure E-P-7. E minus P seasonal anomaly for 1946.

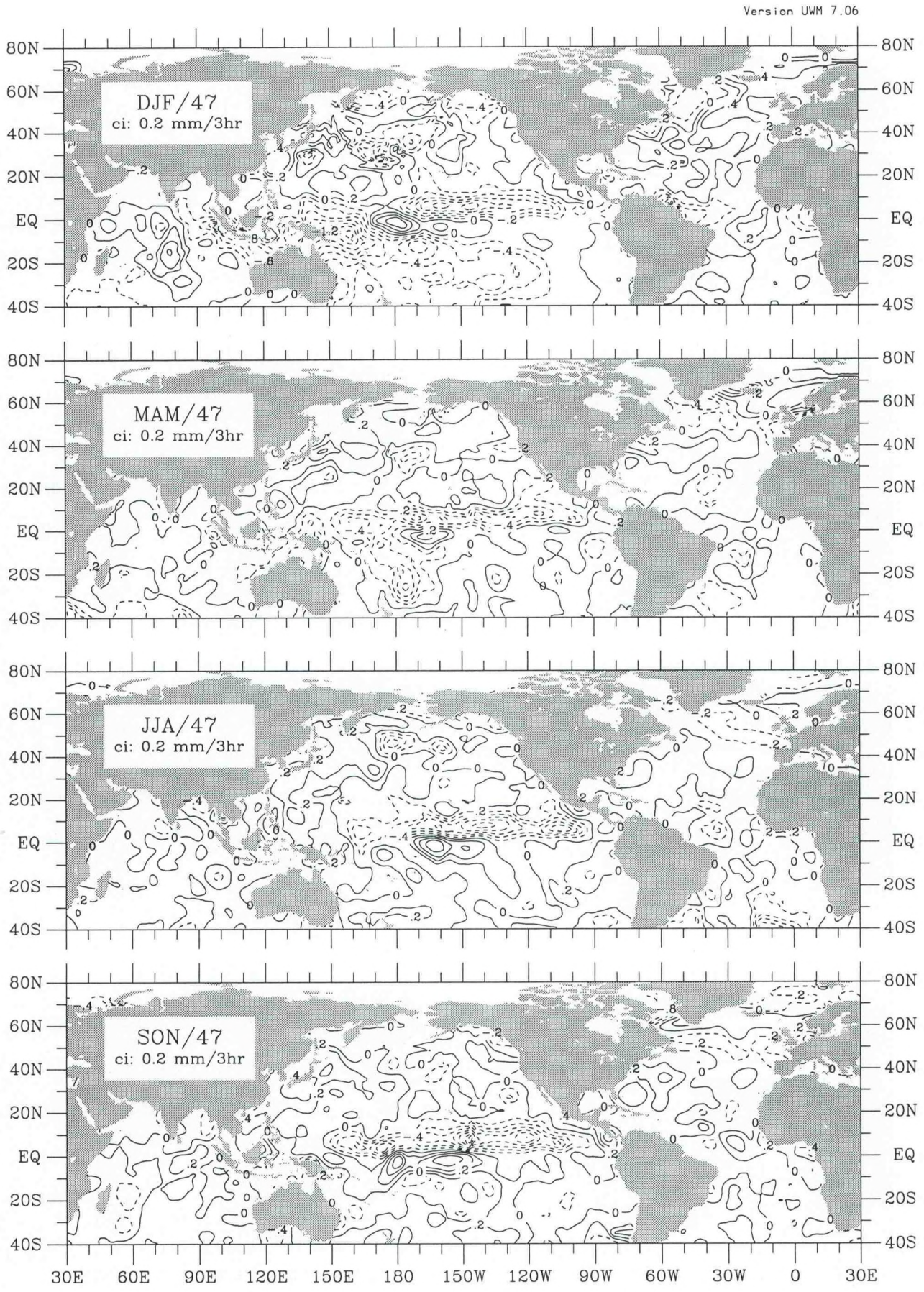

Figure E-P-8. E minus P seasonal anomaly for 1947.

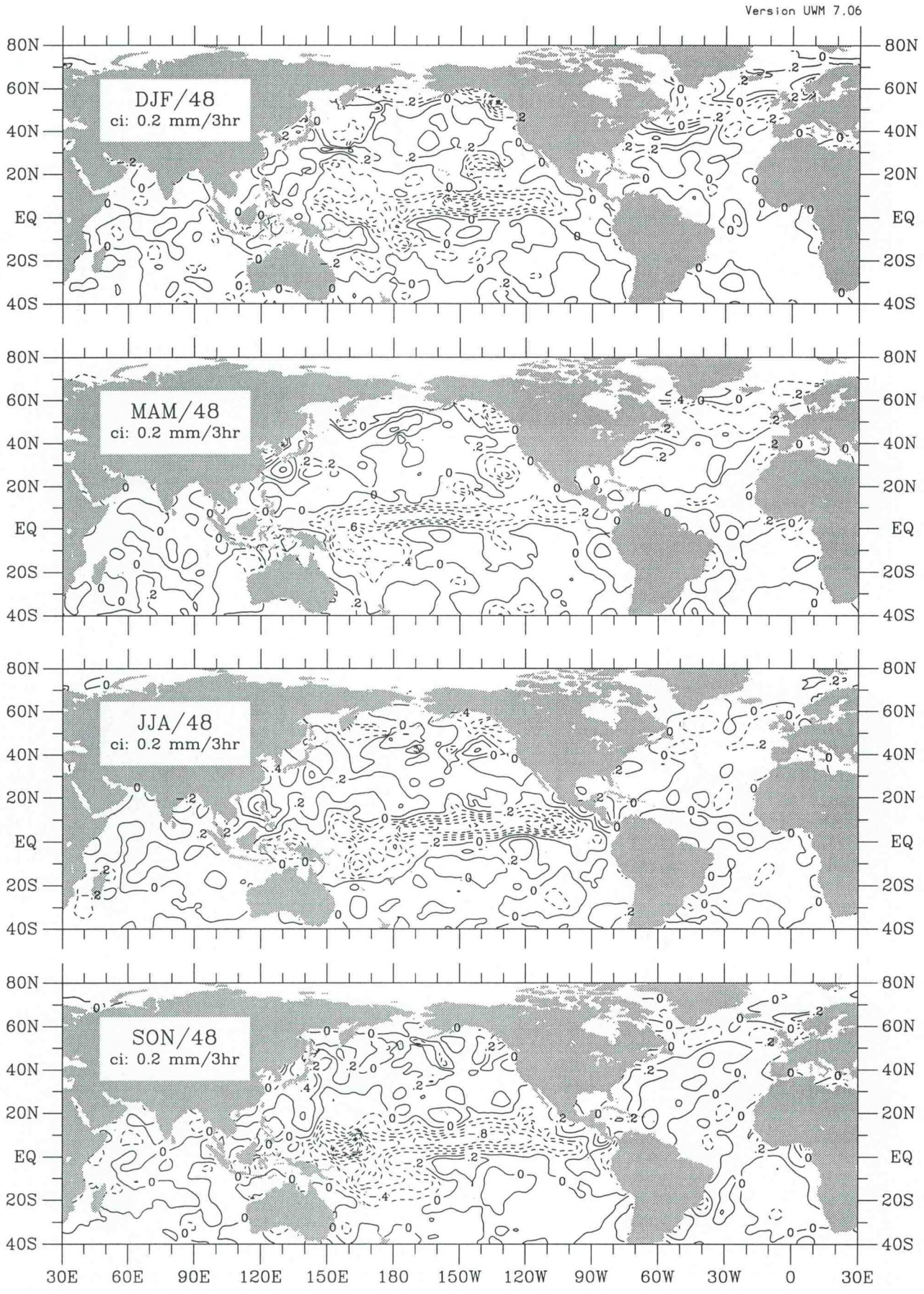

Figure E-P-9. E minus P seasonal anomaly for 1948.

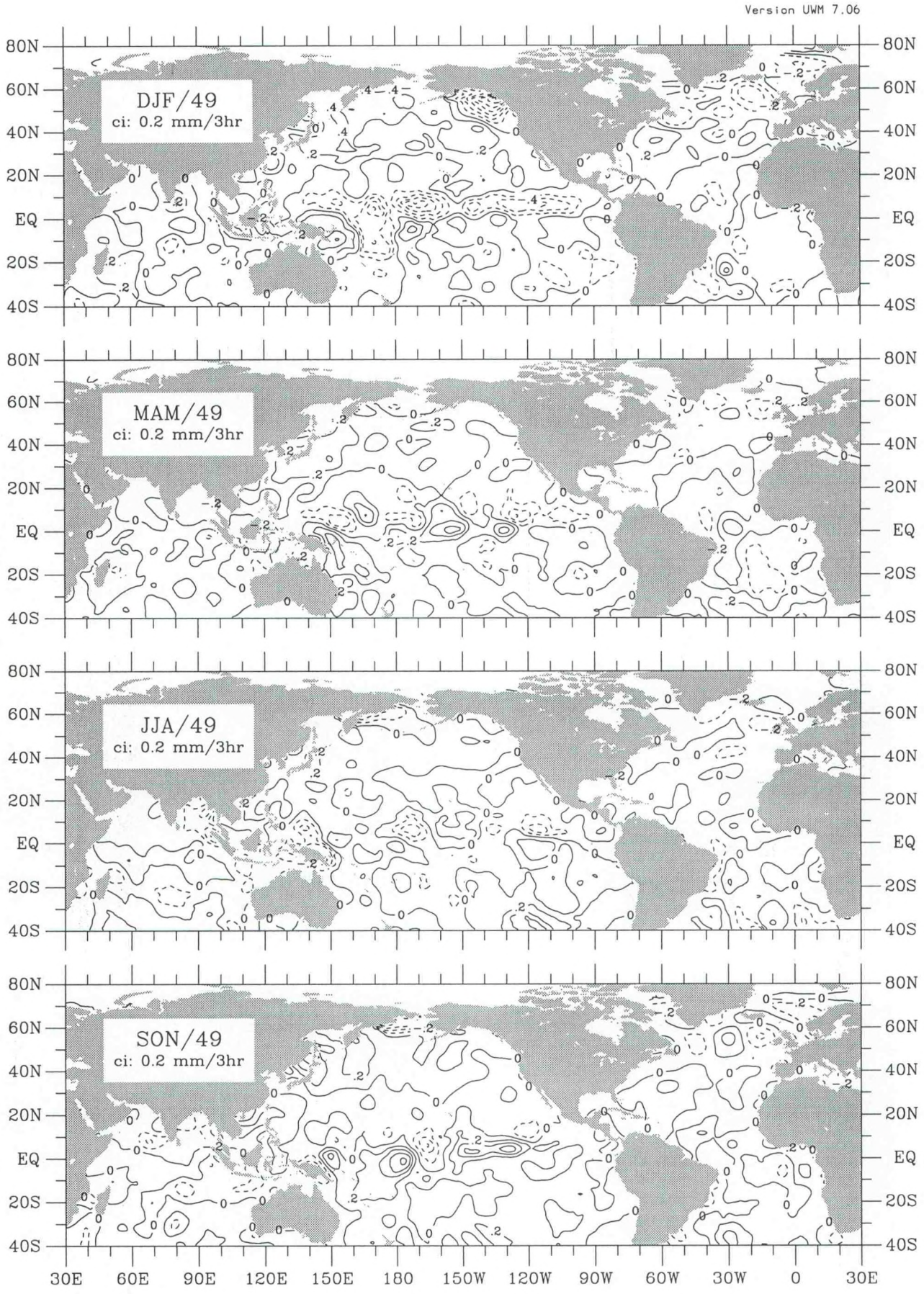

Figure E-P-10. E minus P seasonal anomaly for 1949.

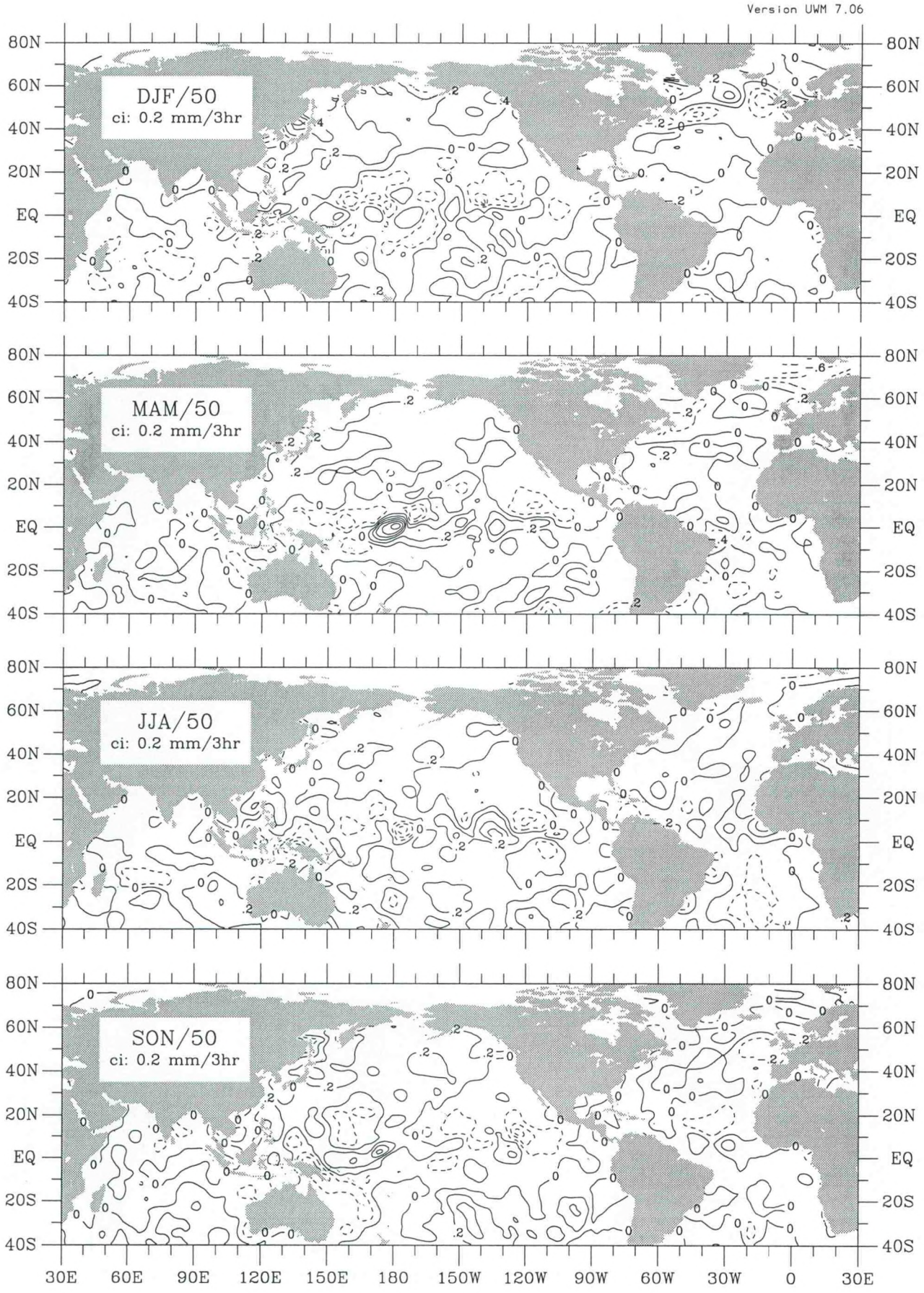

Figure E-P-11. E minus P seasonal anomaly for 1950.

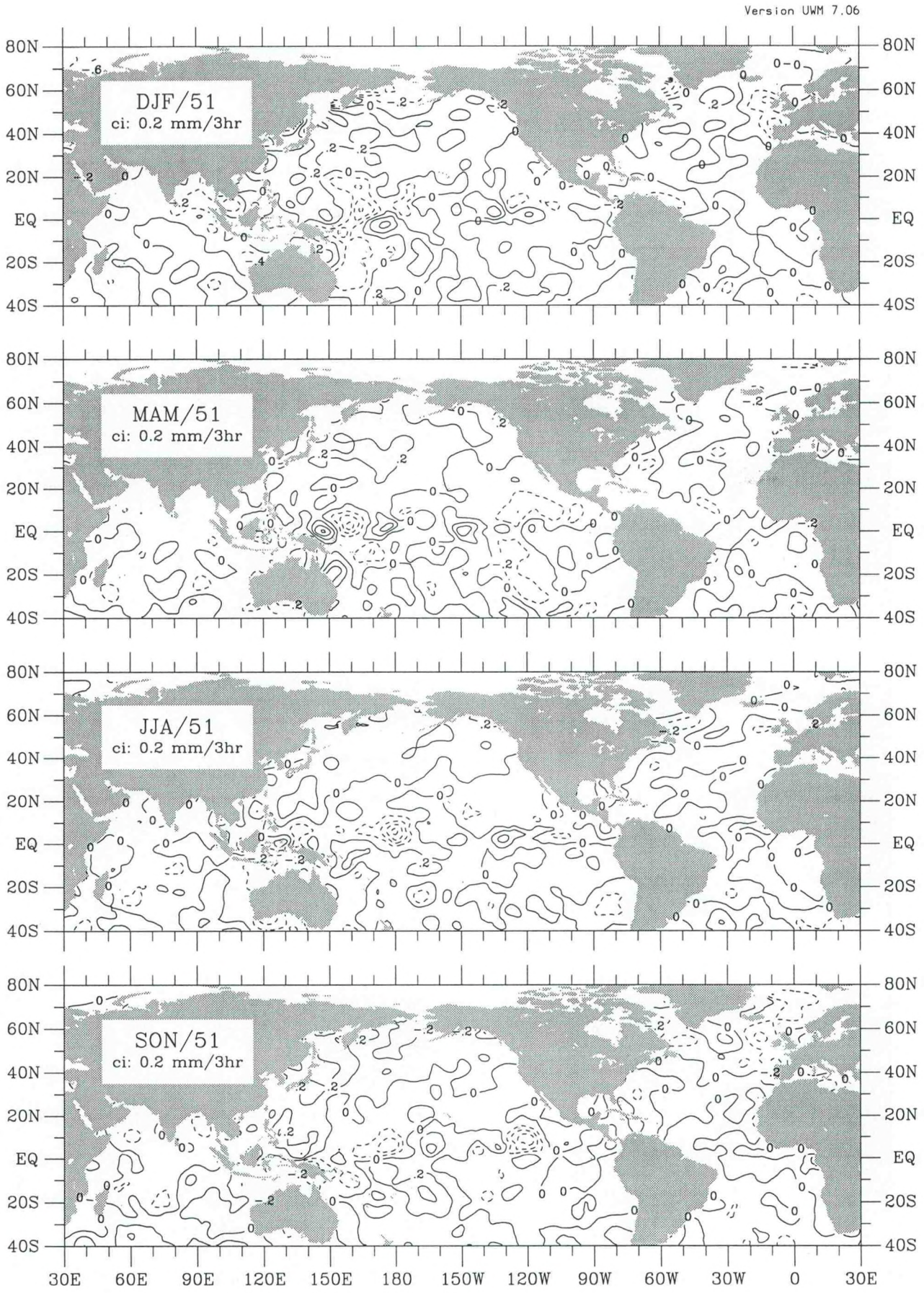

Figure E-P-12. E minus P seasonal anomaly for 1951.

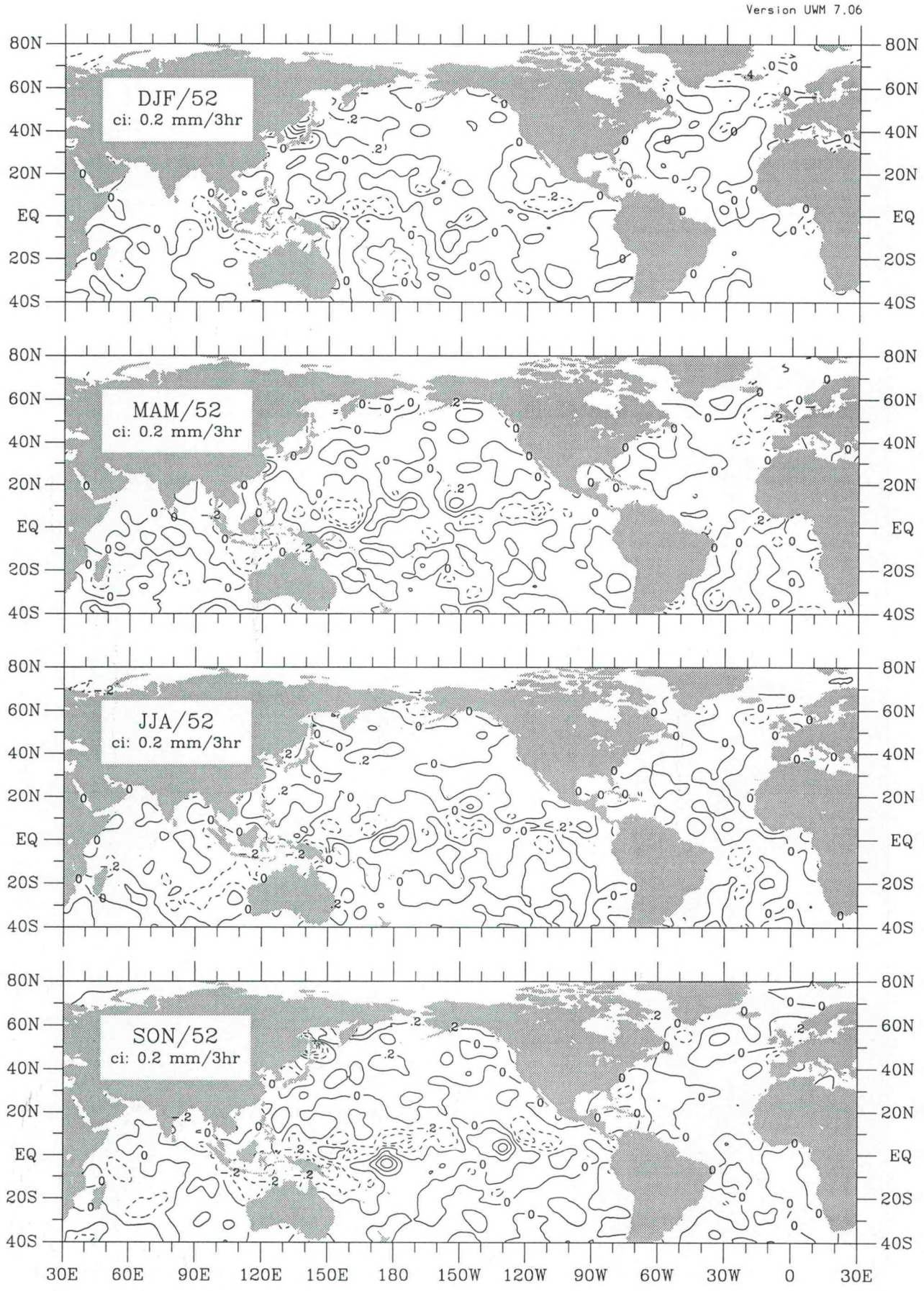

Figure E−P−13. E minus P seasonal anomaly for 1952.

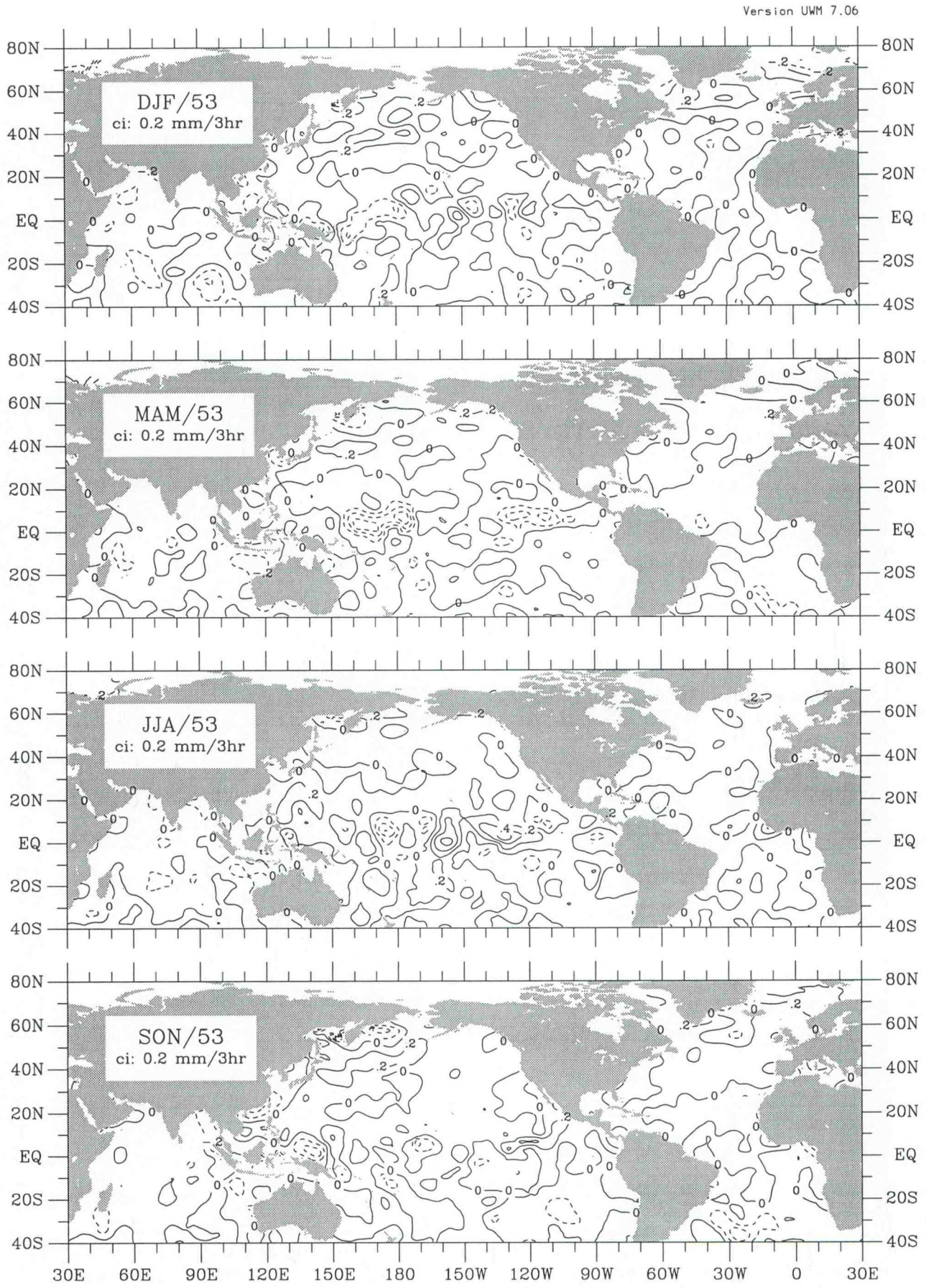

Figure E–P–14. E minus P seasonal anomaly for 1953.

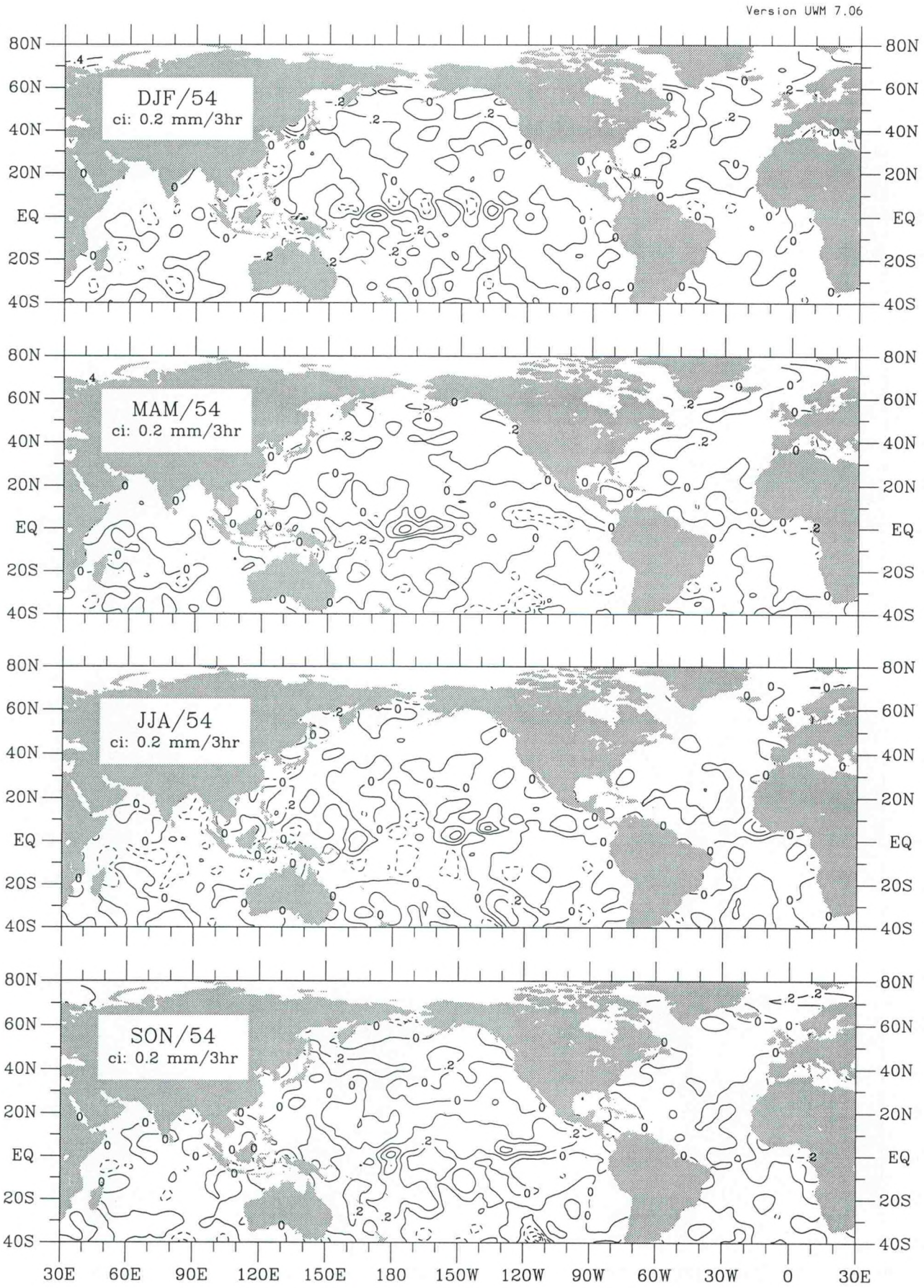

Figure E-P-15. E minus P seasonal anomaly for 1954.

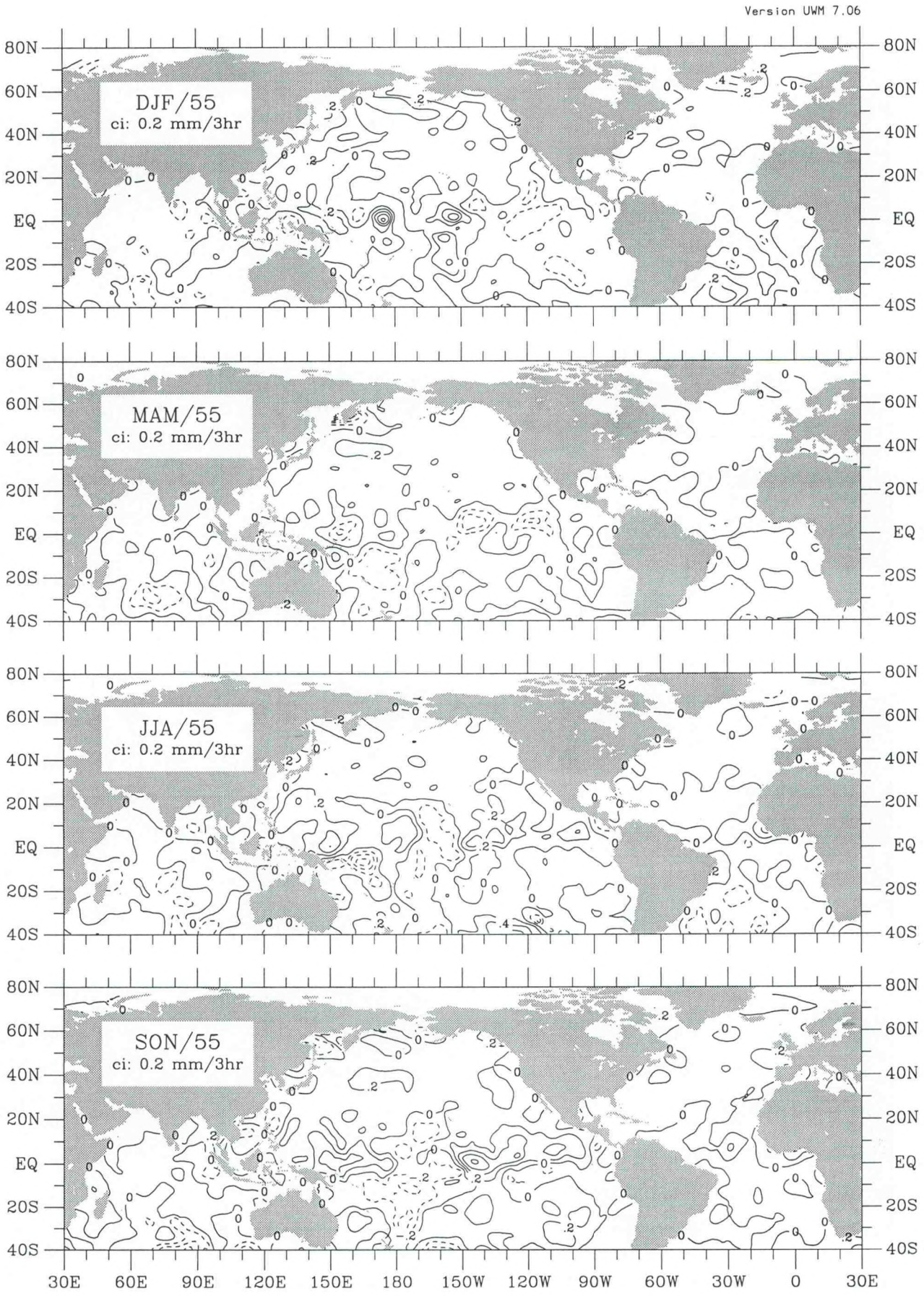

Figure E-P-16. E minus P seasonal anomaly for 1955.

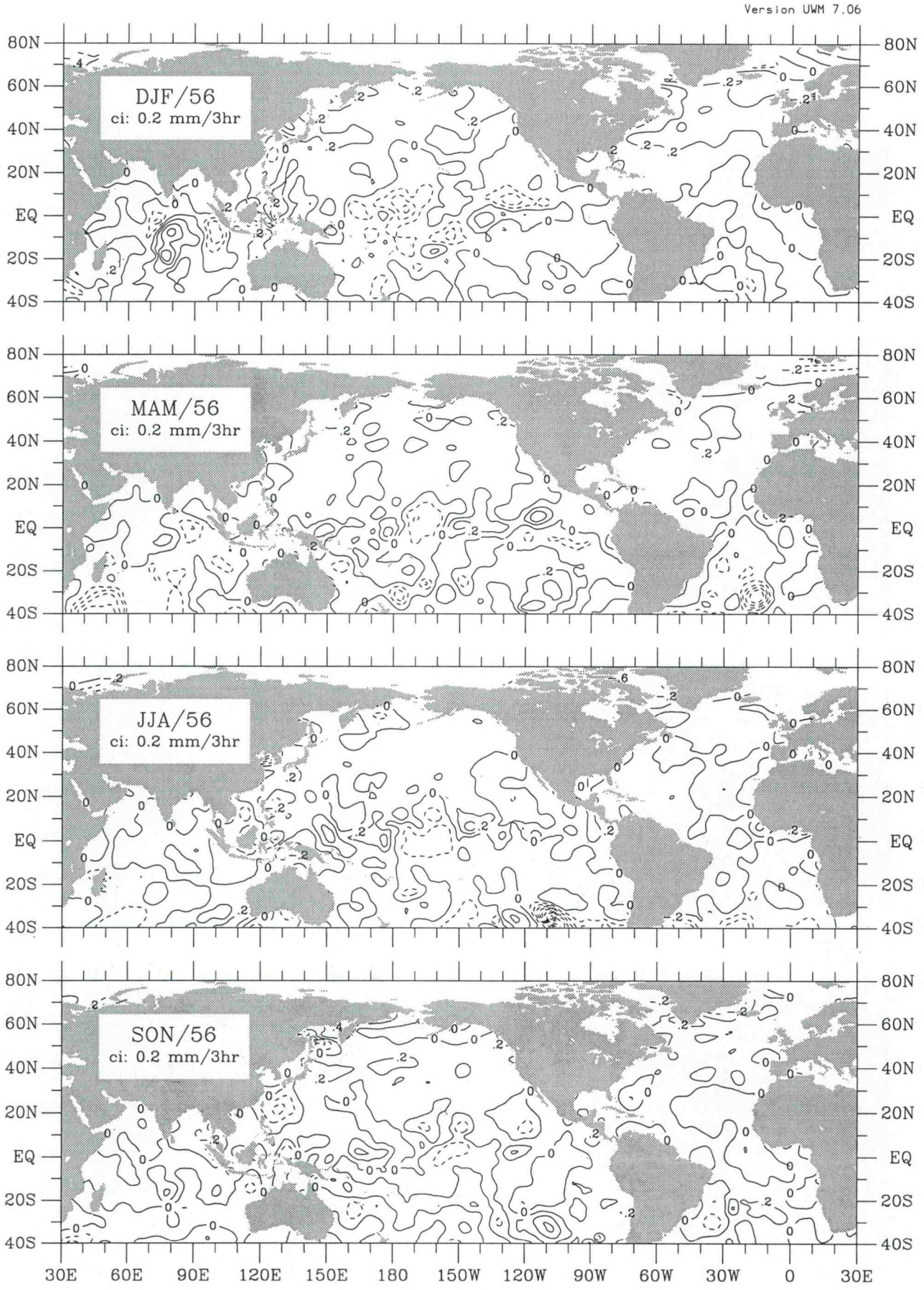

Figure E-P-17. E minus P seasonal anomaly for 1956.

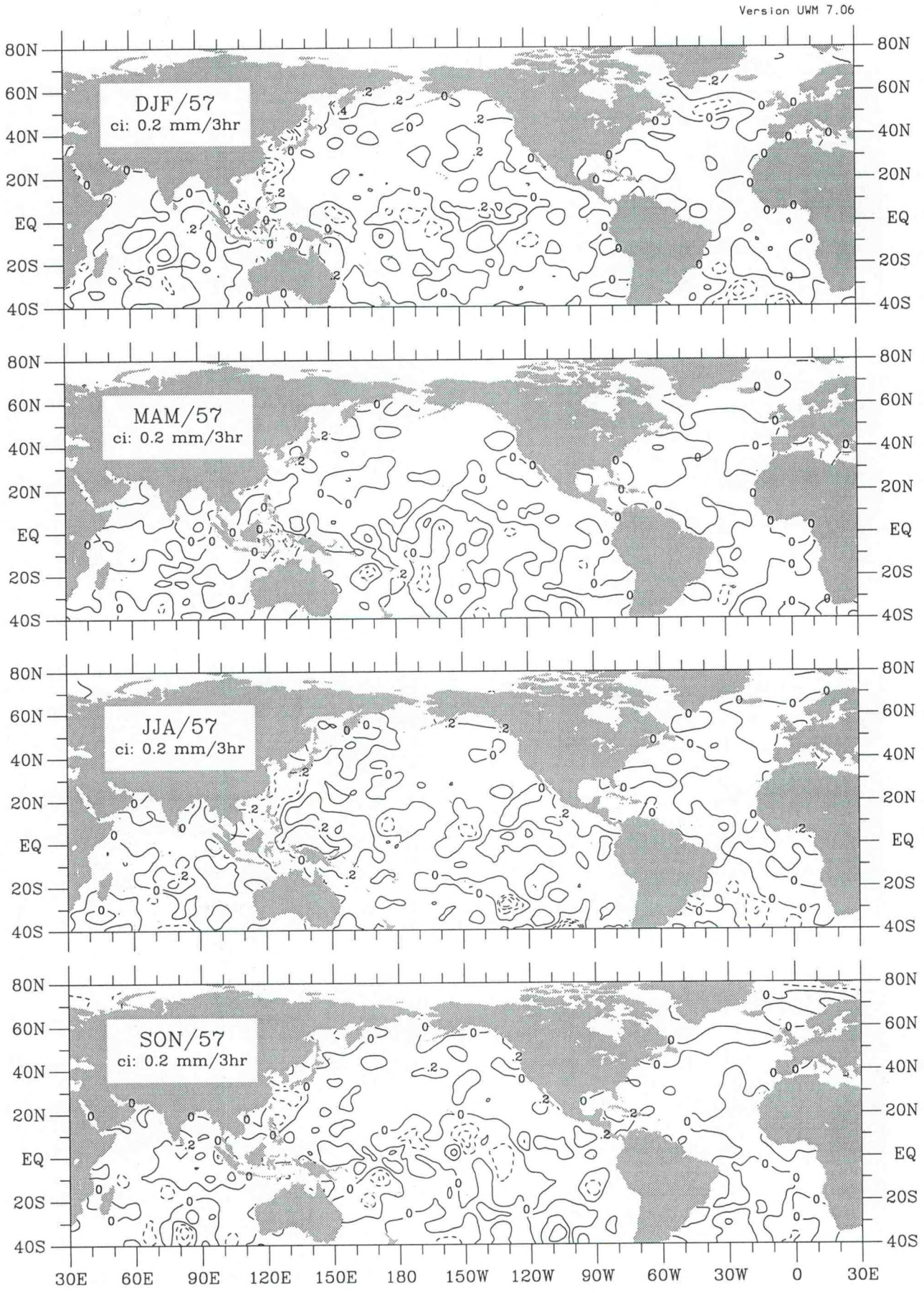

Figure E–P–18. E minus P seasonal anomaly for 1957.

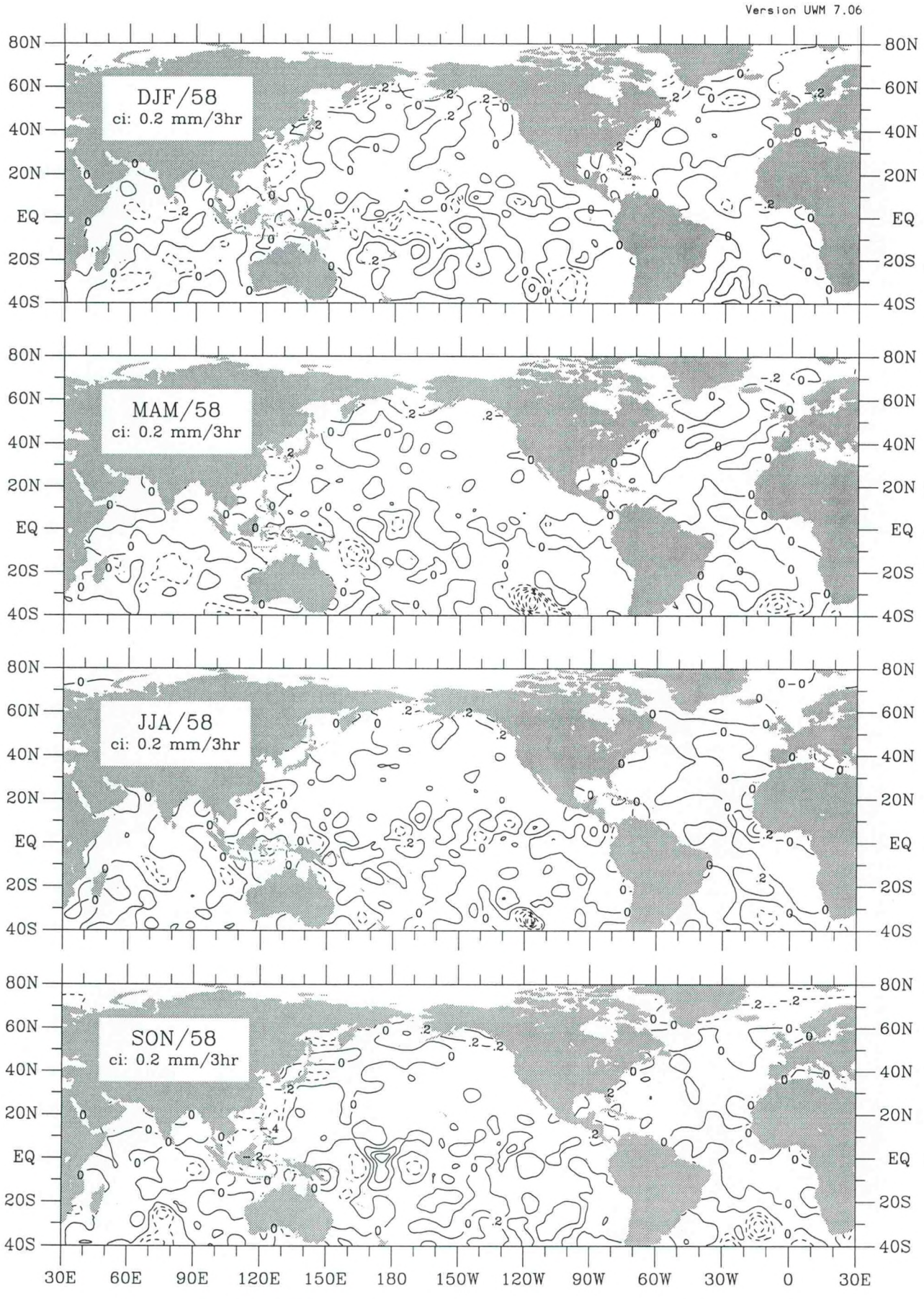

Figure E−P−19. E minus P seasonal anomaly for 1958.

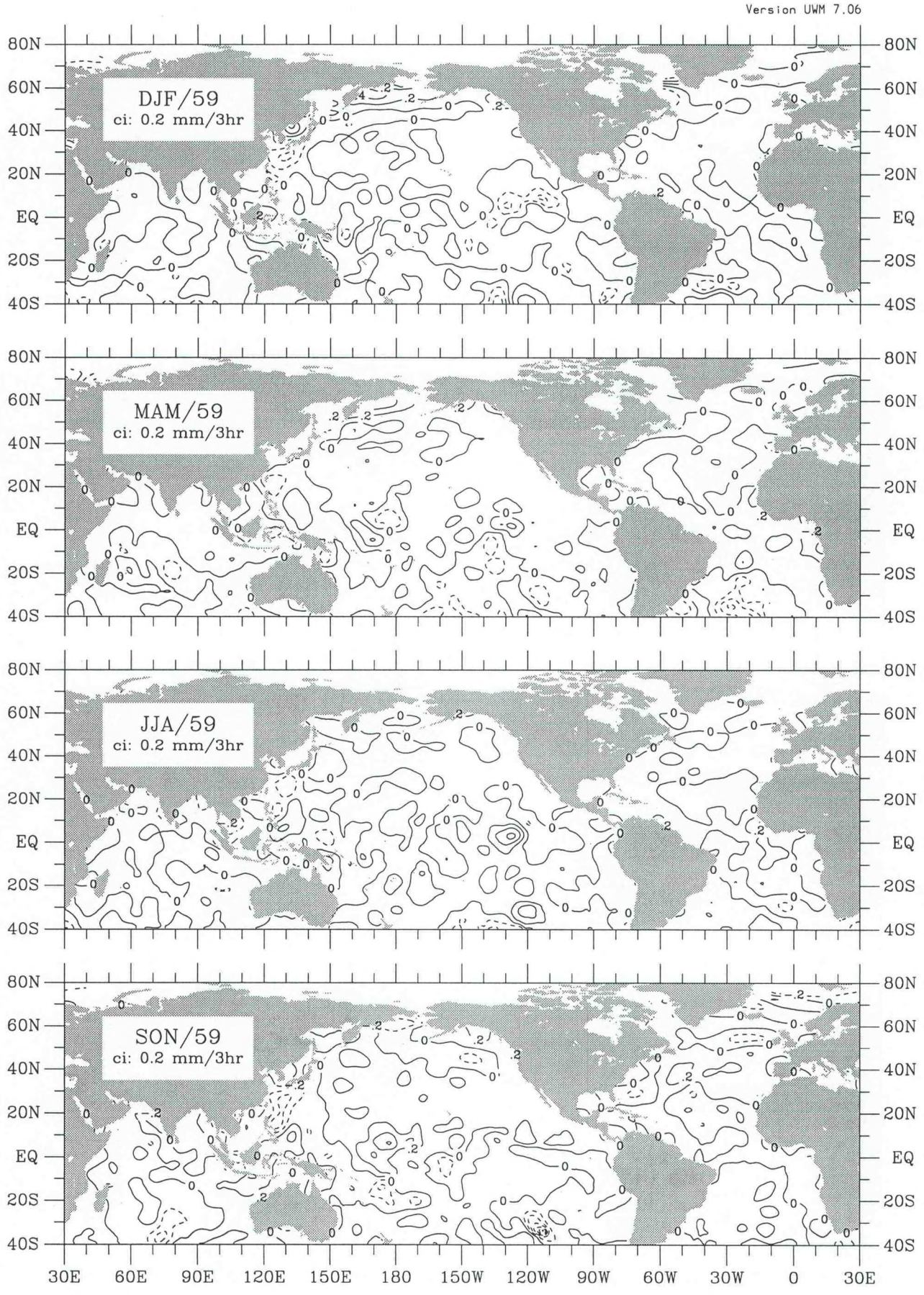

Figure E-P-20. E minus P seasonal anomaly for 1959.

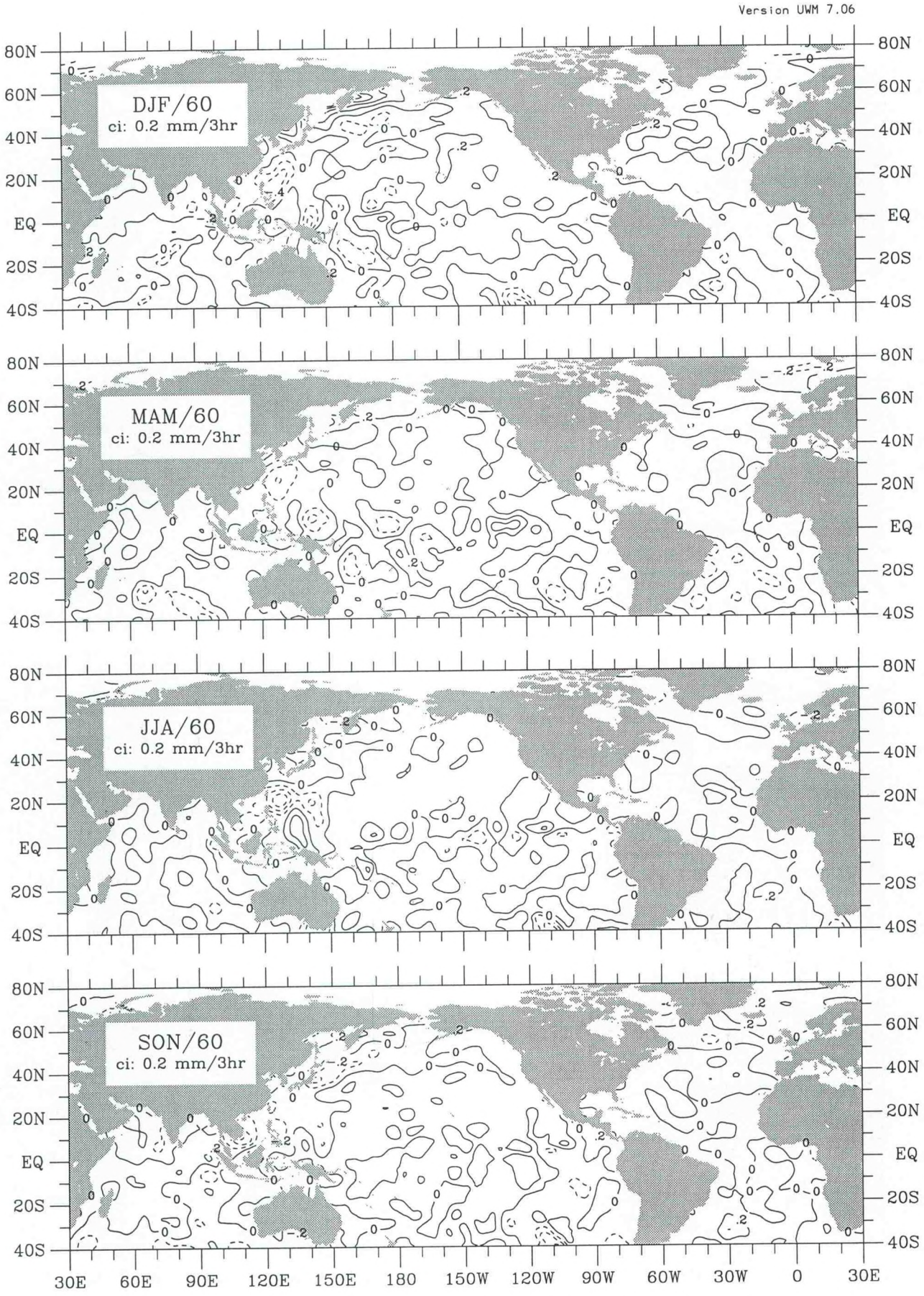

Figure E–P–21. E minus P seasonal anomaly for 1960.

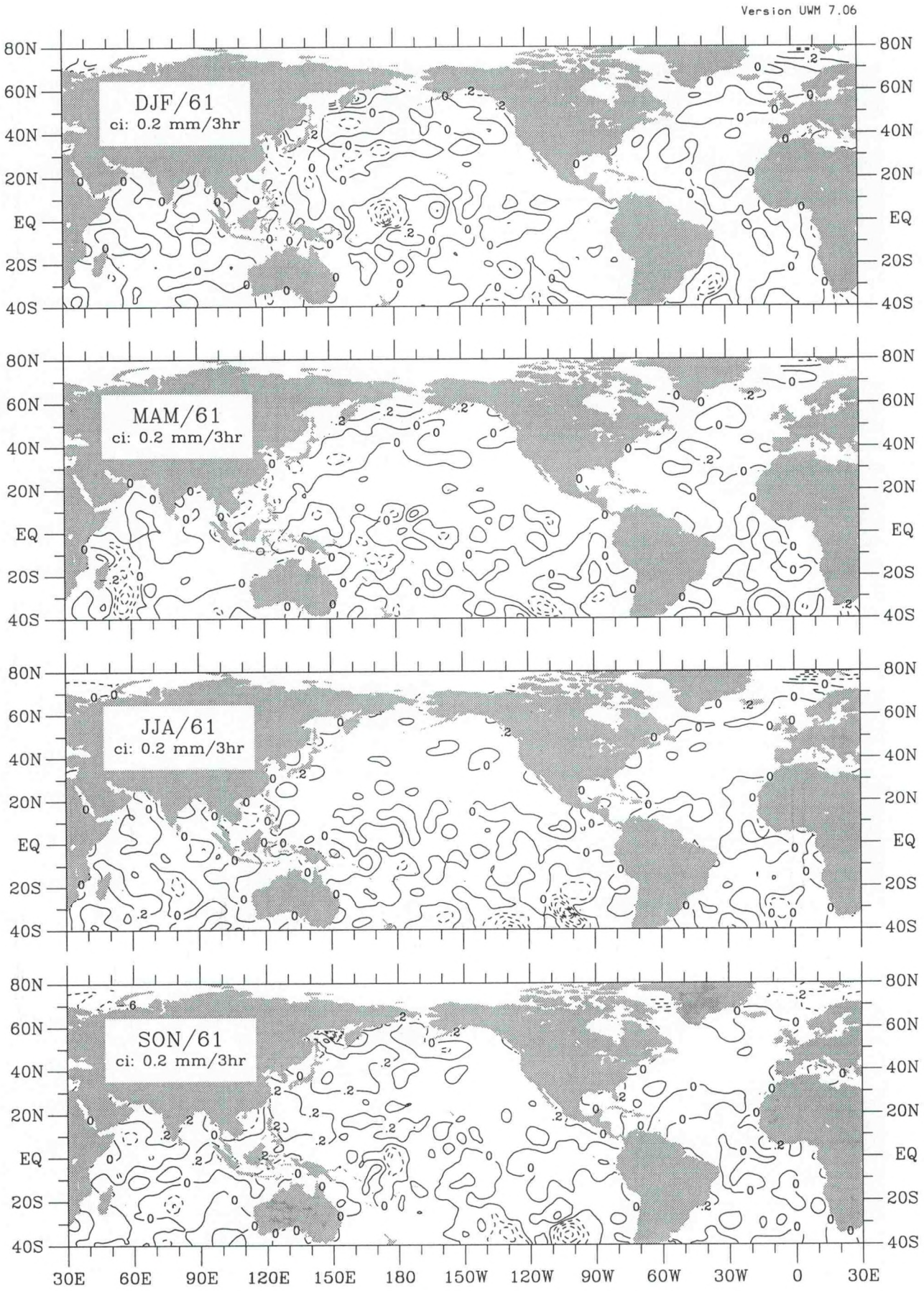

Figure E-P-22. E minus P seasonal anomaly for 1961.

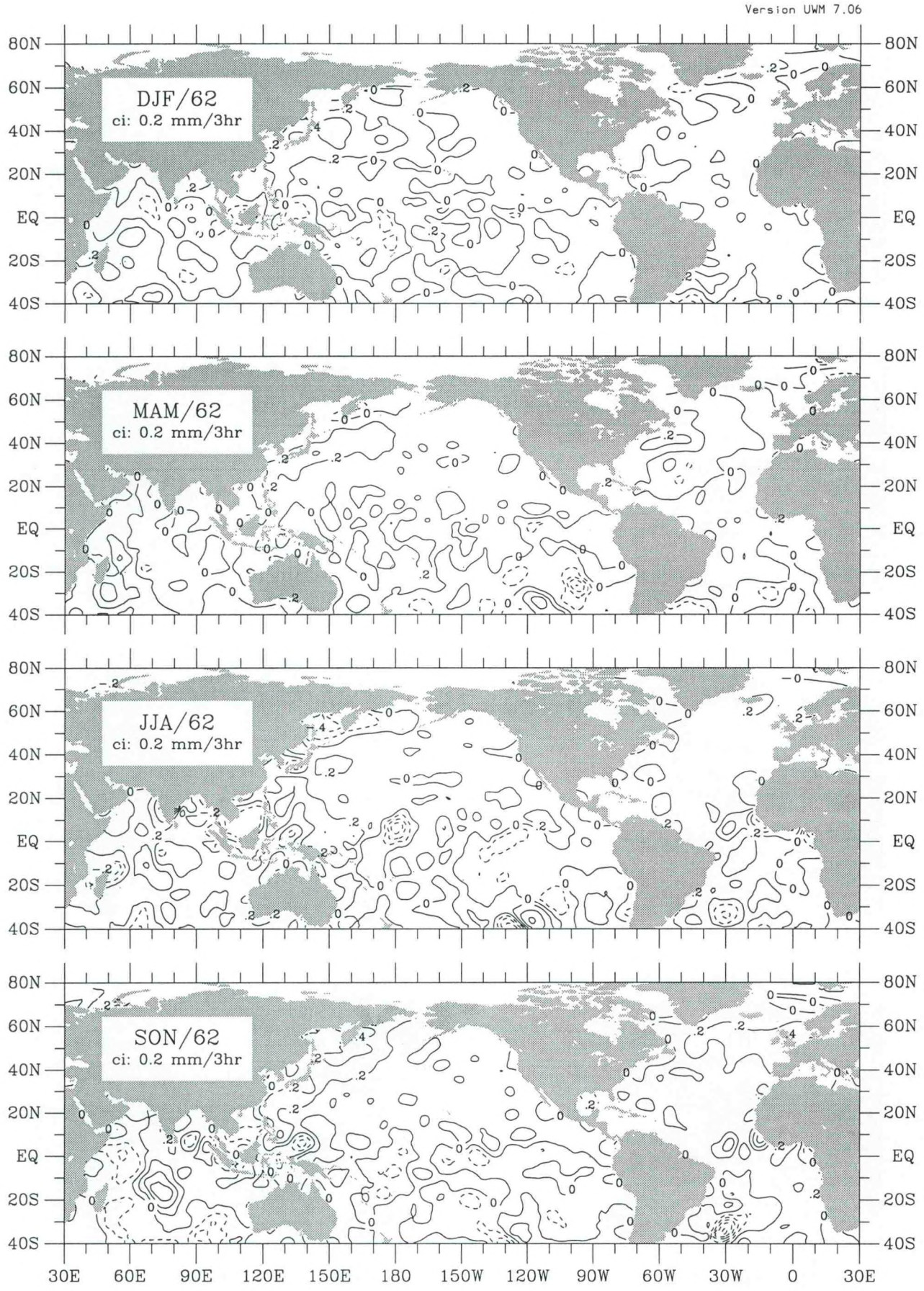

Figure E-P-23. E minus P seasonal anomaly for 1962.

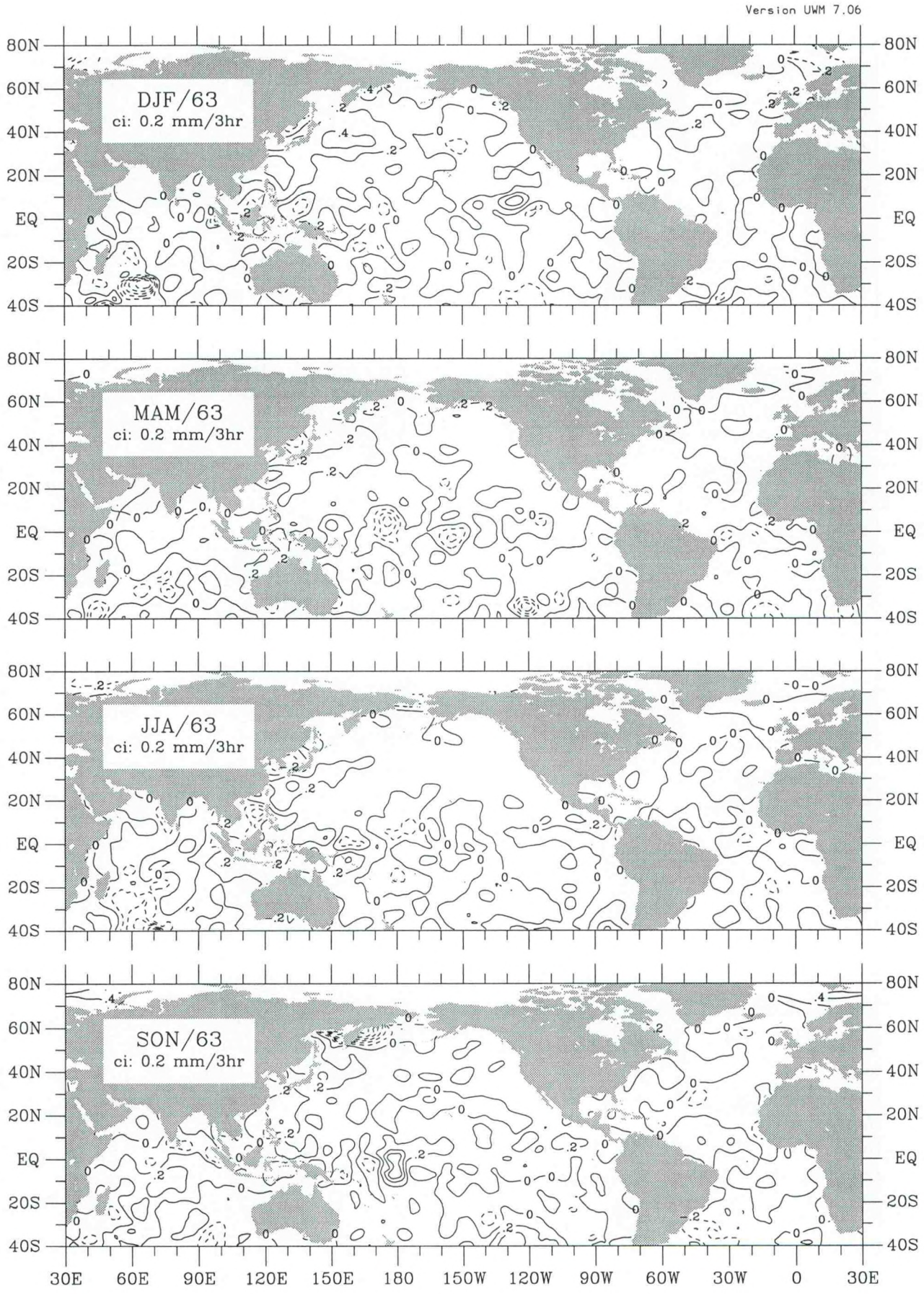

Figure E-P-24. E minus P seasonal anomaly for 1963.

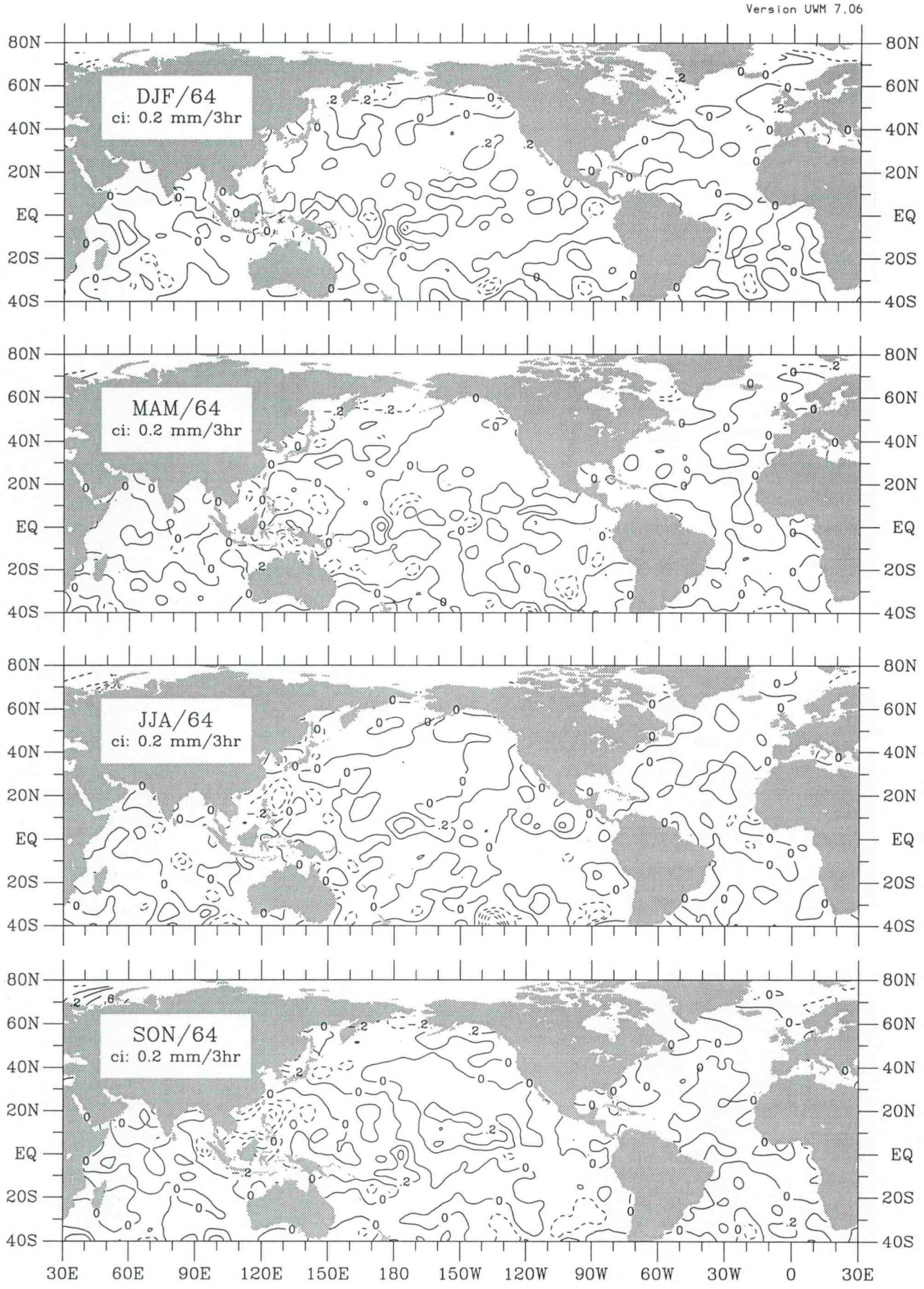

Figure E-P-25. E minus P seasonal anomaly for 1964.

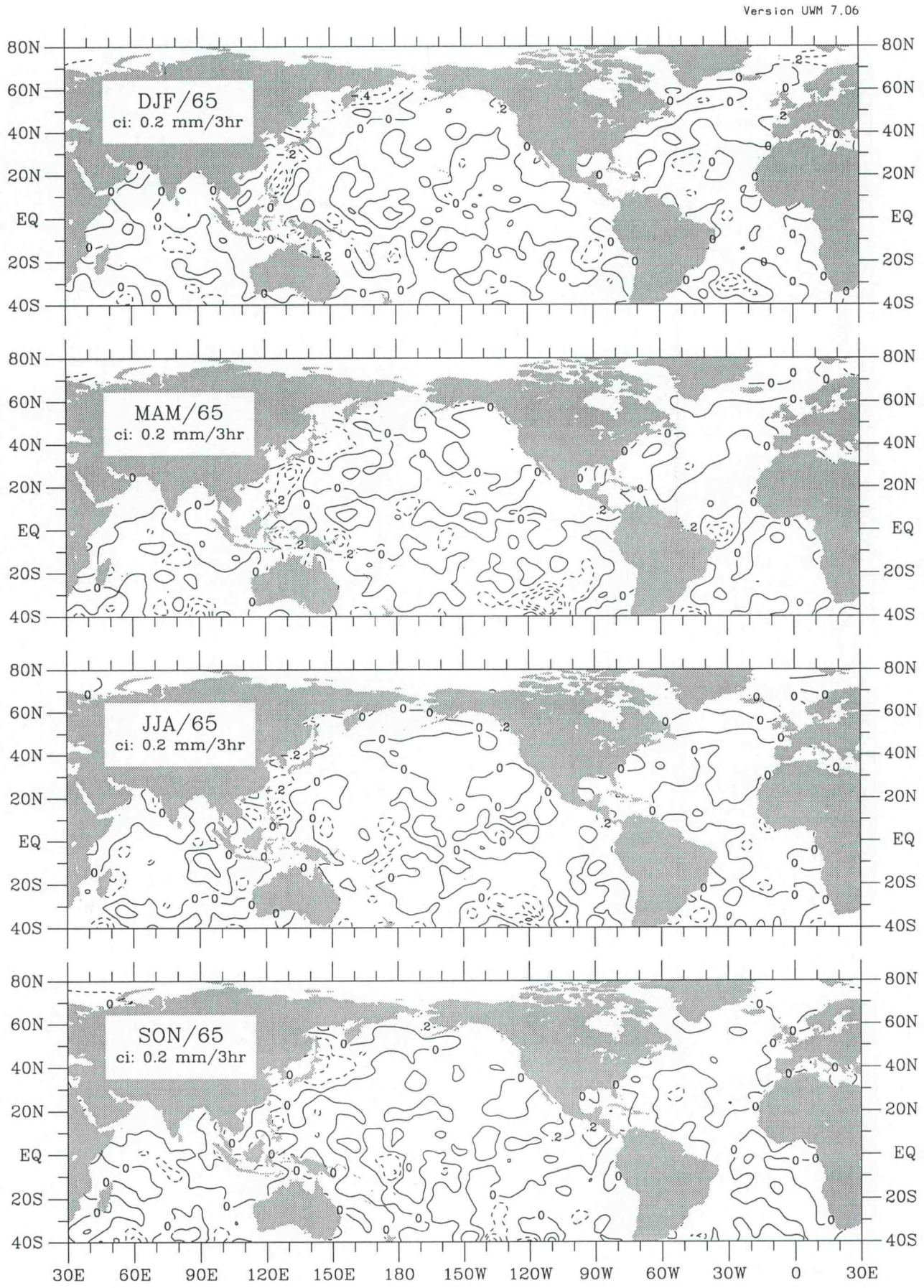

Figure E−P−26. E minus P seasonal anomaly for 1965.

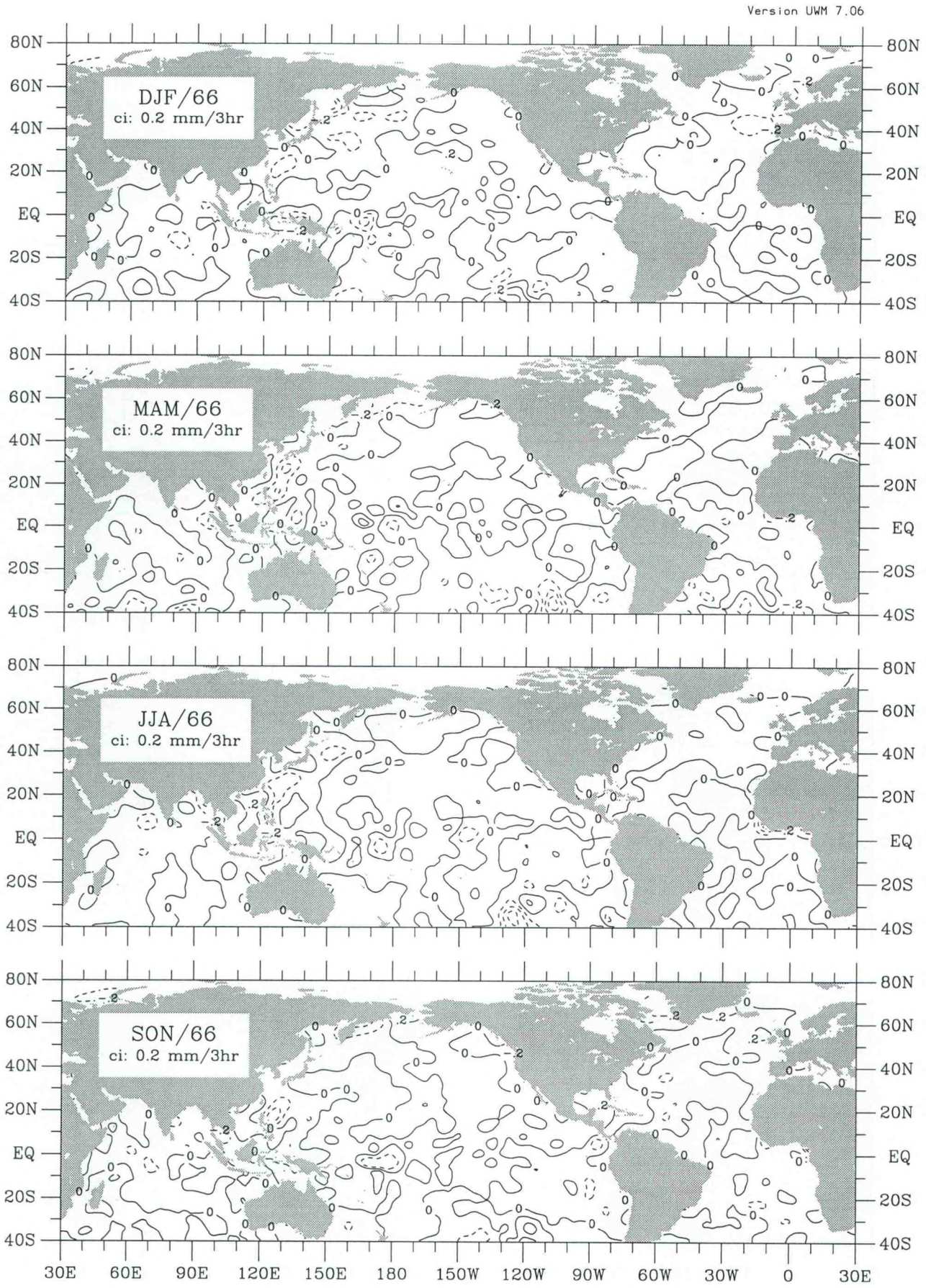

Figure E−P−27. E minus P seasonal anomaly for 1966.

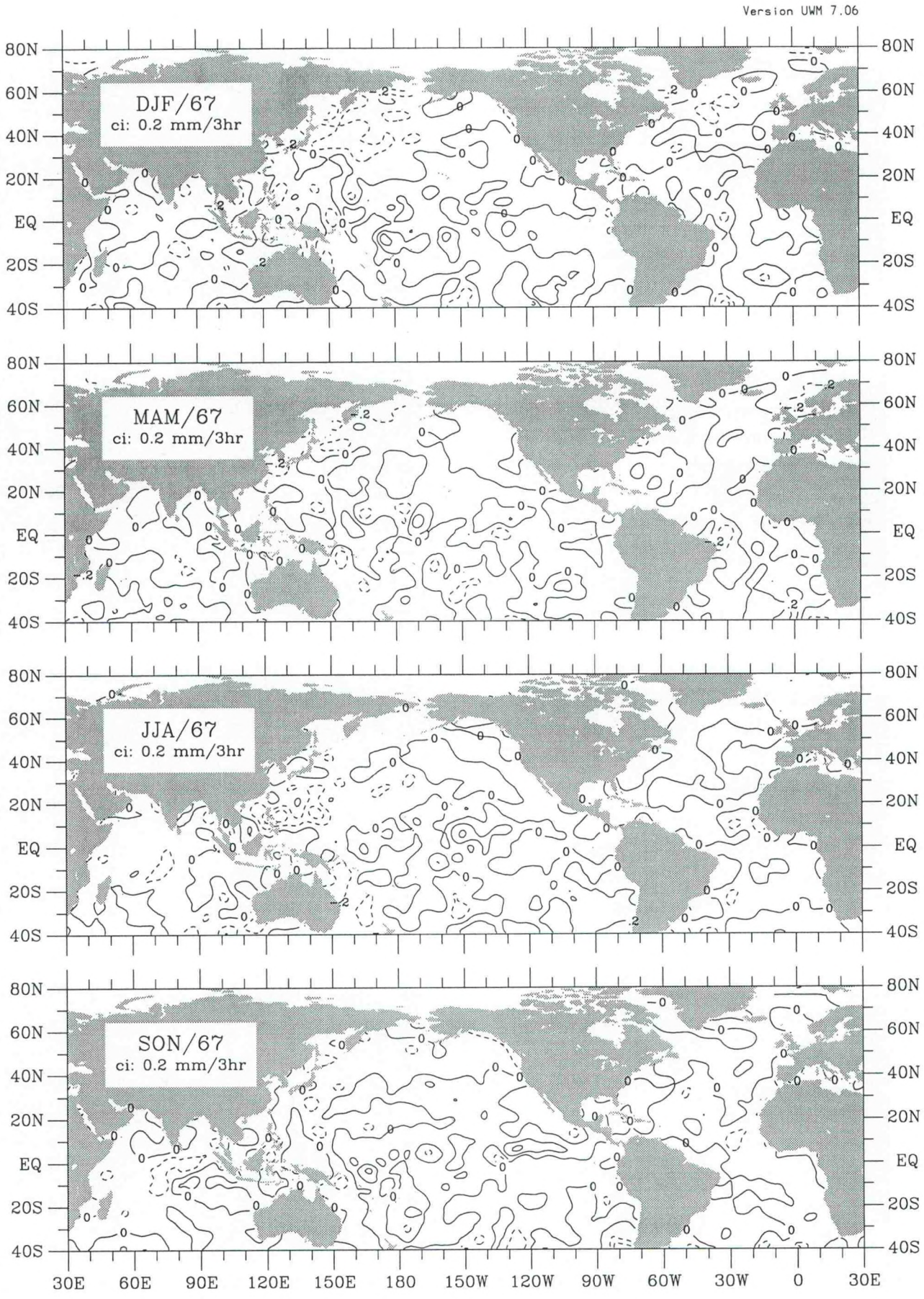

Figure E-P-28. E minus P seasonal anomaly for 1967.

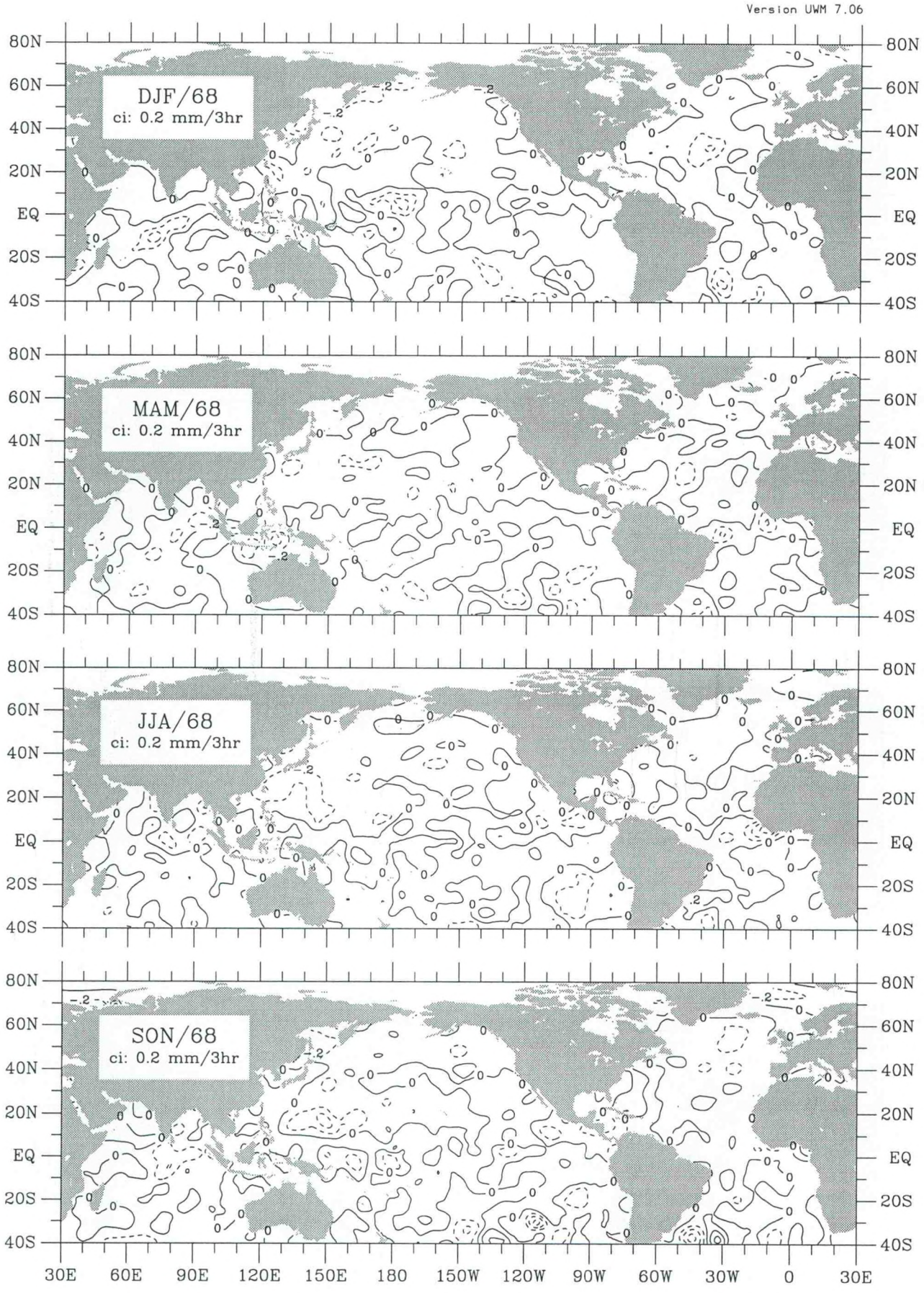

Figure E-P-29. E minus P seasonal anomaly for 1968.

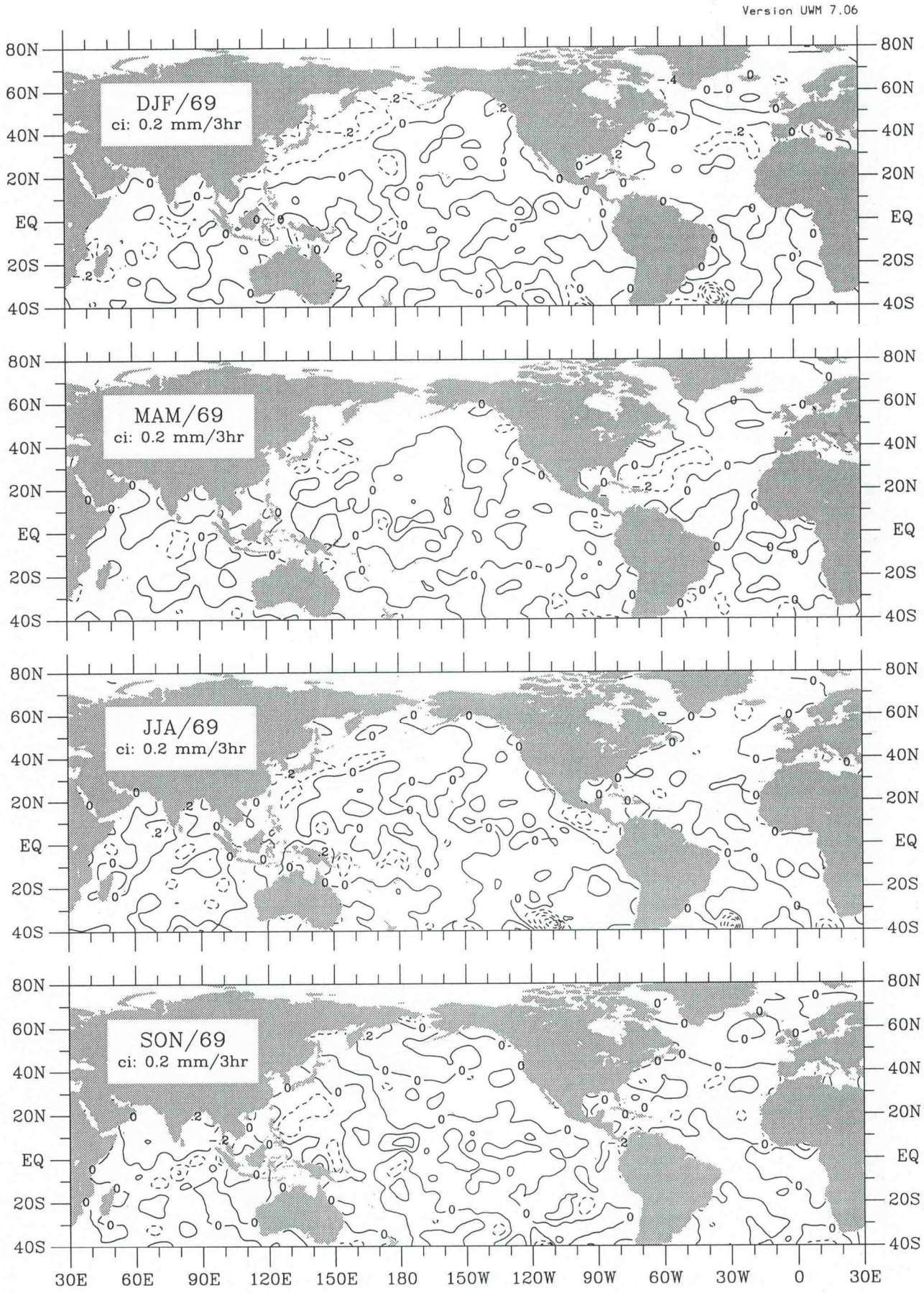

Figure E-P-30. E minus P seasonal anomaly for 1969.

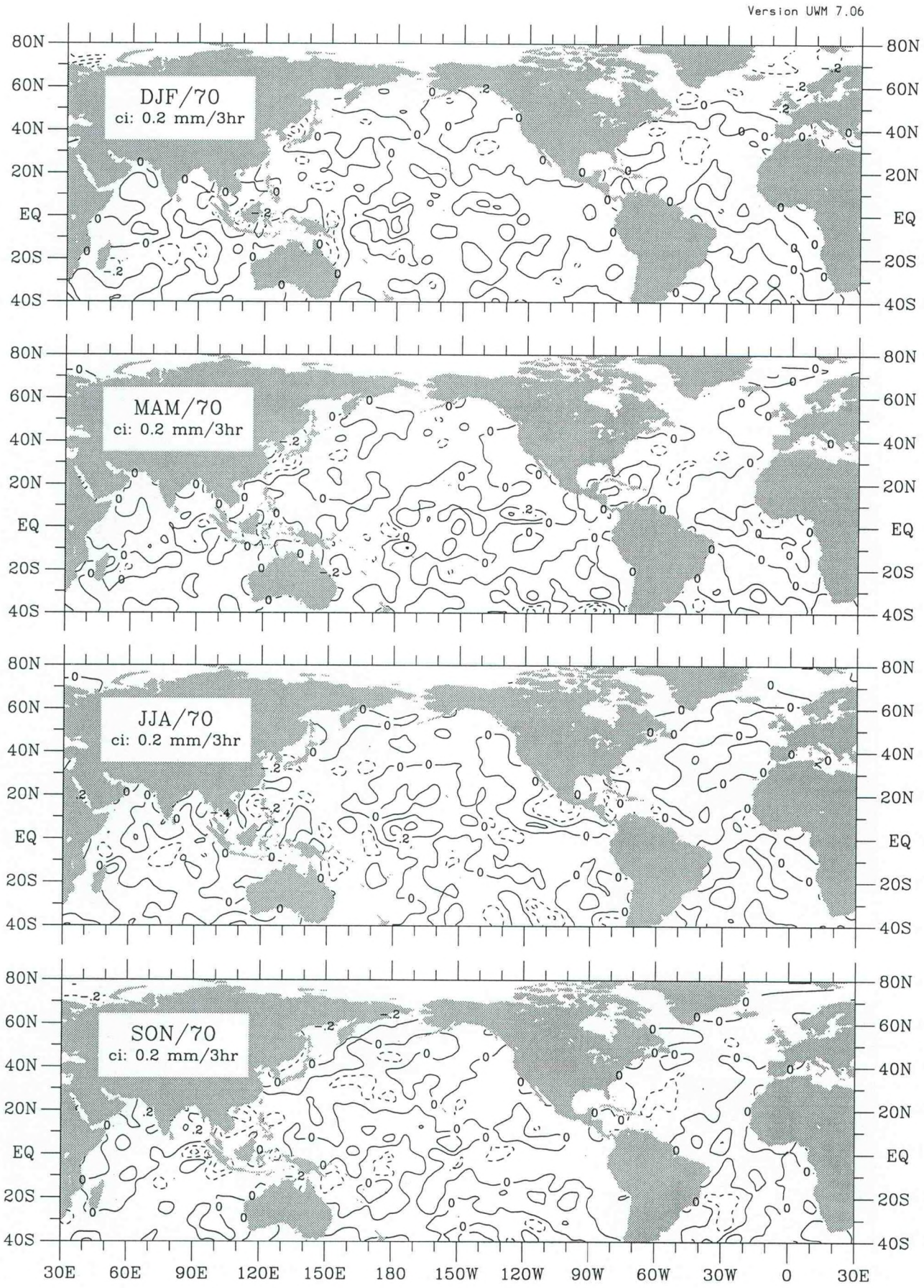

Figure E−P−31. E minus P seasonal anomaly for 1970.

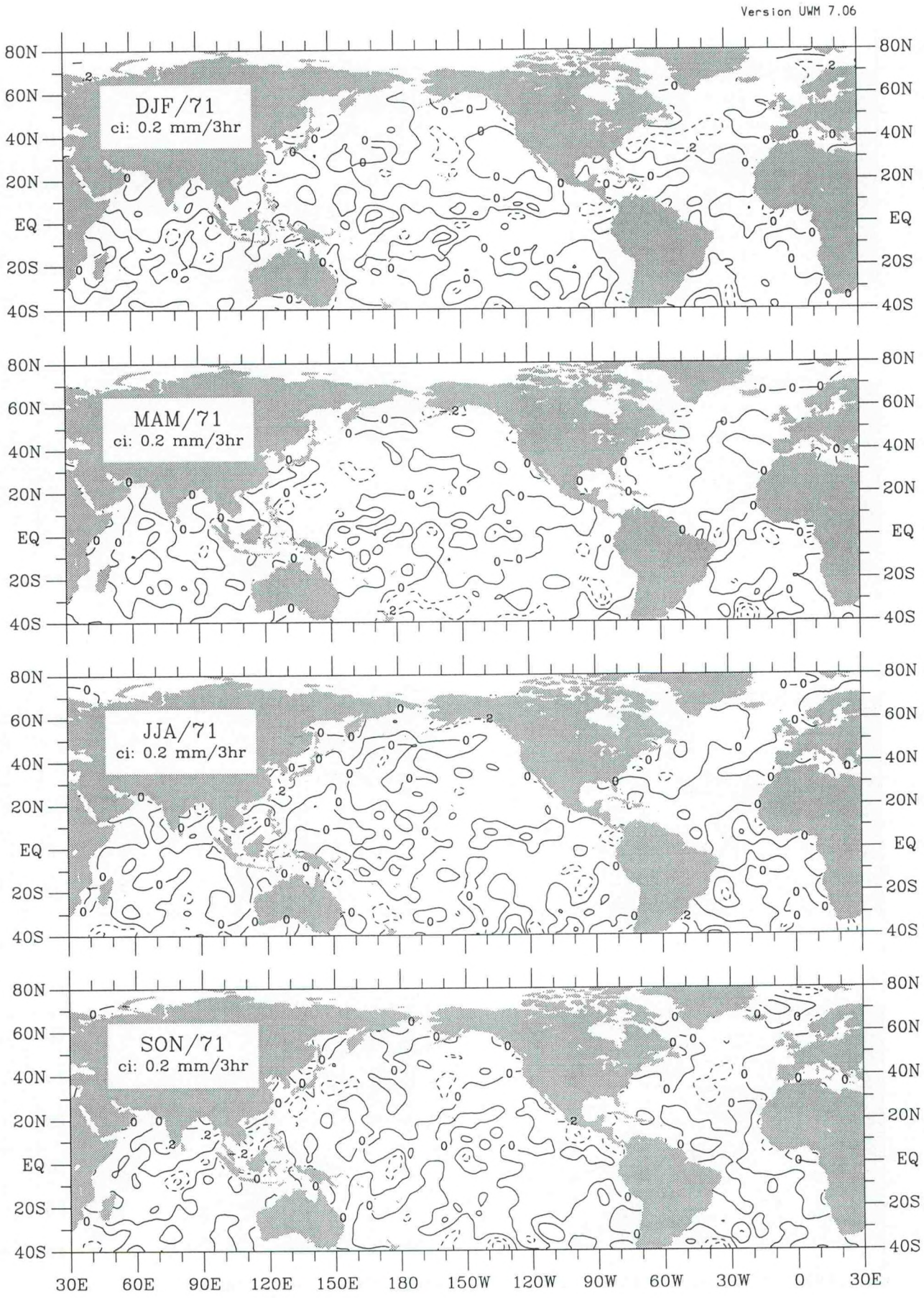

Figure E-P-32. E minus P seasonal anomaly for 1971.

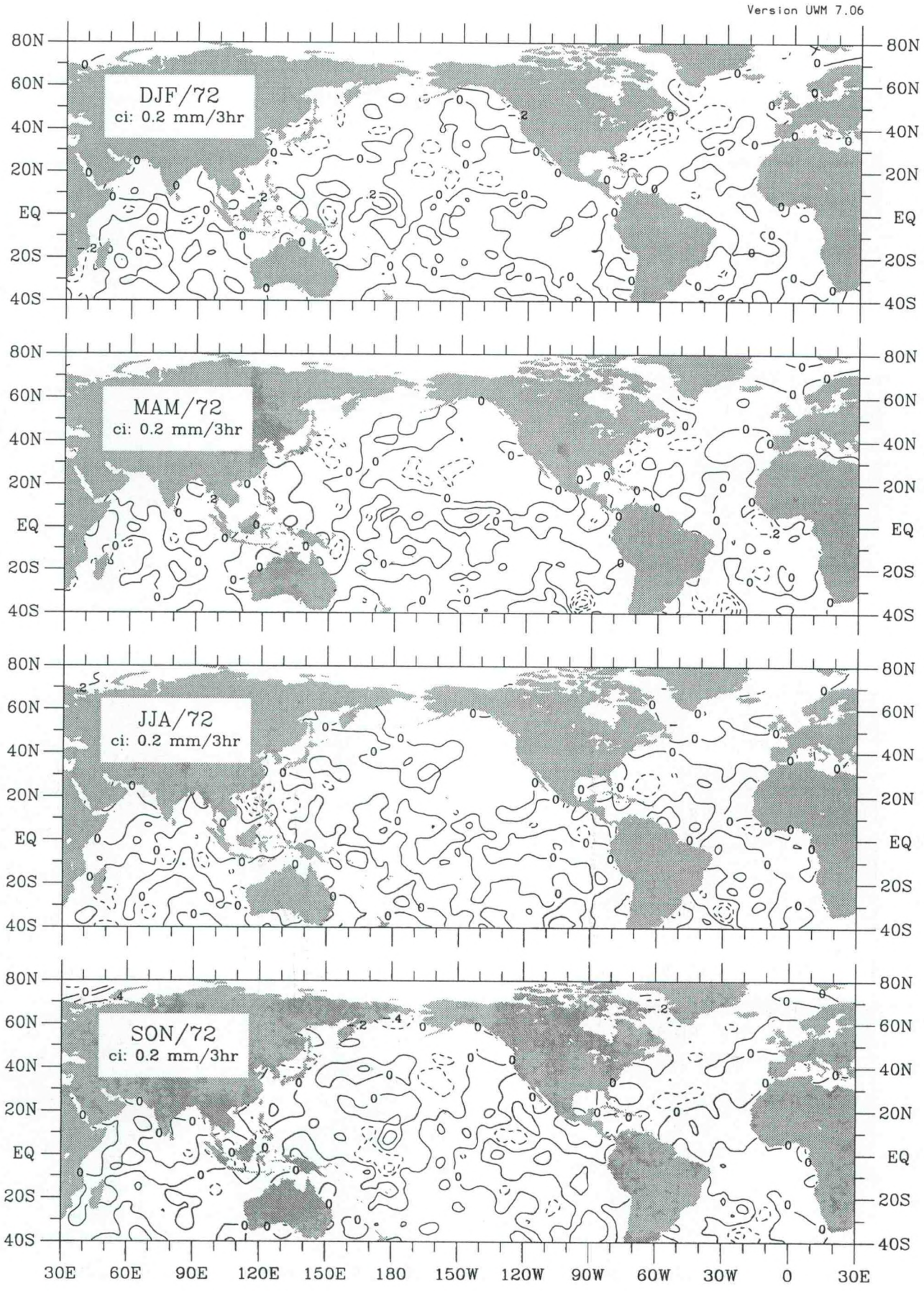

Figure E–P–33. E minus P seasonal anomaly for 1972.

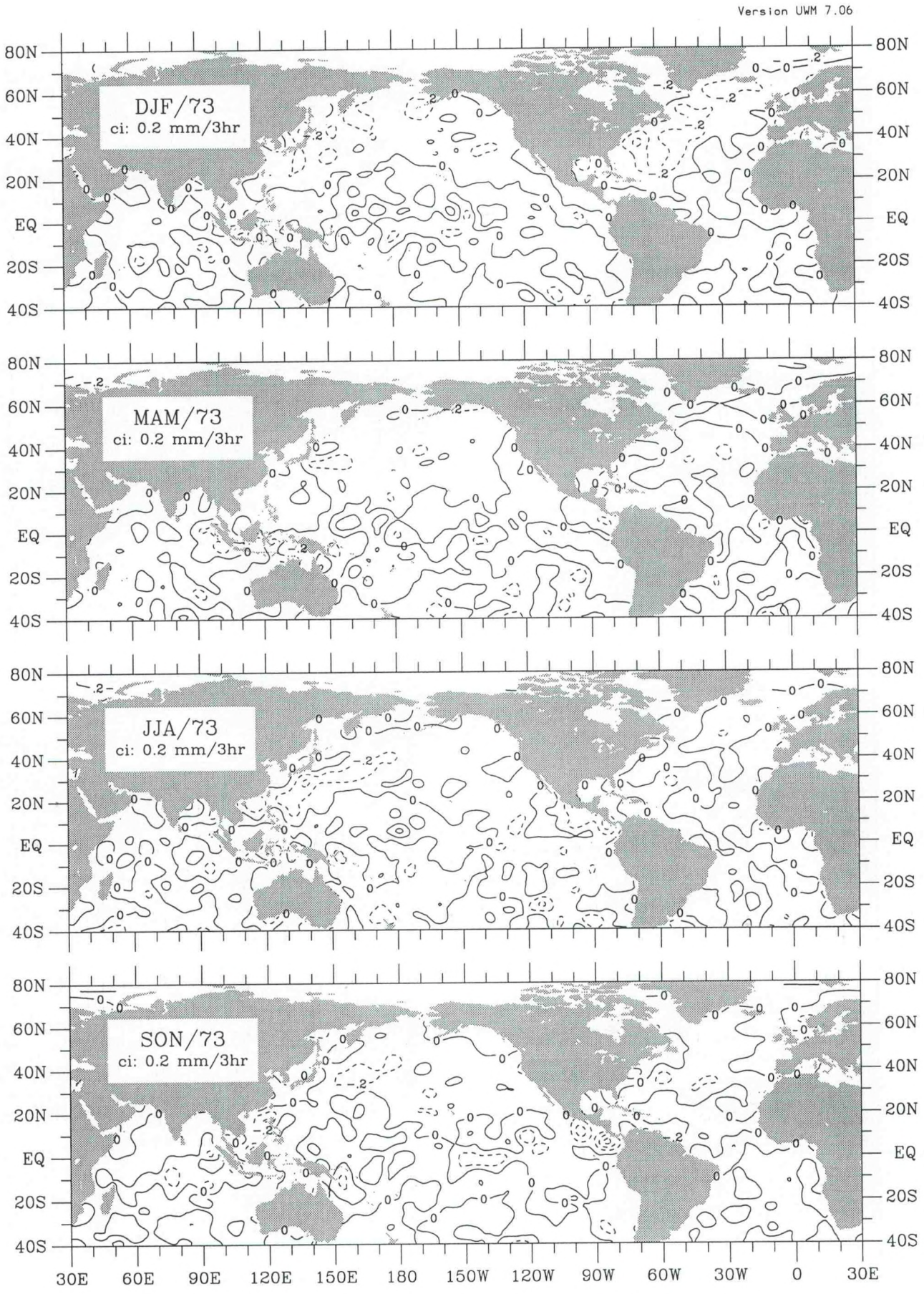

Figure E−P−34. E minus P seasonal anomaly for 1973.

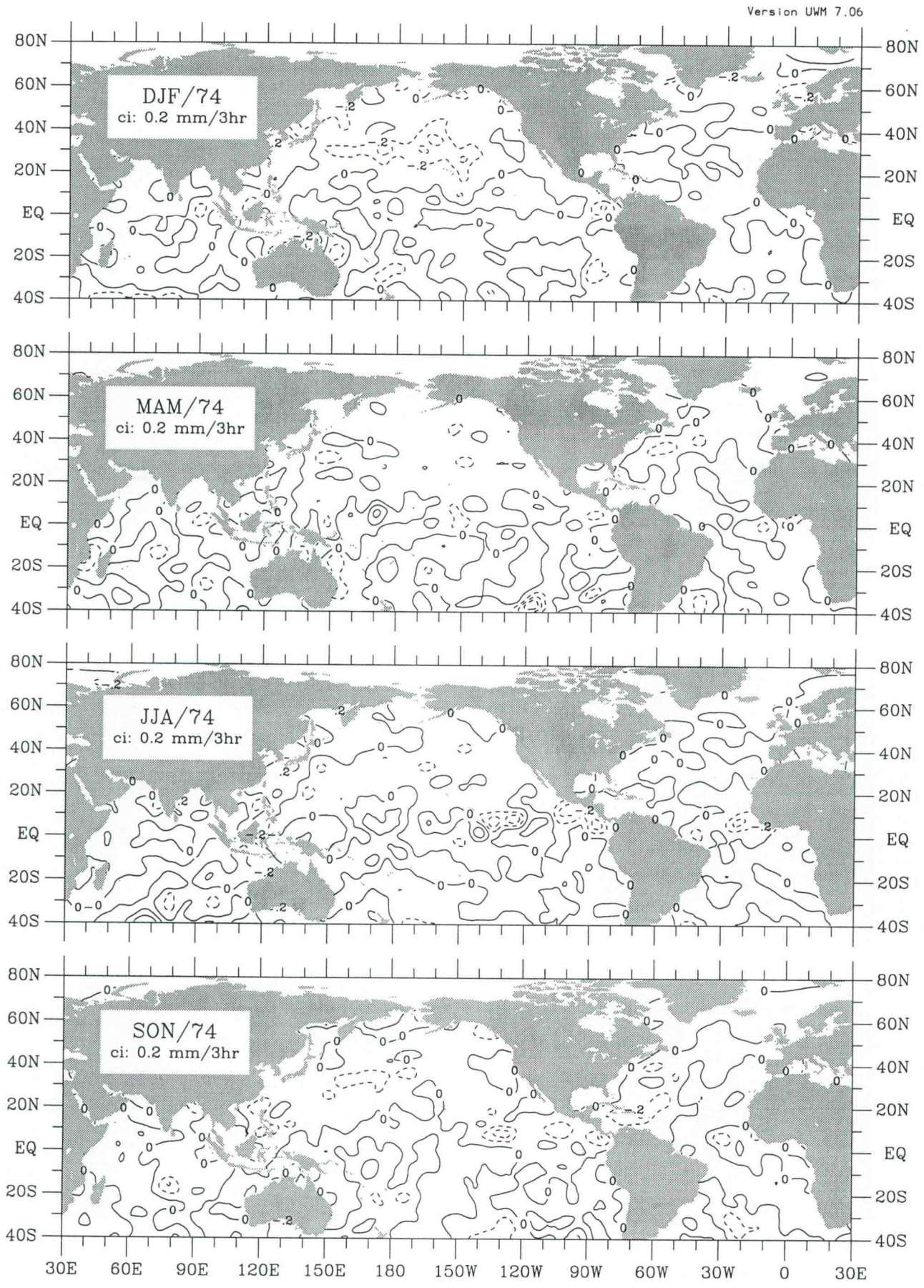

Figure E-P-35. E minus P seasonal anomaly for 1974.

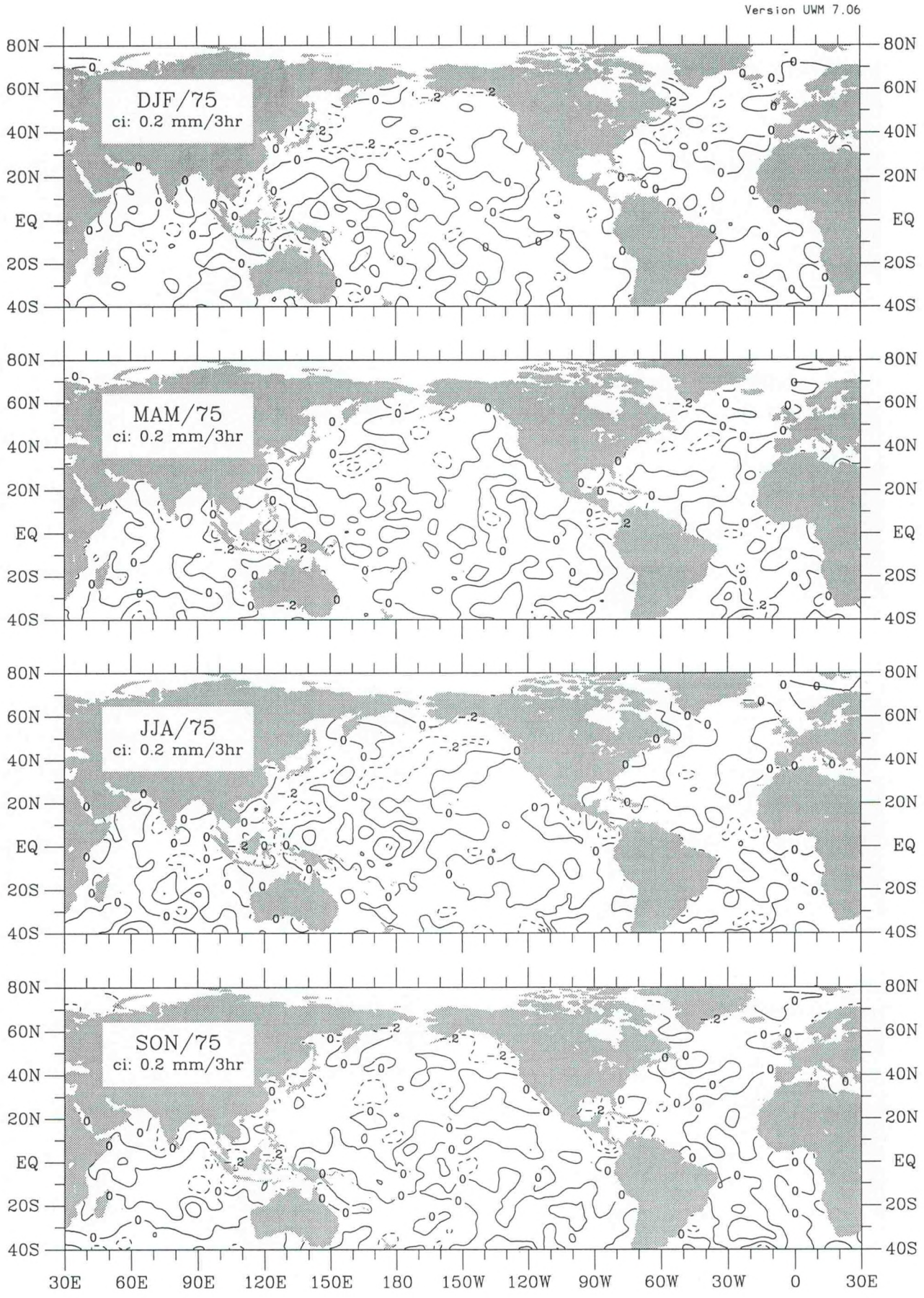

Figure E-P-36. E minus P seasonal anomaly for 1975.

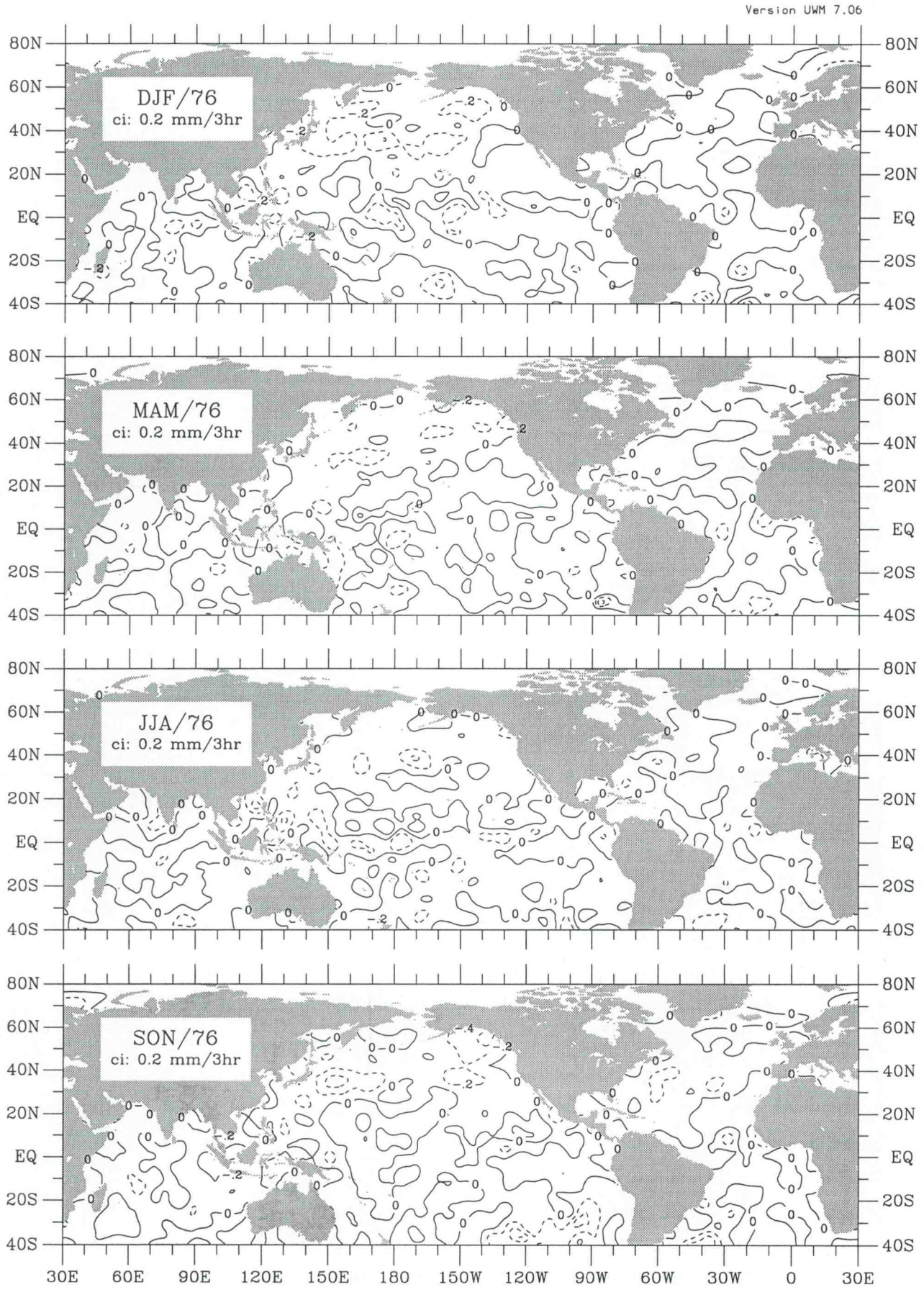

Figure E-P-37. E minus P seasonal anomaly for 1976.

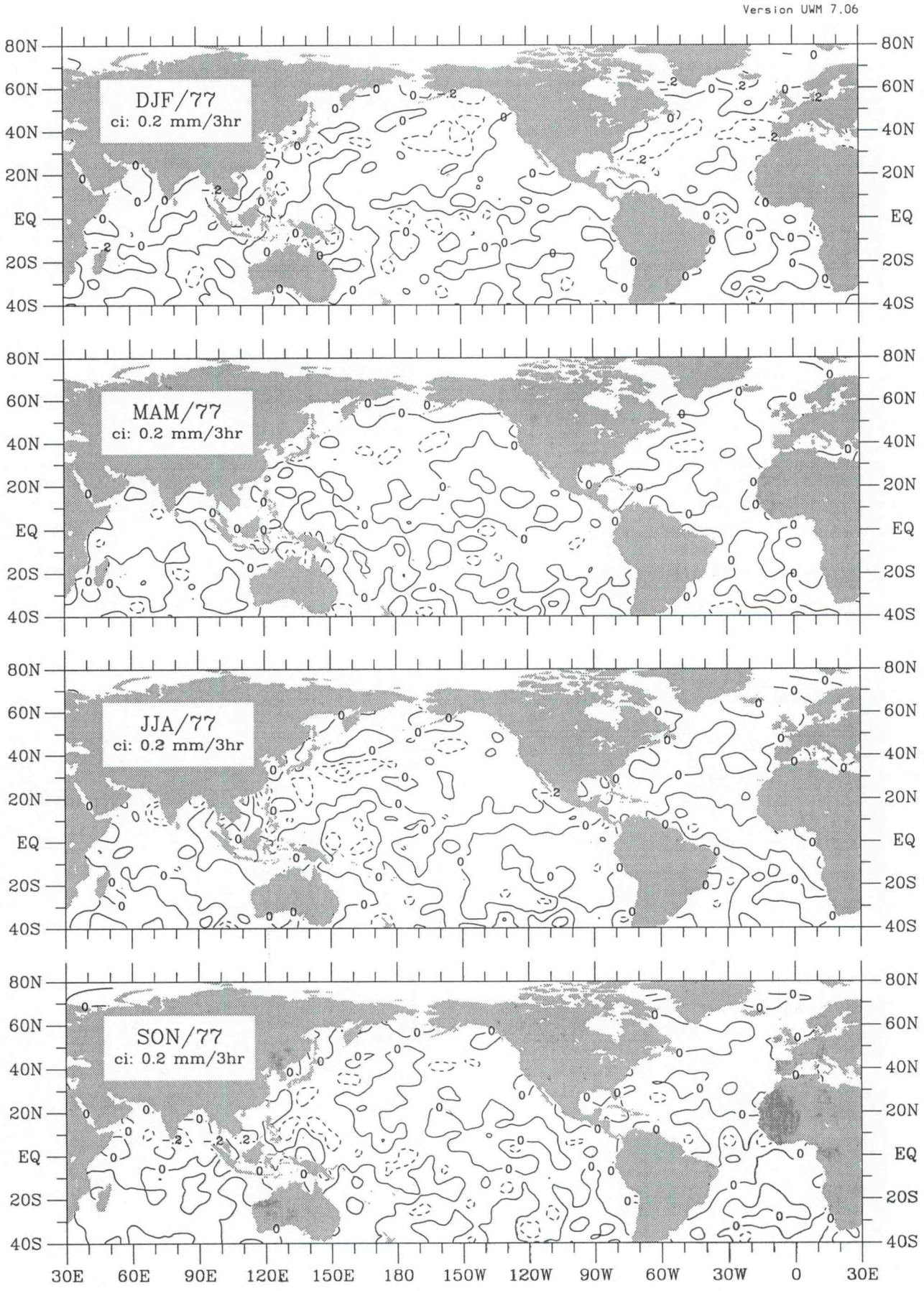

Figure E–P–38. E minus P seasonal anomaly for 1977.

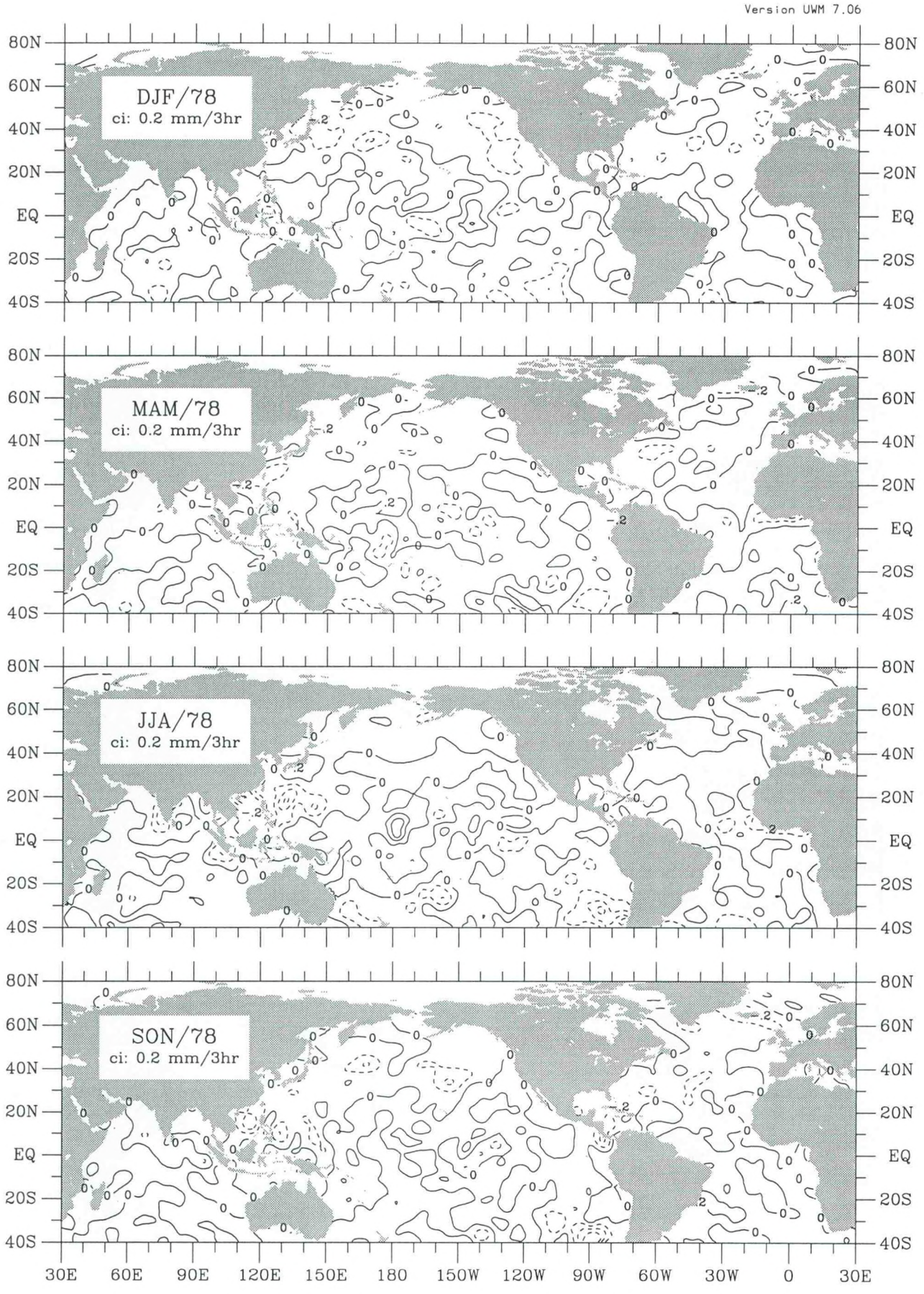

Figure E-P-39. E minus P seasonal anomaly for 1978.

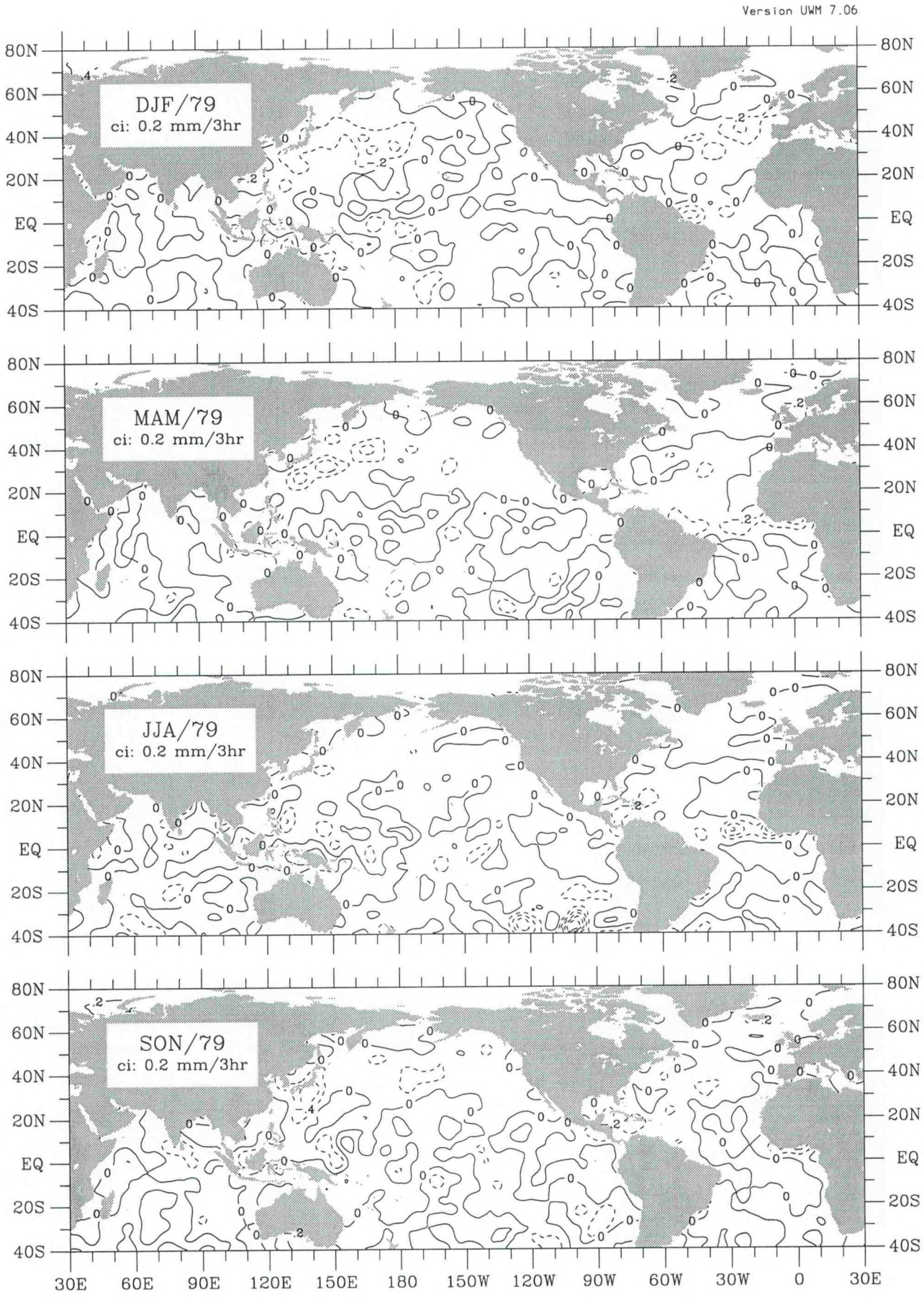

Figure E-P-40. E minus P seasonal anomaly for 1979.

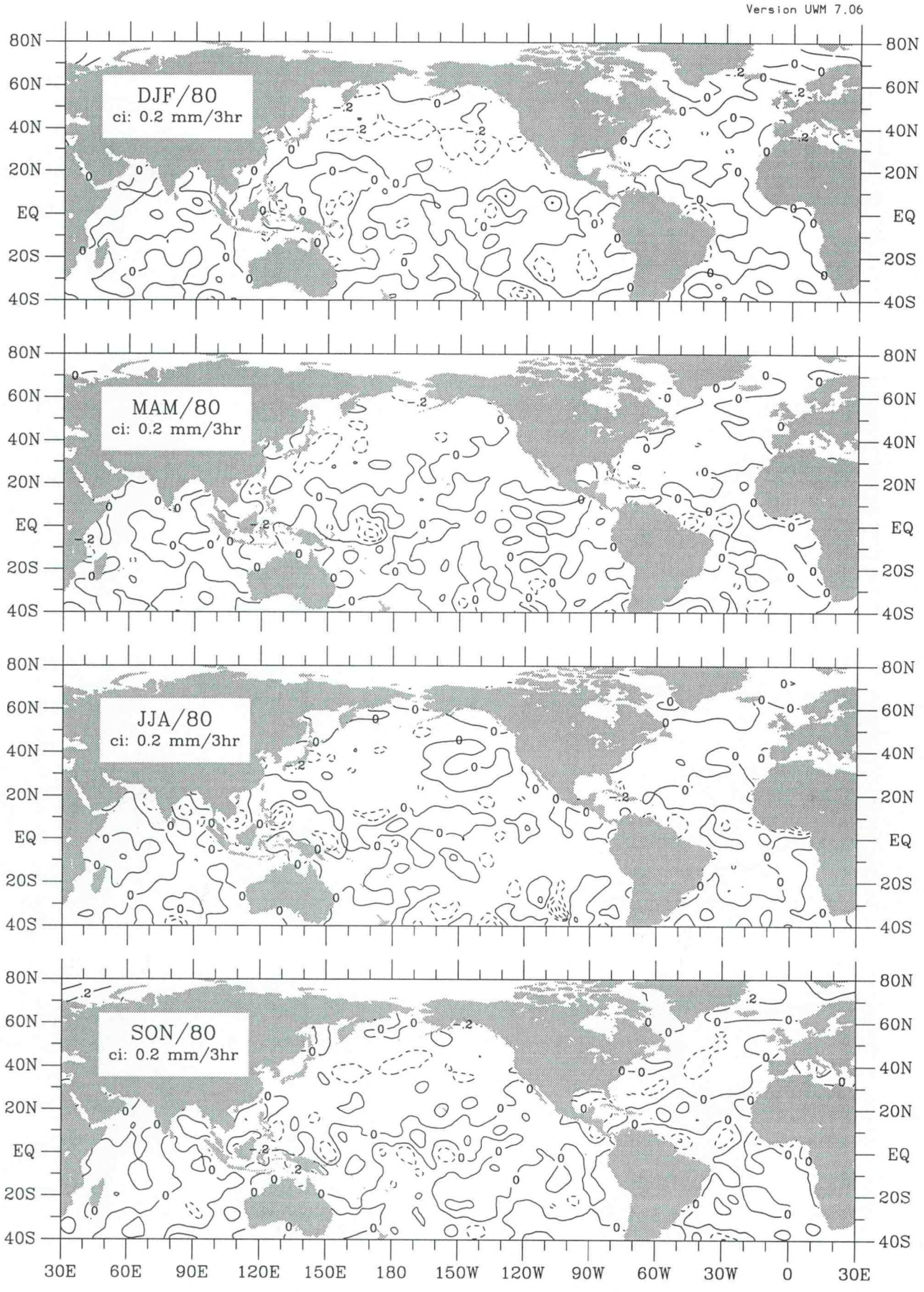

Figure E–P–41. E minus P seasonal anomaly for 1980.

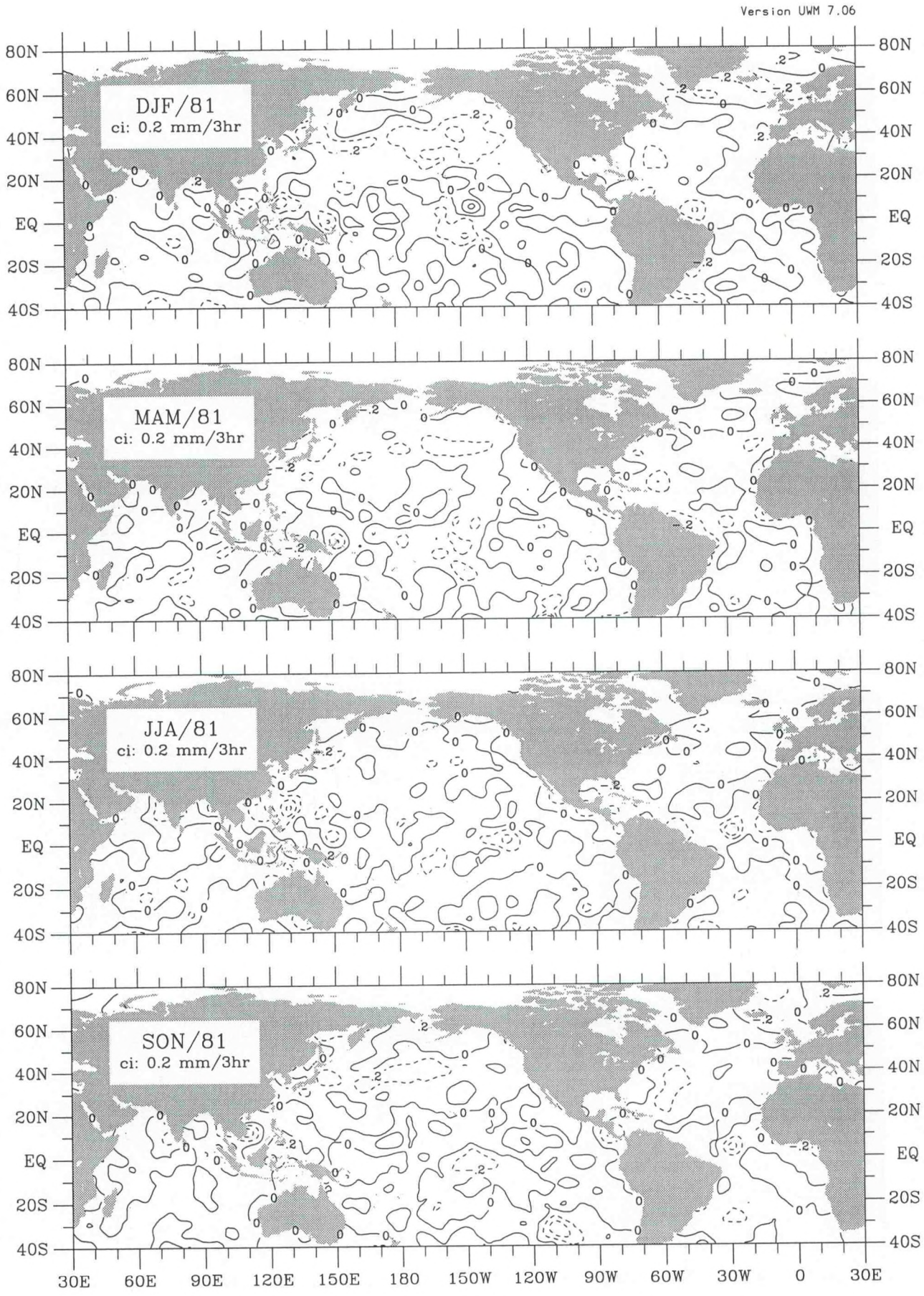

Figure E−P−42. E minus P seasonal anomaly for 1981.

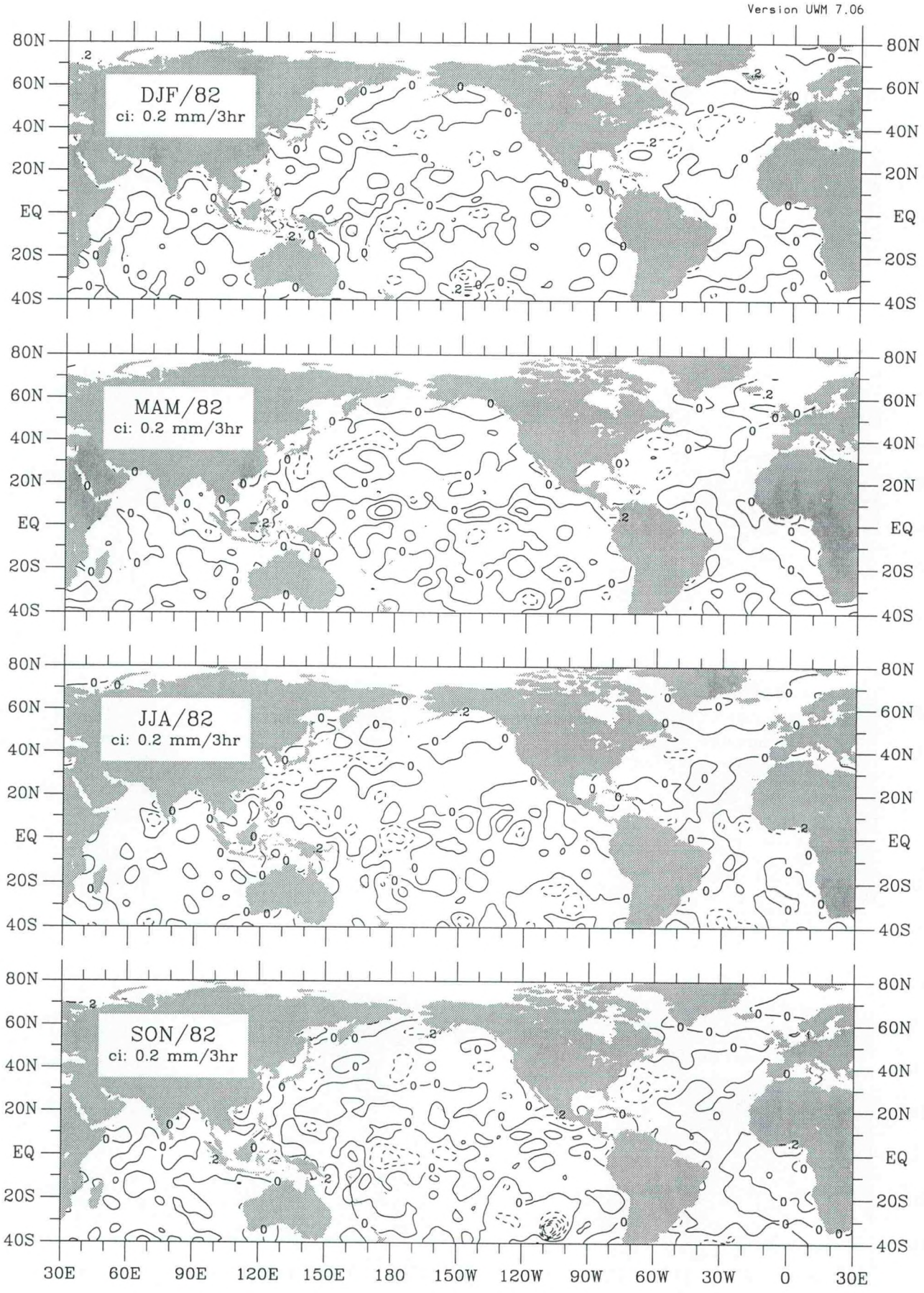

Figure E-P-43. E minus P seasonal anomaly for 1982.

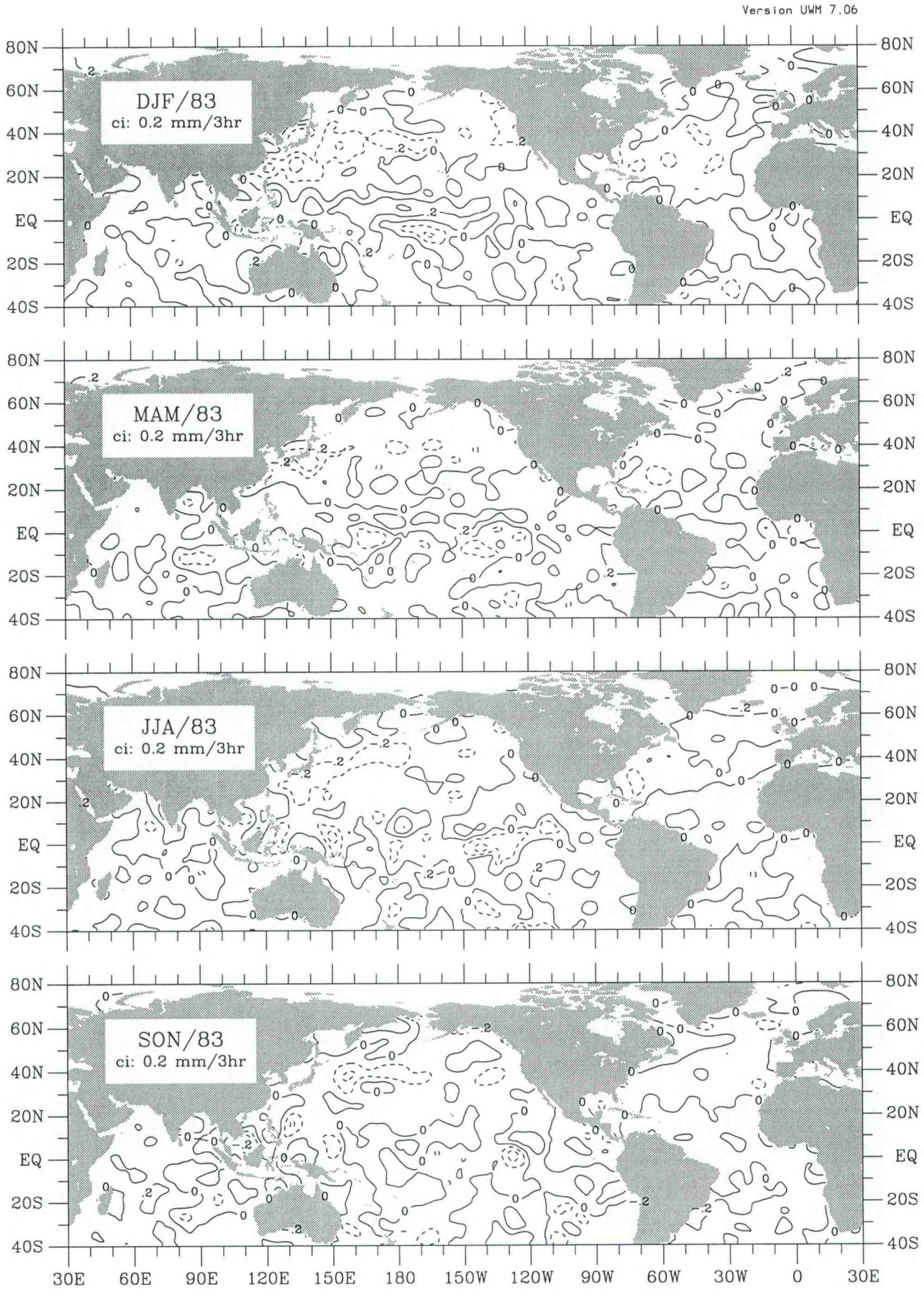

Figure E-P-44. E minus P seasonal anomaly for 1983.

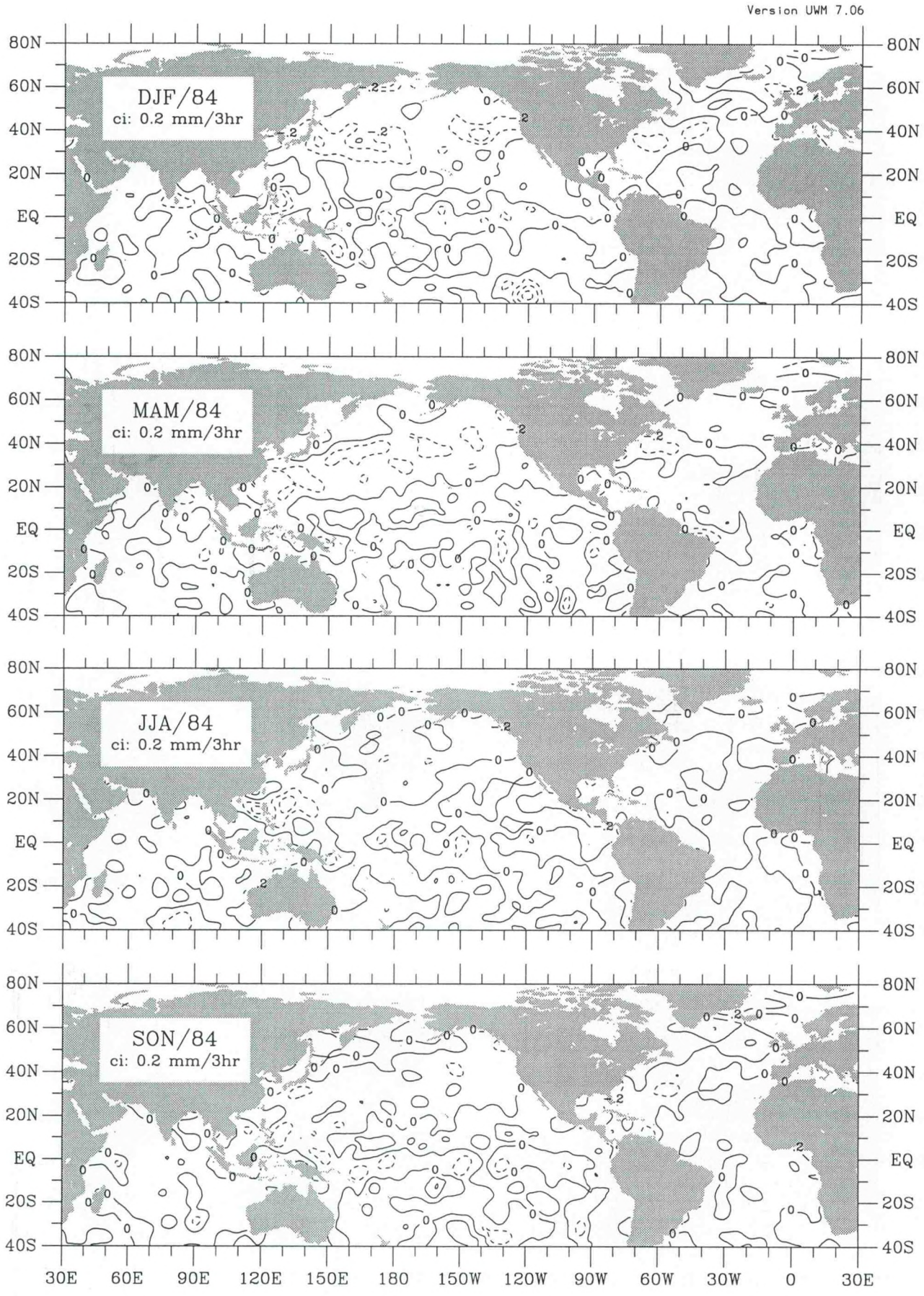

Figure E-P-45. E minus P seasonal anomaly for 1984.

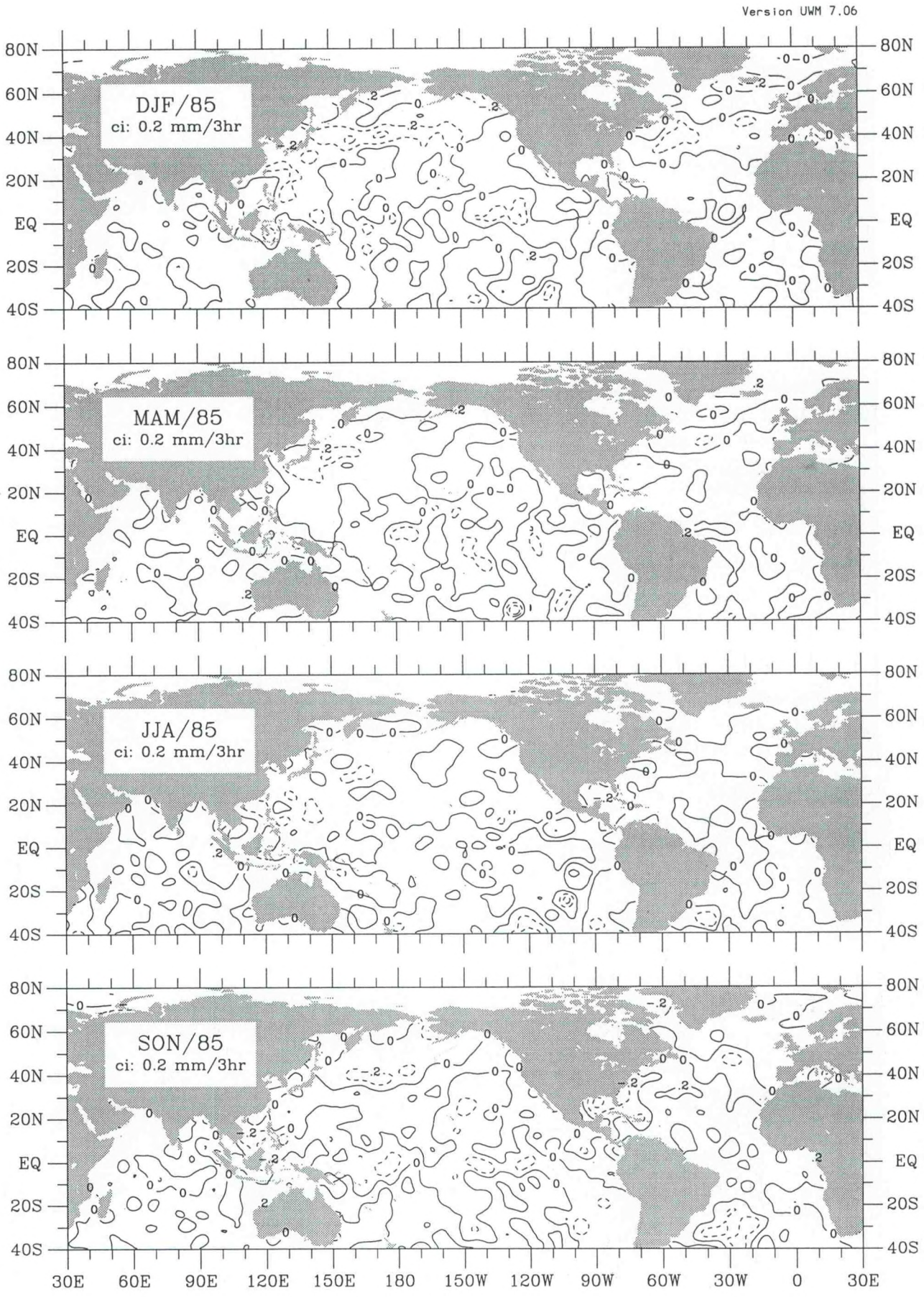

Figure E-P-46. E minus P seasonal anomaly for 1985.

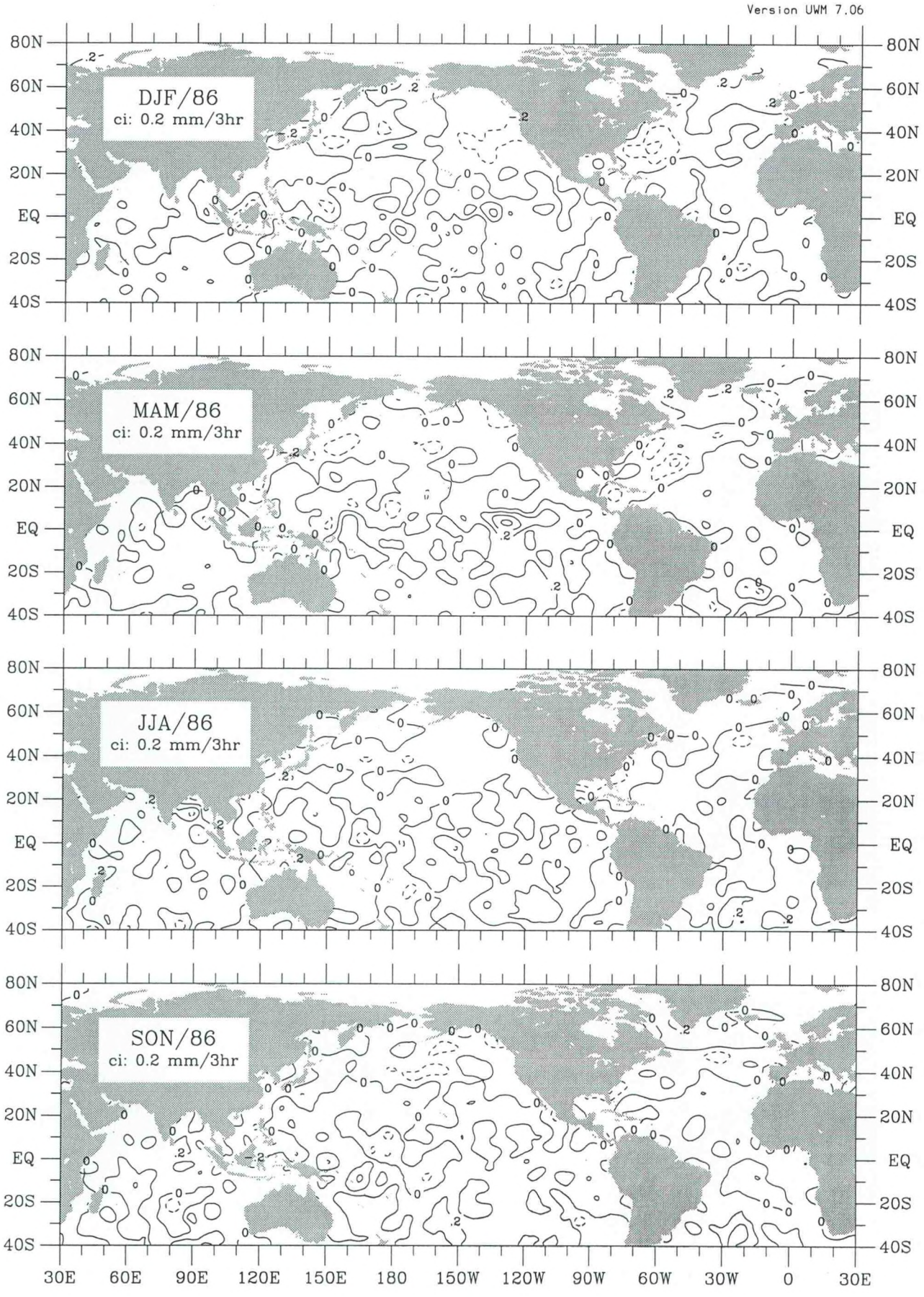

Figure E−P−47. E minus P seasonal anomaly for 1986.

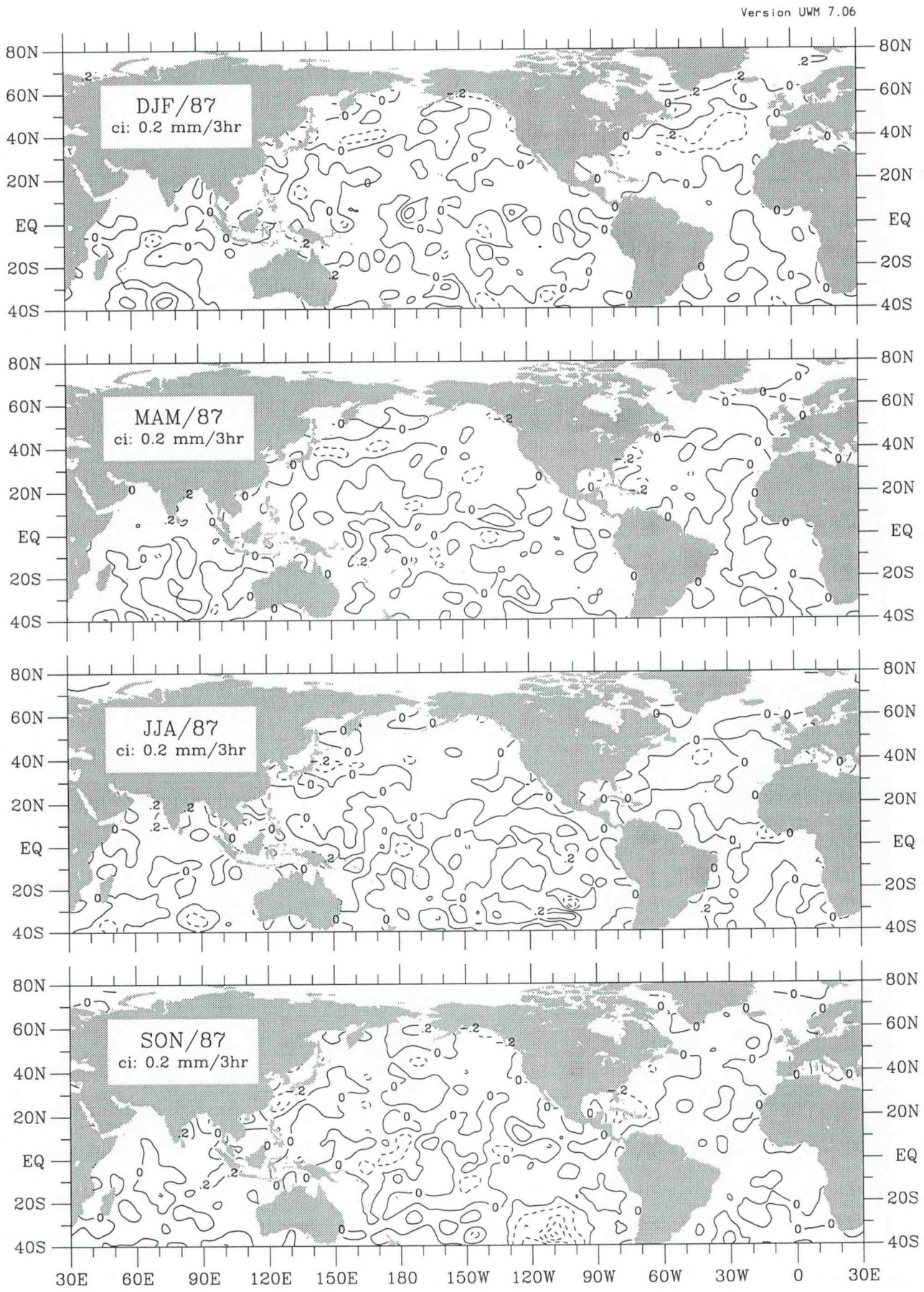

Figure E-P-48. E minus P seasonal anomaly for 1987.

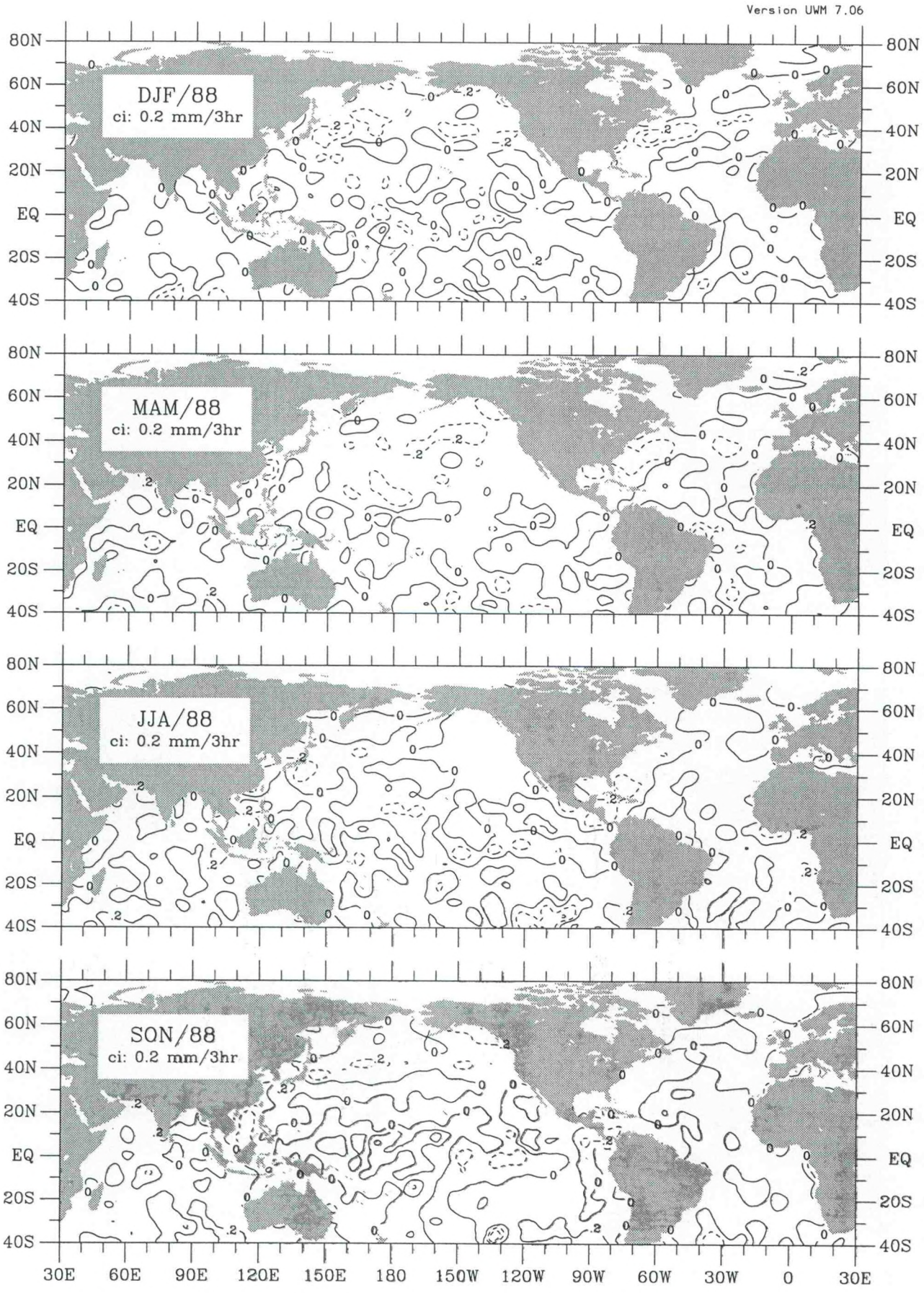

Figure E–P–49. E minus P seasonal anomaly for 1988.

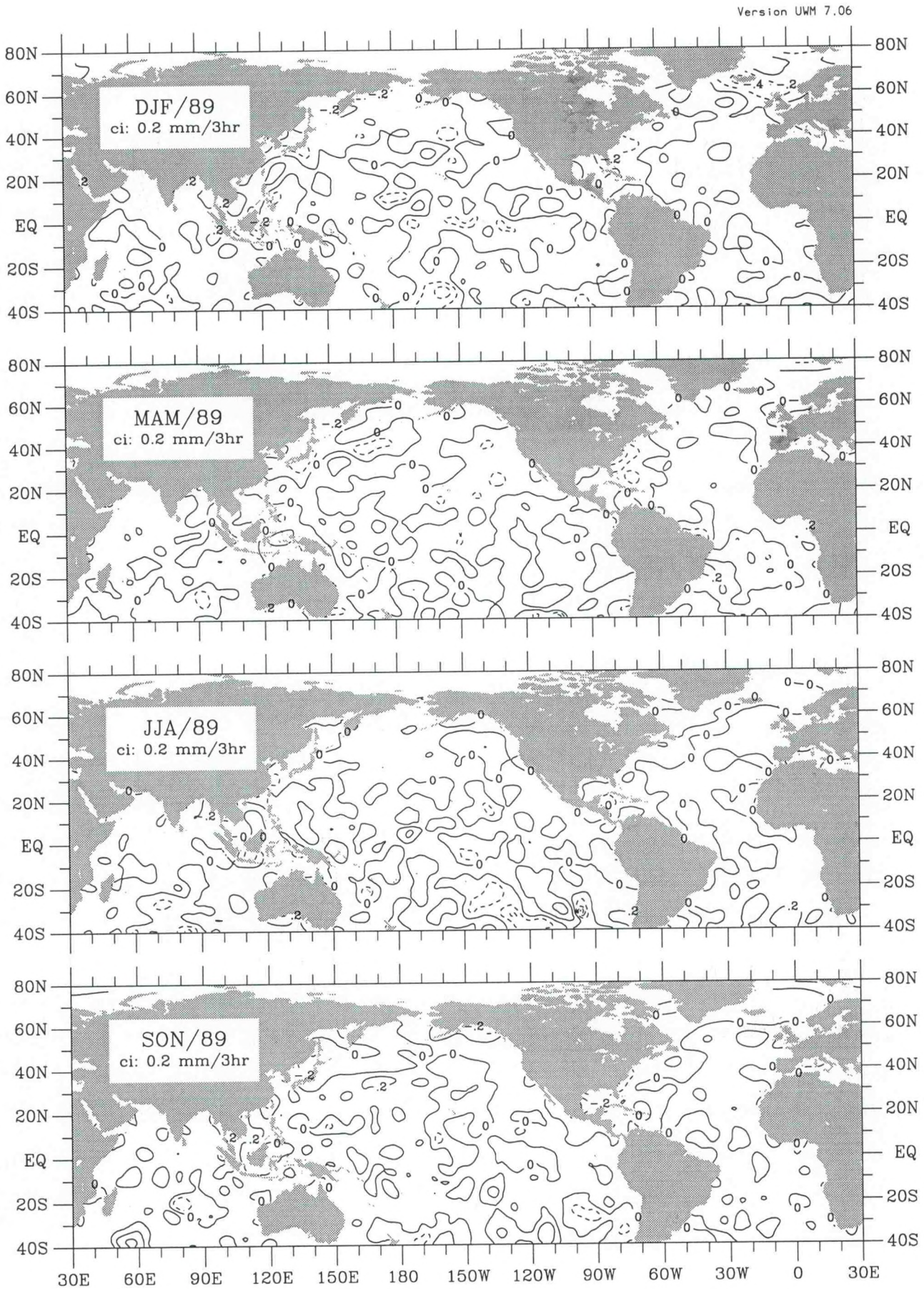

Figure E-P-50. E minus P seasonal anomaly for 1989.

14 Constrained buoyancy flux

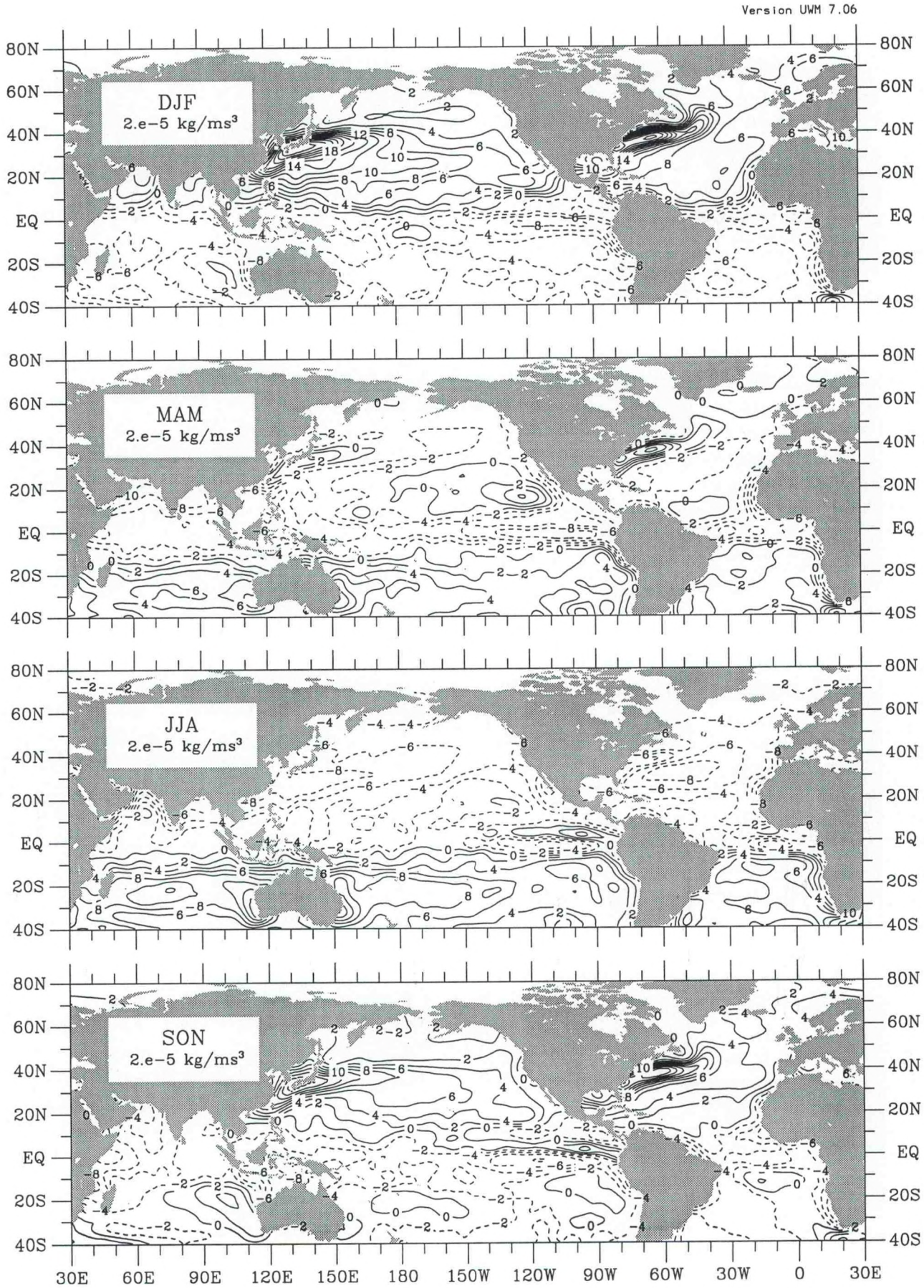

Figure buoy-3. Buoyancy flux seasonal climatology (1945-89).

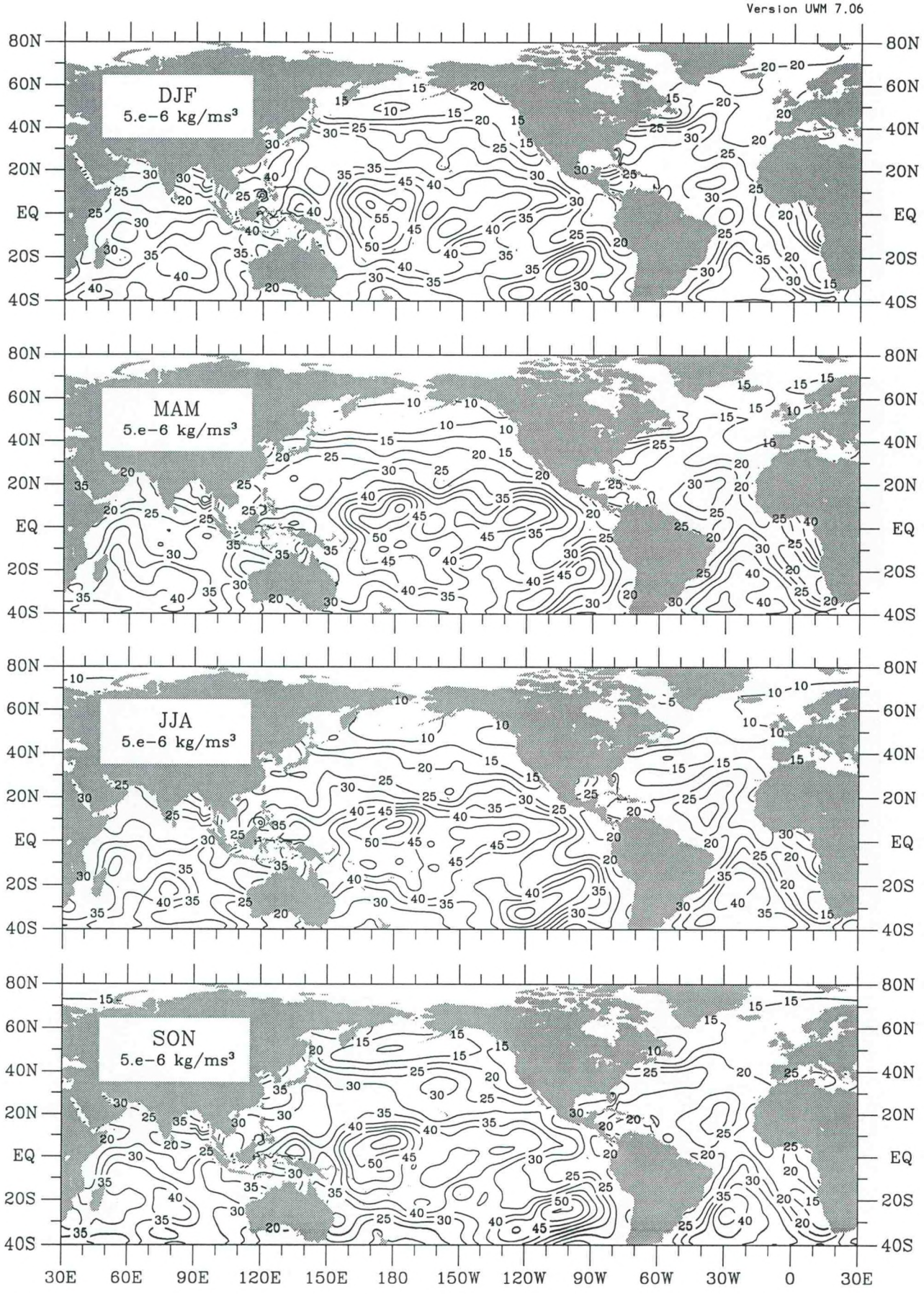

Figure buoy-4. Buoyancy flux seasonal interannual std dev (1945-89).

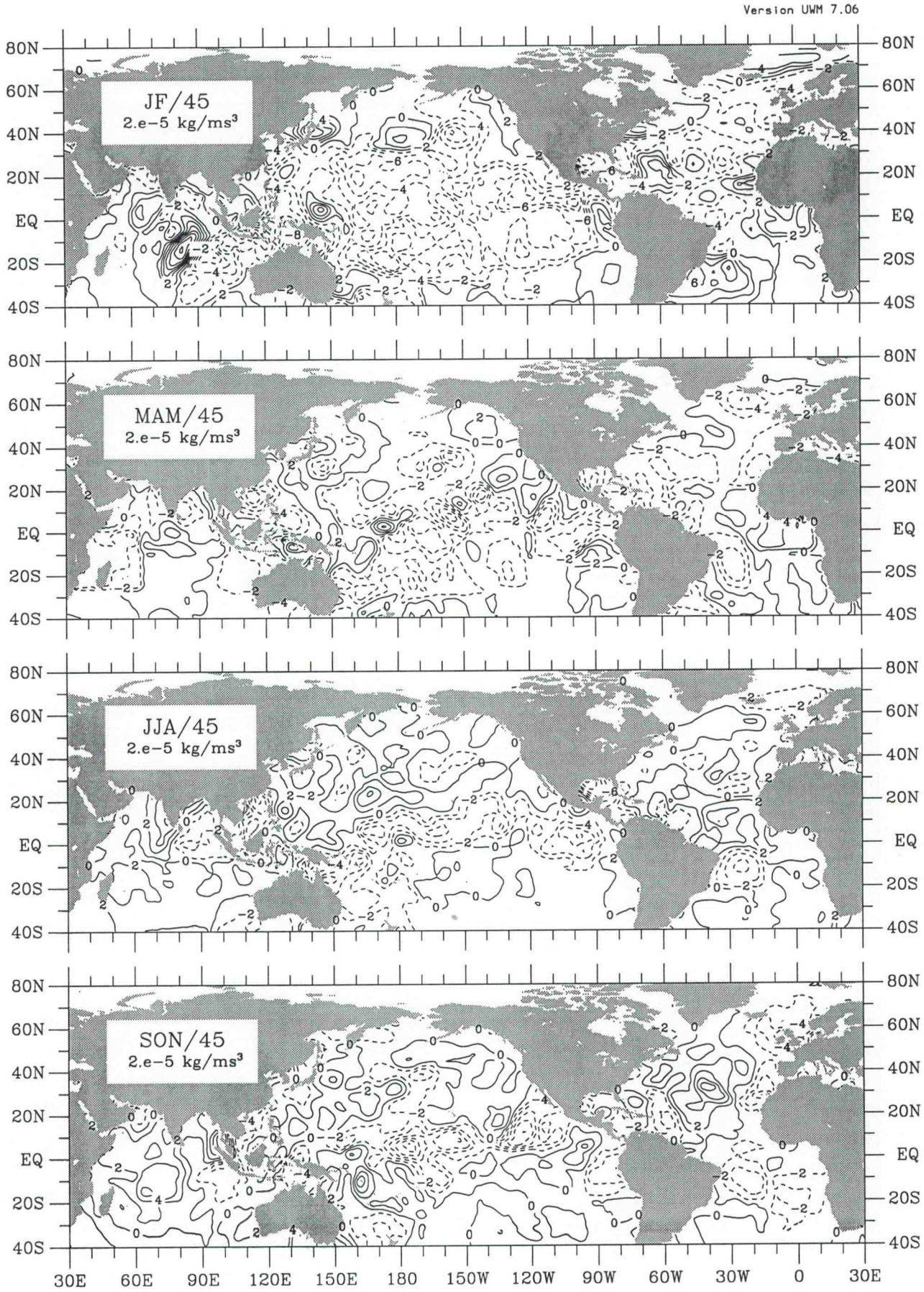

Figure buoy-6. Buoyancy flux seasonal anomaly for 1945.

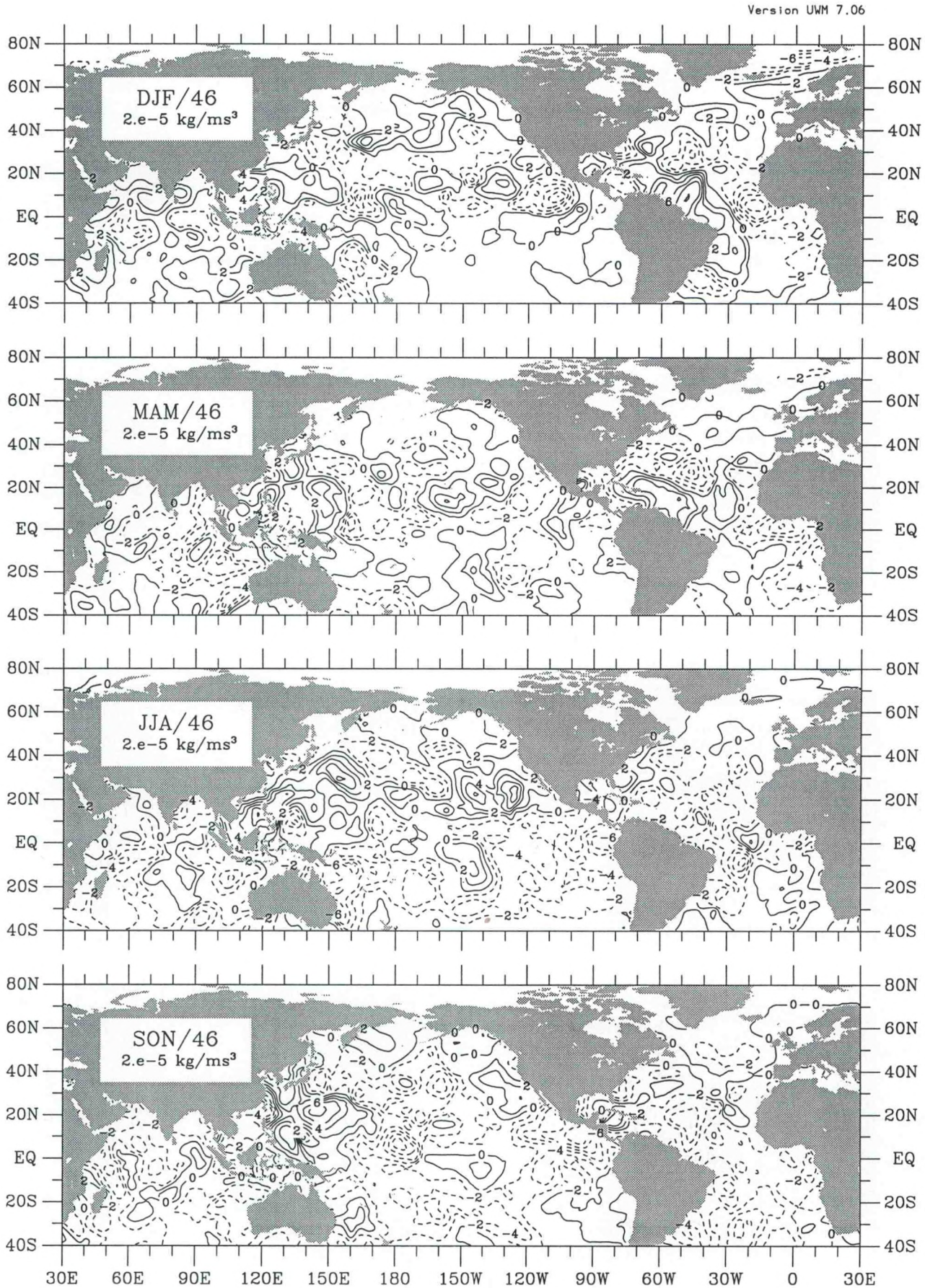

Figure buoy-7. Buoyancy flux seasonal anomaly for 1946.

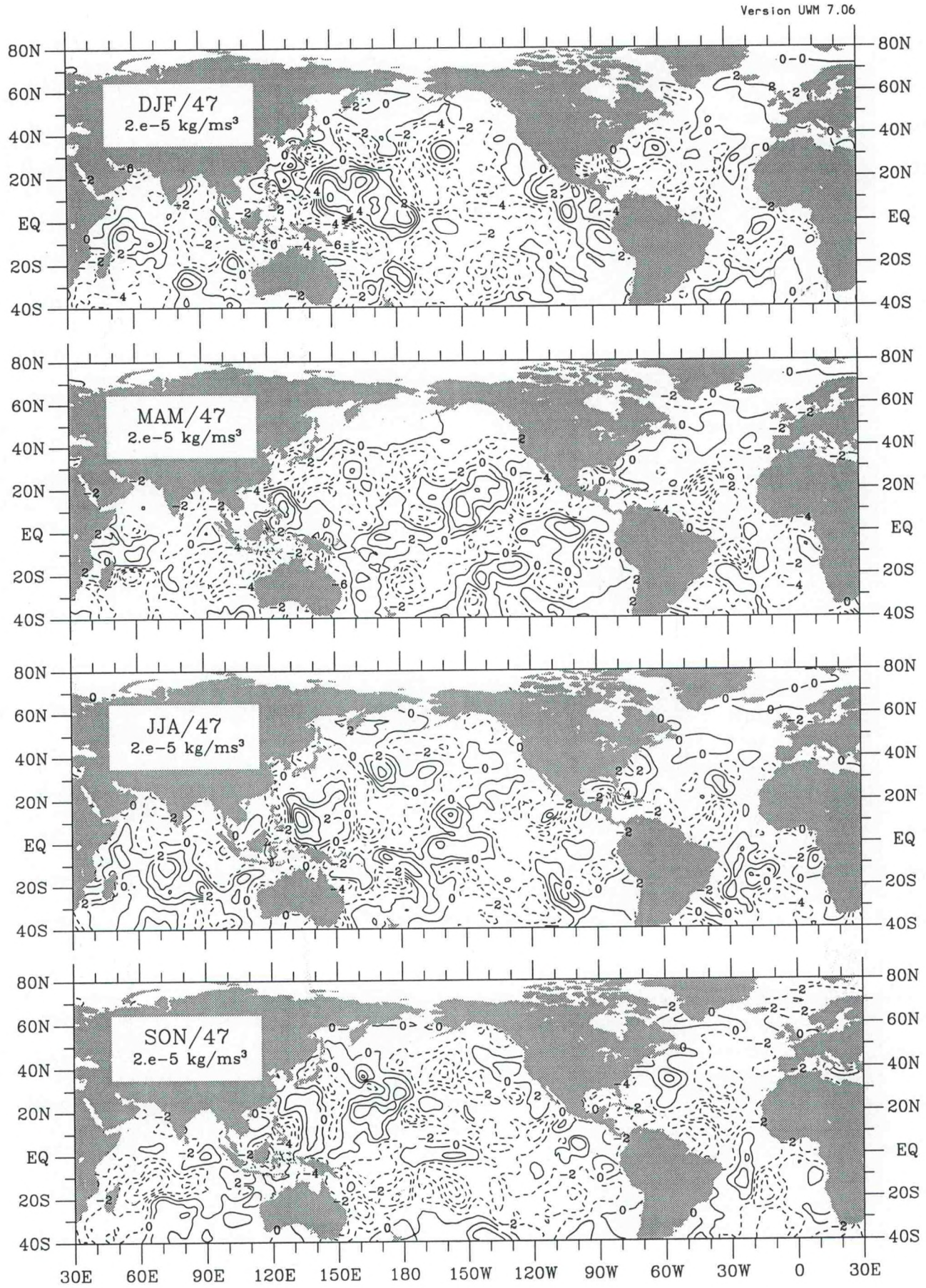

Figure buoy-8. Buoyancy flux seasonal anomaly for 1947.

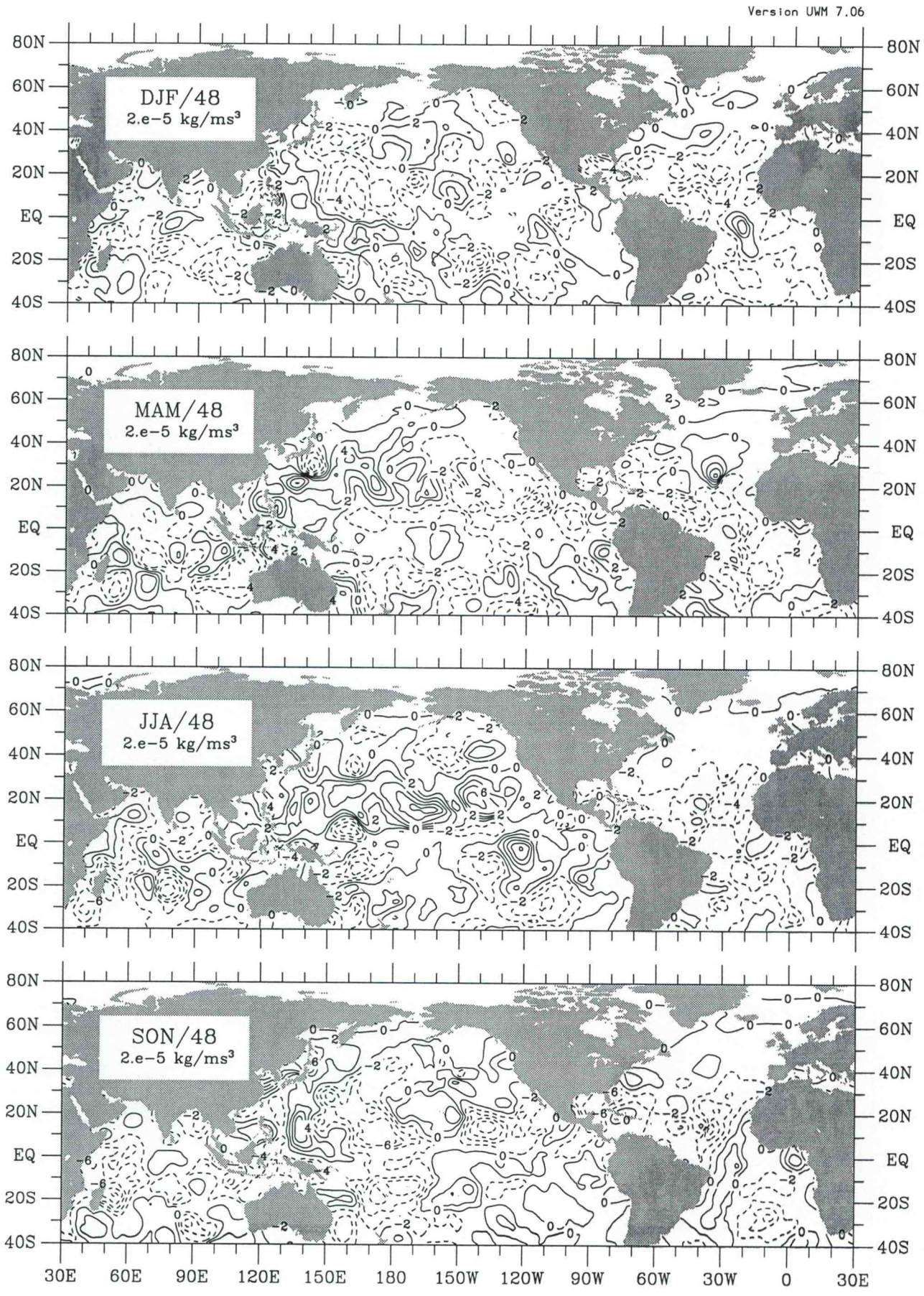

Figure buoy-9. Buoyancy flux seasonal anomaly for 1948.

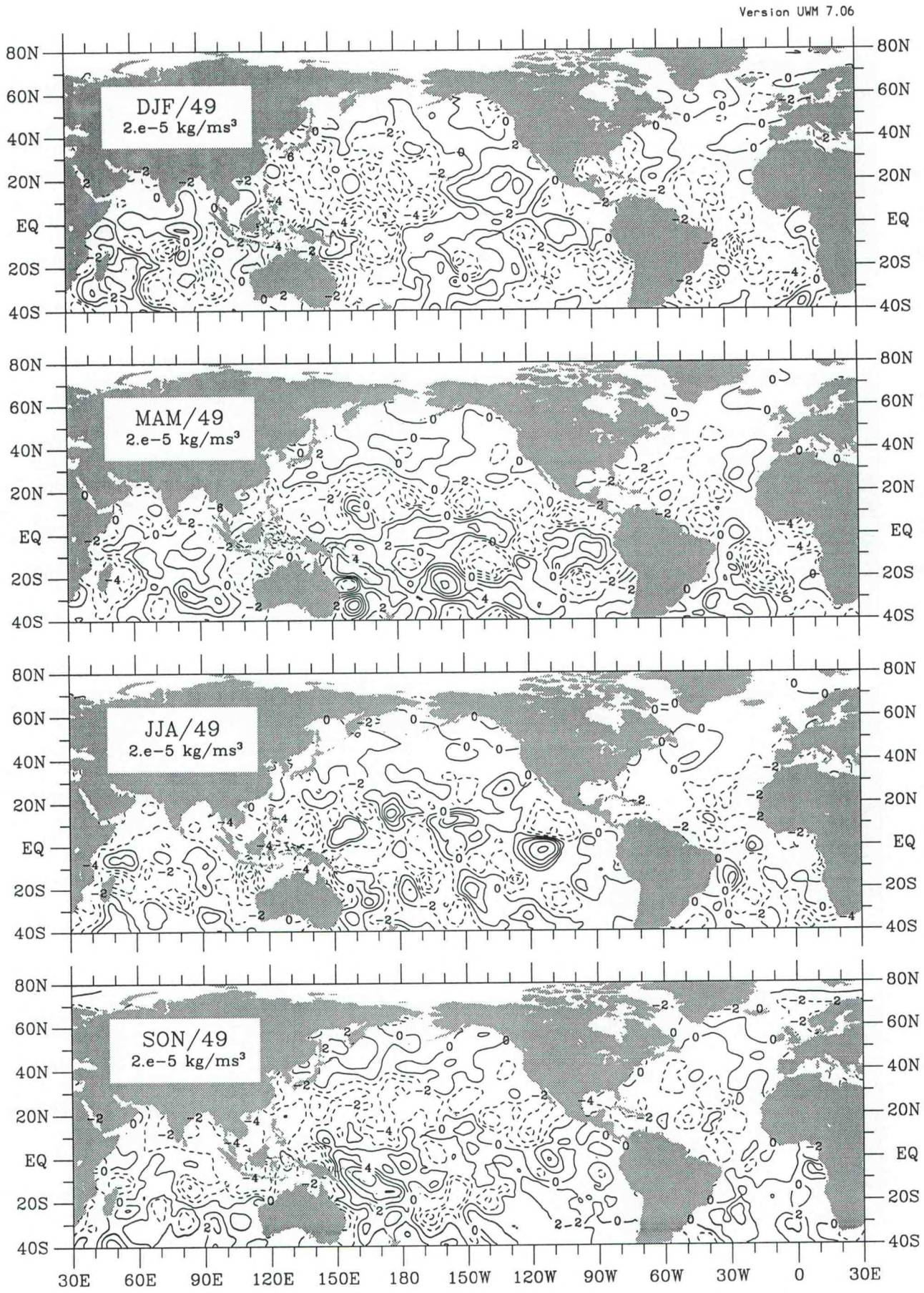

Figure buoy-10. Buoyancy flux seasonal anomaly for 1949.

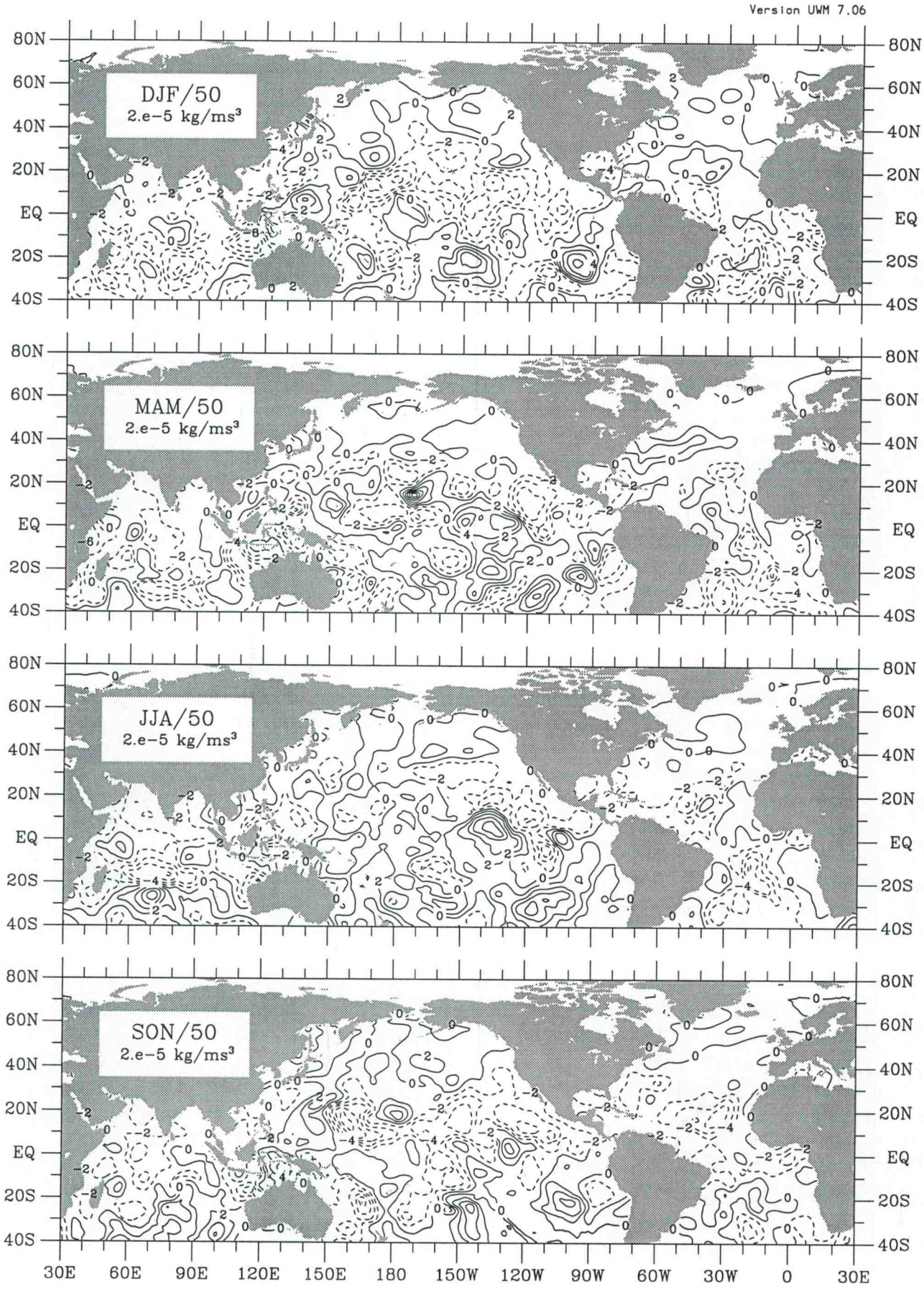

Figure buoy-11. Buoyancy flux seasonal anomaly for 1950.

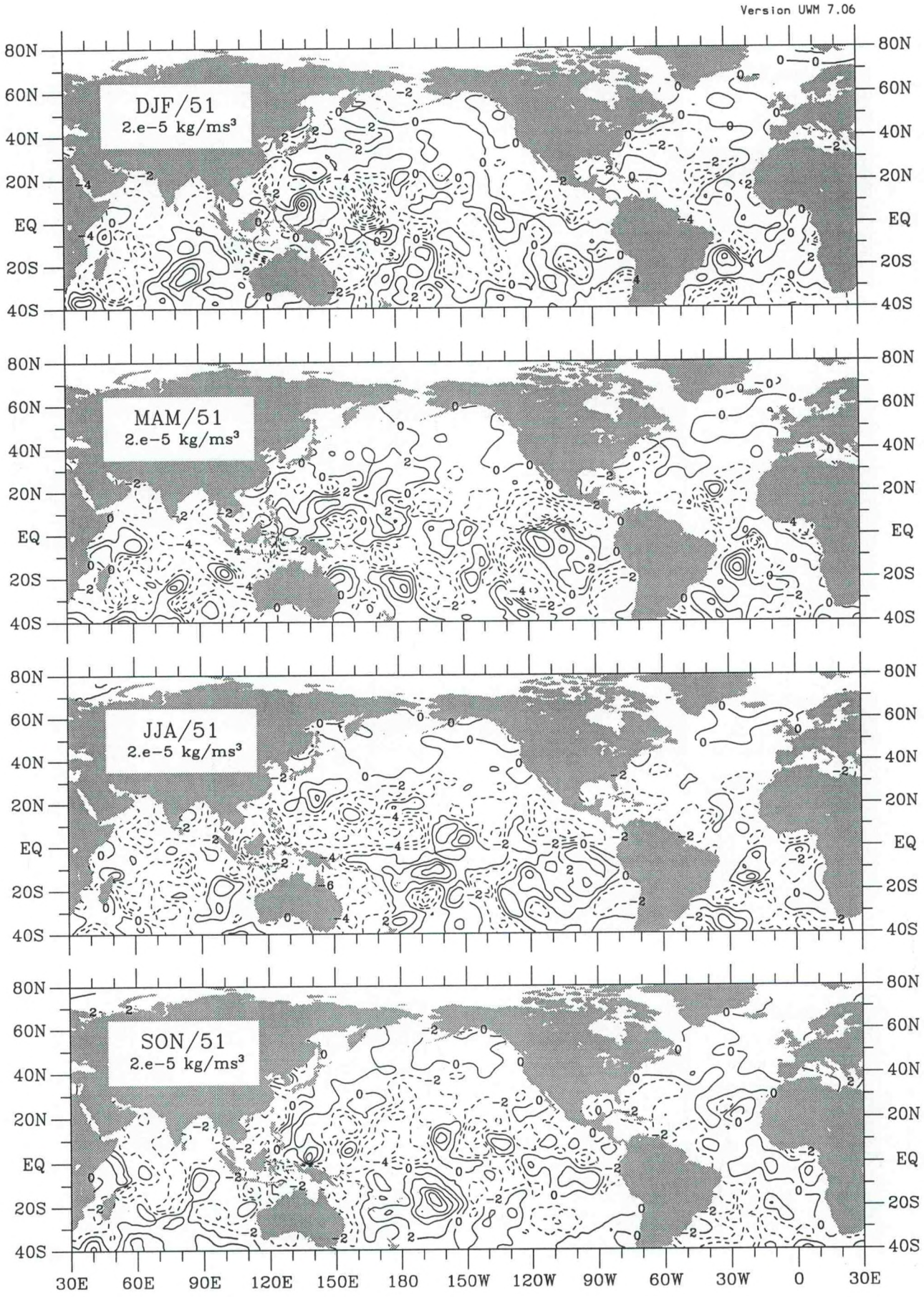

Figure buoy-12. Buoyancy flux seasonal anomaly for 1951.

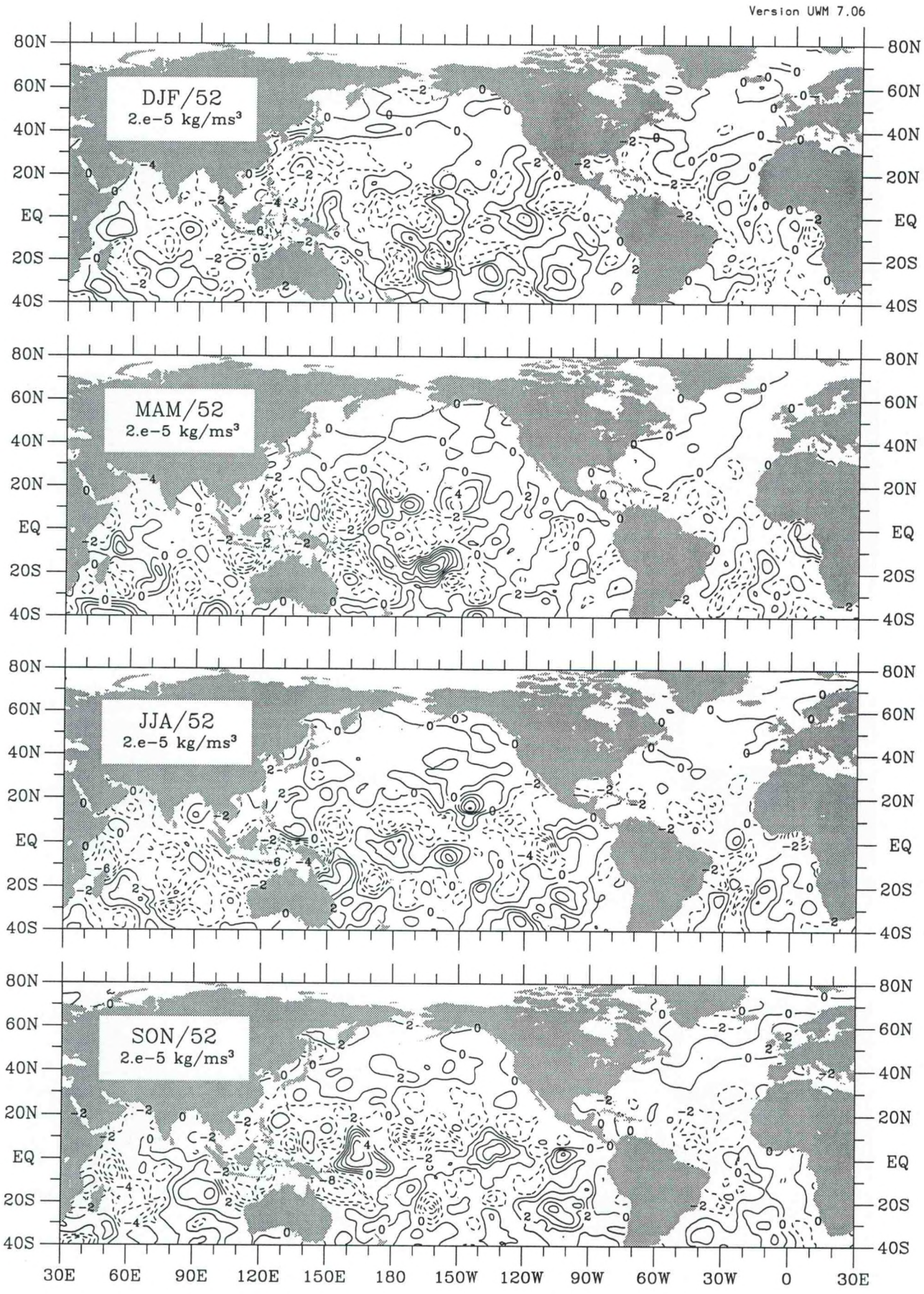

Figure buoy-13. Buoyancy flux seasonal anomaly for 1952.

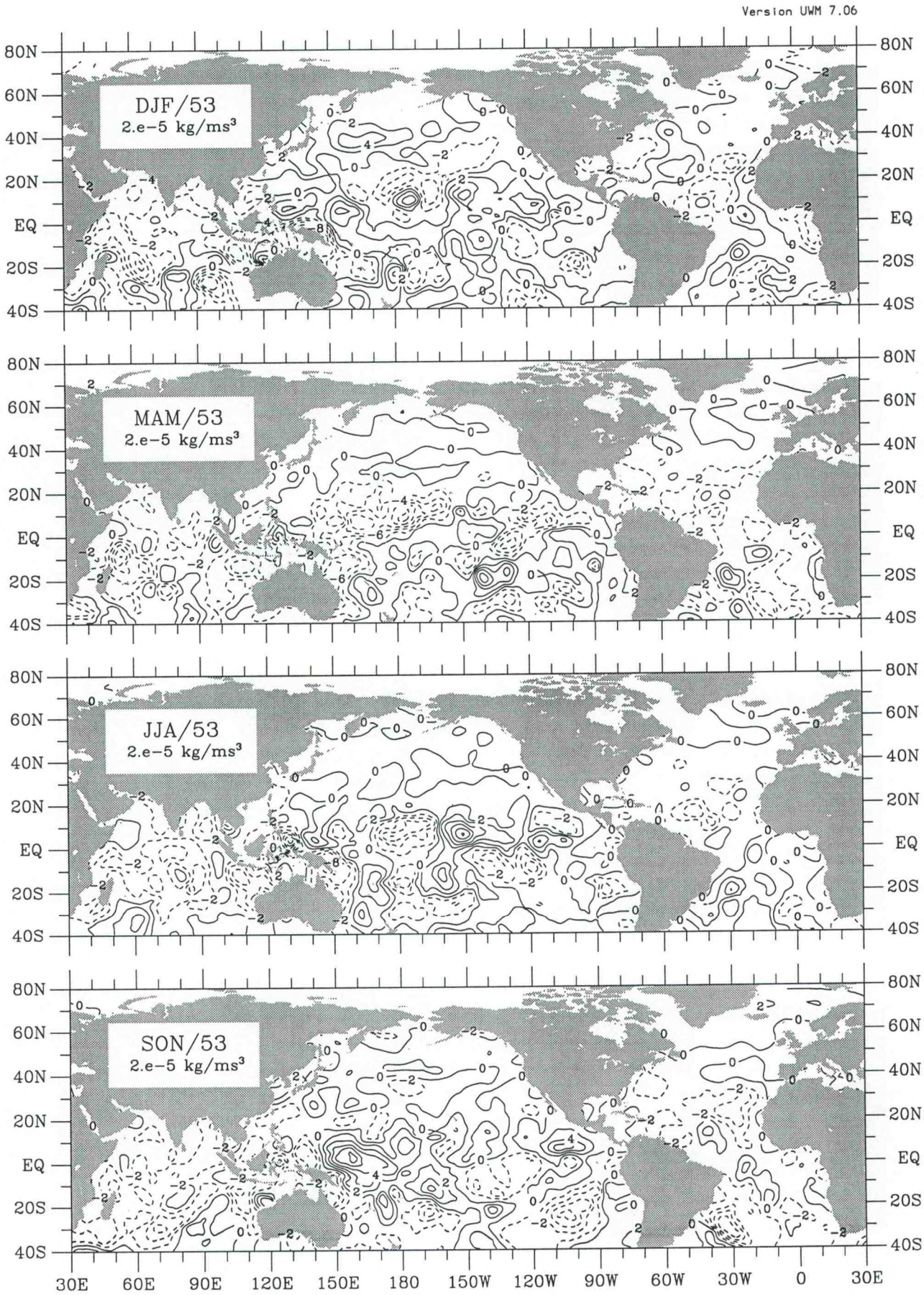

Figure buoy-14. Buoyancy flux seasonal anomaly for 1953.

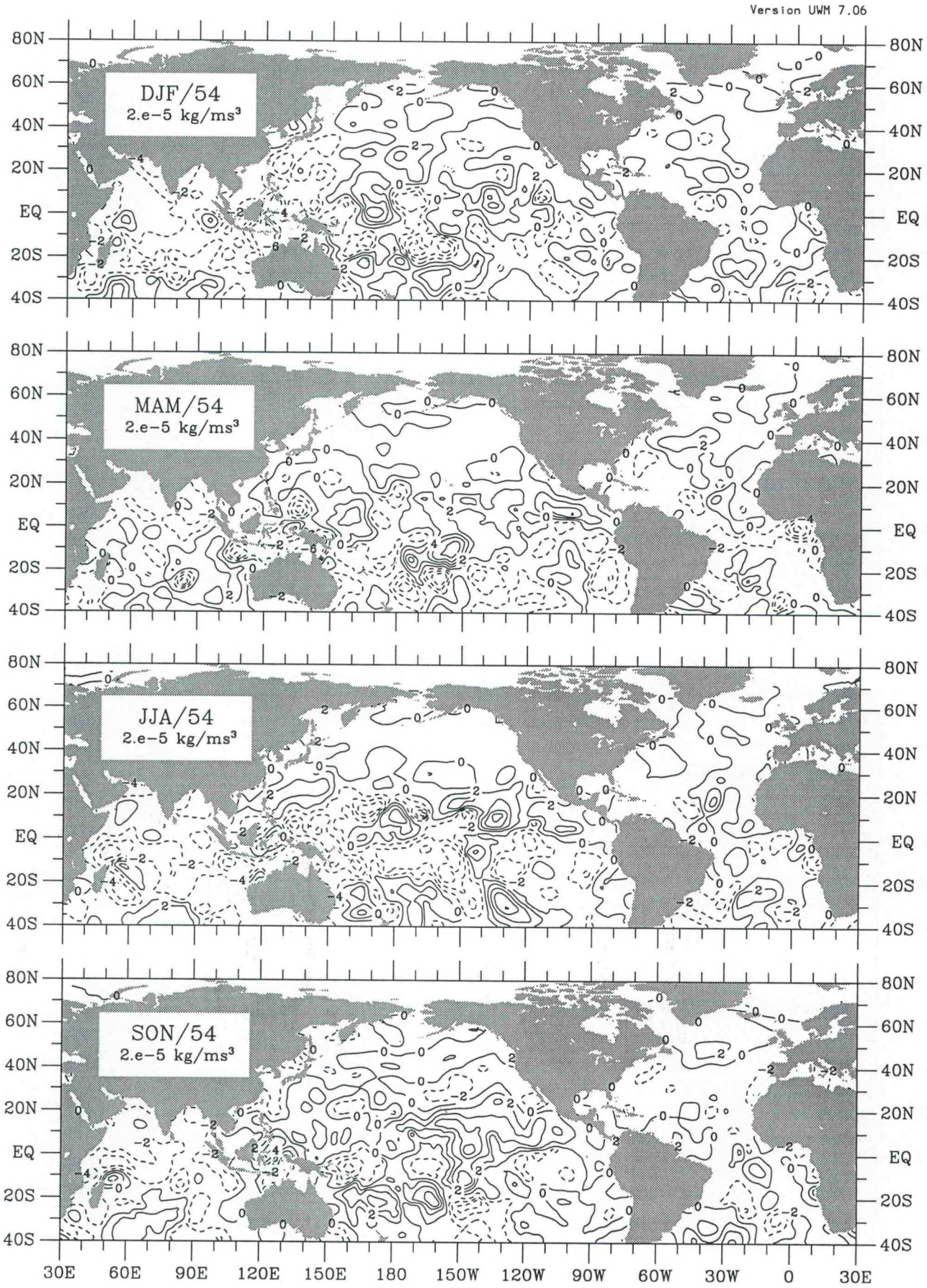

Figure buoy-15. Buoyancy flux seasonal anomaly for 1954.

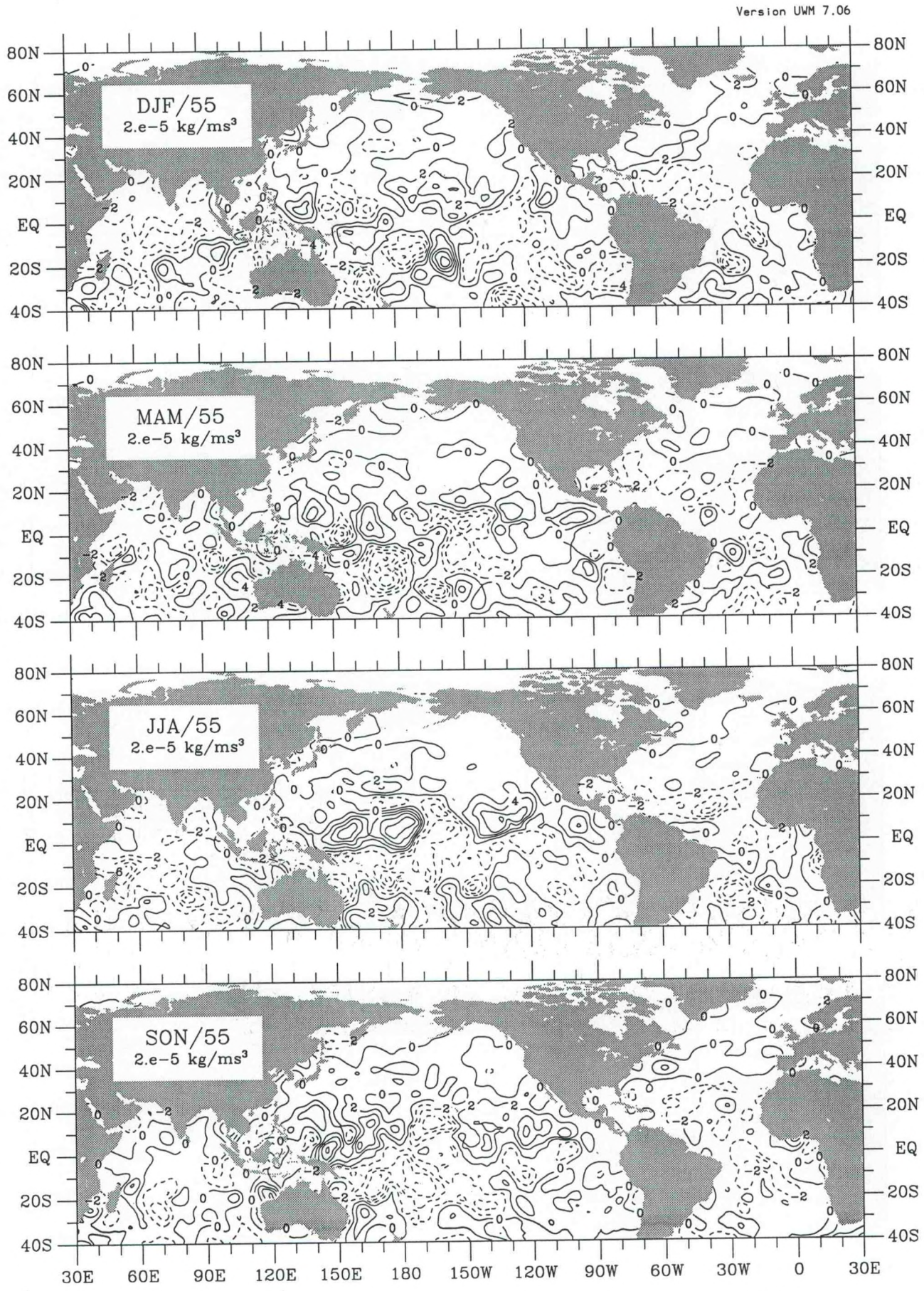

Figure buoy-16. Buoyancy flux seasonal anomaly for 1955.

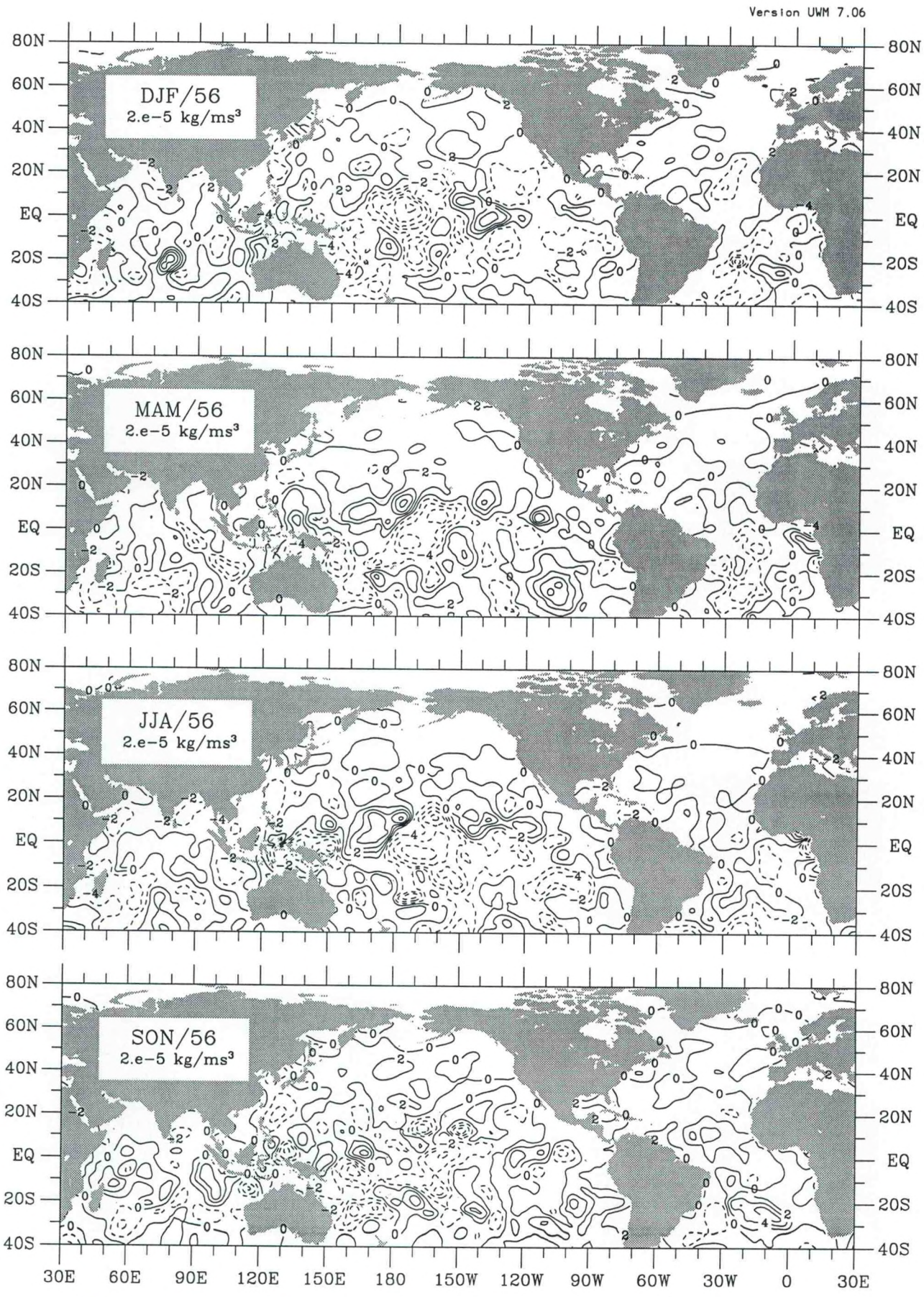

Figure buoy-17. Buoyancy flux seasonal anomaly for 1956.

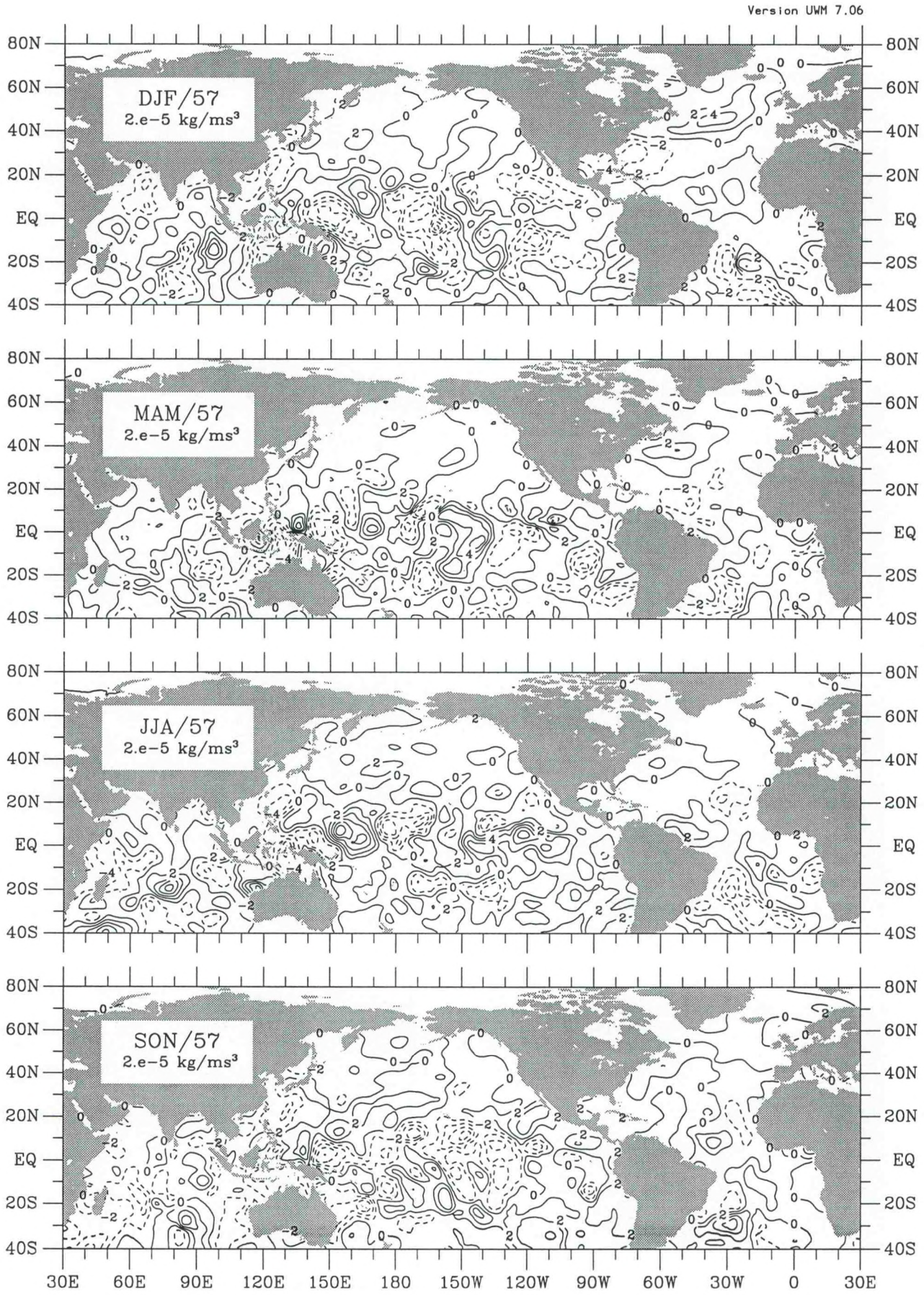

Figure buoy-18. Buoyancy flux seasonal anomaly for 1957.

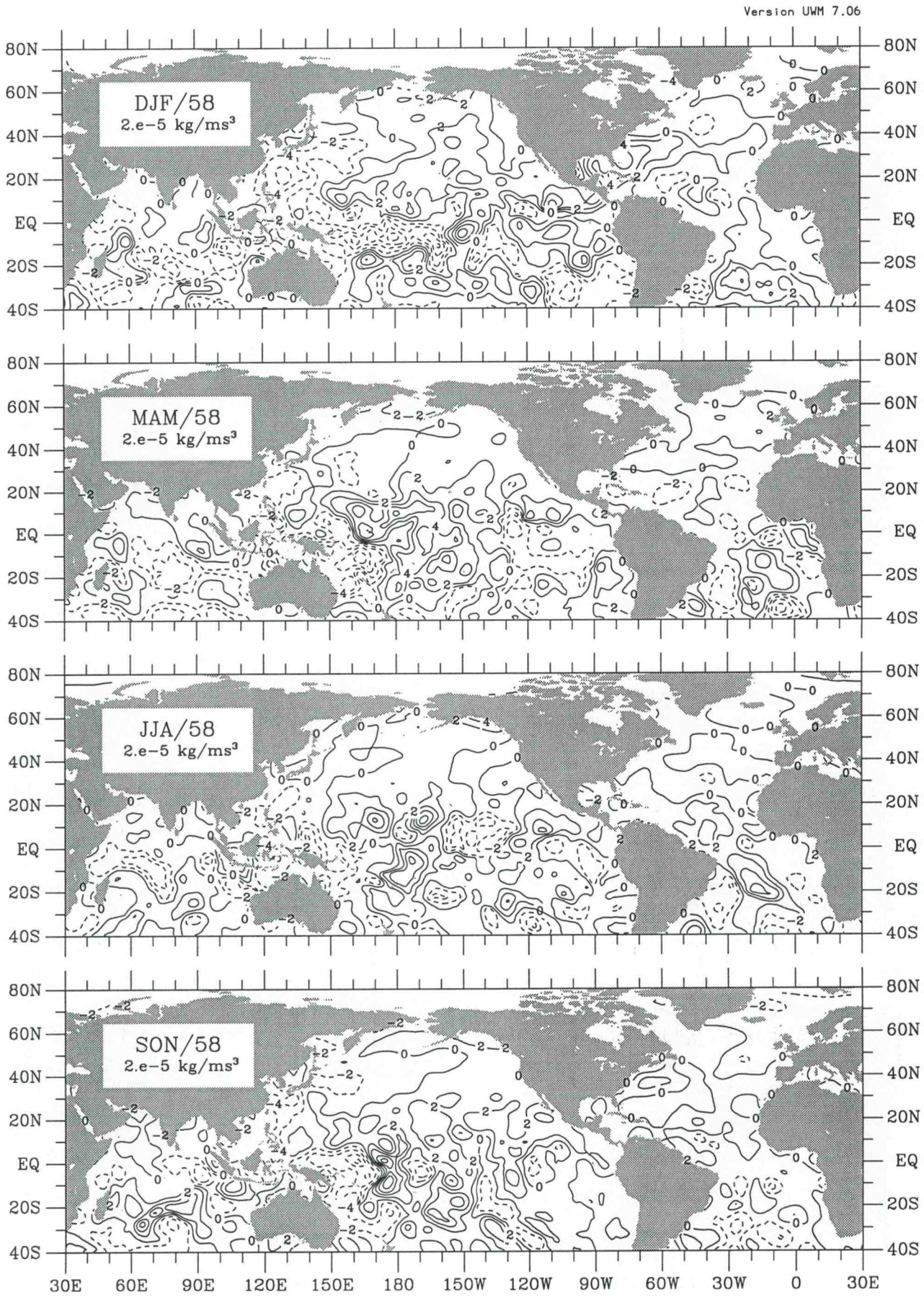

Figure buoy-19. Buoyancy flux seasonal anomaly for 1958.

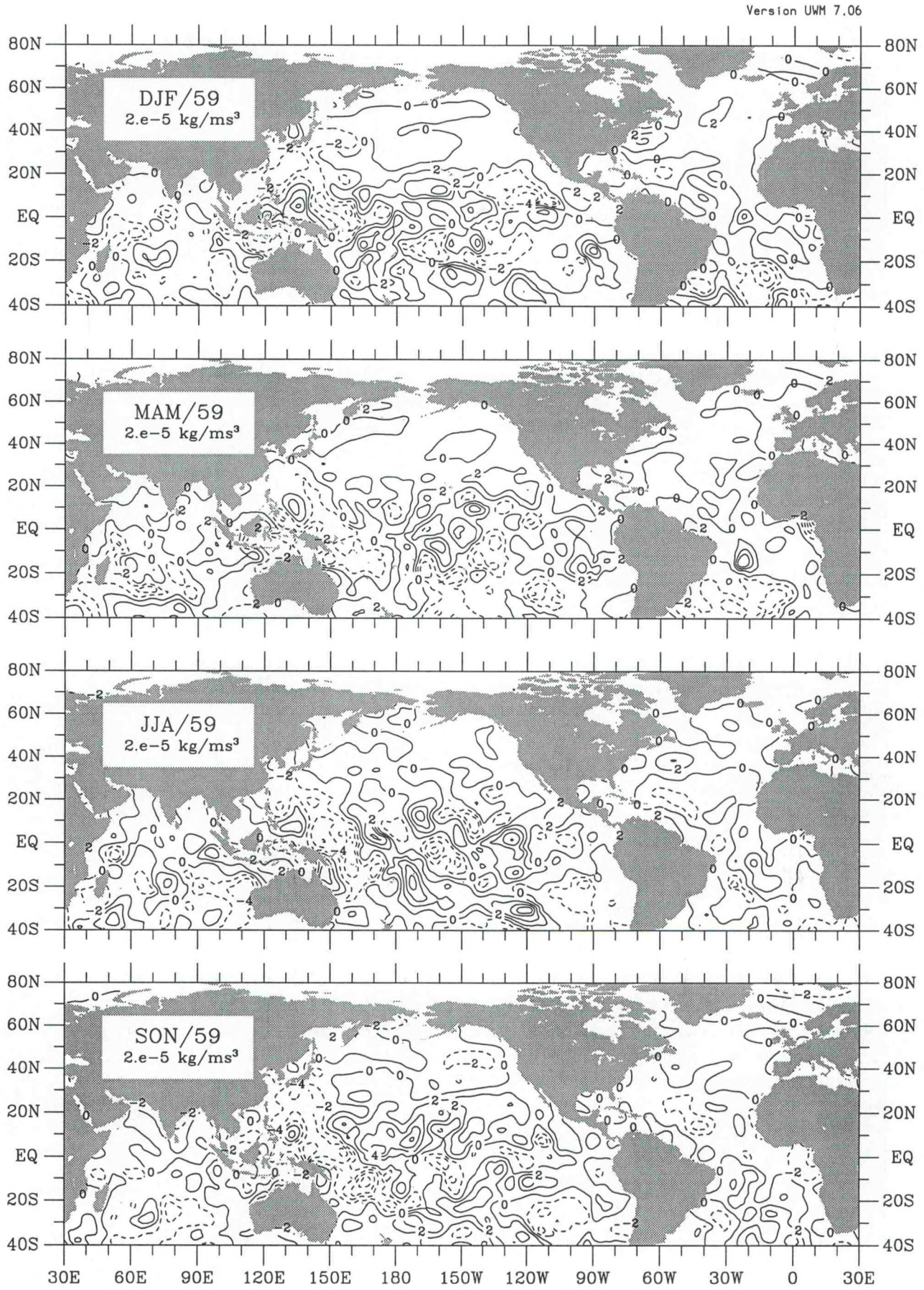

Figure buoy–20. Buoyancy flux seasonal anomaly for 1959.

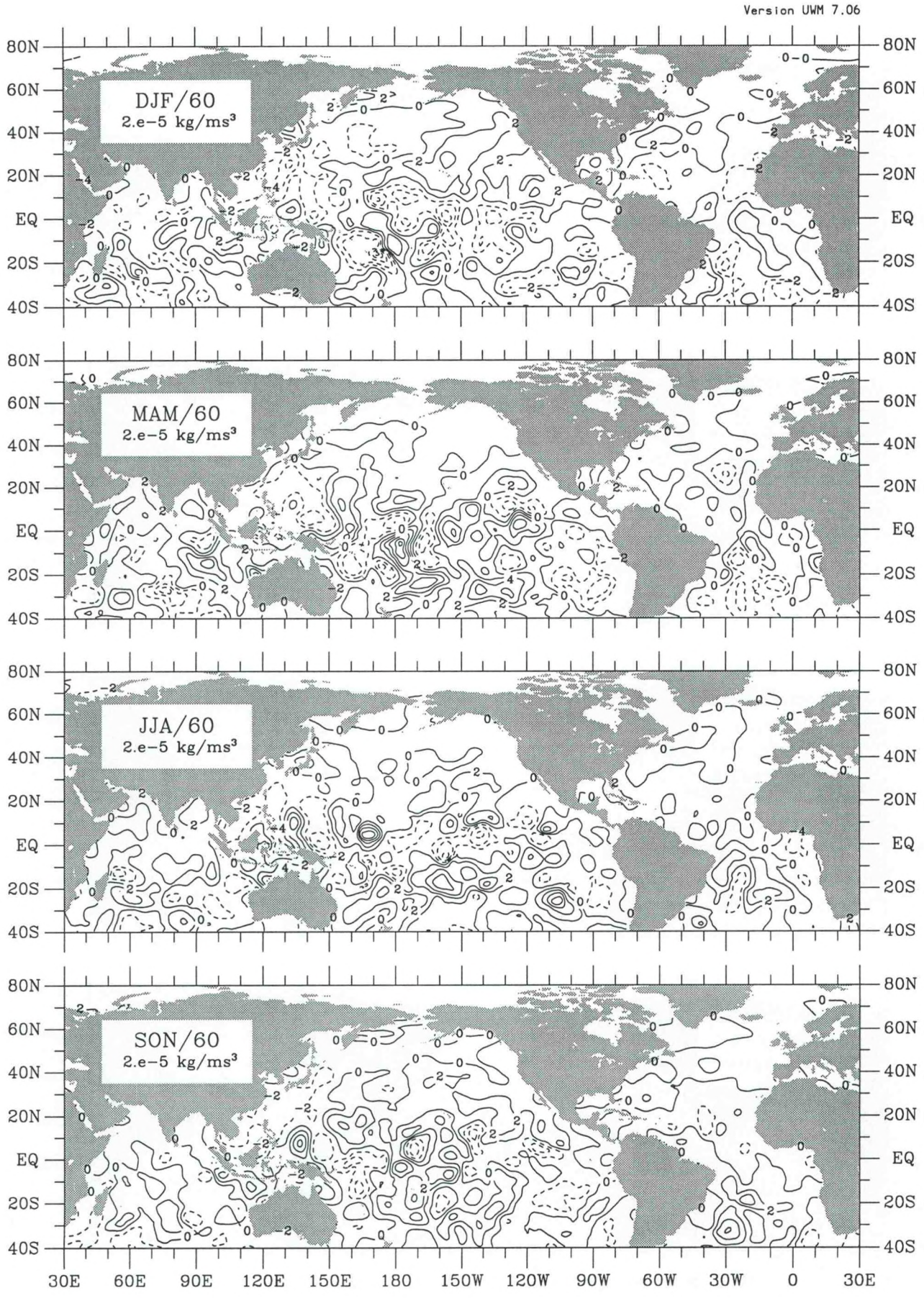

Figure buoy-21. Buoyancy flux seasonal anomaly for 1960.

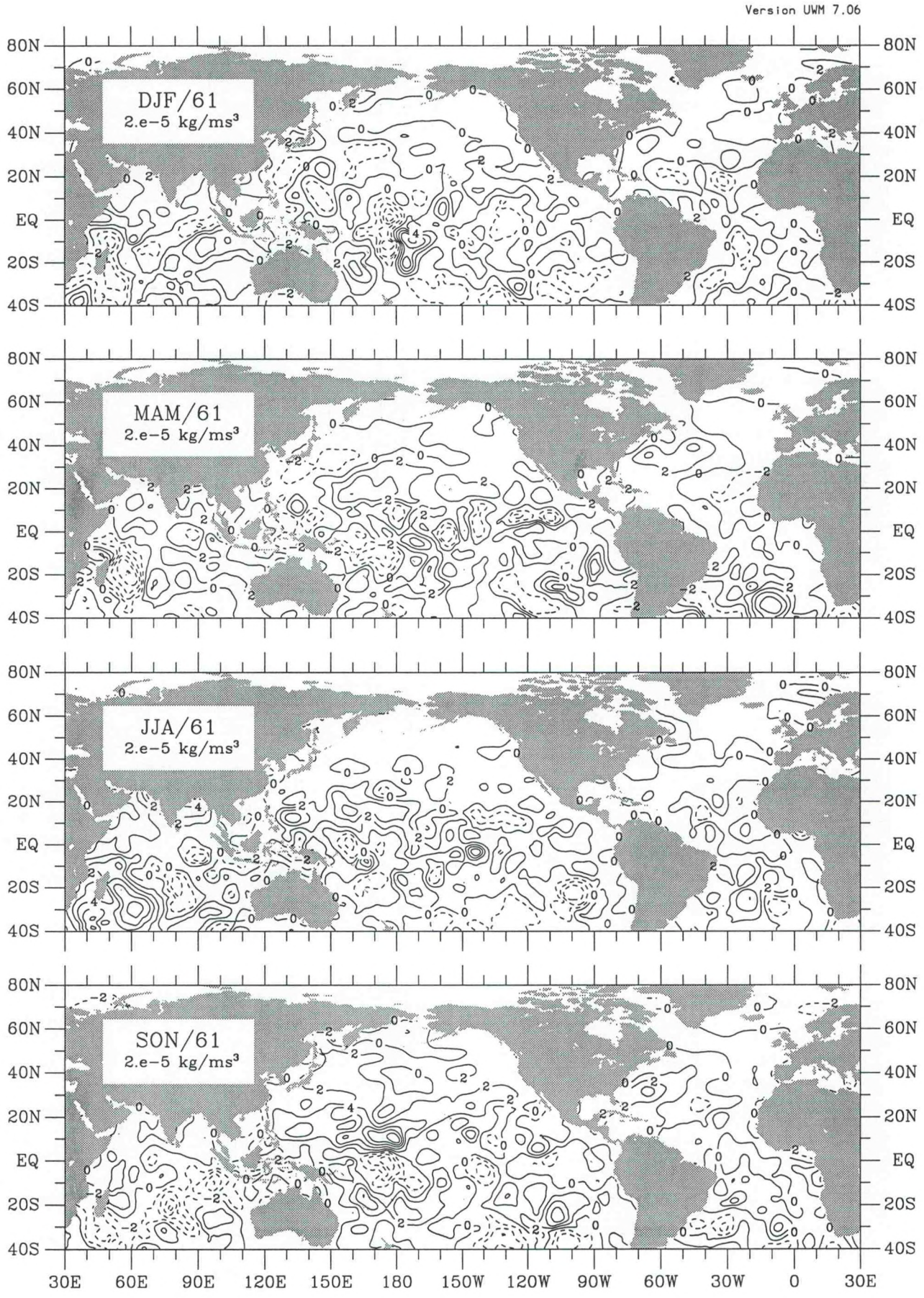

Figure buoy-22. Buoyancy flux seasonal anomaly for 1961.

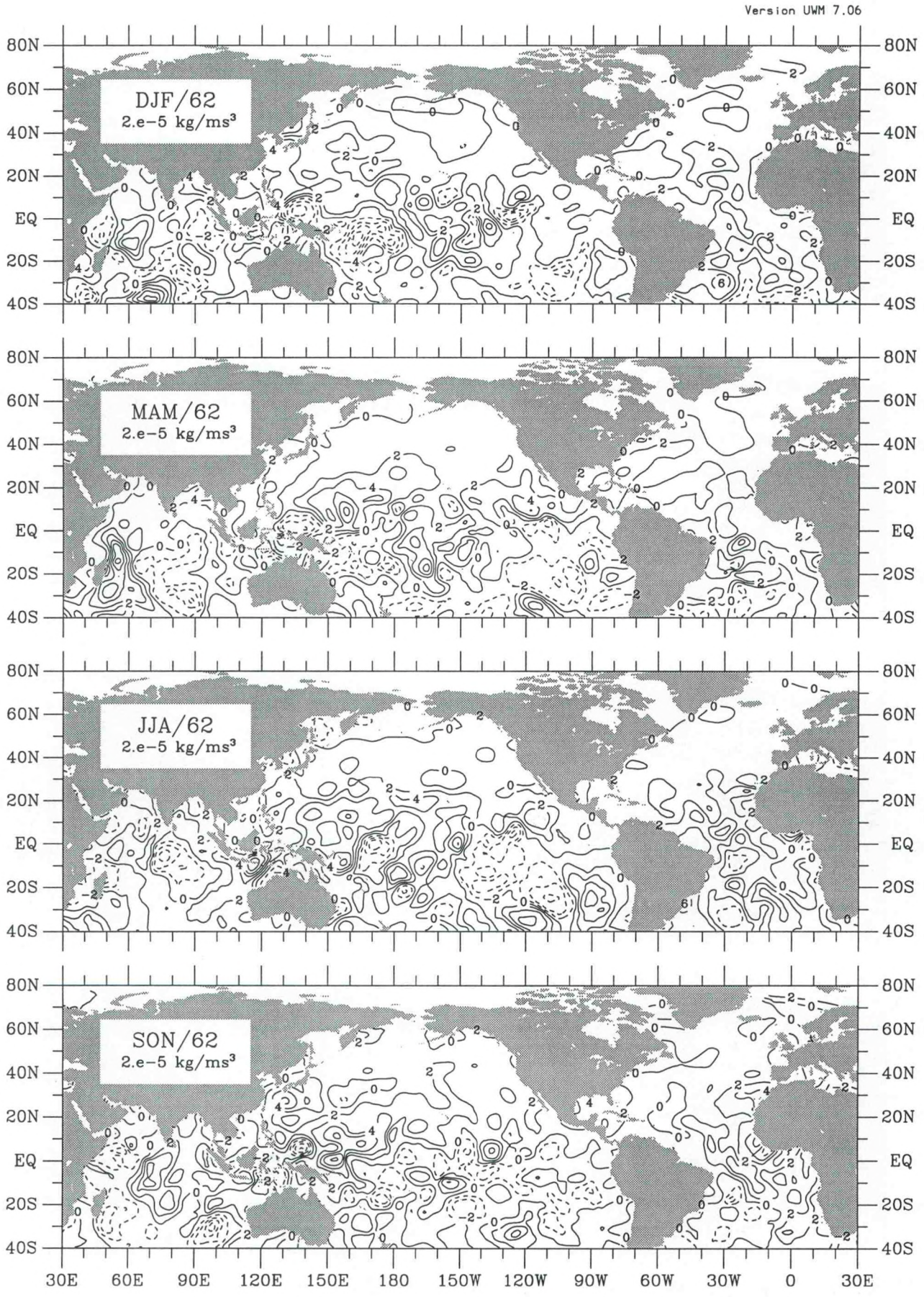

Figure buoy-23. Buoyancy flux seasonal anomaly for 1962.

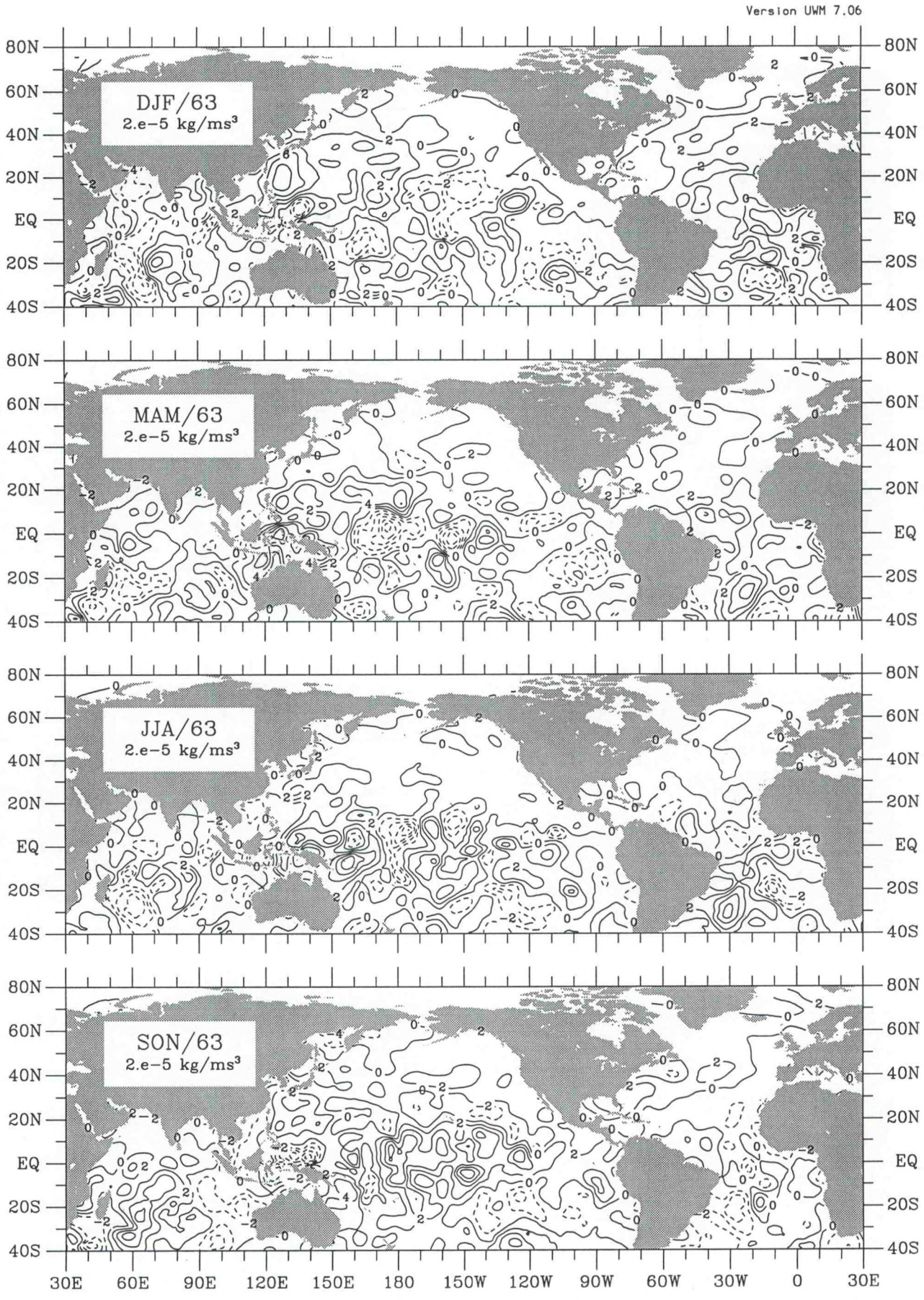

Figure buoy-24. Buoyancy flux seasonal anomaly for 1963.

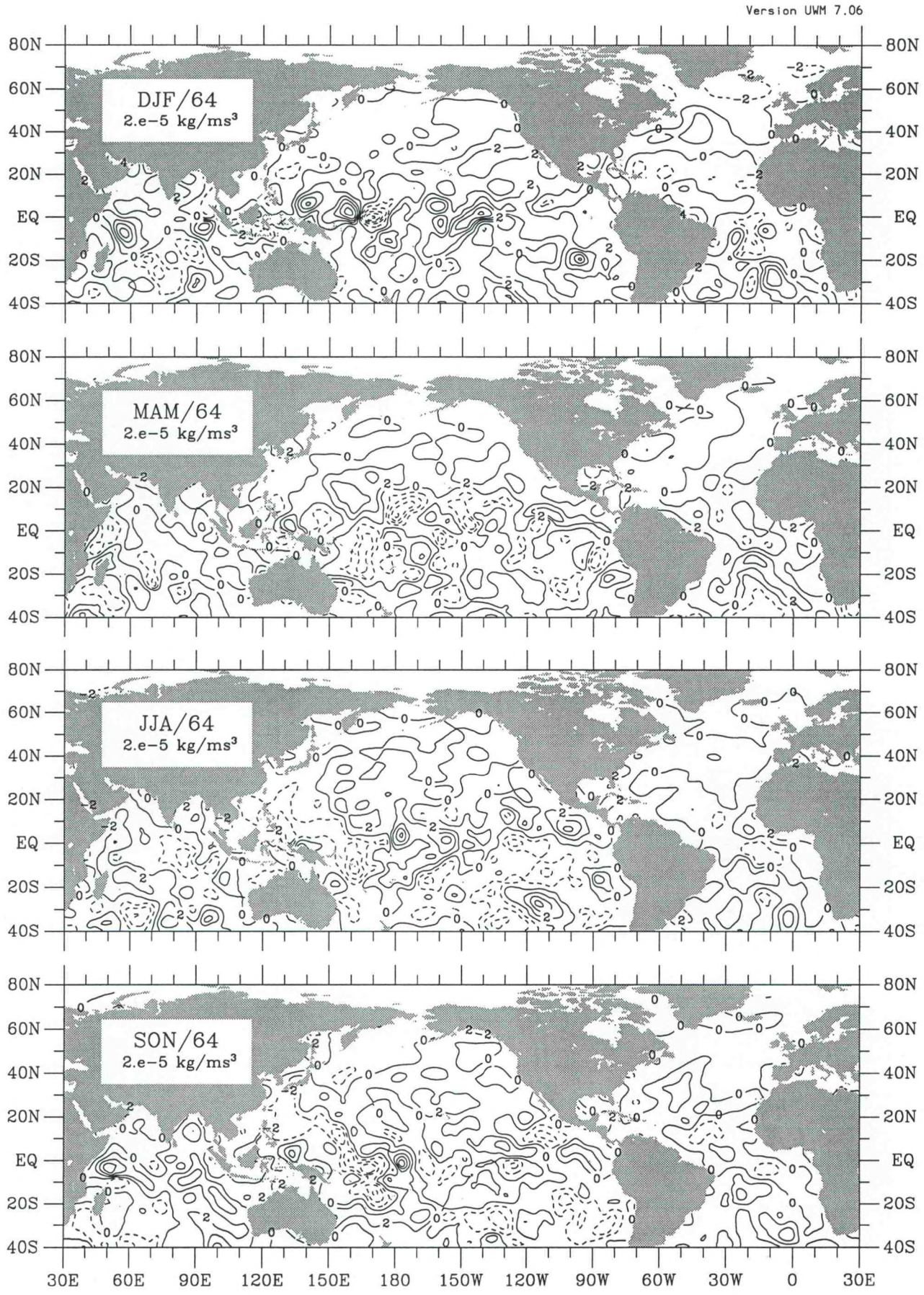

Figure buoy-25. Buoyancy flux seasonal anomaly for 1964.

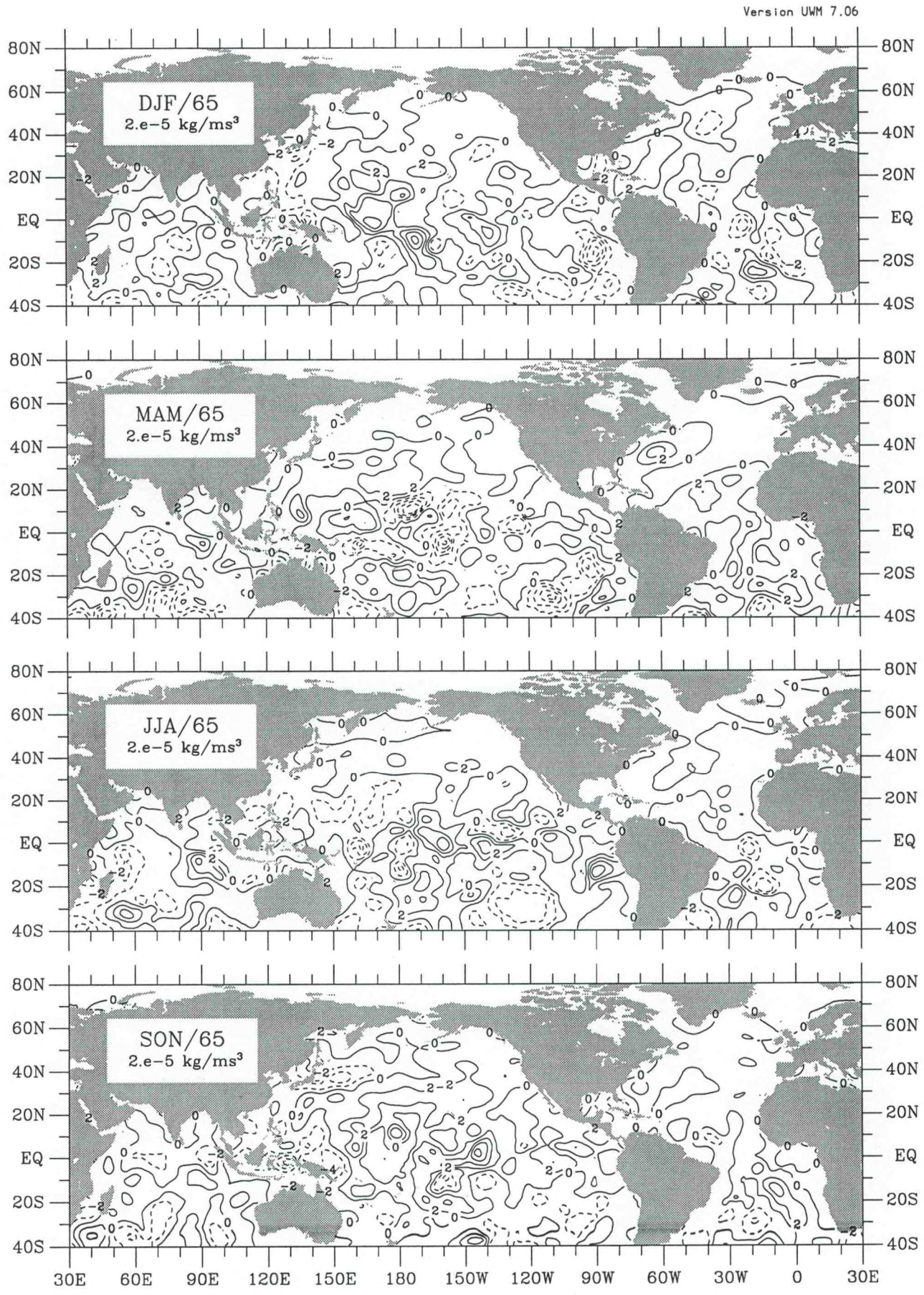

Figure buoy-26. Buoyancy flux seasonal anomaly for 1965.

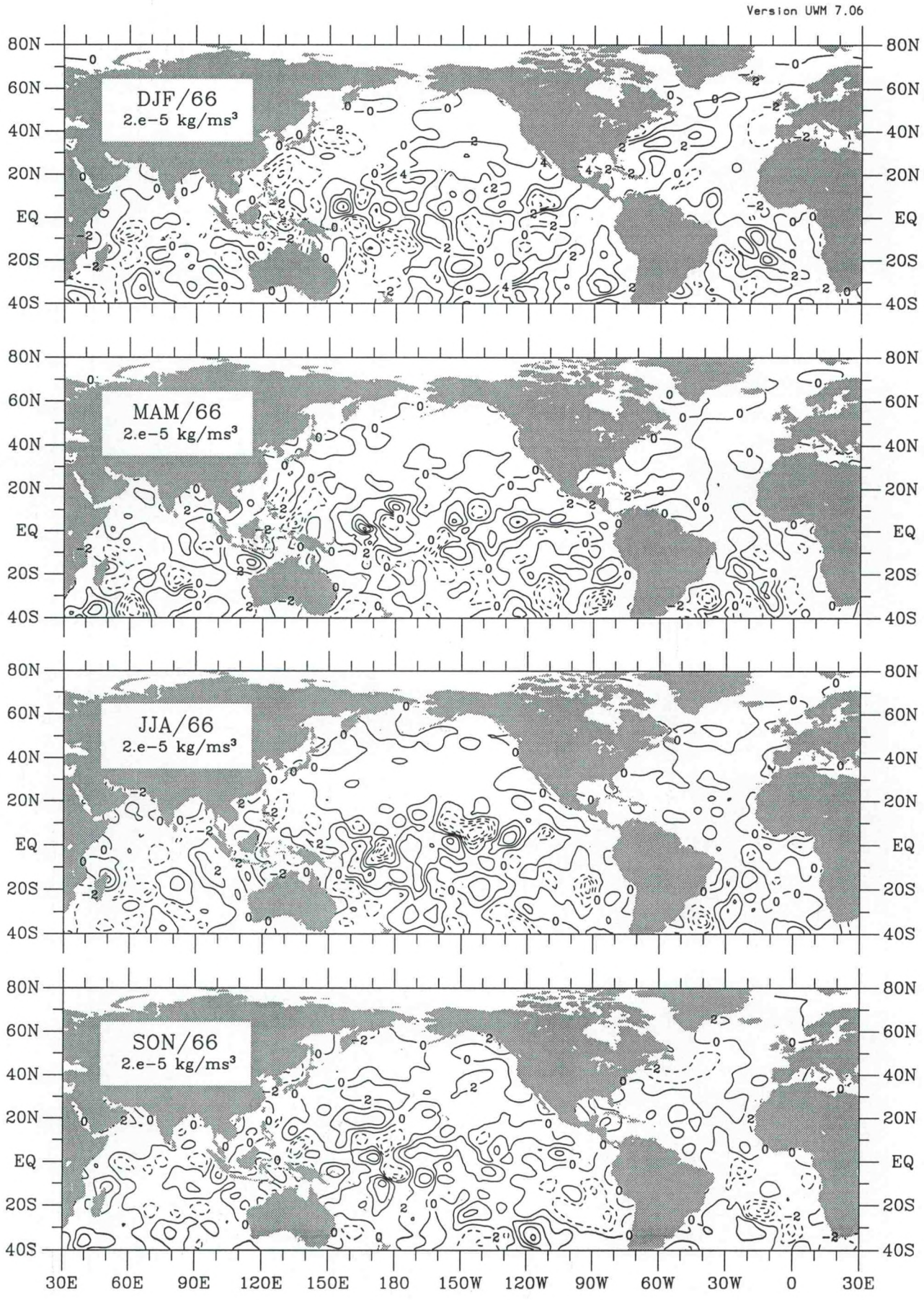

Figure buoy-27. Buoyancy flux seasonal anomaly for 1966.

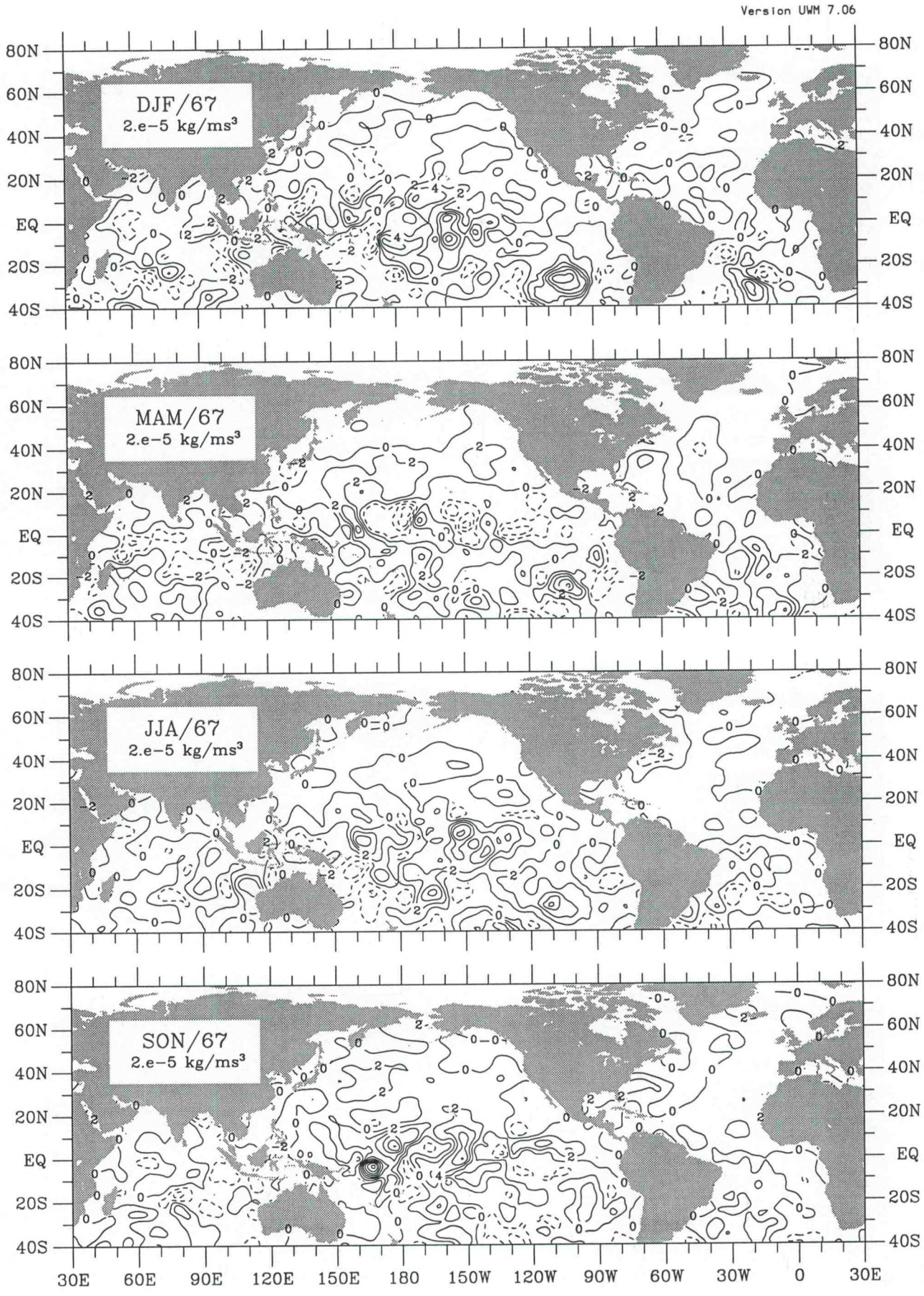

Figure buoy-28. Buoyancy flux seasonal anomaly for 1967.

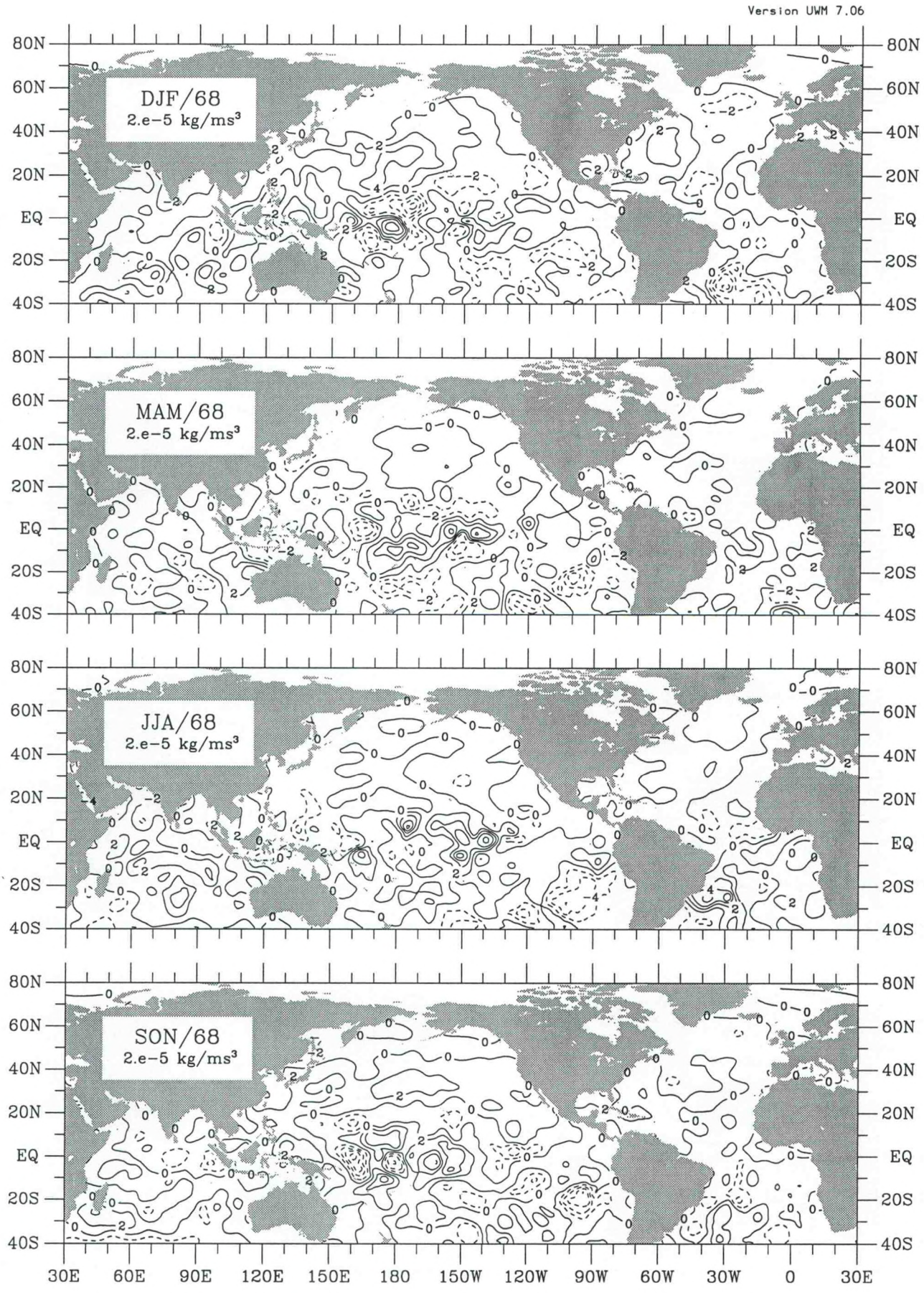

Figure buoy-29. Buoyancy flux seasonal anomaly for 1968.

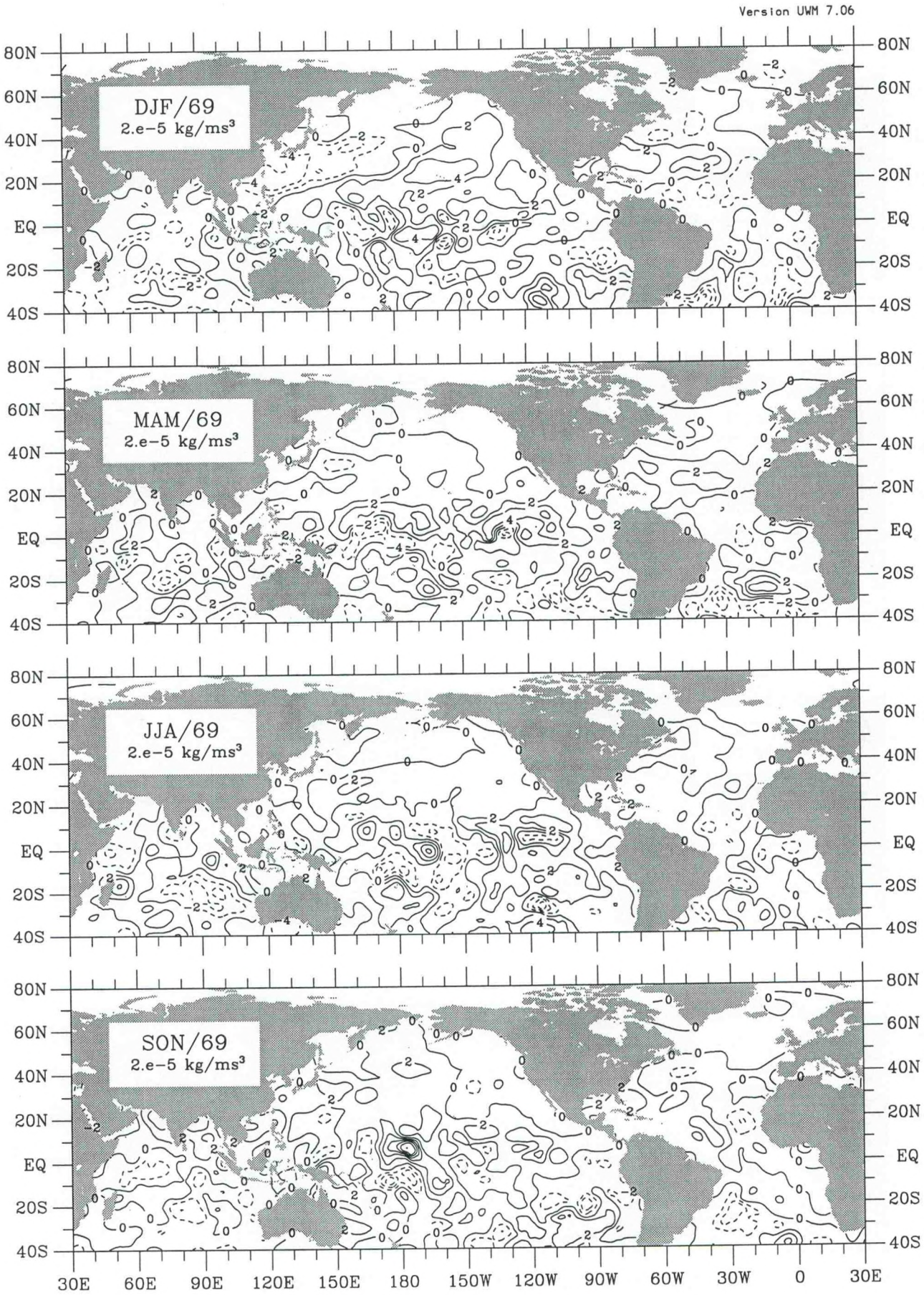

Figure buoy-30. Buoyancy flux seasonal anomaly for 1969.

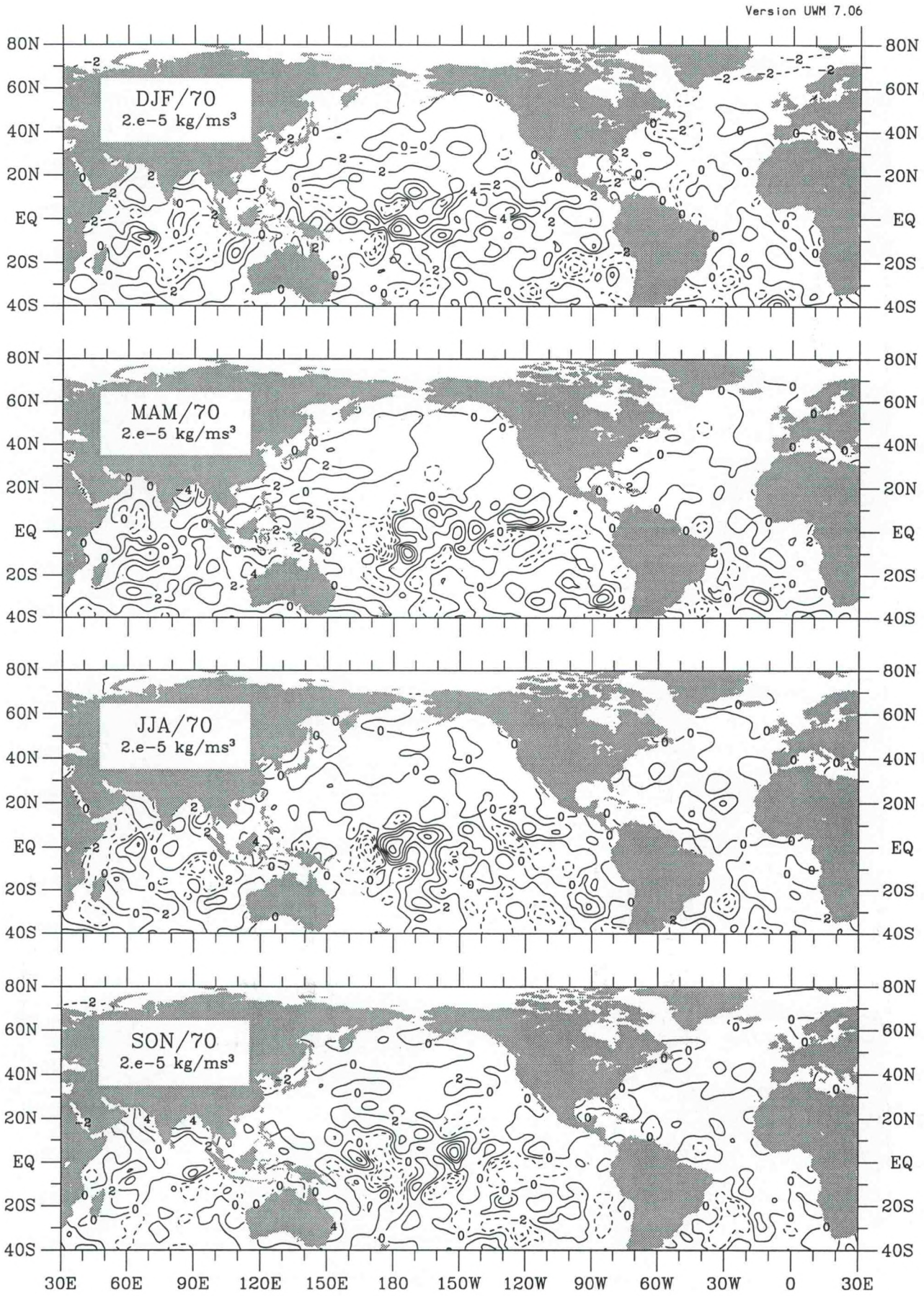

Figure buoy-31. Buoyancy flux seasonal anomaly for 1970.

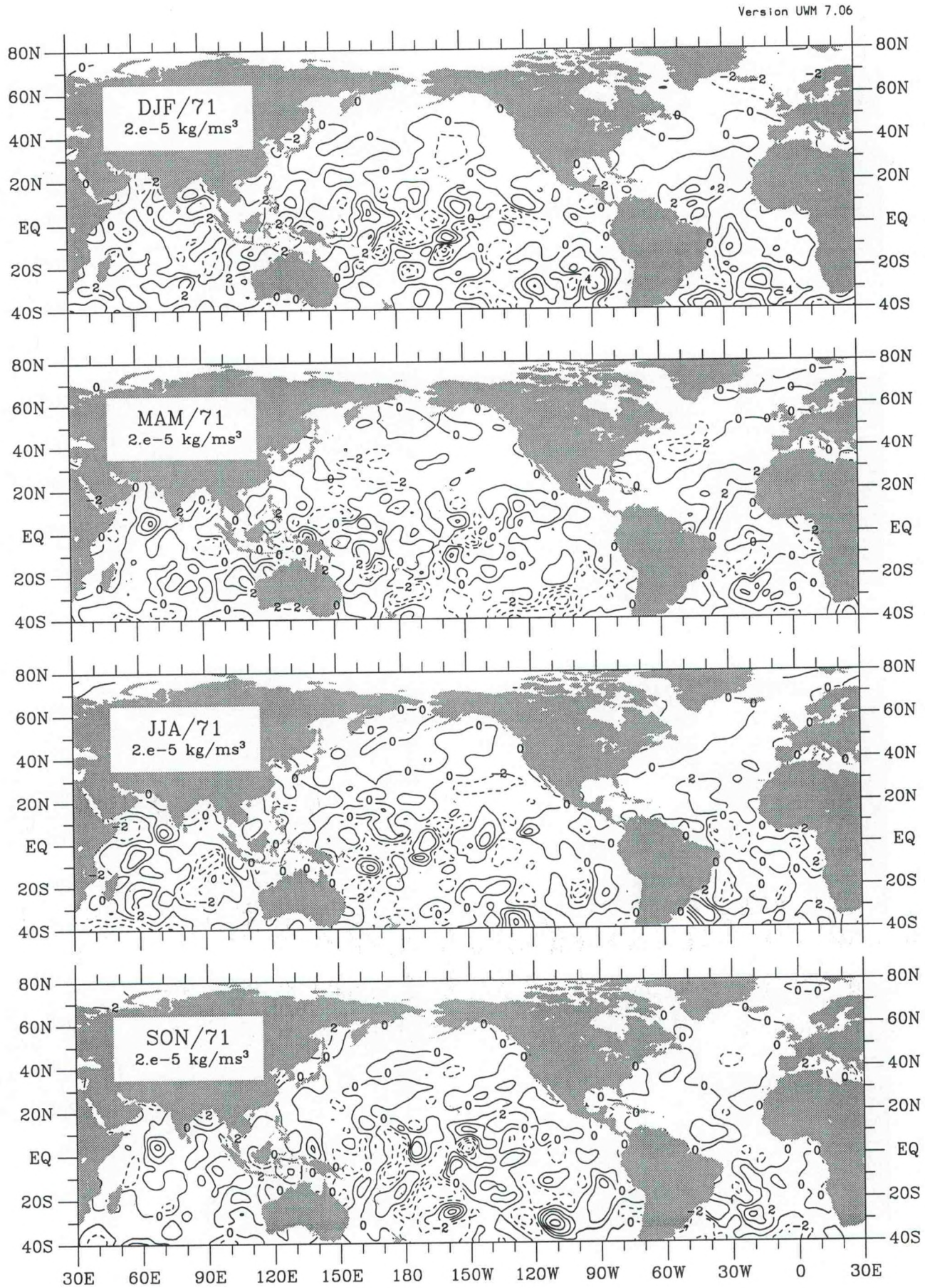

Figure buoy-32. Buoyancy flux seasonal anomaly for 1971.

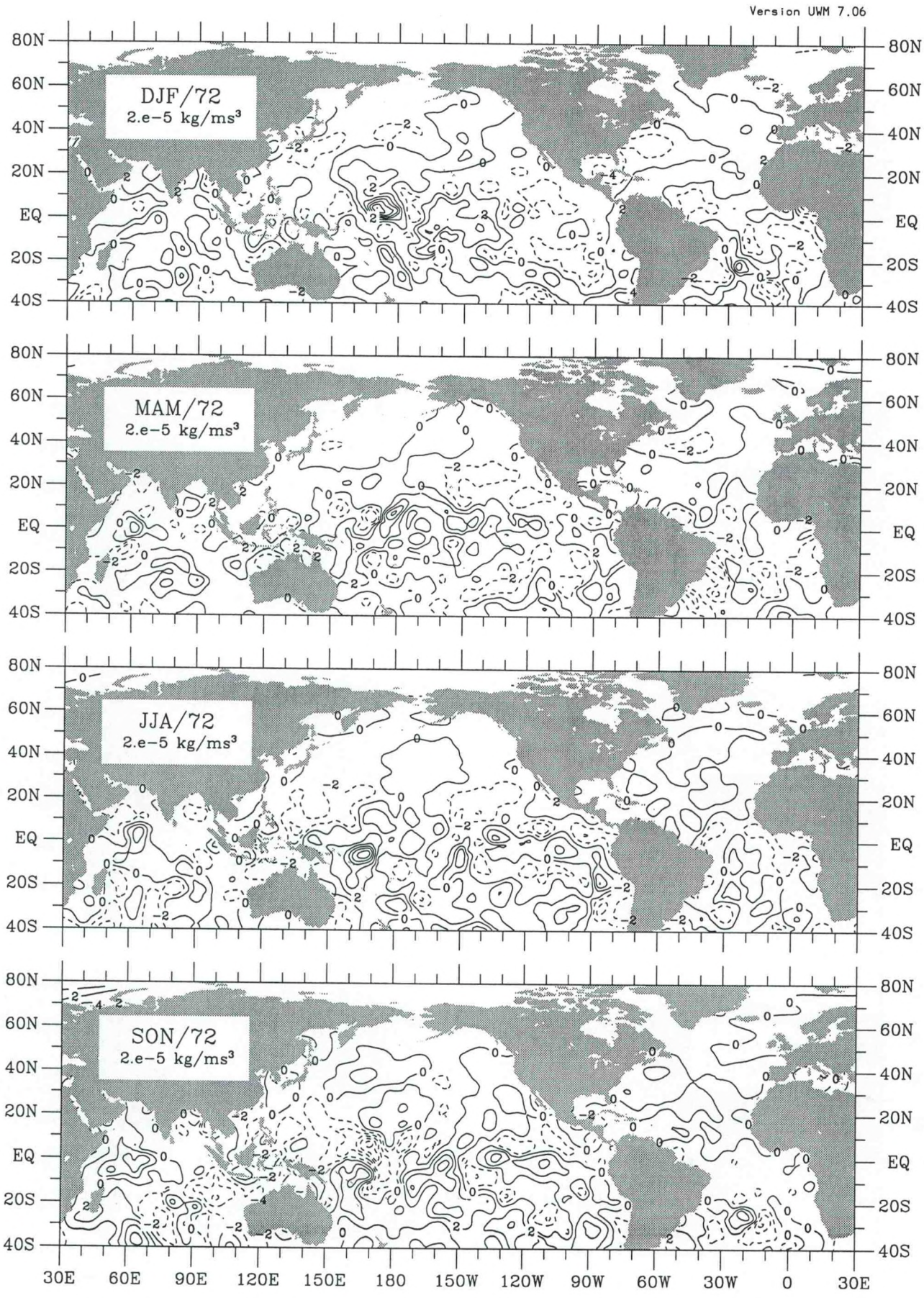

Figure buoy-33. Buoyancy flux seasonal anomaly for 1972.

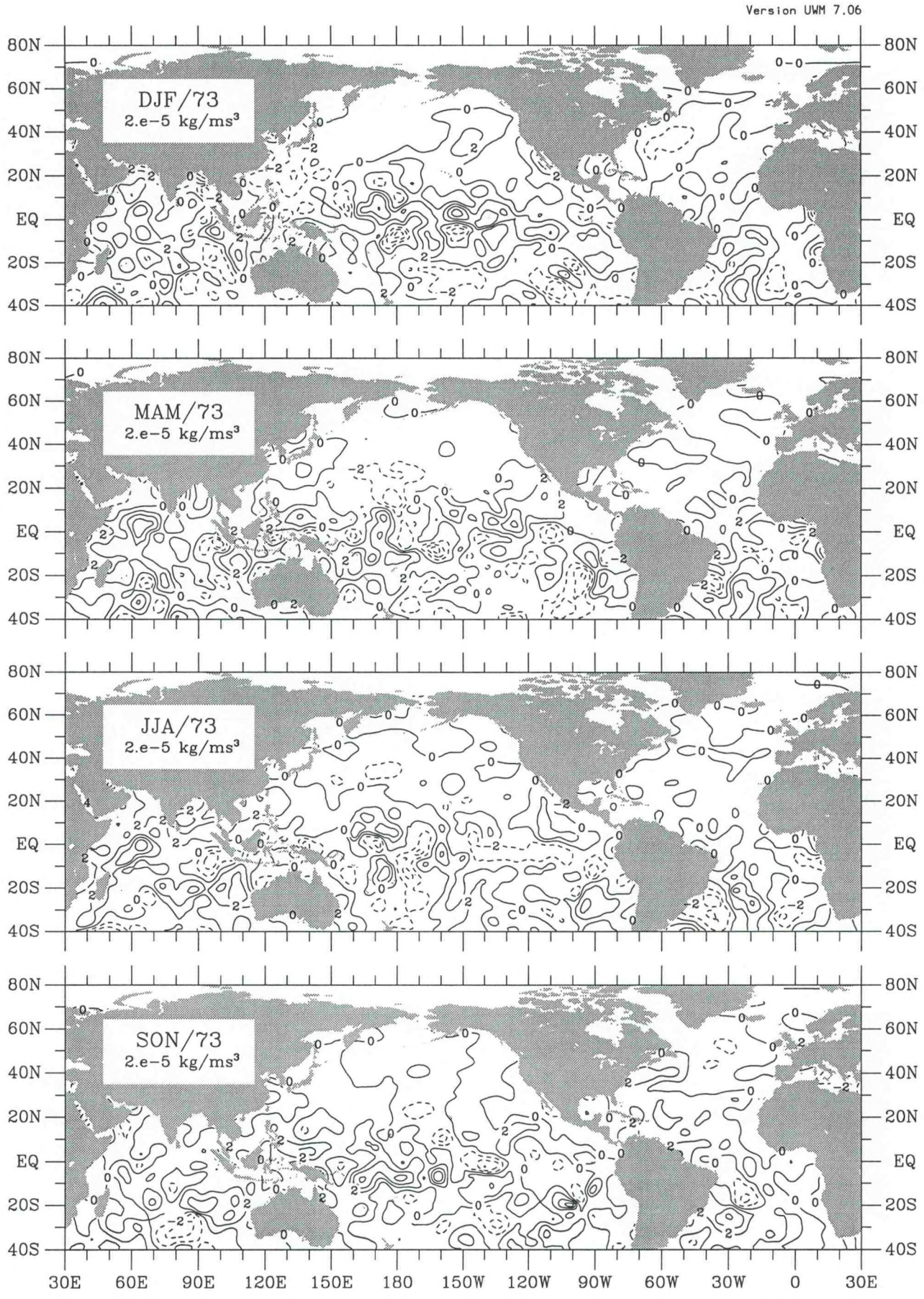

Figure buoy-34. Buoyancy flux seasonal anomaly for 1973.

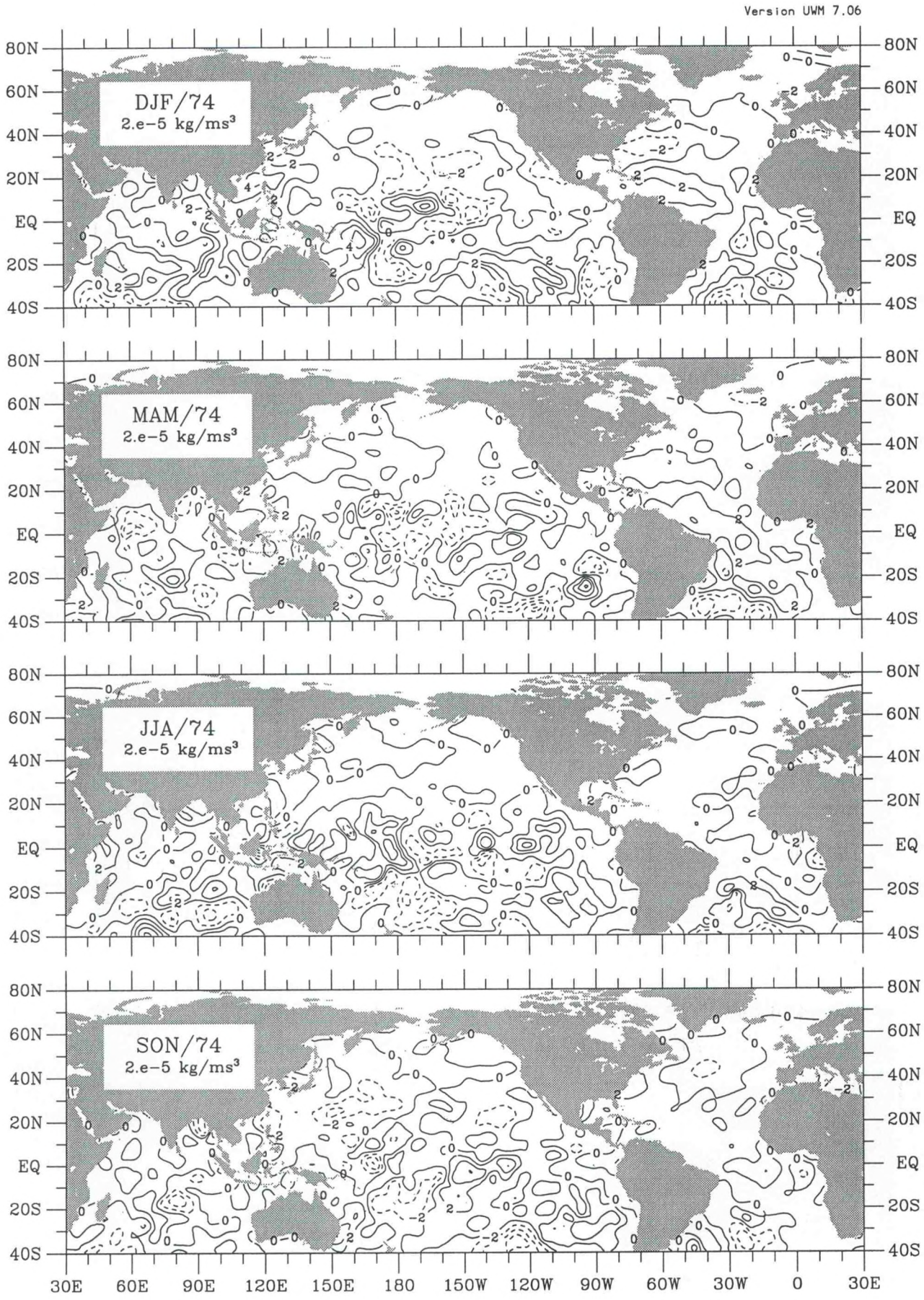

Figure buoy-35. Buoyancy flux seasonal anomaly for 1974.

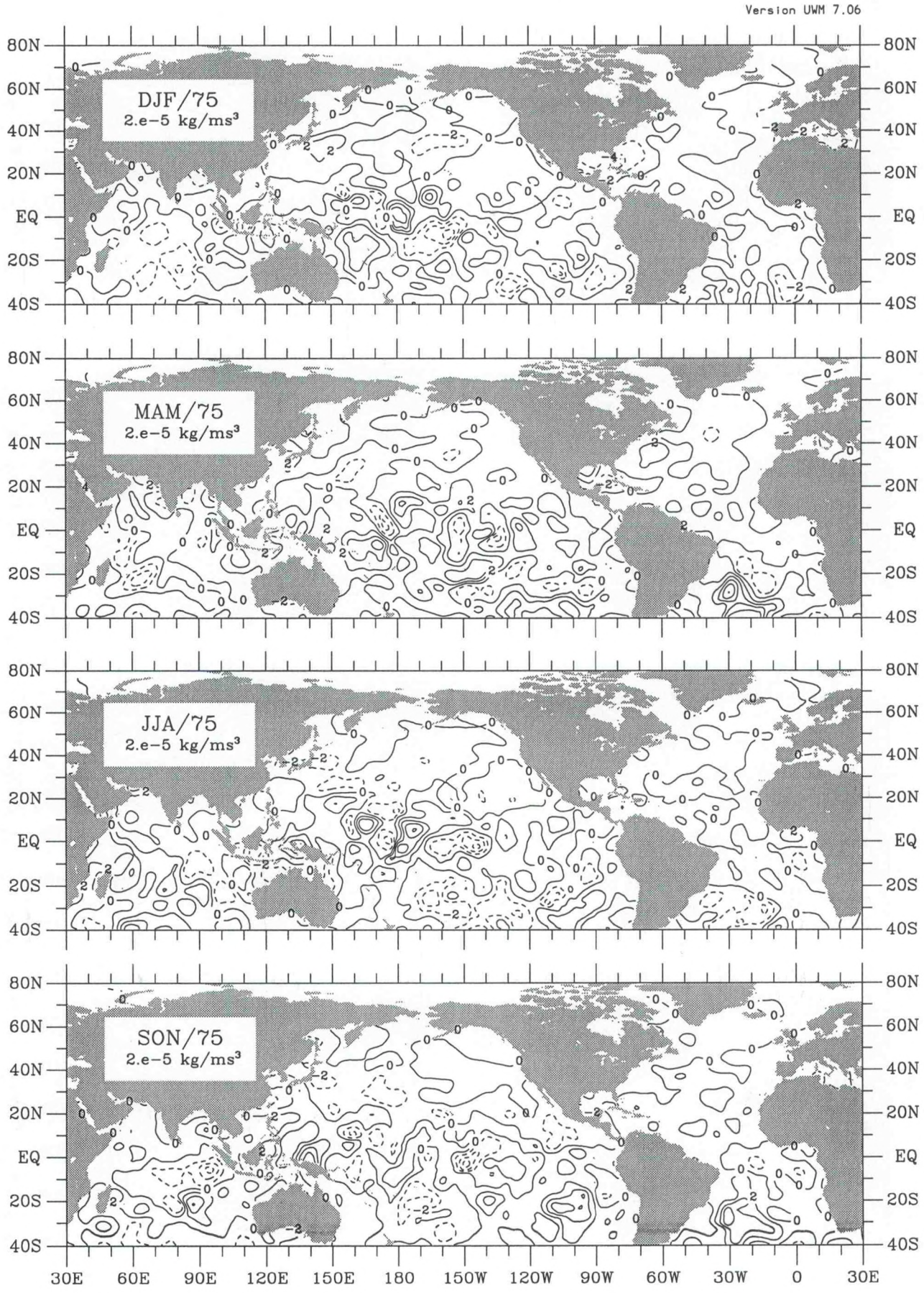

Figure buoy-36. Buoyancy flux seasonal anomaly for 1975.

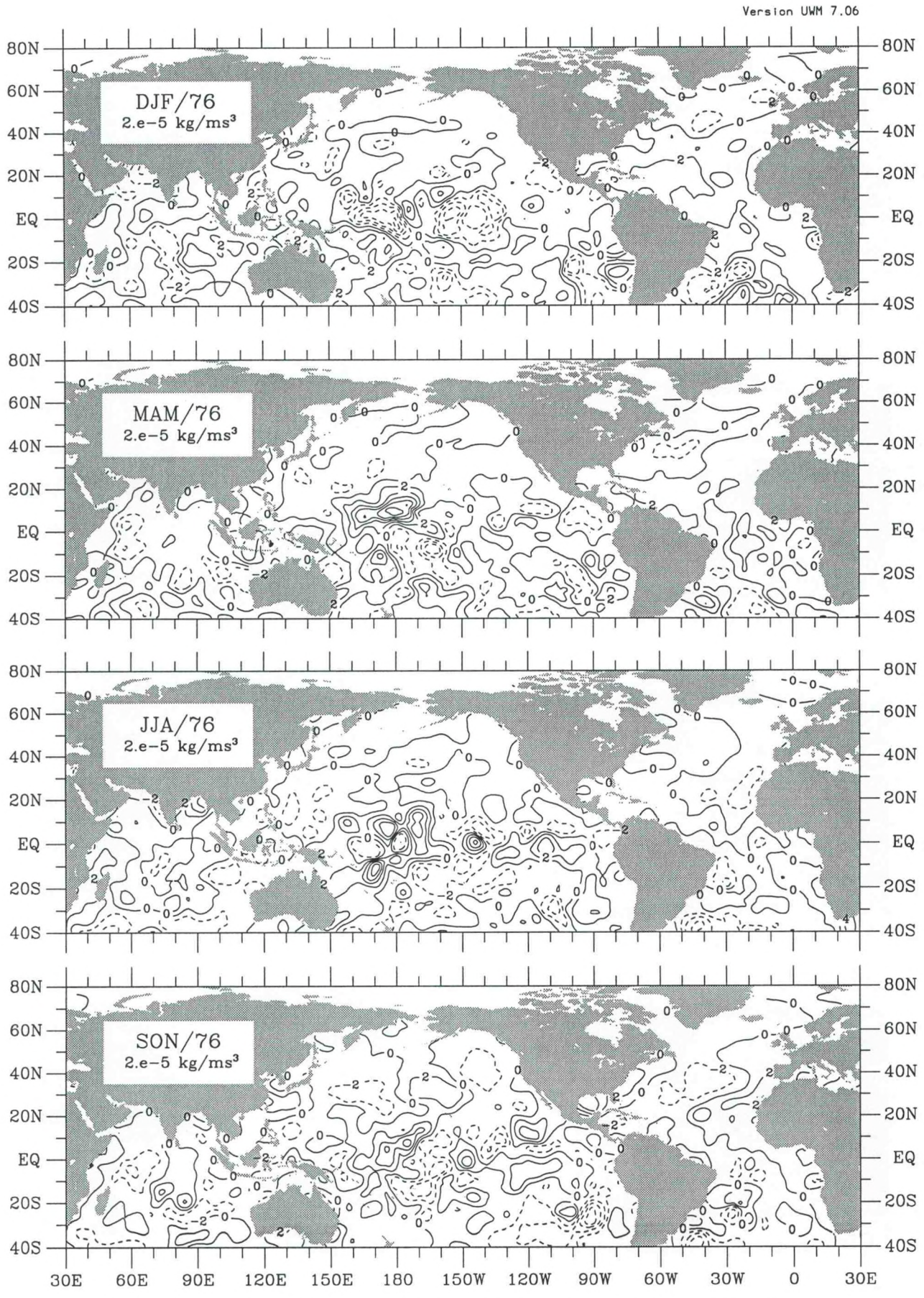

Figure buoy-37. Buoyancy flux seasonal anomaly for 1976.

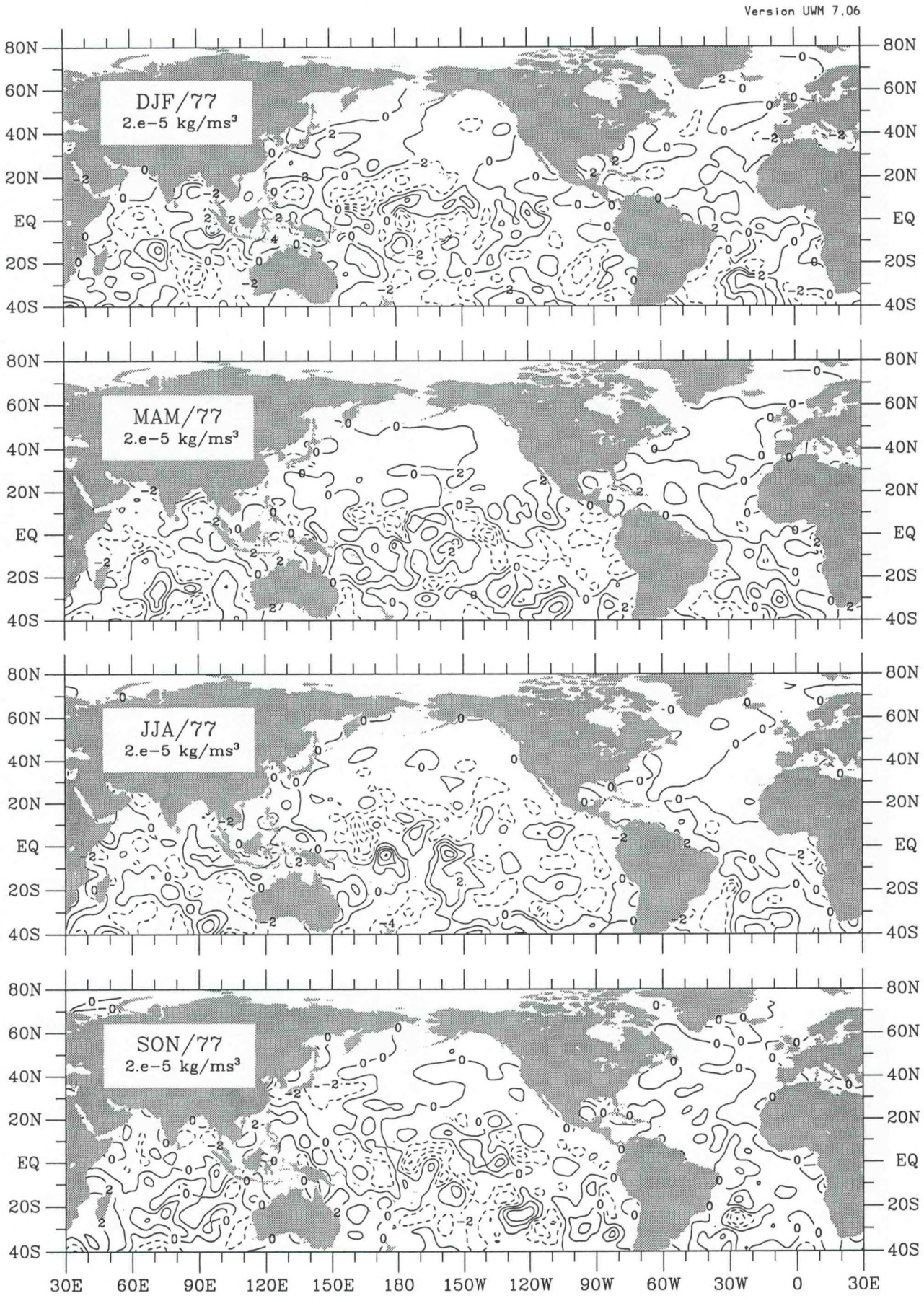

Figure buoy-38. Buoyancy flux seasonal anomaly for 1977.

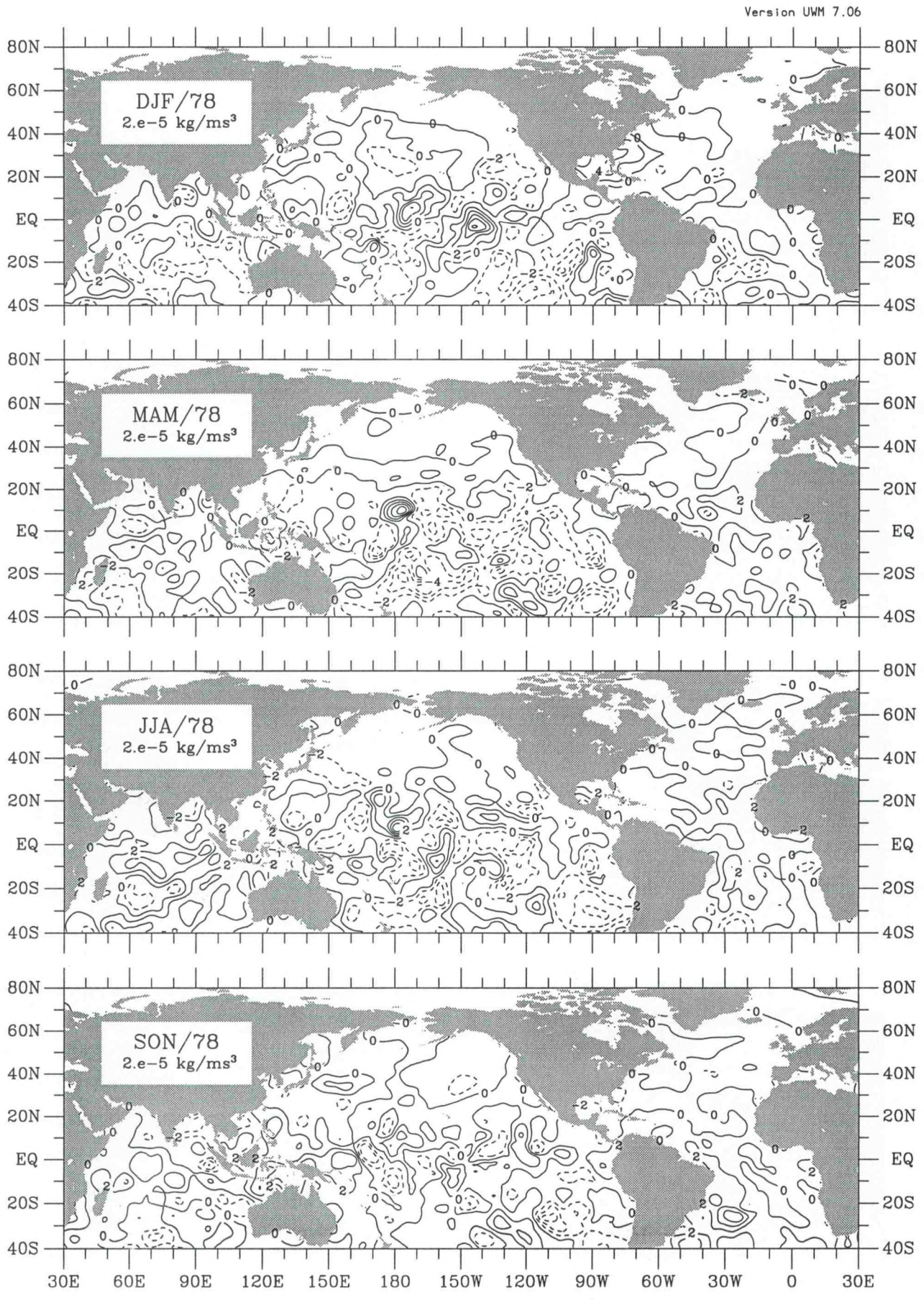

Figure buoy-39. Buoyancy flux seasonal anomaly for 1978.

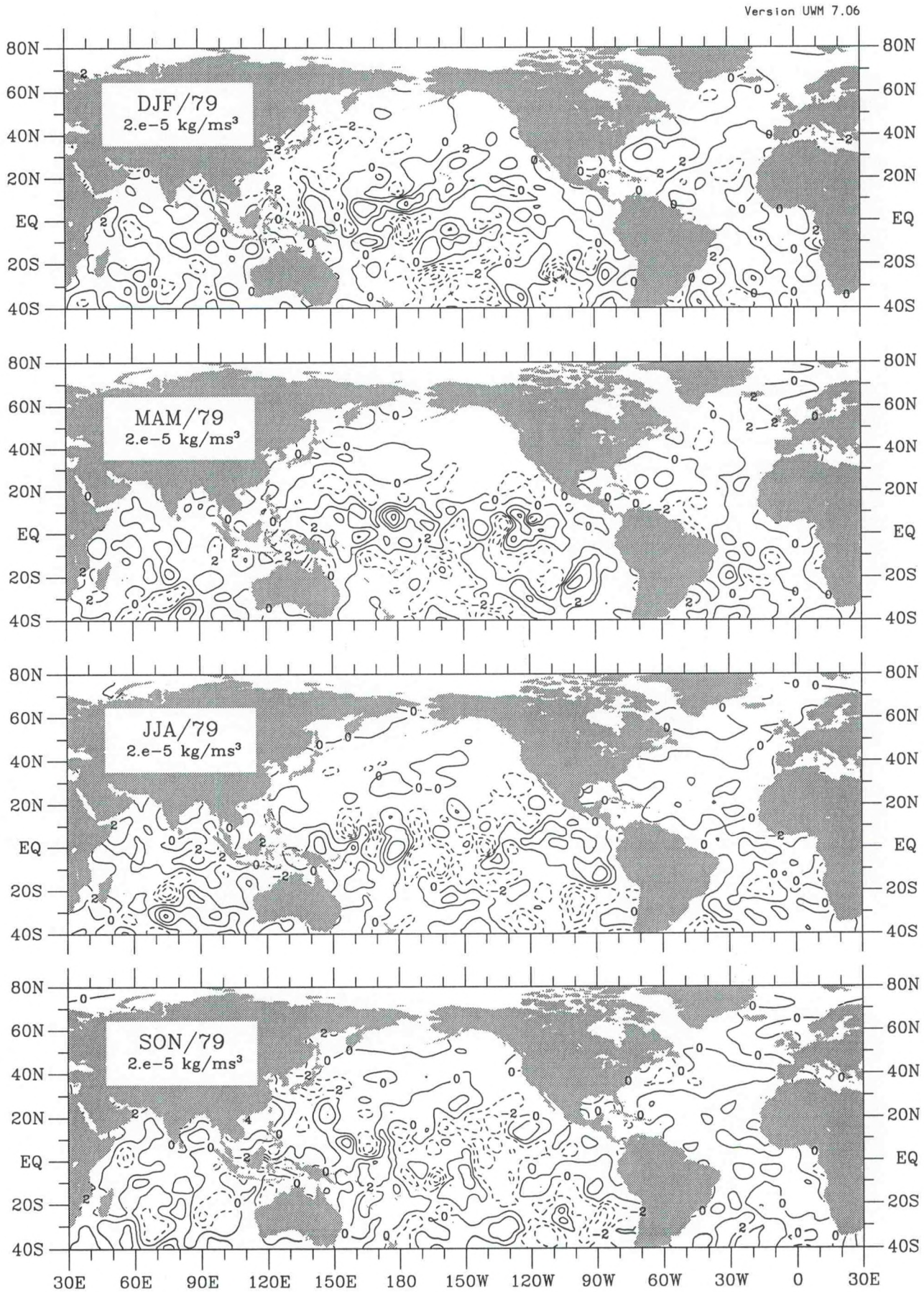

Figure buoy-40. Buoyancy flux seasonal anomaly for 1979.

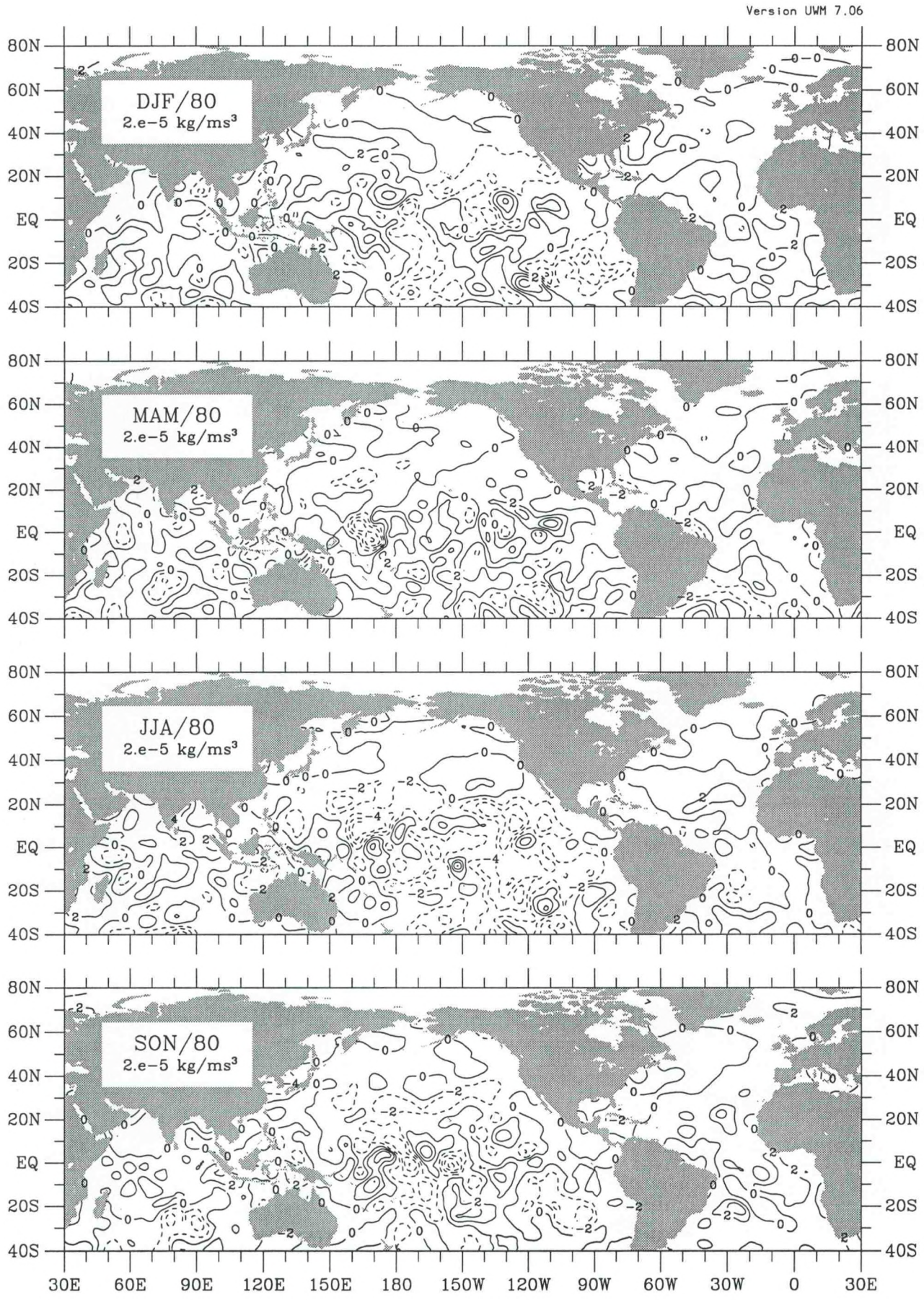

Figure buoy-41. Buoyancy flux seasonal anomaly for 1980.

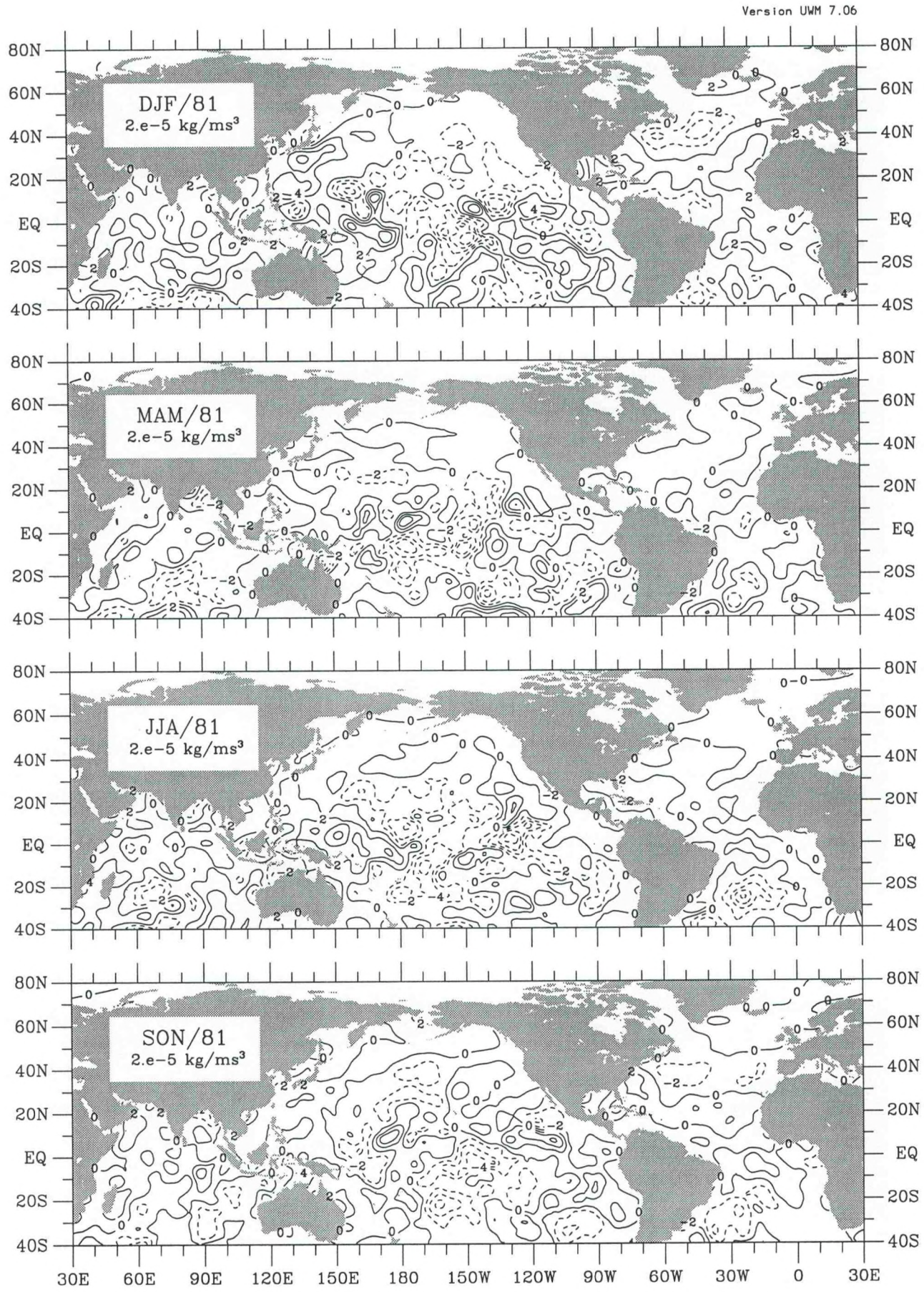

Figure buoy-42. Buoyancy flux seasonal anomaly for 1981.

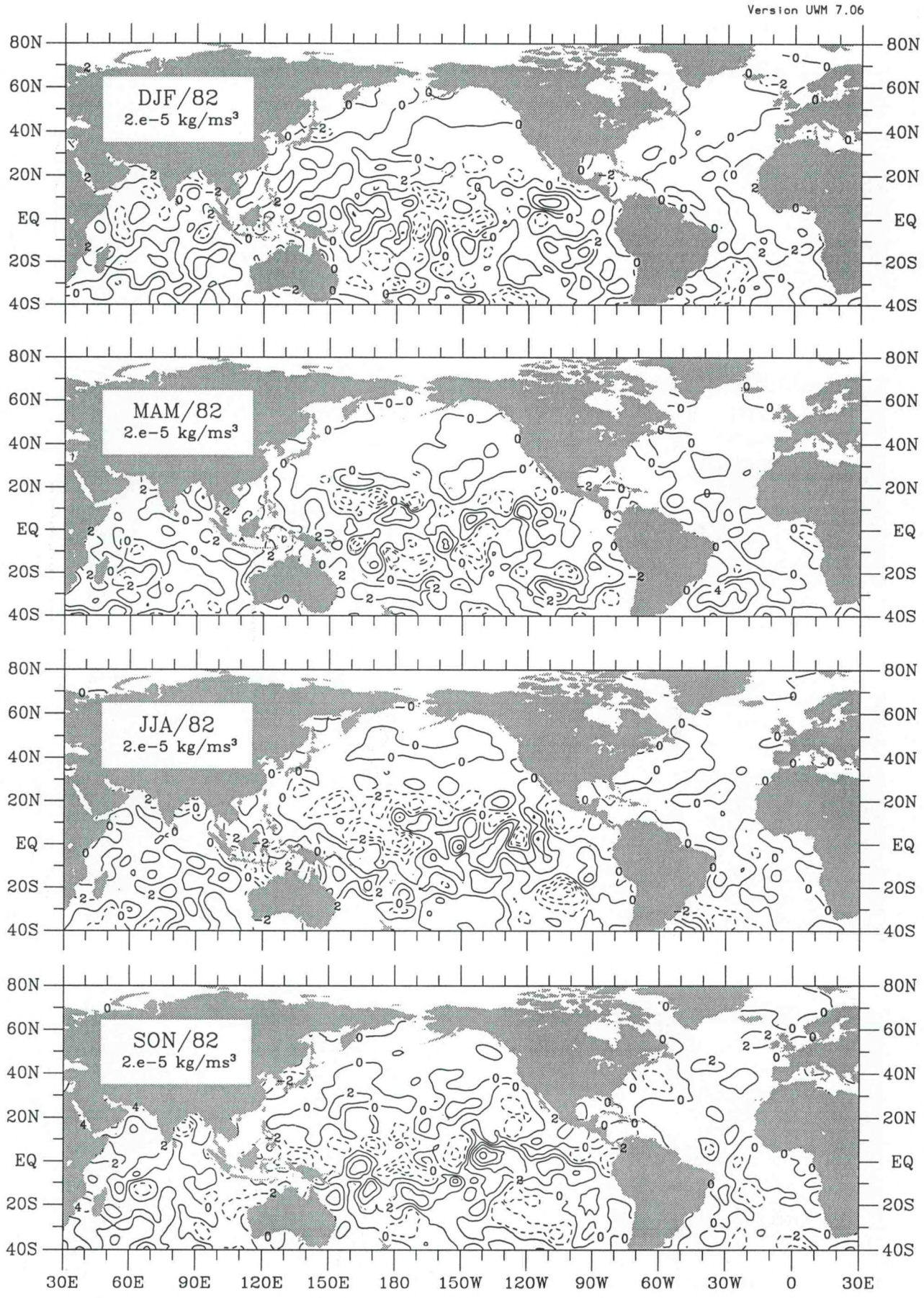

Figure buoy-43. Buoyancy flux seasonal anomaly for 1982.

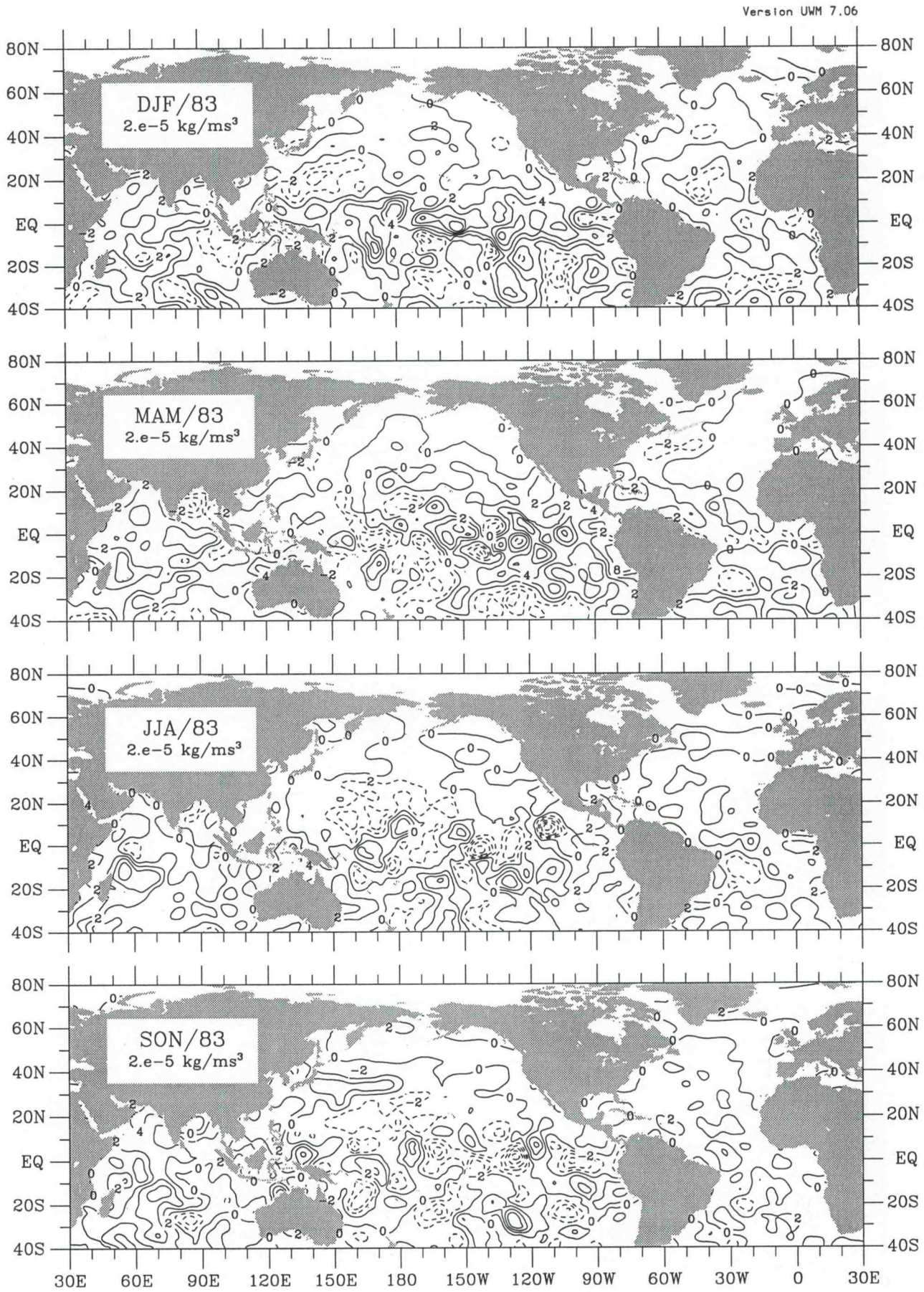

Figure buoy-44. Buoyancy flux seasonal anomaly for 1983.

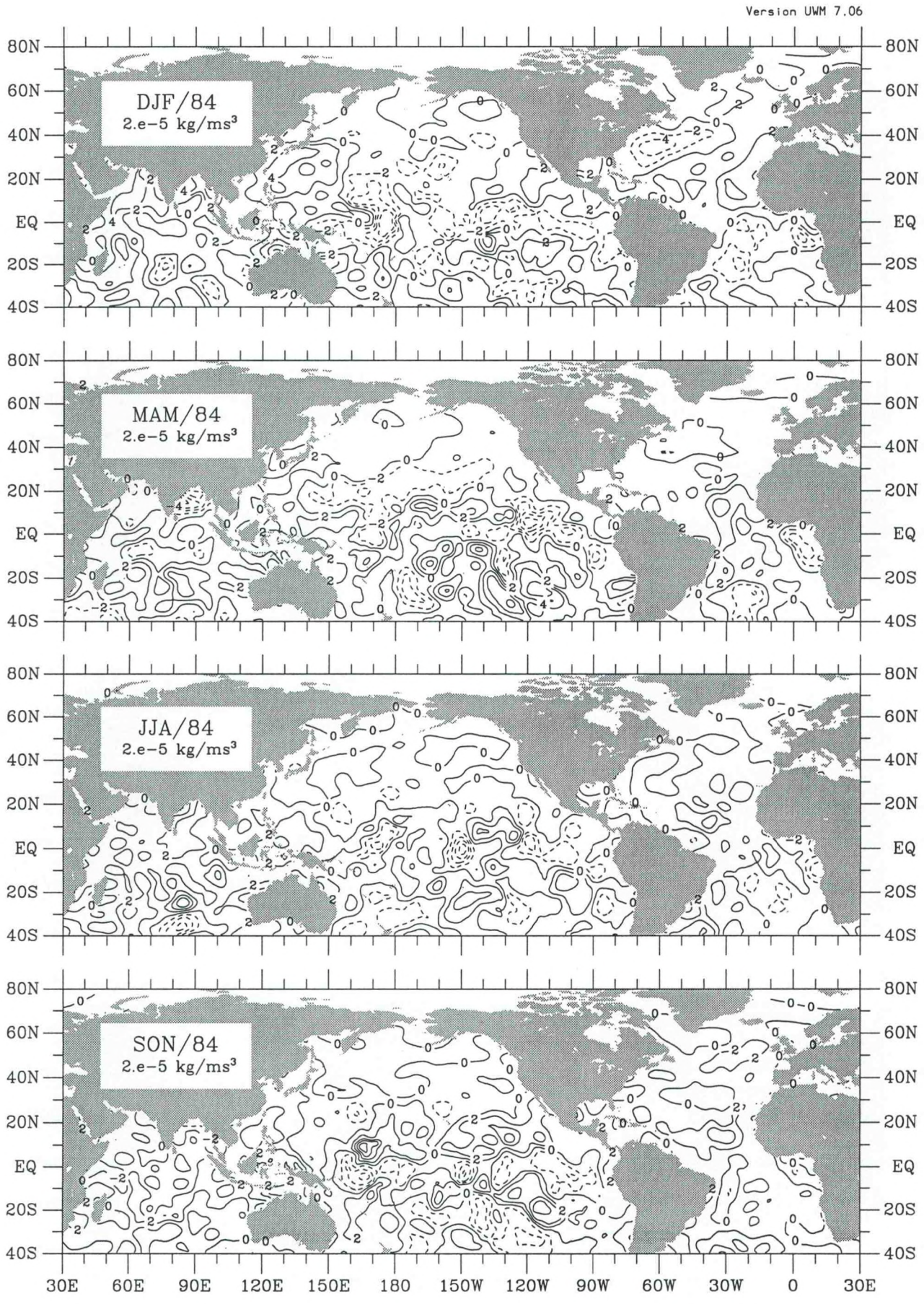

Figure buoy-45. Buoyancy flux seasonal anomaly for 1984.

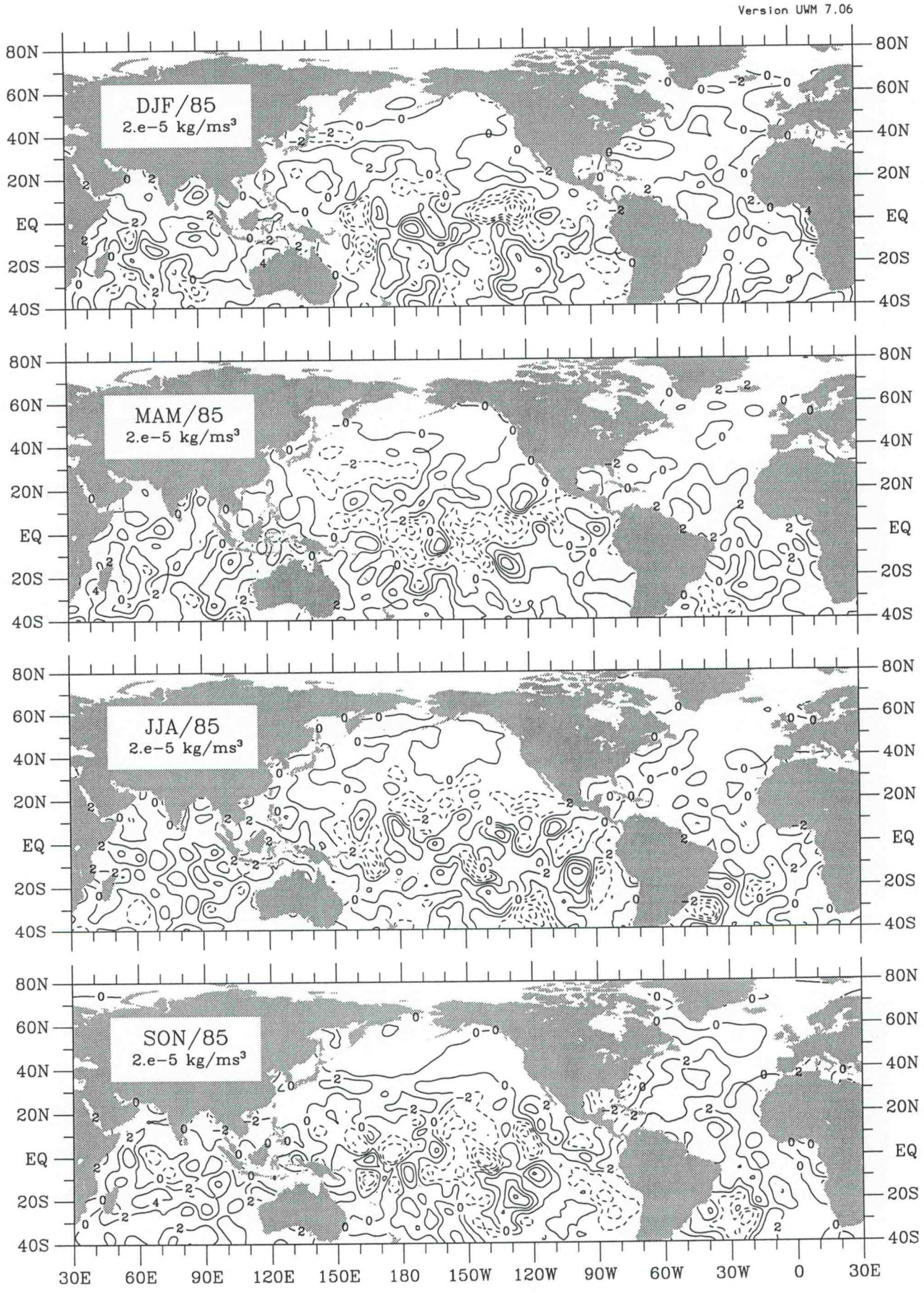

Figure buoy-46. Buoyancy flux seasonal anomaly for 1985.

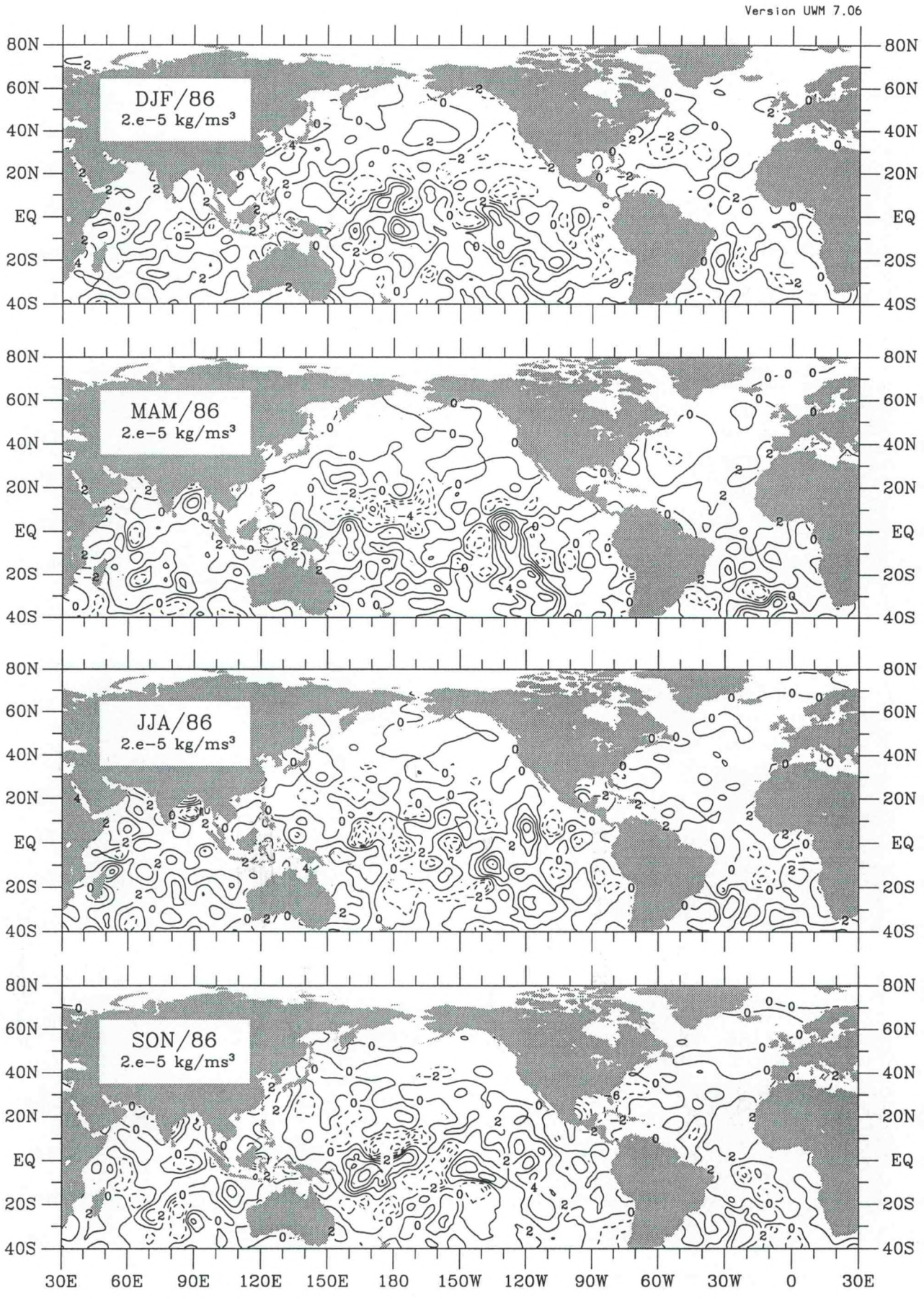

Figure buoy-47. Buoyancy flux seasonal anomaly for 1986.

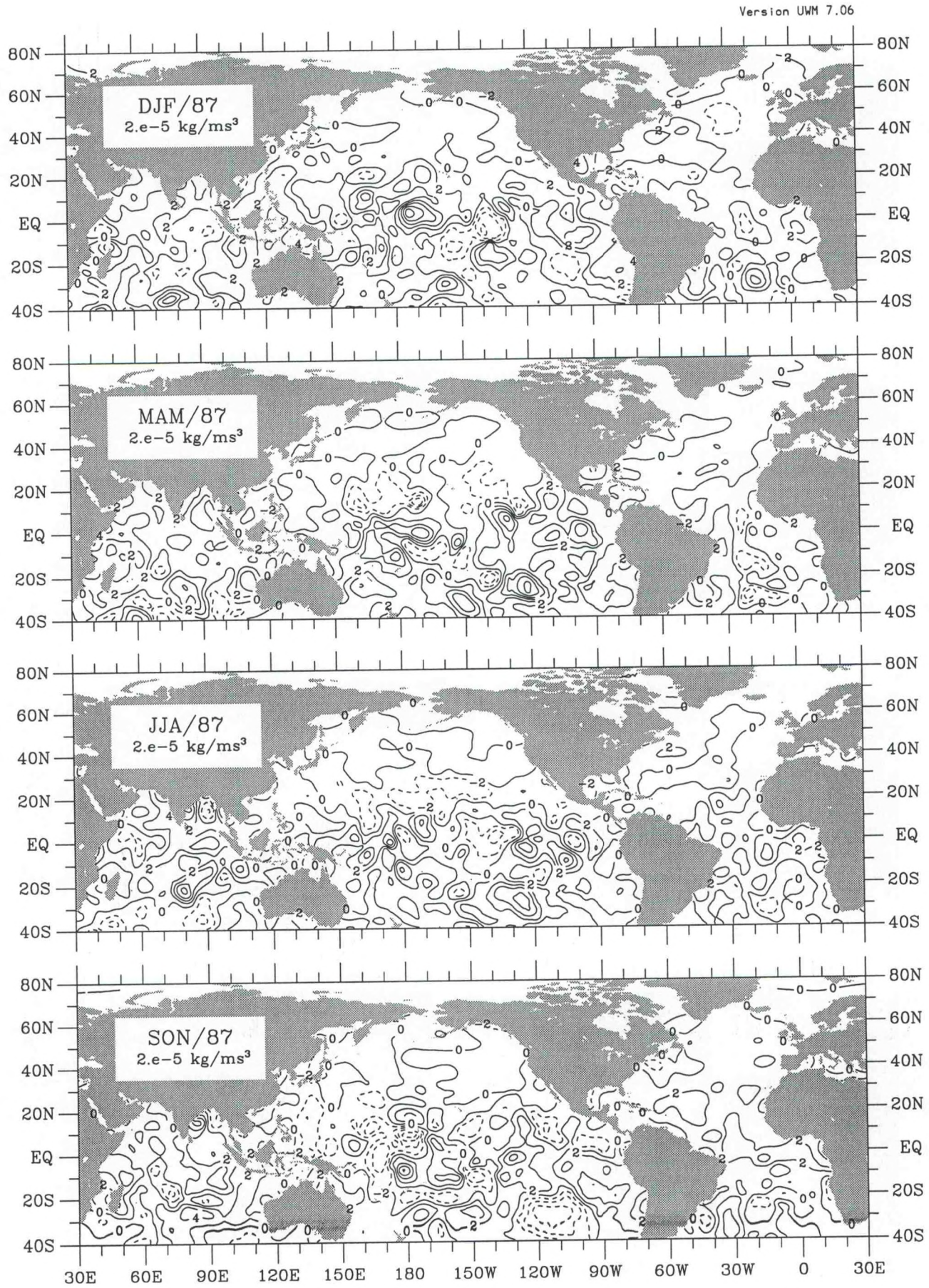

Figure buoy-48. Buoyancy flux seasonal anomaly for 1987.

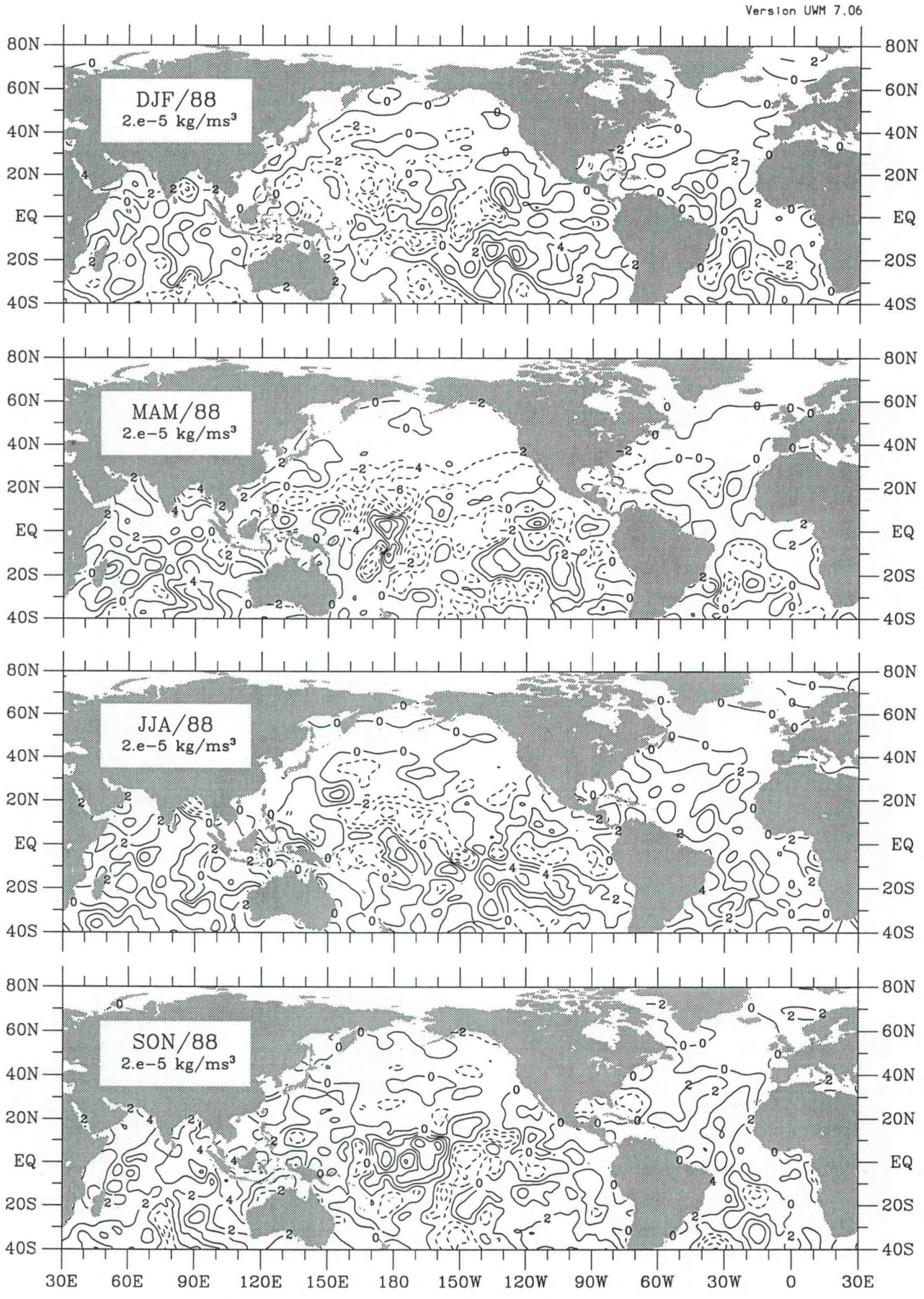

Figure buoy-49. Buoyancy flux seasonal anomaly for 1988.

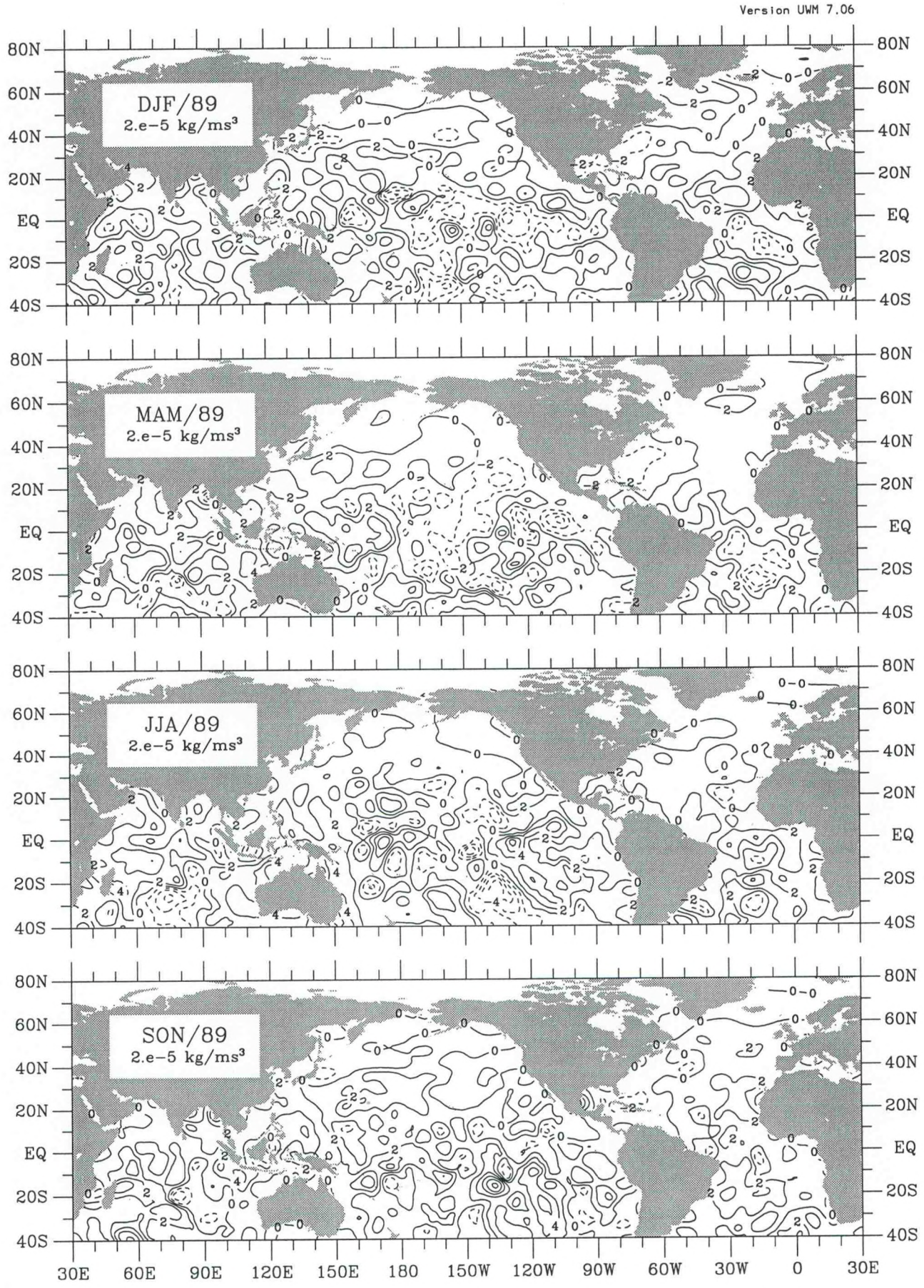

Figure buoy-50. Buoyancy flux seasonal anomaly for 1989.

15 Zonal moisture flux

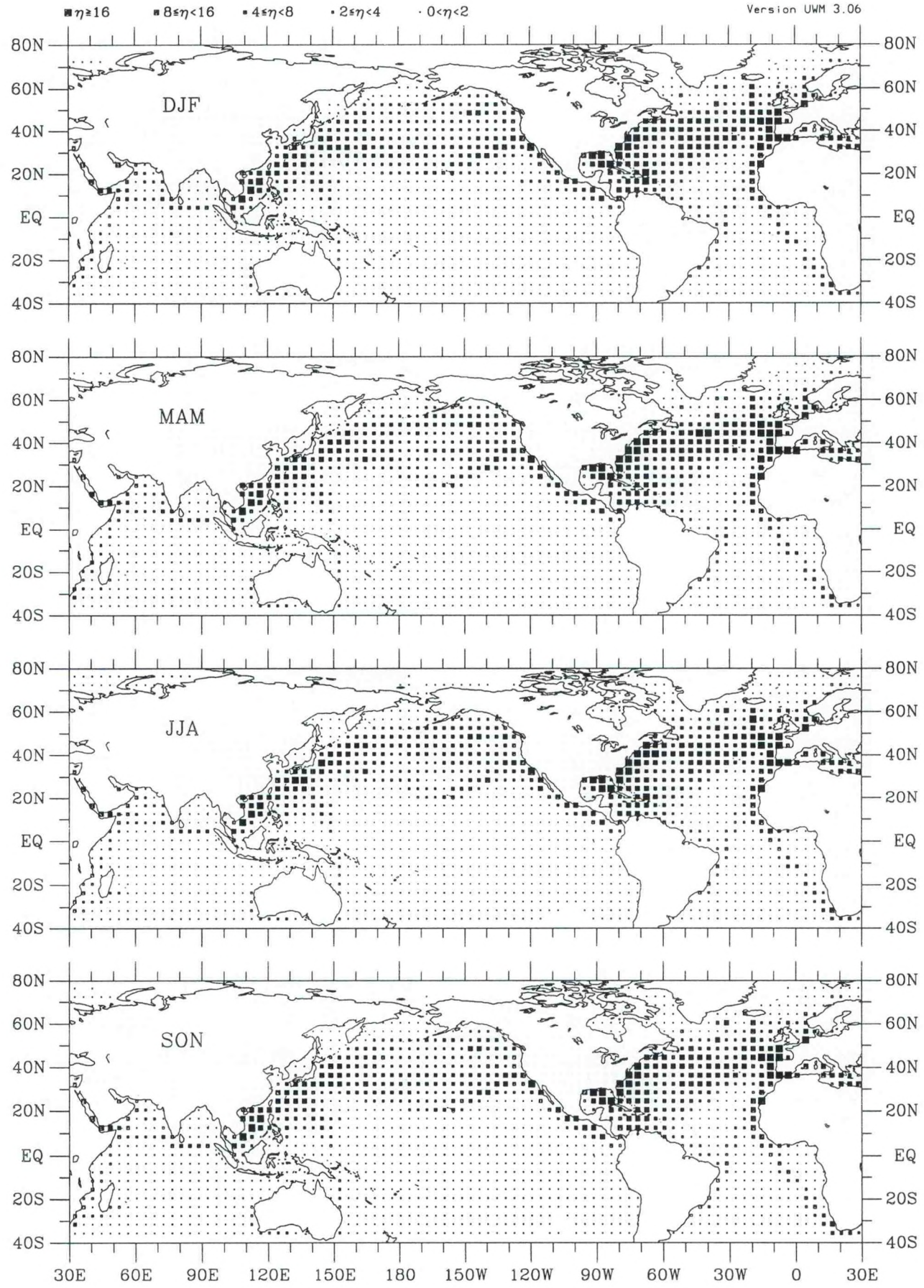

Figure uq-1. Zonal moisture flux seasonal observation density (1945-89).

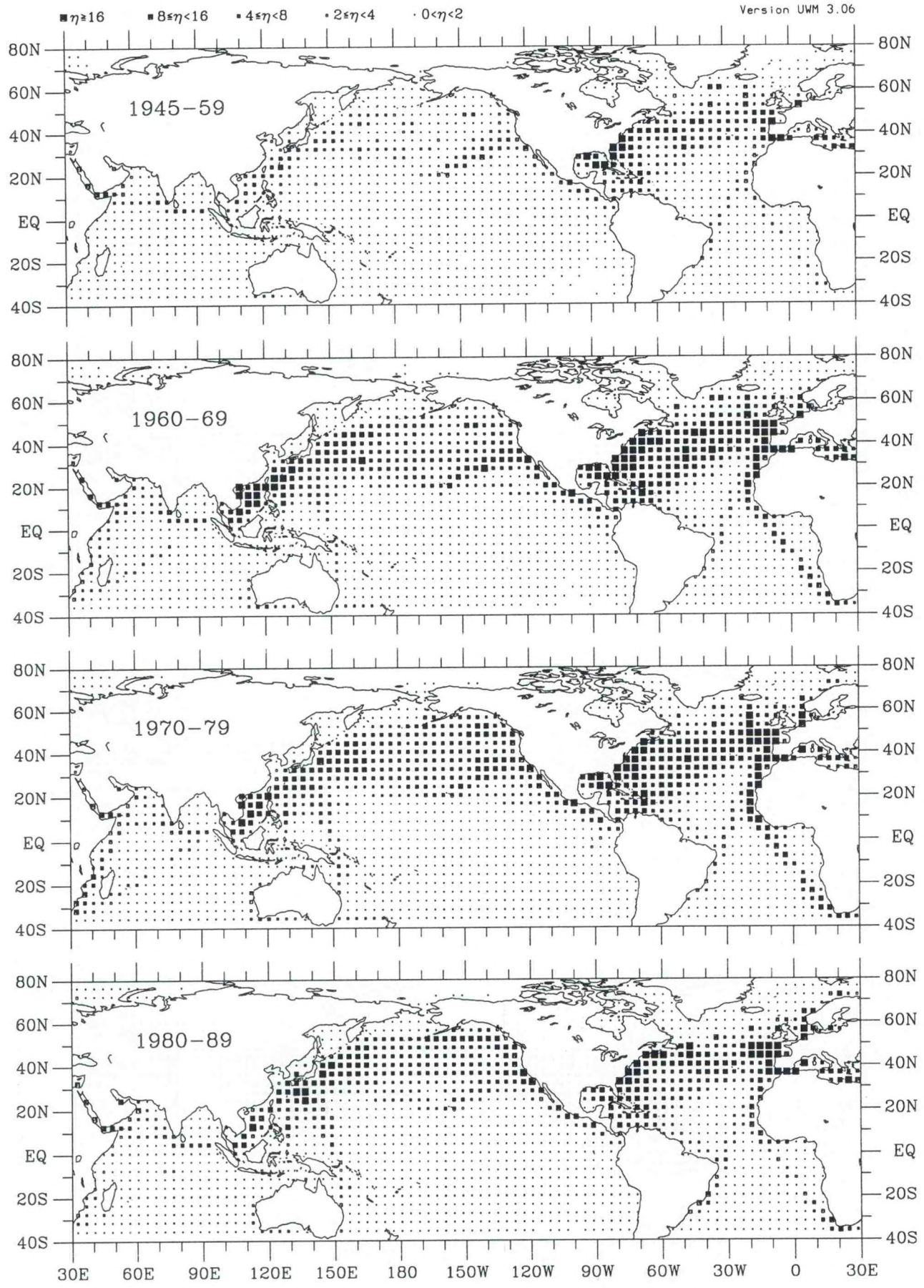

Figure uq–2. Zonal moisture flux decadal observation density.

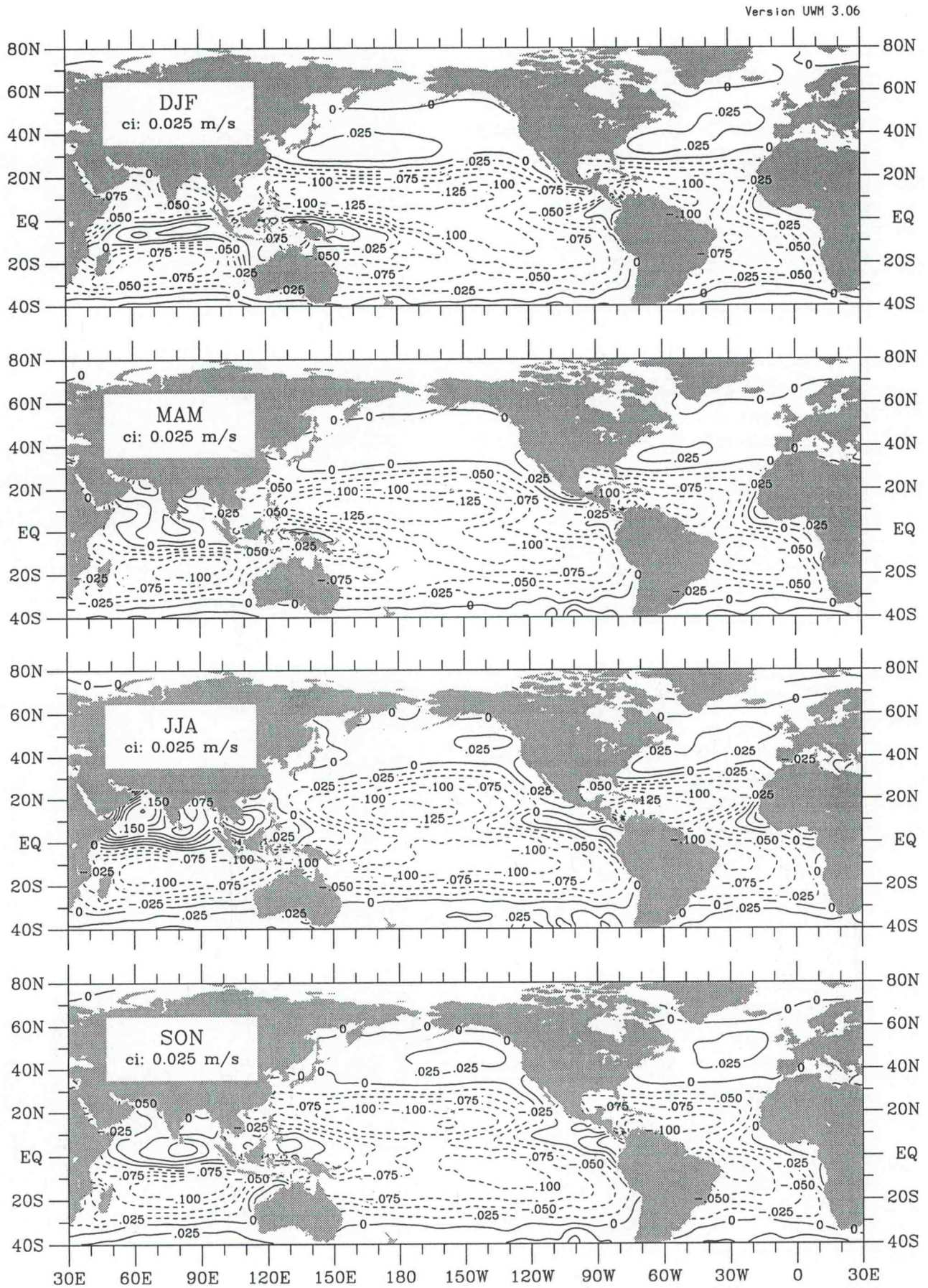

Figure uq-3. Zonal moisture flux seasonal climatology (1945-89).

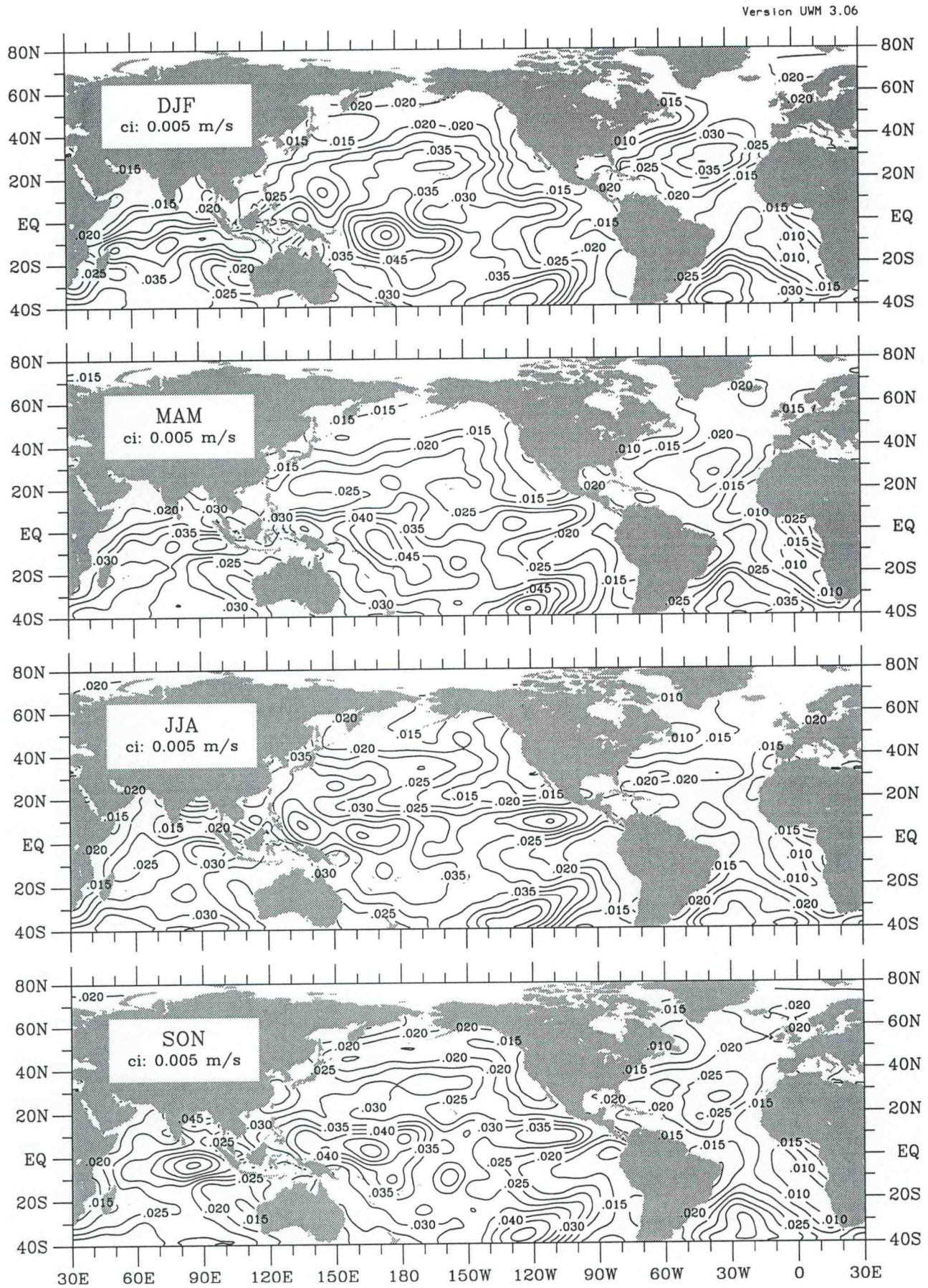

Figure uq-4. Zonal moisture flux seasonal interannual std dev (1945-89).

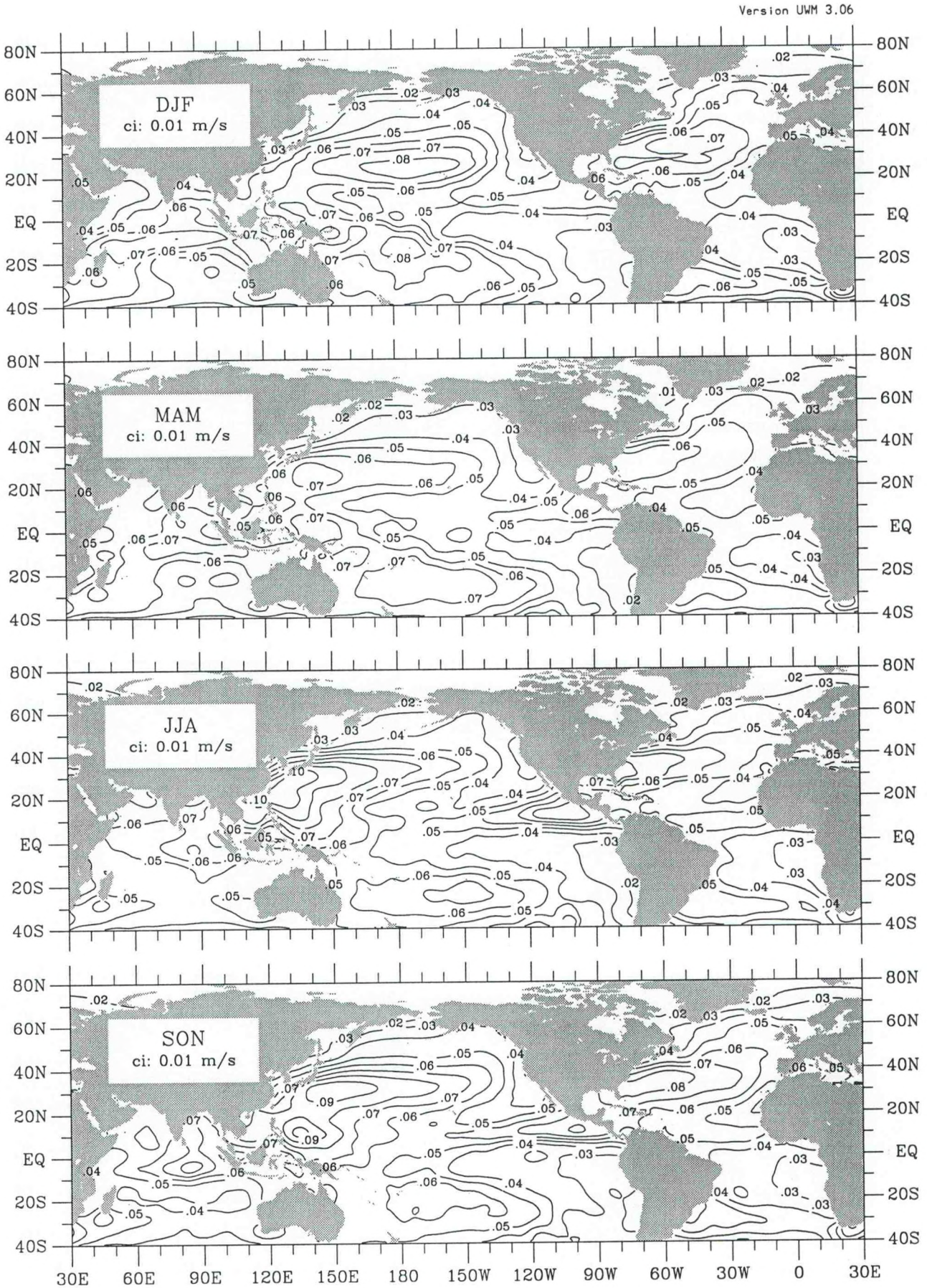

Figure uq-5. Zonal moisture flux seasonal standard deviation (1945-89).

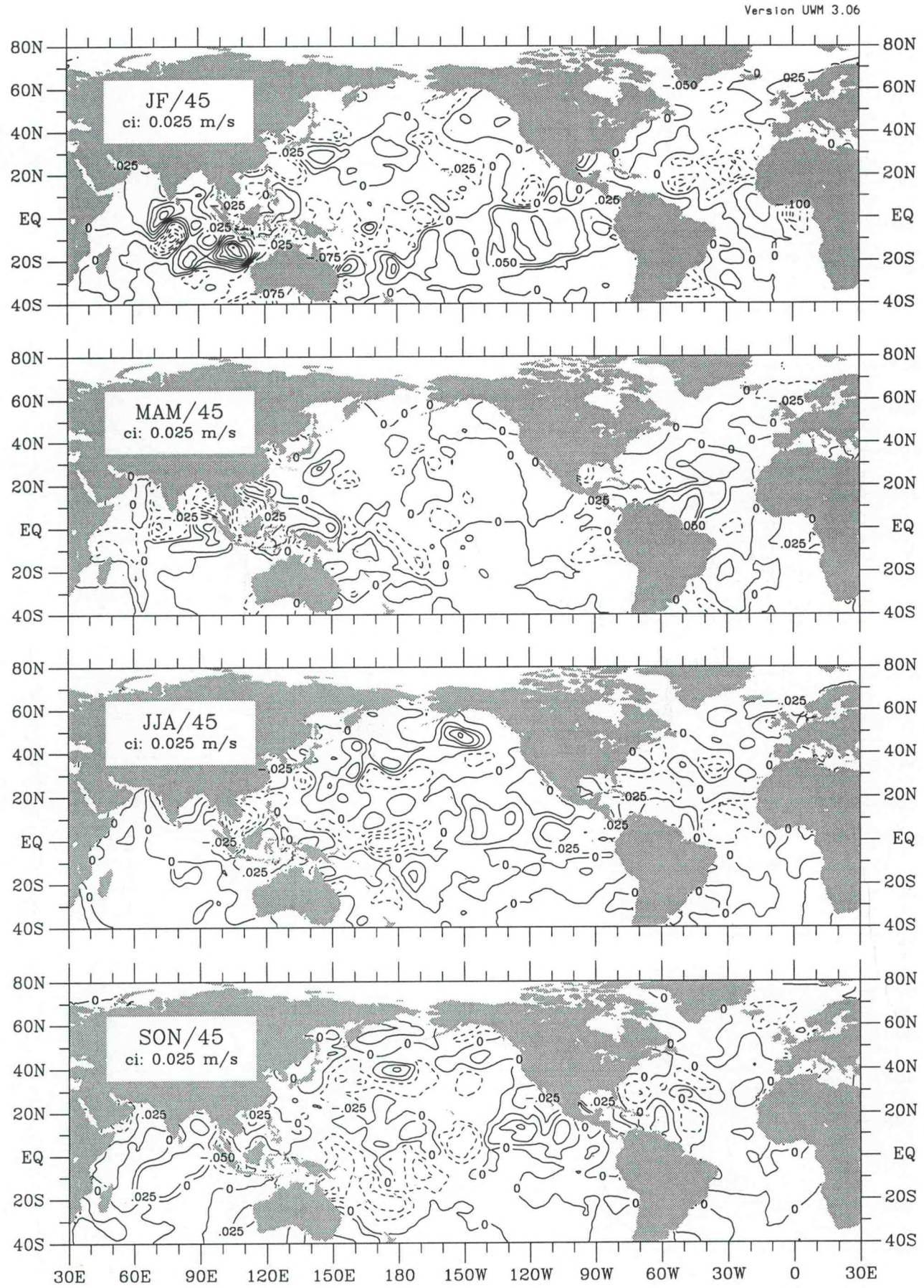

Figure uq-6. Zonal moisture flux seasonal anomaly for 1945.

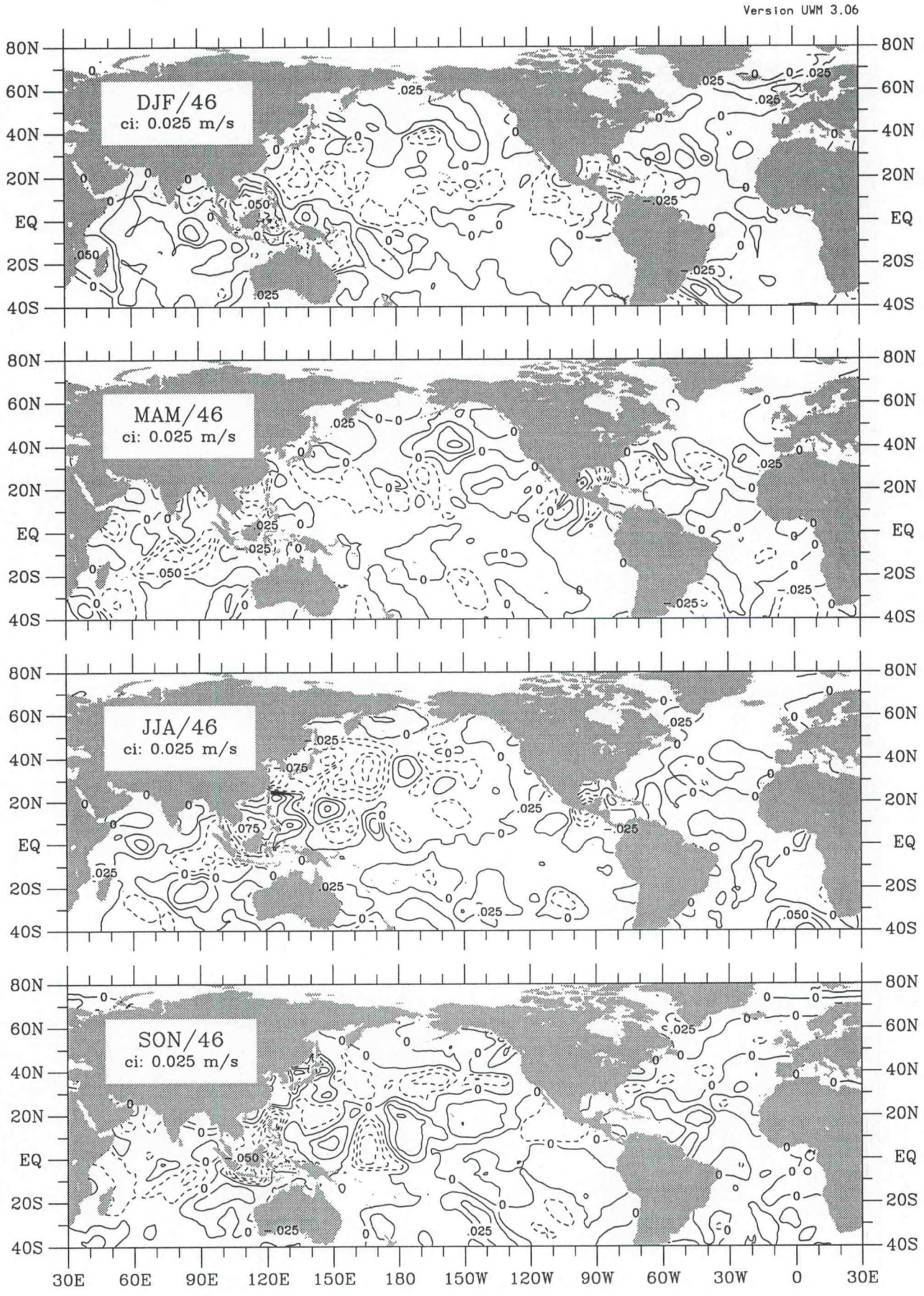

Figure uq-7. Zonal moisture flux seasonal anomaly for 1946.

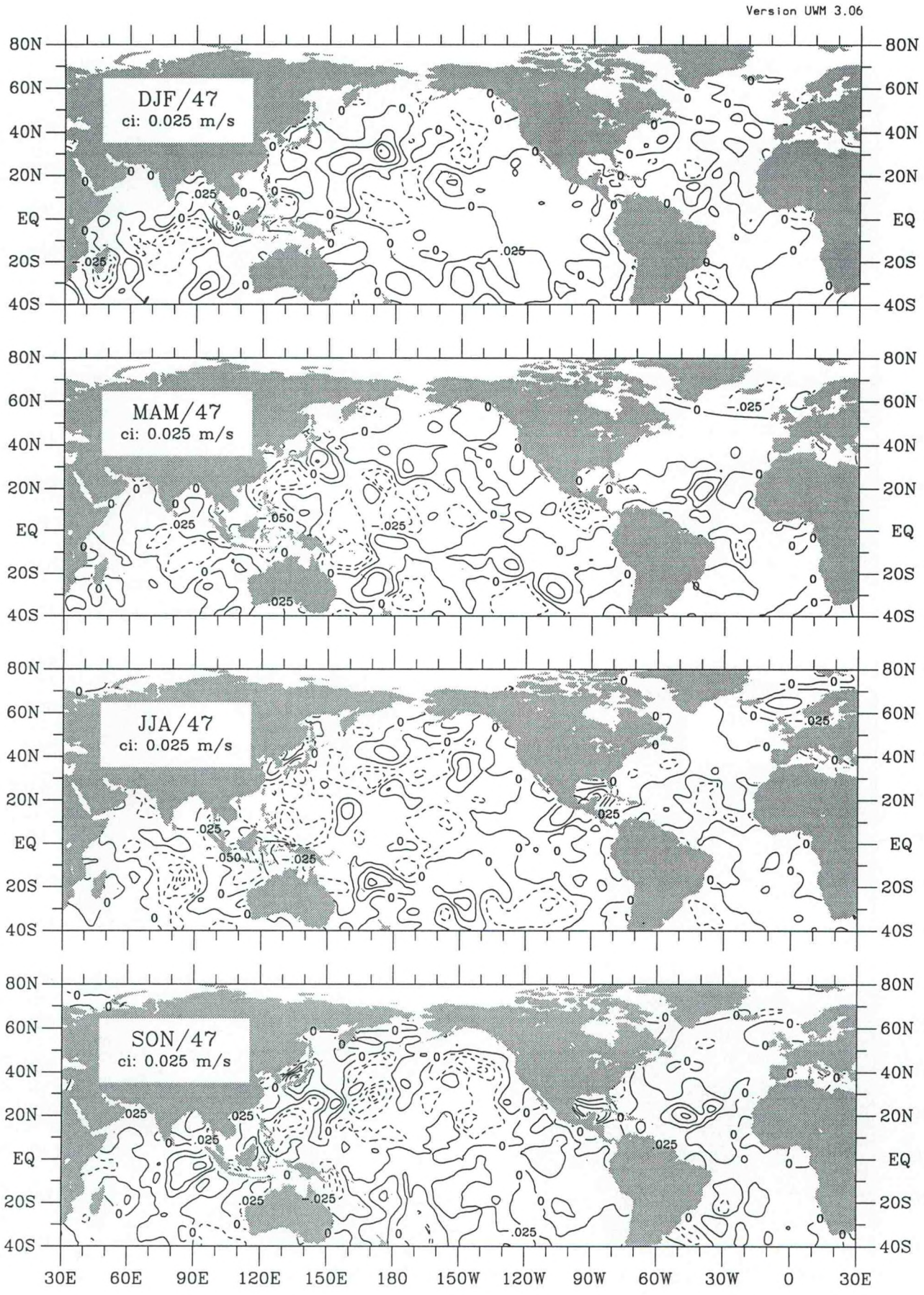

Figure uq-8. Zonal moisture flux seasonal anomaly for 1947.

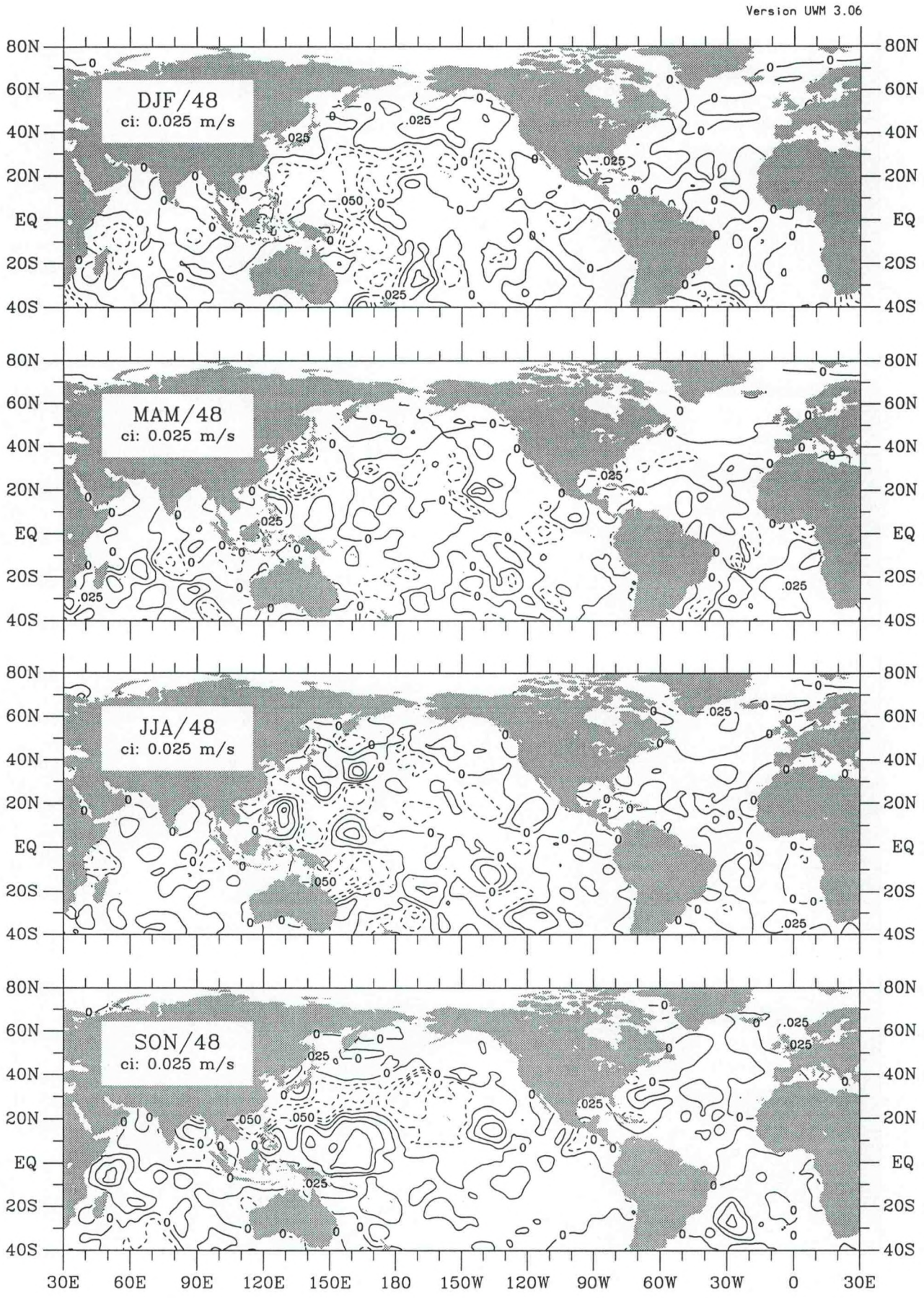

Figure uq-9. Zonal moisture flux seasonal anomaly for 1948.

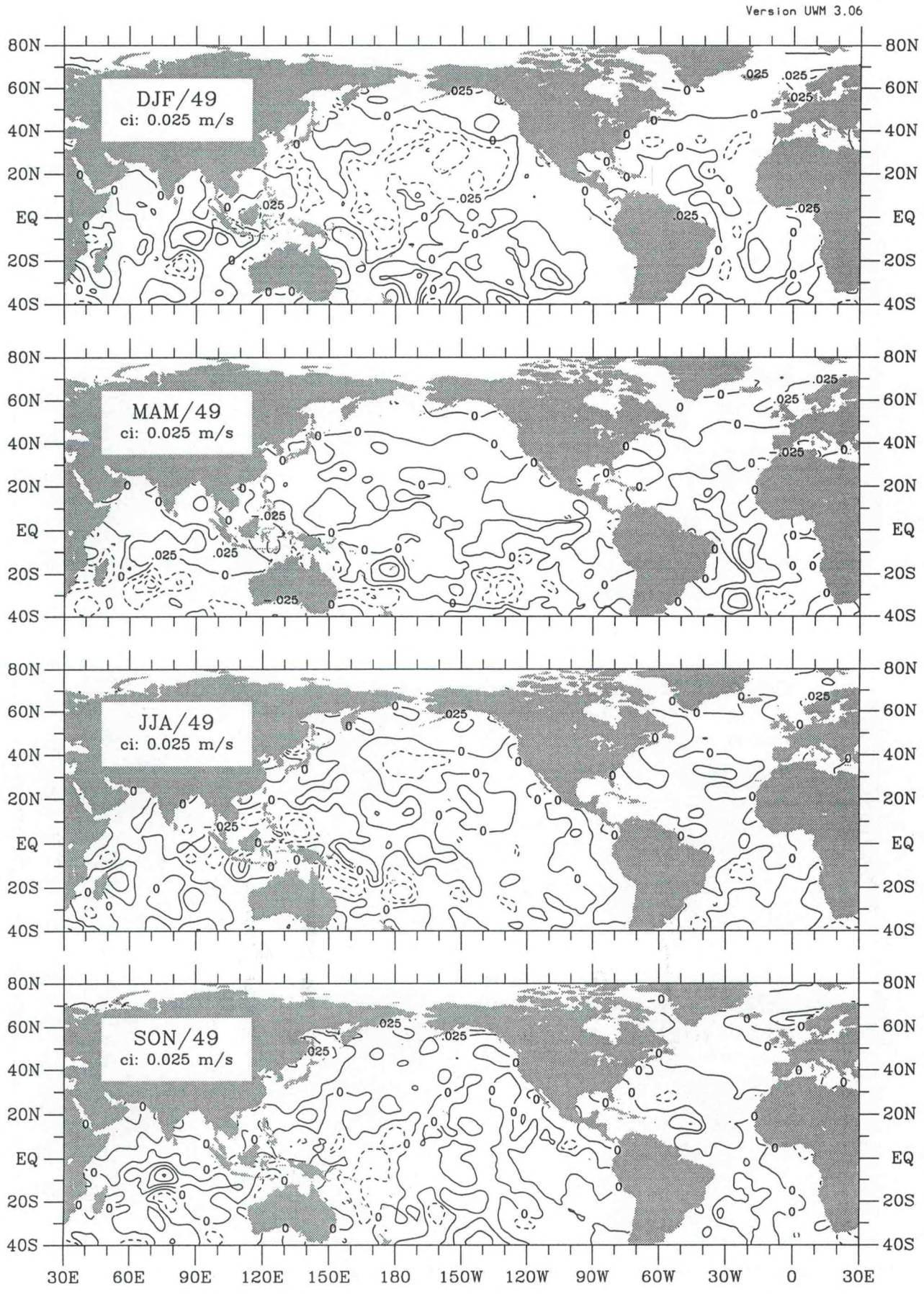

Figure uq-10. Zonal moisture flux seasonal anomaly for 1949.

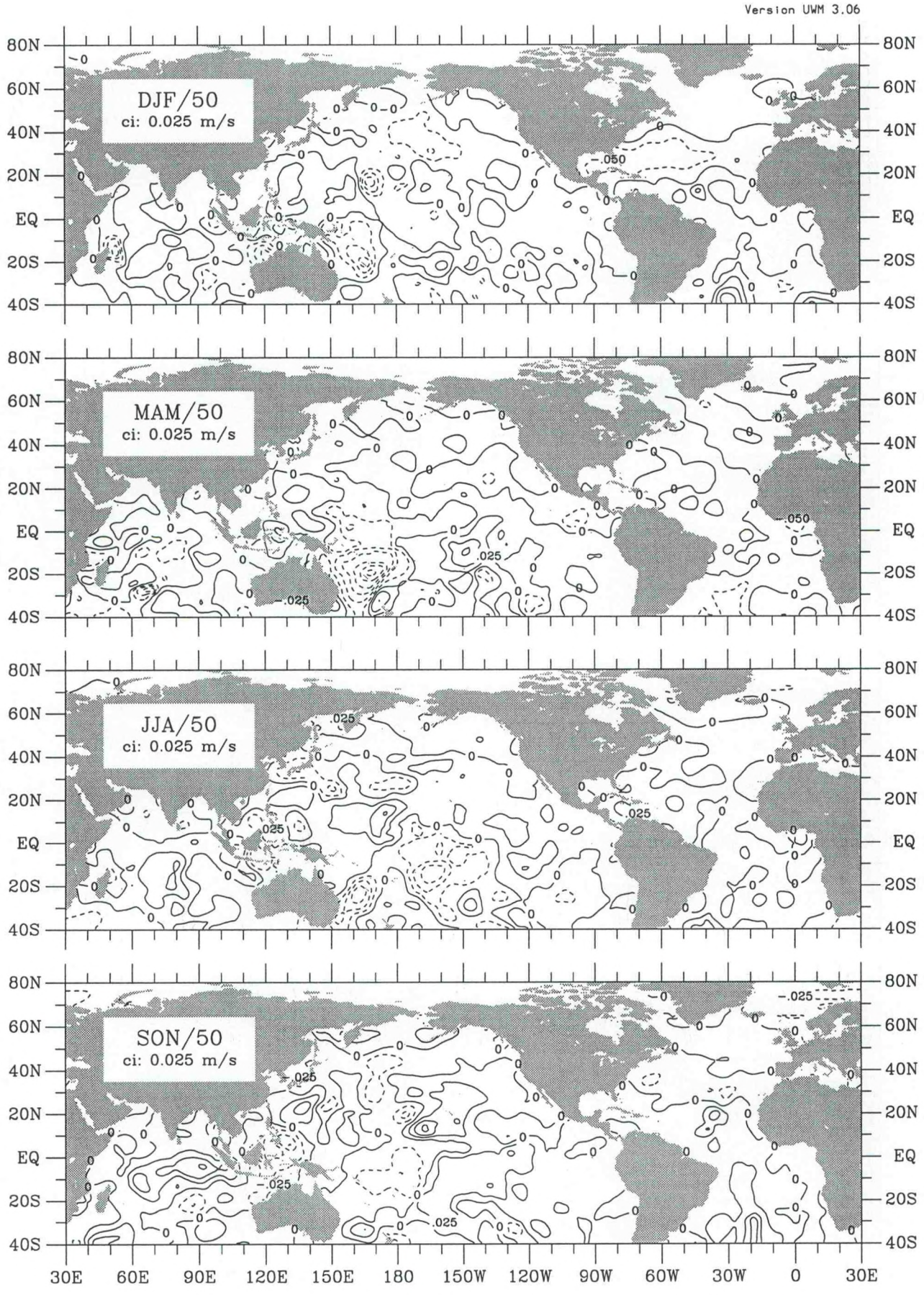

Figure uq-11. Zonal moisture flux seasonal anomaly for 1950.

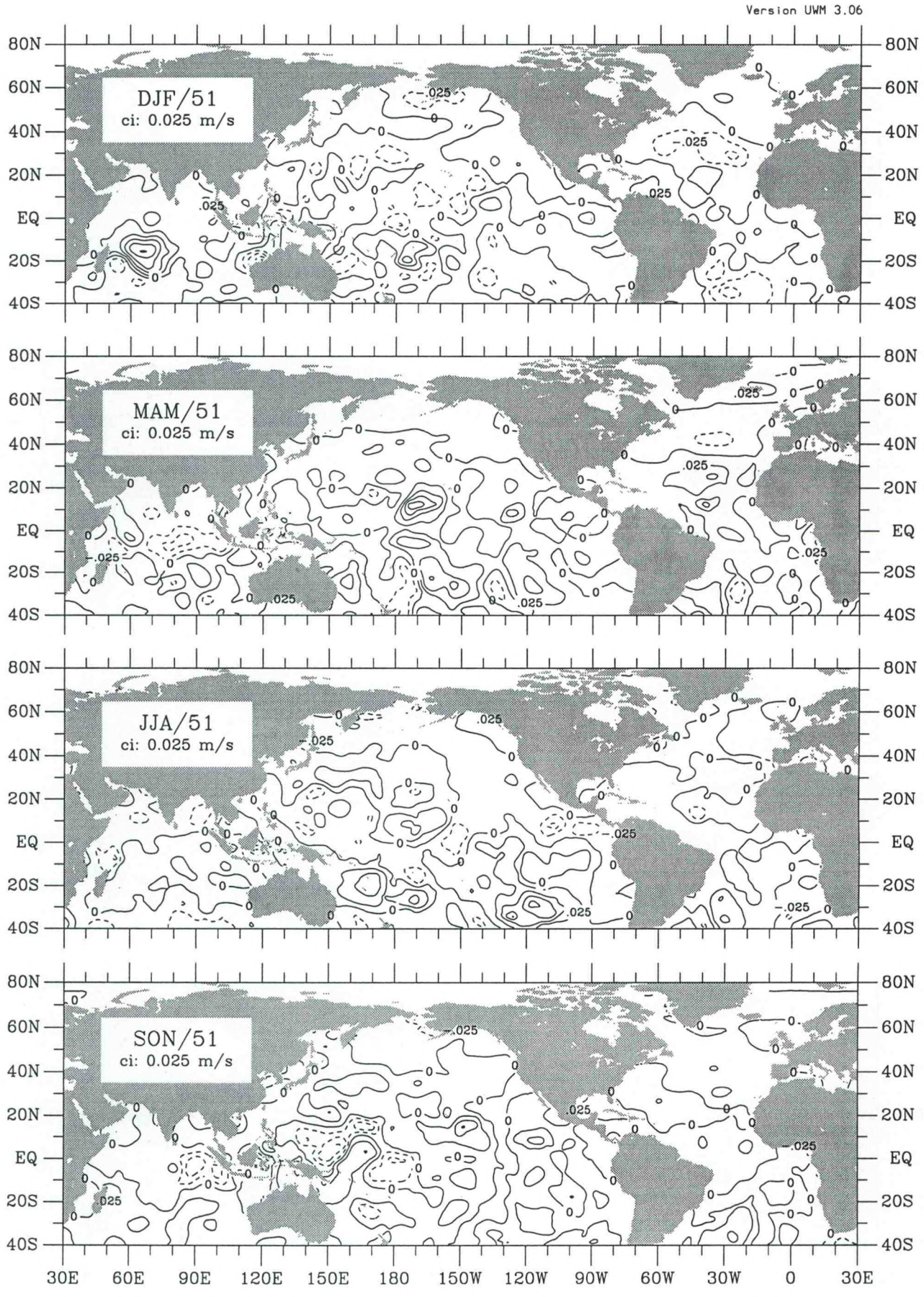

Figure uq-12. Zonal moisture flux seasonal anomaly for 1951.

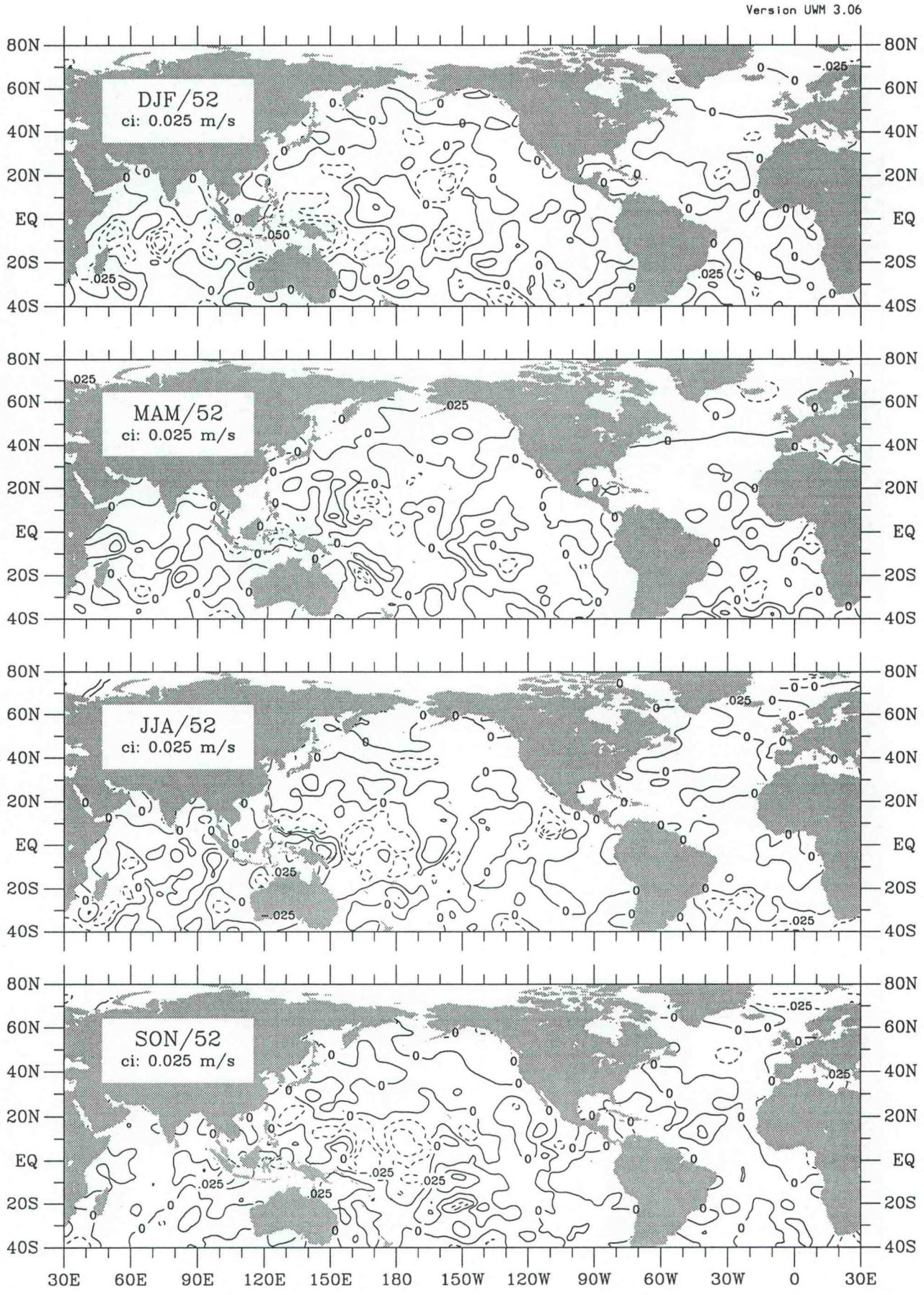

Figure uq-13. Zonal moisture flux seasonal anomaly for 1952.

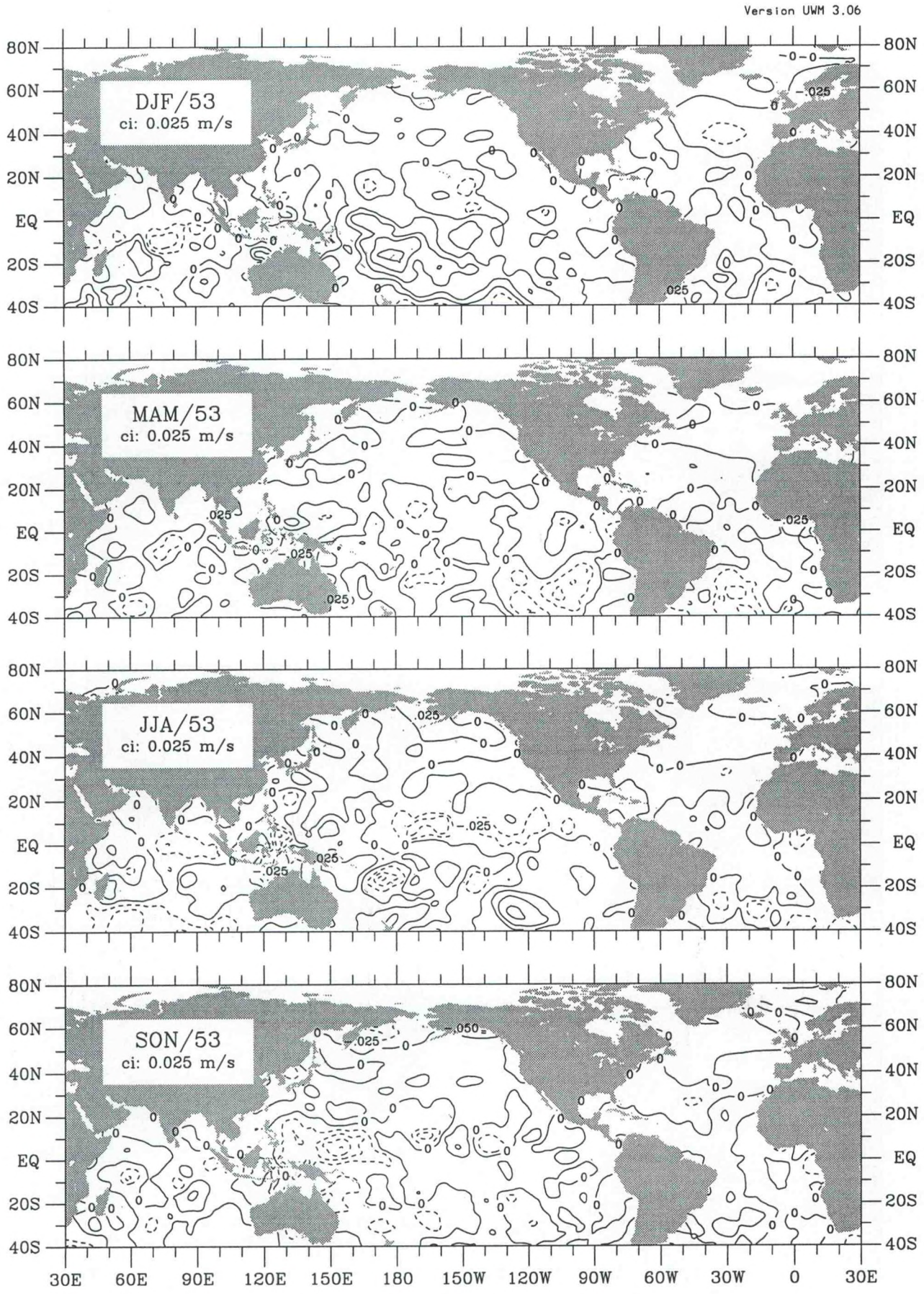

Figure uq-14. Zonal moisture flux seasonal anomaly for 1953.

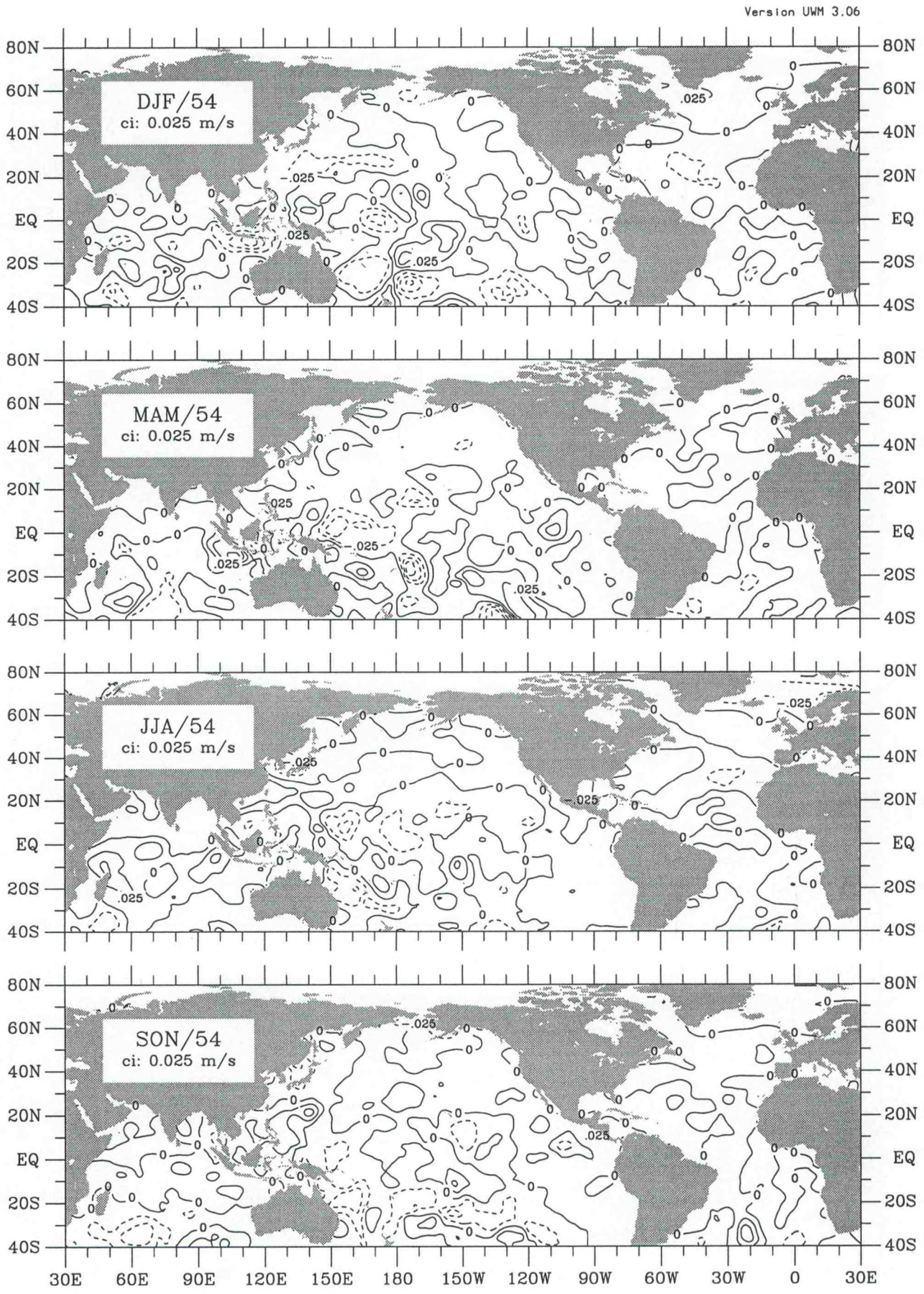

Figure uq-15. Zonal moisture flux seasonal anomaly for 1954.

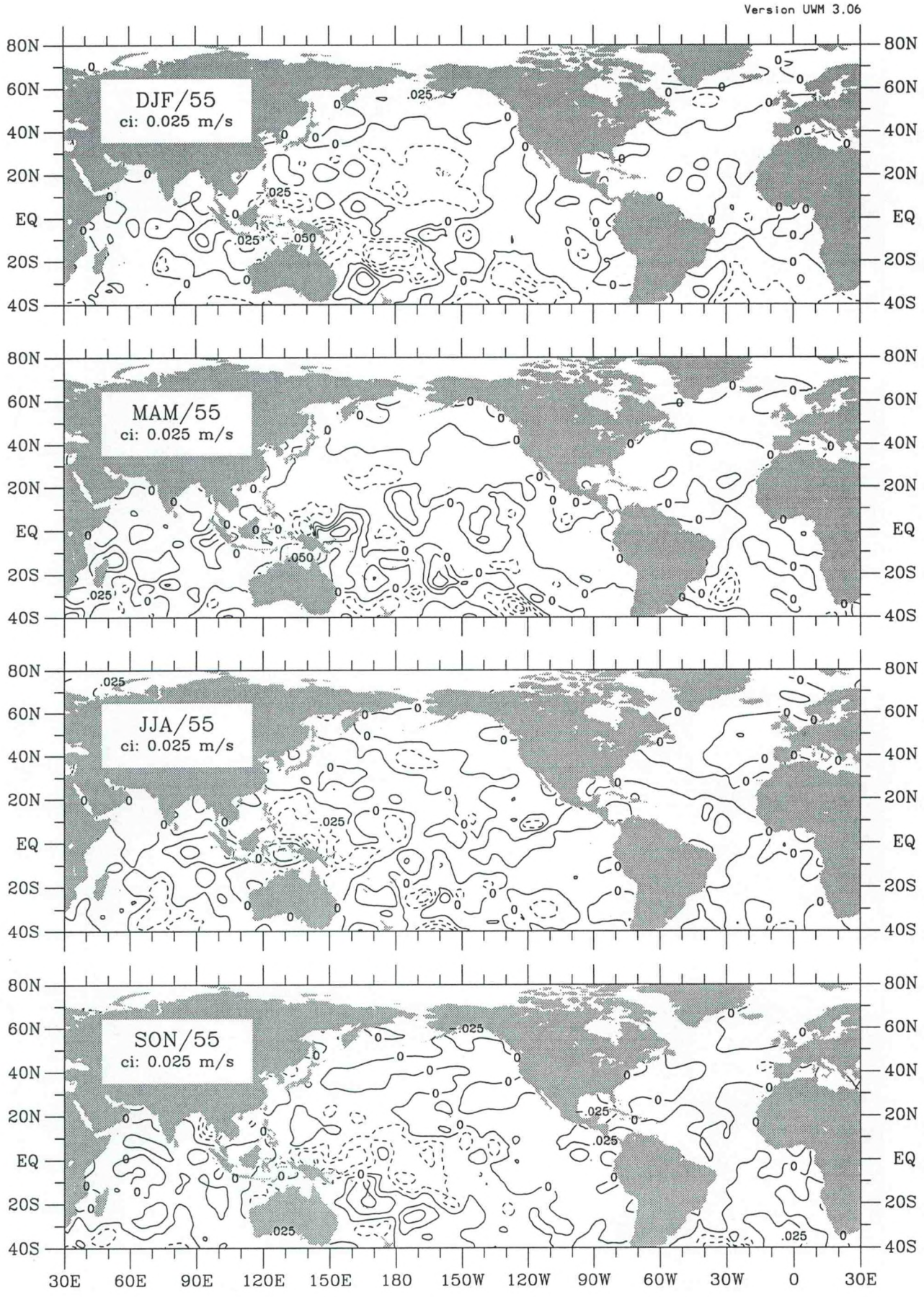

Figure uq-16. Zonal moisture flux seasonal anomaly for 1955.

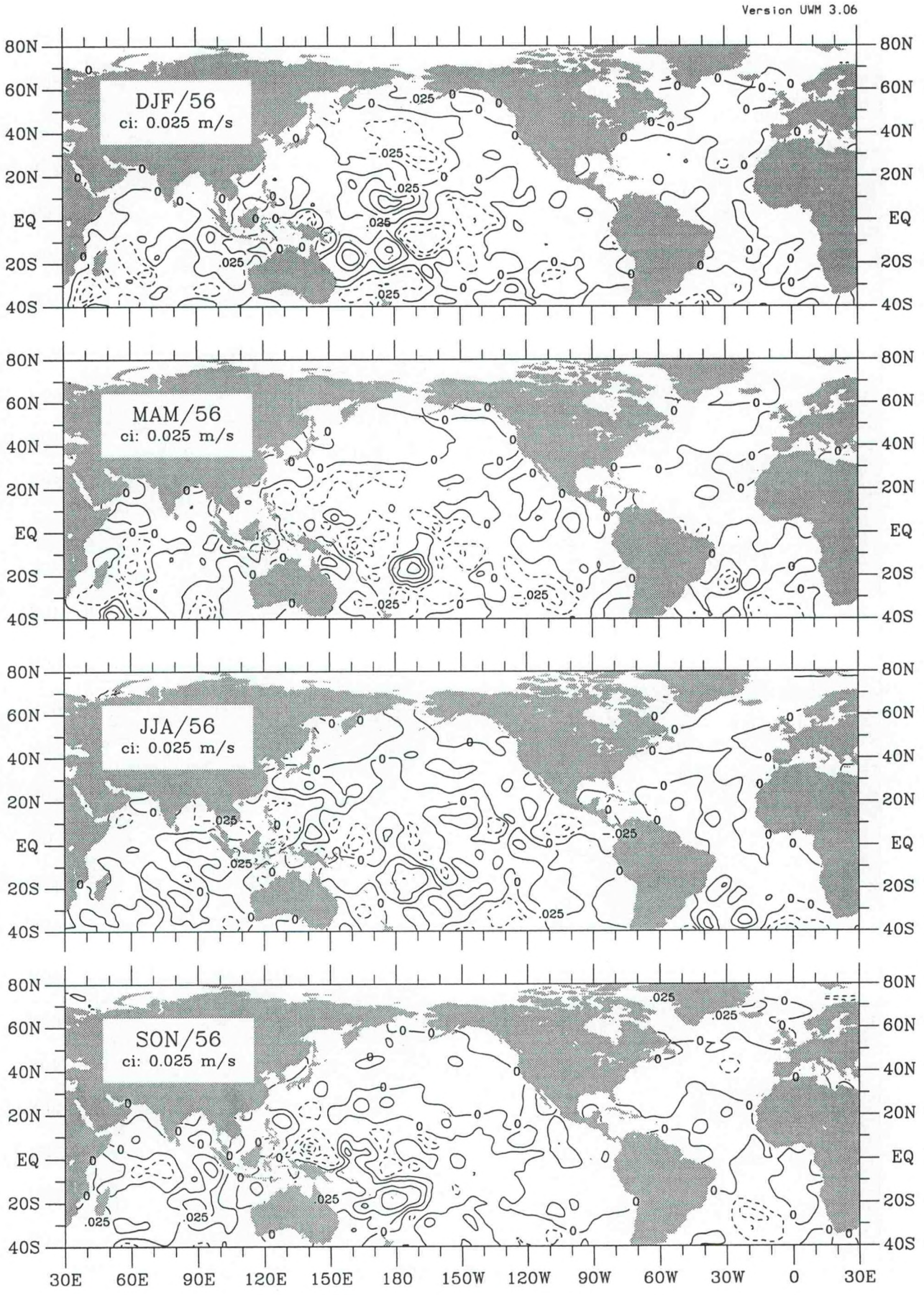

Figure uq-17. Zonal moisture flux seasonal anomaly for 1956.

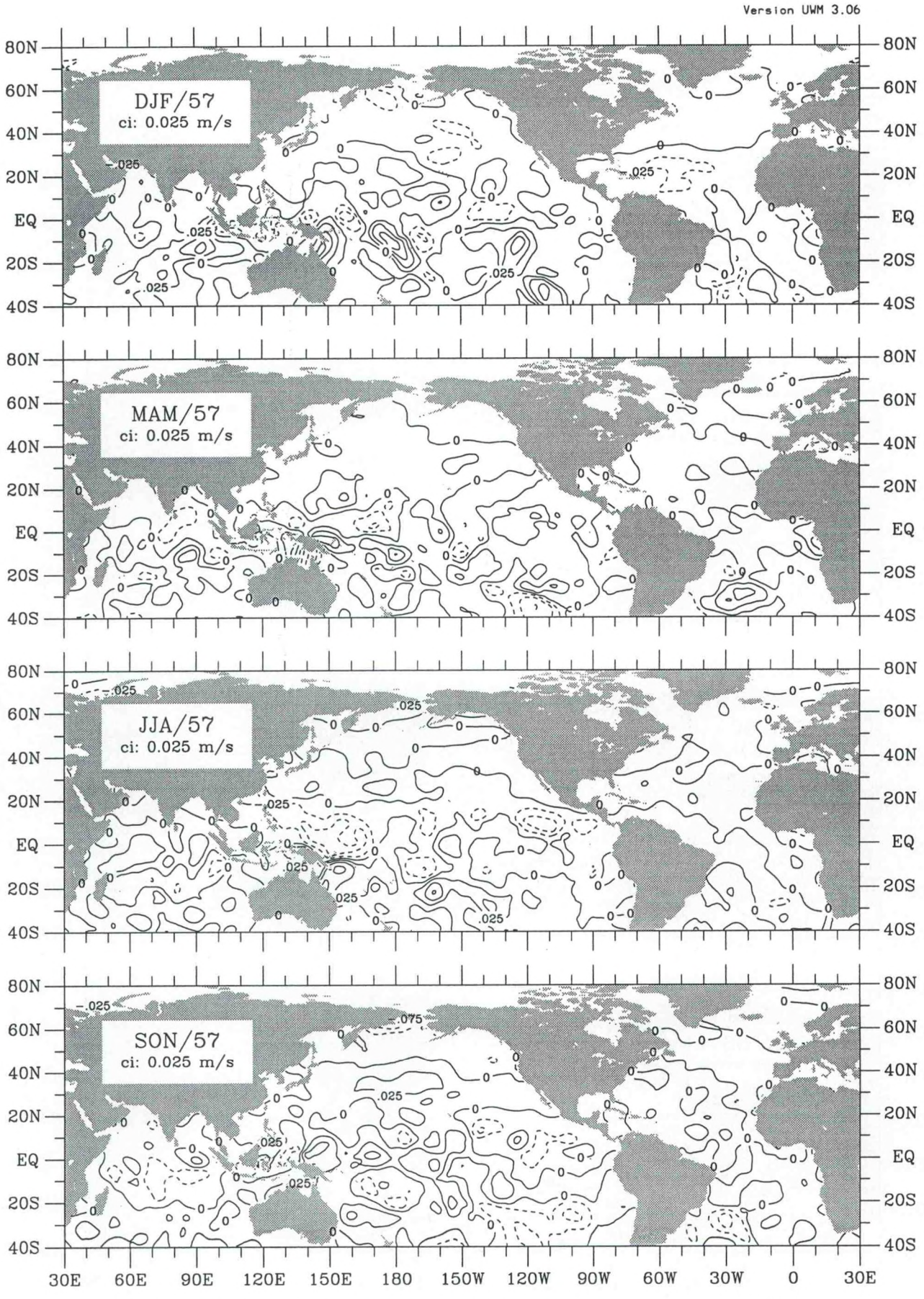

Figure uq-18. Zonal moisture flux seasonal anomaly for 1957.

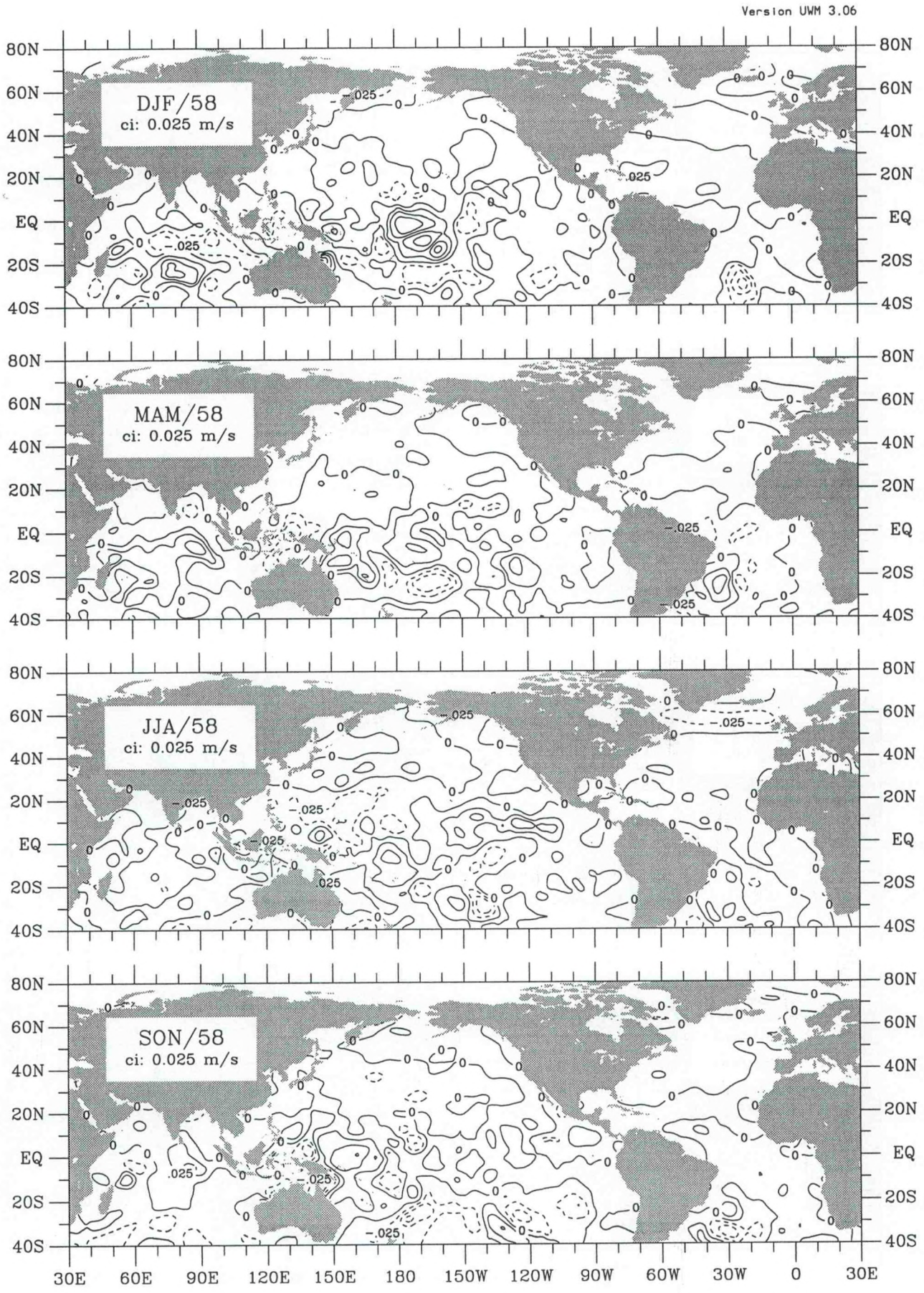

Figure uq-19. Zonal moisture flux seasonal anomaly for 1958.

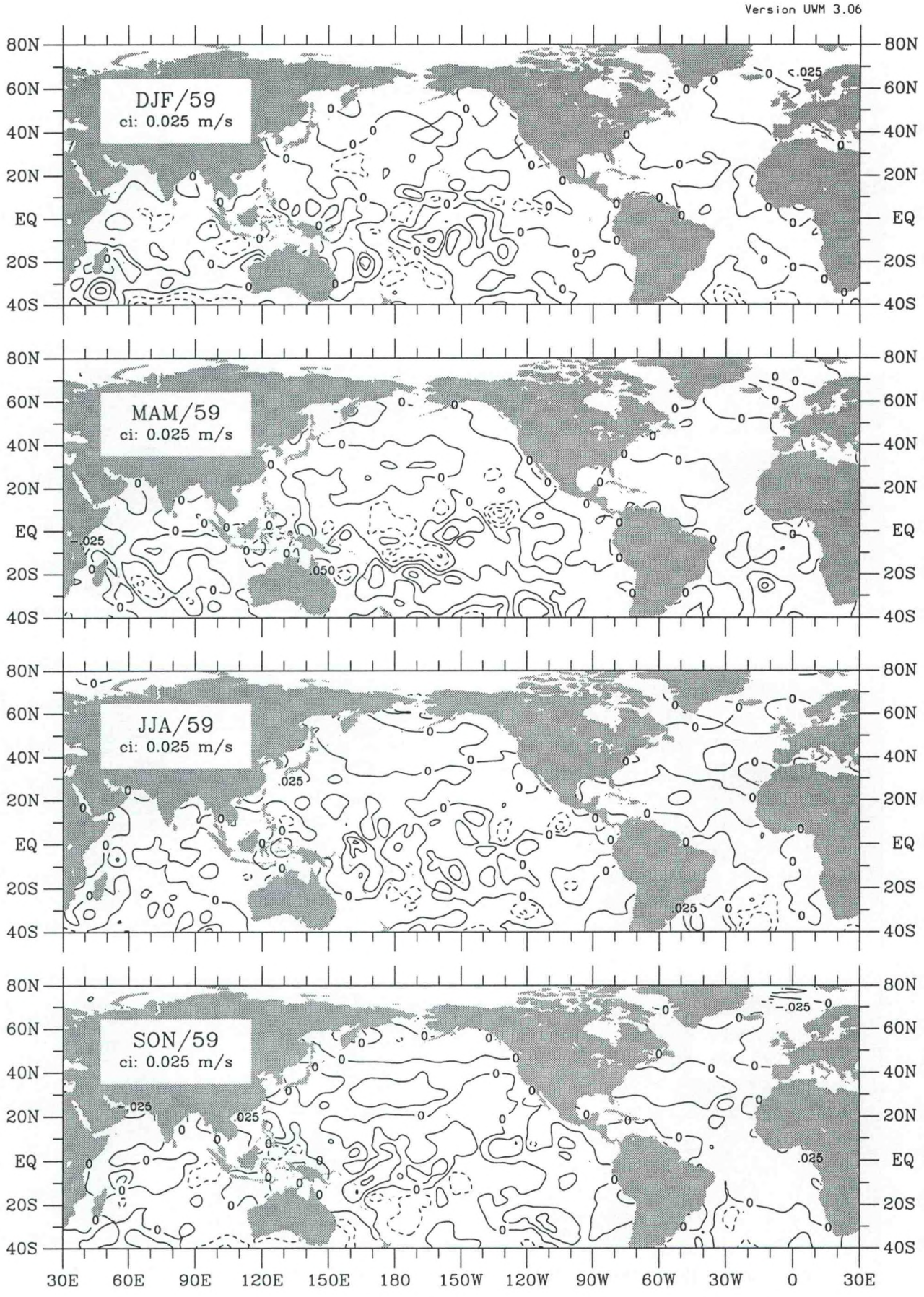

Figure uq-20. Zonal moisture flux seasonal anomaly for 1959.

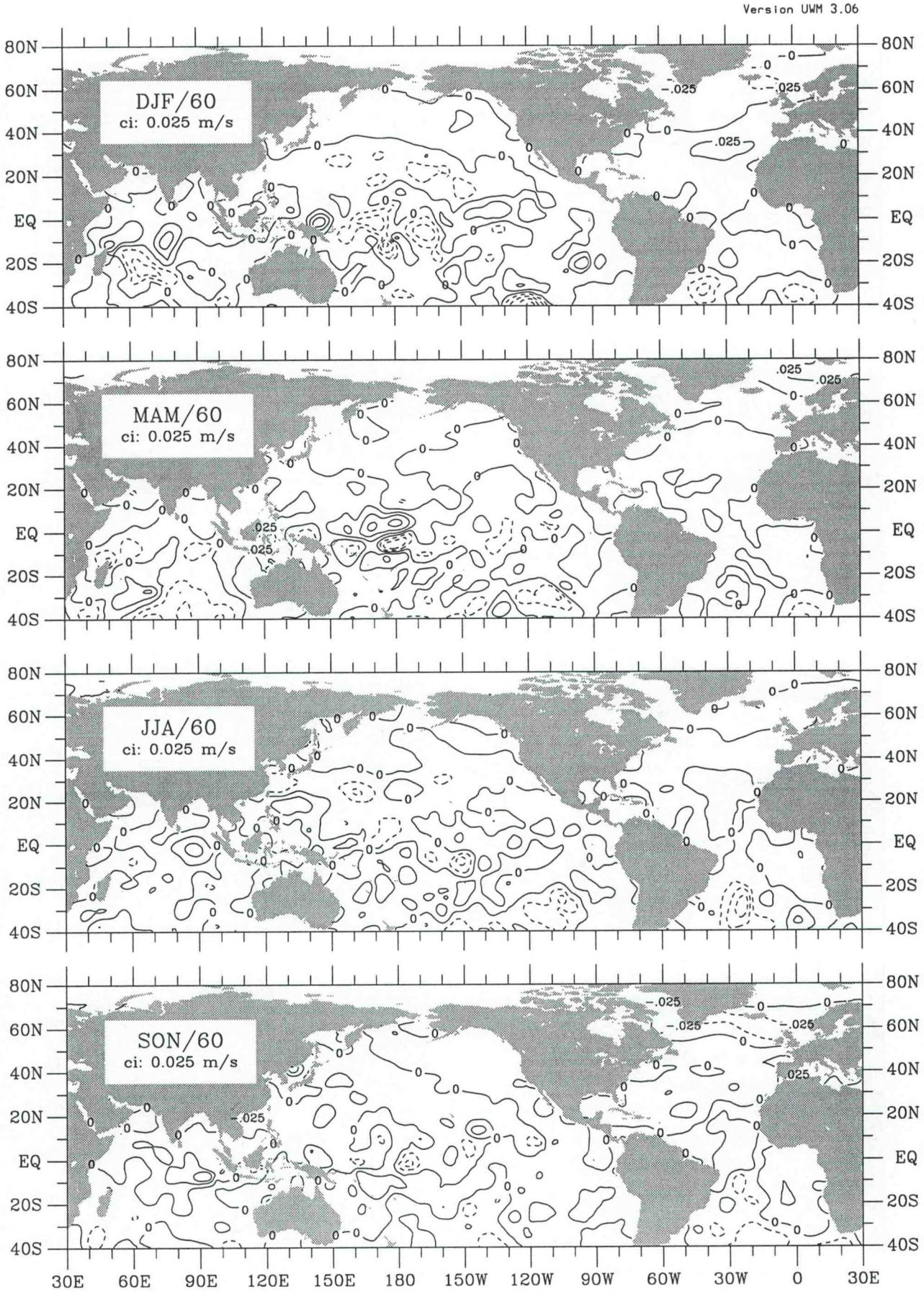

Figure uq-21. Zonal moisture flux seasonal anomaly for 1960.

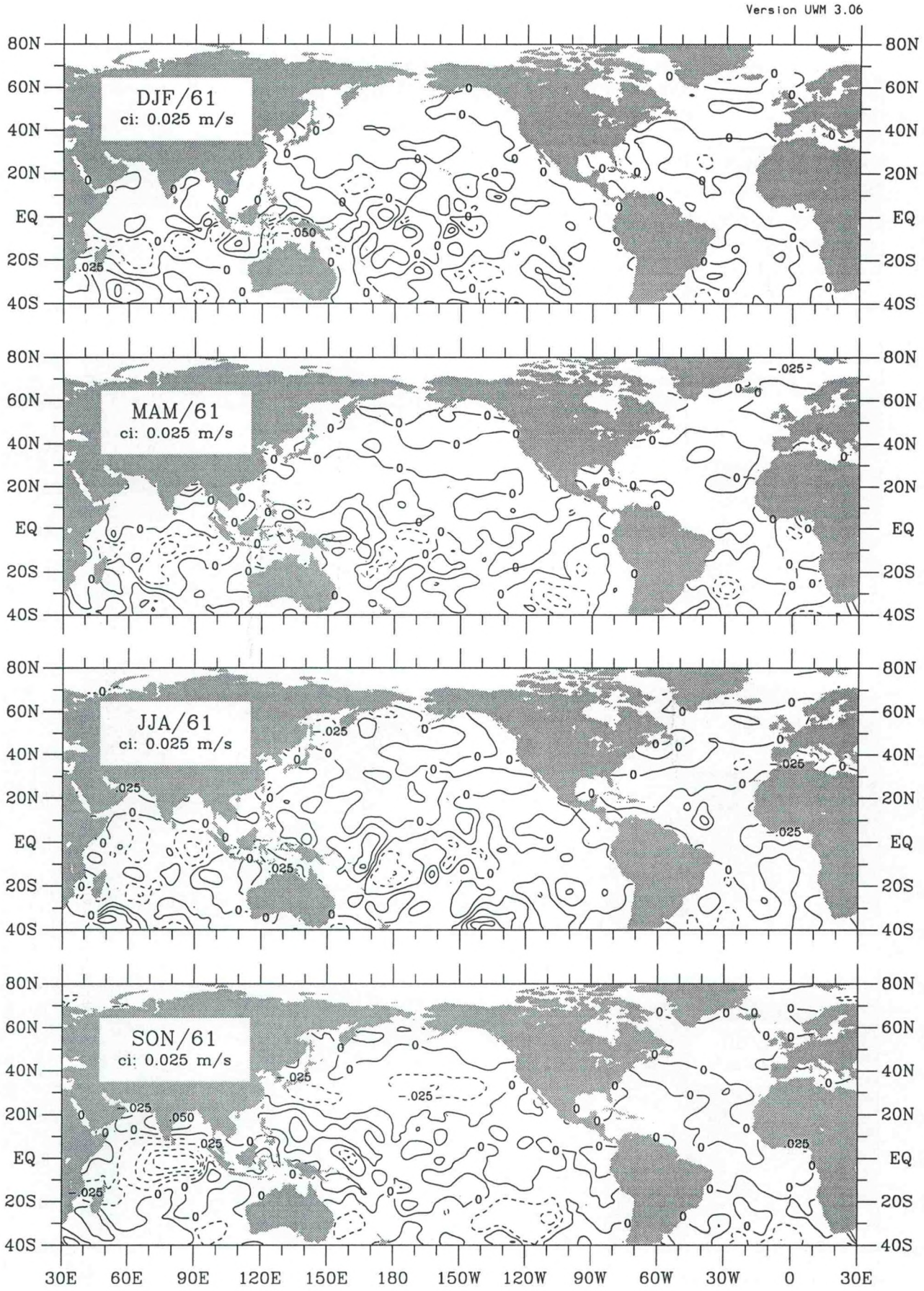

Figure uq-22. Zonal moisture flux seasonal anomaly for 1961.

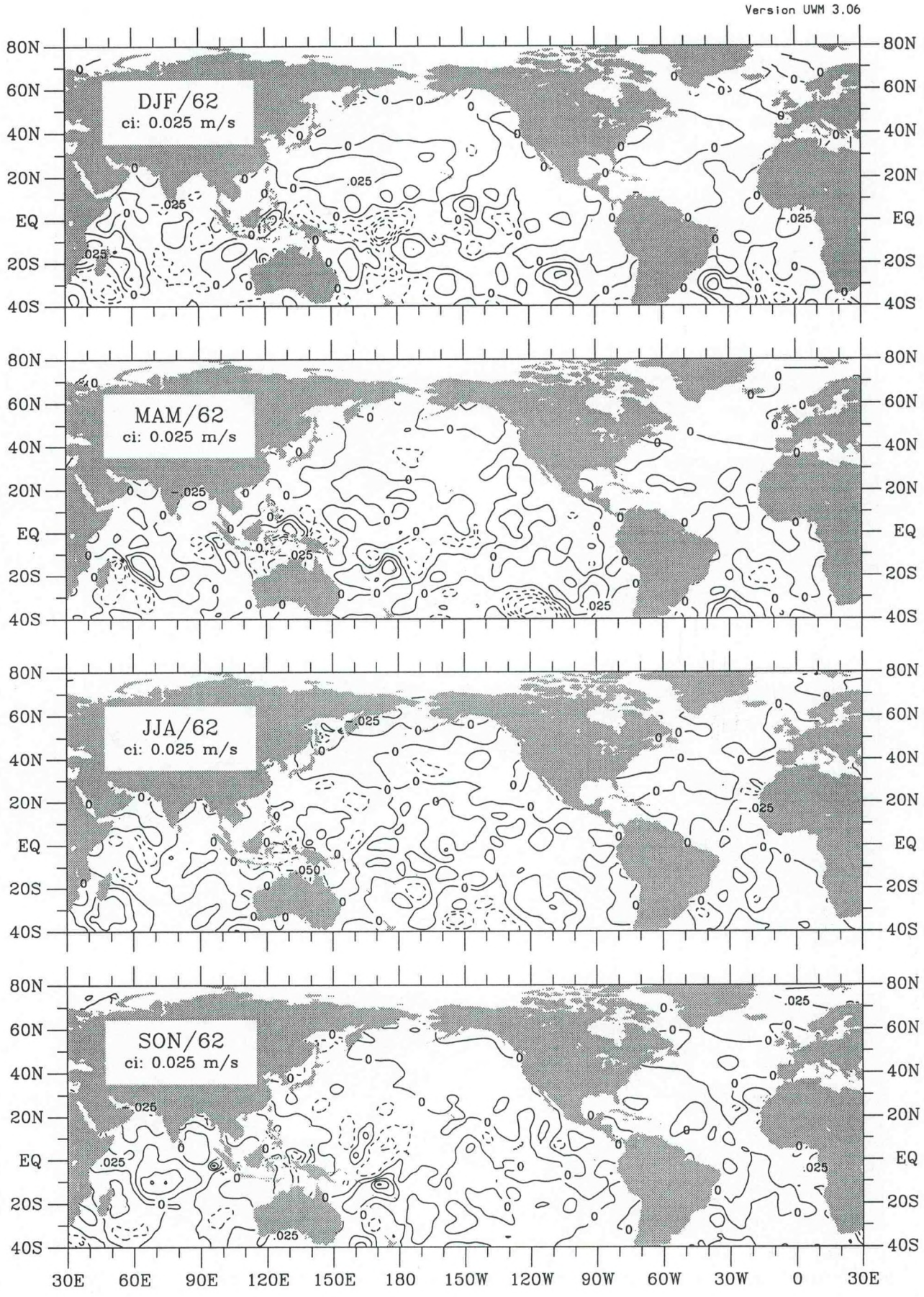

Figure uq-23. Zonal moisture flux seasonal anomaly for 1962.

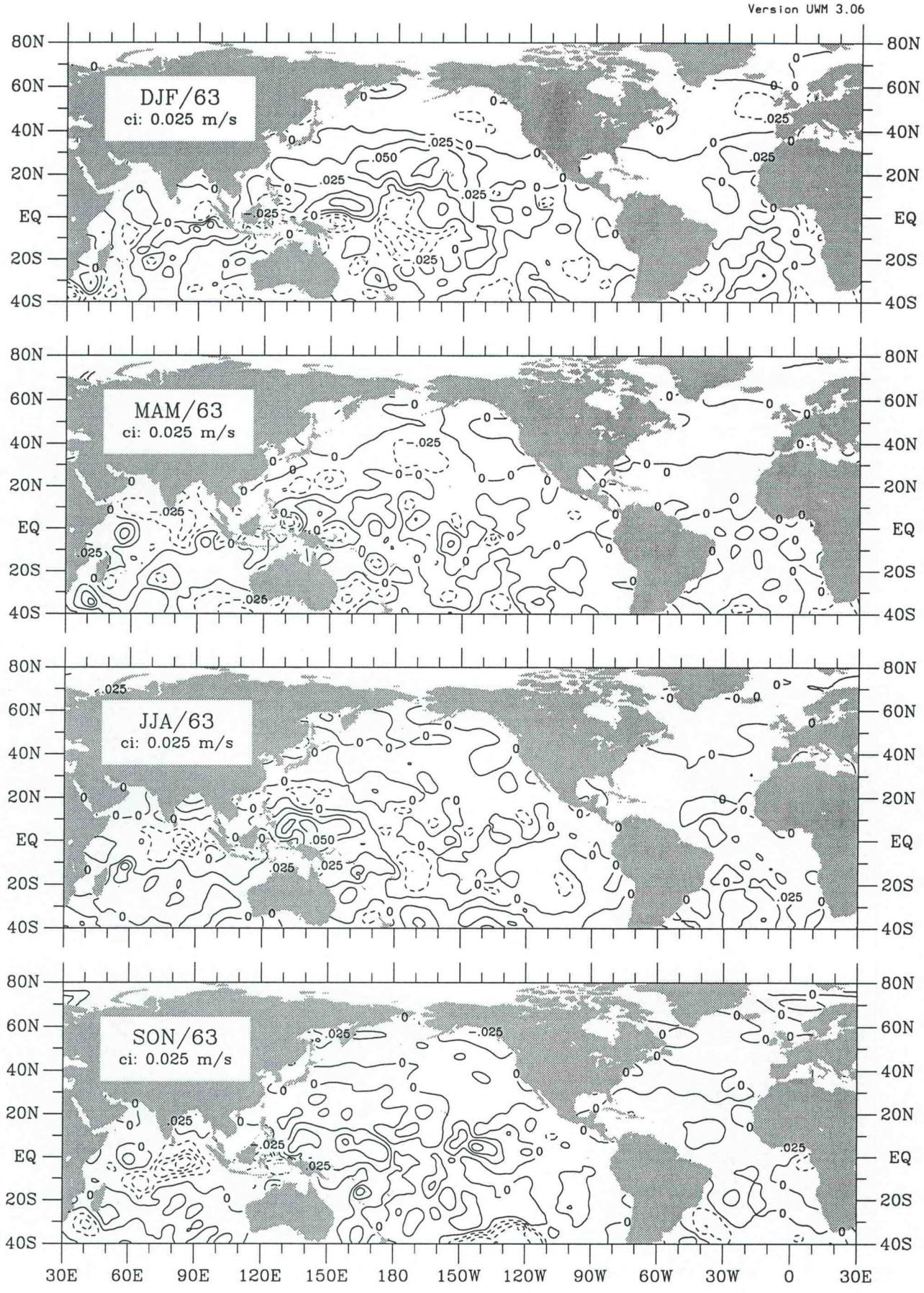

Figure uq-24. Zonal moisture flux seasonal anomaly for 1963.

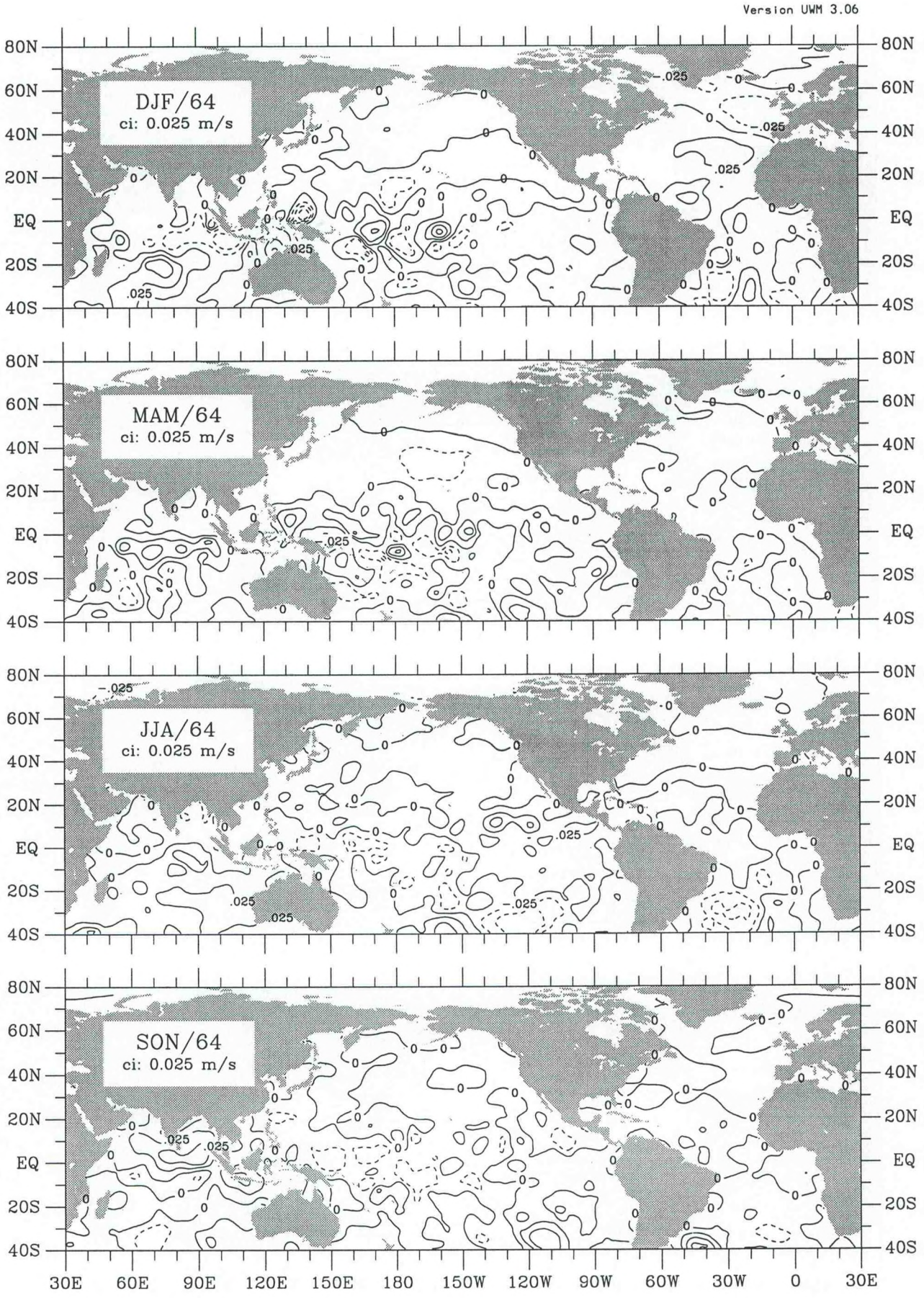

Figure uq-25. Zonal moisture flux seasonal anomaly for 1964.

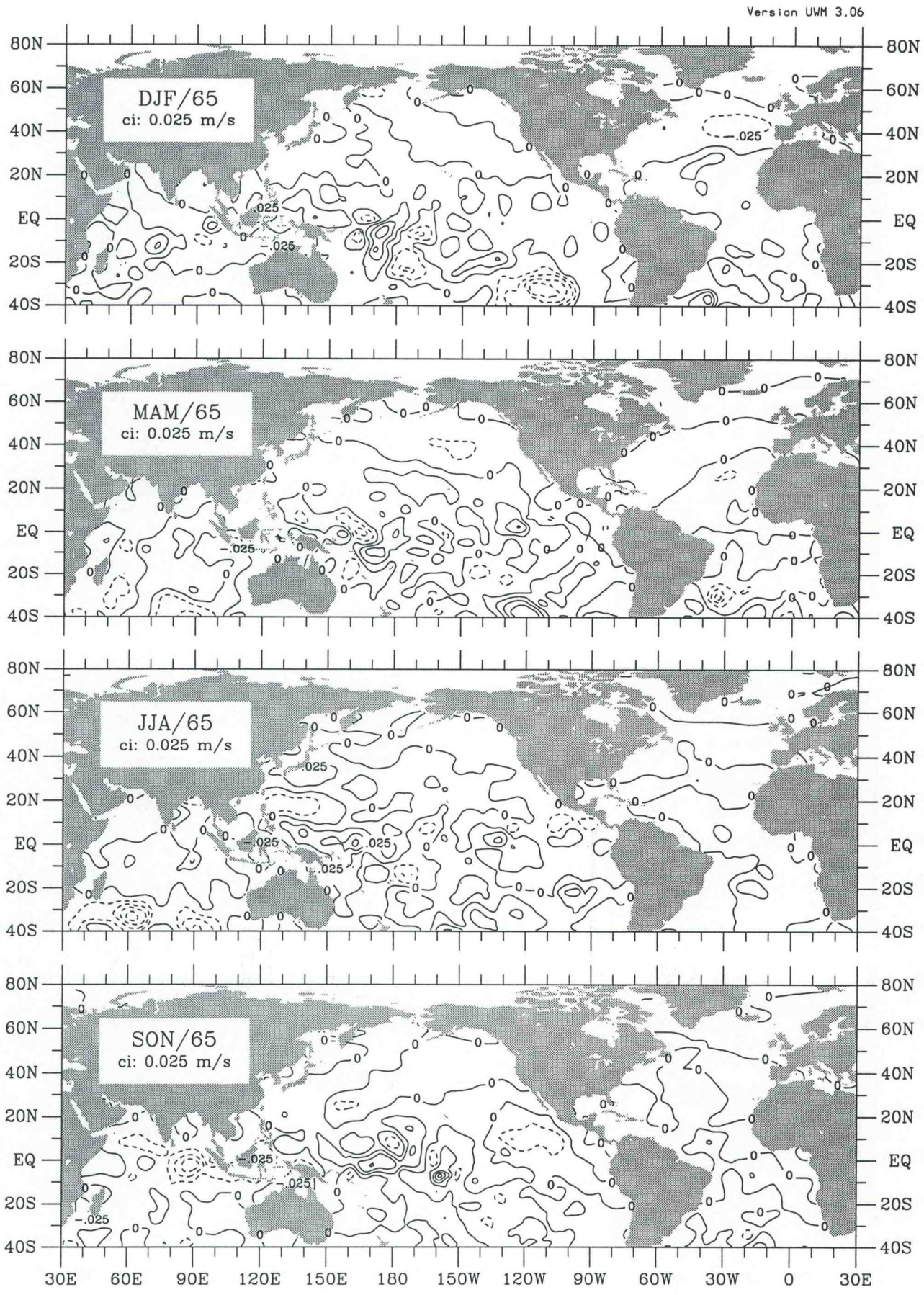

Figure uq-26. Zonal moisture flux seasonal anomaly for 1965.

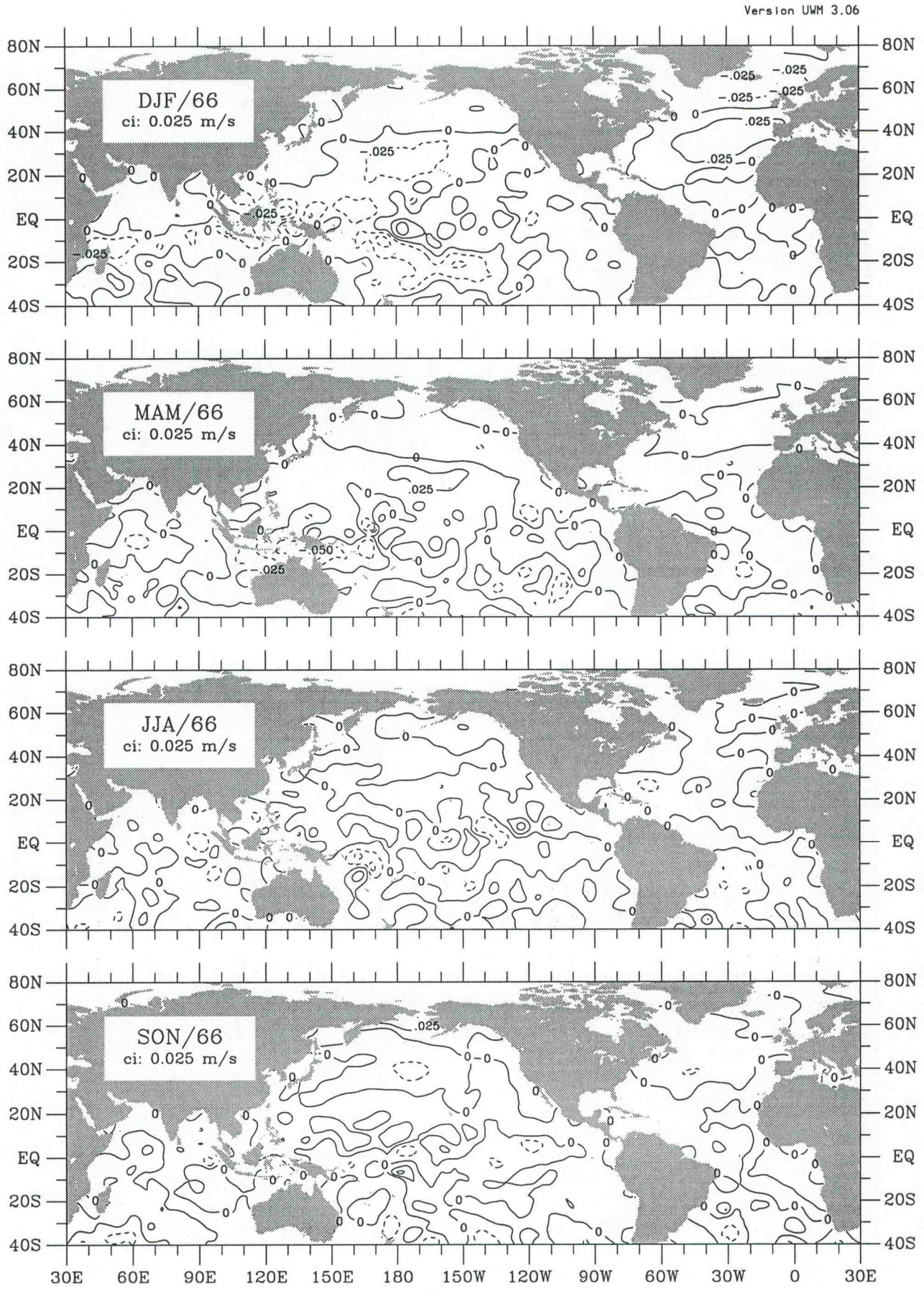

Figure uq-27. Zonal moisture flux seasonal anomaly for 1966.

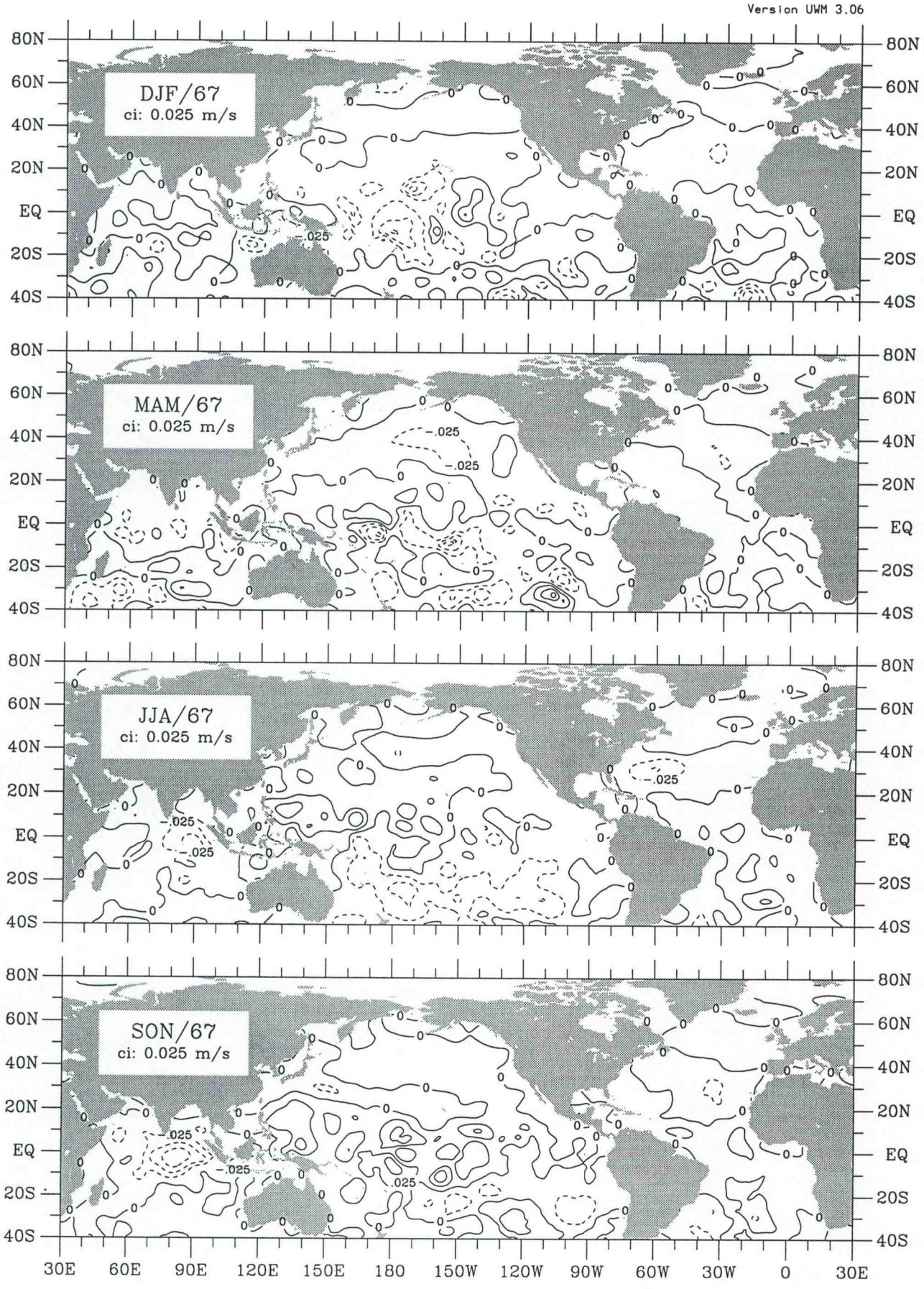

Figure uq-28. Zonal moisture flux seasonal anomaly for 1967.

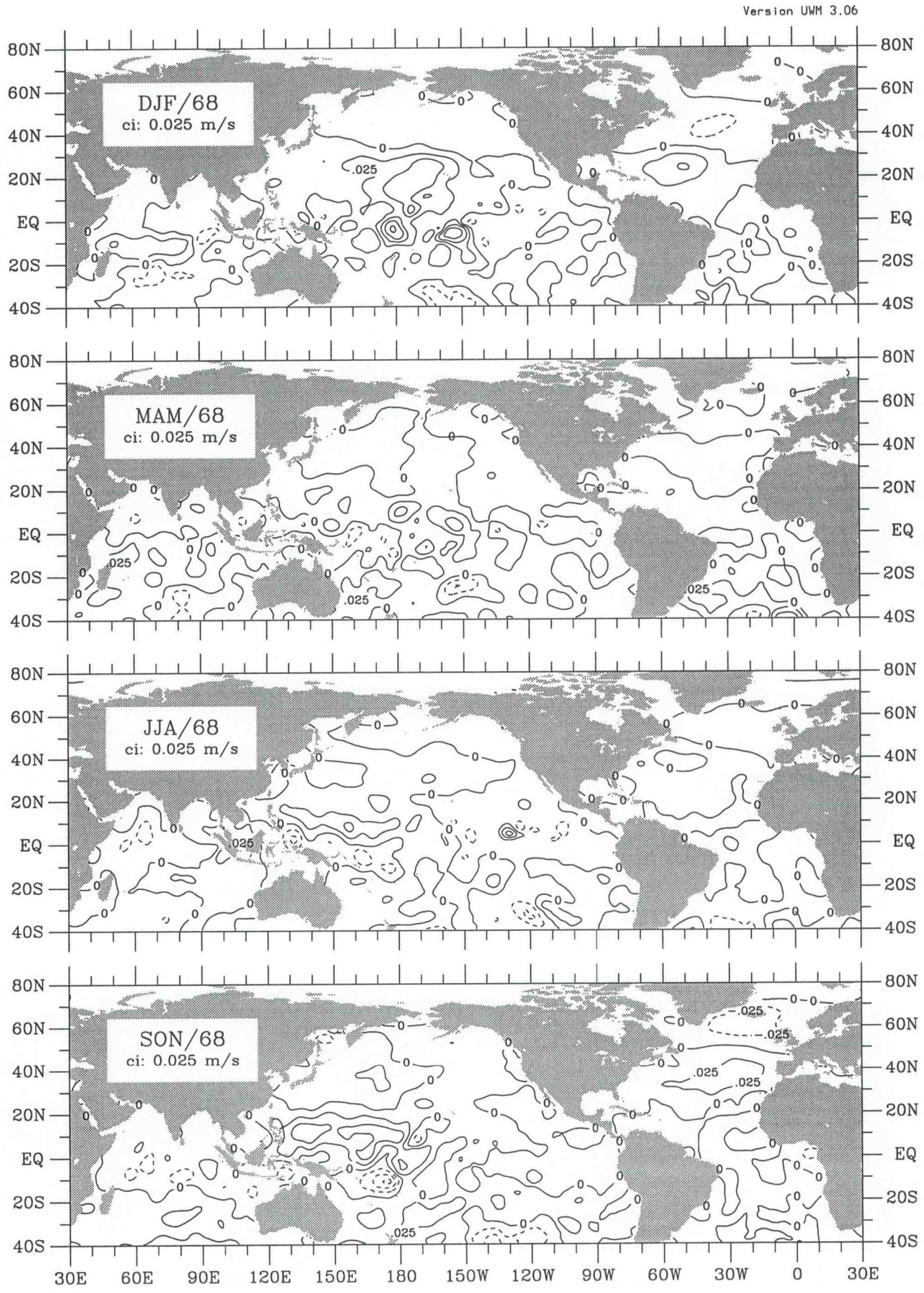

Figure uq-29. Zonal moisture flux seasonal anomaly for 1968.

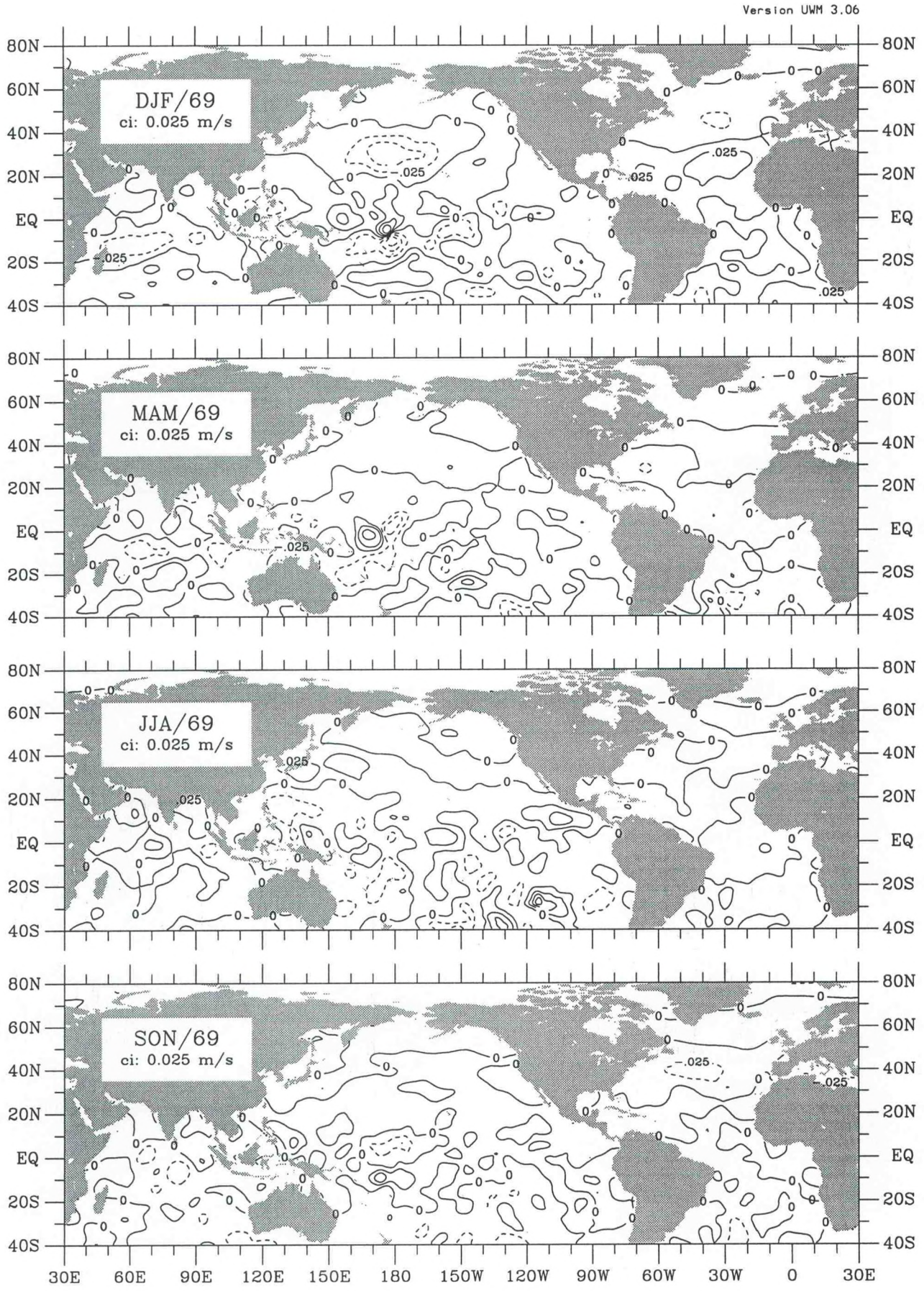

Figure uq-30. Zonal moisture flux seasonal anomaly for 1969.

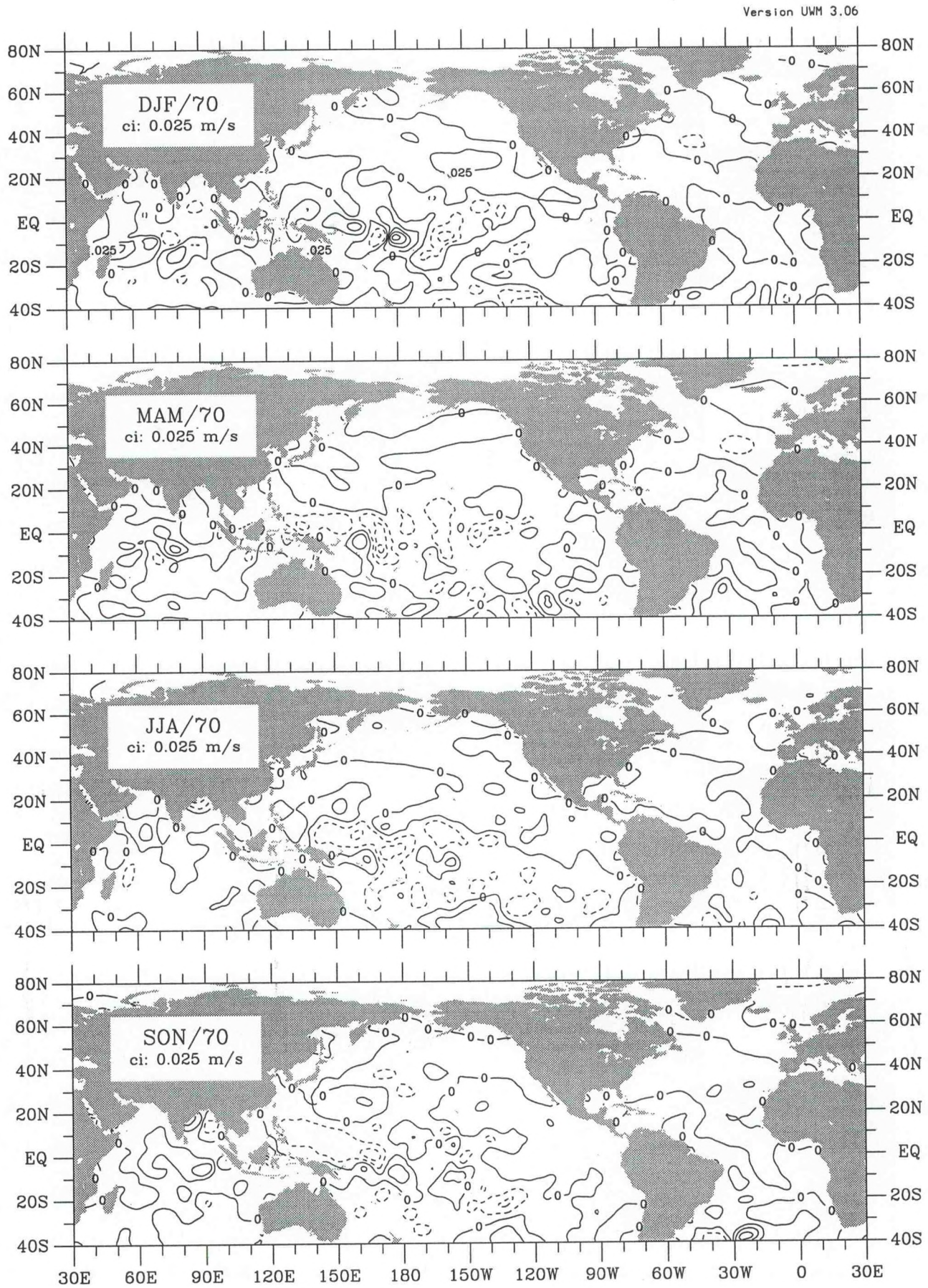

Figure uq-31. Zonal moisture flux seasonal anomaly for 1970.

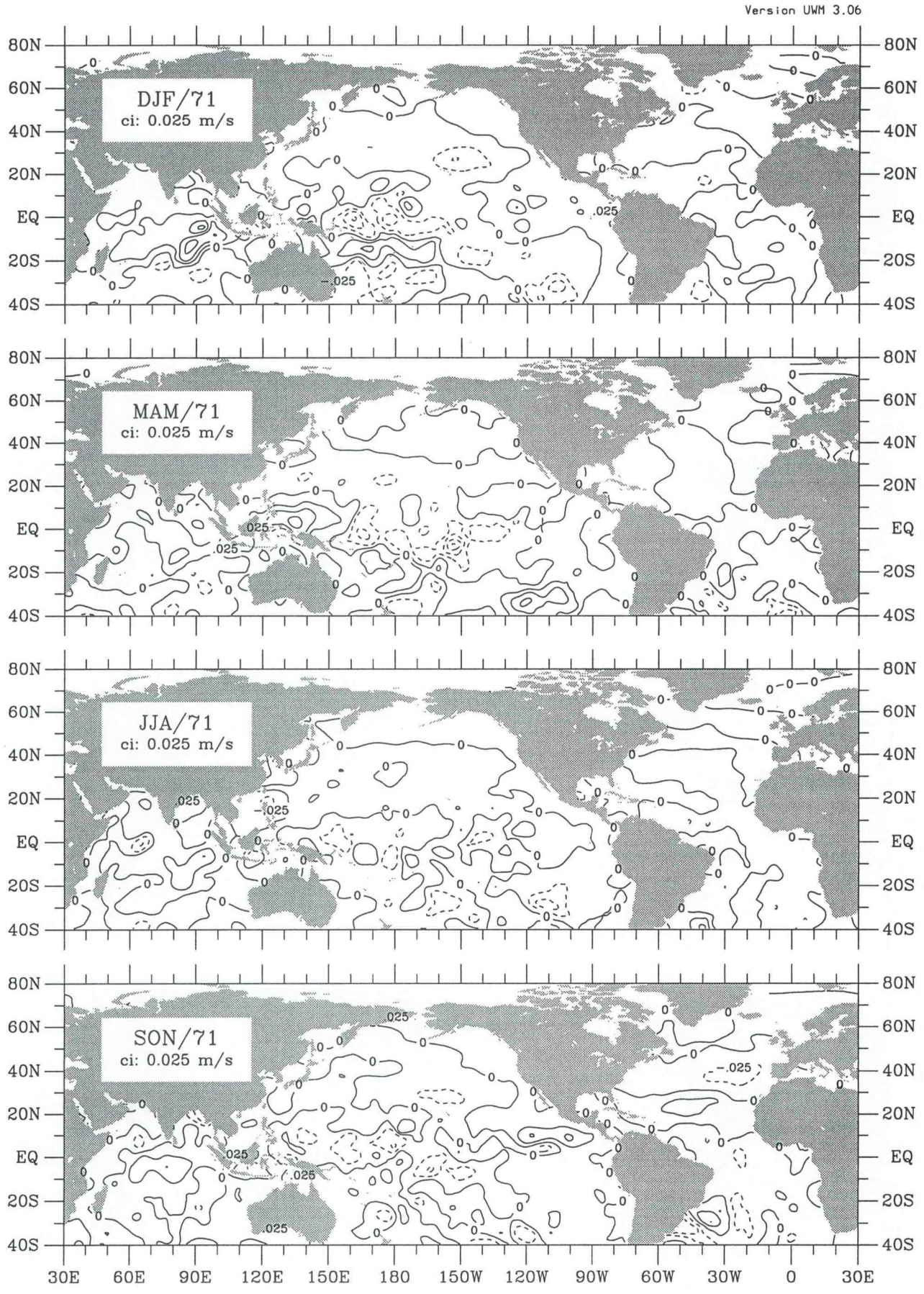

Figure uq-32. Zonal moisture flux seasonal anomaly for 1971.

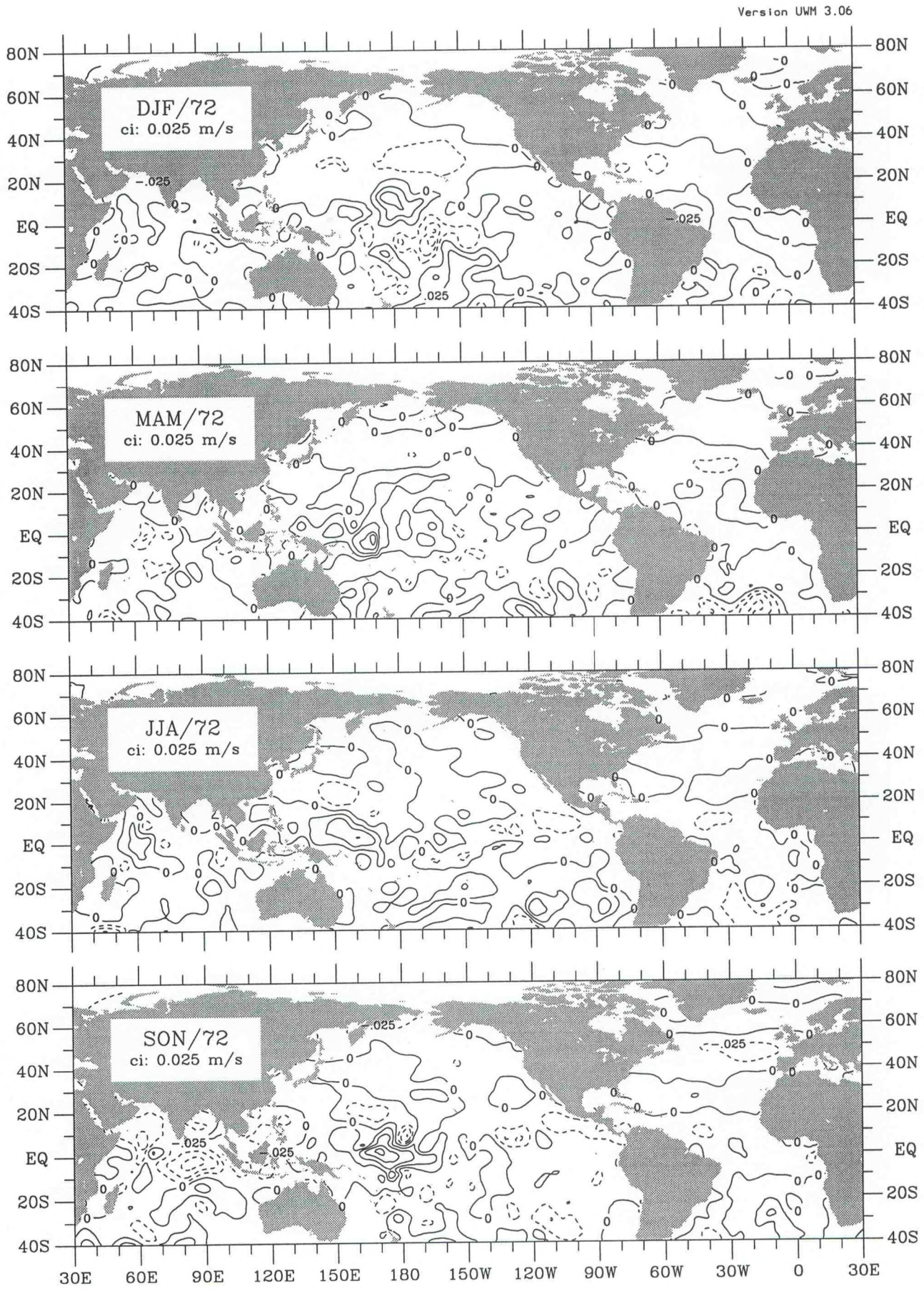

Figure uq-33. Zonal moisture flux seasonal anomaly for 1972.

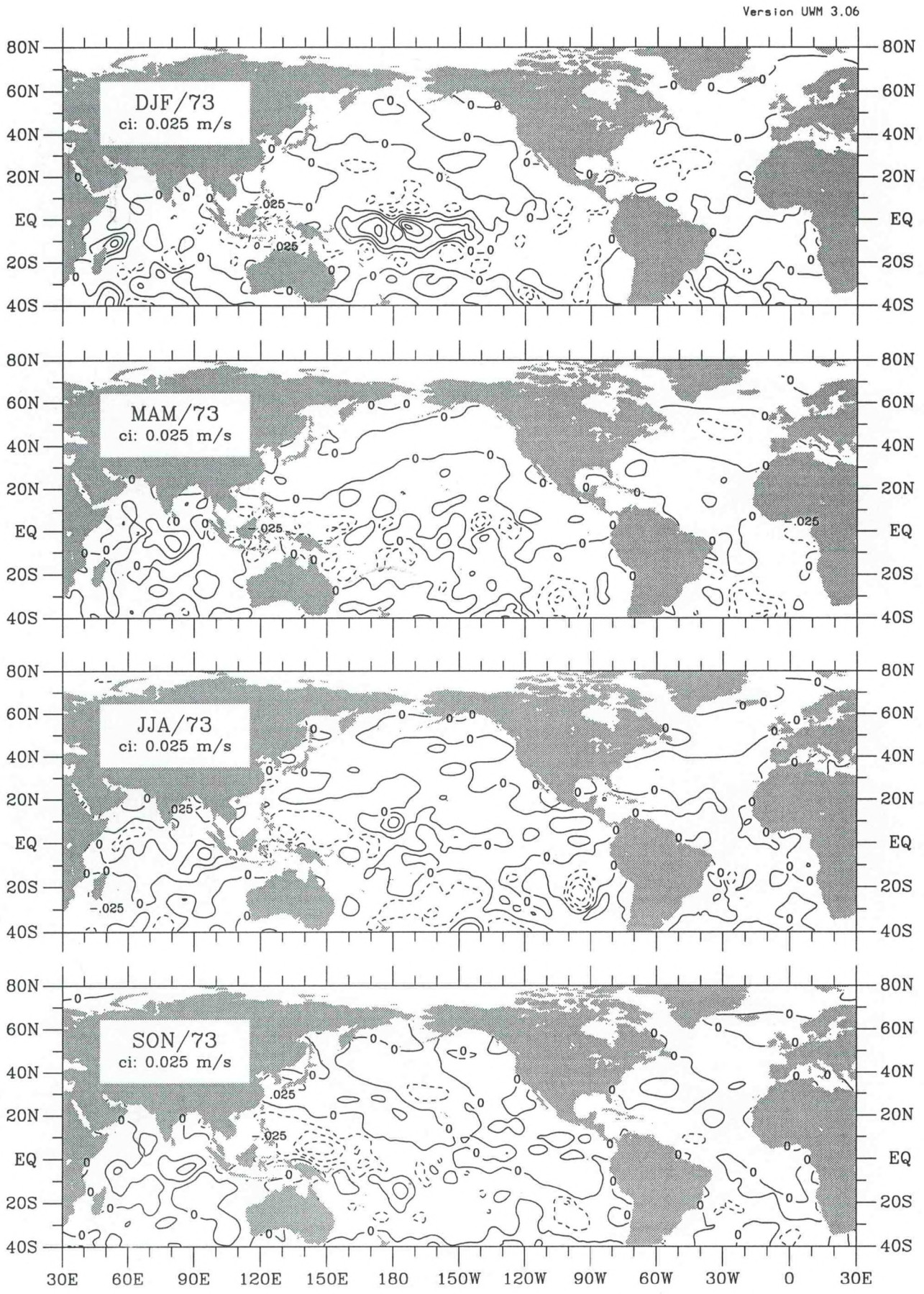

Figure uq-34. Zonal moisture flux seasonal anomaly for 1973.

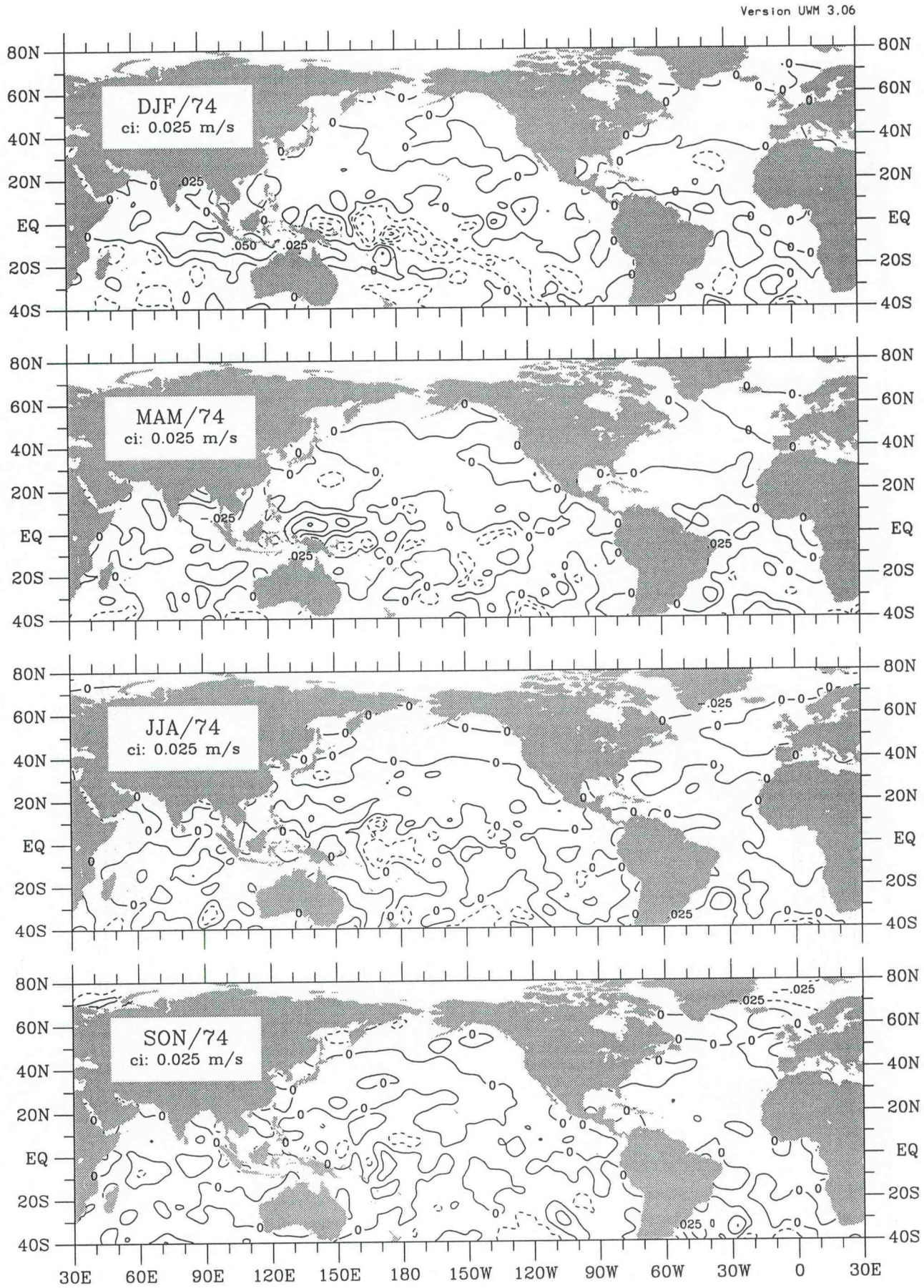

Figure uq-35. Zonal moisture flux seasonal anomaly for 1974.

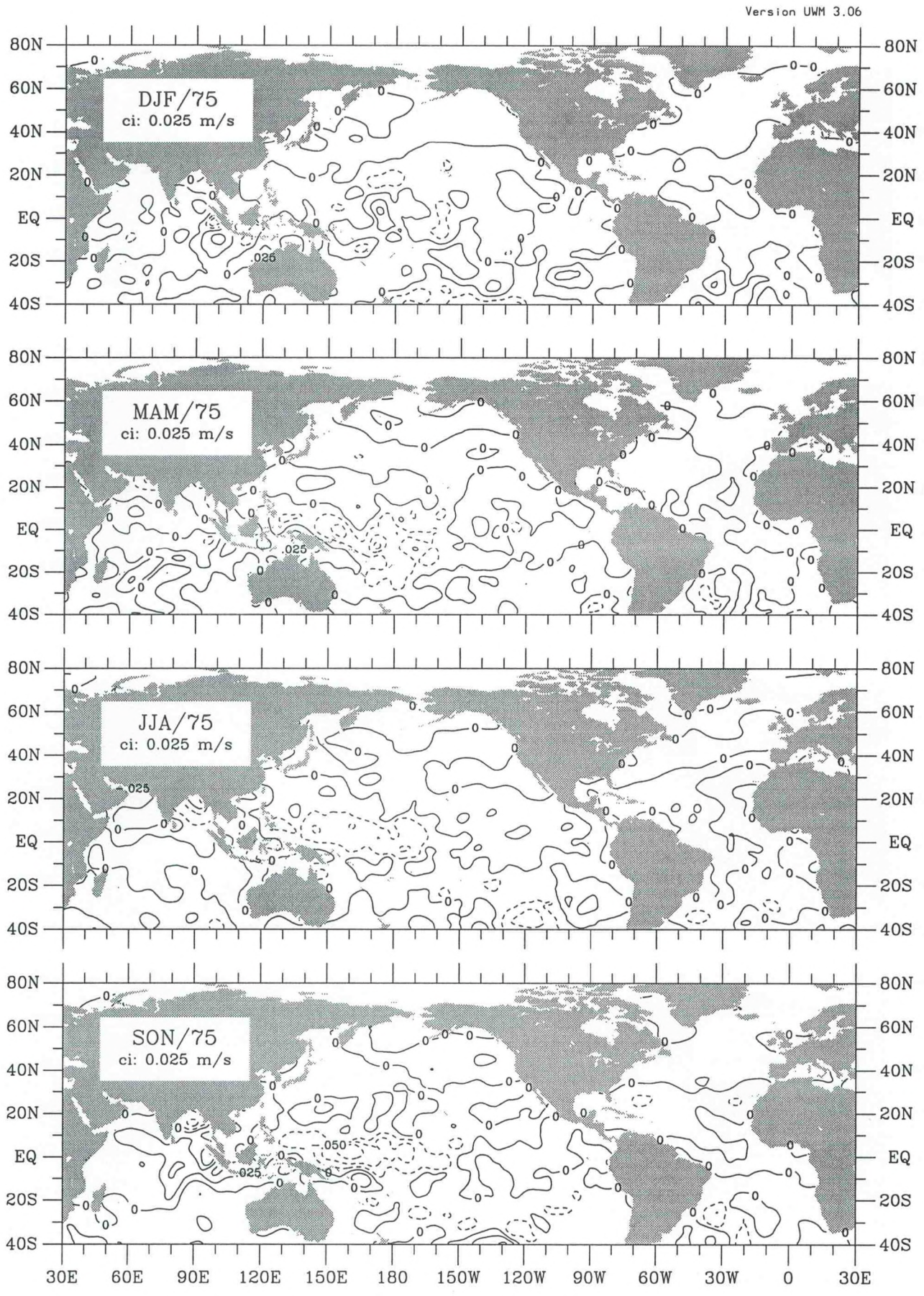

Figure uq-36. Zonal moisture flux seasonal anomaly for 1975.

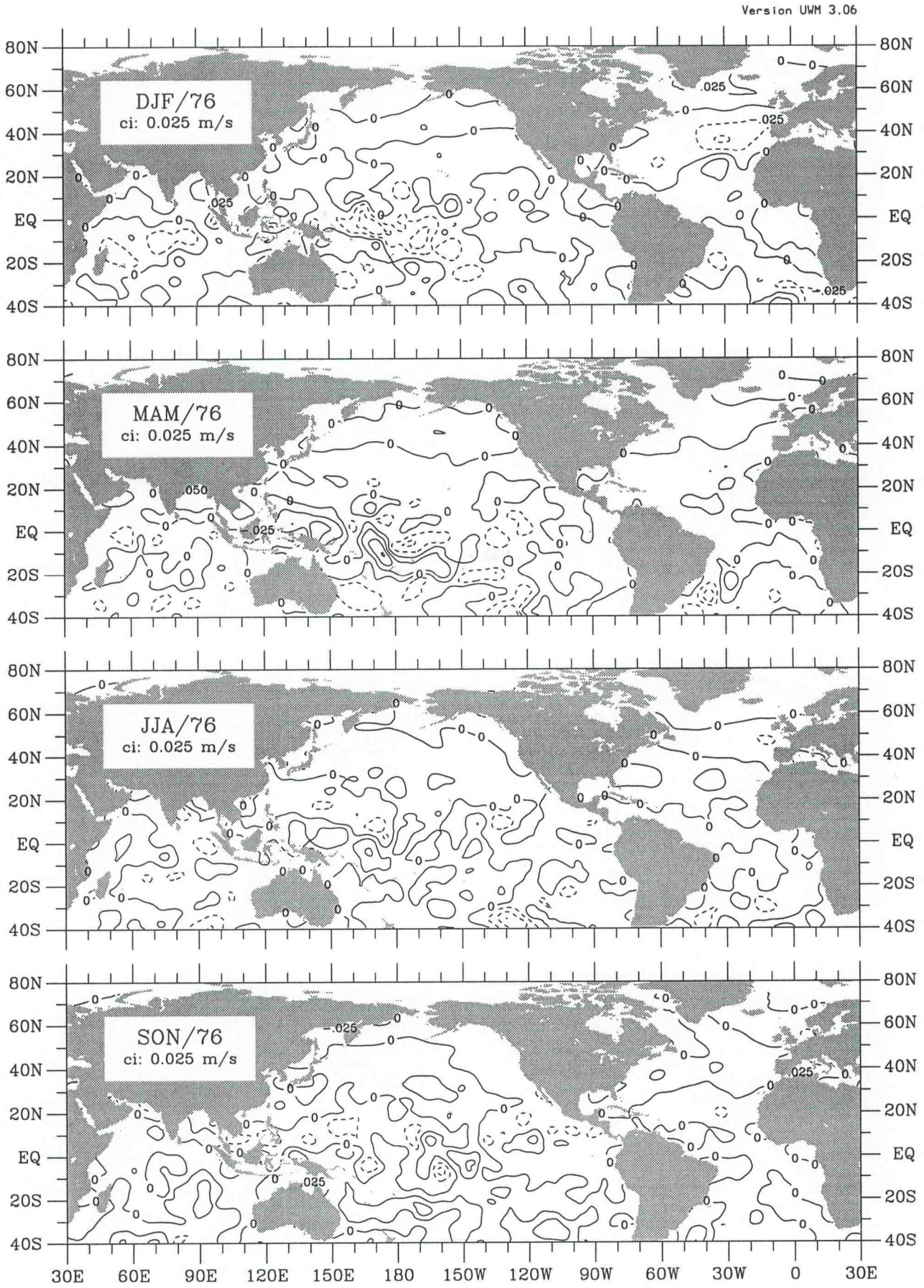

Figure uq-37. Zonal moisture flux seasonal anomaly for 1976.

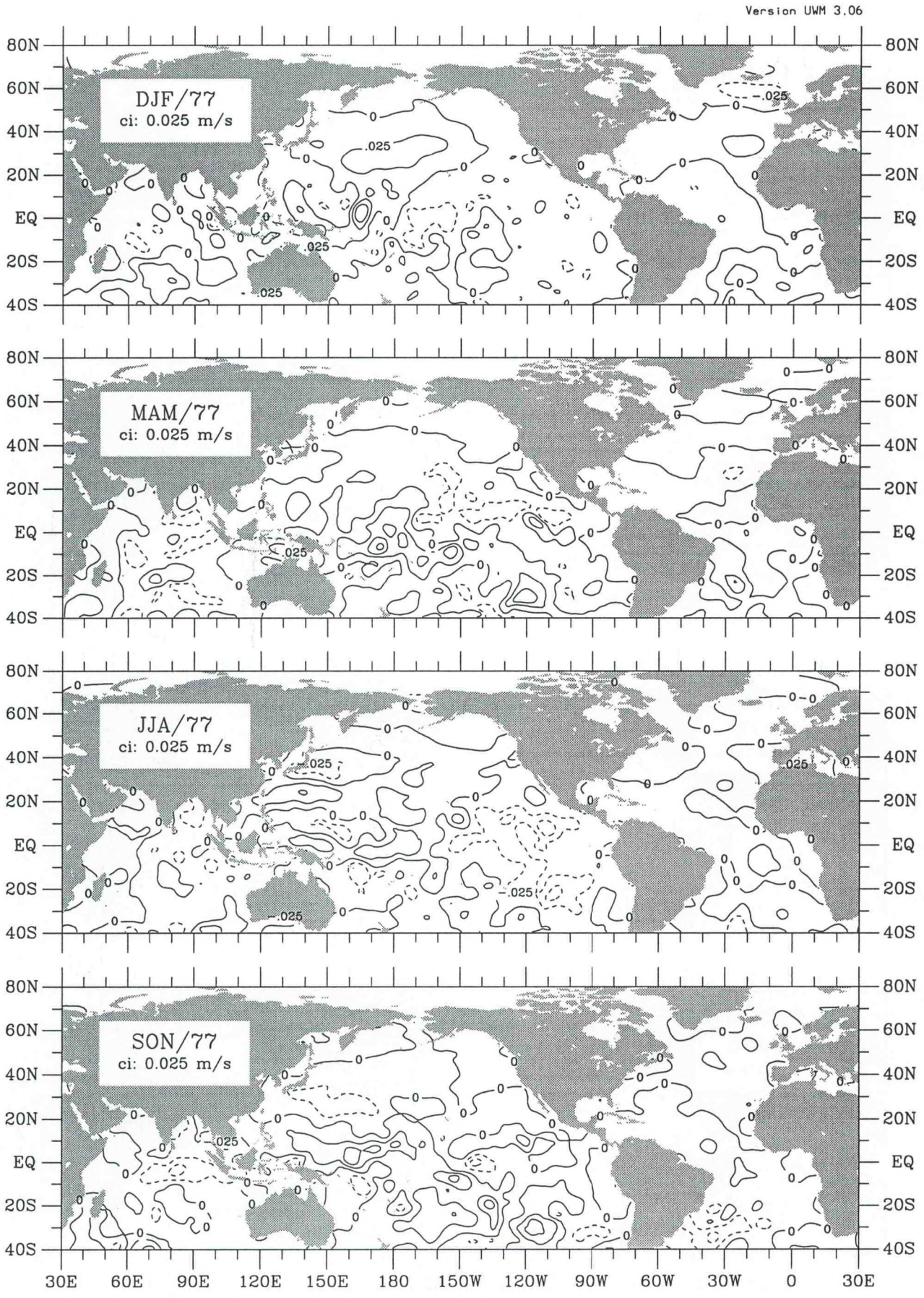

Figure uq-38. Zonal moisture flux seasonal anomaly for 1977.

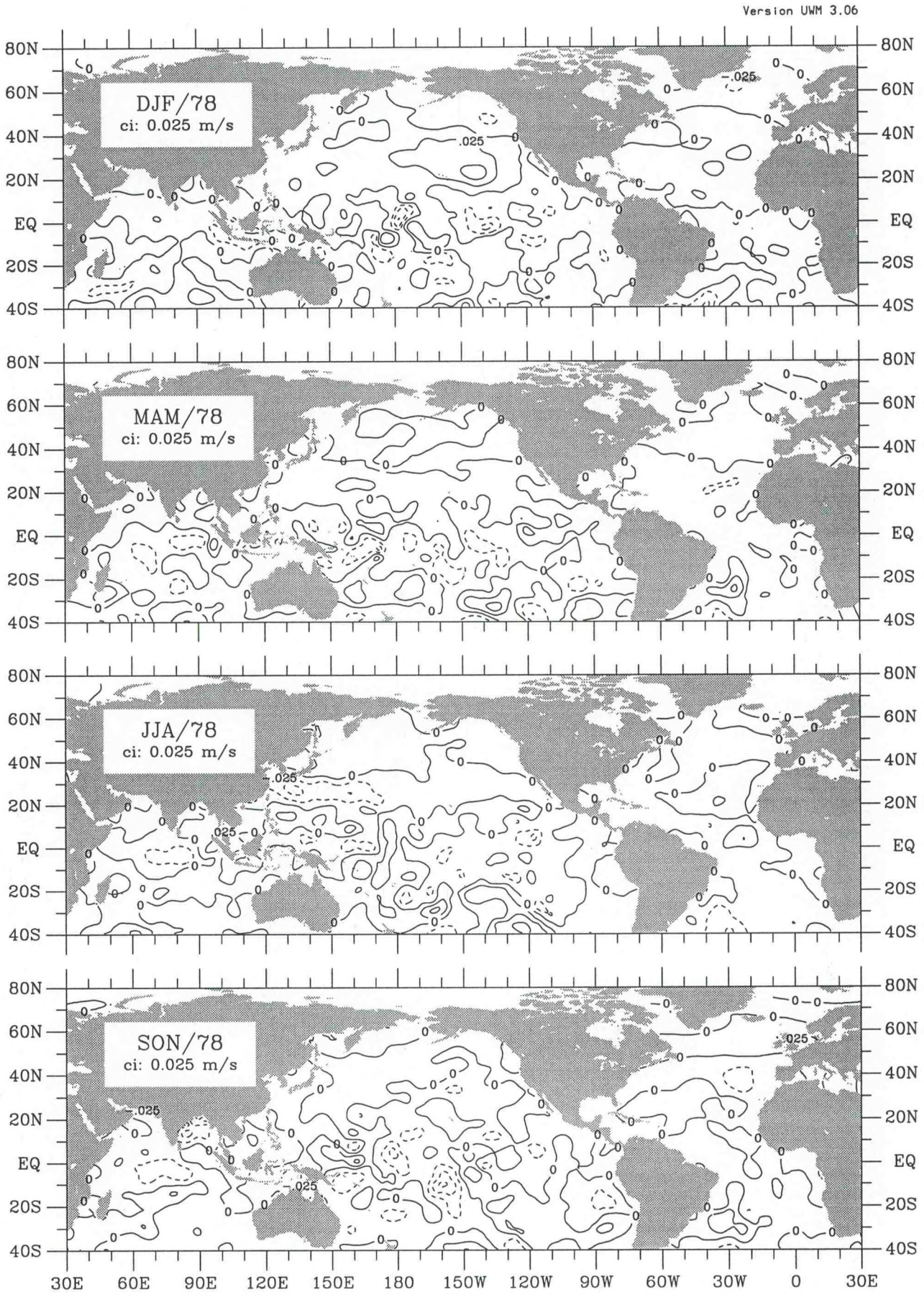

Figure uq-39. Zonal moisture flux seasonal anomaly for 1978.

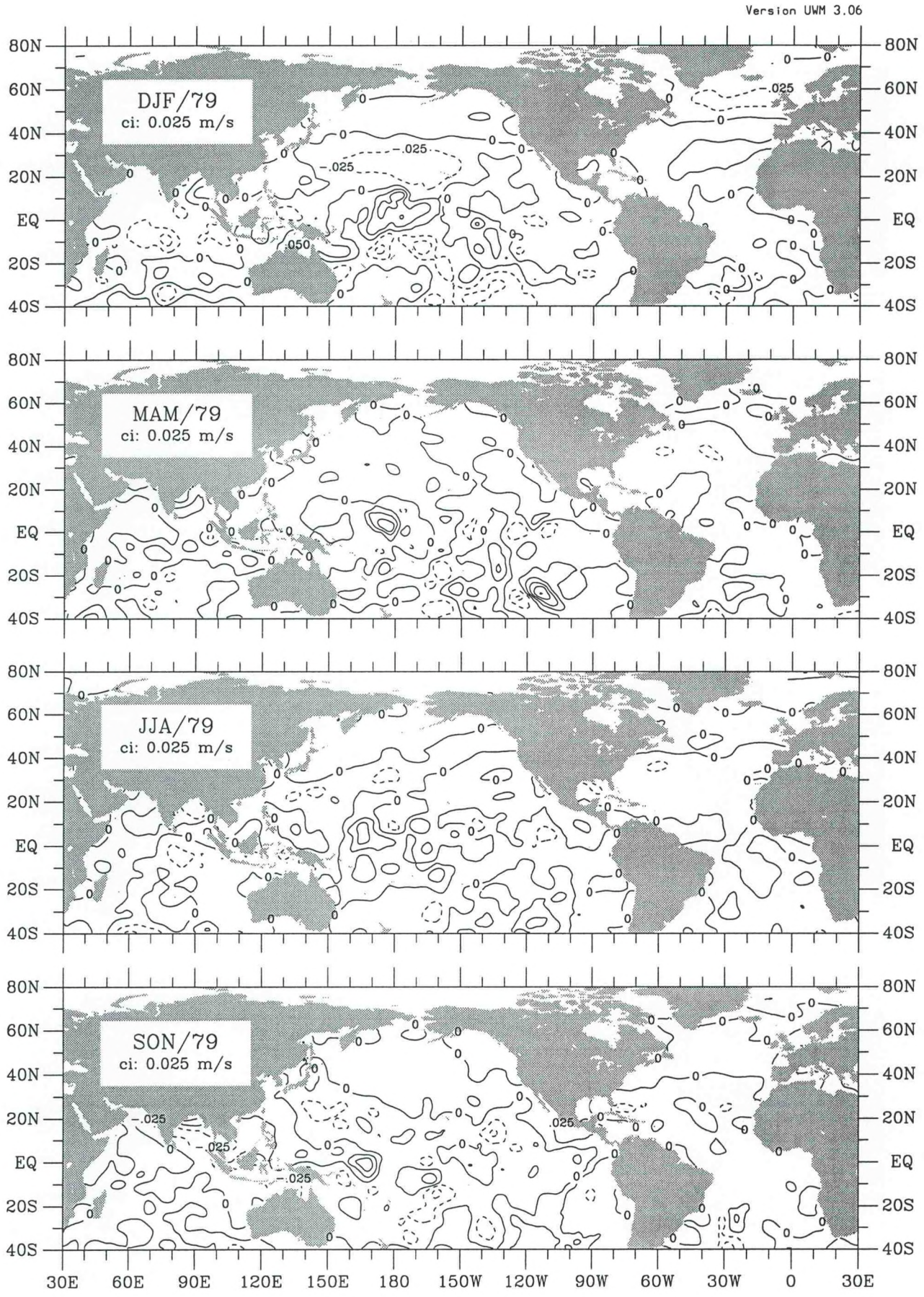

Figure uq-40. Zonal moisture flux seasonal anomaly for 1979.

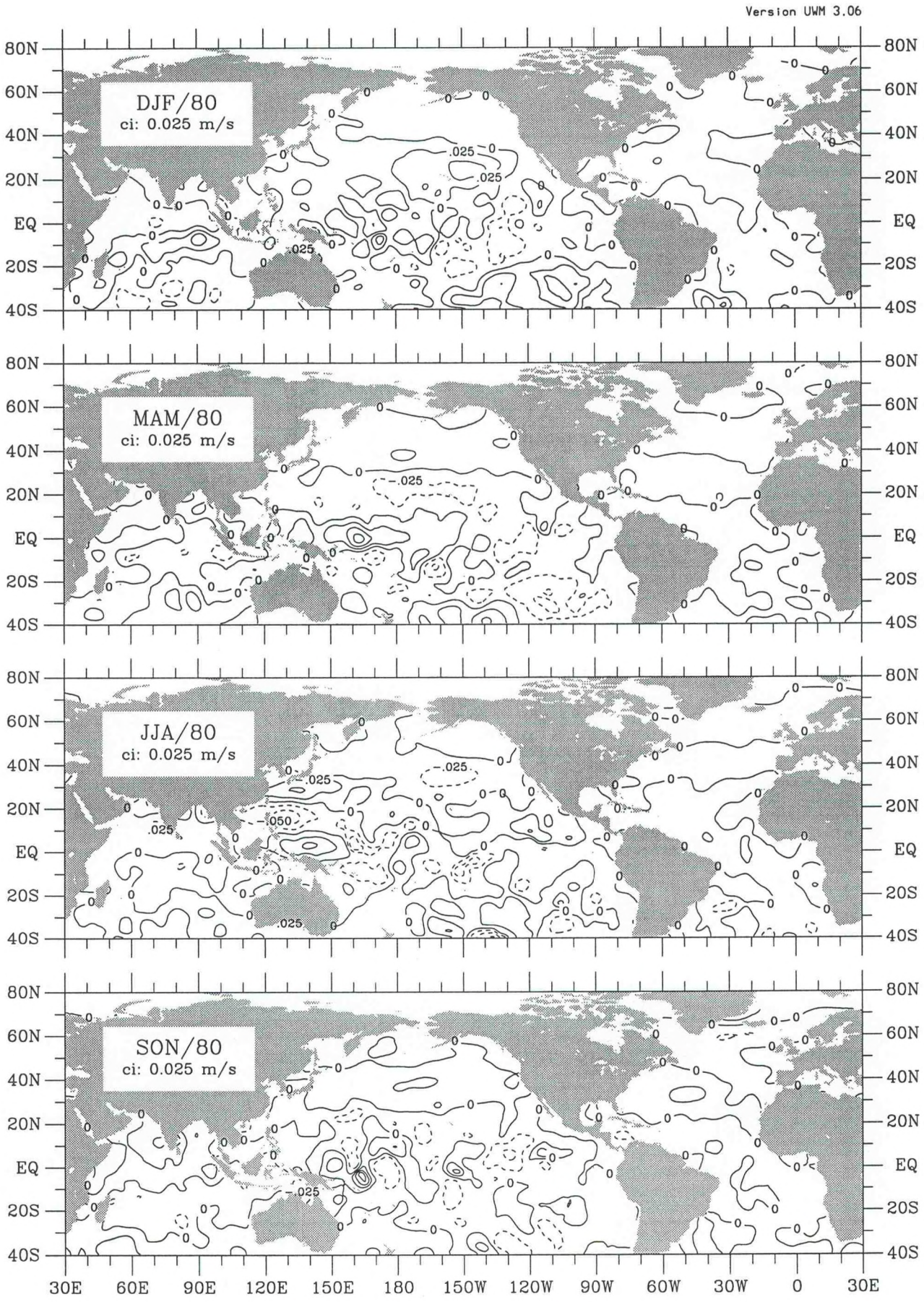

Figure uq-41. Zonal moisture flux seasonal anomaly for 1980.

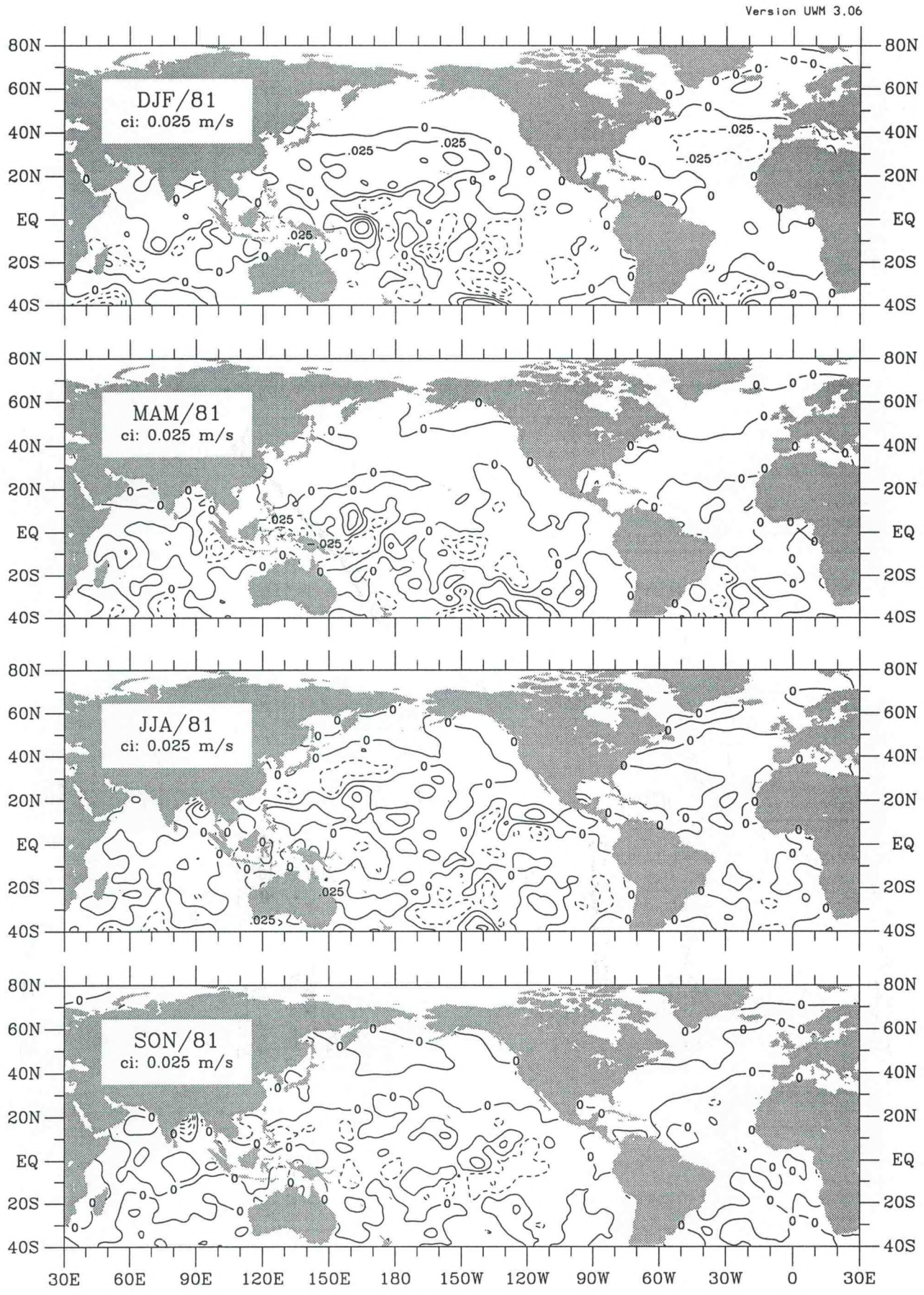

Figure uq-42. Zonal moisture flux seasonal anomaly for 1981.

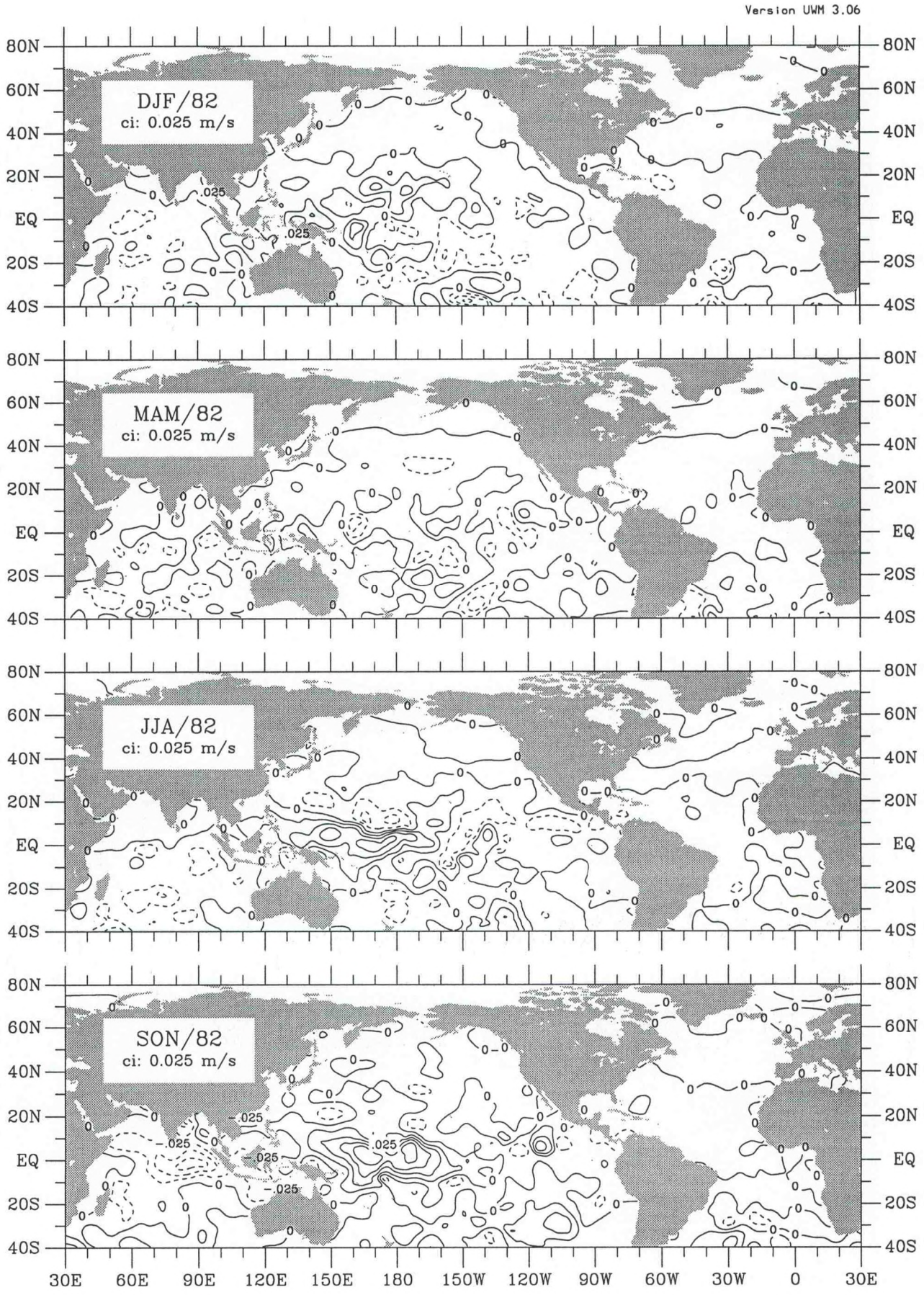

Figure uq-43. Zonal moisture flux seasonal anomaly for 1982.

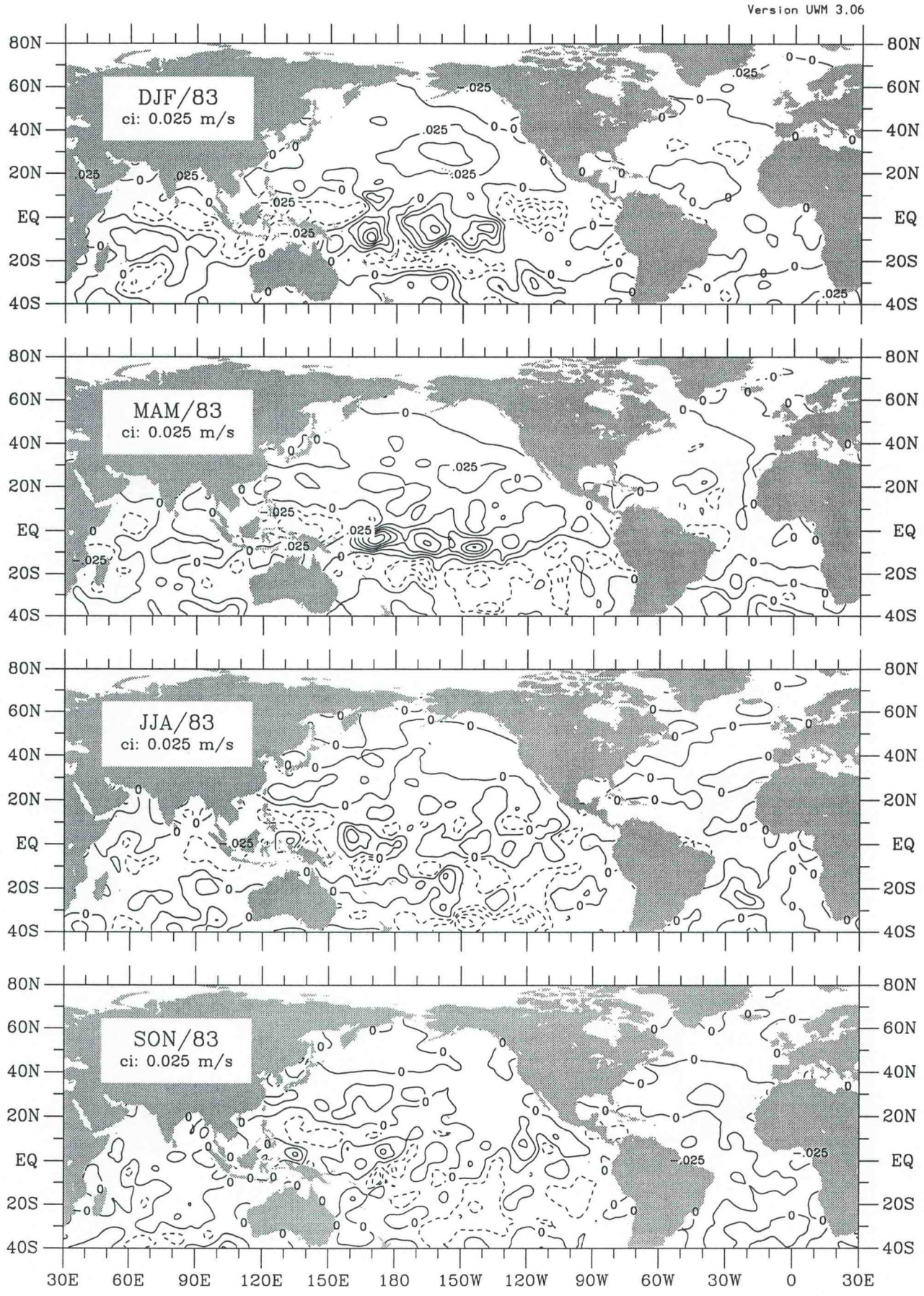

Figure uq-44. Zonal moisture flux seasonal anomaly for 1983.

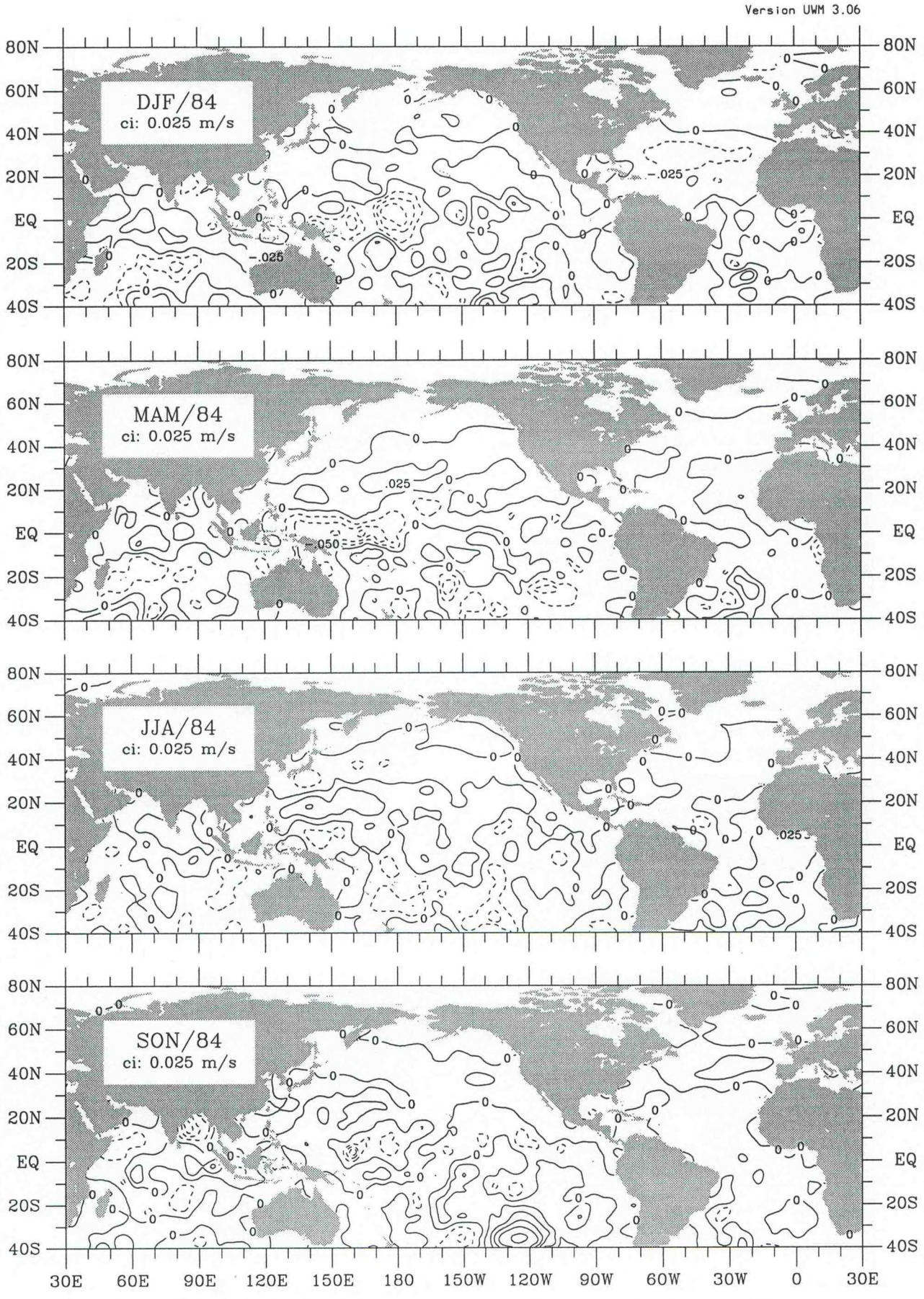

Figure uq-45. Zonal moisture flux seasonal anomaly for 1984.

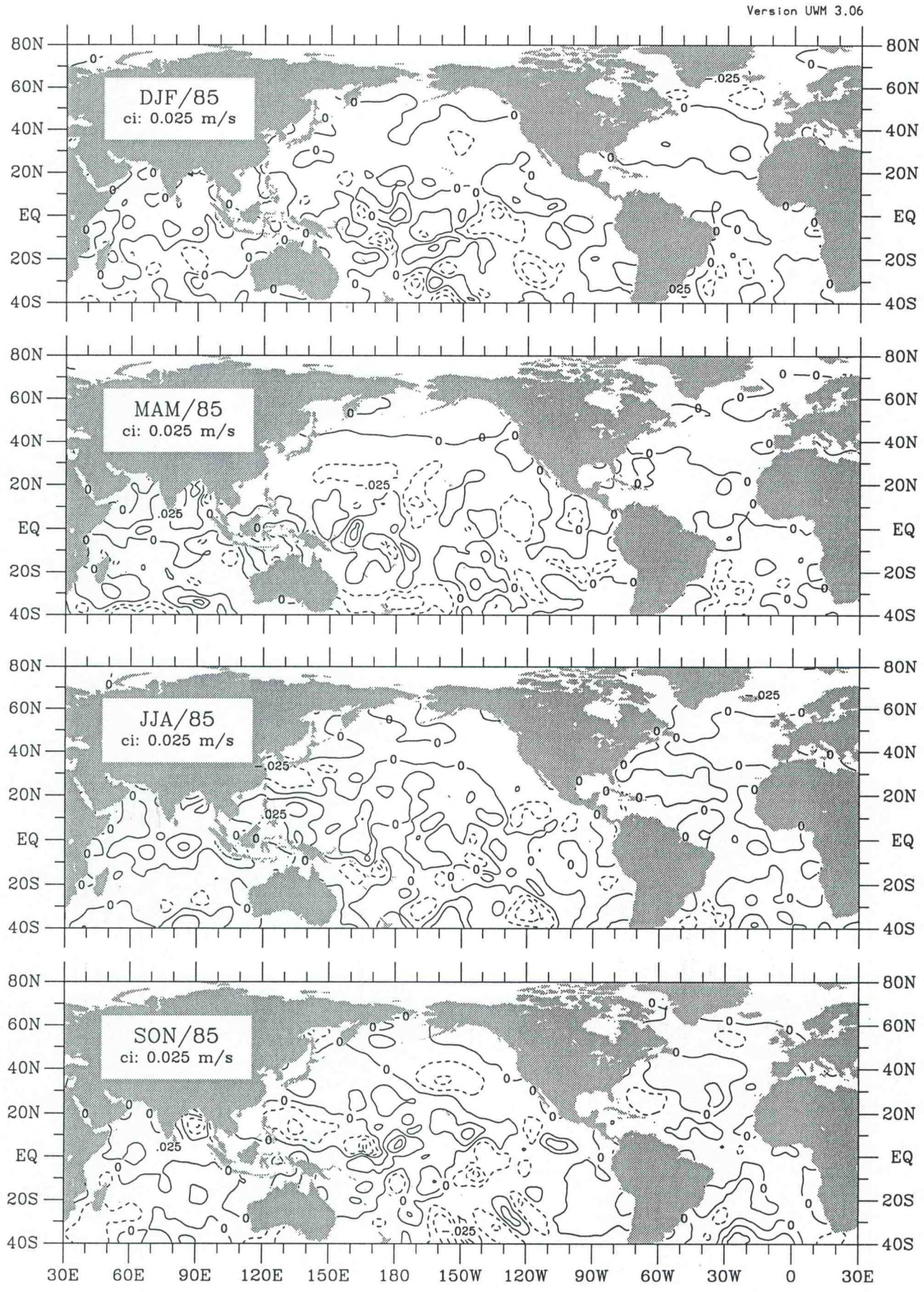

Figure uq-46. Zonal moisture flux seasonal anomaly for 1985.

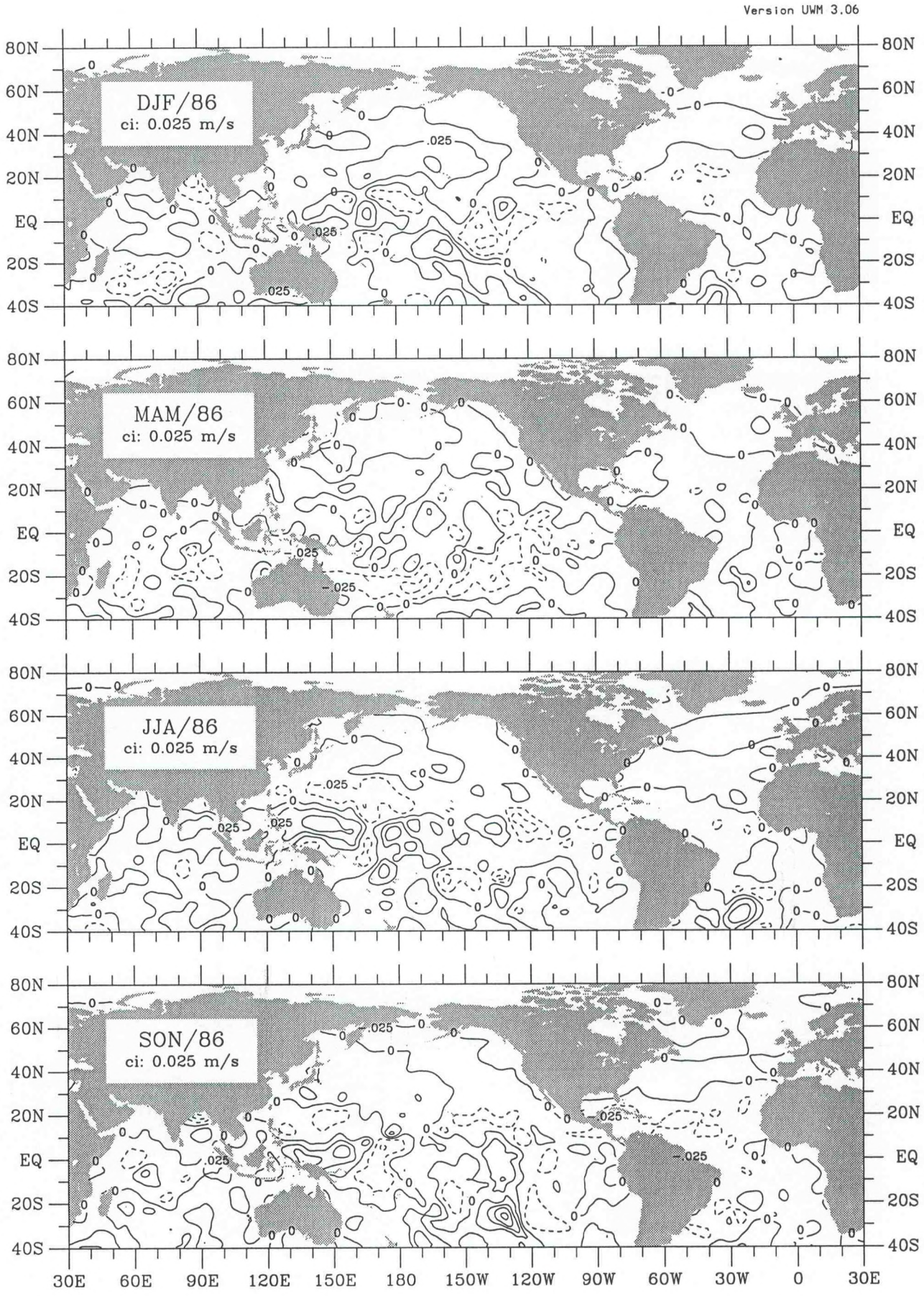

Figure uq-47. Zonal moisture flux seasonal anomaly for 1986.

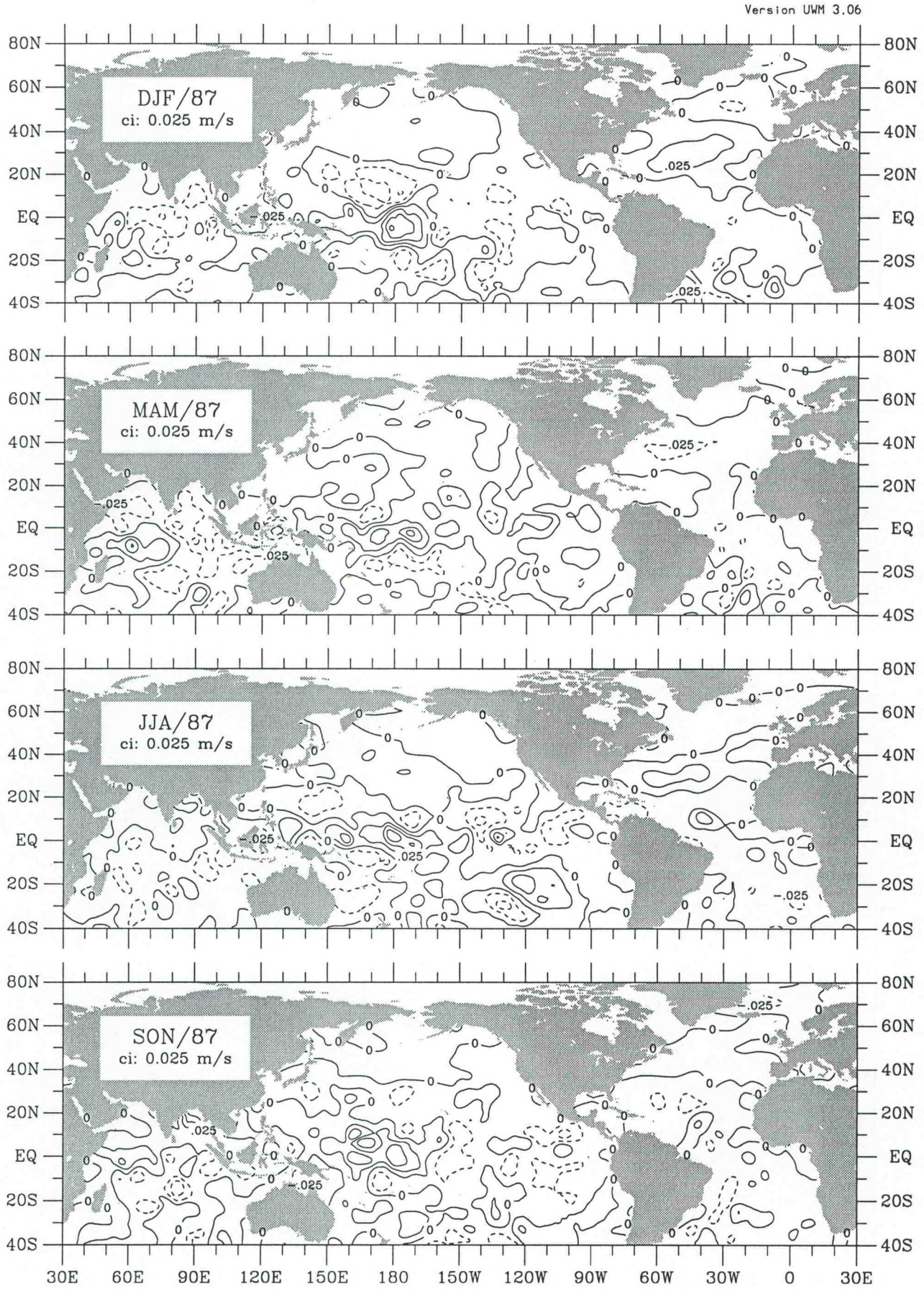

Figure uq-48. Zonal moisture flux seasonal anomaly for 1987.

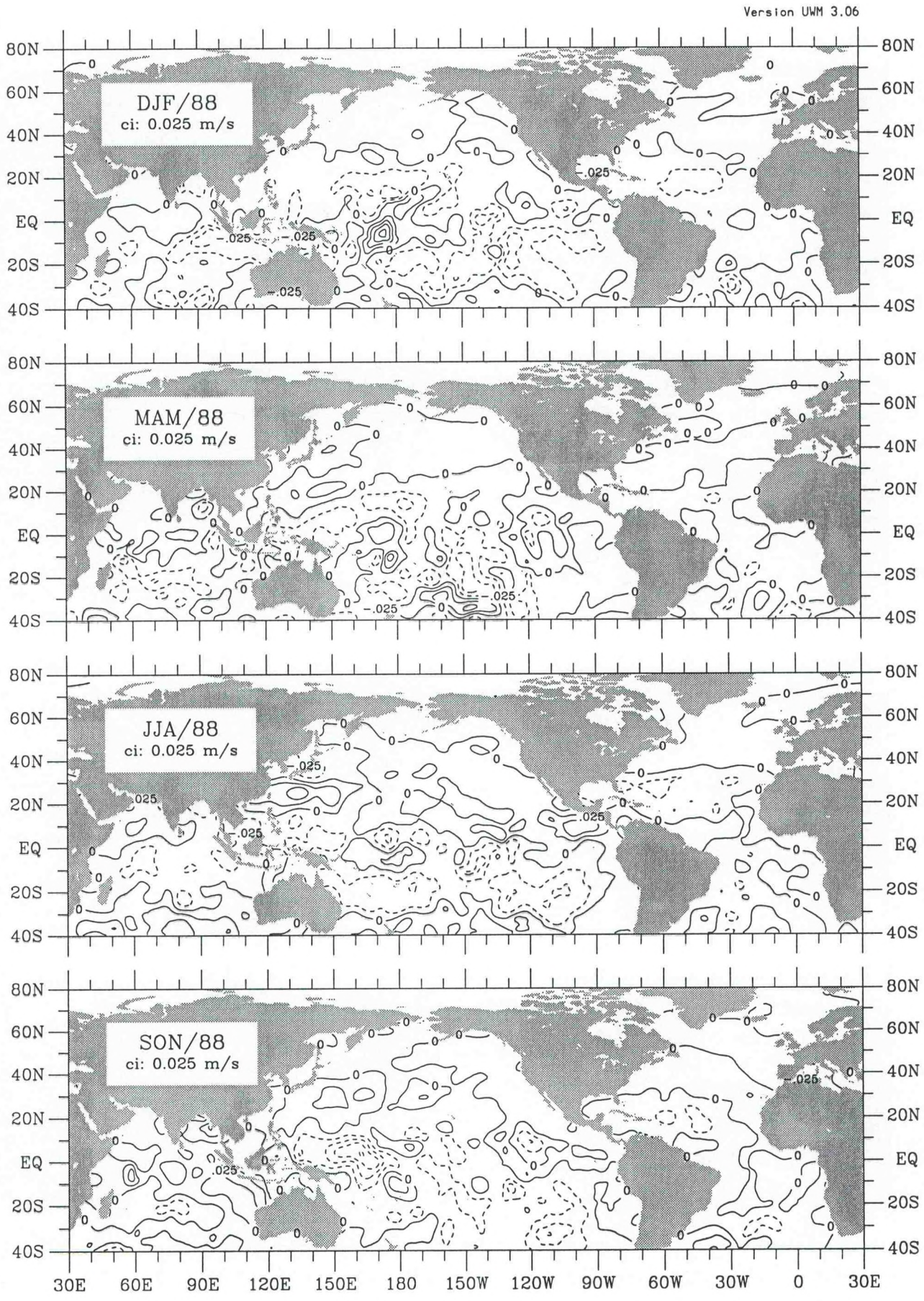

Figure uq-49. Zonal moisture flux seasonal anomaly for 1988.

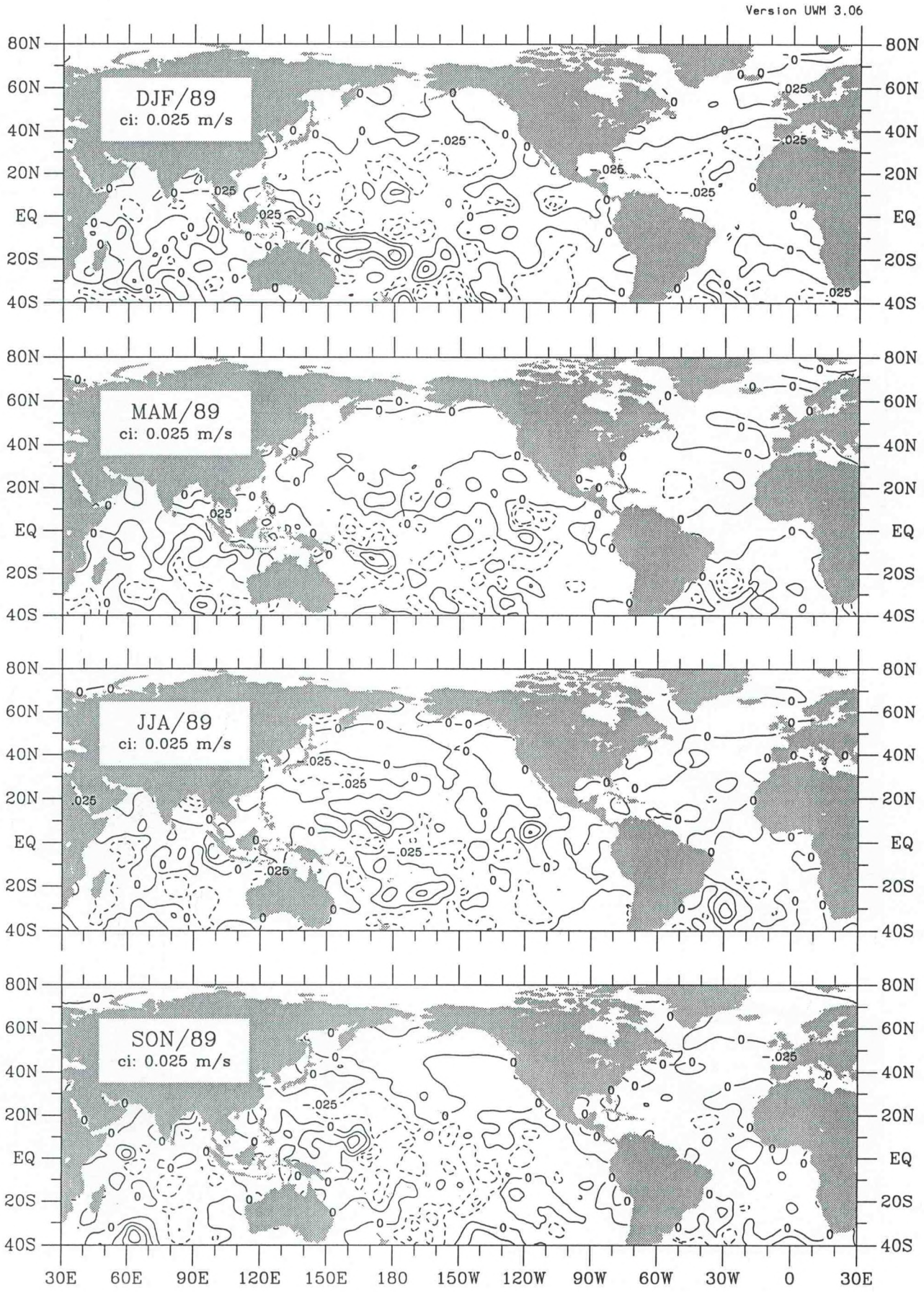

Figure uq-50. Zonal moisture flux seasonal anomaly for 1989.

16 Meridional moisture flux

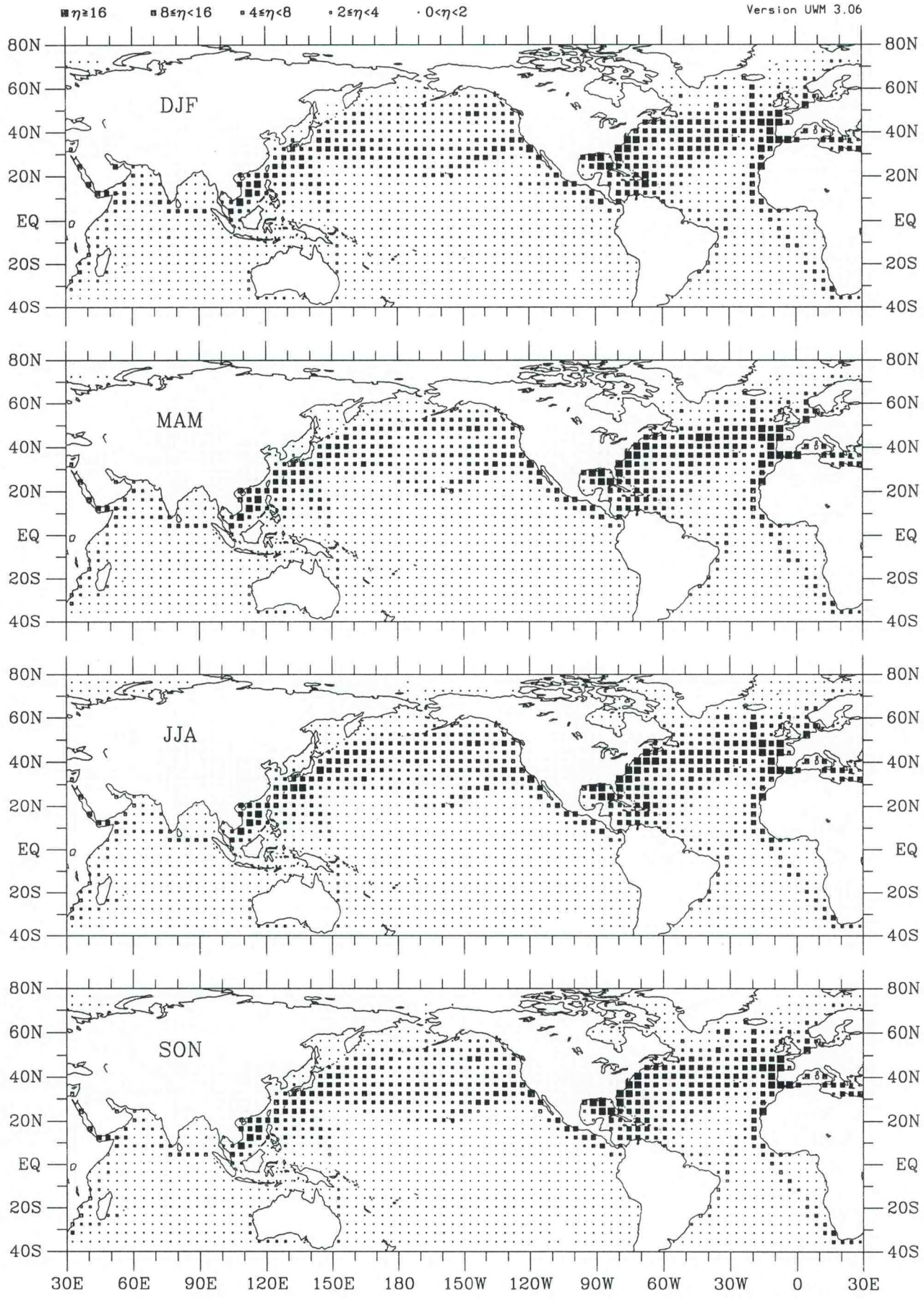

Figure vq-1. Merid. moisture flux seasonal observation density (1945-89).

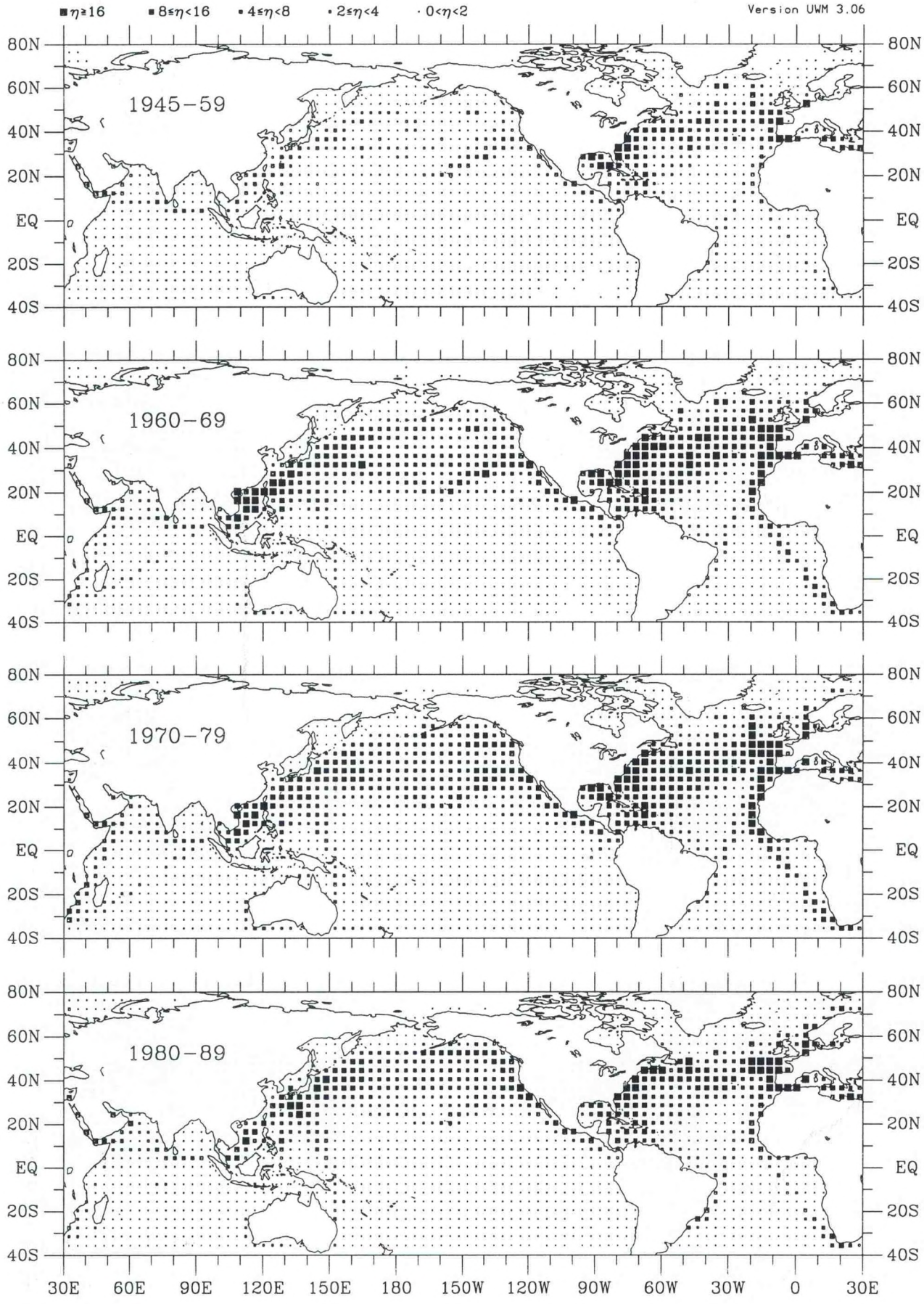

Figure vq-2. Merid. moisture flux decadal observation density.

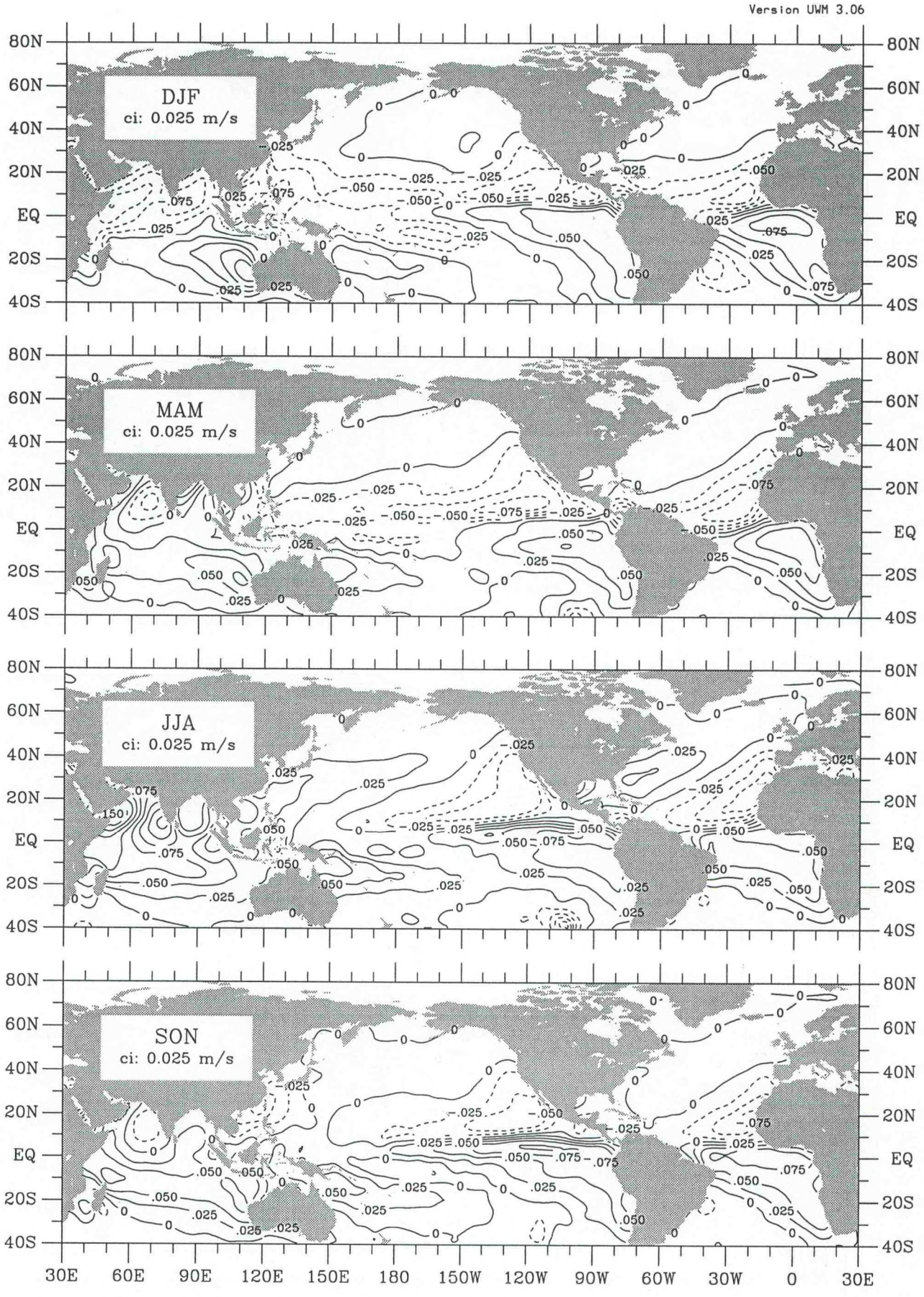

Figure vq-3. Merid. moisture flux seasonal climatology (1945-89).

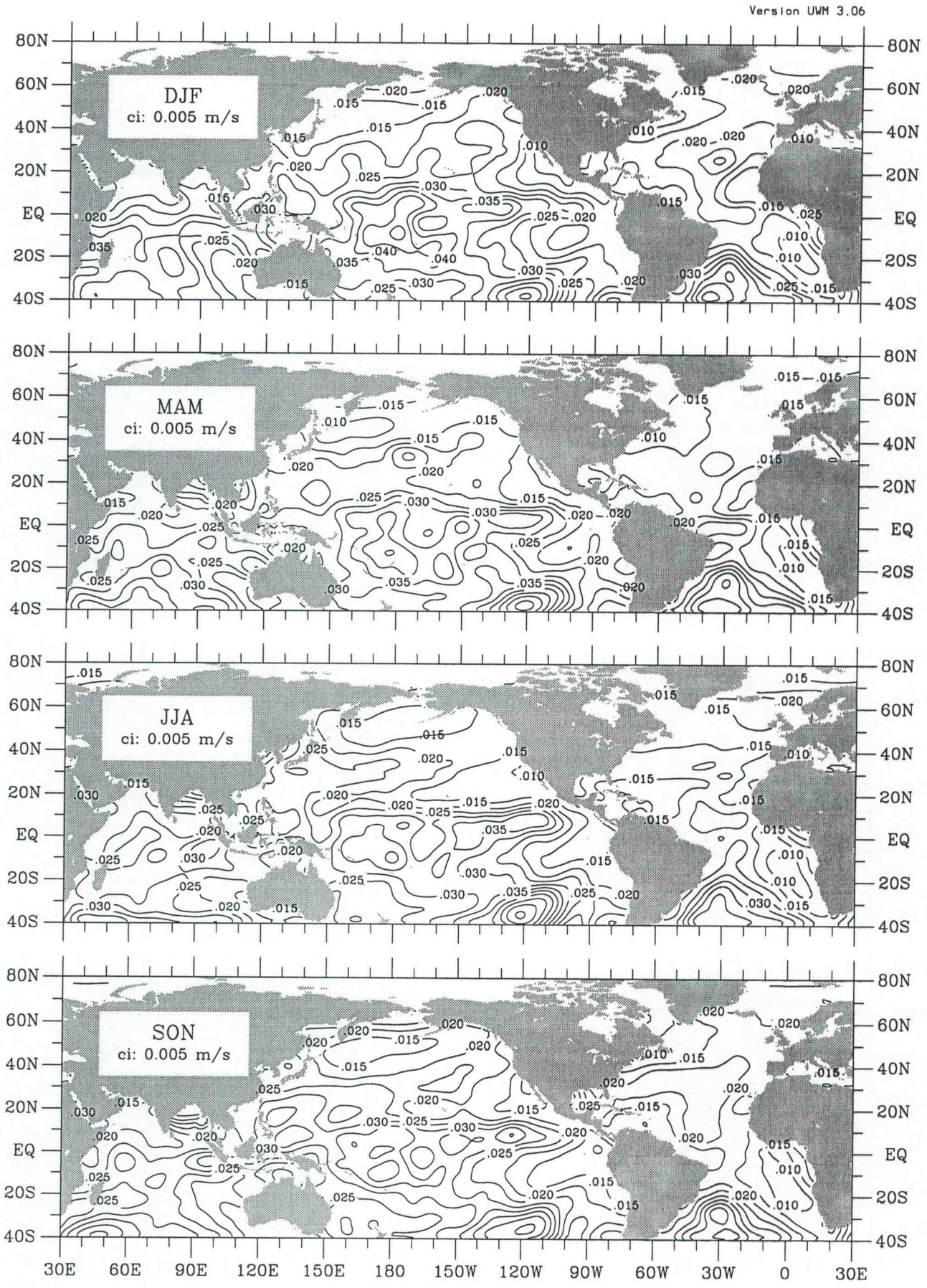

Figure vq-4. Merid. moisture flux seasonal interannual std dev (1945-89).

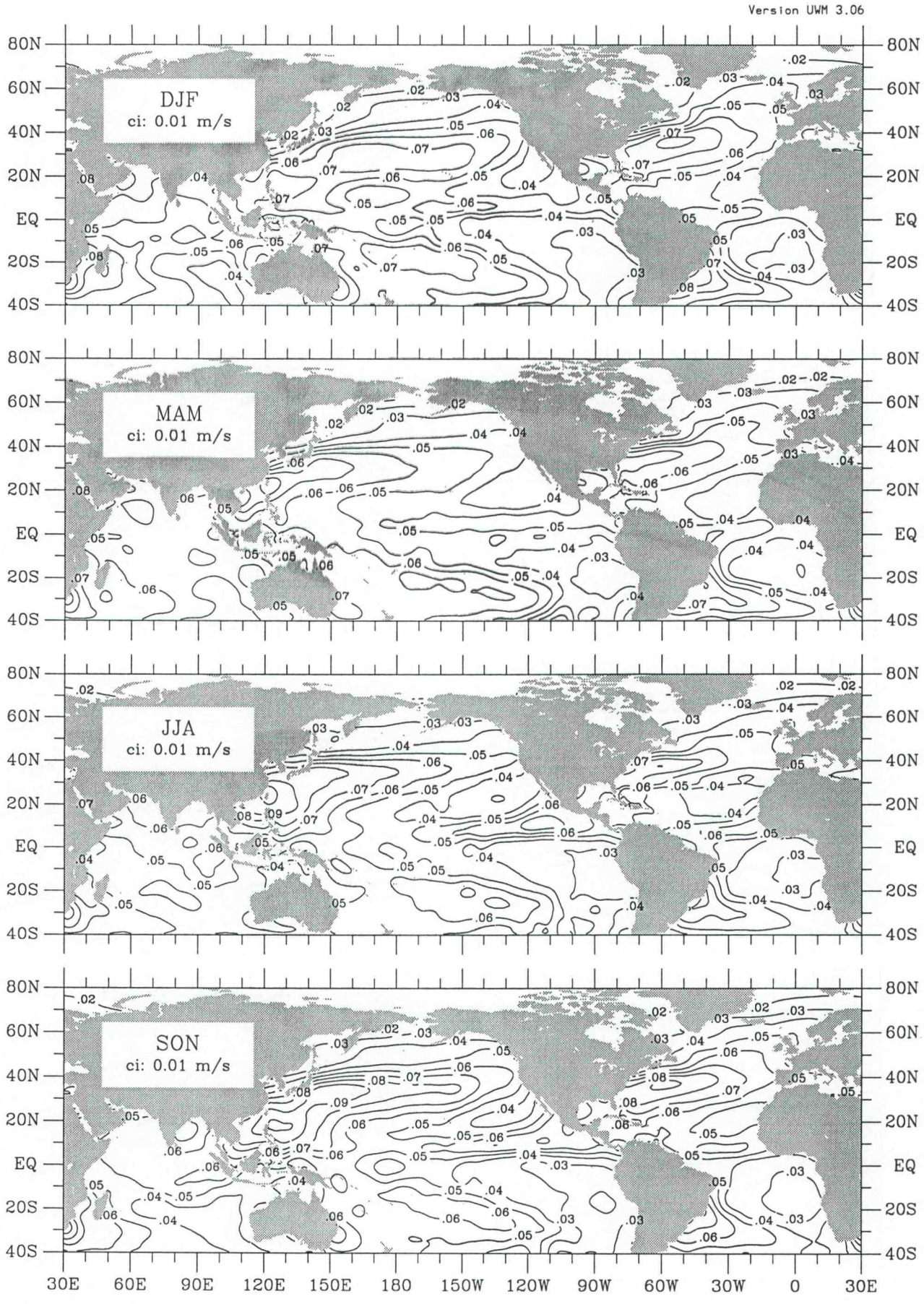

Figure vq-5. Merid. moisture flux seasonal standard deviation (1945-89).

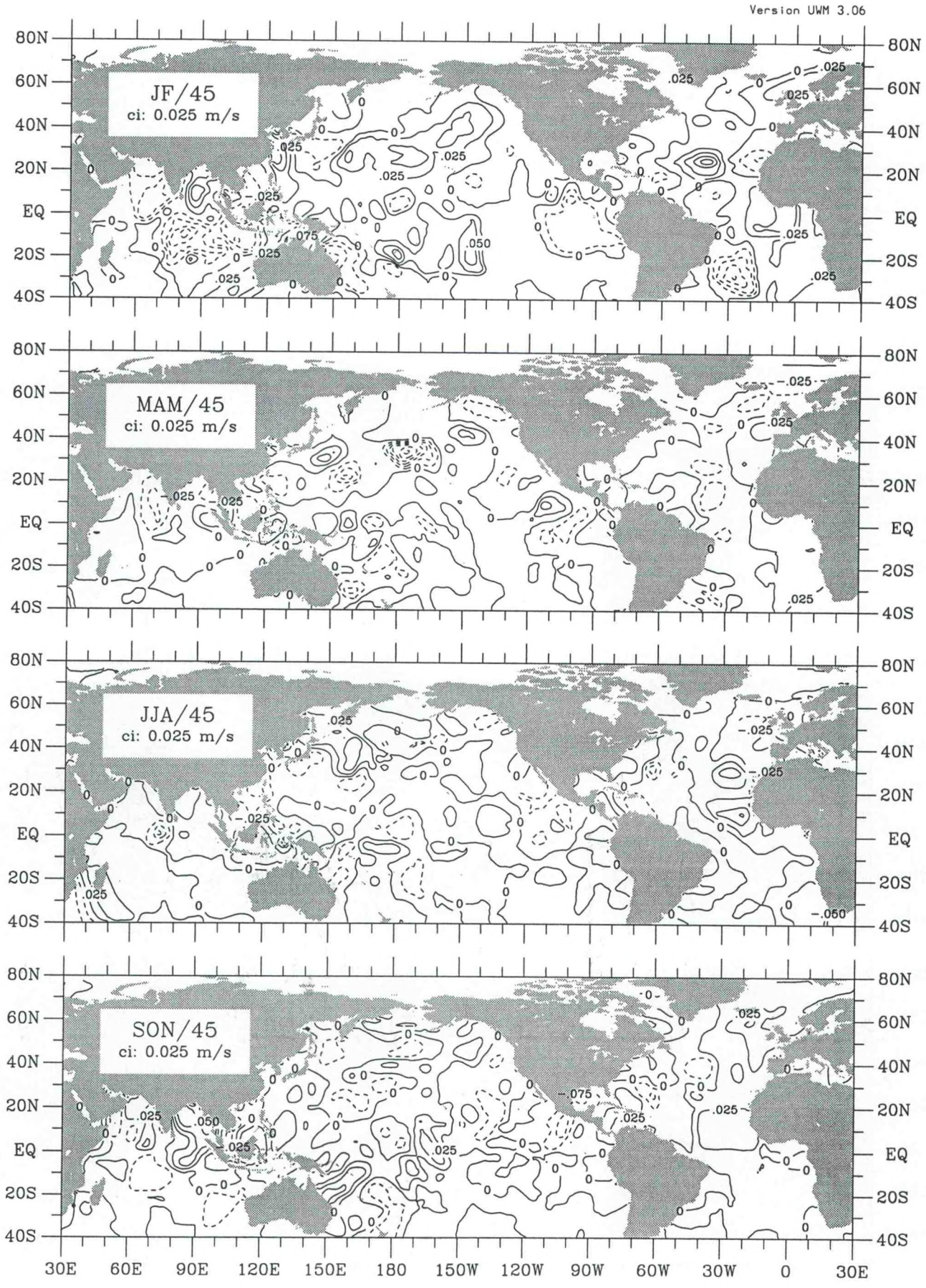

Figure vq-6. Merid. moisture flux seasonal anomaly for 1945.

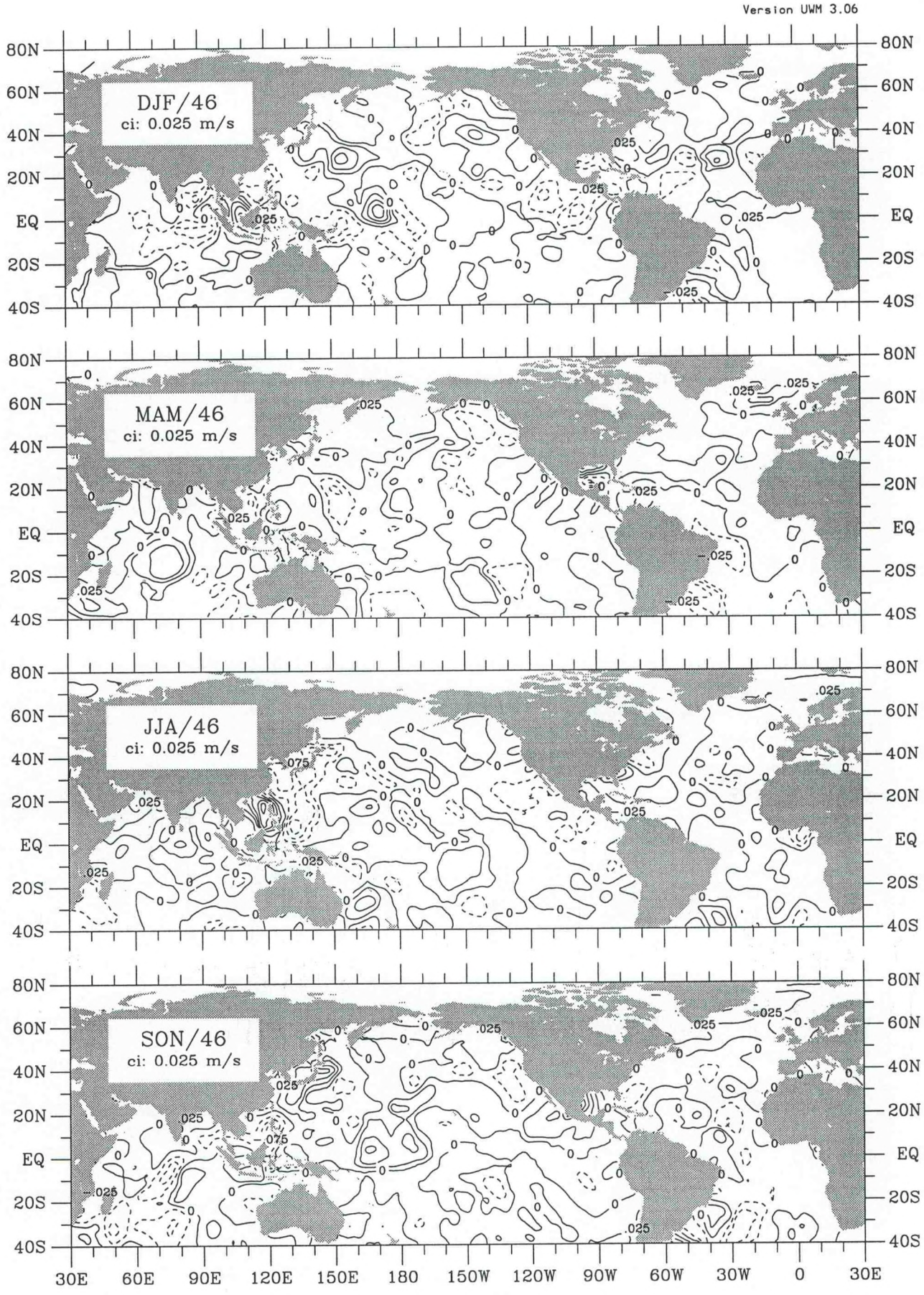

Figure vq-7. Merid. moisture flux seasonal anomaly for 1946.

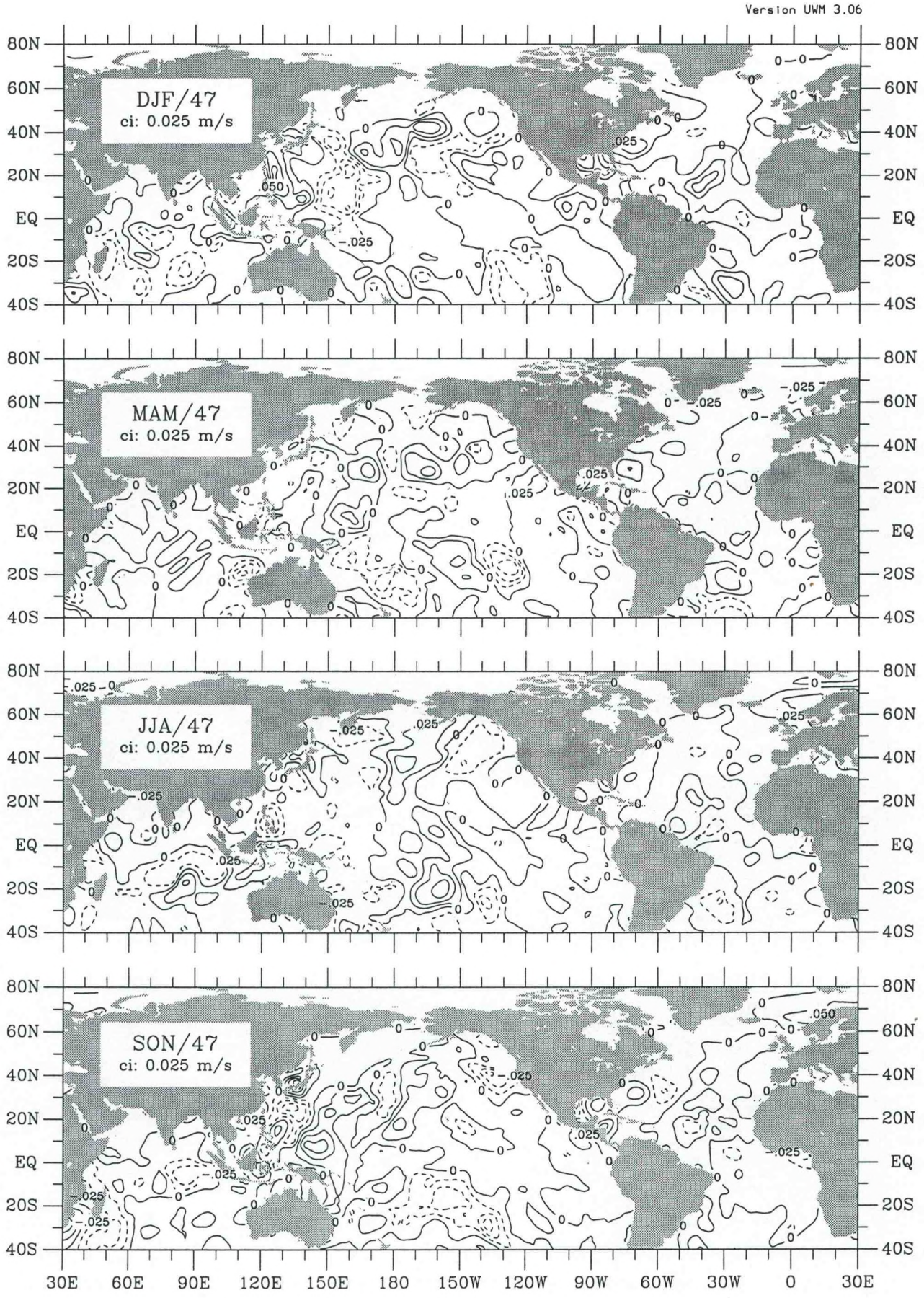

Figure vq-8. Merid. moisture flux seasonal anomaly for 1947.

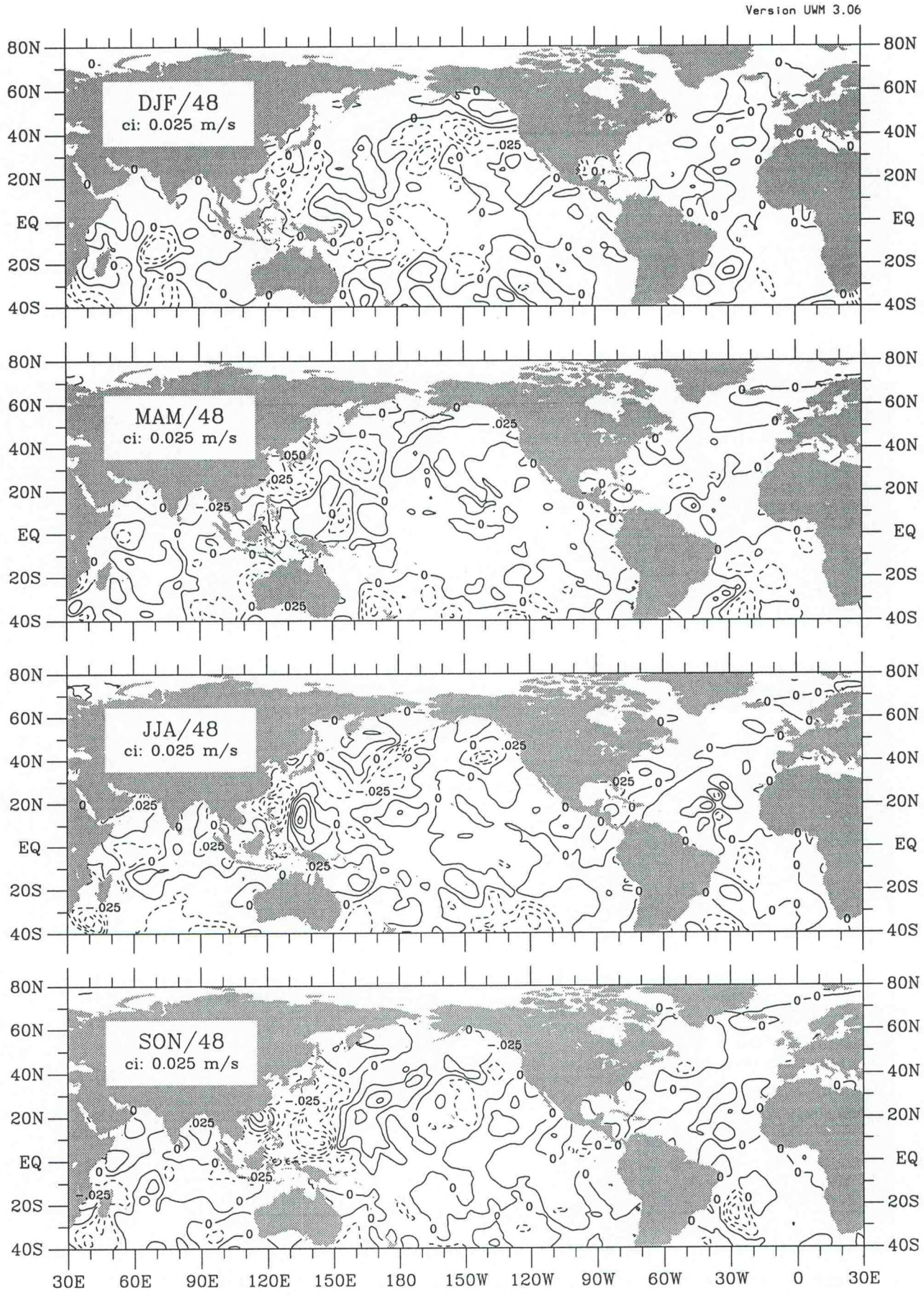

Figure vq-9. Merid. moisture flux seasonal anomaly for 1948.

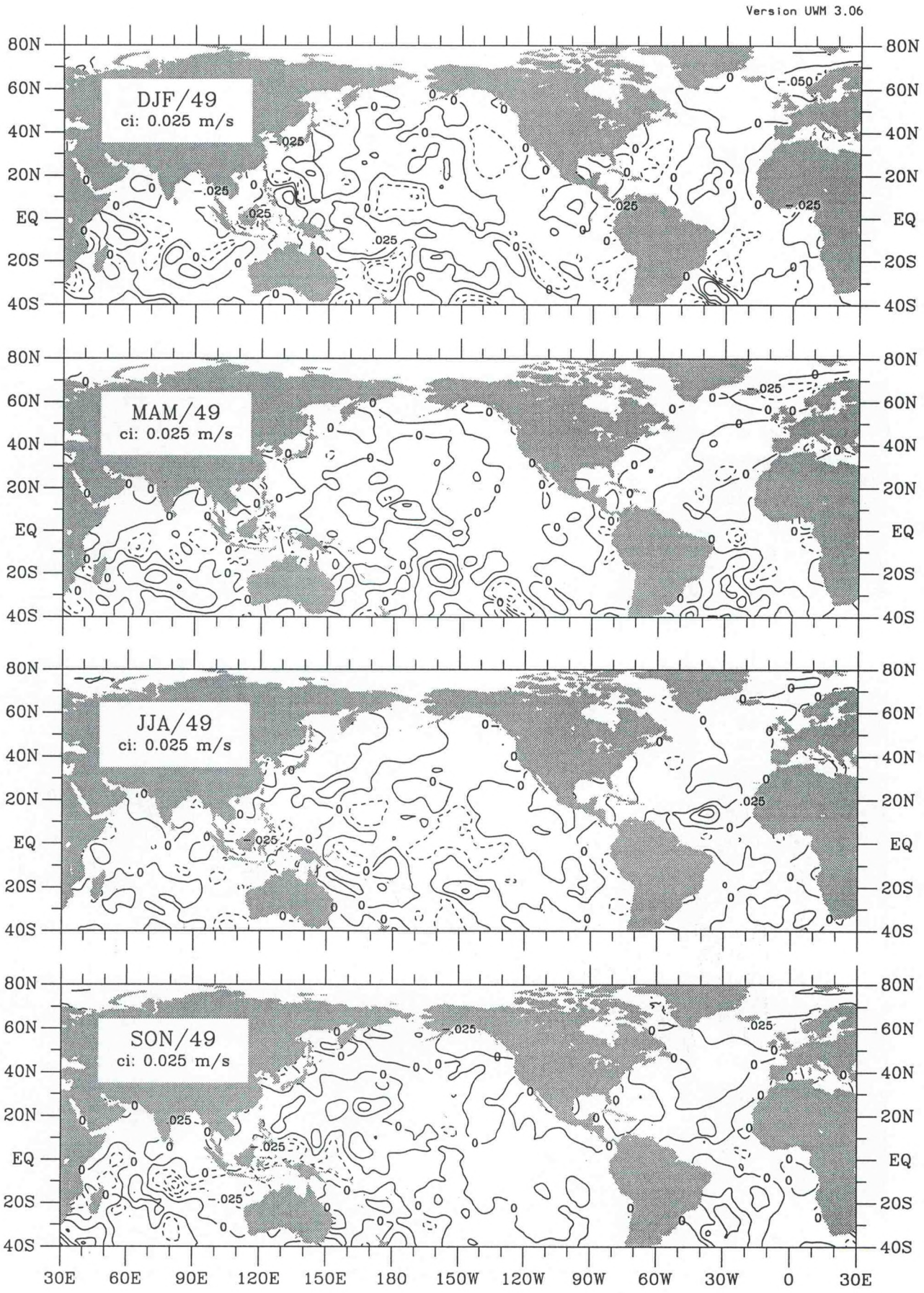

Figure vq-10. Merid. moisture flux seasonal anomaly for 1949.

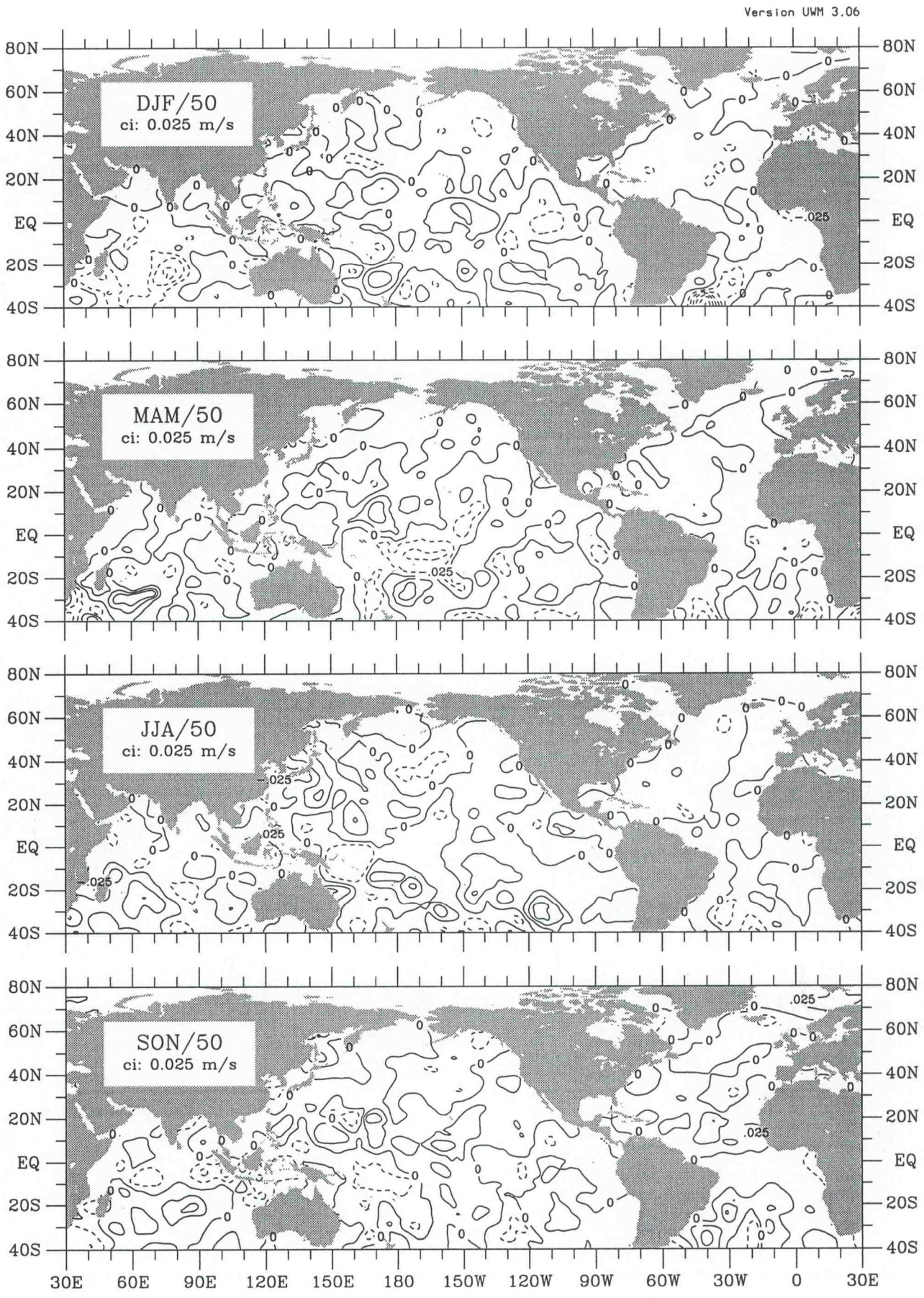

Figure vq-11. Merid. moisture flux seasonal anomaly for 1950.

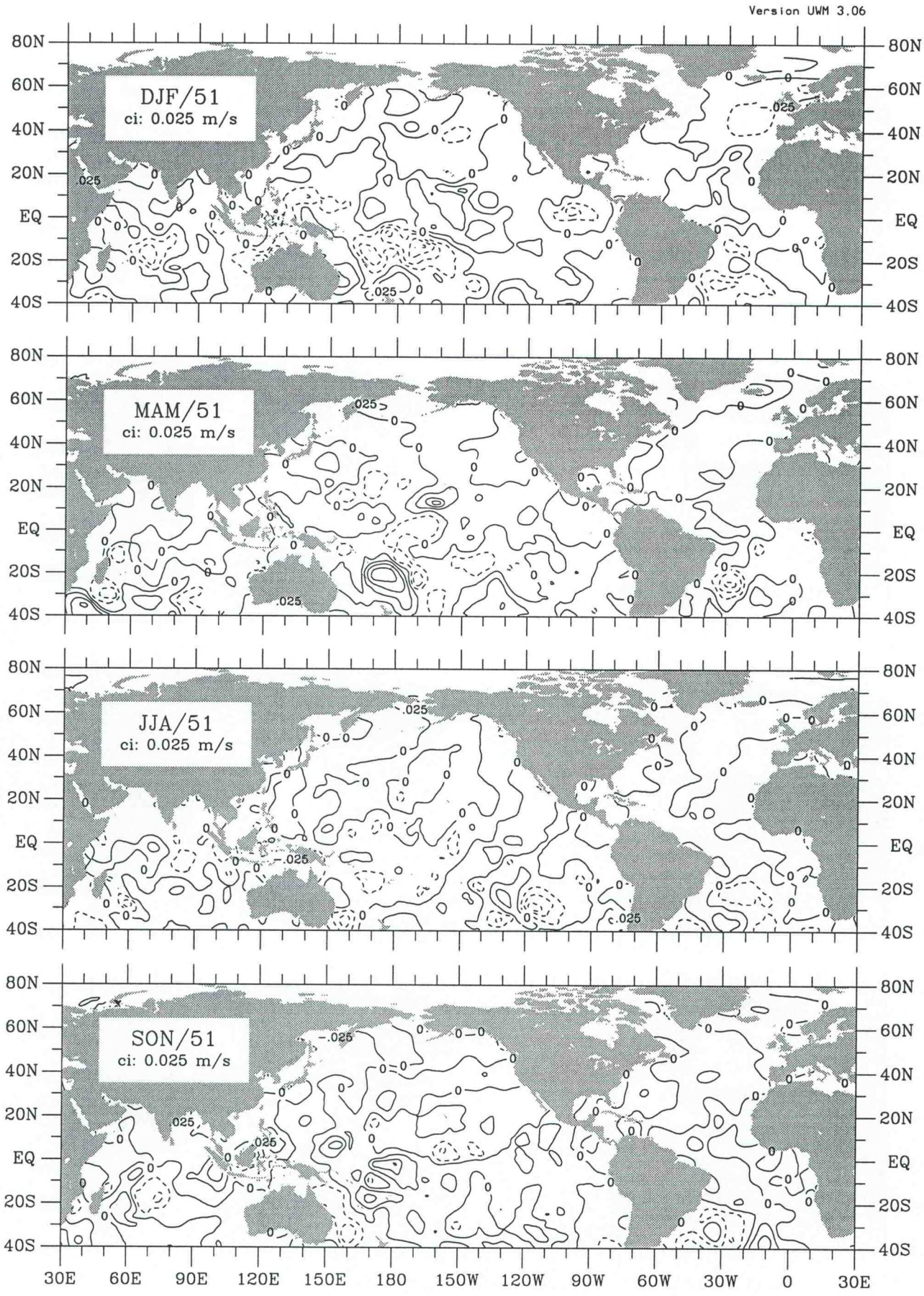

Figure vq-12. Merid. moisture flux seasonal anomaly for 1951.

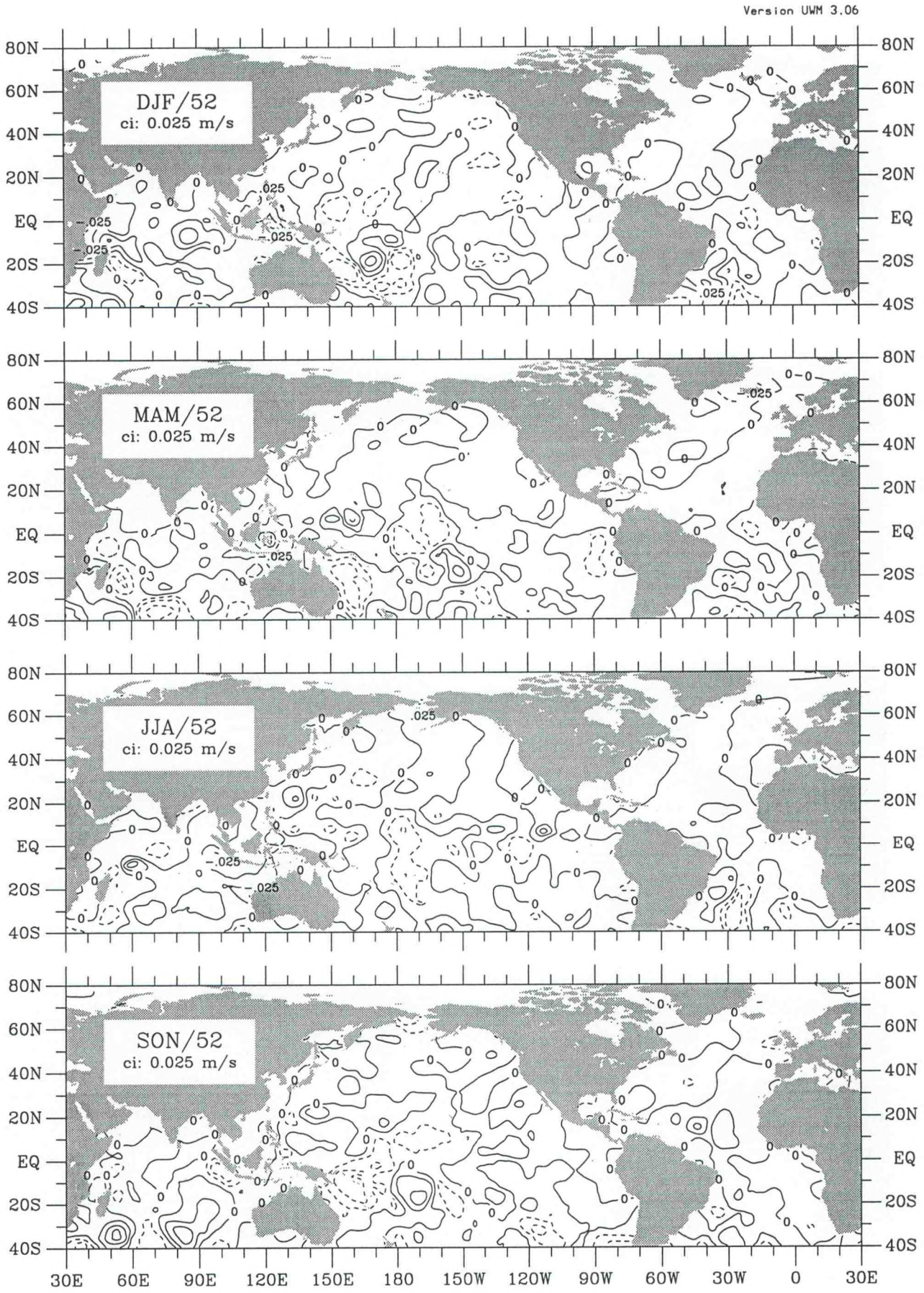

Figure vq-13. Merid. moisture flux seasonal anomaly for 1952.

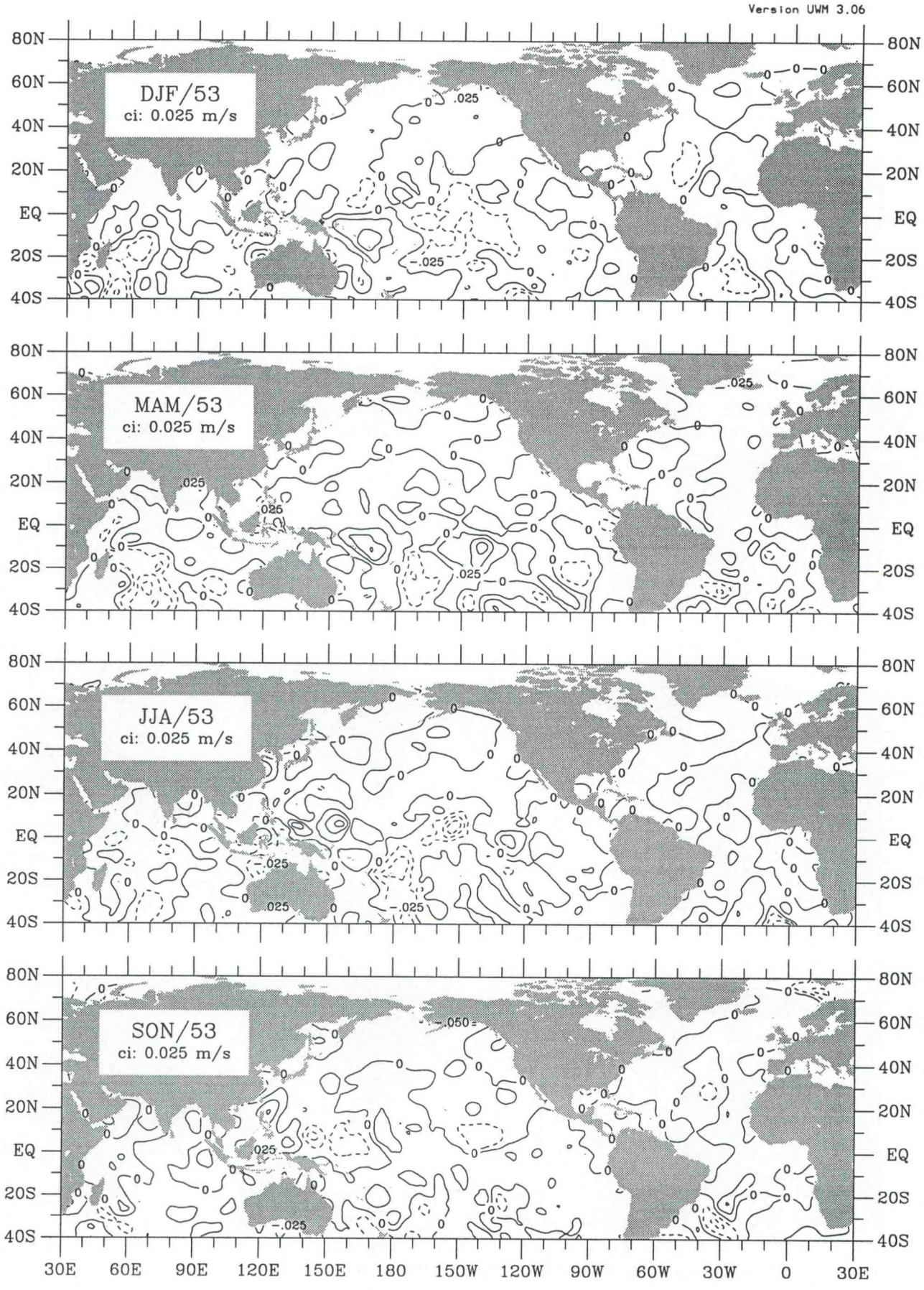

Figure vq-14. Merid. moisture flux seasonal anomaly for 1953.

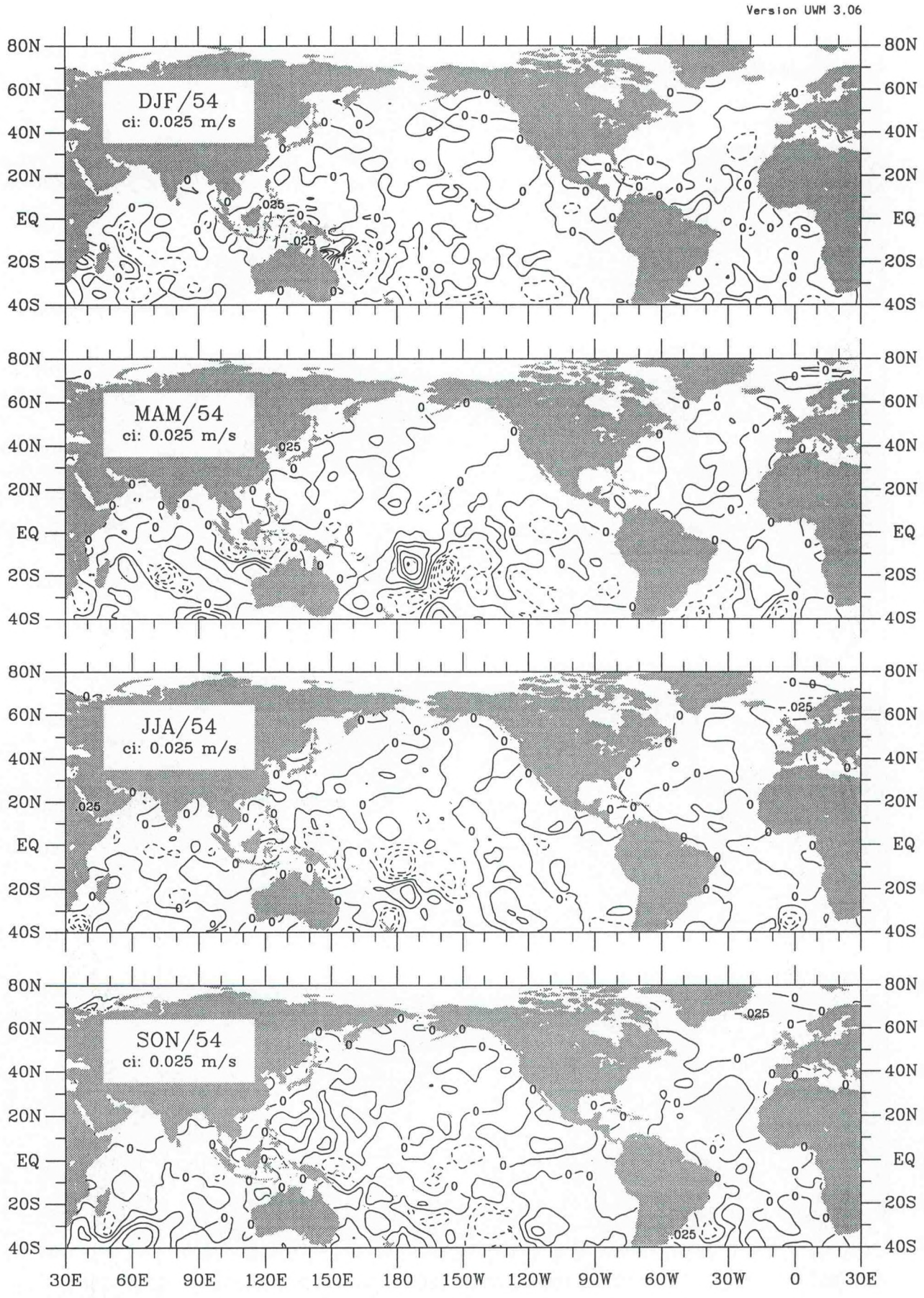

Figure vq-15. Merid. moisture flux seasonal anomaly for 1954.

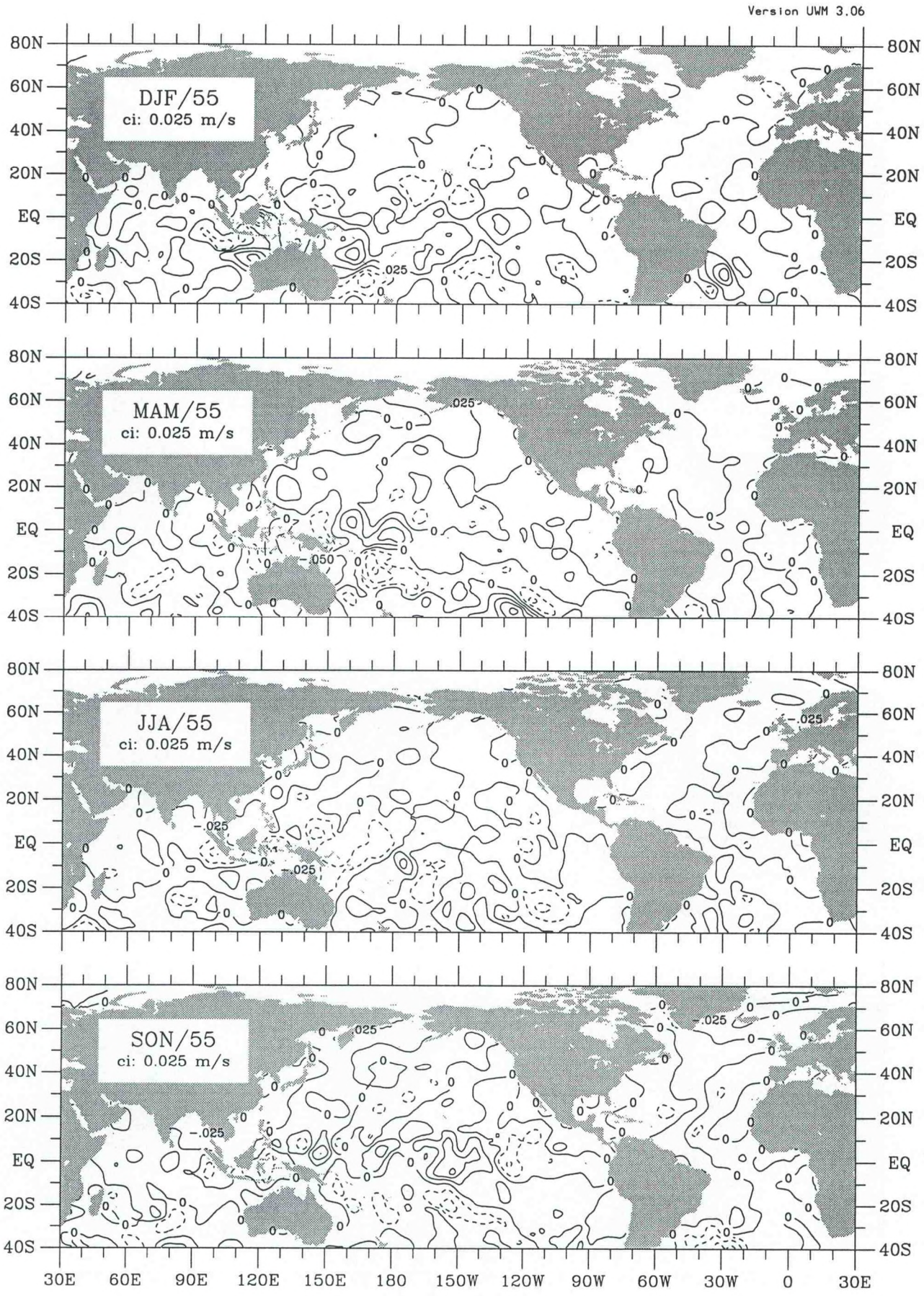

Figure vq-16. Merid. moisture flux seasonal anomaly for 1955.

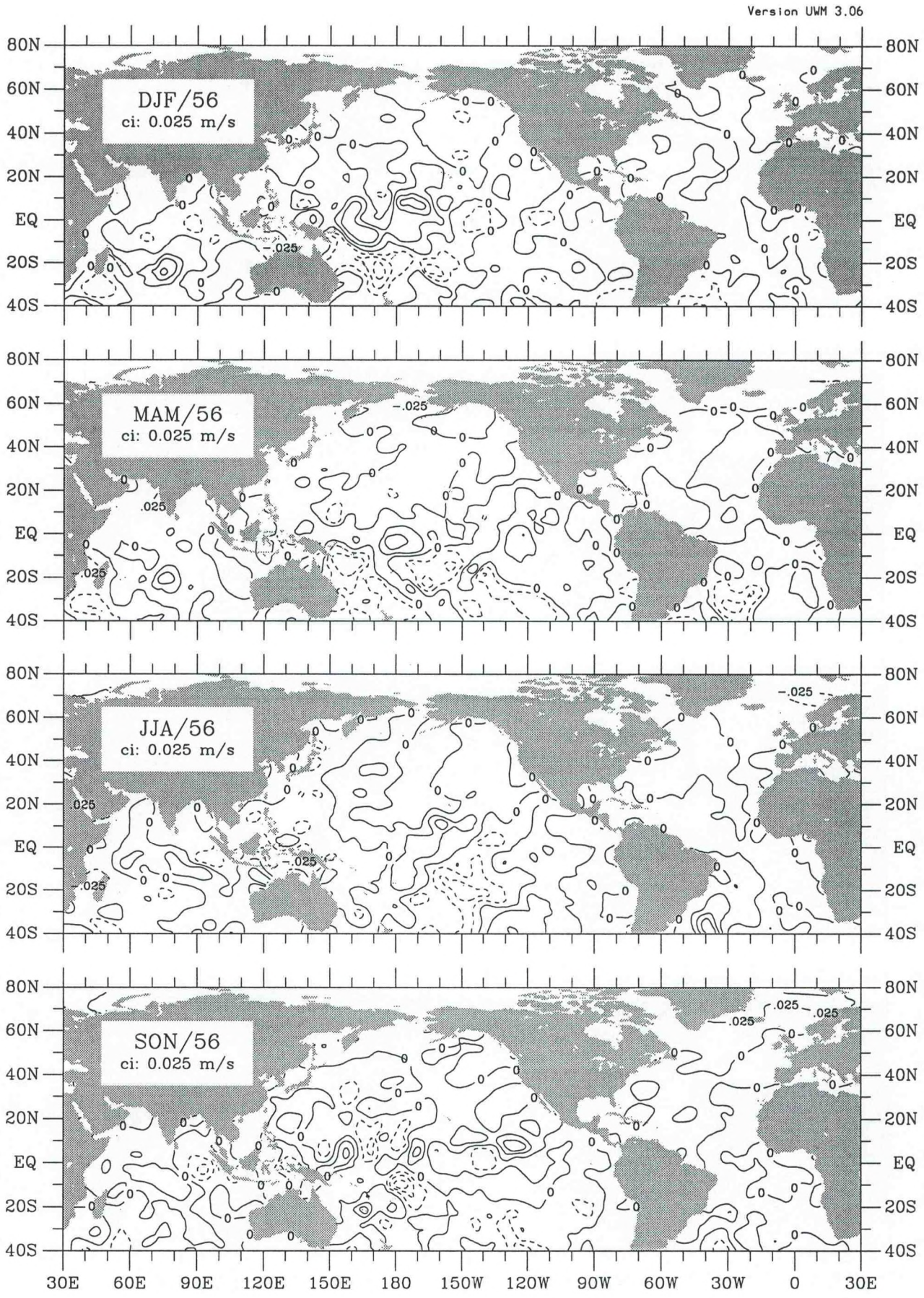

Figure vq-17. Merid. moisture flux seasonal anomaly for 1956.

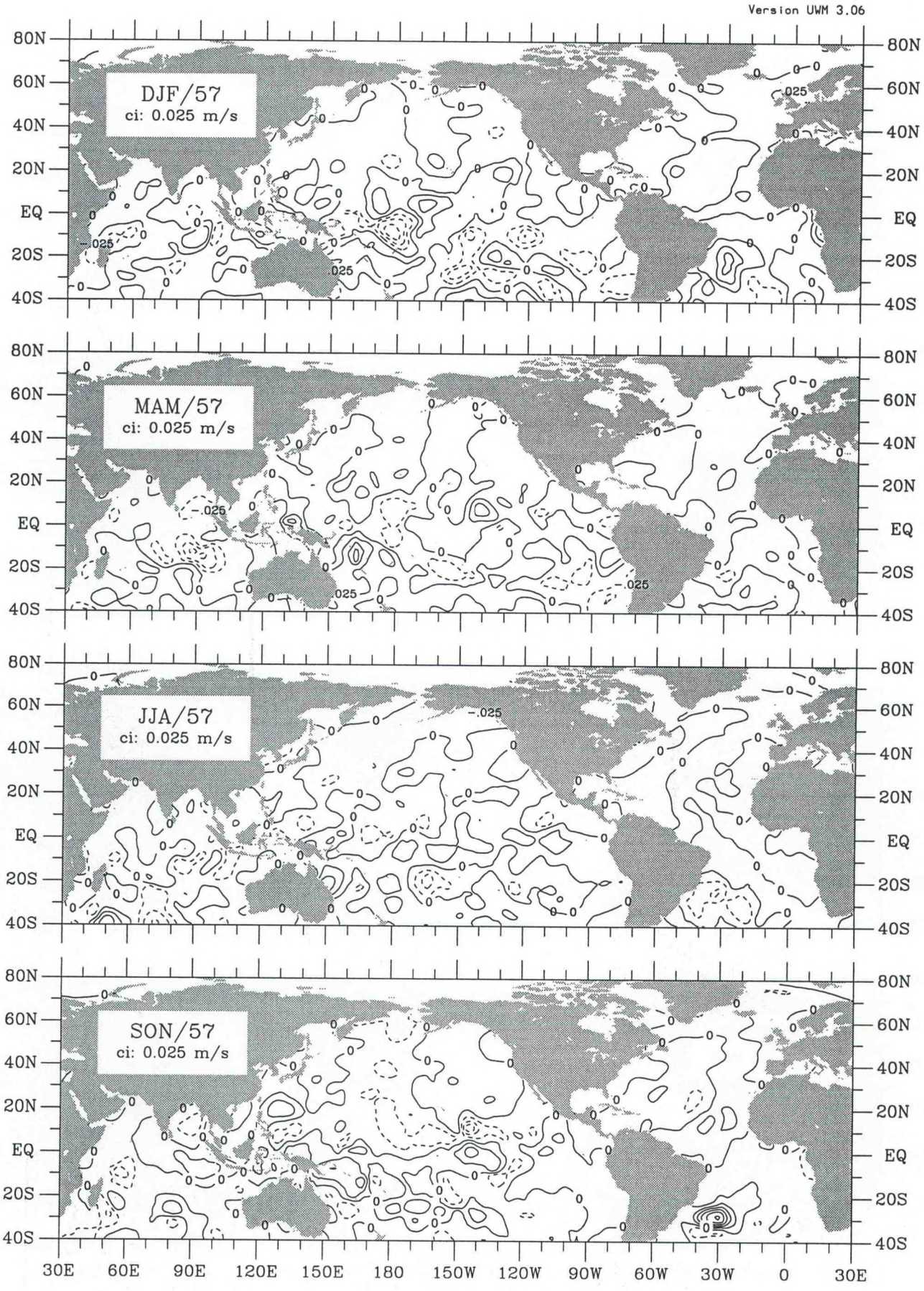

Figure vq-18. Merid. moisture flux seasonal anomaly for 1957.

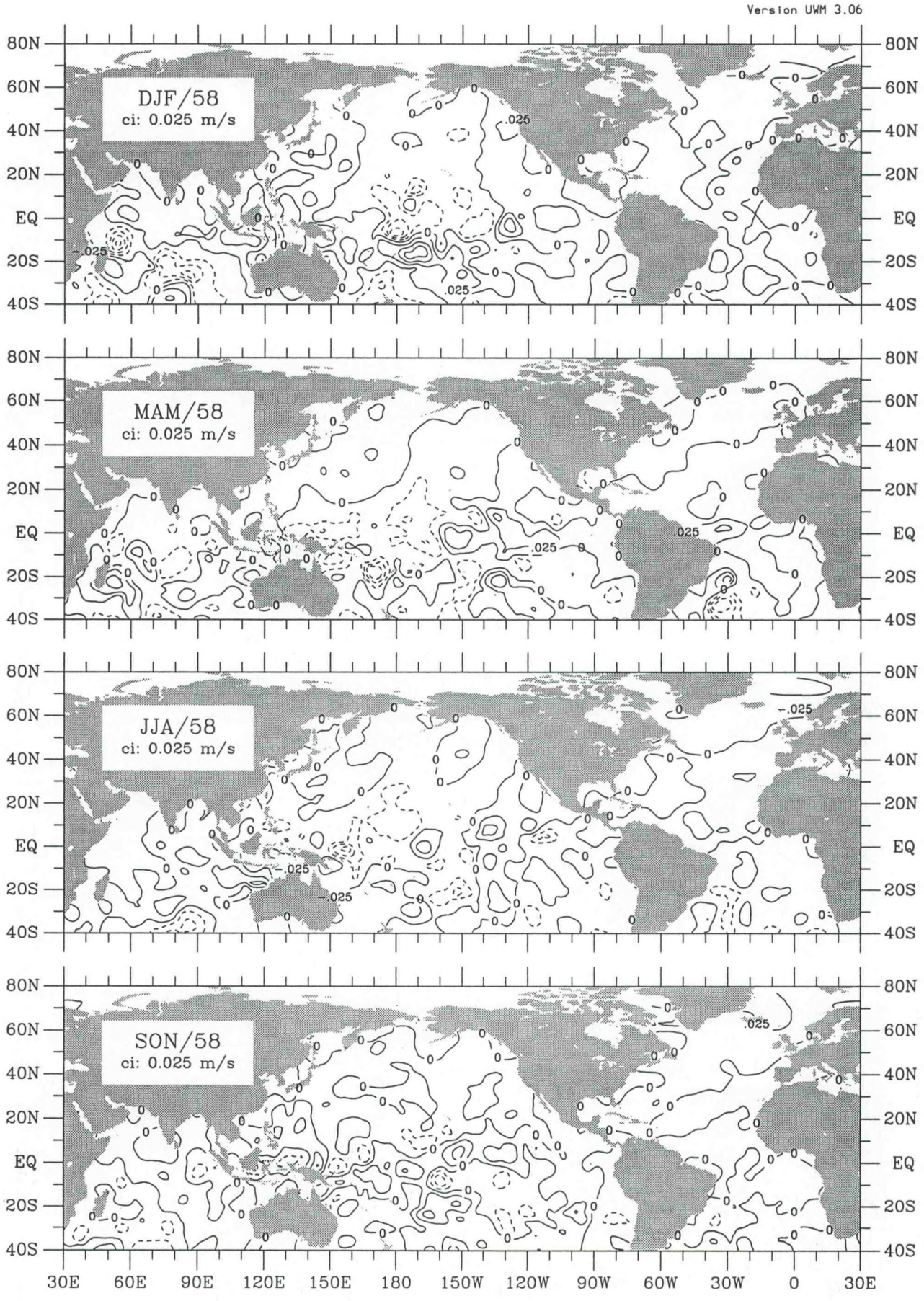

Figure vq-19. Merid. moisture flux seasonal anomaly for 1958.

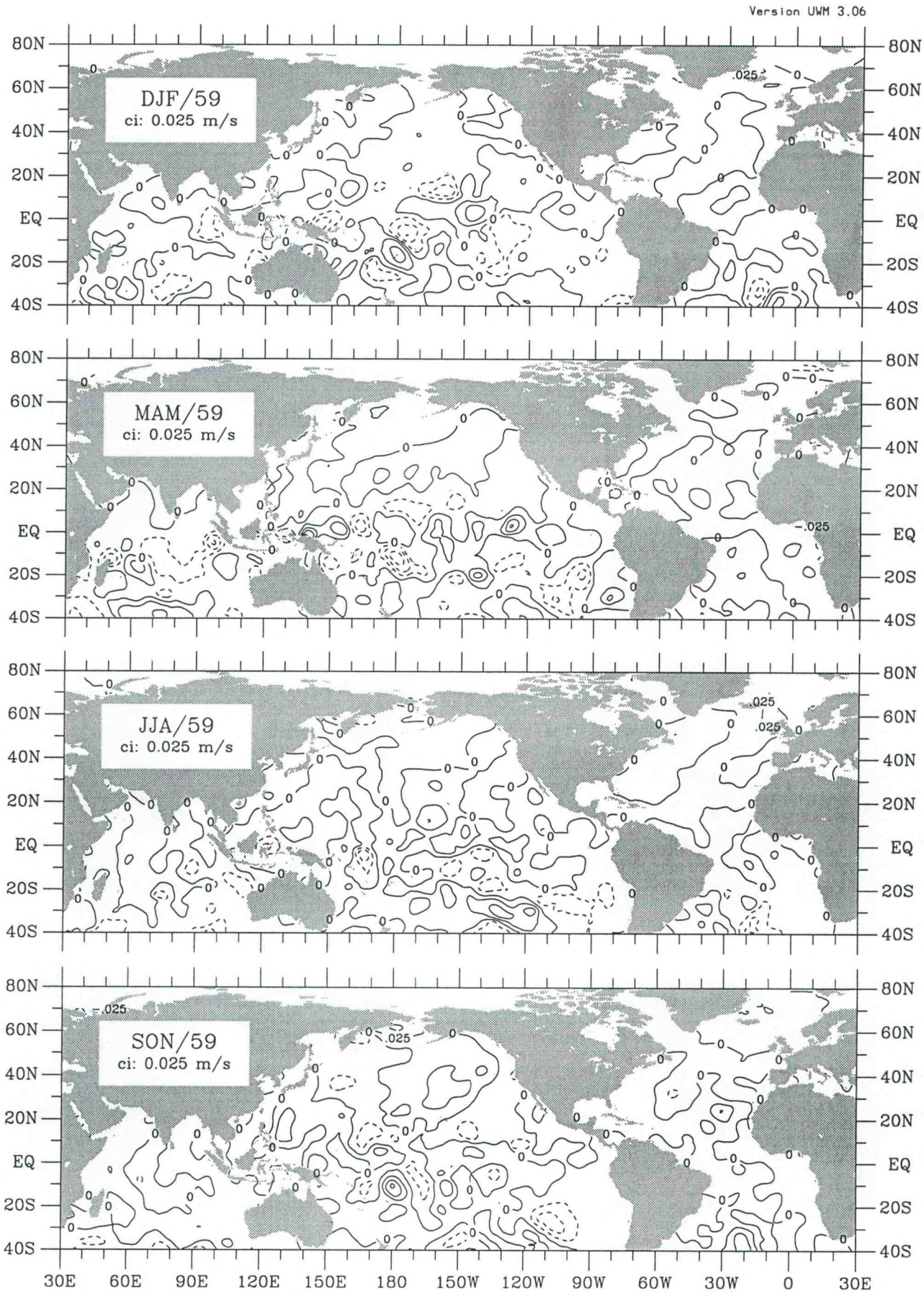

Figure vq-20. Merid. moisture flux seasonal anomaly for 1959.

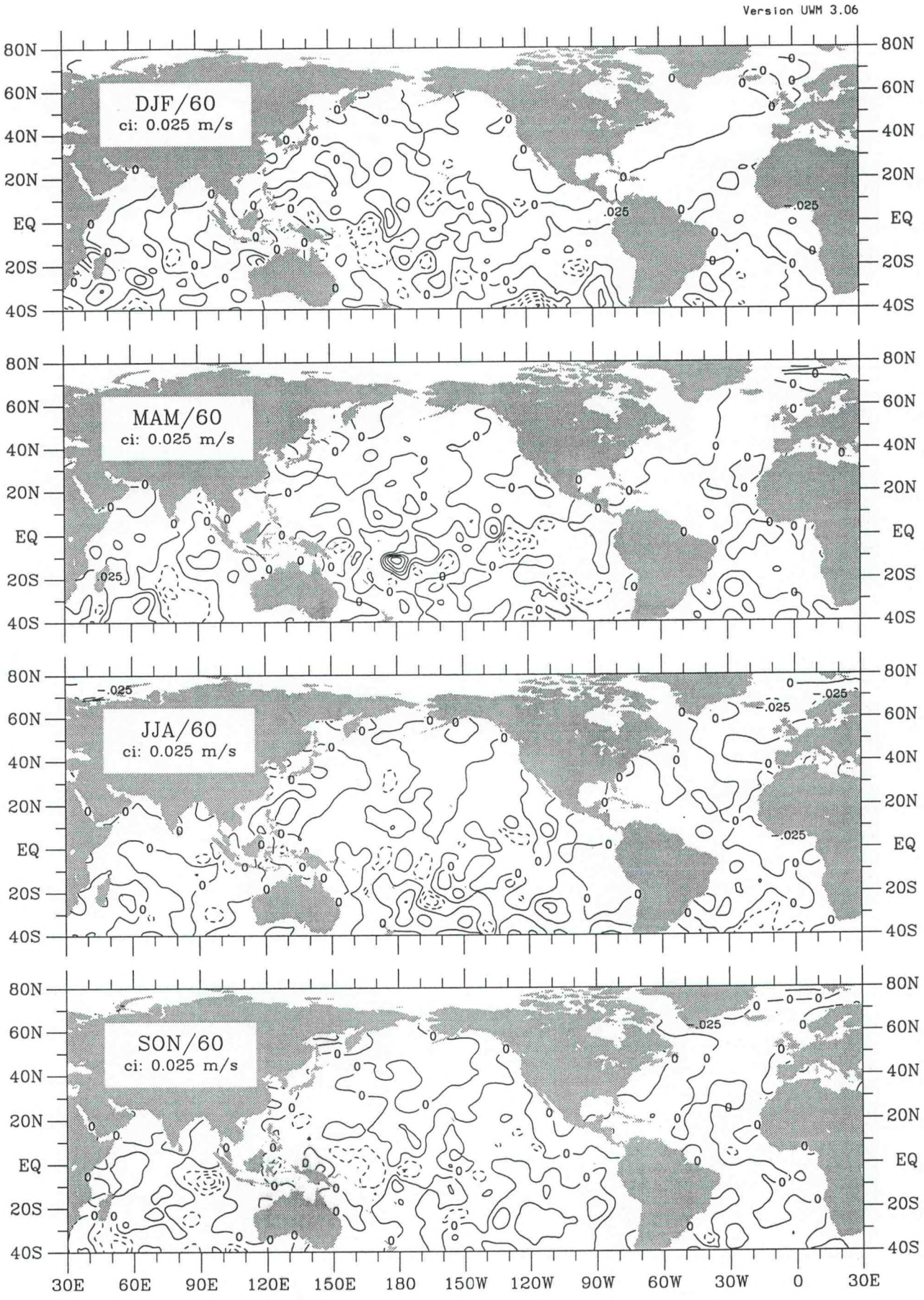

Figure vq-21. Merid. moisture flux seasonal anomaly for 1960.

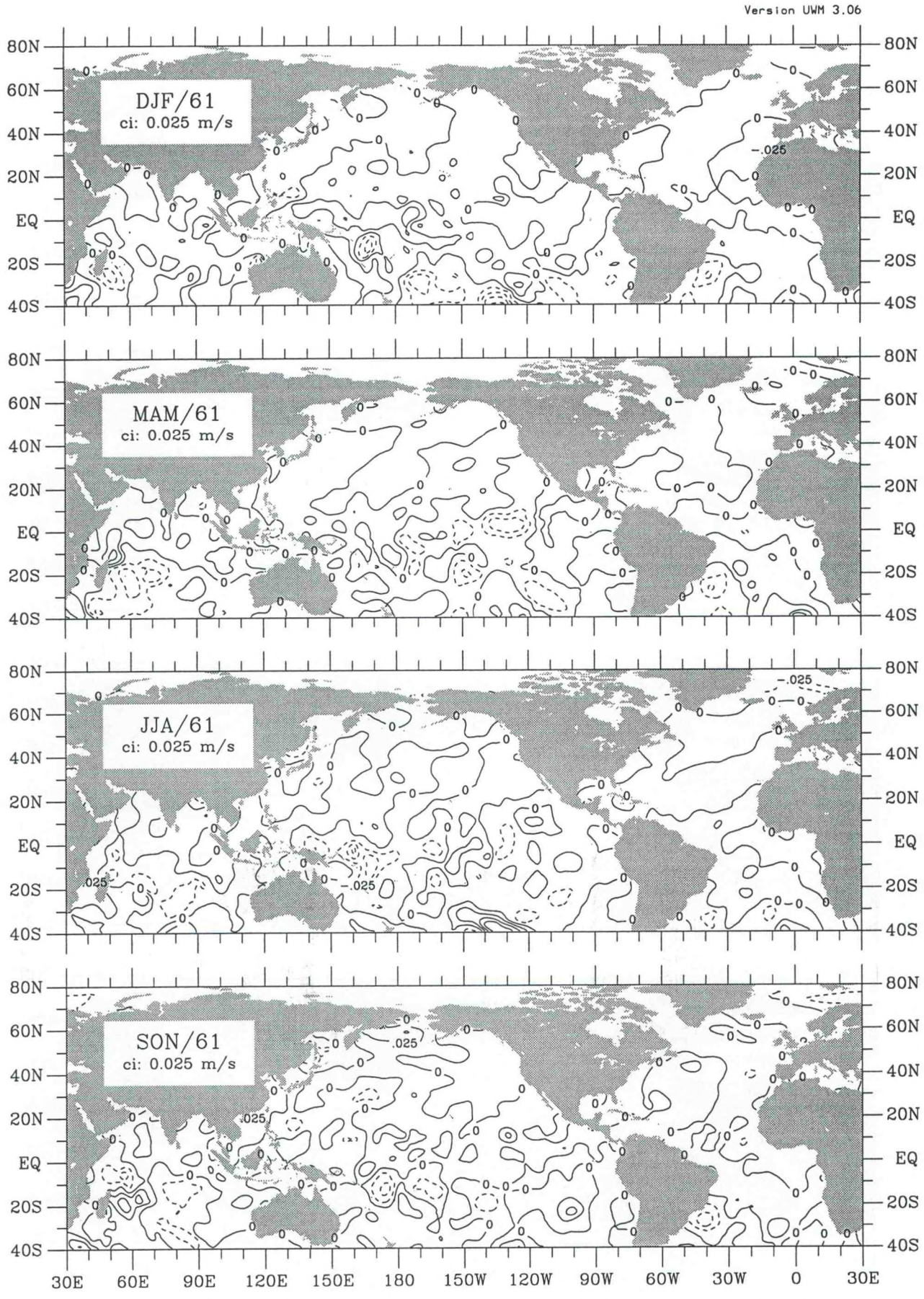

Figure vq-22. Merid. moisture flux seasonal anomaly for 1961.

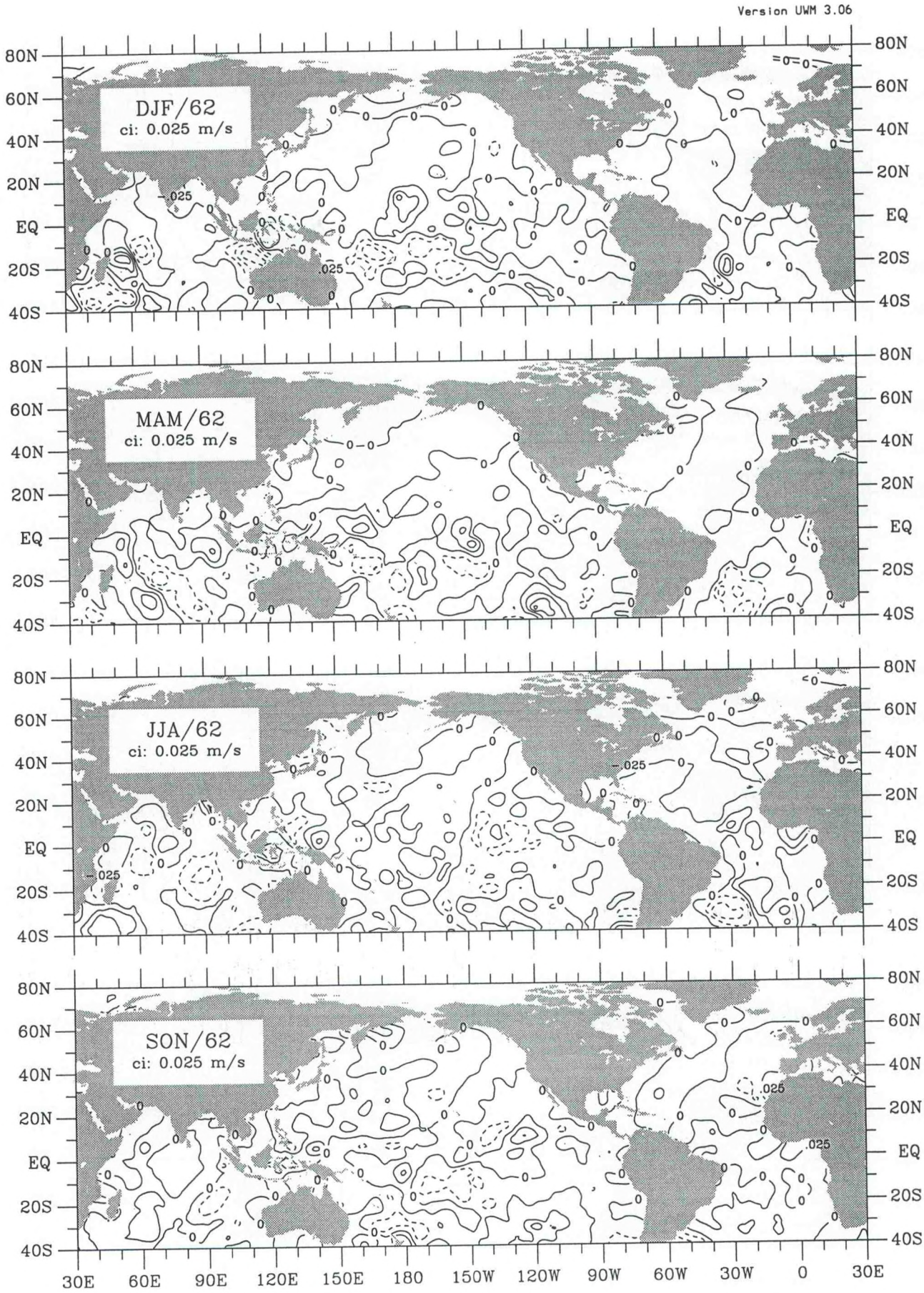

Figure vq-23. Merid. moisture flux seasonal anomaly for 1962.

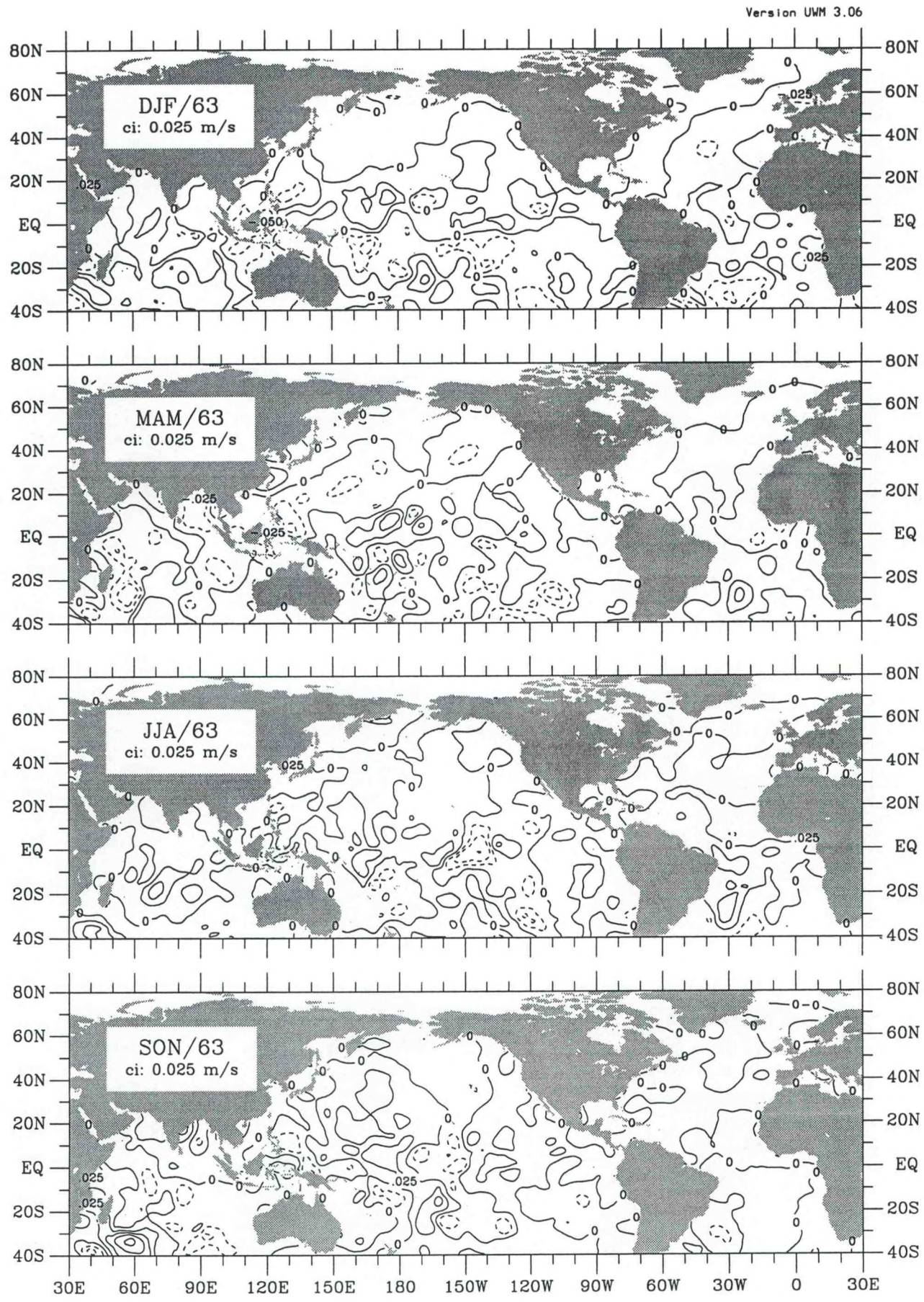

Figure vq-24. Merid. moisture flux seasonal anomaly for 1963.

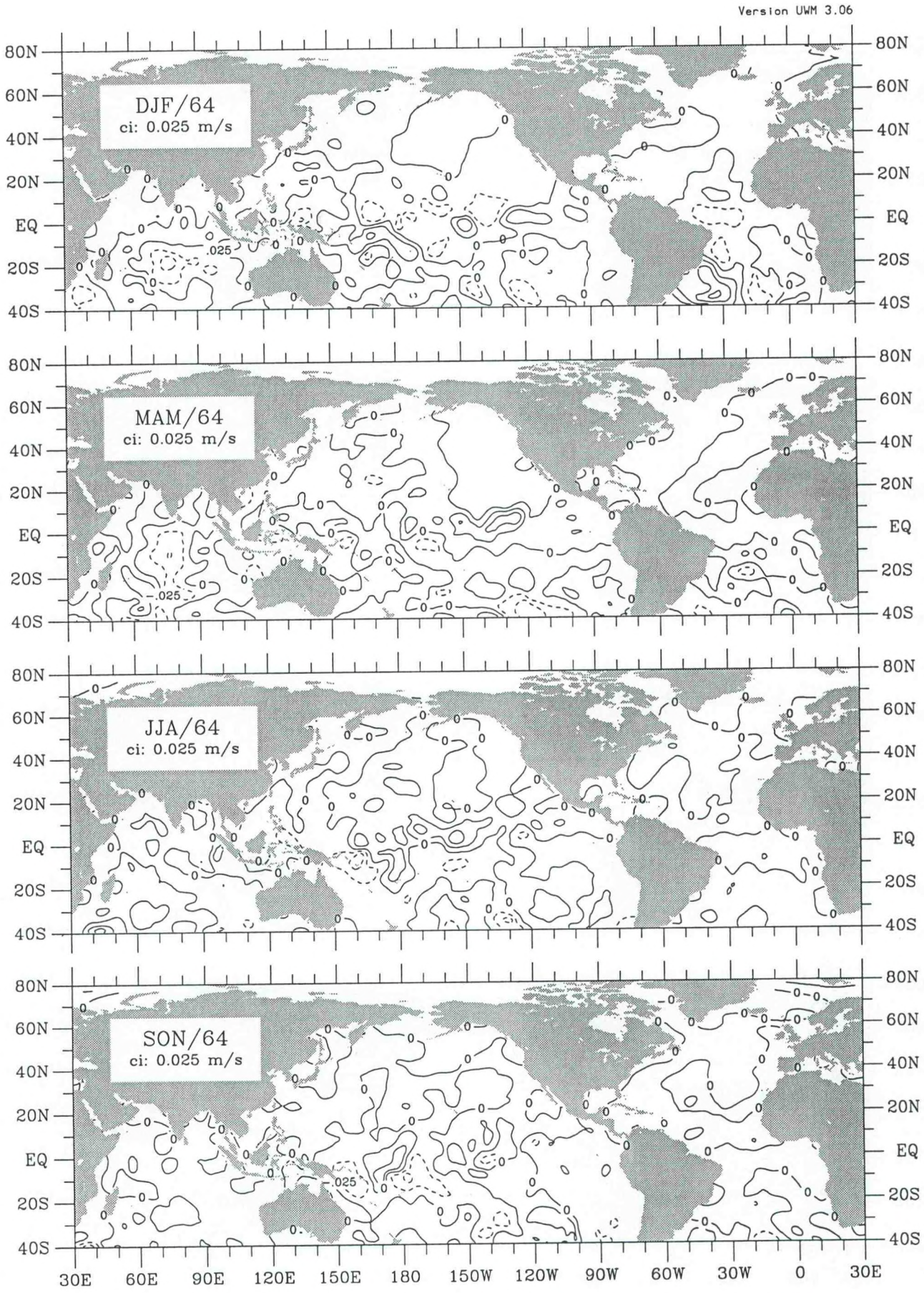

Figure vq-25. Merid. moisture flux seasonal anomaly for 1964.

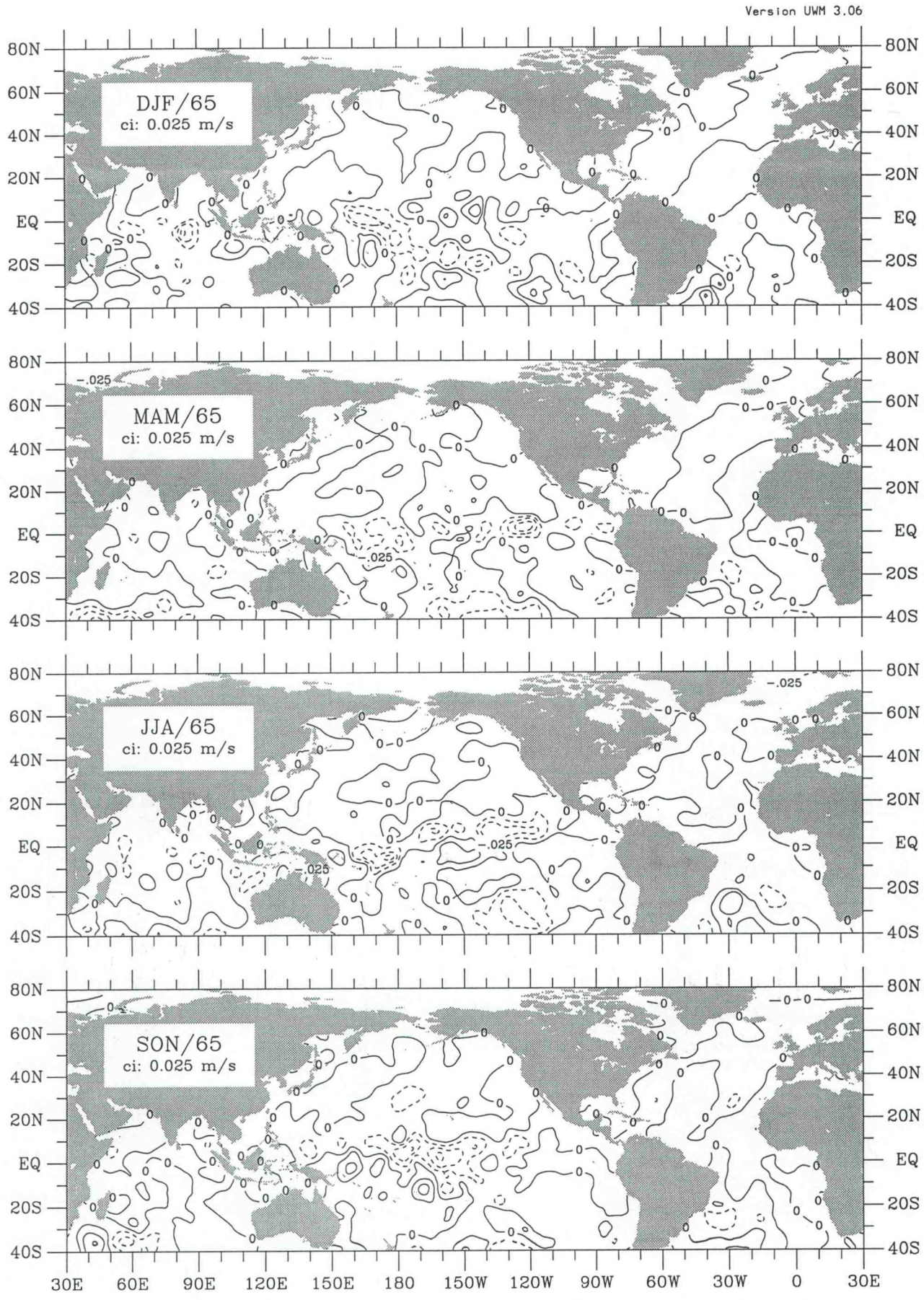

Figure vq-26. Merid. moisture flux seasonal anomaly for 1965.

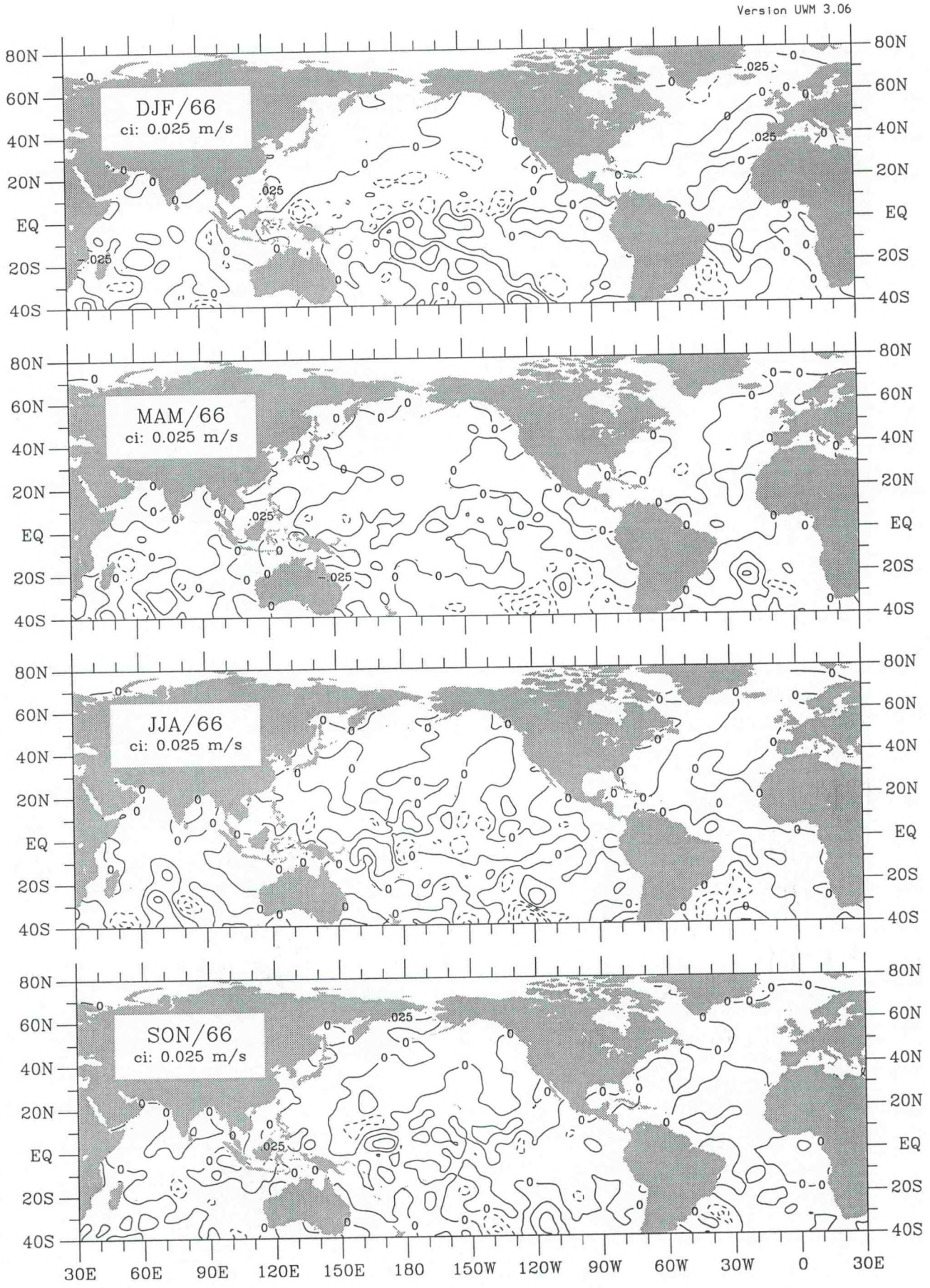

Figure vq-27. Merid. moisture flux seasonal anomaly for 1966.

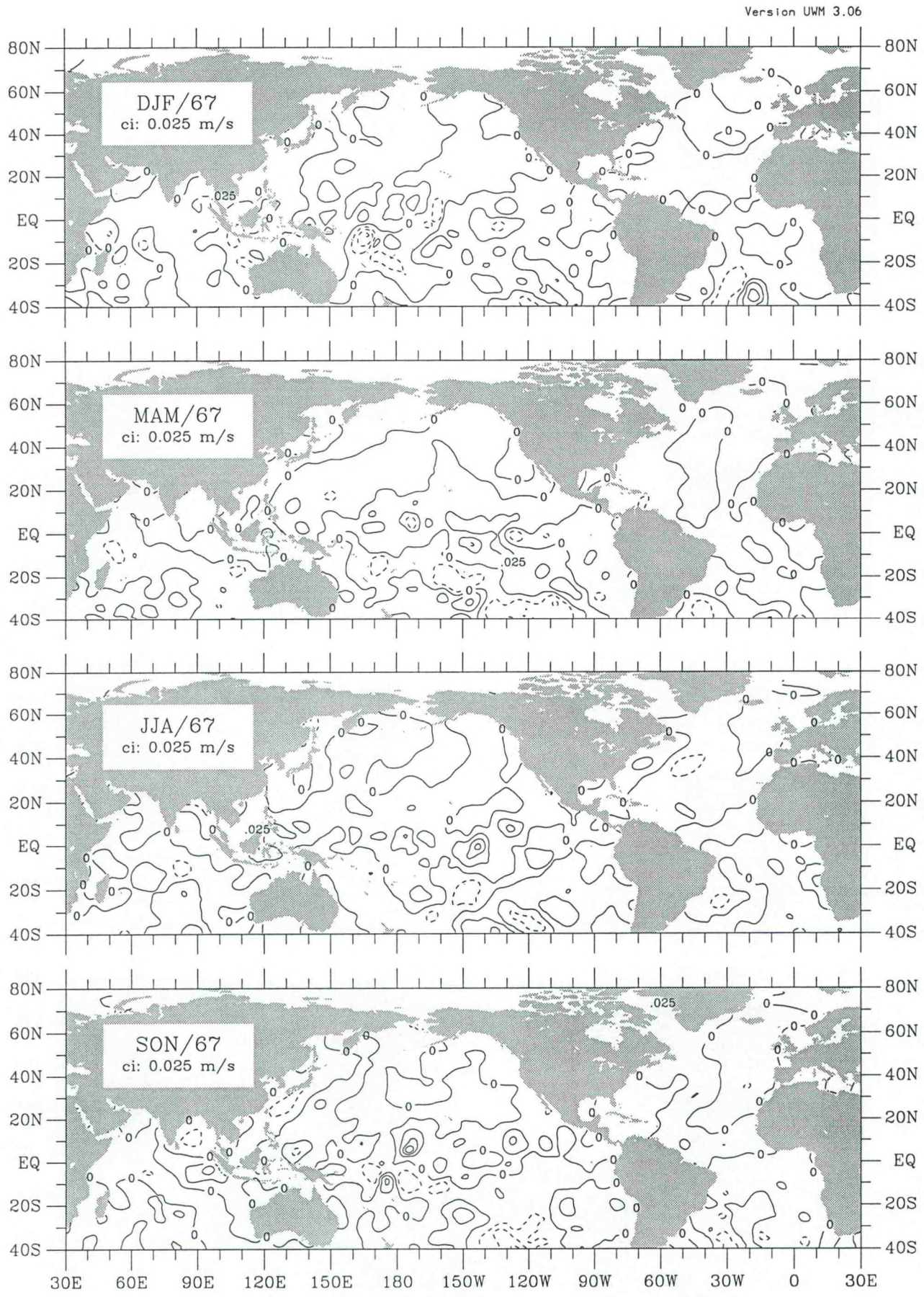

Figure vq-28. Merid. moisture flux seasonal anomaly for 1967.

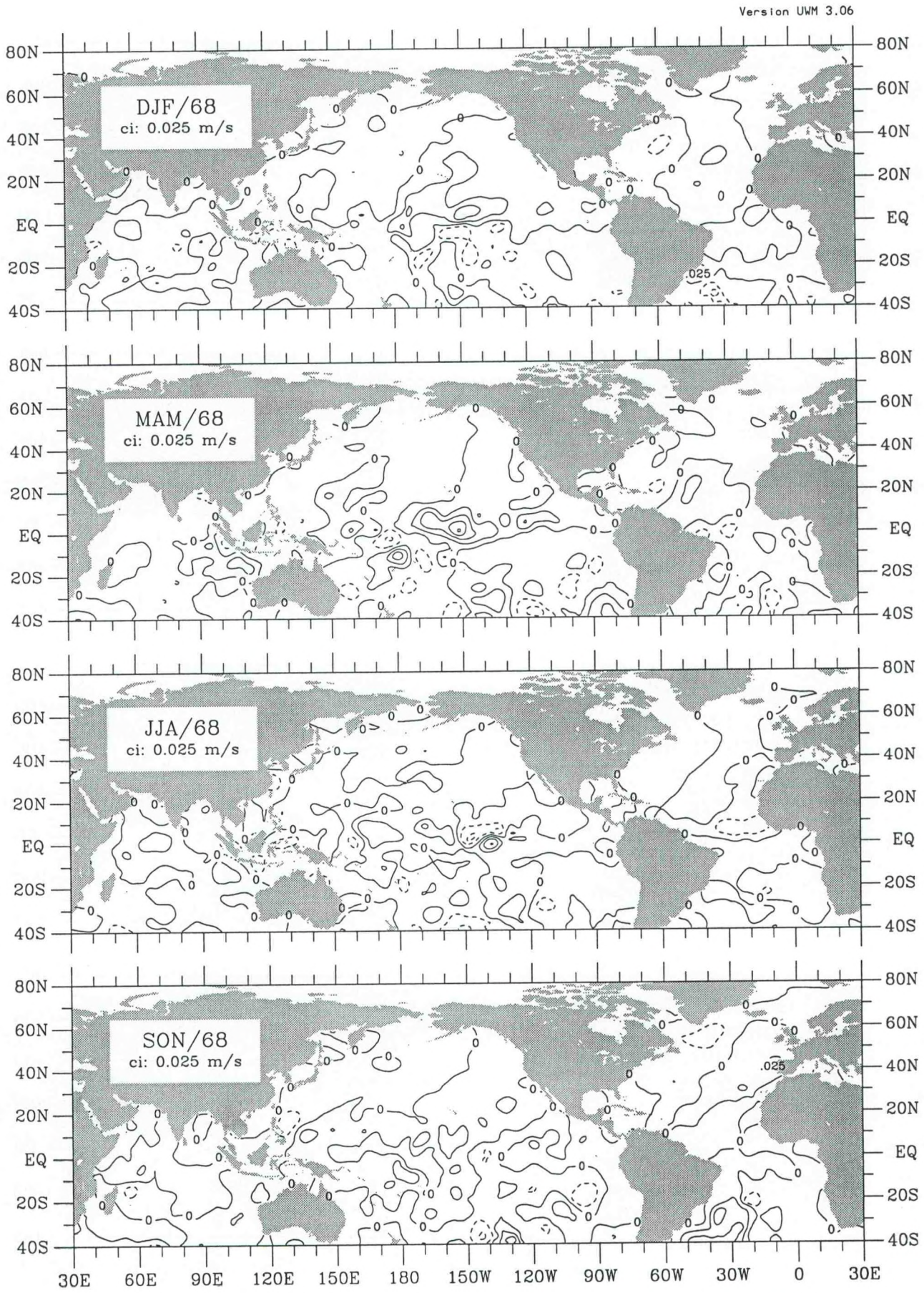

Figure vq-29. Merid. moisture flux seasonal anomaly for 1968.

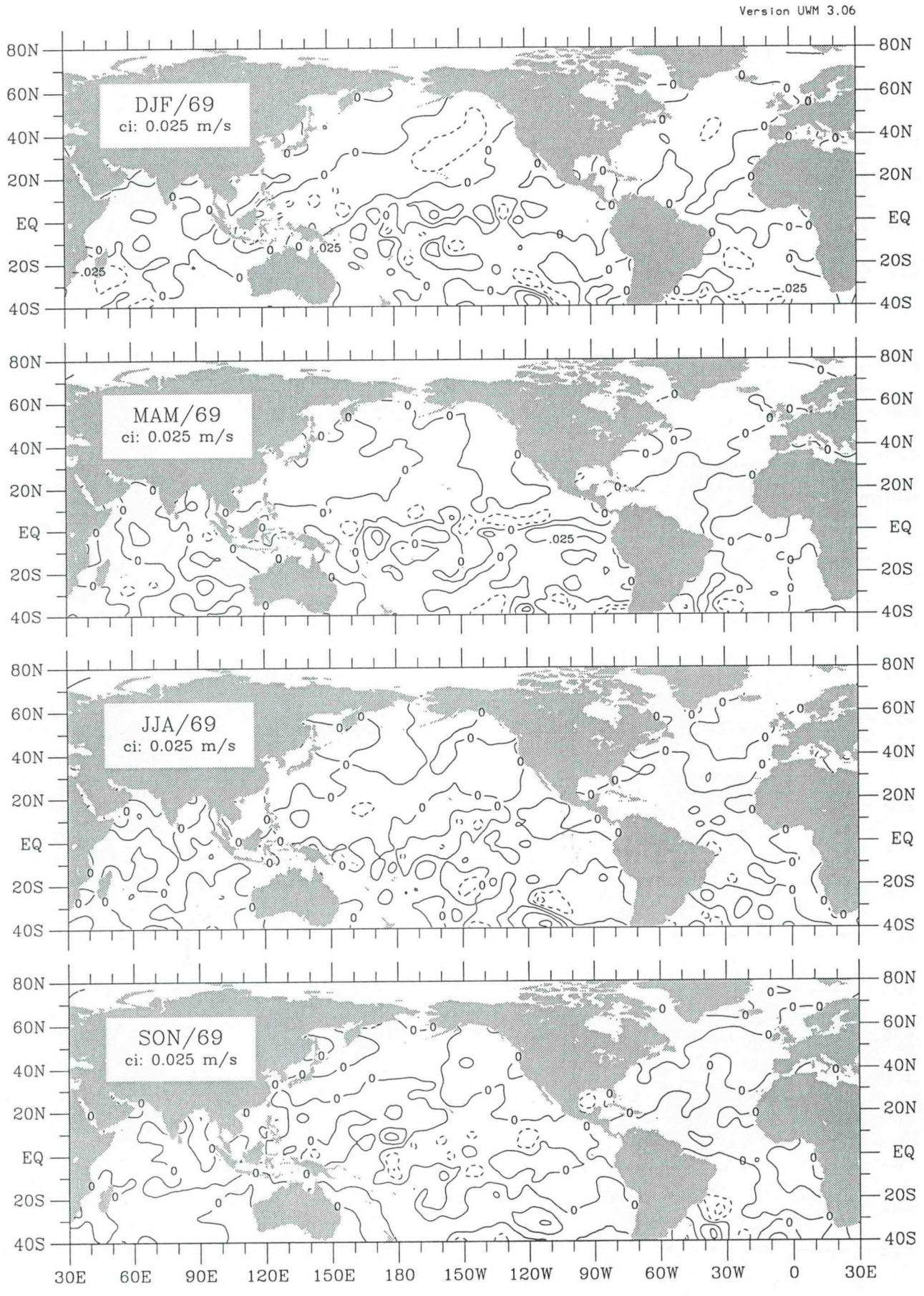

Figure vq-30. Merid. moisture flux seasonal anomaly for 1969.

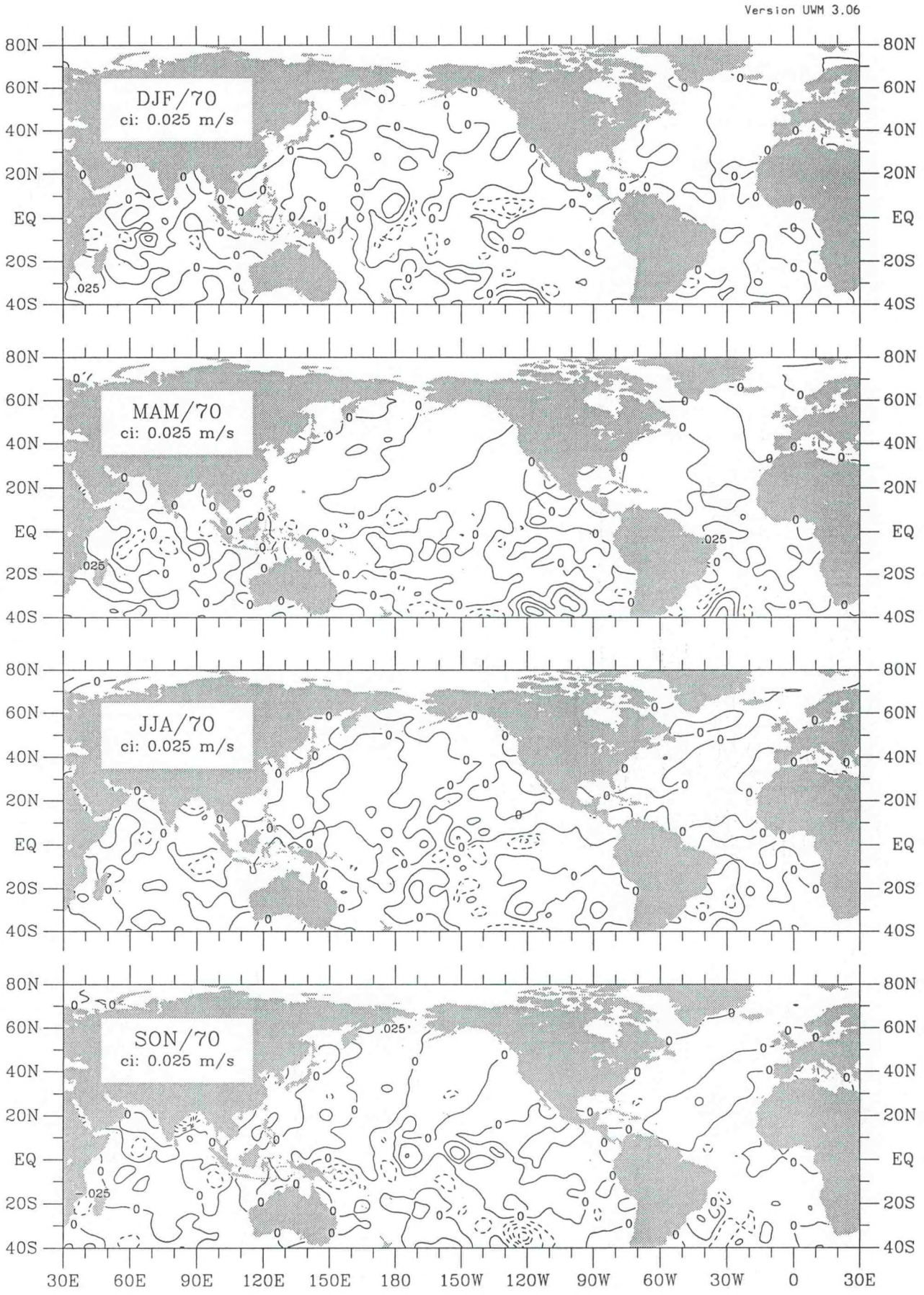

Figure vq-31. Merid. moisture flux seasonal anomaly for 1970.

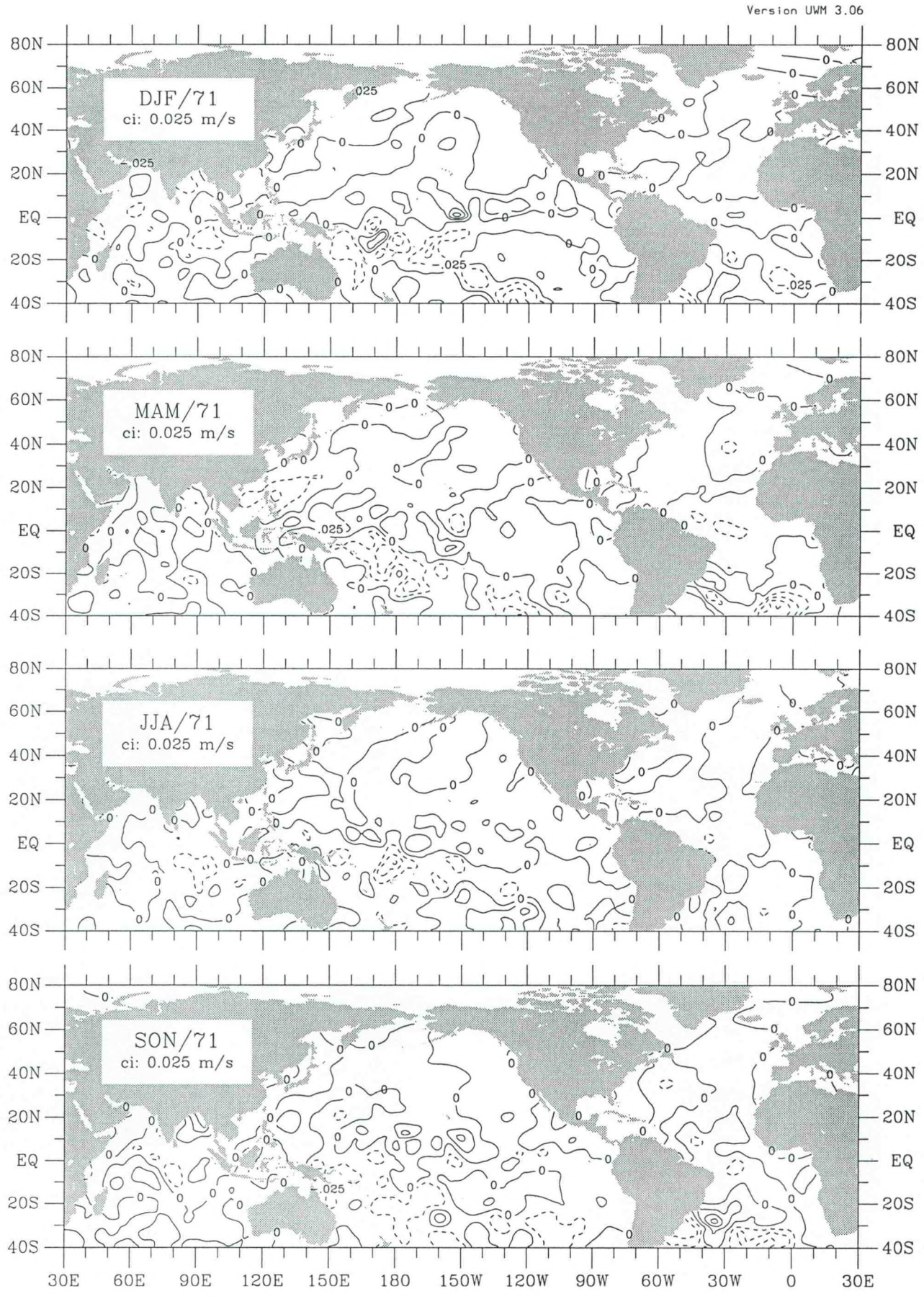

Figure vq-32. Merid. moisture flux seasonal anomaly for 1971.

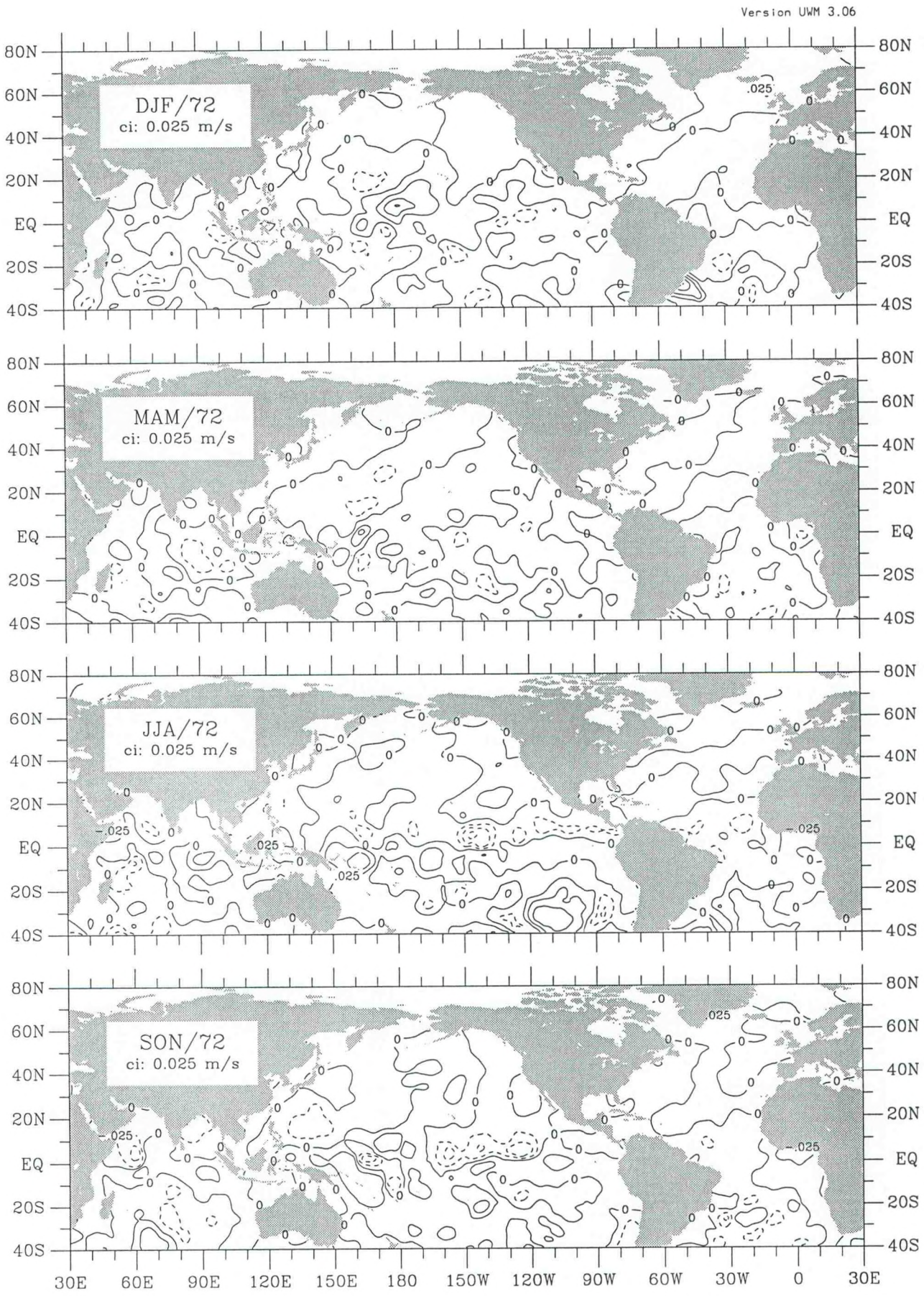

Figure vq-33. Merid. moisture flux seasonal anomaly for 1972.

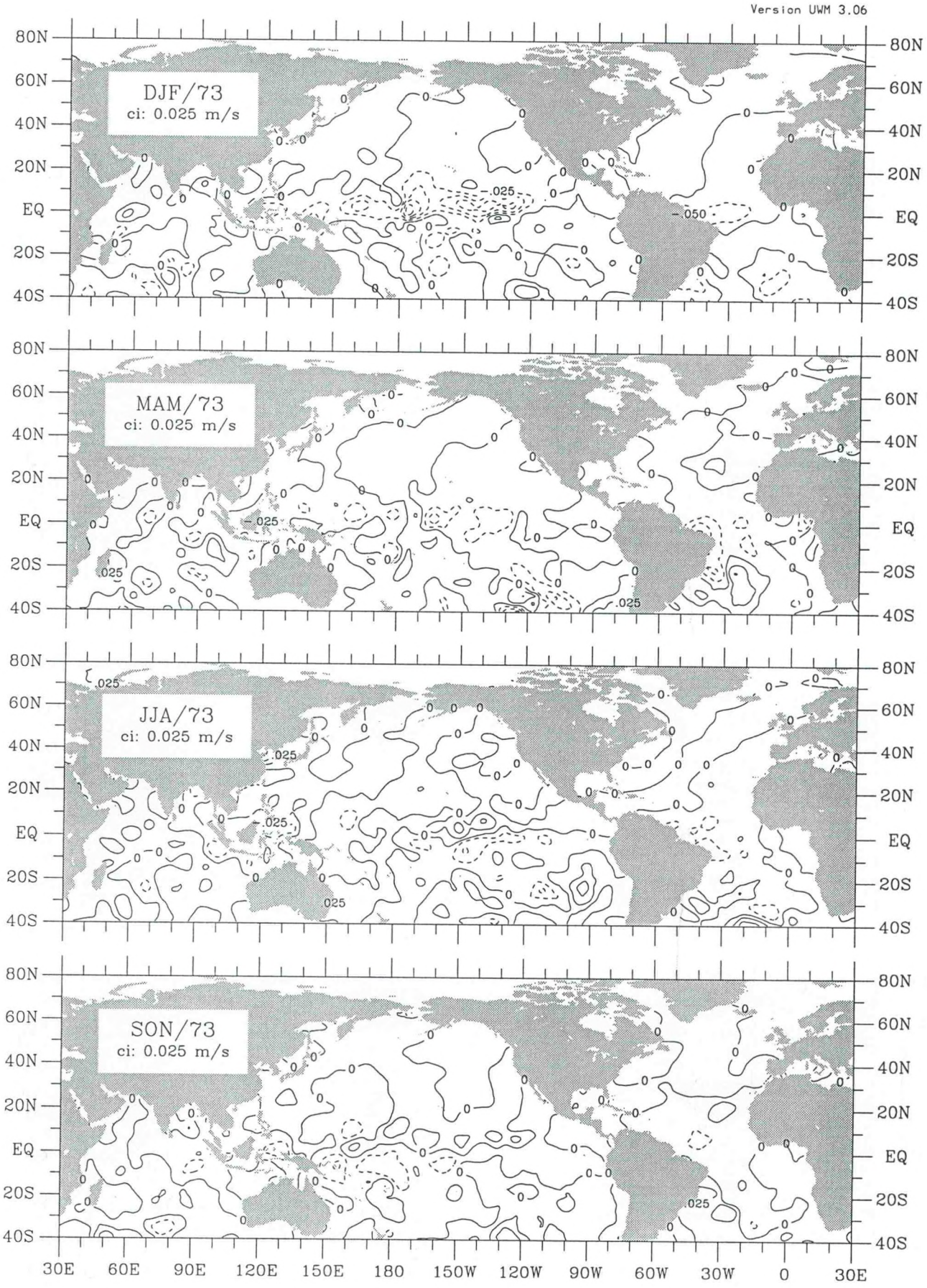

Figure vq-34. Merid. moisture flux seasonal anomaly for 1973.

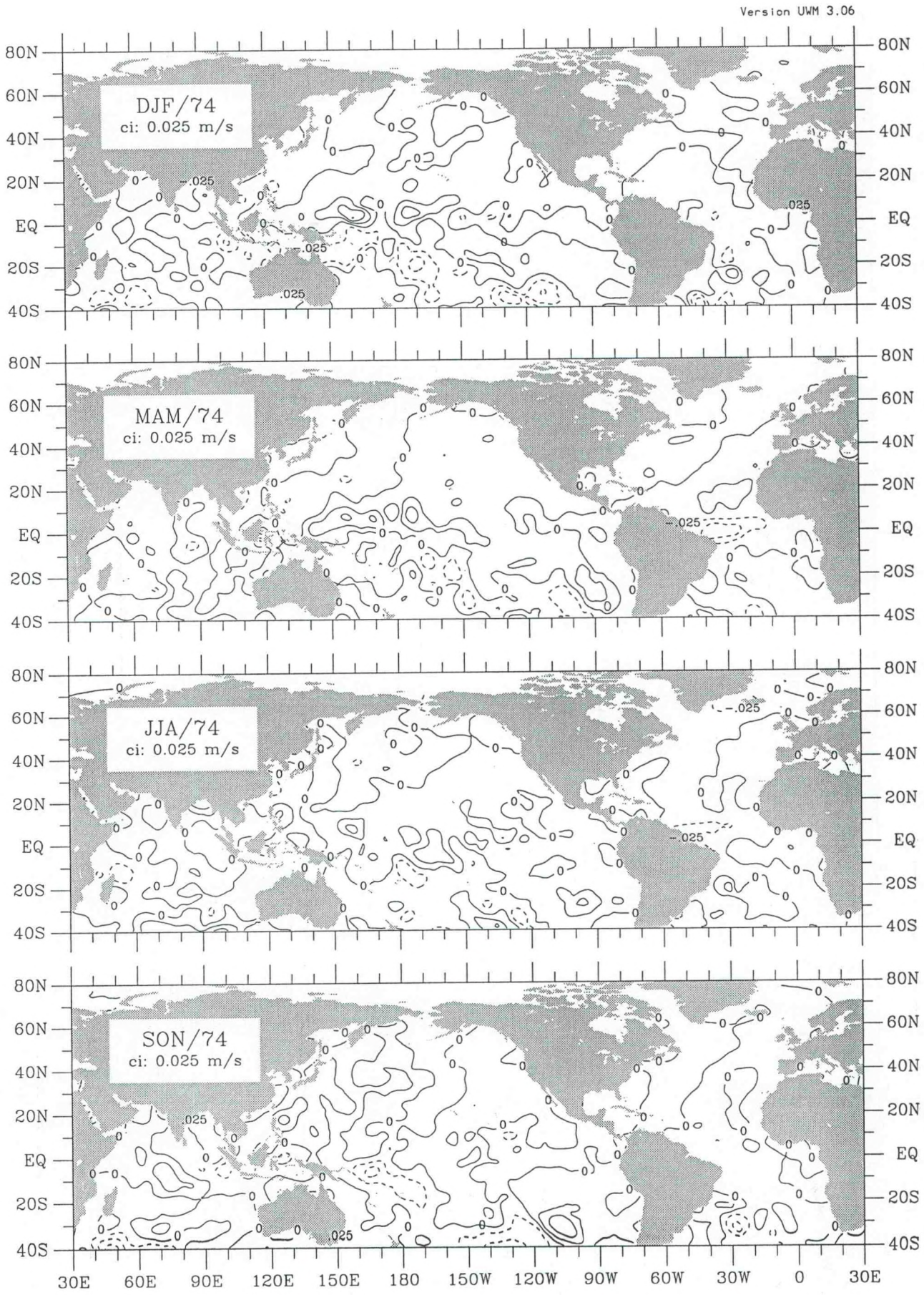

Figure vq-35. Merid. moisture flux seasonal anomaly for 1974.

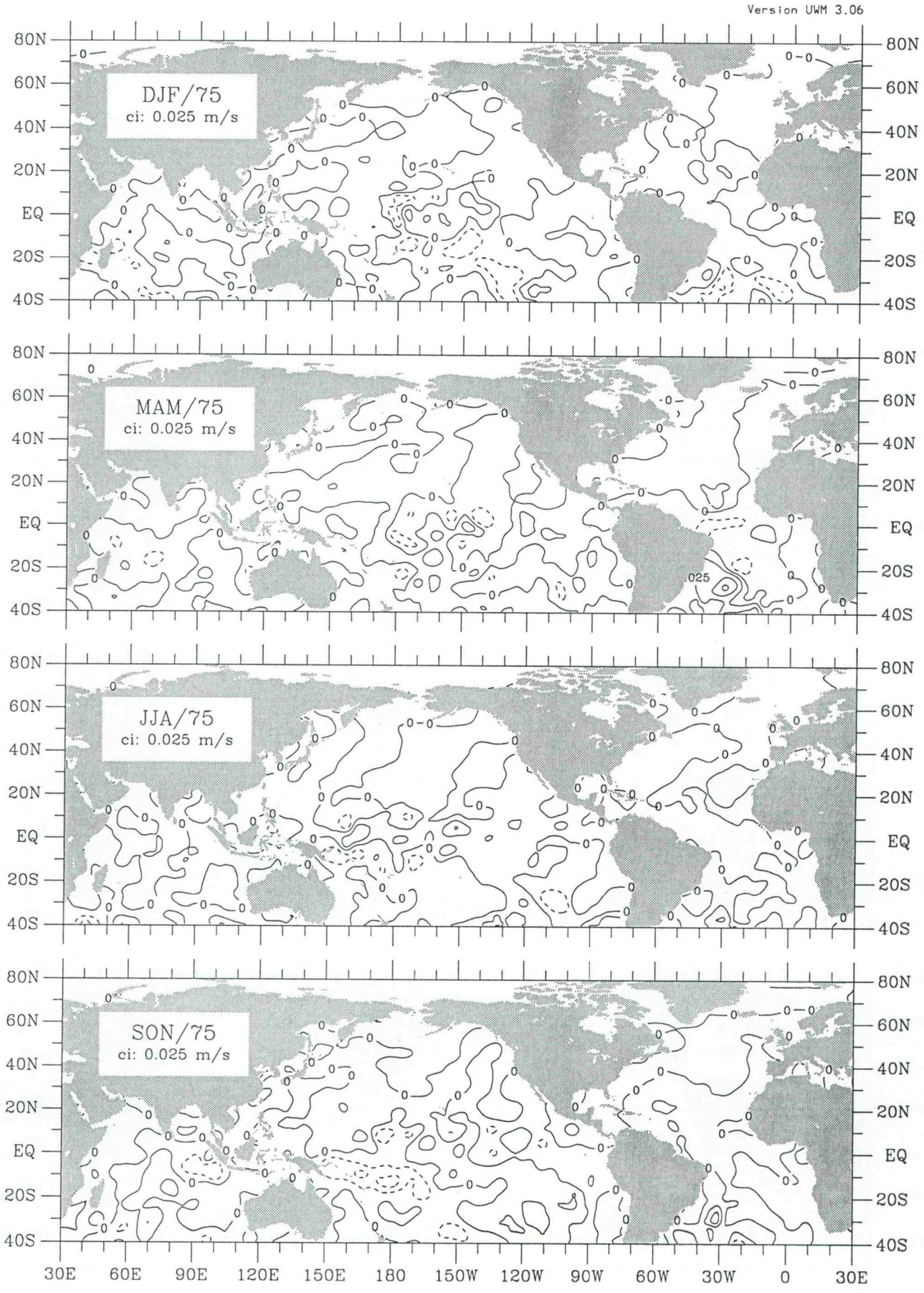

Figure vq-36. Merid. moisture flux seasonal anomaly for 1975.

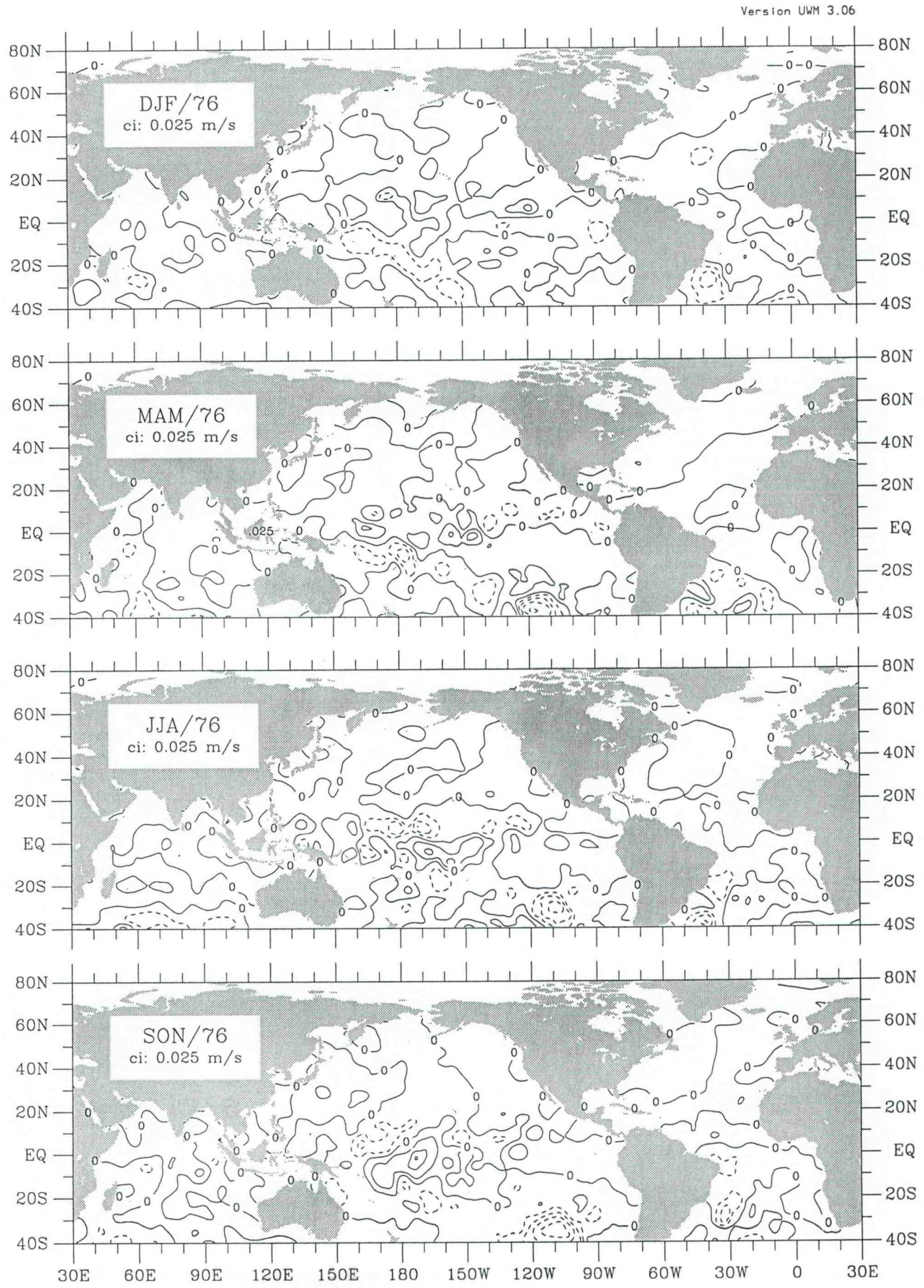

Figure vq-37. Merid. moisture flux seasonal anomaly for 1976.

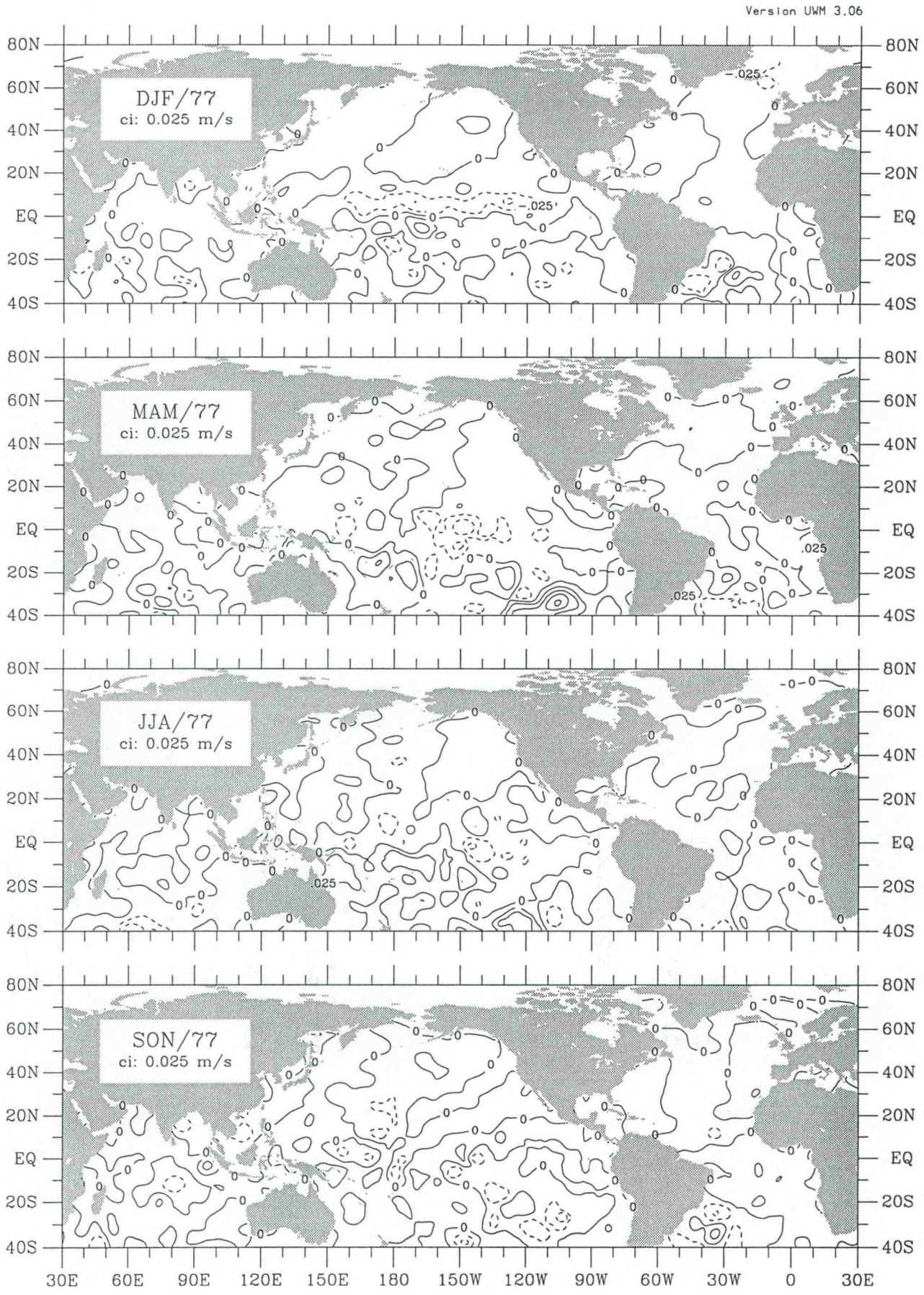

Figure vq-38. Merid. moisture flux seasonal anomaly for 1977.

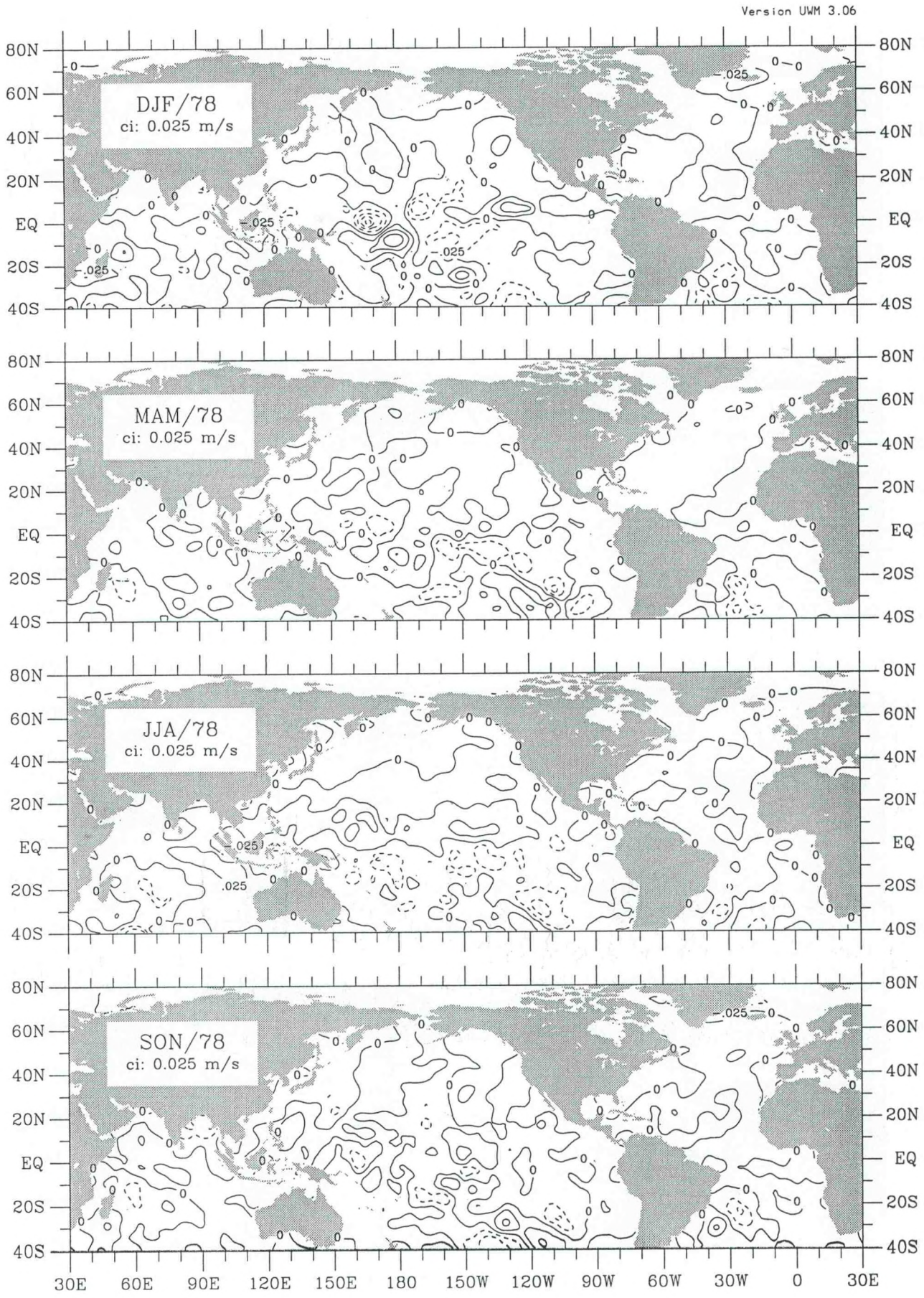

Figure vq-39. Merid. moisture flux seasonal anomaly for 1978.

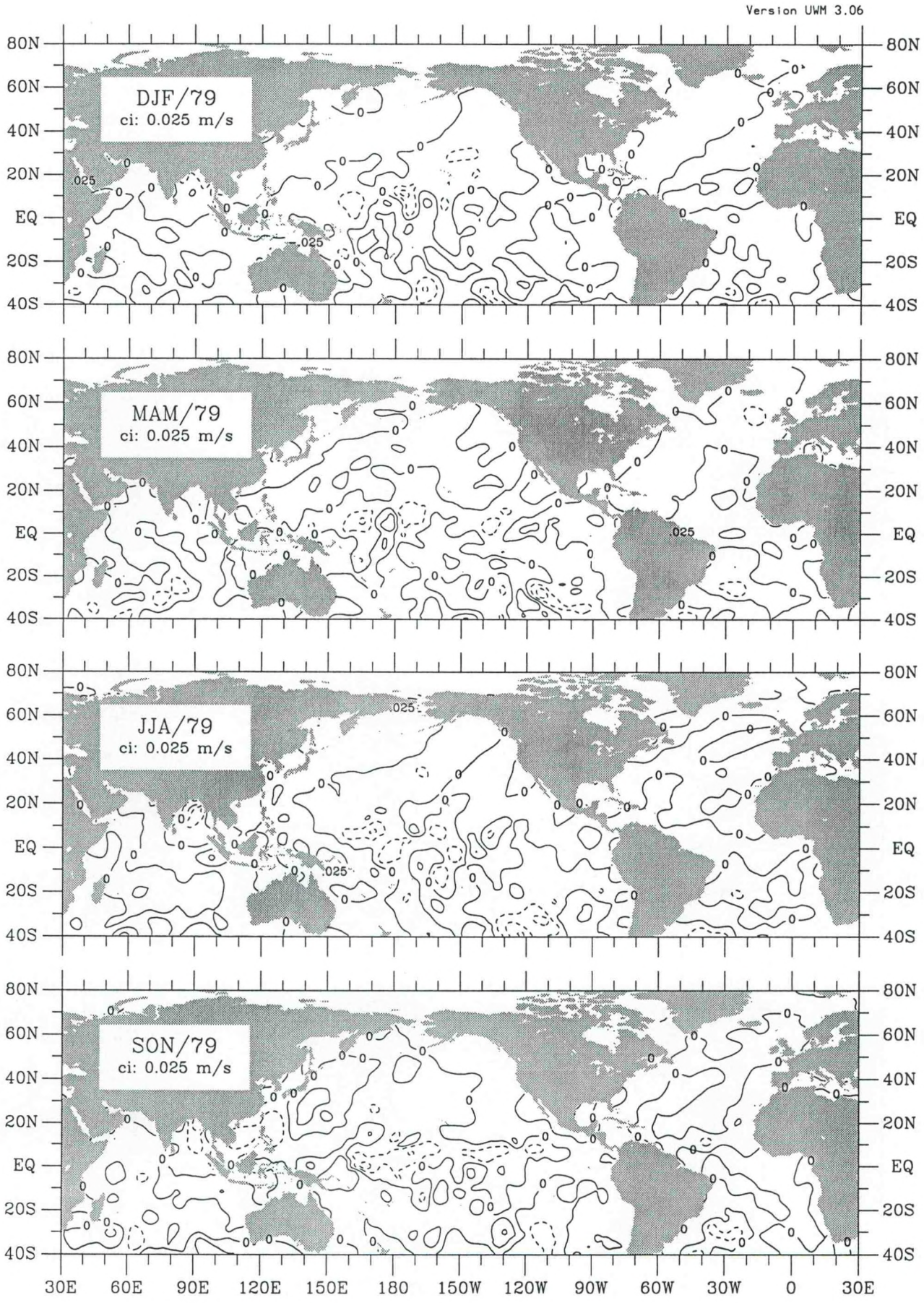

Figure vq-40. Merid. moisture flux seasonal anomaly for 1979.

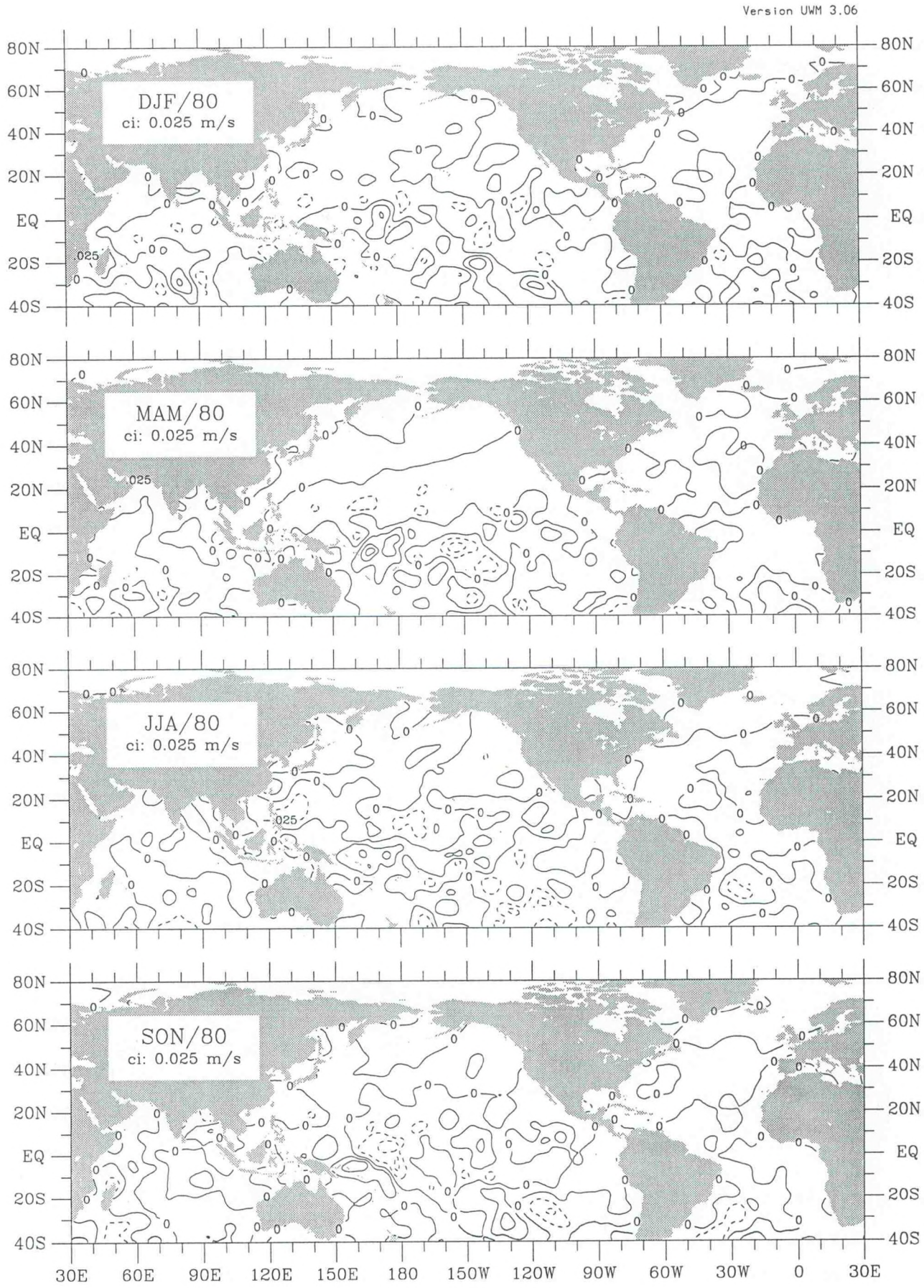

Figure vq-41. Merid. moisture flux seasonal anomaly for 1980.

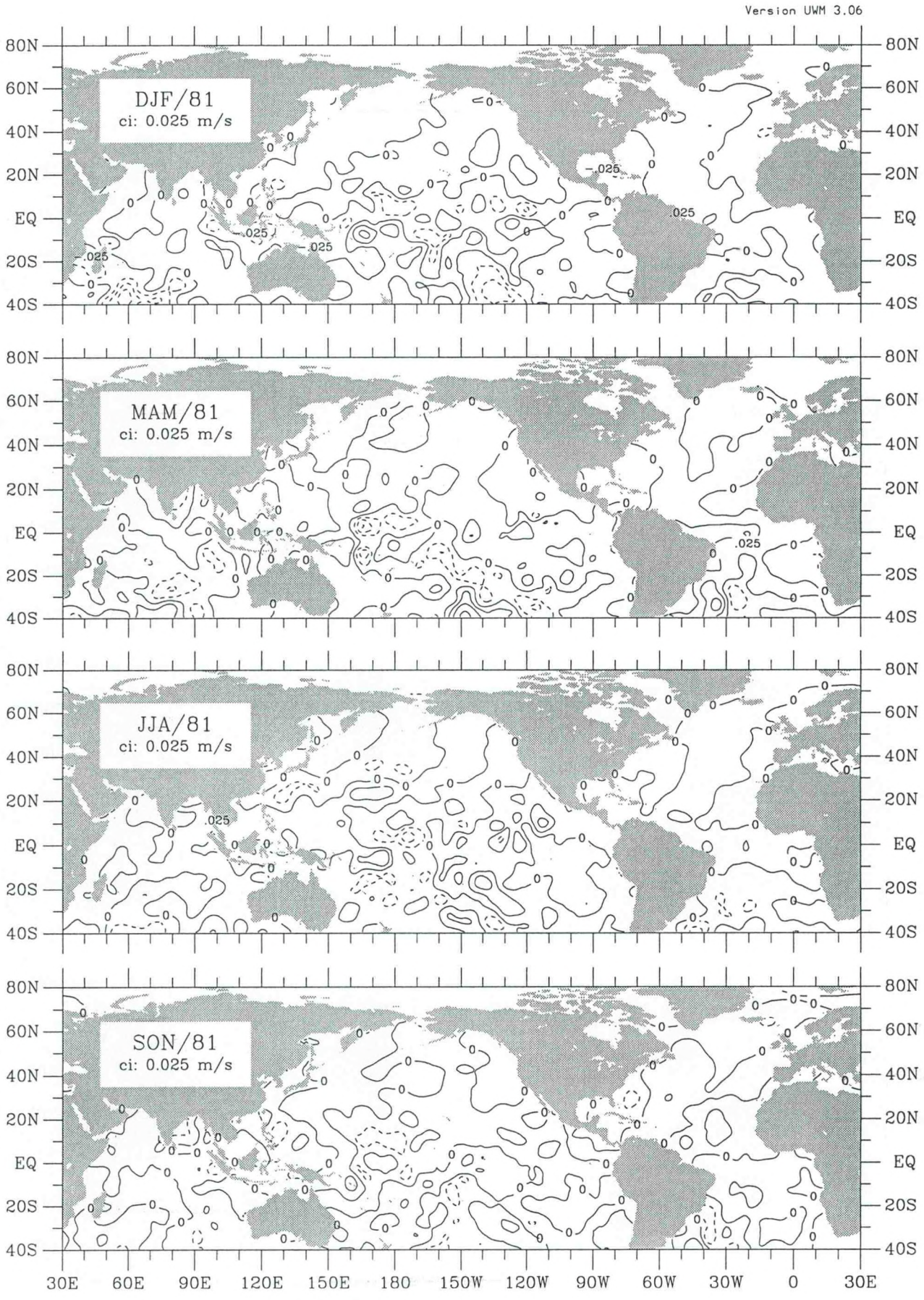

Figure vq-42. Merid. moisture flux seasonal anomaly for 1981.

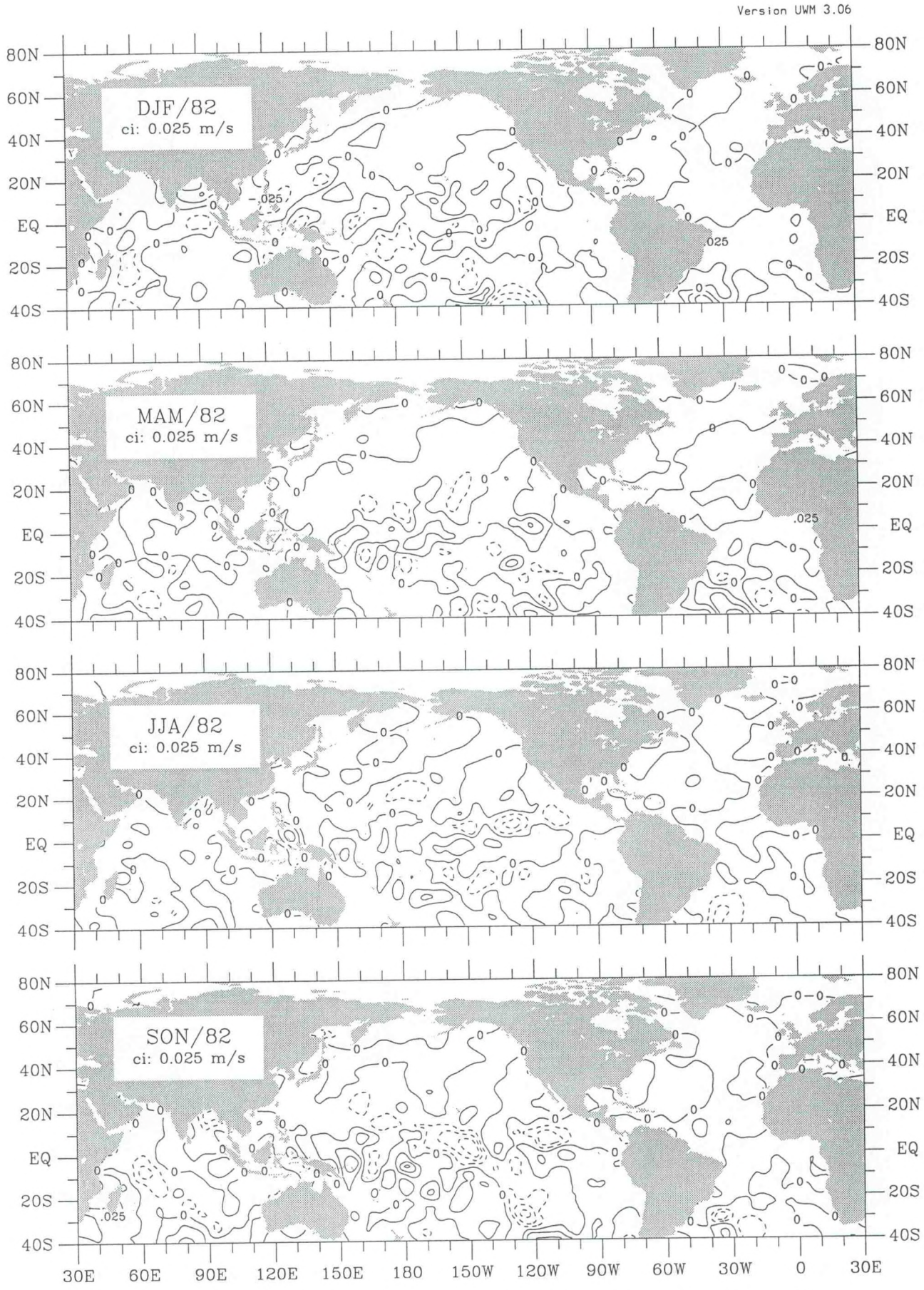

Figure vq-43. Merid. moisture flux seasonal anomaly for 1982.

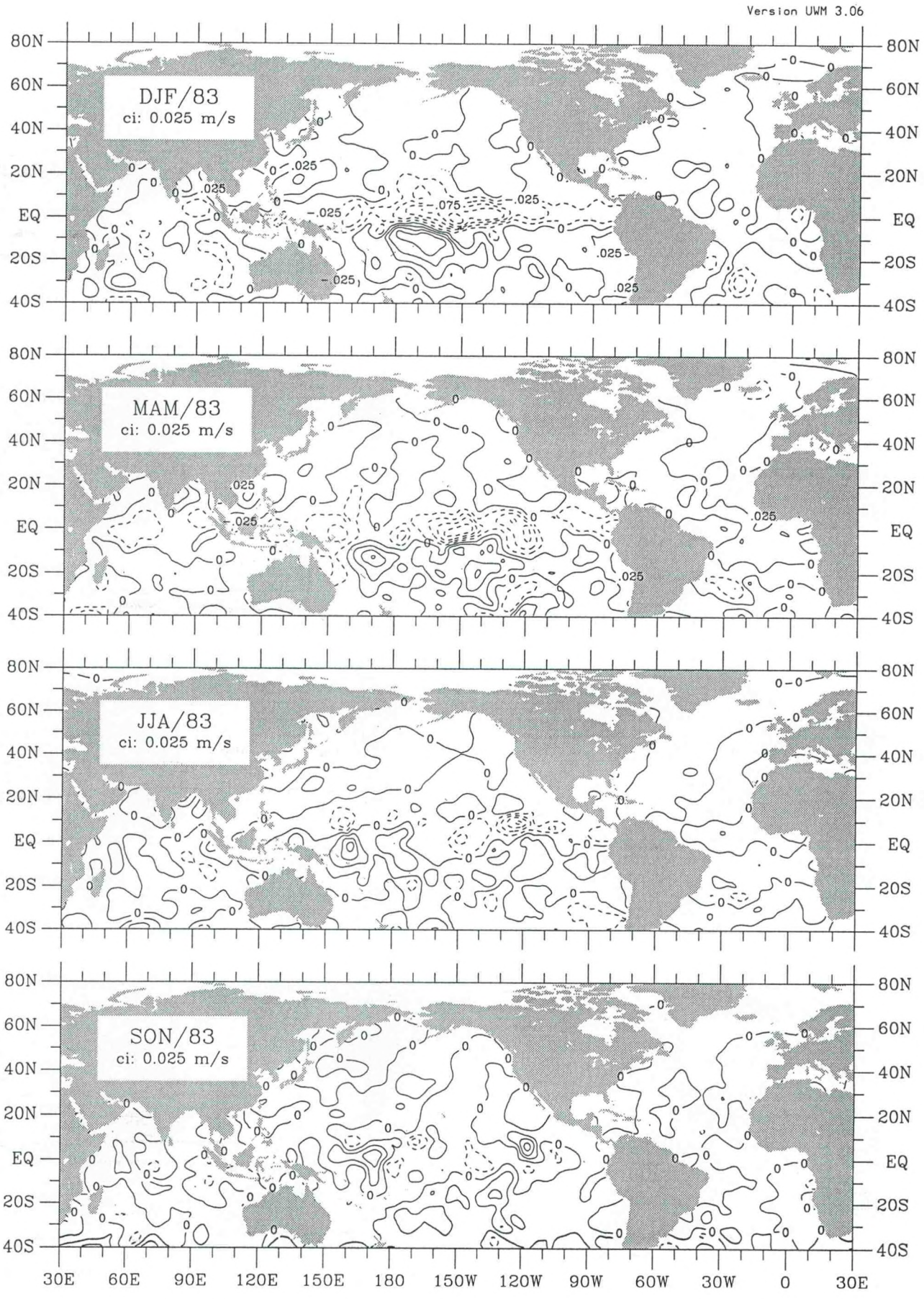

Figure vq-44. Merid. moisture flux seasonal anomaly for 1983.

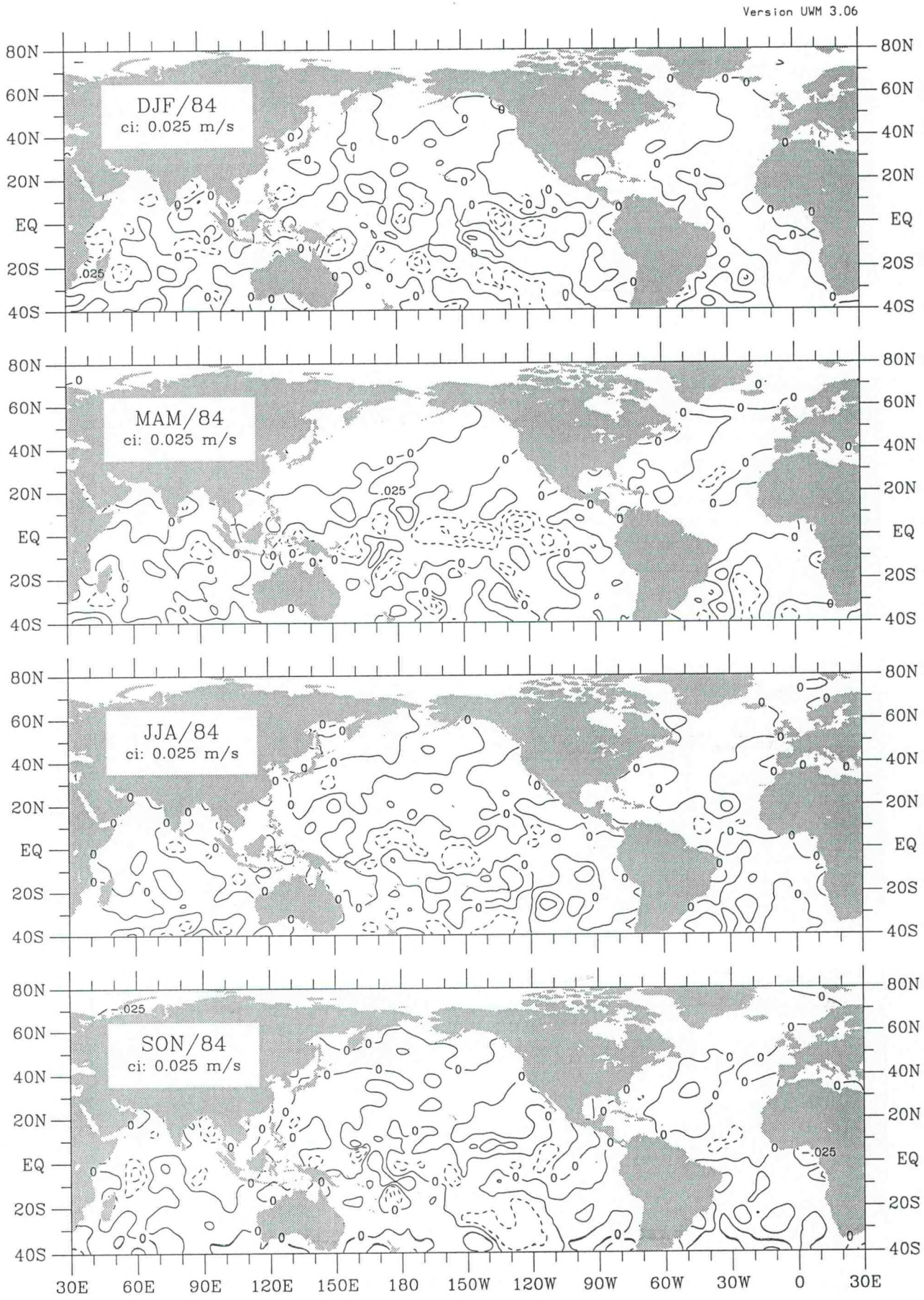

Figure vq-45. Merid. moisture flux seasonal anomaly for 1984.

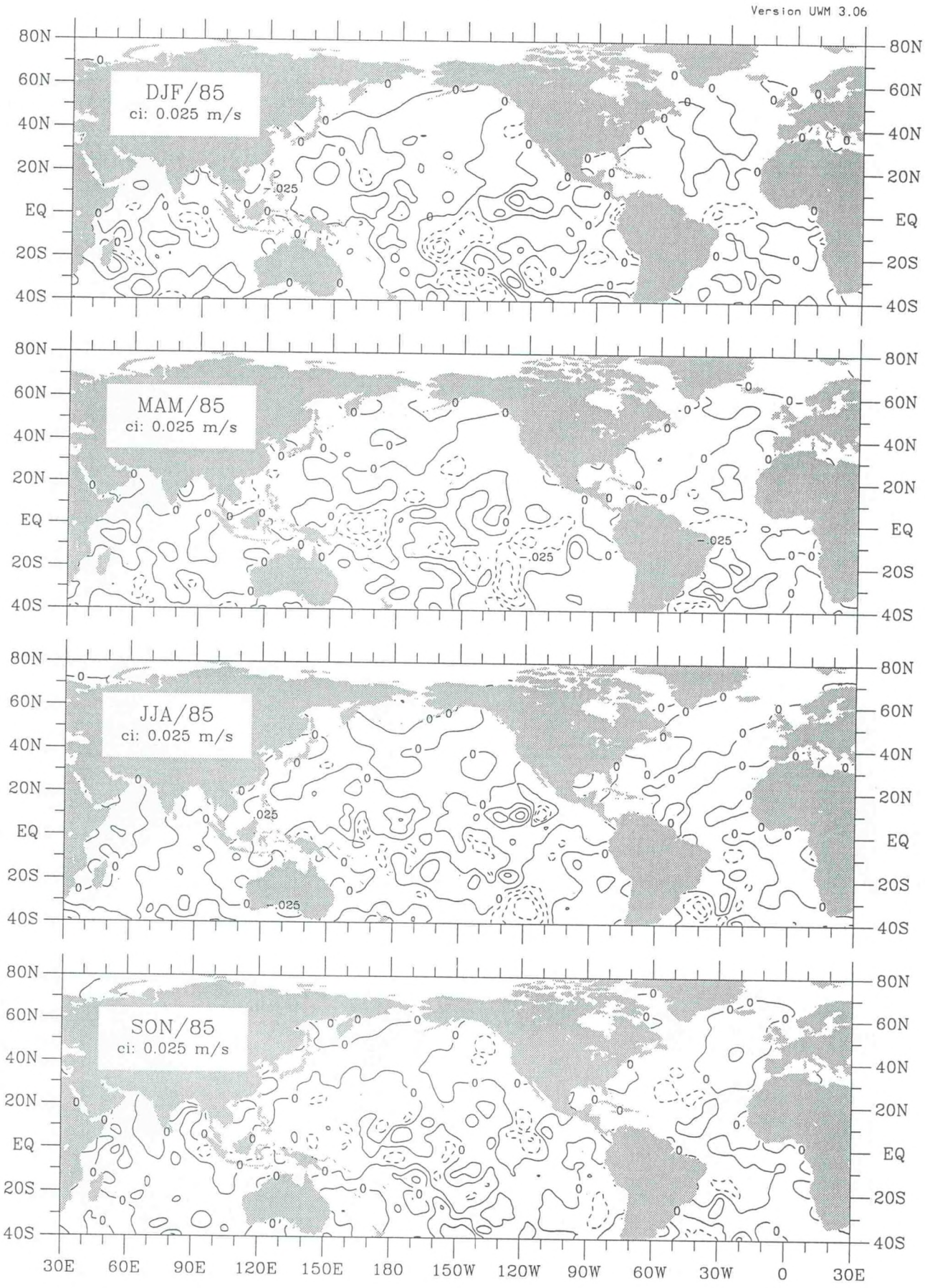

Figure vq-46. Merid. moisture flux seasonal anomaly for 1985.

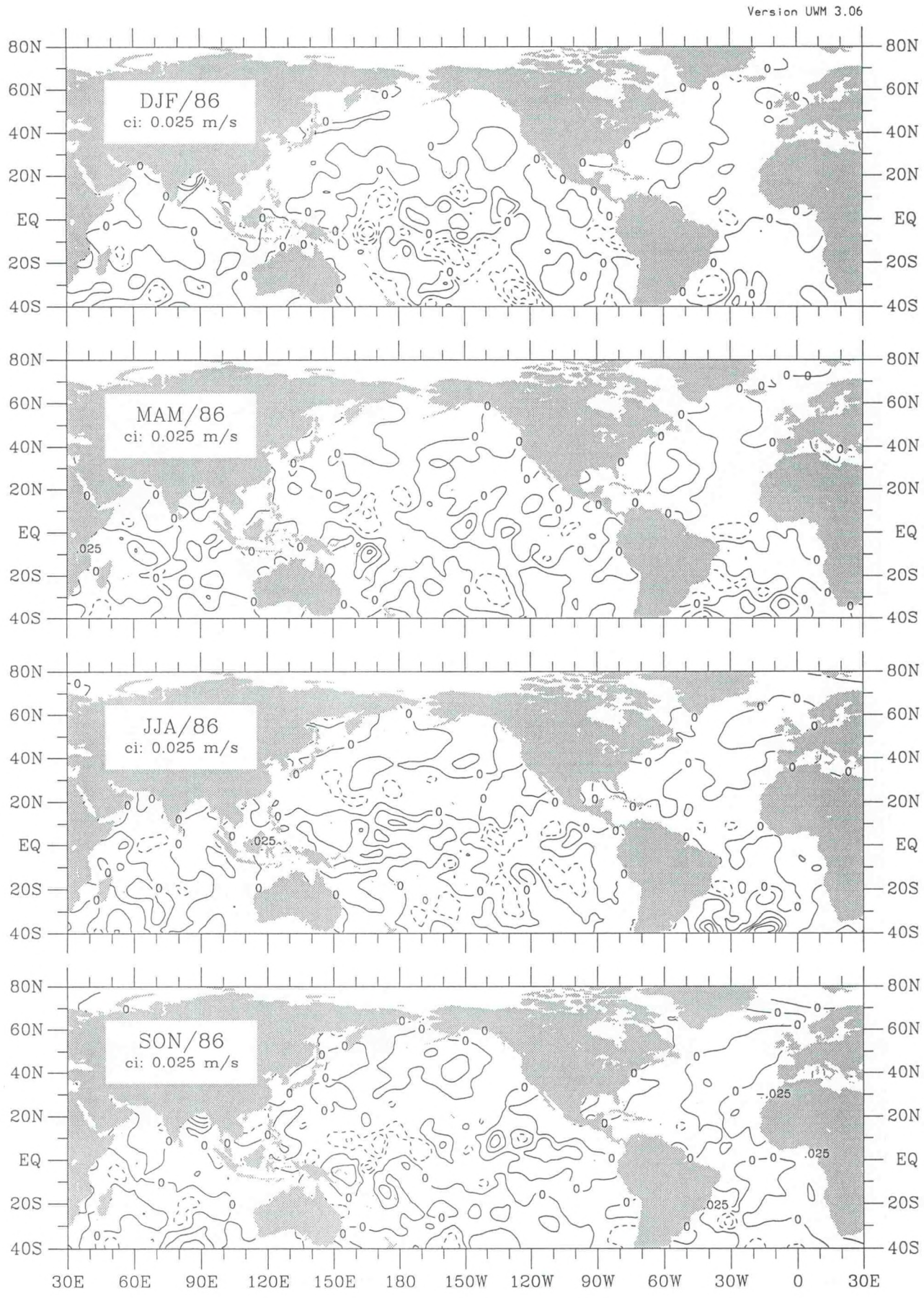

Figure vq-47. Merid. moisture flux seasonal anomaly for 1986.

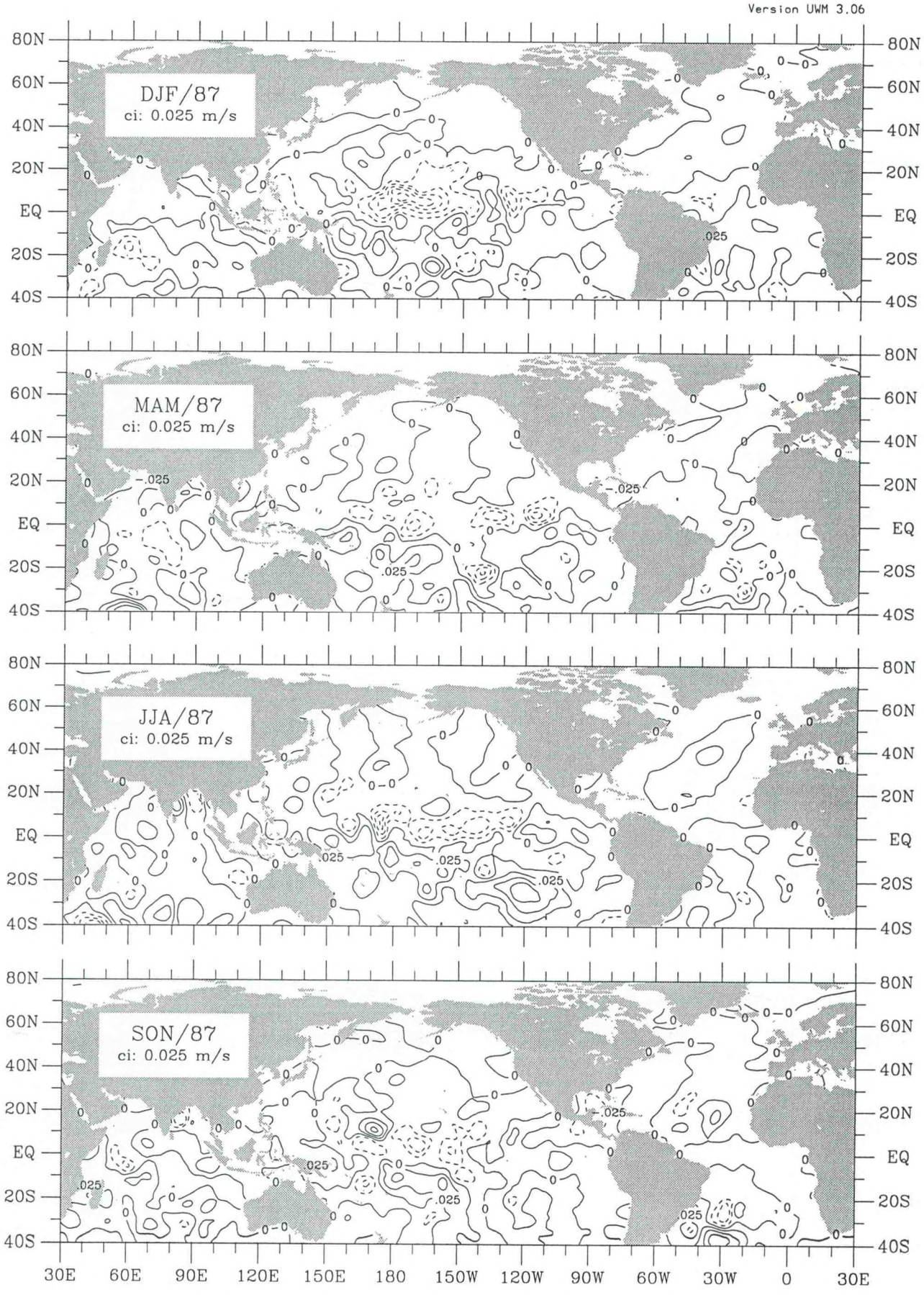

Figure vq-48. Merid. moisture flux seasonal anomaly for 1987.

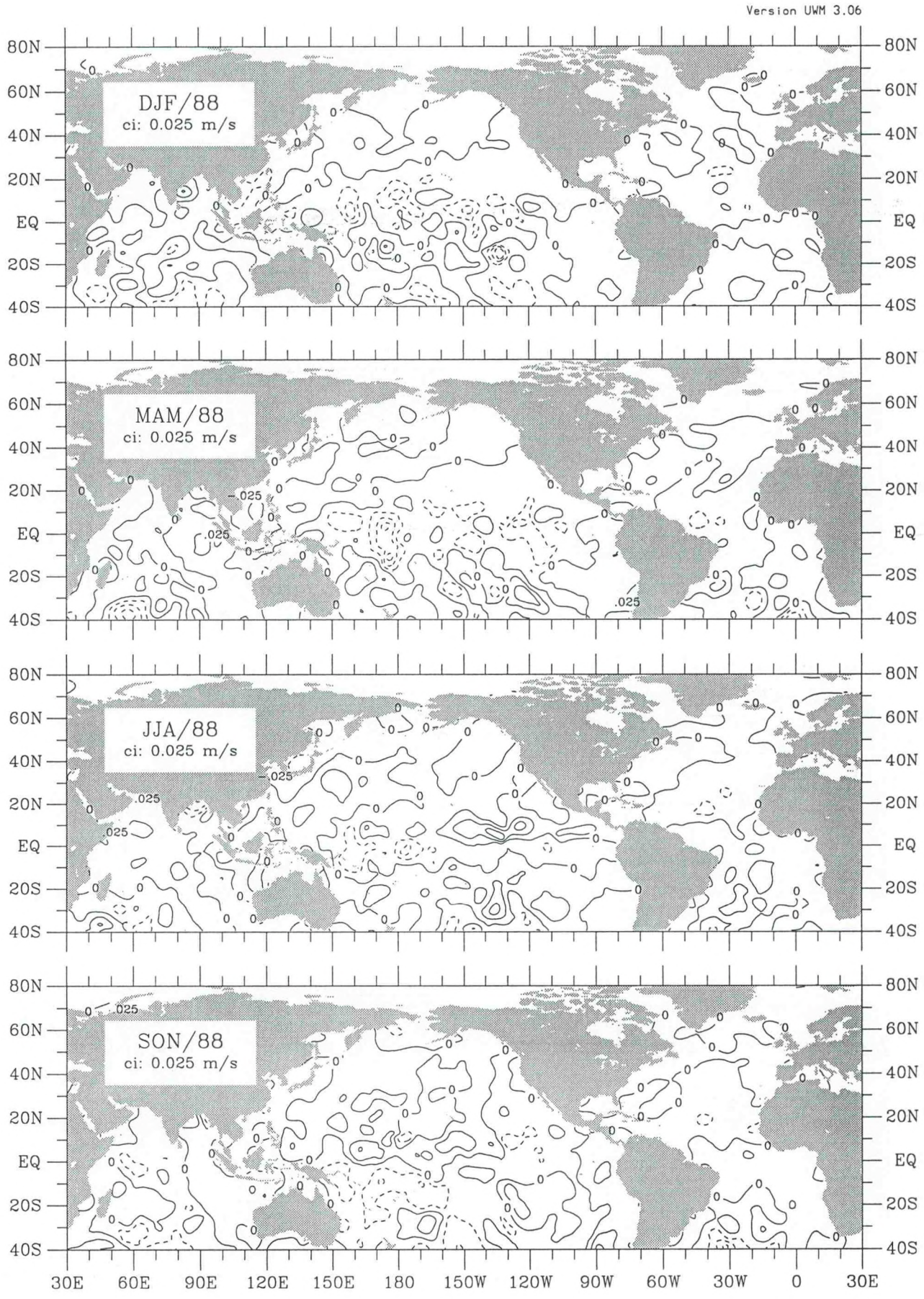

Figure vq-49. Merid. moisture flux seasonal anomaly for 1988.

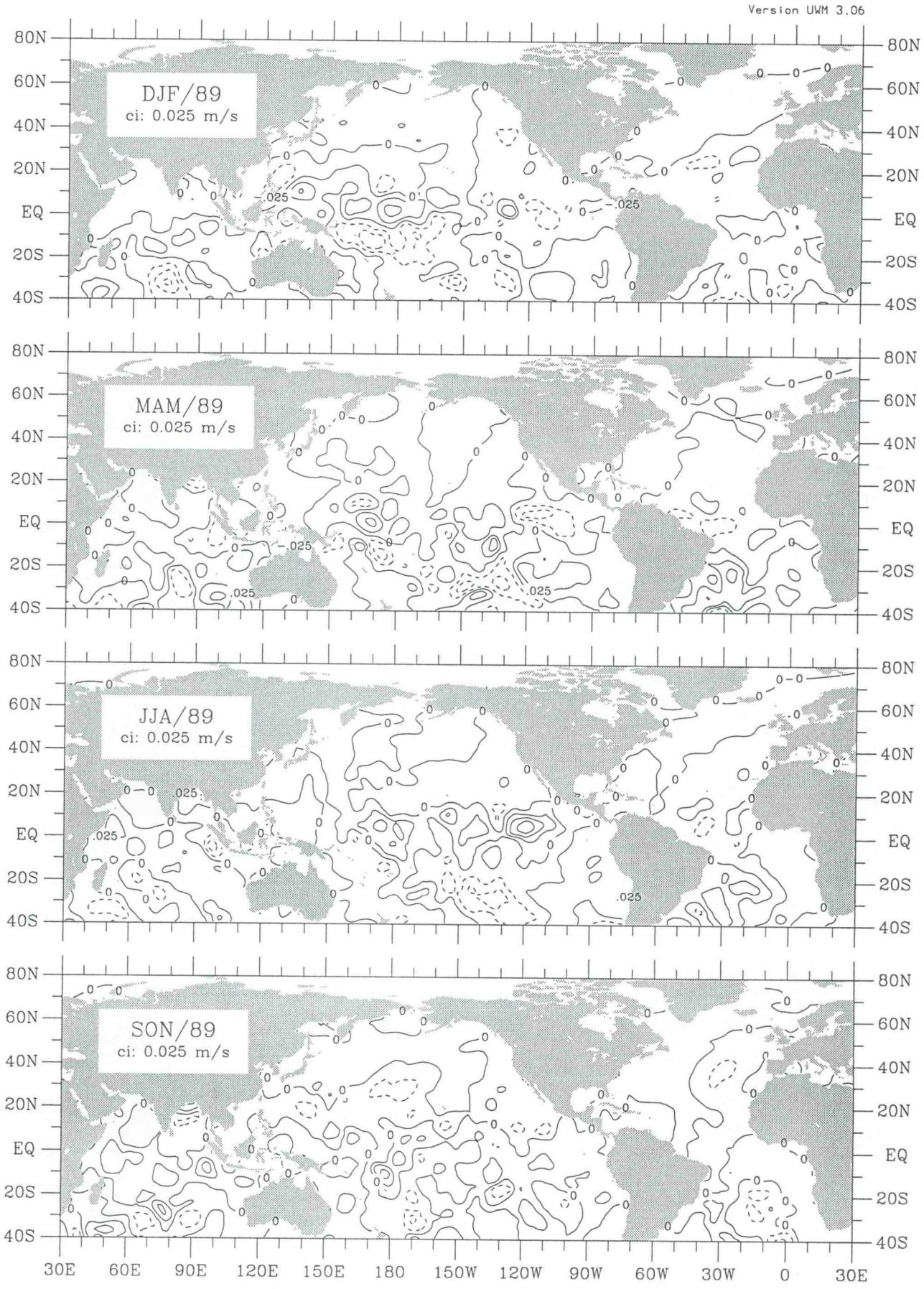

Figure vq-50. Merid. moisture flux seasonal anomaly for 1989.

NOAA SCIENTIFIC AND TECHNICAL PUBLICATIONS

The National Oceanic and Atmospheric Administration was established as part of the Department of Commerce on October 3, 1970. The mission responsibilities of NOAA are to assess the socioeconomic impact of natural and technological changes in the environment and to monitor and predict the state of the solid Earth, the oceans and their living resources, the atmosphere, and the space environment of the Earth.

The major components of NOAA regularly produce various types of scientific and technical information in the following kinds of publications:

PROFESSIONAL PAPERS - Important definitive research results, major techniques, and special investigations.

CONTRACT AND GRANT REPORTS - Reports prepared by contractors or grantees under NOAA sponsorship.

ATLAS - Presentation of analyzed data generally in the form of maps showing distribution of rainfall, chemical and physical conditions of oceans and atmosphere, distribution of fishes and marine mammals, ionospheric conditions, etc.

TECHNICAL SERVICE PUBLICATIONS - Reports containing data, observations, instructions, etc. A partial listing includes data serials; prediction and outlook periodicals; technical manuals, training papers, planning reports, and information serials; and miscellaneous technical publications.

TECHNICAL REPORTS - Journal quality with extensive details, mathematical developments, or data listings.

TECHNICAL MEMORANDUMS - Reports of preliminary, partial, or negative research or technology results, interim instructions, and the like.

U.S. DEPARTMENT OF COMMERCE
National Oceanic and Atmospheric Administration
National Environmental Satellite, Data, and Information Service
Washington, D.C. 20233